PB88-168968

FUNDAMENTAL COMBUSTION RESEARCH APPLIED TO POLLUTION FORMATION
VOLUME III. SUPPORT STUDIES: MEASUREMENT STUDIES

Energy and Environmental Research Corporation
Irvine, CA

Feb 88

U.S. Department of Commerce
National Technical Information Service
NTIS

PB88-168968

EPA/600/7-88/002
February 1988

FUNDAMENTAL COMBUSTION RESEARCH APPLIED TO POLLUTION FORMATION

VOLUME III. SUPPORT STUDIES: MEASUREMENT STUDIES

by

W. R. Seeker and M. P. Heap

Energy and Environmental Research Corporation
18 Mason
Irvine, California 92714

EPA Contract No. 68-02-2631
EPA Project Officer: W. Steven Lanier
Air and Energy Engineering Research Laboratory
Research Triangle Park, North Carolina 27711

AIR AND ENERGY ENGINEERING RESEARCH LABORATORY
OFFICE OF RESEARCH AND DEVELOPMENT
U.S. ENVIRONMENTAL PROTECTION AGENCY
RESEARCH TRIANGLE PARK, NC 27711

REPRODUCED BY
U.S. DEPARTMENT OF COMMERCE
NATIONAL TECHNICAL
INFORMATION SERVICE
SPRINGFIELD, VA. 22161

TECHNICAL REPORT DATA
(Please read Instructions on the reverse before completing)

1. REPORT NO. EPA/600/7-88/002
2.
3. RECIPIENT'S ACCESSION NO. PB88 168968/AS
4. TITLE AND SUBTITLE Fundamental Combustion Research Applied to Pollution Formation; Volume III. Support Studies: Measurement Studies
5. REPORT DATE February 1988
6. PERFORMING ORGANIZATION CODE
7. AUTHOR(S) W. R. Seeker and M. P. Heap
8. PERFORMING ORGANIZATION REPORT NO.
9. PERFORMING ORGANIZATION NAME AND ADDRESS
Energy and Environmental Research Corporation
18 Mason
Irvine, California 92718
10. PROGRAM ELEMENT NO.
11. CONTRACT/GRANT NO. 68-02-2631
12. SPONSORING AGENCY NAME AND ADDRESS
EPA, Office of Research and Development
Air and Energy Engineering Research Laboratory
Research Triangle Park, NC 27711
13. TYPE OF REPORT AND PERIOD COVERED Final: 1/77 - 9/80
14. SPONSORING AGENCY CODE EPA/600/13
15. SUPPLEMENTARY NOTES AEERL project officer W. S. Lanier is no longer with the Agency; for details contact William P. Linak, Mail Drop 65, 919/541-5792.

16. ABSTRACT The report, one of four volumes describing research performed under EPA's Fundamental Combustion Research (FCR) Applied to Pollution Formation Program, gives results of three studies related to measurement system evaluations. Section I documents an evaluation of the performance and potential measurement biases of chemiluminescent NOx analyzers. The study evaluates commercial instruments operating with low- and atmospheric-pressure reaction chambers. Section II documents an assessment of various techniques used to measure nitrogenous intermediates from staged combustion processes. The study focuses on an evaluation of specific ion electrodes for measurement of hydrogen cyanide and ammonia concentrations generated in staged combustion flames. Emphasis was on development of sampling techniques and evaluation of potential biases in specific ion electrode analysis. Section III documents an evaluation of three laser-based techniques (based on interferometry, holography, and laser diffraction) for measuring characteristics of sprays. Results are presented from application of these techniques for measurement of droplet size distribution produced by a commercial liquid spray nozzle.

17. KEY WORDS AND DOCUMENT ANALYSIS

a. DESCRIPTORS		b. IDENTIFIERS/OPEN ENDED TERMS	c. COSATI Field/Group	
Pollution	Interferometers	Pollution Control	13B	
Combustion	Holography	Stationary Sources	21B	14E
Research	Lasers	Fundamental Research	14F	20E
Measurement	Hydrogen Cyanide	Staged Combustion	14G	
Nitrogen Oxides	Ammonia		07B	
Chemiluminescence	Drops (Liquids)		07D, 20F	

18. DISTRIBUTION STATEMENT Release to Public
19. SECURITY CLASS (This Report) Unclassified
20. SECURITY CLASS (This page) Unclassified
21. NO. OF PAGES 497
22. PRICE PC $38.95 / MF $6.95

EPA Form 2220-1 (9-73)

ABSTRACT

This document is the third volume in a four volume series describing research work performed under the Fundamental Combustion Research (FCR) Applied to Pollution Formation Program (EPA contract 68-20-2631). The FCR program was structured under a master contract concept with Energy and Environmental Research (EER) as the prime contractor. Individual research studies were performed by EER directly, under subcontract, or as joint EER/subcontractor efforts. Volume III of the final report series compiles reports from three studies related to measurement system evaluations. Section I documents a study conducted directly by EER to evaluate performance and potential measurement biases of chemiluminescent NO_x analyzers. The study presents results from an evaluation of commercial instruments operating with low pressure and atmospheric pressure reaction chambers. Section II documents results from an FCR subcontract with the University of Utah to assess various techniques being used to measure nitrogenous intermediates from staged combustion processes. The study focuses on an evaluation of specific ion electrodes for measurement of hydrogen cyanide and ammonia concentrations generated in staged combustion flames. Emphasis was placed on development of appropriate sampling techniques and evaluation of potential biases in specific ion electrode analysis. Section III documents results from a joint study conducted by EER and Spectron Development Laboratories to evaluate three laser based techniques for measuring characteristics of sprays. The three techniques evaluated included processes based on interferometry, holography, and laser diffraction. Results are presented from application of these techniques for measurement of droplet size distribution produced by a commercial liquid spray nozzle.

```
     ACCESSION NUMBER: PB88144001          U8806            14:27:42-03/01/88

(05) ENERGY AND ENVIRONMENTAL RESEARCH CORP.,           C    211
IRVINE, CA.*ENVIRONMENTAL PROTECTION AGENCY,
RESEARCH TRIANGLE PARK, NC. AIR AND ENERGY        BA    2595      5190       0
ENGINEERING RESEARCH LAB.
(06) FUNDAMENTAL COMBUSTION RESEARCH APPLIED TO   MA     695      1390
POLLUTION FORMATION. VOLUME 4. ENGINEERING
ANALYSIS.
(09) FINAL REPT. JAN 77--SEP 80,
(10) C. J. KAU;  M. P. HEAP;  W. R. SEEKER;
T. J. TYSON  (11) DEC 87,  (12) 211P
(15)(CN )EPA-68-02-2631
(18)EPA/600/7-87/ 27;  (18A)
(21) <SEE ALSO VOLUME 1, PB86-122660.> SPONSORED
 BY ENVIRONMENTAL PROTECTION AGENCY, RESEARCH
TRIANGLE PARK, NC. AIR AND ENERGY ENGINEERING
RESEARCH LAB.

                                                  MESSAGE: ENTER: "END" FOR
                                                  MENU.
```

NOTICE

This document has been reviewed in accordance with U.S. Environmental Protection Agency policy and approved for publication. Mention of trade names or commercial products does not constitute endorsement or recommendation for use.

TABLE OF CONTENTS*

ABSTRACT iii

INTRODUCTION 1

1.0 The FCR Program and Measurement Studies 1

2.0 Chemiluminescent Measurement of Nitric Oxide 3

3.0 Measurement of Nitrogenous Intermediates to Optimize a Staged Combustion System 11

4.0 Spray Characterization 13

5.0 References 20

Part I. Chemiluminescent Measurement of Nitric Oxide in Combustion Products (EER) .... I-i

Part II. Measurement of Nitrogenous Intermediates to Optimize a Staged Combustion System (U. of Utah) .... II-i

Part III. Spray Characterization (EER) .... III-i

LIST OF FIGURES

Figure 1. Example: Correcting Data for Background Gas Composition 8

Figure 2. NO_x Emissions From a Firetube Combustor 14

Figure 3. NO_x Emissions From a Tunnel Furnace 15

Figure 4. Experimental Facility 17

LIST OF TABLES

Table 1. Combustion Experiment Example 6

---

*Each part of this volume has its own separate detailed Table of Contents and lists of Figures and Tables.

INTRODUCTION

1.0 THE FCR PROGRAM AND MEASUREMENT STUDIES

The Fundamental Combustion Research applied to Pollution Control Program (FCR) was focused upon research areas related to nitrogen oxide (NO_x) formation and control in pulverized coal and heavy oil flames. It was a subcontractor oriented program and the Energy and Environmental Research Corporation (EER) was the Prime Contractor responsible for planning, management review of the total program and for the execution of certain tasks. The FCR program had three major objectives, namely:

- To generate the understanding of combustor behavior necessary to aid the Combustion Research Branch (CRB) in the development of control strategies to minimize NO_x emissions from stationary sources.

- To develop engineering models which would allow effective utilization of a large body of fundamental information in the development of new NO_x control techniques.

- To identify critical information necessary for low-NO_x combustor development and to generate it in a time frame which was consistent with the needs of the CRB technology development programs.

The overall goal of the CRB, and hence for the FCR program, is to provide the technology for the maximum control of NO_x emissions from stationary sources. The intent of FCR was to develop a focused program directed at the important issues relevant to the CRB's goals in order that the results could be applied in a relatively short time period. The program plan emphasized well-defined priority target areas, and the ensuing research effort was always guided towards engineering solutions to specific problems.

The FCR program was divided into three program areas and two support areas. The major program areas were concerned with (1) gas phase chemistry,

(2) the physics and chemistry of two phase systems, and (3) transport processes in reacting systems. This organization was designed to address the critical phenomena that occurred during the combustion of solid or liquid fuels in turbulent diffusion flames in order to describe fuel NO formation. The two support areas were: (1) studies related to measurement techniques and (2) the development of analytical tools required during the program and for future investigations.

This volume of the final report describes three studies which were carried out in the measurement techniques area, namely:

- A study of the potential errors involved in the chemiluminescent measurement of nitric oxide in combustion products.
- An assessment of the procedures required to measure nitrogeneous intermediates involved in staged combustion.
- An evaluation of techniques available for the characterization of liquid sprays.

2.0 CHEMILUMINESCENT MEASUREMENT OF NITRIC OXIDE IN COMBUSTION PRODUCTS

B. A. Folsom and C. W. Courtney
Energy and Environmental Research Corporation

2.1 Introduction

The measurement of nitric oxide (NO) concentrations in combustion products [1,2,3] by chemiluminescence has several advantages over alternative methods and as a result the chemiluminescent NO analyzer (CLA) has become a standard instrument for most laboratory and field emission tests. The usual procedure for CLA calibration is to set the instrument zero and span with high purity nitrogen (N_2) and a known concentration of NO in N_2, respectively. The instrument is then used to measure NO in combustion products. Ideally the composition of the combustion products, which varies according to fuel type and excess air level, will not affect the measurement of NO. However, several investigators have found that background gas composition can measurably affect the NO concentration indicated by a CLA. [3,4,5] Extrapolating these results to typical combustion product compositions indicates that the common procedure of neglecting background gas composition variations could introduce errors as large as 23% in indicated NO concentrations.[5] The objectives of this study were to:

o Assess the accuracy of commercial CLAs measuring NO in combustion products following the procedures recommended by the instrument manufacturers.

o Examine methods of correctly CLA indicated NO concentrations for the effects of background gas composition variations.

o Examine methods to improve calibration procedures.

Two commercially available CLAs were zeroed and spanned with N_2 and NO in N_2, respectively, and then used to measure known concentrations of NO in a variety of background gases. The gas mixtures were prepared by blending high purity gases and mixtures of NO in carrier gases in a precision flow metering system. The gas mixtures simulated combustion products from a wide range of fuel compositions and combustor operating conditions. Binary mixtures were also tested. The NO concentrations indicated by the CLAs were then compared with the actual NO concentrations to determine the effects of background gas composition.

In these tests the CLAs were operated without modifications strictly according to the manufacturers recommendations. The results may be applied to emission tests where CLAs were operated in this manner. The results should not be applied to emission tests where CLAs were modified such as low pressure flat flame experiments where the CLA sample metering systems are modified or removed.

2.2 Results

The results of this study indicated that commercial CLAs generally indicate NO concentrations lower than actual when spanned with mixtures of NO in N_2 and used to sample NO in combustion products. The errors introduced by neglecting sample background gas composition variations cover the following ranges:

COMBUSTION PRODUCTS FROM FUEL AND:	ERROR %	
	TECO	BECKMAN
21% O_2/N_2	+ 1 to - 5	+ 2 to -11
21% O_2/Ar	-11 to -16	- 6 to -14
21% O_2/21% CO_2/Ar	-12 to -15	-15 to -20

These results apply directly to the two CLAs tested but are probably representative of the performance of other instruments of similar design as well. Both instruments utilize capillaries to control sample flowrates. The TECO reaction chamber operates at approximately 9 torr while the Beckman reaction chamber operates at atmospheric pressure.

The gases responsible for the majority of the errors are CO_2, H_2O, O_2 and Ar. Each of these gases decreases the CLA's sensitivity to NO. Carbon dioxide is often present at high concentrations in combustion products and accounts for the majority of the errors at near stoichiometric conditions. Water vapor has a much higher quenching efficiency than N_2. At the low H_2O concentrations typical of combustion products dried in an ice bath, the quenching effects far outweigh the effects of viscosity. Sample dewpoint variations can change CLA response to NO by several percent. For oxygen the effects of viscosity and quenching variations are additive and this combined with the high concentrations of O_2 present in lean combustion products results in errors as high as 4%.

The effects of viscosity and quenching variations are opposite for Ar. In the CLAs tested here, the viscosity related variations over compensated the quenching variations resulting in a decrease in CLA sensitivity to NO with increasing Ar concentration. In the experiments reported in Reference 5, the sample flowrate was maintained constant and the results did not include the viscosity related flowrate variations present in these experiments. This accounts for the reported opposite effect of Ar on CLA response to NO. In combustion experiments utilizing O_2/Ar or O_2/CO_2/Ar as the oxidant, the concentration of Ar in the combustion products is high and results in CLA errors as high as 20%.

The variations in CLA response due to background gas composition variations were generally smaller with the TECO than with the Beckman except for Ar. Based upon these results a low reaction chamber pressure CLA such as the TECO would be preferred to monitor products of combustion of fuels burned in air. However, the choice of instruments for experiments involving O_2/Ar or O_2/CO_2/Ar oxidants is unclear. The following example illustrates these points.

A fuel containing bound nitrogen is burned in three oxidants: air, O_2/Ar and O_2/CO_2/Ar. It is assumed that 500 ppm of NO are formed from fuel bound N_2 independent of oxidant composition. It is further assumed that an additional 500 ppm of NO are formed from N_2 when the fuel is burned in air. Ideally, the experimental results should indicate 1000 ppm in the air experiment and 500 ppm in both Ar experiments. The thermal NO could then be calculated as the difference in NO concentrations (500 ppm).

Table 1 shows the results which would be obtained in this experiment utilizing the TECO and Beckman CLAs but without correcting the results for background gas

Table 1. Combustion Experiment Example

OXIDANT	NO SOURCE	INDICATED NO CONCENTRATIONS (PPM)	
		BECKMAN	TECO
Air	Fuel + Thermal	890	970
O_2/Ar	Fuel	430	430
O_2/Ar	Thermal (By Difference)	460	540
O_2/CO_2/Ar	Fuel	395	430
O_2/CO_2/Ar	Thermal (By Difference)	495	540

composition variations. The fuel was assumed to be C burning at 100% theoretical oxidant and the instrument response was taken from the results in sections I.5.2 and I.5.6.

In the air experiments, the TECO reads closer to the correct concentration. However, with the O_2/Ar oxidant both CLA's indicate incorrectly by the same amount. The thermal NO concentrations calculated by subtracting the NO concentrations are in error by equal amounts for both CLAs but the errors are in opposite directions. With the O_2/CO_2/Ar oxidant the TECO reads closer to the correct concentration. However, the Beckman yields better results for the thermal NO. This example shows no clear cut advantage for either instrument design.

The results of this study can be used to correct the results of NO emission tests for the effects of background gas composition variations. Accurate corrections can be made if:

- The CLA utilized in the emission tests was one of those tested here.
- The CLA was operated according to the manufacturer's recommendations.
- The combustion product composition is known.

Figure 1 shows the application of the results of this study to an actual NO emission test. A No. 6 oil was fired in a bench scale furnace over a range of excess O_2 with air and O_2/CO_2/Ar oxidants. Nitrogen oxides (NO_x) were measured with a TECO CLA equipped with a stainless steel converter to reduce NO2 to NO. The indicated NO_x concentrations were corrected for background gas composition variations by applying the results in sections I.5.2 and I.5.6. The C and CH_4 data were interpolated to account for the oil's H/C ratio and the results obtained for 21% O_2, 21% CO_2 balance Ar were used (neglecting the difference between 20 and 21% CO_2 in the oxidant). Application of these results to the experimental data slightly increases the NO_x concentration for combustion in air and substantially increases (60 ppm) the NO_x concentration for combustion in the oxidant containing Ar. The conversion of fuel nitrogen to NO_x is higher and the thermal NO_x formation is lower than if the effects of background gas

Argon Furnace, Sonicore Ultasonic Atomizer, No Swirl Air,
No. 6 Alaskan/North Slope Oil - 0.51% N - 100% Conversion = 815 ppm (Dry 0% O_2)

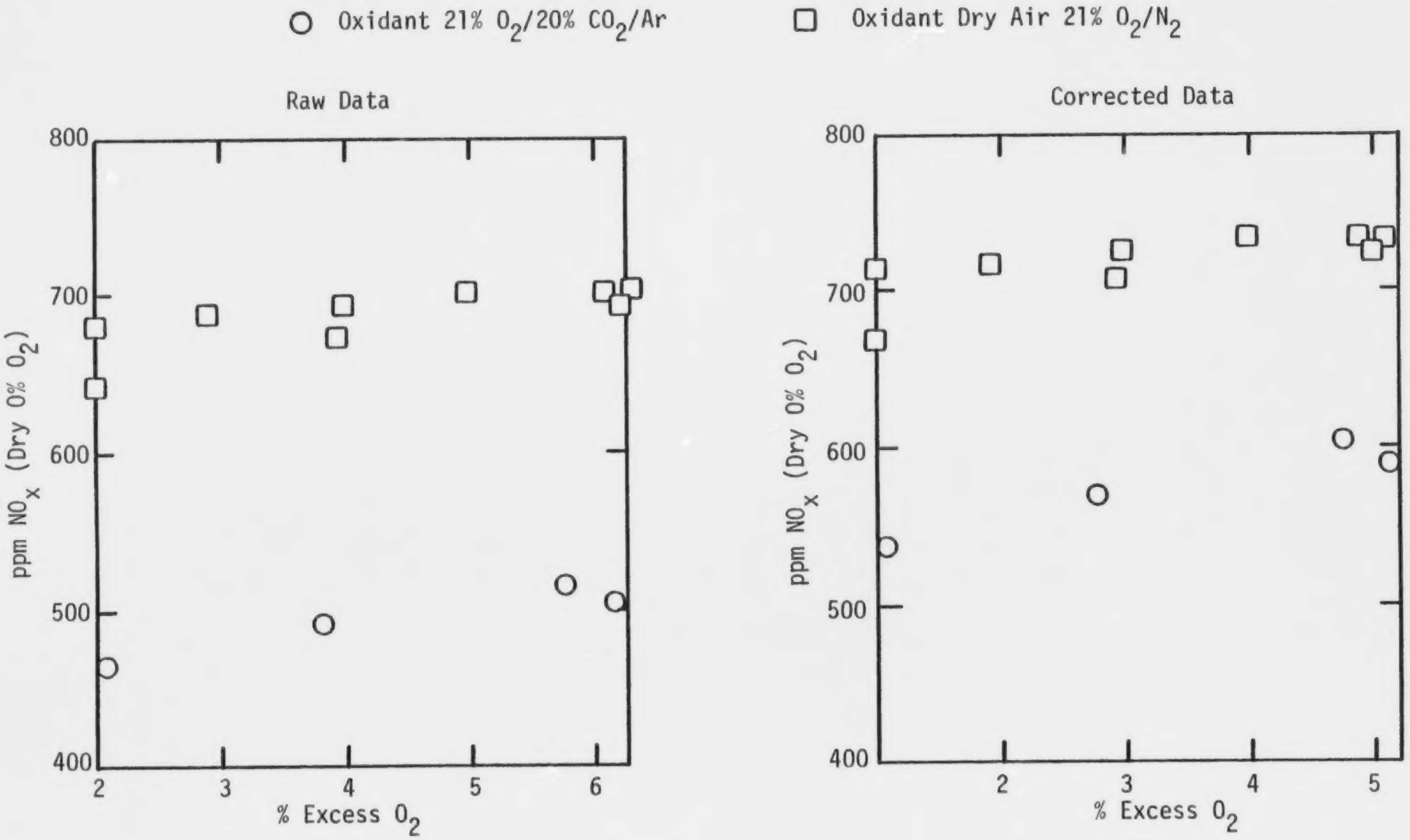

Figure 1. Example: Correcting Data for Background Gas Composition.

2.3 Recommendations

In many laboratory and field emissions tests the variability in operating conditions and other factors introduce errors of the same order of magnitude or larger than the errors produced by background gas composition variations. Under these conditions it is recommended that the NO concentrations indicated by the CLAs be used directly without corrections recognizing that the results will tend to be low by a few percent.

If the experimental errors in the emissions tests are small compared to the errors produced by background gas composition variations, the indicated NO concentrations should be corrected. However, the results of this investigation can only be applied to CLAs designed and operated similar to those tested. In low pressure flat flame experiments where the CLA sample gas metering system (capillary) is replaced by a different type of metering system, the effects of background gas composition variations on sample flowrate may be significantly different. Under these conditions the results of this investigation cannot be applied. It is recommended that either the effects of background composition variations on sample gas flowrate be evaluated and quenching data such as Reference 5 be applied, or the overall effects of background composition variations be empirically determined as in this investigation.

As an alternative to correcting the indicated NO concentrations, the CLA could be operated so as to minimize the effects of background gas composition variations. Three methods for accomplishing this are to:

- Calibrate the CLA with NO in a background gas similar to the anticipated combustion products.
- Dilute the sample with a known amount of N_2. Dry the sample to a low dewpoint.

Calibrating the CLA with NO in a background gas with a composition identical to the combustion products to be sampled would eliminate these problems. However, the concentration of NO in the mixture must be accurately known. Some gas mixture suppliers determine the concentration of NO in their mixtures by using a CLA. This introduces errors similar to calibrating the laboratory CLA on NO in N_2.

If the sample gas is diluted with a large amount of N_2, variations in sample gas compositions will have less effect on the flowrate into the reaction chamber and quenching. For this technique to be effective the dilution factor must be large (such as 10/1) and precisely known independent of sample gas composition variations. This accurate dilution is difficult to achieve in practice and has the further disadvantage of reducing the overall sensitivity of the CLA by the dilution factor.

The sample gas must be dried to a dewpoint less than the CLA operating temperature to avoid plugging the sample capillary with condensation. However, at 293 K dewpoint the sample gas contains 2.3% H_2O vapor and as a result the CLA will indicate less than the actual NO concentration due to background and dilution effects. Lowering the dewpoint to 273 K reduces the H_2O vapor concentration to 0.60% and reduces the error in indicated NO concentration.

In experiments involving combustion products of fuels in air, a low pressure reaction chamber CLA such as the TECO is preferred. However in experiments involving combustion in O_2/Ar or O_2/CO_2/Ar oxidants, high and low reaction chamber pressure CLAs perform equally well.

Small variations in CLA operating conditions such as adjustment of the sample gas or ozone flowrates and changes in the reaction chamber pressure do not have any clear advantages in reducing the effects of background gas composition variations. However, if the reaction chamber pressure is maintained low, the sample gas flowrate is maintained constant and the ratio of O_2 to sample gas flowrates is high, the effects of background gas composition variations could be significantly reduced.

3.0 MEASUREMENT OF NITROGENEOUS INTERMEDIATES TO OPTIMIZE A STAGED COMBUSTION SYSTEM

R. M. Winter and D. W. Pershing
University of Utah

3.1 Purpose and Scope

The design of a staged combustion system involves the establishment of a fuel rich zone to promote the formation of molecular nitrogen from the fuel nitrogen fragments. In an optimized system the sum of the total fixed nitrogen species (NO, NH_3, and HCN) are minimized in order to minimize exhaust NO levels.

The overall objective of this work was to investigate the role of the thermal environment in the furnace proper on the optimization of staged combustion for NO_x emissions control. The research concentrated on controlling first-stage thermal environment and evaluating the impact of step changes in the thermal environment on first-stage NO, NH_3, and HCN and exhaust NO.

A supporting objective was to evaluate current NH_3 and HCN analytical technology and thereby experimentally define the techniques appropriate for the measurement of TFN species in a rich flame. Several analytical techniques had been previously implemented to detect NH_3 and HCN, but a detailed evaluation of the accuracy of the methods as applied to the detection of these species in furnace systems had not been completed. Therefore, prior to conducting the experimental studies on the influence of thermal environment in a staged combustor, it was necessary to develop and verify analytical techniques for HCN and NH_3.

The approach was experimental, utilizing a 25.5 kW (70 x 10^3 Btu/hr) refractory-walled laboratory combustor. Natural gas was the fuel, with air supplying the oxidizing agent. Pure ammonia gas was utilized as a nitrogen additive to the fuel. Analytical technique development for NH_3 and HCN centered around the use of specific ion electrodes.

3.2 Conclusions

The following conclusions may be drawn from the results of this experimental study:

1. Gas-phase NH_3 concentration measurements can be made accurately and expeditiously with a gas-sensing, ion-specific electrode. The collection system should include a stainless-steel liquid spray probe, two 500 ml, fritted cylinder impingers and associated flowmetering equipment. The scrubbing solution of choice is 0.1 N H2SO4 and the gas flow rate should be approximately 5 l/min. Collection efficiencies in excess of 98 percent can be expected with this system.
2. HCN can be successfully measured with either an ion-specific electrode system. HCN liquid-phase collection efficiencies are slightly lower (85 percent) than those observed with NH_3.
3. The conversion of HCN to NO in the second stage of a staged combustor is very low.
4. Thermal formation of NO in the second stage was insignificant in the experimental system studied.
5. Limited (12 percent) first stage cooling retards the rate of decay of NO to near zero if the gas temperatures are reduced below 1200°C.
6. Limited cooling in the first stage of CH_4/NH_3/air flames increases NO in the exhaust because the rate of NO destruction is significantly slowed in the first stage.
7. Additional cooling of CH_4/NH_3/air flames provides slightly lower emissions than initial cooling because the temperature minimum is reached in the second stage flame, where NO, NH_3, and O_2 are reduced in a homogeneous gas-phase reaction. This produces lower NO levels in the exhaust.

These results suggest that the optimum staged combustion system is one in which the first stage is operated essentially adiabatically to maximize TFN decay. Interstage cooling should also be used to reduce the second stage flame temperature to below 1540°C, thereby minimizing thermal NO formation in the second stage.

4.0 SPRAY CHARACTERIZATION

W. R. Seeker and G. S. Samuelsen
Energy and Environmental Research Corporation

4.1 Introduction

The results from recent EPA Combustion Research Branch (CRB) studies indicate that the emission of NO_x from oil-fired furnaces and boilers are influenced by the type of nozzle employed, the operating condition of the nozzle, and the swirl of primary air.[6,7] For example, the data of Figure 2 were obtained from a firetube boiler simulator operating with a variety of nozzle types under three swirl conditions. At low swirl, an increase in swirl number produces sharp reductions in the NO_x emitted. For most of the nozzles, NO_x then increases as the swirl number is raised to 0.8. A notable exception is the Monarch nozzle, the emissions of which continue to decrease as the swirl number is raised.

A second example (Figure 3) are data obtained from a tunnel furnace that was operated (a) in the absence of swirl, and (b) with a zero-nitrogen oxidizer as well as air to isolate the fuel NO_x produced. Here, the operating condition of the nozzle is shown to also influence the NO_x emission. Thermal NO_x, for example, decreases dramatically as atomizing pressure is reduced.

These data identify the need for characterizing those properties of sprays (e.g., droplet size distribution, droplet velocity, gas velocity, evaporation rate) that likely dictate the NO_x produced. Characterizations of this type require the measurement of local droplet size, local droplet velocities, and local gas velocities. Of the variety of techniques available to measure spray properties, only laser interferometry has the immediate potential to measure simultaneously the properties of interest. The present FCR study was established to test the applicability of laser interferometry in measuring spray properties for a variety of conditions, and to compare the results against the following two more conventional and extensively used, but less versatile techniques: laser diffraction, and laser holography. As a result, this study represents the first to systematically assess the performance of laser interferometry against that of laser diffraction and laser holography.

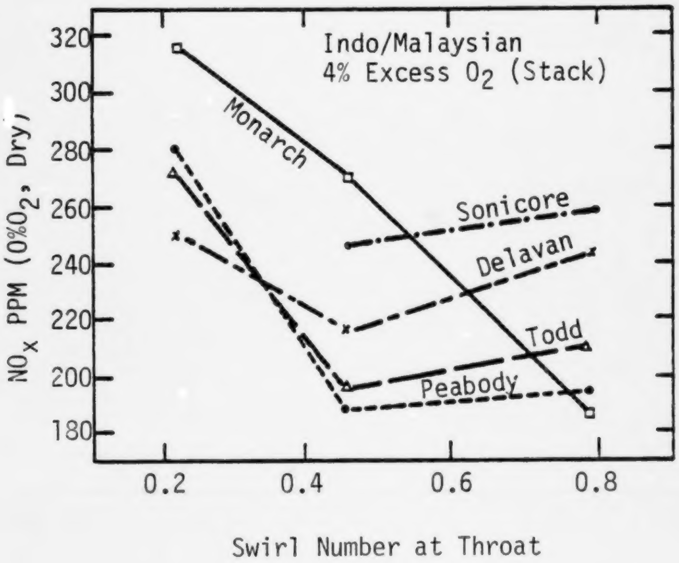

Figure 2. NO_x Emissions From a Firetube Combustor.(6)

(a) Tunnel Furnace

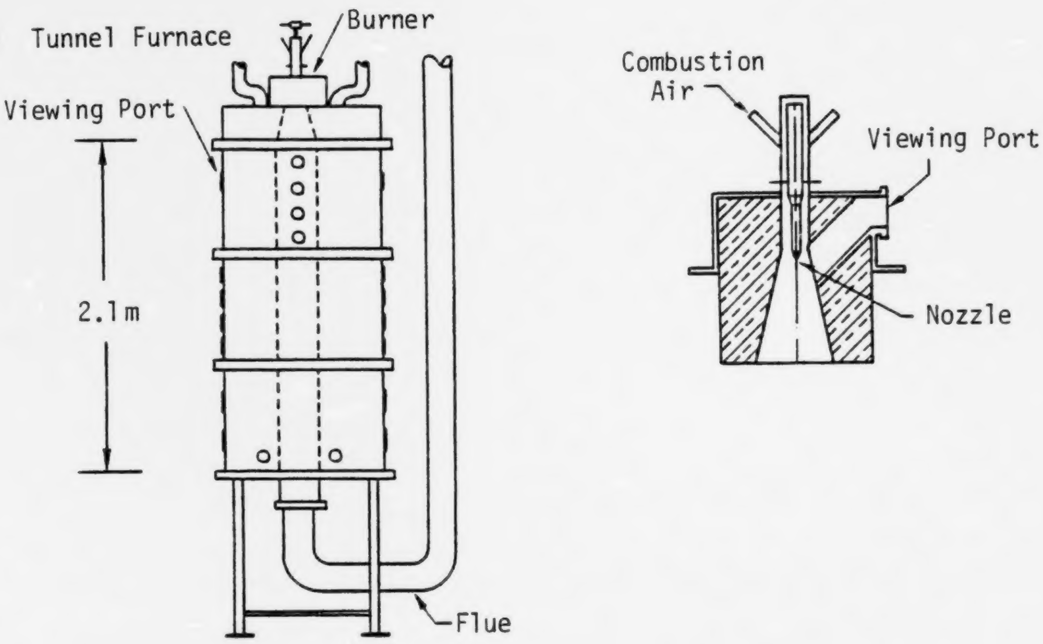
Burner
Viewing Port
2.1m
Flue
Combustion Air
Viewing Port
Nozzle

(b) NO_x Emissions

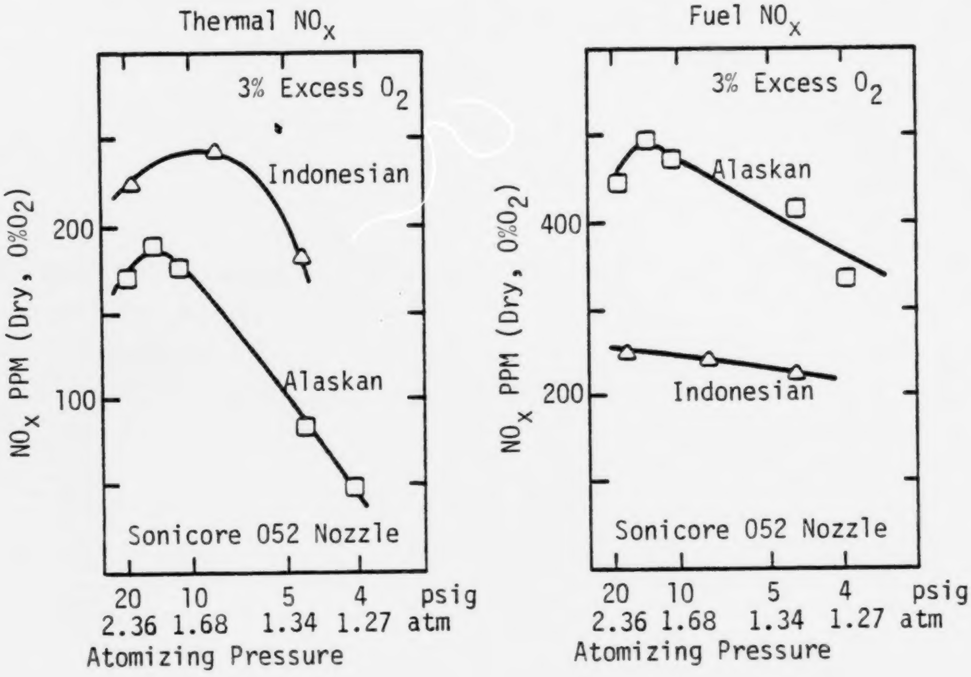

Figure 3. NO_x Emissions From a Tunnel Furnace.(7)

4.2 Approach

The approach adopted for the present study was to obtain spray measurements under cold conditions in a chamber patterned after the firetube combustor (from which the data of Figure 2 were obtained) with respect to the diameter and the ability to later accommodate a variety of inlet geometries and swirl levels. Schematics of both the spray chamber and the firetube combustor are shown in Figure 4. The spray in the cold chamber is downward injected from a movable platform with respect to a fixed observation position.

The following three nonintrusive laser techniques were used to characterize spray performance:

- interferometry
- holography
- diffraction

Interferometry is a point measurement technique and was selected because of the potential to (1) measure simultaneously droplet size and velocity, and (2) resolve spatially droplet size and velocity distributions. Holography provides an instantaneous, three-dimensional "picture" of the droplet field and was selected as a check for the interferometric and diffraction techniques. Diffraction was selected because, although velocity and spatial resolution are not provided, the technique has been extensively tested (e.g., Negus and Azzopardi, 1978) and is relatively fast in providing processed data. In addition, because diffraction was employed in the IFRF studies,[8] the adaptation of diffraction to the present study had the added advantage of providing a check on reproducibility between two laboratories, including evaluation of chamber size.

4.3 Conclusions

The present study was undertaken to explore the utility and applicability of laser interferometry as a result of its potential to:

- Make point rather than path measurements and thereby provide spatial resolution.

(a) Cold Chamber

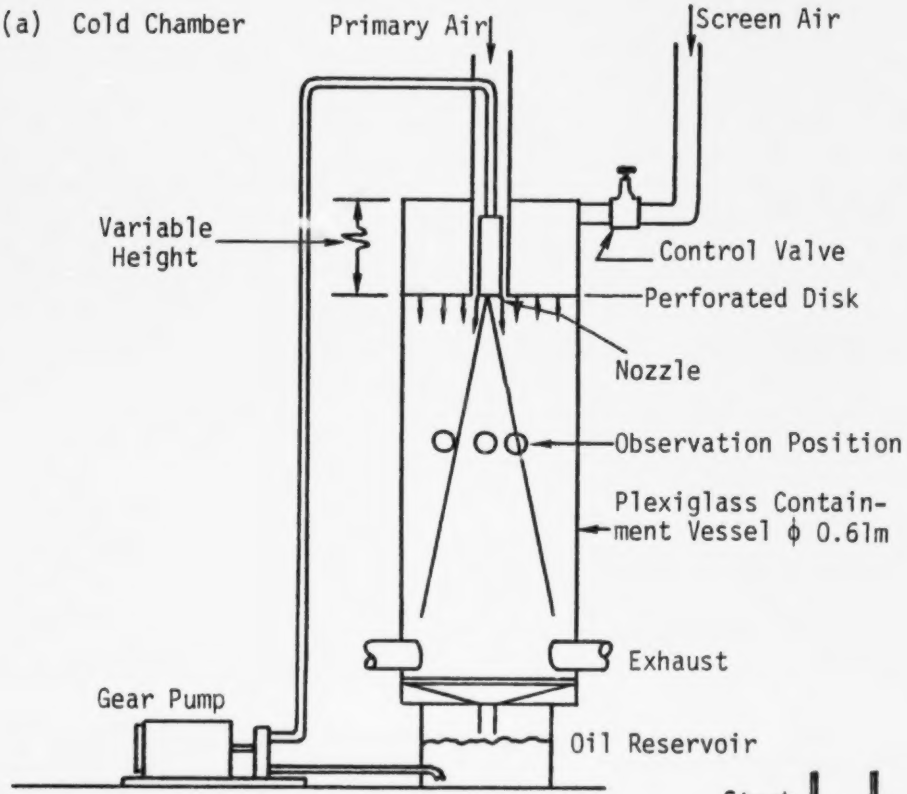
Primary Air
Screen Air
Variable Height
Control Valve
Perforated Disk
Nozzle
Observation Position
Plexiglass Containment Vessel ϕ 0.61m
Exhaust
Gear Pump
Oil Reservoir

(b) Firetube Combustor

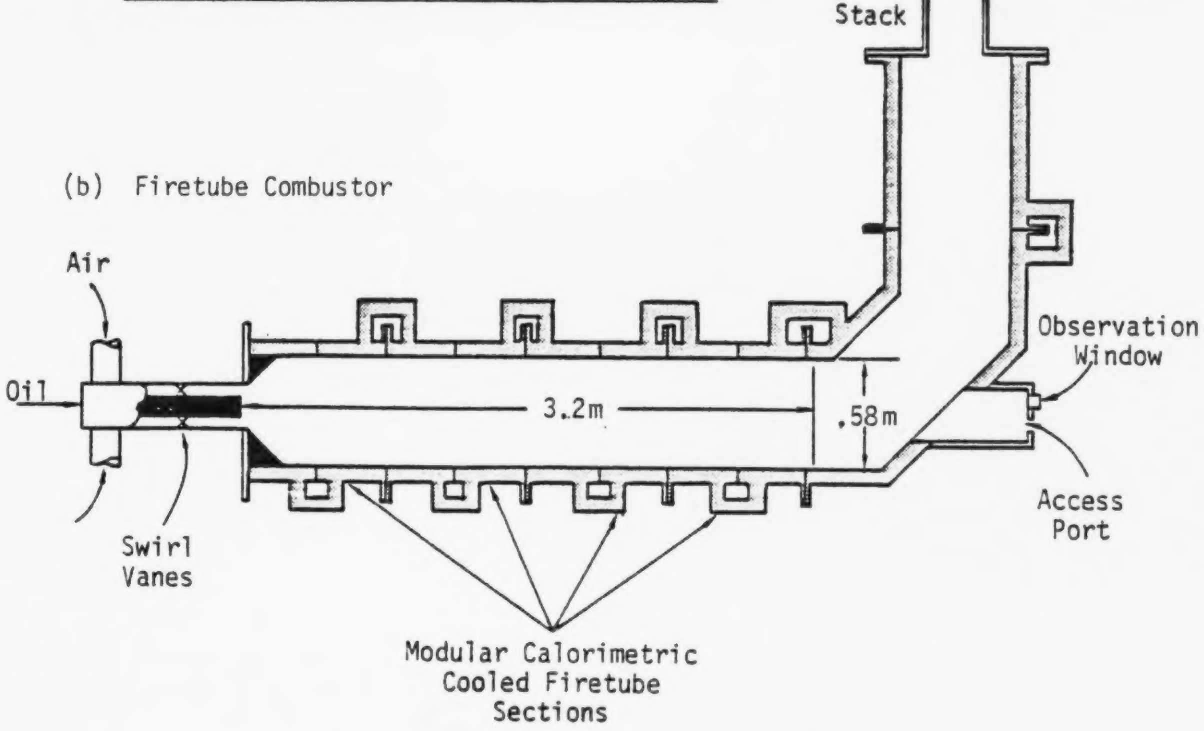
Stack
Air
Oil
3.2m
.58m
Observation Window
Access Port
Swirl Vanes
Modular Calorimetric Cooled Firetube Sections

Figure 4. Experimental Facility.

- Measure single droplets rather than aggregates of droplets and thereby measure droplet velocity as well as exactly measure the number density.

- Measure droplet velocity and thereby obtain information concerning droplet ballistics and gas/droplet interaction.

- Measure gas velocity and thereby measure the aerodynamic flow activity on the droplet.

These types of measurements are necessary to the exploration of pollutant formation in combustors and boilers operating on both conventional and alternative fuels.

The conclusions of the study are:

1. Interferometry has a high potential for making the measurements described above.
2. Application of the technique requires that the dynamic range (10:1) of the instrument be changed to accommodate large droplets (which are especially important to weight density distribution) and small droplets (which are especially important to number density distribution).
3. Both optical techniques used to assess the performance of the laser interferometric system in the present study established that the dynamic range was limited on the large droplet end (dp 90 um) and, as a result, the laser interferometric technique failed to measure large droplets.
4. The laser diffraction technique, in addition, indicated that droplets were indeed present below the lower cutoff (dp = 15 to 20 um) limit of both the holography and interferometry methods.
5. The interferometric operator must be very aware of the sensitivity limit range and the saturation limit range. It may require several measurements with different PMT bias levels and fringe

developed to measure the distribution by continually shifting the valid range and then combining results.

5.0 REFERENCES

1. Clough, P. N., and Thrush, B. A. "Mechanism of Chemiluminescent Reaction Between Nitric Oxide and Ozone." Transactions of the Faraday Society, Vol. 63, No. 494, Part 4, p. 915, April 1967.

2. Fontijn, A., Sabadell, A. J., and Ronco, J. "Homogeneous Chemiluminescent Measurement of Nitric Oxide with Ozone." Analytical Chemistry, Vol. 42, p. 575, 1970.

3. Niki, H., Warnick, A., and Lord, R. "An Ozone-NO Chemiluminescence Method for NO Analysis in Piston and Turbine Engines." Proceedings of Automotive Engineering Congress, p. 246, Detroit, Michigan, 1971.

4. Maahs, H. G. "Interference of Oxygen, Carbon Dioxide and Water Vapor on the Analysis for Oxides of Nitrogen by Chemiluminescence." NASA Technical Memorandum, NASA TM X-3229, August 1975.

5. Mathews, R. D., Sawyer, R. F., and Schefer, R. W. "Interferences in Chemiluminescent Measurement of NO and NO2 Emissions from Combustion Systems." Environmental Science and Technology, Vol. 11, No. 12, p. 1092, November 1977.

6. England, G. C., Heap, M. P., Horton, R. T., Pershing, D. W., and Flament, G. "The Control of Pollutant Formation in Fuel Oil Flames--The Influence of Oil Properties and Spray Characteristics." Proceedings of the Third Stationary Source Combustion Symposium, Vol. II, Advanced Processes and Special Topics, EPA-600/7-79-050b (NTIS PB292540), p. 41, 1979.

7. Heap, M. P., Pershing, D. W., England, G. C., Lee, J. W., and Chen, S. L., "The Influence of Fuel Characteristics on Nitrogen Oxide Formation-Bench-Scale Studies." Proceedings of the Third Stationary Source Combustion Symposium, Vol. II, Advanced Processes and Special Topics, EPA-600/7-79-050b (NTIS PB292540), p. 3, 1979.

8. England, G. C., Pershing, D. W., Heap, M. P., and Cichanowicz, J. E. , "Effects of Fuel Properties and Atomization Parameters on NO_x Control for Heavy Liquid Fuel Fired Package Boilers," EPA-600/7-82-029 (NTIS PB82-230715), April 1982.

I. CHEMILUMINESCENT MEASUREMENT OF NITRIC OXIDE IN COMBUSTION PRODUCTS

By

BLAIR A. FOLSOM and CRAIG W. COURTNEY

ENERGY AND ENVIRONMENTAL RESEARCH CORPORATION
8001 IRVINE BOULEVARD
SANTA ANA, CALIFORNIA 92705

ABSTRACT

The response of commercially-available chemiluminescent NO_x analyzers to simulated combustion products containing NO was investigated. An accurate flow metering system was used to combine O_2, CO_2, CO, N_2, A, H_2O, CH_4, and H_2 into simulated combustion products modeling a wide range of fuels and excess air conditions. The simulated combustion products were doped with known amounts of NO and then monitored by two commercial chemiluminescent NO_x analyzers.

The results indicate that chemiluminescent analyzers spanned with NO/N_2 generally indicate less than the actual amount of NO in sampled combustion products. The errors range from one to 20 percent depending upon fuel type, oxidant composition and the sample conditioning system.

TABLE OF CONTENTS

Section		Page
1.0	INTRODUCTION	I-1
2.0	CHEMILUMINESCENT MEASUREMENT OF NO	I-2
3.0	PROCEDURE	I-11
4.0	EXPERIMENTAL APPARATUS	I-19
	4.1 High Accuracy Metering System	I-19
	4.2 Water Addition System	I-23
	4.3 Gases	I-23
	4.4 Instruments	I-24
5.0	RESULTS	I-29
	5.1 Experiment No. 1 - Binary Background Gases	I-29
	5.2 Experiment No. 2 - Lean Complete Combustion Products (Dry)	I-32
	5.3 Experiment No. 3 - Lean Complete Combustion Products (Wet)	I-34
	5.4 Experiment No. 4 - Incomplete Lean Combustion Products (Dry)	I-34
	5.5 Experiment No. 5 - Rich Combustion Products (Dry)	I-34
	5.6 Experiment No. 6 and 7 - Combustion Products in Atmospheres (Dry)	I-38
	5.7 Experiment No. 8 - Off Design Point CLA Operation	I-38
6.0	DISCUSSION	I-42
7.0	RECOMMENDATIONS	I-47
8.0	APPENDIX	I-49
9.0	REFERENCES	I-65

LIST OF FIGURES

Figure		Page (I-)
1	Chemiluminescent Measurement of NO	3
2	Relative Intensity of Chemiluminescent Emission for Six Different Third Bodies as a Function of Third Body Concentration in Sample Mixture	8
3	Complete Dry Products of Combustion from Burning CH_x in Air	14
4	Simulated Fuel Rich Dry Combustion Products from Burning CH_x in Air	16
5	Experimental Apparatus	20
6	Critical Orifice Metering System	21
7	Gas Supply and Metering System	22
8	TECO Model 10A	26
9	Beckman Model 951	28
10	Experiment No. 1: Binary Background Gases	30
11	Experiment No. 1 (continued): Binary Background Gases	31
12	Experiment No. 2: Lean Complete Combustion Products Burning Fuels in Air (dry)	33
13	Experiment No. 3: Lean Complete Combustion Products from Burning C in Air (wet)	35
14	Experiment No. 4: Incomplete Lean Combustion Products Burning C in Air (dry)	36
15	Experiment No. 5: Rich Combustion Products Burning Fuels in Air (dry)	37
16	Experiment No. 6: Lean Complete Combustion Products Burning Fuels in O_2/A and O_2/CO_2/A Oxidants (dry)	39
17	Experiment No. 7: Rich Combustion Products Burning C in O_2/A and O_2/CO_2/A Oxidants (dry)	40
18	Experiment No. 8: Off Design Point CLA Operation Burning C at 125% Theoretical Oxidant (dry)	41
19	Example: Correcting Data for Background Gas Composition	46

LIST OF TABLES

Table		Page (I-)
1	Estimated Effect of Sample Viscosity on CLA Response	6
2	Effects of Quenching and Viscosity on CLA Response	10
3	Test Matrix	13
4	Gas Analysis Instruments	25

ACKNOWLEDGEMENT

The work upon which this publication is based was conducted under Contract No. 68-02-2631 with the Environmental Protection Agency. The authors wish to express their appreciation to W. S. Lanier of the Environmental Protection Agency and to M. P. Heap, J. S. Johnsen and J. M. Keene of Energy and Environmental Research Corporation for their assistance in various portions of the work.

1.0 INTRODUCTION

The measurement of nitric oxide (NO) concentrations in combustion products by chemiluminescence has several advantages over alternative methods(1,2,3) and as a result the chemiluminescent NO analyzer (CLA) has become a standard instrument for most laboratory and field emission tests. The usual procedure for CLA calibration is to set the instrument zero and span with high purity nitrogen (N_2) and a known concentration of NO in N_2 respectively. The instrument is then used to measure NO in combustion products. Ideally the composition of the combustion products, which varies according to fuel type and excess air level, will not affect the measurement of NO. However, several investigators have found that background gas composition can measurably affect the NO concentration indicated by a CLA.(3,4,5) Extrapolating these results to typical combustion product compositions indicates that the common procedure of neglecting background gas composition variations could introduce errors as large as 28% in indicated NO concentrations.(5) The objectives of this study were to:

- Assess the accuracy of commercial CLAs measuring NO in combustion products following the procedures recommended by the instrument manufacturers
- Examine methods of correcting CLA indicated NO concentrations for the effects of background gas composition variations
- Examine methods to improve calibration procedures

Two commercially available CLAs were zeroed and spanned with N_2 and NO in N_2 respectively and then used to measure known concentrations of NO in a variety of background gases. The gas mixtures were prepared by blending high purity gases and mixtures of NO in carrier gases in a precision flow metering system. The gas mixtures simulated combustion products from a wide range of fuel compositions and combustor operating conditions. Binary mixtures were also tested. The NO concentrations indicated by the CLAs were then compared with the actual NO concentrations to determine the effects of background gas composition.

In these tests the CLAs were operated without modifications strictly according to the manufacturers recommendations. The results may be applied to emission tests where CLAs were operated in this manner. The results should not be applied to emission tests where CLAs were modified such as low pressure flat flame experiments where the CLA sample metering systems are modified or removed.

2.0 CHEMILUMINESCENT MEASUREMENT OF NO

The chemiluminescent measurement of NO is based upon the following four reactions:

$$NO + O_3 \longrightarrow NO_2^* + O_2 \qquad (1)$$

$$NO + O_3 \longrightarrow NO_2 + O_2 \qquad (2)$$

$$NO_2^* \longrightarrow NO_2 + h\nu \qquad (3)$$

$$NO_2^* + M \longrightarrow NO_2 + M \qquad (4)$$

Nitric oxide and ozone (O_3) react readily to form nitrogen dioxide (NO_2) in either an excited state (NO_2*) or a ground level state (NO_2). The yield of NO_2* is about 10% at ambient temperatures and increases with temperature by approximately 0.9%/K(3). The excited molecules can decay to ground state giving off light of a characteristic frequency (chemiluminescence) or can collide with any third body (M) and decay to ground state without chemiluminescence (quenching). The relative importance of the chemiluminescent and quenching reactions depends upon the temperature and the amount and types of molecules available for quenching. If these factors are constant and the amount of O_3 present is large, the intensity of chemiluminescence is directly proportional to NO concentration.

Figure 1 is a simplified schematic diagram of a NO analyzer based upon this reaction scheme. A sample gas containing NO is metered into a reaction chamber at a constant rate by a suitable flow metering system. Ozone produced from O_2 is also metered into the reaction chamber at a constant rate. The O_2 flowrate is selected to produce a reaction chamber O_3 concentration many times the maximum anticipated NO concentration. Thus the reaction between NO and O_3 does not measurably deplete the O_3 concentration and the intensity of chemiluminescence is directly proportional to NO concentration in the sample gas. The chemiluminescent emission is filtered to remove extraneous light and directed upon a photomultiplier tube (PMT). The PMT output is amplified and suitably scaled to read out directly in concentration units (PPM). The amplifier zero offset and gain are adjustable to permit calibration with standard gases. High purity N_2 (free from NO) is used to set the zero offset. This allows the PMT dark current which varies with PMT

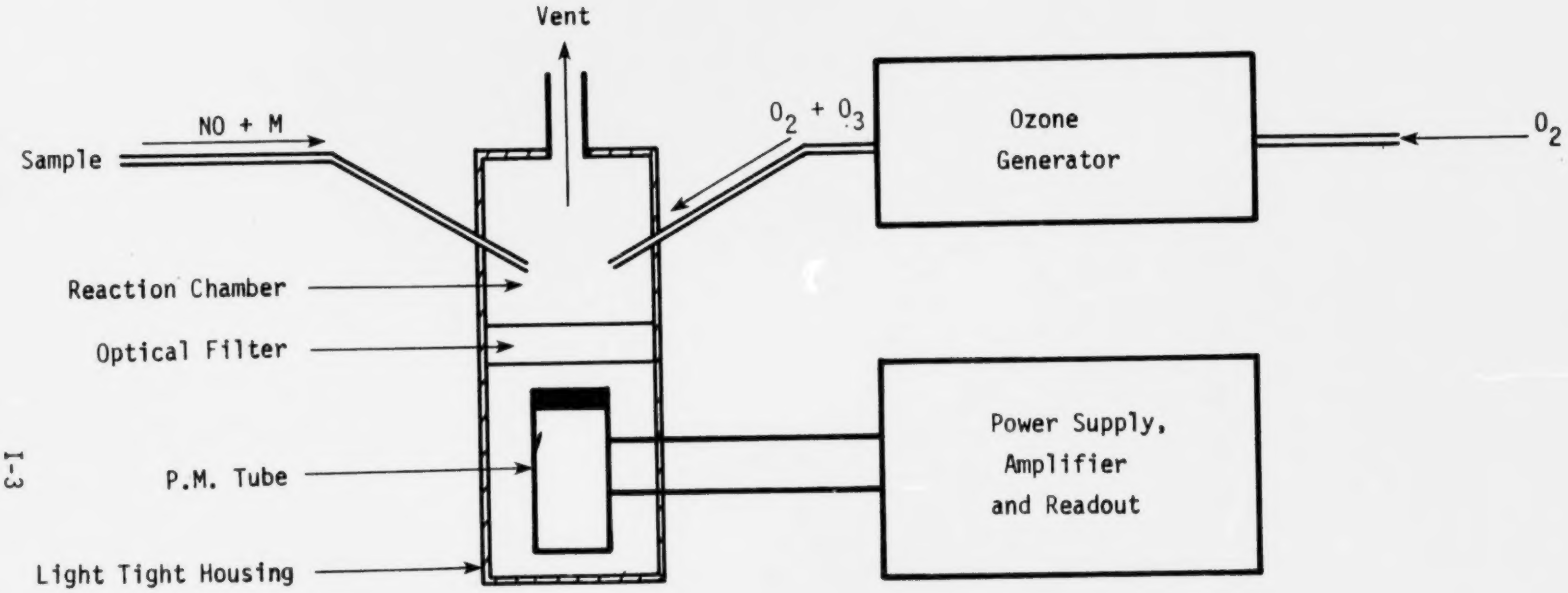
Vent
Sample
NO + M
$O_2 + O_3$
Ozone Generator
O_2
Reaction Chamber
Optical Filter
P.M. Tube
Light Tight Housing
Power Supply, Amplifier and Readout

Figure 1. Chemiluminescent Measurement of NO.

age and temperature to be nulled out. A known concentration of NO in N_2 background gas is used to adjust the instrument gain or span.

Commercial CLA s are designed and constructed to maintain the variables affecting instrument calibration very close to constant. Calibration drift on state-of-the-art instruments is usually less than 3% of span per day. A CLA calibrated as described above will indicate the correct NO concentration (within about 1%) of any mixture of NO in N_2 within instrument range. However if the sample gas contains species other than NO or N_2, these gases could cause the instrument to read incorrectly.

There are four potential ways in which sample gas composition variations can alter CLA response to NO; these are:

- Depletion of O_3 by chemical reaction
- Chemiluminescence of gases other than NO within the optical filter band width
- Sample flowrate variations due to sample gas property changes
- Quenching efficiency of sample gas species different from N_2

The flowrate of O_3 into the reaction chamber is many times the amount required to oxidize the highest anticipated NO concentration. However if other species which react with O_3 are introduced with the sample gas in sufficient quantities, the O_3 concentration might be depleted enough to decrease the instrument's sensitivity to NO. Assuming that one molecule of O_3 reacts with one molecule of reactive specie, concentrations of reactive species greater than the maximum anticipated NO concentration would be required to measurably reduce instrument sensitivity. The decrease in sensitivity to NO would be directly proportional to the reactive specie concentration in the sample gas. Ozone is a strong oxidizer and reacts readily with many materials including hydrocarbons such as ethylene(6).

The CLA includes an optical filter which transmits light in the frequency range produced by the decay of NO_2^* (0.6 to 3.0μ)(1) and absorbs light outside this range. If a specie introduced with the sample gas undergoes a chemiluminescent reaction with emission in this range, the CLA will indicate an erroneously high NO concentration. Apparently iron carbonyls interfere with the CLA by undergoing chemiluminescent reaction with O_3. These compounds are formed when carbon monoxide (CO) comes in contact with materials containing iron. Carbon monoxide stored in pressurized steel cylinders often contains substantial amounts of iron carbonyls(7) and if the CO is used as a sample gas directly from the cylinder, the CLA may read an erroneous NO concentration of several hundred ppm. The carbon monoxide may be freed from iron carbonyls by passing it over activated charcoal or through a heated tube. The decomposition temperature at 1.0 atmosphere is 453K.(8)

The CLA measures the number of NO molecules entering the reaction chamber per unit time. If the sample gas flowrate is constant, the number of molecules of NO entering the reaction chamber per unit time is directly proportional to the NO concentration. The sample gas flowrate in many commercial CLA s is maintained constant by passing the sample gas through a capillary and regulating the capillary pressure drop. However, the volumetric flowrate through a capillary with fixed pressure drop is inversely proportional to the sample gas dynamic viscosity (μ). Thus sample gas compositions with viscosity different from that of N_2 will result in sample gas flowrates different from N_2 and therefore the CLA will not respond properly to NO. Sample gases with low viscosity will result in indicated NO concentrations greater than actual and vice versa.

Table 1 lists the dynamic viscosities of several gases commonly found in combustion products. The ratios of the viscosity of N_2 to the viscosity of mixtures of various gases in N_2 are also shown. These ratios indicate the approximate relative CLA response due to viscosity variations while sampling gas mixtures (containing NO) compared with the response sampling NO in N_2. Viscosity variations are clearly important. If a CLA were spanned with NO in N_2 and then used to sample NO in H_2, the indicated NO concentration would be nearly twice the actual value. If the sample were NO in Argon (A) the indicated NO concentration would be more than 20% lower than actual.

The products of combustion of hydrocarbon fuels burned in air usually contain in excess of 75% N_2 and are dried before entering a CLA. Thus the maximum variation in CLA response due to viscosity changes relative to N_2 is +8 to -4%.

Table 1. Estimated Effect of Sample Viscosity on CLA Response

Gas M	Dynamic Viscosity Micropoise	Response of CLA to Mixture/Response to N_2				
		5% M/N_2	10% M/N_2	25% M/N_2	50% M/N_2	100% M
H_2	83.5	1.007	1.015	1.042	1.117	1.990
H_2O	88.0	1.019	1.040	1.110	1.264	1.886
CH_4	102.6	1.015	1.030	1.083	1.197	1.618
CO_2	139.0	1.010	1.020	1.050	1.099	1.194
CO	166.0	1.000	1.000	1.000	1.000	1.000
N_2	166.0	1.000	1.000	1.000	1.000	1.000
Air	170.8	0.999	0.997	0.993	0.986	0.972
O_2	189.0	0.993	0.986	0.965	0.933	0.878
A	209.6	0.985	0.970	0.930	0.875	0.792

NOTES

1. The response of CLA with mixture/response with N_2 is the ratio of viscosity of N_2 to viscosity of mixture.
2. Viscosities of the mixtures were calculated according to Reference 9.

Several investigators have recently studied the combustion of fuels with O_2/A or $O_2/A/CO_2$ oxidants to eliminate the formation of NO from N_2 and to thus isolate NO formed from fuel nitrogen compounds. Combustion products from these experiments contain negligible concentrations of N_2 and high concentrations (50 to 90%) of A. Spanning a CLA with NO in N_2 and measuring NO in combustion products from these experiments could introduce viscosity related errors greater than 20%.

The NO_2^* produced by reaction of NO and O_3 can either decay to the ground-state producing chemiluminescence or transfer energy to other molecules (M) without chemiluminescence (quenching). Some quenching is unavoidable due to the finite probability of NO_2^* molecules colliding with other molecules in the reaction chamber. The rate of the quenching reaction depends upon the amount and types of molecules in the reaction chamber. Reaction chamber pressure affects quenching by altering the mean free path and collision frequency. Low pressure tends to reduce quenching and several commercial CLAs operate with reaction chamber pressures less than 10 torr. The quenching reaction rate affects the intensity of chemiluminescence and hence variations in the quenching reaction rate will alter CLA response to NO.

The quenching reaction rate is significantly influenced by the type of molecules in the reaction chamber. Experimental evidence confirms that the rate of quenching increases with the number of degrees of freedom of the molecules present in the reaction chamber(4). Mathews et al(5) recently compiled quenching data from several investigators. Figure 2 shows these data in the form of chemiluminescent intensity with N_2 as the background gas normalized by the chemiluminescent intensity from mixtures of M in N_2. These data were taken from a CLA operated at reaction chamber pressures in the range 1.3 to 14.0 torr. The CLAs were zeroed with N_2, spanned with NO in N_2 and then the gas mixtures were sampled. The sample gas flowrates were constant for all conditions thus eliminating the viscosity related effects discussed above(10). The gas molecules in the reaction chamber consist of sample gas species as well as the O_3/O_2 mixture. Thus changes in the sample gas and O_3/O_2 mixture will also result in quenching reaction rate variations.

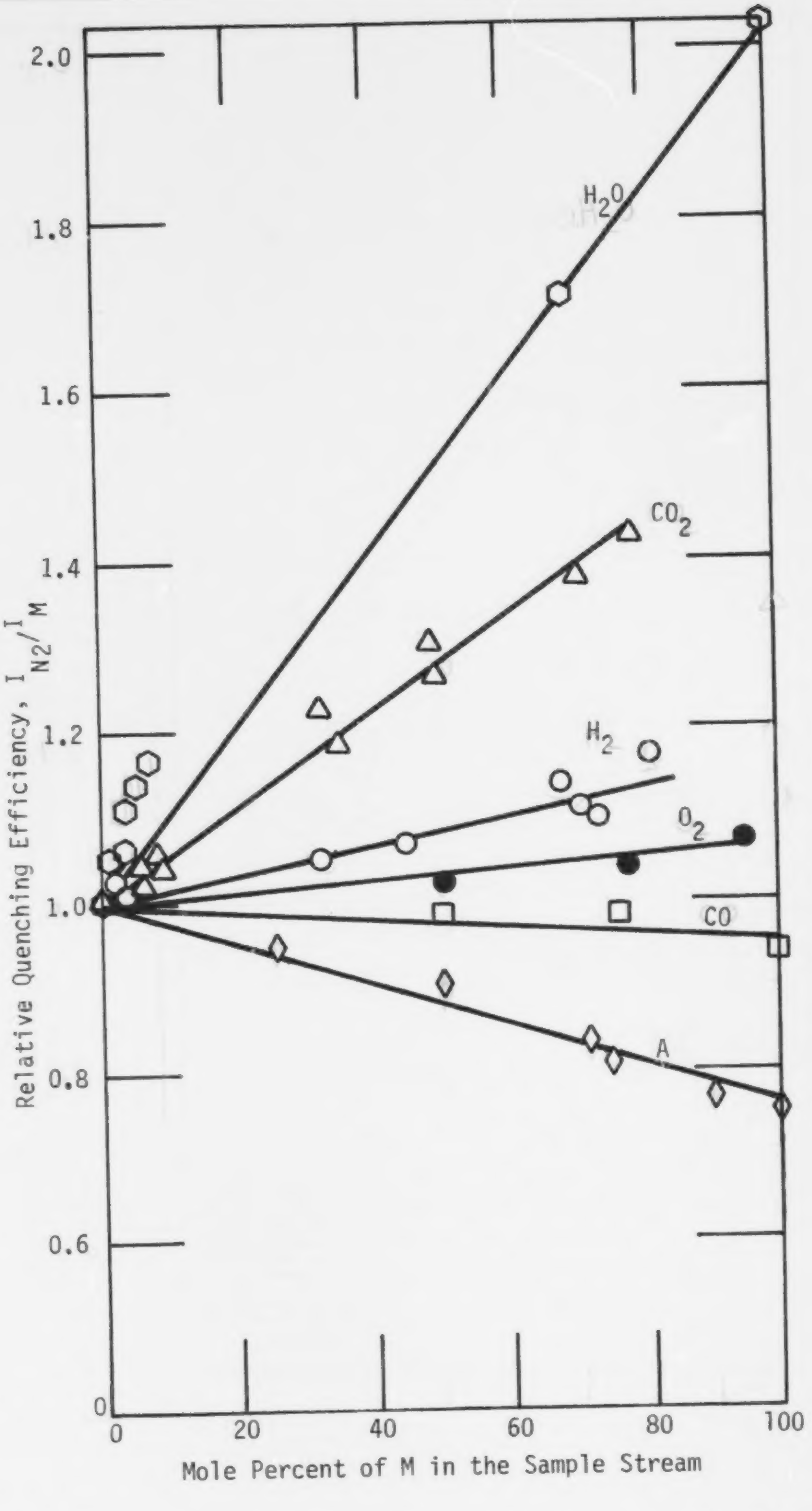

Figure 2. Relative Intensity of Chemiluminescent Emission for Six Different Third Bodies as a Function of Third Body Concentration in Sample Mixture.

The variations in chemiluminescent response to NO due to quenching and viscosity effects are generally of the same order of magnitude. However, the magnitude and direction of the effects vary for specific gases. Table 2 shows the quenching and viscosity effects for a CLA spanned with NO in N_2 and used to sample NO in another gas M. The viscosity effect was calculated assuming 100% M in the sample gas and constant capillary pressure drop. The quenching effect was calculated by extrapolating the data in Figure 2 to 100% M. This applies to a low reaction chamber pressure with a ratio of sample to O_2/O_3 flowrates of 83%. For some gases (H_2 and O_2) the combined effects of quenching and viscosity result in a greater error than for quenching alone. For other gases (H_2O, CO_2 and A) the error is reduced by inclusion of viscosity effects.

Table 2. Effects of Quenching and Viscosity on CLA Response

Relative CLA Response Spanning on NO/N_2 and Sampling NO/M			
Gas M	Relative Response Due to Quenching	Relative Response Due to Viscosity	Relative Response Due to Both Effects
H_2	0.86	1.99	1.72
H_2O	0.49	1.89	0.92
CH_4	*	1.62	*
CO_2	0.64	1.19	0.76
CO	1.06	1.00	1.06
N_2	1.00	1.00	1.00
O_2	0.94	0.88	0.83
A	1.33	0.79	1.06

---

* Quenching efficiency not determined in Reference 5.

3.0 PROCEDURE

The preceeding section discussed the design and operation of CLAs and identified four mechanisms by which sample gas composition variations could affect CLA response to NO. The objective of this investigation was to access the cumulative effects of these mechanisms on commercially available CLAs operated in accordance with the manufacturers' instructions sampling combustion products.

Two CLAs were selected for evaluation:

- Beckman Model 951
- Thermal Electron Corporation (TECO) Model 10A

The Beckman analyzer utilizes an atmospheric reaction chamber. Sample gas and ozone flows are controlled by regulating the pressure drop across capillaries. Sample pressure is provided by an internal sample pump.

The TECO analyzer utilizes a subatmospheric pressure reaction chamber operating at nominally 9 torr. As with the Beckman analyzer, flowrates in the TECO are controlled by capillaries. A vacuum pump exhausts the reaction chamber and creates the pressure drop across the capillaries. The use of a subatmospheric reaction chamber adds considerable complexity to the instrument but reduces the importance of quenching thus increasing sensitivity to low NO concentrations.

The manufacturers' instructions for both CLAs include detailed operating information specifying the proper pressures, flowrates and calibration procedures. Filtering and drying the sample gas to a dewpoint less than operating temperature is required to prevent sample capillary blockage.

The operating procedure used by technicians in laboratory and field tests varies somewhat with sample train design and test conditions. Most commonly the instrument is utilized intact, operated according to the manufacturers' instructions and zeroed and spanned with N_2 and NO in N_2 respectively. This was the procedure utilized in this investigation. However, in tests of subatmospheric combustors such as flat flames a low reaction chamber pressure CLA (such as the TECO) is often used without the sample gas capillary. This allows the sample gas to pass directly from the probe to the reaction chamber without water removal. Sample flowrate is controlled by the probe tip which acts as a sonic flow orifice. The results of this investigation cannot be directly applied to CLAs operated in this manner.

Table 3 shows the gas mixtures tested in this investigation. These mixtures were prepared by blending high purity gases and mixtures of NO in N_2 or A with a precision gas flow metering system. Nitric oxide in N_2 span gases were prepared similarly so that inaccuracies in mixed gases supplied in cylinders could not affect the CLAs' relative responses to span gases and sample gases.

For each experiment in Table 3, the CLAs were adjusted to read correctly on N_2 with no NO and a mixture of NO in N_2. The instruments were then used to measure the concentrations of NO in the mixture compositions tested. The actual concentrations of NO in span and test gases were identical so that the ratios of indicated NO measured in the test gases to actual NO concentrations were direct measurements of background gas composition effects. The CLAs' responses to N_2 zero and NO in N_2 span gases were checked after each datum point. Concentrations of O_2, CO and CO_2 in zero, span and test gases were also monitored as a check on metering system accuracy and to verify no leaks in the sampling train.

In the first experiment the test gases were mixtures of NO in two component (binary) background gases. This is similar to the experiments reported by Mathews et al(5) except that these experiments measure the response of the CLAs in toto while Mathews et al only measured the effects of quenching variations. The NO concentration was 200 ppm and the background gases tested were various concentrations of O_2, CO, CO_2, CH_4, H_2 or A in N_2.

In the second experiment the test gases simulated complete dry products of combustion from burning a hydrocarbon fuel, CH_x, in air. To simulate a wide range of hydrocarbon fuels, X was chosen as either zero (pure carbon) or 4 (methane). Figure 3 shows the concentrations of CO_2 and O_2 in these mixtures as functions of the stoichiometry of the combustion process. The balance of the mixtures are N_2 (and of course trace amounts of NO). At 100% theoretical air the complete products of combustion are N_2 and CO_2 (since H_2O has been assumed to be removed). At leaner stoichiometries the concentration of CO_2 is lower and some residual O_2 remains in the products. As the percent theoretical air is increased towards infinity, the concentrations of CO_2

Table 3. Test Matrix

EXPERIMENT NUMBER	CONDITIONS SIMULATED	FUELS	OXIDANTS	STOICHIOMETRY % T.A.	COMMENTS
1	Binary Background Gases				O_2,CO,CO_2,CH_4, H_2 or A in N_2
2	Lean Complete Combustion Product - Dry	C, CH_4	21% O_2/N_2	100 - ∞	
3	Lean Complete Combustion Product - Wet	C	21% O_2/N_2	100, 250, 500	Dry to 294 K Dewpoint
4	Lean Incomplete Combustion Product - Dry	C	21% O_2/N_2	125 - 300	20% $CO_2 \rightarrow CO + 1/2\ O_2$
5	Rich Combustion Product - Dry	C, CH_4	21% O_2/N_2	50 - 100	$[O_2] = 0$, Relative C and H Stoichiometries Equal, No Soot or $H_x\ C_y$
6	Lean Complete Combustion Product - Dry	C, CH_4	21% O_2/A 21% O_2/21% CO_2/A	100 - ∞	
7	Rich Combustion Product - Dry	C	21% O_2/A 21% O_2/21% CO_2/A	60 - 100	$[O_2] = 0$, Relative C and H Stoichiometries Equal, No Soot or $H_x\ C_y$
8	Lean Complete Combustion Product - Dry	C	21% O_2/N_2 21% O_2/A	125	Instruments Operated Off Design Points

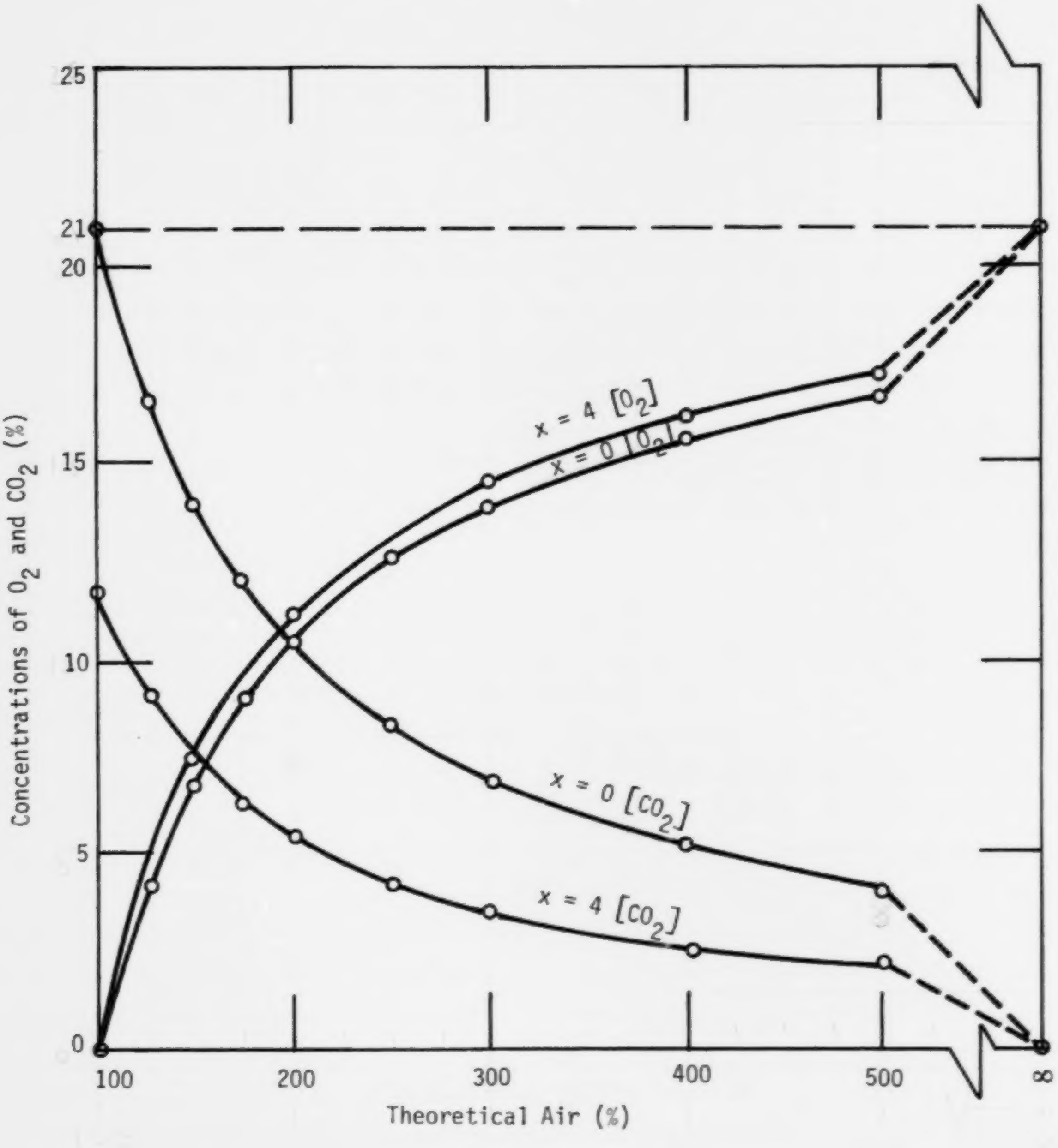

Figure 3. Complete Dry Products of Combustion from Burning CH_x in Air.

approach zero and the concentrations of O_2 approach 21.0% (the concentration of O_2 in the air).

The gases blended to form these "dry" mixtures typically contained about 3 ppm H_2O. This corresponds to a dew point (ice point) of 205K at atmospheric pressure. Sample trains utilizing CLAs usually contain a water trap which reduces the combustion product dew point to between 273 and 293K. This corresponds to 6000 to 23,050 ppm H_2O at atmospheric pressure. In experiment number 3, H_2O was added to the dry gases to raise the dewpoint to this range.

In experiment number 4 incomplete combustion products were simulated by replacing 20% of the CO_2 in the complete products with CO and O_2 according to the following reaction:

$$CO_2 \longrightarrow CO + 1/2\ O_2 \qquad 5$$

Incomplete combustion products from practical systems may also contain hydrogen, unburned hydrocarbons and soot. These were not included in the simulation.

The composition of combustion products from combustion systems operating fuel rich depends strongly upon combustor design and operating conditions. Oxygen concentrations are generally near zero and substantial concentrations of H_2, CO, hydrocarbons, H_2 and soot may be present. In experiment number 5 the combustion products from burning C and CH_4 in air were simulated subject to the following assumptions:

- All O_2 in the reactants is converted to either CO, CO_2 or H_2O. The residual O_2 concentration is zero
- All carbon in the reactants is converted to a mixture of CO and CO_2
- All H_2 in the reactants is converted to a mixture of H_2 and H_2O (H_2O was eliminated to simulate dry combustion products)
- NO soot or hydrocarbons are produced
- The stoichiometries of hydrogen and carbon atom combustion are equal

These simulated combustion products were mixtures of N_2, CO, CO_2 and H_2 and are shown in Figure 4.

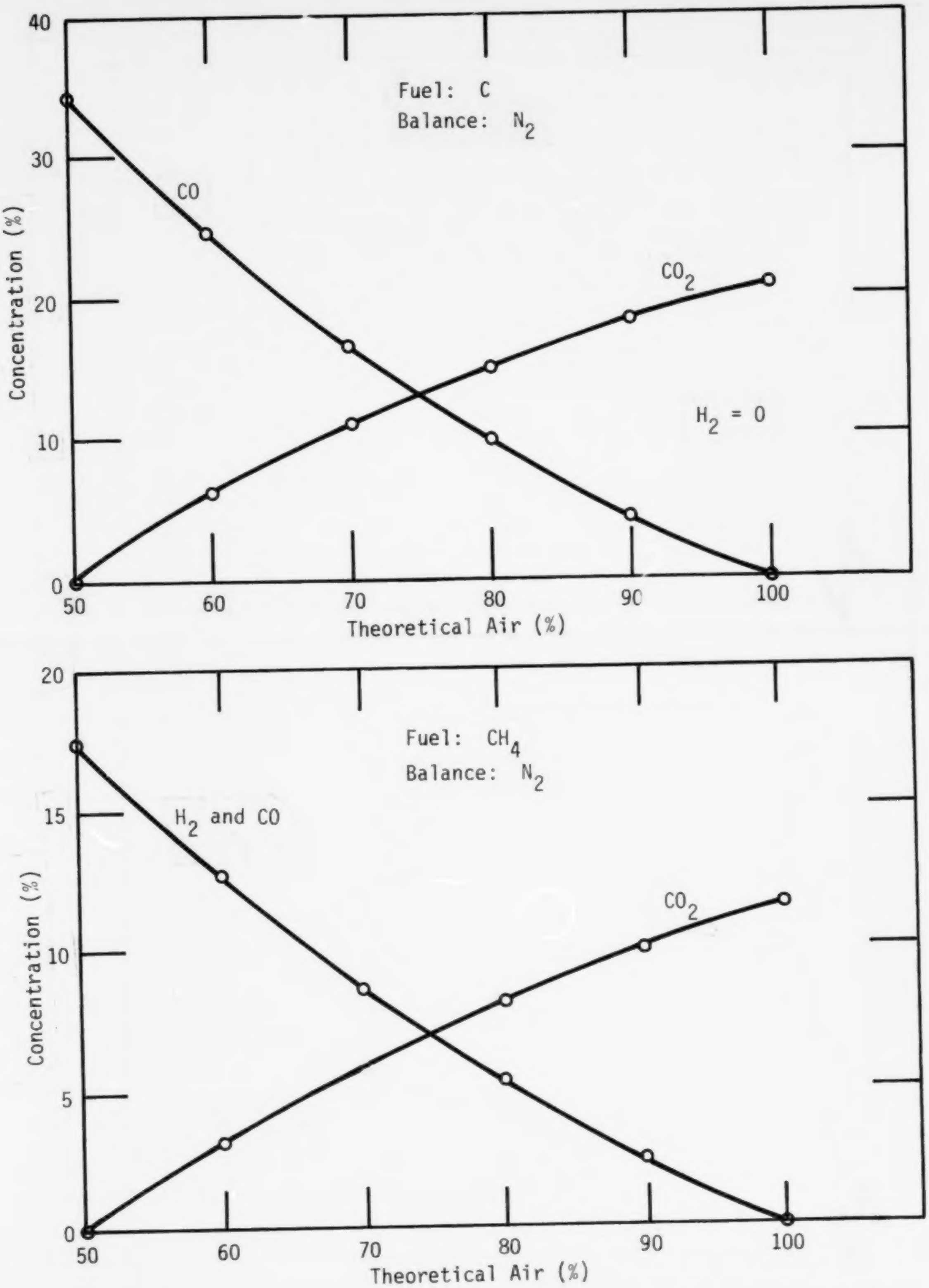

Figure 4. Simulated Fuel Rich Dry Combustion Products from Burning CH_x in Air.

It should be noted that the products of combustion from practical combustors operated fuel rich will generally be different from the compositions listed in Figure 4. These simulated combustion product compositions were selected for simplicity and to give an approximate indication of the CLA performance sampling rich products.

In experiments involving combustion of fuels containing bound nitrogen it is difficult to differentiate between NO formed from atmospheric N_2 and NO formed from nitrogen bound in the fuel. Several investigators have recently combusted fuels containing bound nitrogen in an oxidant containing only O_2, CO_2 and A to eliminate NO formation from N_2. The oxidant mixtures most commonly used are 21% O_2 balance A and 21% O_2, X% CO_2 balance A. Carbon dioxide is sometimes added to adjust the flame temperature to match the flame temperature produced with air as the oxidant. The concentration of CO_2 required is usually about 20%.

Experiments 6 and 7 are identical to experiments 4 and 5 except that the oxidant was 21% O_2 balance A and 21% O_2, 21% CO_2 balance A.

In the first seven experiments the CLAs were operated strictly according to the manufacturers' recommendations. In experiment 8 the CLA operating conditions were varied over wide ranges to determine if:

- The results obtained were sensitive to CLA operating conditions
- The variations in CLA response due to sample gas composition variations could be minimized by judicious choice of CLA operating conditions

The dry complete products of combustion of burning carbon with 125% theoretical oxidant were simulated. The oxidants tested were 21% O_2 balance N_2 or A. For each test, the CLAs' operating parameters were adjusted to specific off design point conditions and the CLAs were zeroed and spanned with N_2 and NO in N_2 respectively and used to measure NO in the simulated combustion products. The variable operating parameters for the CLA's included:

- BECKMAN
  - sample pressure
  - oxygen pressure

- TECO
    - sample vacuum
    - oxygen pressure

In the TECO, these variations also caused the reaction chamber pressure to vary.

4.0 EXPERIMENTAL APPARATUS

A schematic diagram of the experimental apparatus is shown in Figure 5. The gas mixtures were generated by blending high purity gases and mixtures of NO in N_2 or A from cylinders with a high accuracy metering system. Water vapor was added by bubbling some of the gases (O_2 and N_2) through distilled water. Contacting of the NO mixtures with O_2 and H_2O was controlled by maintaining the NO mixtures separate from the O_2 and H_2O. The two streams were blended immediately upstream of the instruments in a short length of teflon tubing. The instruments included Beckman and TECO CLAs and other instruments to measure O_2, CO, CO_2 and dewpoint. The following subsections describe the experimental apparatus in more detail.

4.1 High Accuracy Metering System

A maximum number of eight gases was metered at one time with two flow systems designed to handle corrosive gases, such as NO mixtures. These mixtures only came in contact with stainless steel and teflon while the other gases also came in contact with brass.

Figure 6 shows a typical metering system with four orifices of varying sizes. The flowrate is nearly directly proportional to the upstream pressure and inversely proportional to the square root of the upstream temperature. Pressures were measured with high accuracy (± 0.11% full scale) variable capacitance pressure transducers and temperatures were maintained constant at 366K by a hot water tank. The pressures downstream from the orifices are second order variables but were also maintained constant with back pressure relief valves. The pressure transducers were mounted in an insulated box to minimize the drift associated with temperature and humidity variations.

The 32 critical orifices were Gatti Sapphire Orifice Jewels and range in size from 0.076 to 0.640 mm diameter. Utilizing these orifices individually or in combination and varying upstream pressures by a factor of two gave a total metering range of 54.0 to 1.0.

Figure 7 gives an overall picture of the gas supply and metering system. For any desired combination of gases and flowrates, the required orifices were selected with ball valves and the pressure regulators adjusted to the desired

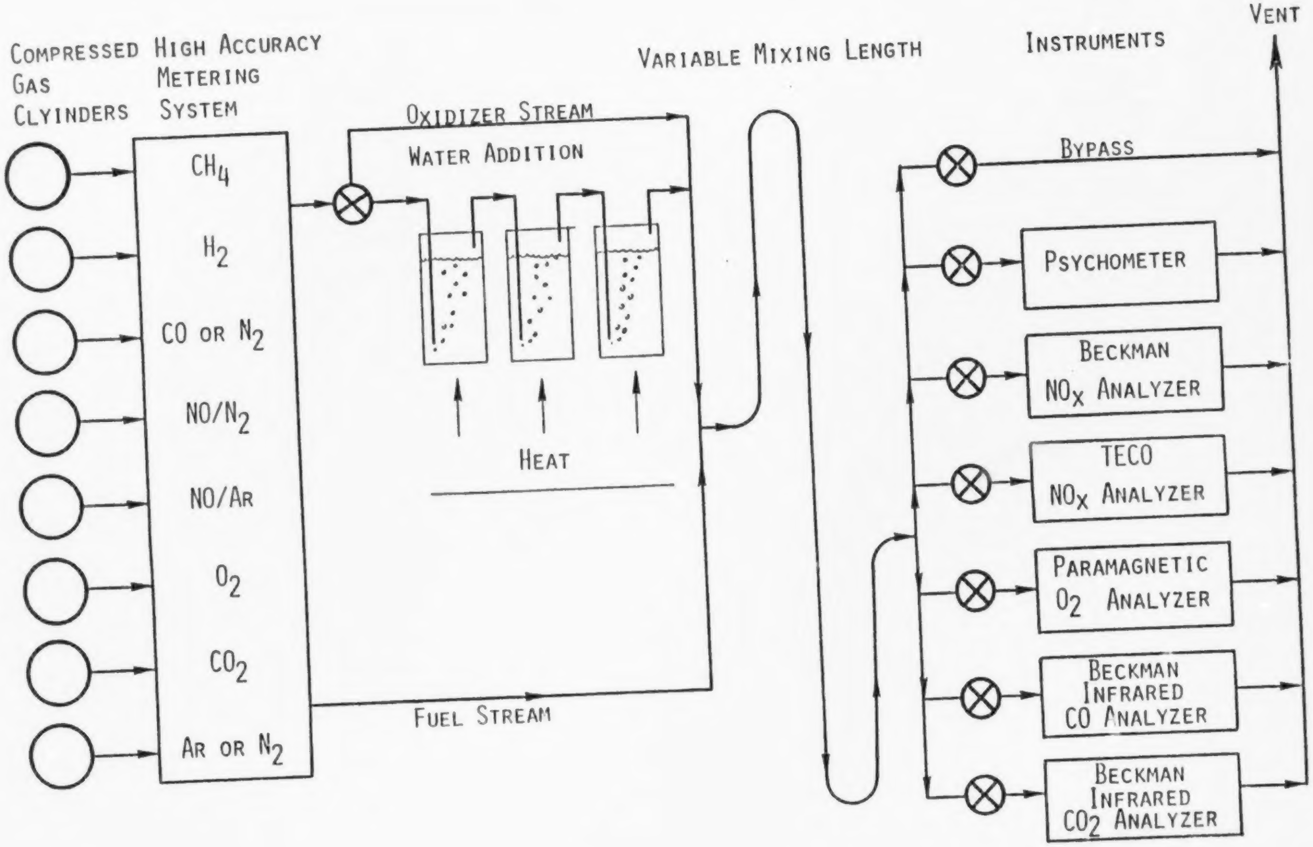
Compressed Gas Clyinders
High Accuracy Metering System
CH_4
H_2
CO or N_2
NO/N_2
NO/Ar
O_2
CO_2
Ar or N_2
Oxidizer Stream
Water Addition
Heat
Fuel Stream
Variable Mixing Length
Instruments
Vent
Bypass
Psychometer
Beckman NO_x Analyzer
TECO NO_x Analyzer
Paramagnetic O_2 Analyzer
Beckman Infrared CO Analyzer
Beckman Infrared CO_2 Analyzer

Figure 5. Experimental Apparatus.

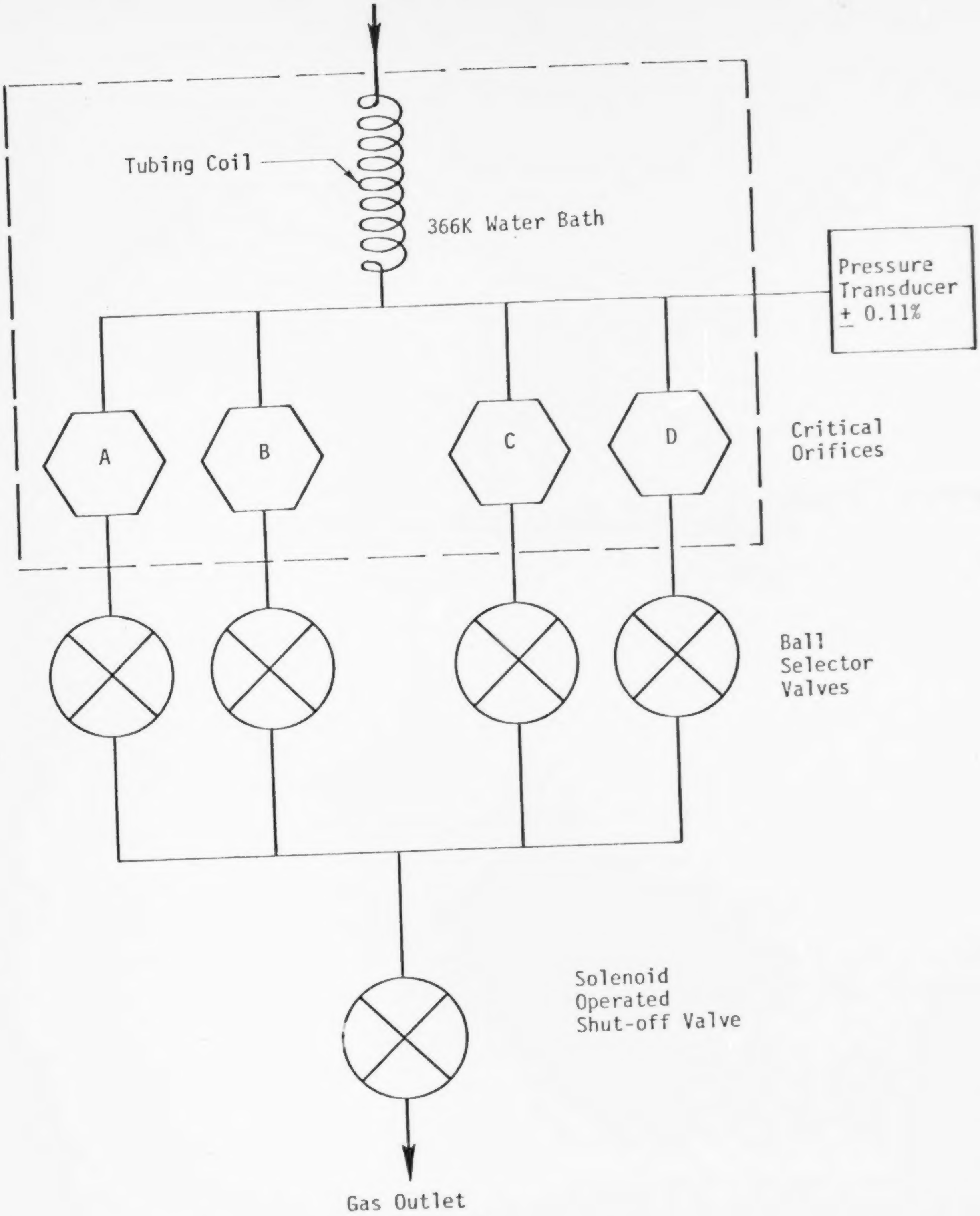
Tubing Coil
366K Water Bath
Pressure Transducer ± 0.11%
A
B
C
D
Critical Orifices
Ball Selector Valves
Solenoid Operated Shut-off Valve
Gas Outlet

Figure 6. Critical Orifice Metering System.

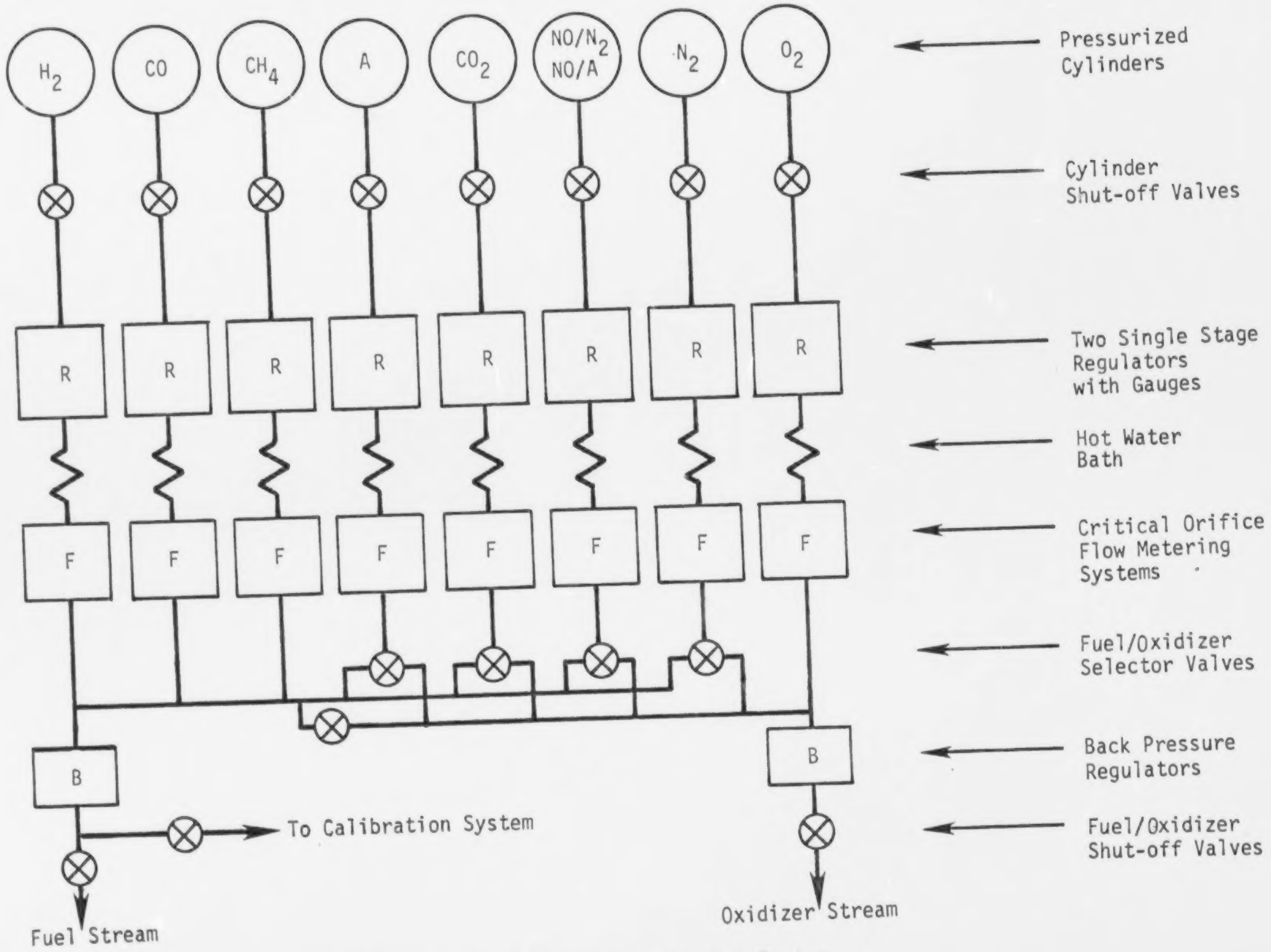
H2
CO
CH4
A
CO2
NO/N2
NO/A
N2
O2
Pressurized Cylinders
Cylinder Shut-off Valves
R
Two Single Stage Regulators with Gauges
Hot Water Bath
F
Critical Orifice Flow Metering Systems
Fuel/Oxidizer Selector Valves
B
Back Pressure Regulators
Fuel/Oxidizer Shut-off Valves
To Calibration System
Fuel Stream
Oxidizer Stream

Figure 7. Gas Supply and Metering System.

pressures. Solenoid operated shutoff valves in each metering system allowed the gas flows to be joined to either the fuel or oxidizer streams as required.

The critical orifice flow metering system was stable and accurate well within 0.5% as determined by a built in calibration system. The pressure transducers were calibrated with a precision Heise pressure gauge. During calibration, the gas metering system valves connected all pressure transducers to a common plenum joining the Heise gauge and thus all transducers were calibrated simultaneously. Each critical orifice was calibrated by measuring the time required to fill an evacuated tank, the final tank temperature and pressure and the tank volume. This procedure was performed at three upstream pressures over the range of operating conditions and the best straight line correlation was determined by a least squares fit. The calibration system was carefully designed and operated to minimize starting and ending transients and other error sources.

4.2 Water Addition System

Moisture was added to the oxidizer stream by bubbling the non-soluble gases, such as nitrogen and oxygen, through three heated flasks containing distilled water. The excess flow from the metering system was passed over a psychrometer which measured the wet and dry bulb temperatues of the gas mixture. The actual NO concentration was corrected for the water addition and the dewpoint was determined by applying a correction factor to the pyschrometric chart. This factor was based on the individual gaseous components for each simulated product composition. The dewpoint was varied from 266K to 294K with the upper limit resulting from potential condensation in the mixing section and the instruments.

4.3 Gases

All gases were high purity grade (99.97% or better) with the exception of CO (99.0%). NO was supplied as mixtures in N_2 and A (± 5% accuracy) to facilitate metering. All mixed gases were calibrated against a National Bureau of Standards (NBS) traceable mixture. To confirm the concentrations of NO in the test gas mixtures, several gas mixtures were analyzed utilizing the phenolydsulfonic acid (PDSA) method. The maximum deviation between calculated and PDSA measured concentrations was 3.0%.

4.4 Instruments

The gas analysis instruments utilized in these tests are listed in Table 4. The O_2, CO and CO_2 instruments were operated according to the manufacturers' recommendations and were utilized to verify the accuracy of the flow metering system and to check for leaks. The CLAs are discussed in the following paragraphs.

Figure 8 is a simplified schematic diagram of the TECO Model 10A CLA. The flow of gases through the instrument is provided by an oil sealed vacuum pump and a diaphram bypass pump. The reaction chamber operates at sub-atmospheric pressure and flowrates of sample gas and ozone are controlled by regulating the pressure drop across capillaries. The gas sample to be analyzed is supplied to the instrument at near atmospheric pressure and drawn through the main capillary by the bypass pump. The sample pressure regulator bleeds in additional filtered ambient air to maintain the pressure at point A essentially constant. The sample pressure regulator is referenced to the reaction chamber pressure so that it maintains the difference between the pressure at point A and the reaction chamber pressure constant. Since the pressure drop across the bypass flowmeter is small and constant, the system effectively maintains the pressure drop across the sample capillary constant. Under normal operating conditions the flowrate through the sample capillary is approximately 4.0% of the total flow through the main capillary. The bypass flowrate is adjusted with an external valve on the sample inlet to be constant at 15.7 cm^3/sec (2.0 scfh).

Oxygen is supplied to the instrument and regulated to a small positive pressure by the ozone pressure regulator. Ozone is generated as the O_2 passes through a silent discharge tube and the flowrate of the O_2/O_3 mixture is regulated by the ozone capillary.

The sample gas and O_2/O_3 mixtures are drawn into the reaction chamber by an oil sealed vacuum pump. The reaction chamber pressure is determined by the pump speed and the flowrates of gases into the reaction chamber. Under typical operating conditions the reaction chamber pressures is 5 to 12 torr.

Table 4. Gas Analysis Instruments

GAS	RANGES	TYPE	MANUFACTURER	MODEL
O_2	10, 25, 100%	Paramagnetic	Taylor Servomex	OA250
CO	0.3, 1.2, 3.0, 12.0%	NDIR	Beckman	315B
CO_2	2.0, 5.0, 15.0%	NDIR	Beckman	315B
NO	2.5, 10, 25, 100, 250, 1000, 2500, 10,000 ppm	CLA	TECO	10A
NO	10, 25, 100, 250, 1000, 2500, 10,000 ppm	CLA	Beckman	951

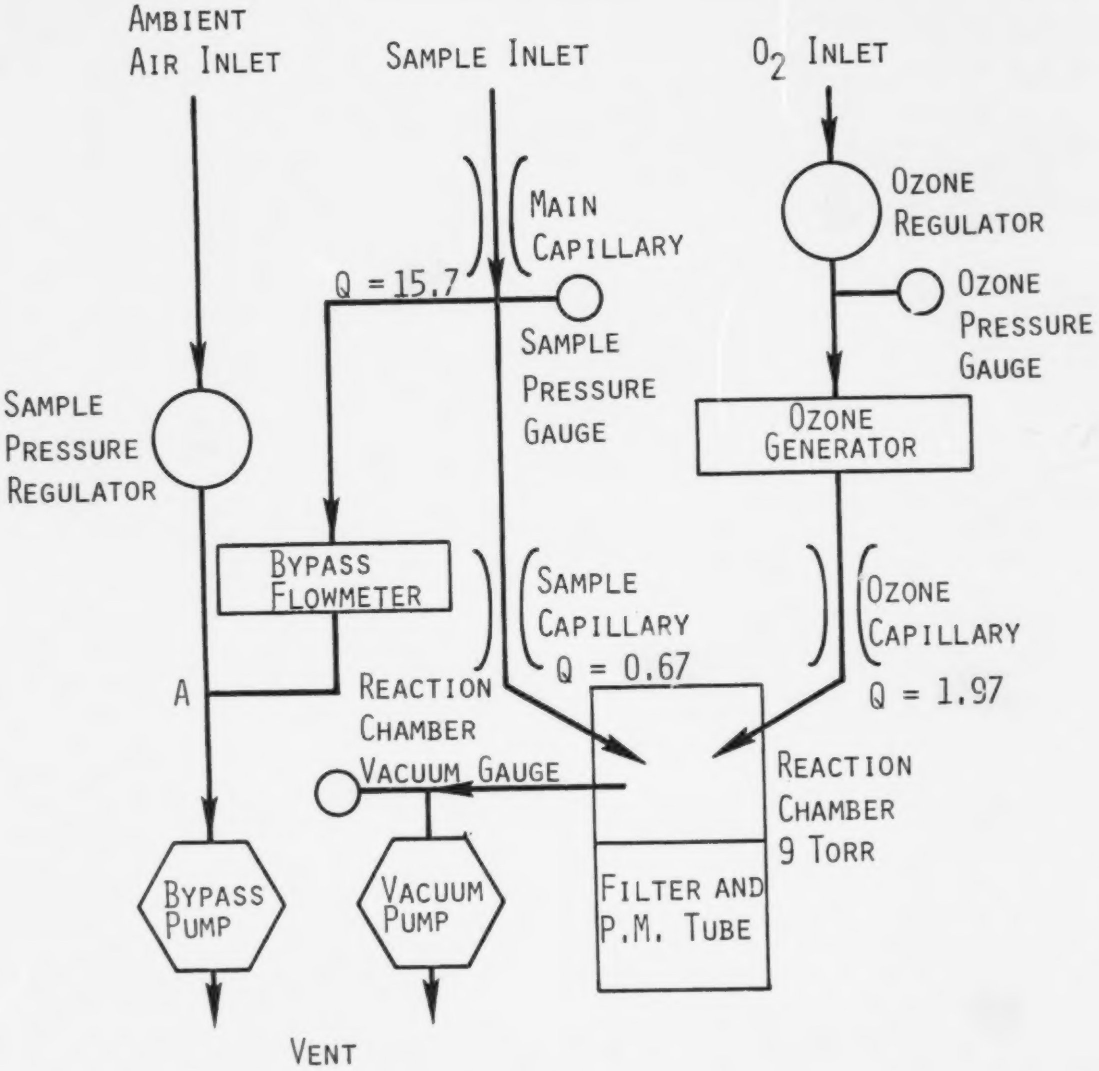
AMBIENT AIR INLET
SAMPLE INLET
O2 INLET
MAIN CAPILLARY
Q = 15.7
SAMPLE PRESSURE GAUGE
OZONE REGULATOR
OZONE PRESSURE GAUGE
OZONE GENERATOR
SAMPLE PRESSURE REGULATOR
BYPASS FLOWMETER
SAMPLE CAPILLARY
Q = 0.67
OZONE CAPILLARY
Q = 1.97
A
REACTION CHAMBER VACUUM GAUGE
REACTION CHAMBER 9 TORR
FILTER AND P.M. TUBE
BYPASS PUMP
VACUUM PUMP
VENT

NOTE: Q = FLOWRATE CM^3/SEC.

Figure 8. TECO Model 10A.

The independent operating parameters for the TECO Model 10A and the recommended operating conditions are as follows:

- Sample Vacuum: 83,300 Pa (5.0 in. Hg vacuum)
- Sample Bypass Flowrate: 15.7 cm^3/sec (2.0 scfh)
- Oxygen Pressure: 1.2×10^5 Pa (3.0 psig)

These conditions resulted in a reaction chamber pressure of 9 torr with the CLA used in these tests.

Figure 9 is a simplified schematic diagram of the Beckman Model 951 CLA. As with the TECO, this CLA utilizes capillaries to control flowrates into the reaction chamber. However, the Beckman CLA incorporates a teflon lined sample pump which provides the pressure to force sample gas through the sample capillary. A back pressure relief valve bypasses most of the sample gas through a flowmeter to a vent and maintains the pressure upstream of the sample capillary constant.

The ozone flow control system is similar to that employed in the TECO except that ozone is generated by ultraviolet light. The reaction chamber vent is unrestricted and the reaction chamber operates at essentially atmospheric pressure independent of the gas flowrates into the reaction chamber. Since the pressure regulators are referenced to atmospheric pressure, they function to maintain the differential pressures across the capillaries constant.

The independent operating parameters for the Beckman Model 951 and the recommended operating conditions are as follows:

- Sample Pressure: 1.3×10^5 Pa (4 psig)
- Sample Bypass Flowrate: 33.3 cm^3/sec (2 lpm)
- Oxygen Pressure 2.4×10^5 Pa (20 psig)

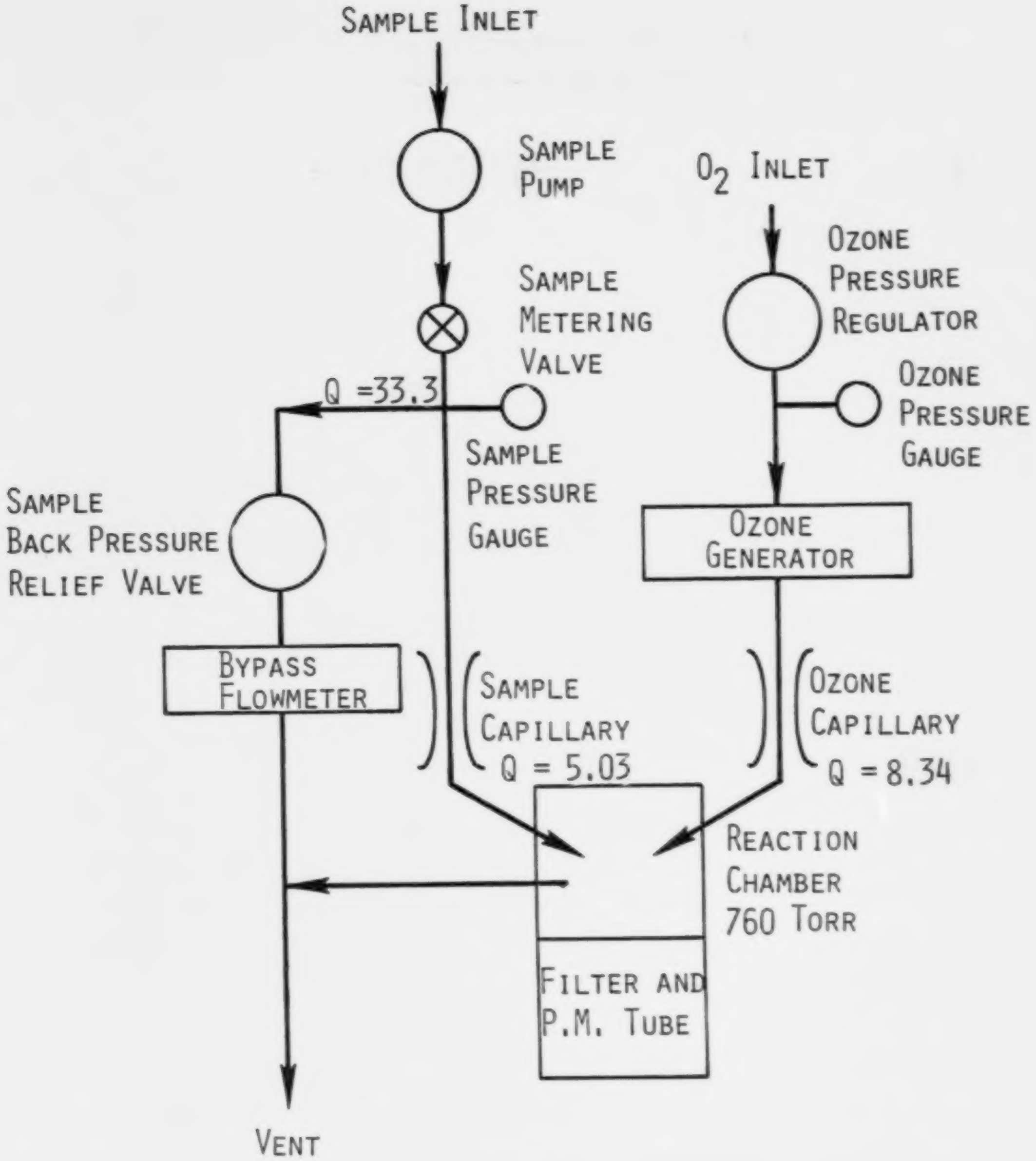
Sample Inlet
Sample Pump
Sample Metering Valve
Q = 33.3
Sample Pressure Gauge
Sample Back Pressure Relief Valve
Bypass Flowmeter
Sample Capillary Q = 5.03
O$_2$ Inlet
Ozone Pressure Regulator
Ozone Pressure Gauge
Ozone Generator
Ozone Capillary Q = 8.34
Reaction Chamber 760 Torr
Filter and P.M. Tube
Vent

NOTE: Q = FLOWRATE CM^3/SEC.

Figure 9. Beckman Model 951.

5.0 RESULTS

The experimental results plotted in this section are expressed as the ratios of the NO concentrations indicated by the CLA to the actual NO concentrations in the sample gas mixtures. The actual NO concentrations in the binary gas mixtures and simulated products of combustion for fuels burning in air were calculated from the reported NO concentrations in the compressed gas cylinders as diluted by the gas metering system. Since the span gas mixtures were produced from the same cylinder of NO in N_2 as the sample gases, errors in reported NO concentrations in the cylinders do not affect the ratios of indicated to actual NO concentrations plotted here as results.

For the tests involving simulated products of combustion for fuels burning in O_2/A or $O_2/CO_2/A$ atmospheres, the sample and span gases were produced from two separate cylinders containing NO mixtures. The concentrations in the cylinders were compared following the method discussed in section 4.3 and the "actual" NO concentration in the sample gas was calculated accordingly.

The raw data for all tests are listed in the Appendix.

5.1 Experiment No. 1 - Binary Background Gases

Figures 10 and 11 show the results of the binary background gas tests as the ratios of indicated to actual NO concentrations as functions of the concentrations of gases in the M/N_2 mixtures. As the concentration of gas M approaches zero, the ratio of indicated to actual concentration must approach 1.0 since 100% N_2 was the background gas used for spanning the instruments.

The results for all gases except H_2 at high concentrations show either negligible changes or decreases in the ratios of indicated to actual NO concentrations as the concentrations of the gases in the background mixtures increase. The results for CO and H_2 are similar for both CLAs. This is expected since the quenching data presented in section 2.0 indicates that the relative quenching efficiency of CO, H_2 and N_2 are nearly the same. Carbon monoxide has the same viscosity as N_2 and thus the viscosities of CO/N_2 mixtures are the same as N_2. This accounts for the negligible effects of CO concentration in the background gas on the ratios of indicated to actual NO concentrations. H_2 has a viscosity much smaller than N_2 and the viscosities of mixtures of H_2 in N_2

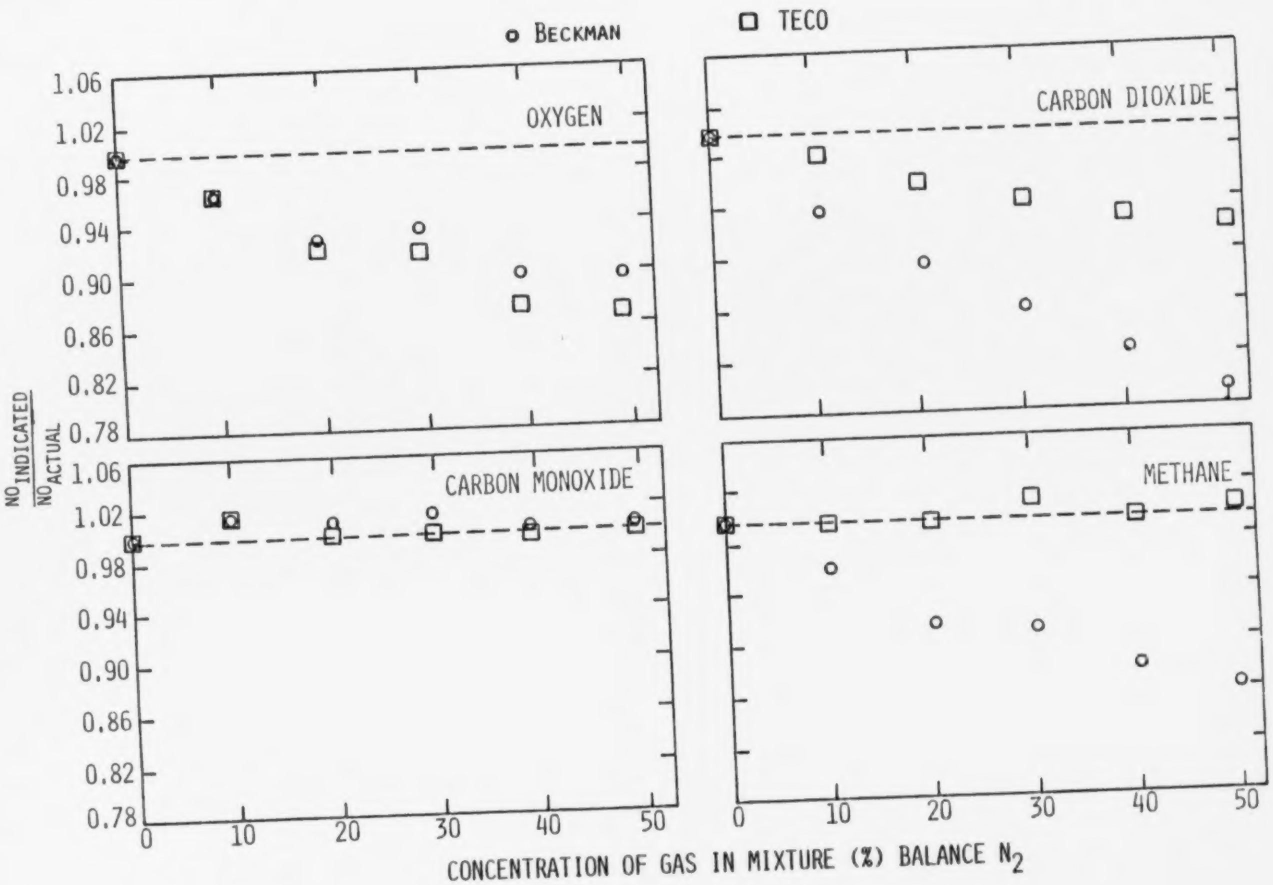

Figure 10. Experiment No. 1: Binary Background Gases

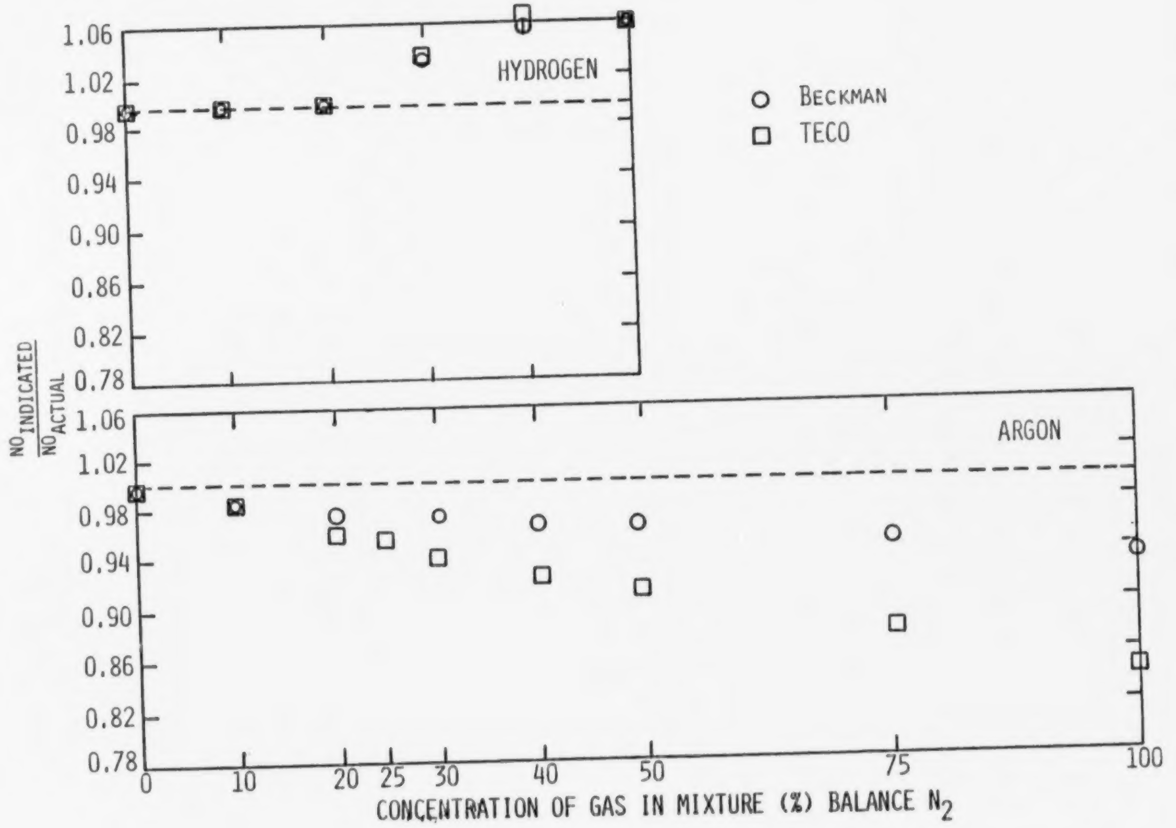

Figure 11. Experiment No. 1 (continued): Binary Background Gases.

decrease rapidly as the concentration of H_2 increases above 20% (see Table 1). This accounts for the increase in the ratio of indicated to actual NO concentration at high H_2 concentrations.

The results for the other binary background gas mixtures in Figures 10 and 11 can also be explained by examining the combined effects of viscosity related flowrate variations and quenching efficiency variations. For example, CH_4 has a viscosity less than N_2 and the viscosity related flowrate variations with CH_4/N_2 mixtures tend to increase the ratio of indicated to actual NO concentrations as the concentration of CH_4 increases. However, since CH_4 has more degrees of freedom than N_2, its quenching efficiency should be greater tending to decrease the ratio of indicated to actual NO concentration as the concentration of CH_4 increases. The results in Figure 10 show that the combined effects of quenching and viscosity variations produce a nearly flat response with the TECO. With the Beckman, the quenching efficiency effects are much larger (due to the higher reaction chamber pressure) and over compensate the viscosity effects to produce a decrease in ratio of indicated to actual NO concentration as CH_4 concentration increases.

5.2 Experiment No. 2 - Lean Complete Combustion Products (Dry)

Figure 12 shows the results of tests on the simulated complete dry combustion products from burning C and CH_4 in air. These background gas mixtures contained O_2, CO_2 and N_2 and were calculated as discussed in section 3.0. In all tests the ratio of indicated to actual NO concentration was less than 1.0 The TECO generally indicated NO concentrations closer to the actual levels than the Beckman. This is consistent with the results of experiment No. 1. For both instruments, the simulated combustion products from C exhibit more deviation than those from CH_4. This is a direct result of the higher CO_2 concentration in the simulated combustion products from C (see Figure 3).

These experiments were conducted with two concentrations of NO in the sample and span gas mixtures. Figures 12A and B show the results for 200 ppm NO for C and CH_4 fuels. Figure 12C compares the results for C as the fuel with 100 and 200 ppm NO and shows that the ratio of indicated to actual NO concentration is independent of the NO doping level.

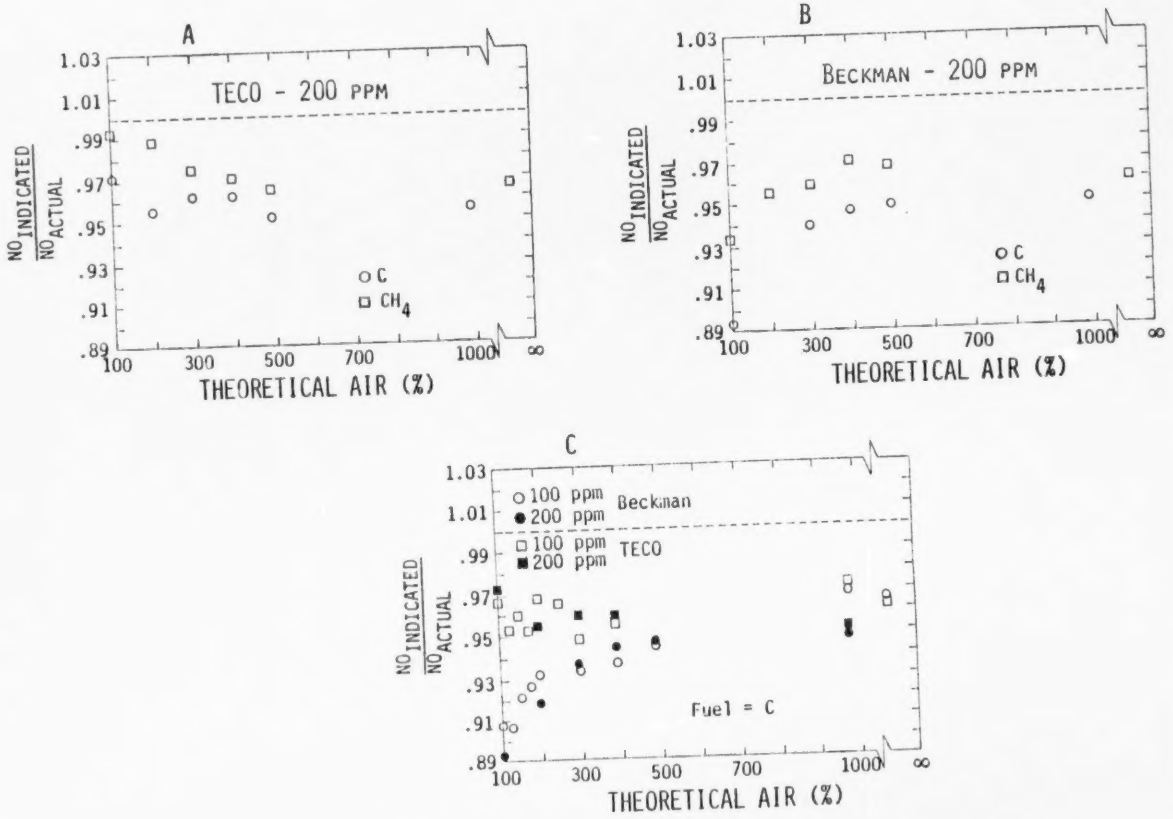

Figure 12. Experiment No. 2: Lean Complete Combustion Products Burning Fuels in Air (dry).

5.3 Experiment No. 3 - Lean Complete Combustion Products (Wet)

The previous experiments were conducted with dry sample gas mixtures prepared by blending dry compressed gases from cylinders. The dewpoints of these mixtures were about 205K. In laboratory and field emissions tests the combustion products generally contain several percent H_2O and the dewpoint may be as high as 350K. The usual procedure is to draw the sample gas through an ice bath to remove most of the H_2O and reduce the dewpoint beneath ambient temperature. This prevents condensation in the sample capillary and the associated plugging.

In this experiment the water vapor was added to the dry simulated combustion products to produce dewpoints in the range of 275 to 294K. Figure 13 shows the results for C burning in air at 100, 250 and 500% theoretical air. At each stoichiometry increasing the dewpoint decreased the ratio of indicated to actual NO concentration. The effect was small for the TECO (1.0 to 2.0%) but substantial for the Beckman (up to 6.0%).

5.4 Experiment No. 4 - Incomplete Lean Combustion Products (Dry)

The method of simulating incomplete combustion products utilized in these tests was to allow 20% of the CO_2 in the simulated complete combustion products to be reduced to CO and O_2. Figure 14 shows the results for simulated combustion products burning C in air assuming complete and incomplete combustion. The TECO's performance is essentially unaffected while the Beckman's improves with incomplete combustion. This is a result of the decrease in CO_2 concentration.

5.5 Experiment No. 5 - Rich Combustion Products (Dry)

The simulated rich combustion product mixtures contained CO, CO_2, H_2 and N_2 and the compositions were calculated as discussed in section 3.0. The results of those tests are shown in Figure 15. As with the lean combustion products, the TECO generally indicated closer to the actual NO concentration than the Beckman. Largest deviations were at near stoichiometric conditions with C as the fuel. Under very rich conditions (50%

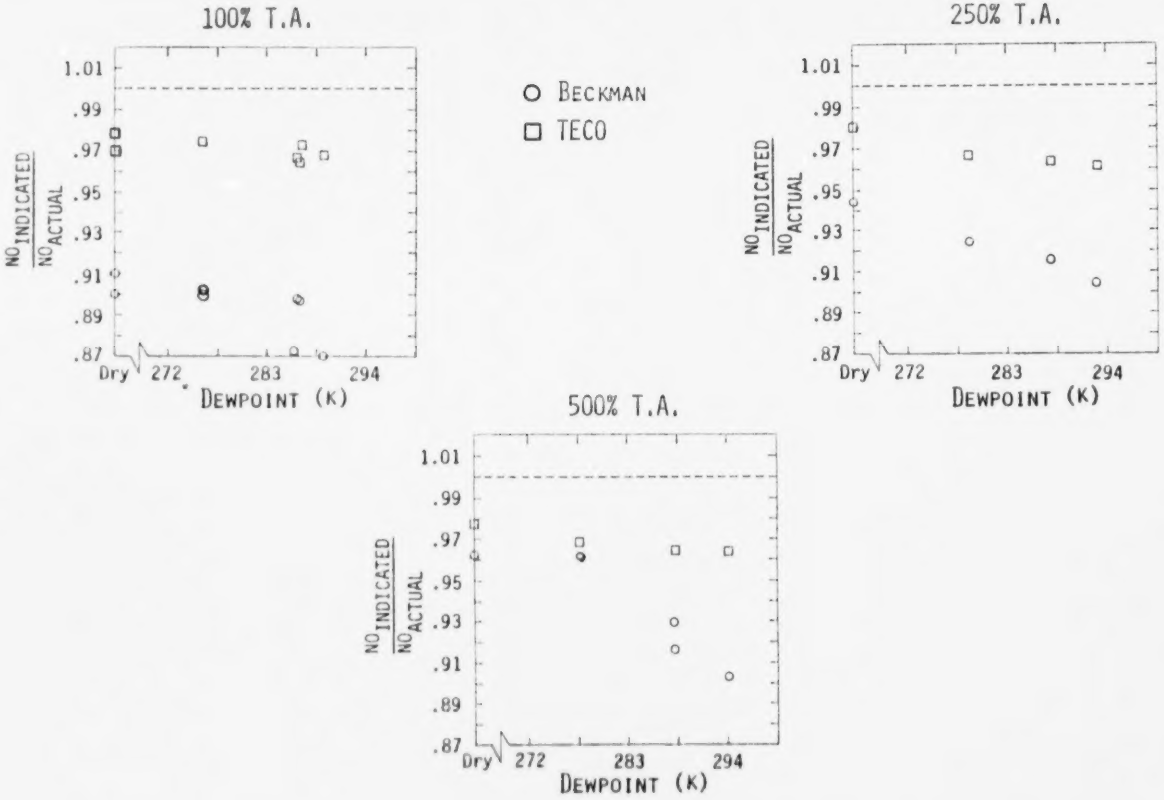

Figure 13. Experiment No. 3: Lean Complete Combustion Products from Burning C in Air (wet).

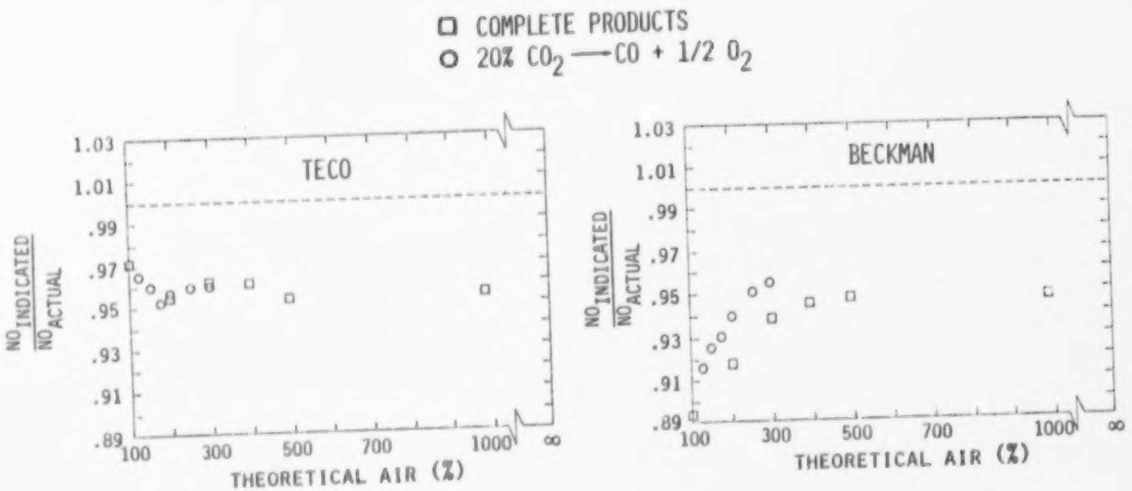

Figure 14. Experiment No. 4: Incomplete Lean Combustion Products Burning C in Air (dry).

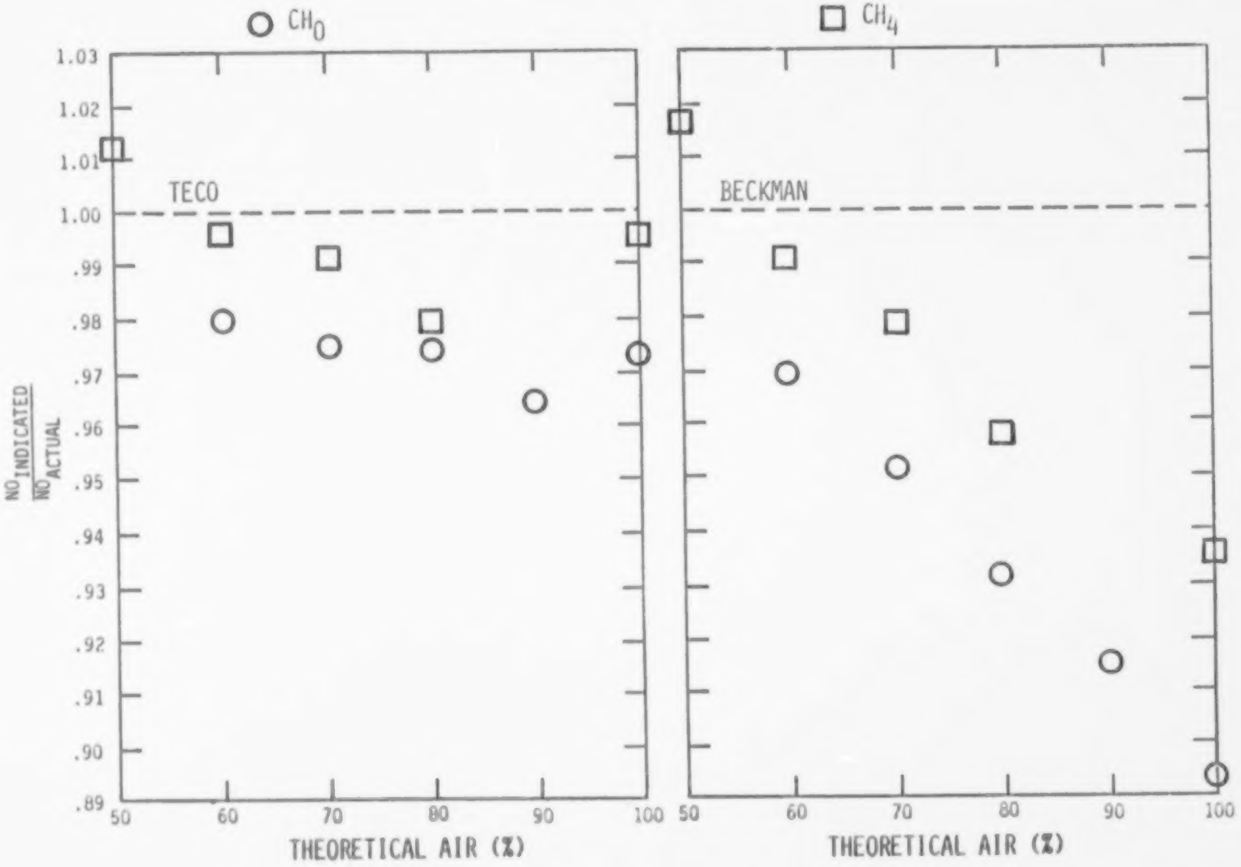

Figure 15. Experiment No. 5: Rich Combustion Products Burning Fuels in Air (dry).

theoretical air) with CH_4 as the fuel, both CLAs indicated slightly higher than the actual concentration of NO. At 50% theoretical air the concentrations of H_2 is over 17% and the binary background gas tests demonstrated that high concentrations of H_2 result in indicated NO concentrations greater than actual (see Figure 11).

5.6 Experiment No. 6 and 7 - Combustion Products in A Atmospheres (Dry)

Experiments 4 and 5 were repeated with O_2/A and $O_2/CO_2/A$ as the oxidant and the results are shown in Figures 16 and 17. The results for lean combustion products obtained with the TECO are essentially independent of stoichiometry, oxidant (O_2/A or $O_2/CO_2/A$) and fuel (C or CH_4). However, while similar results for combustion of fuels in air gave ratios of indicated to actual NO concentrations of 0.95 to 0.99, these results are much lower (0.82 to 0.87).

The results for lean combustion products obtained with the Beckman are also lower than comparable results obtained with air as the oxidant but the differences are smaller than with the TECO. The Beckman results are also affected by the CO_2 content of the oxidant with increasing CO_2 concentration decreasing the ratio of indicated to actual NO concentrations as expected.

The results of the rich combustion products tests shown in Figure 17 show the same general trends as the lean tests: the TECO response is nearly constant independent of stoichiometry and oxidant under rich conditions and the Beckman results are very sensitive to the concentration of CO_2 in the oxidant.

5.7 Experiment No. 8 - Off Design Point CLA Operation

All of the previous experiments were conducted with the CLAs operated strictly according to the manufacturers' instructions. Figure 18 shows the results of operating the CLAs under other conditions. Simulated combustion products from burning C in air and O_2/A oxidants were utilized and the CLAs were zeroed, spanned and used to measure these sample gases with the operating parameters set at several conditions. The effect of each independent variable on instrument response is shown in the raw data in the Appendix. Figure 18 shows the ranges of instrument response observed as the independent parameters were varied. In all cases, variations in the operating parameters resulted in only minor changes (± 3%) in instrument response.

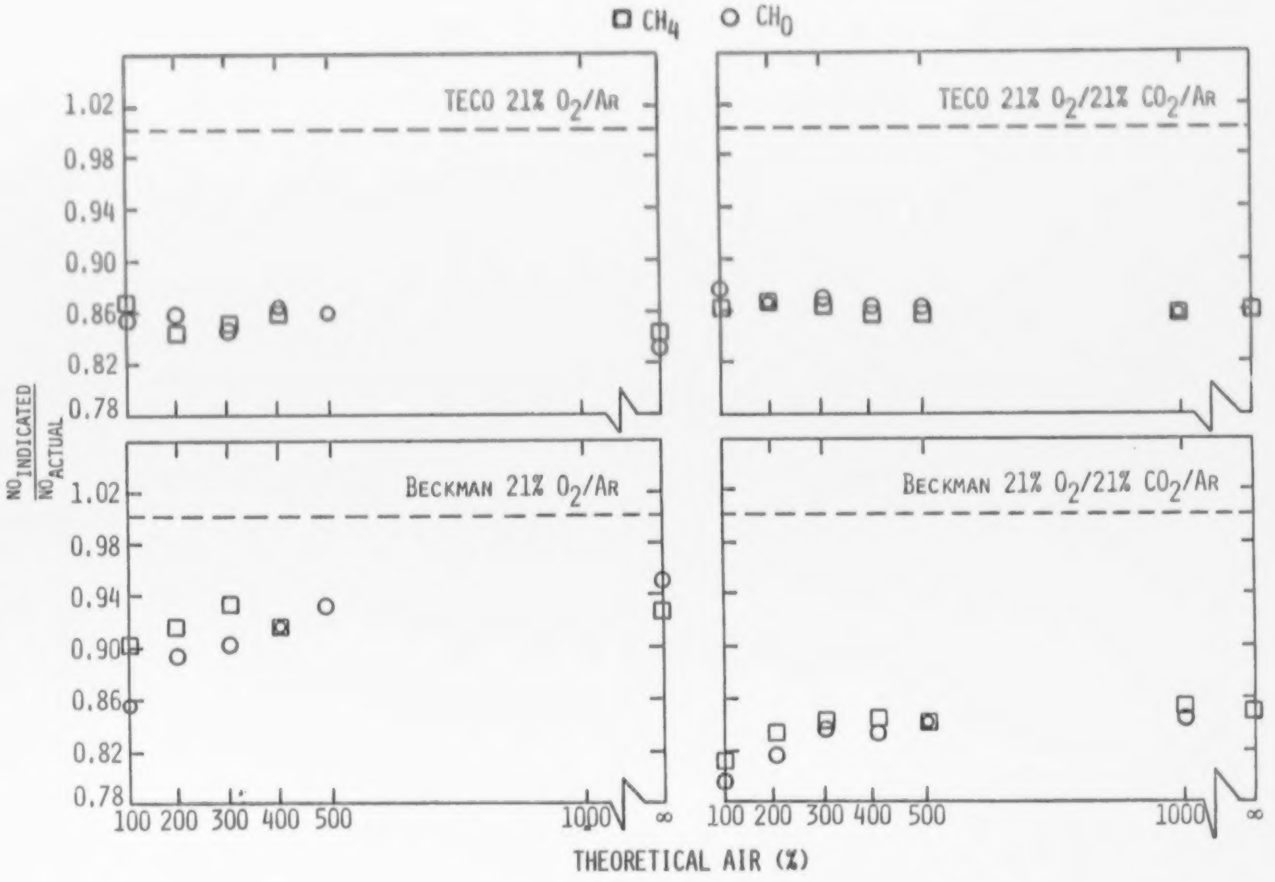

Figure 16. Experiment No. 6: Lean Complete Combustion Products Burning Fuels in O_2/Ar and O_2/CO_2/Ar Oxidants (dry).

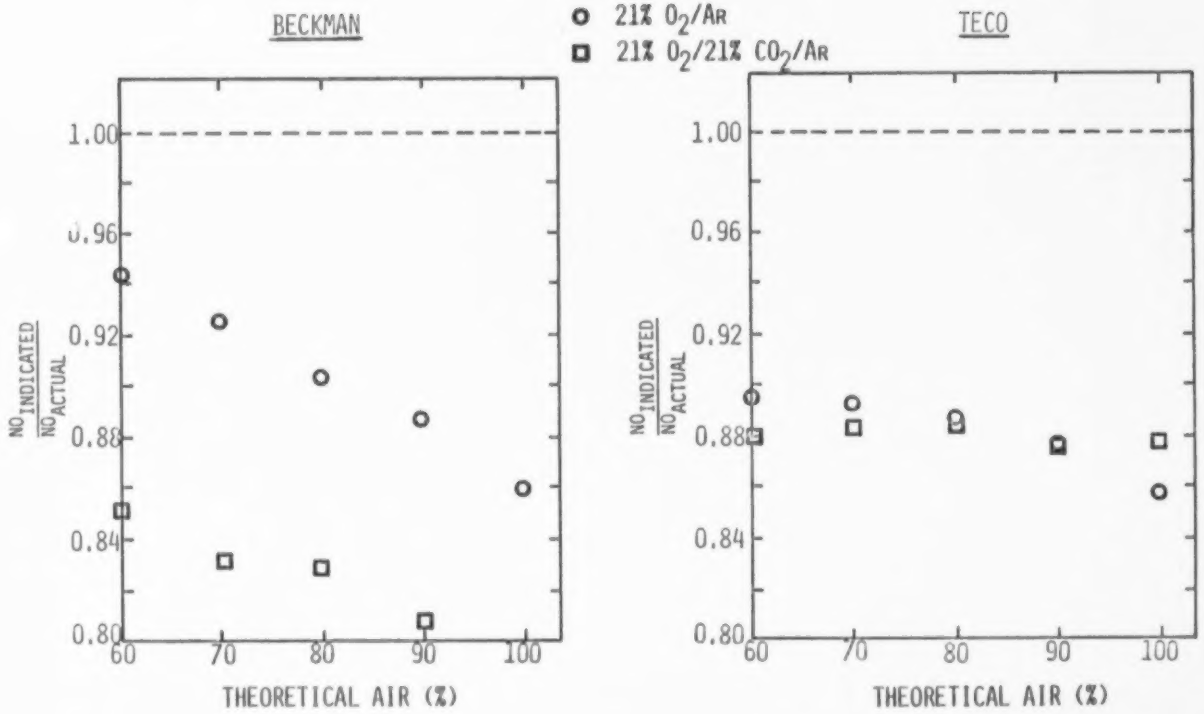

Figure 17. Experiment No. 7: Rich Combustion Products Burning C in O_2/Ar and O_2/CO_2/Ar Oxidants (dry).

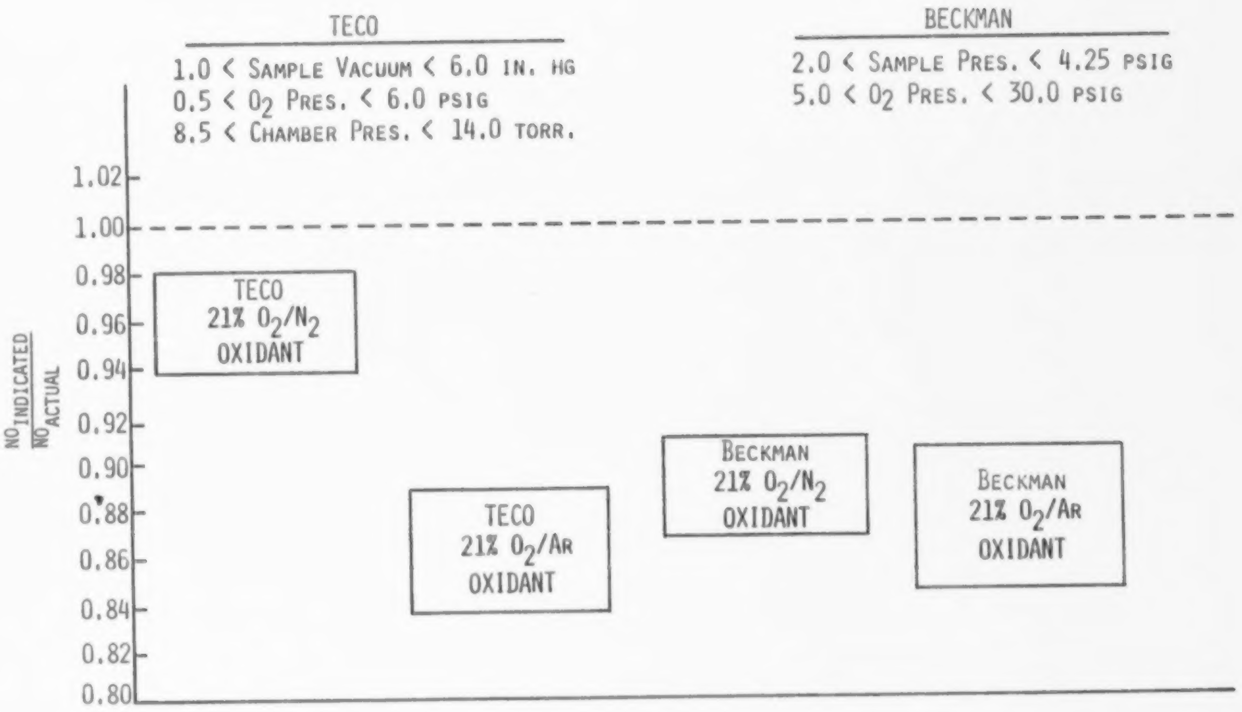

Figure 18. Experiment No. 8: Off Design Point CLA Operation Burning C at 125% Theoretical Oxidant (dry).

6.0 DISCUSSION

The objectives of this study were to:

- Assess the accuracy of commercial CLAs measuring NO in combustion products following the procedures recommended by the instrument manufacturers
- Examine methods of correcting CLA indicated NO concentrations for the effects of background gas composition variations
- Examine methods to improve calibration procedures

The results of the experiments discussed above show that commercial CLAs generally indicate NO concentrations lower than actual when spanned with mixtures of NO in N_2 and used to sample NO in combustion products. The errors introduced by neglecting sample background gas composition variations cover the following ranges:

COMBUSTION PRODUCTS FROM FUEL AND:	ERROR % TECO	BECKMAN
21% O_2/N_2	+1 to -5	+2 to -11
21% O_2/Ar	-11 to -16	-6 to -14
21% O_2/21% CO_2/Ar	-12 to -15	-15 to -20

These results apply directly to the two CLAs tested but are probably representative of the performance of other instruments of similar design as well. Both instruments utilize capillaries to control sample flowrates. The TECO reaction chamber operates at approximately 9 torr while the Beckman reaction chamber operates at atmospheric pressure.

The gases responsible for the majority of the errors are CO_2, H_2O, O_2 and Ar. Each of these gases decrease the CLA's sensitivity to NO. Carbon dioxide is often present at high concentrations in combustion products and accounts for the majority of the errors at near stoichiometric conditions. Water vapor has a much higher quenching efficiency than N_2. At the low H_2O concentrations typical of combustion products dried in an ice bath, the quenching effects far outweight the effects of viscosity. Sample dewpoint variations can change CLA response to NO by several percent. For oxygen the effects of viscosity and quenching variations are additive and this combined with the high concentrations of O_2 present in lean combustion products results in errors as high as 4%.

The effects of viscosity and quenching variations are opposite for Ar. In the CLAs tested here, the viscosity related variations over compensated the quenching variations resulting in a decrease in CLA sensitivity to NO with increasing Ar concentration. In the experiments reported in Reference 5, the sample flowrate was maintained constant and the results did not include the viscosity related flowrate variations present in these experiments. This accounts for the reported opposite effect of Ar on CLA response to NO. In combustion experiments utilizing O_2/Ar or O_2/CO_2/Ar as the oxidant, the concentration of Ar in the combustion products is high and results in CLA errors as high as 20%.

The variations in CLA response due to background gas composition variations were generally smaller with the TECO than with the Beckman except for Ar. Based upon these results a low reaction chamber pressure CLA such as the TECO would be preferred to monitor products of combustion of fuels burned in air. However, the choice of instruments for experiments involving O_2/Ar or O_2/CO_2/Ar oxidants is unclear. The following example illustrates these points.

A fuel containing bound nitrogen is burned in three oxidants: air, O_2/Ar and O_2/CO_2/Ar. It is assumed that 500 ppm of NO are formed from fuel bound N_2 independent of oxidant composition. It is further assumed that an additional 500 ppm of NO are formed from N_2 when the fuel is burned in air. Ideally, the experimental results should indicate 1000 ppm in the air experiment and 500 ppm in both Ar experiments. The thermal NO could then be calculated as the difference in NO concentrations (500 ppm).

Table 5 shows the results which would be obtained in this experiment utilizing the TECO and Beckman CLAs but without correcting the results for background gas composition variations. The fuel was assumed to be C burning at 100% theoretical oxidant and the instrument response was taken from the results in sections 5.2 and 5.6.

In the air experiments the TECO reads closer to the correct concentration. However, with the O_2/Ar oxidant both CLAs indicate incorrectly by the

Table 5. Combustion Experiment Example

OXIDANT	NO SOURCE	INDICATED NO CONCENTRATIONS (PPM)	
		BECKMAN	TECO
Air	Fuel + Thermal	890	970
O_2/Ar	Fuel	430	430
O_2/Ar	Thermal (By Difference)	460	540
O_2/CO_2/Ar	Fuel	395	430
O_2/CO_2/Ar	Thermal (By Difference)	495	540

same amount. The thermal NO concentrations calculated by subtracting the NO concentrations are in error by equal amounts for both CLAs but the errors are in opposite directions. With the $O_2/CO_2/Ar$ oxidant the TECO reads closer to the correct concentration. However, the Beckman yields better results for the thermal NO. This example shows no clear cut advantage for either instrument design.

The results of this study can be used to correct the results of NO emission tests for the effects of background gas composition variations. Accurate corrections can be made if:

- The CLA utilized in the emission tests was one of those tested here.
- The CLA was operated according to the manufacturer's recommendations.
- The combustion product composition is known.

Figure 19 shows the application of the results of this study to an actual NO emission test conducted at Energy and Environmental Research Corporation. A No. 6 oil was fired in a bench scale furnace over a range of excess O_2 with air and $O_2/CO_2/Ar$ oxidants. Nitrogen oxides (NO_x) were measured with a TECO CLA equipped with a stainless steel converter to reduce NO_2 to NO. The indicated NO_x concentrations were corrected for background gas composition variations by applying the results in sections 5.2 and 5.6. The C and CH_4 data were interpolated to account for the oil's H/C ratio and the results obtained for 21% O_2, 21% CO_2, and the balance Ar were used (neglecting the difference between 20 and 21% CO_2 in the oxidant). Application of these results to the experimental data slightly increases the NO_x concentration for combustion in air and substantially increases (60 ppm) the NO_x concentration for combustion in the oxidant containing Ar. The conversion of fuel nitrogen to NO_x is higher and the thermal NO_x formation is lower than if the effects of background gas composition variations had been neglected.

Argon Furnace, Sonicore Ultasonic Atomizer, No Swirl Air,
No. 6 Alaskan/North Slope Oil - 0.51% N - 100% Conversion = 815 ppm (Dry 0% O_2)

○ Oxidant 21% O_2/20% CO_2/Ar ☐ Oxidant Dry Air 21% O_2/N_2

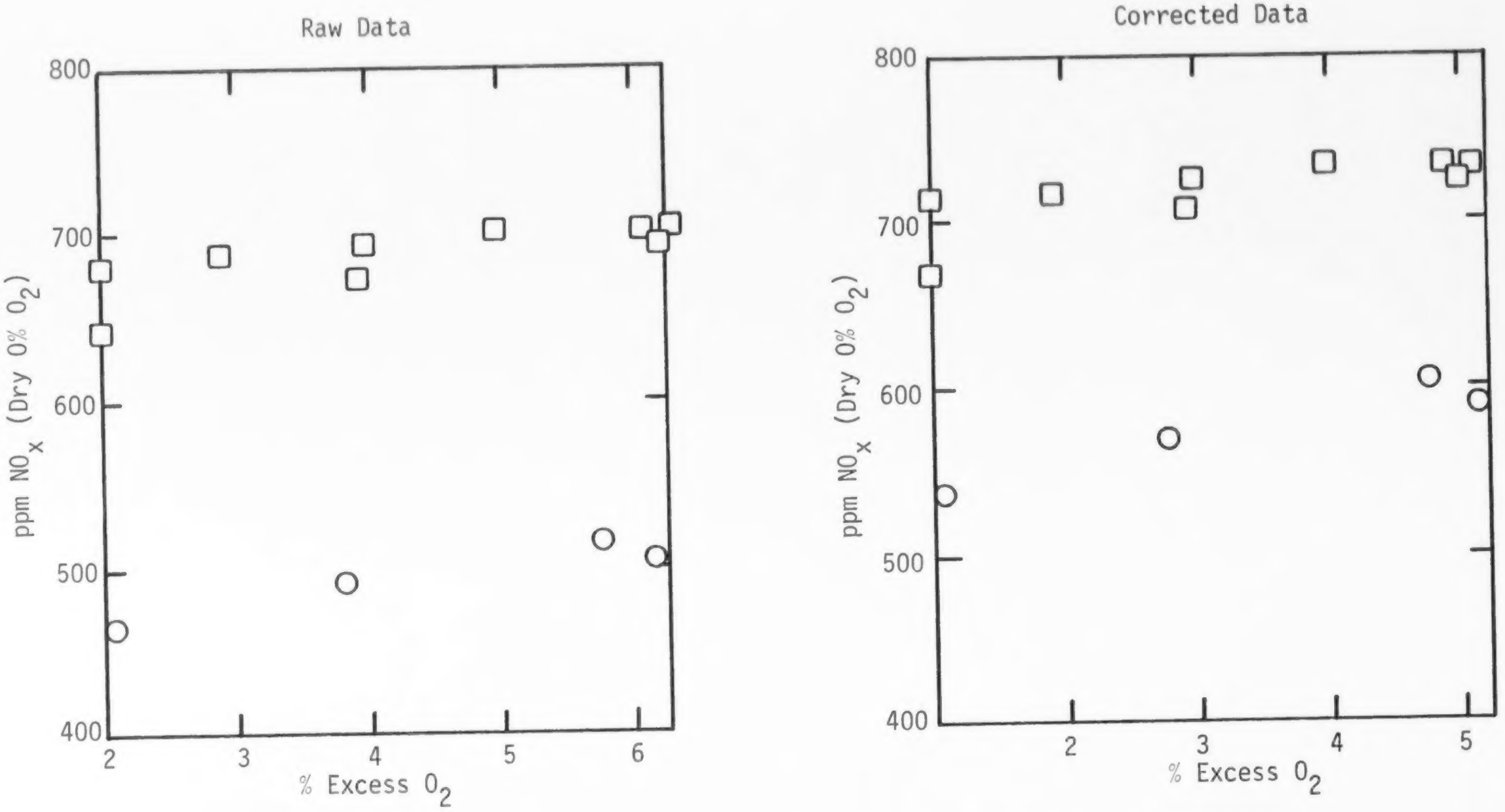

Figure 19. Example: Correcting Data for Background Gas Composition.

7.0 RECOMMENDATIONS

In many laboratory and field emissions tests the variability in operating conditions and other factors introduce errors of the same order of magnitude or larger than the errors produced by background gas composition variations. Under these conditions it is recommended that the NO concentrations indicated by the CLAs be used directly without corrections recognizing that the results will tend to be low by a few percent.

If the experimental errors in the emissions tests are small compared to the errors produced by background gas composition variations, the indicated NO concentrations should be corrected as discussed in the previous section. However the results of this investigation can only be applied to CLAs designed and operated similar to those tested. In low pressure flat flame experiments where the CLA sample gas metering system (capillary) is replaced by a different type of metering system, the effects of background gas composition variations on sample flowrate may be significantly different. Under these conditions the results of this investigation cannot be applied. It is recommended that either the effects of background composition variations on sample gas flowrate be evaluated and quenching data such as Reference 5 be applied, or the overall effects of background composition variations be emperically determined as in this investigation.

As an alternative to correcting the indicated NO concentrations, the CLA could be operated so as to minimize the effects of background gas composition variations. Three methods for accomplishing this are to:

- Calibrate the CLA with NO in a background gas similar to the anticipated combustion products
- Dilute the sample with a known amount of N_2
- Dry the sample to a low dewpoint

Calibrating the CLA with NO in a background gas with a composition identical to the combustion products to be sampled would eliminate these problems. However, the concentration of NO in the mixture must be accurately known. Some gas mixture suppliers determine the concentration of NO in their mixtures by using a CLA. This introduces errors similar to calibrating the laboratory CLA on NO in N_2.

If the sample gas is diluted with a large amount of N_2, variations in sample gas compositions will have less effect on the flowrate into the reaction chamber and quenching. For this technique to be effective the dilution factor must be large (such as 10/1) and precisely known independent of sample gas composition variations. This accurate dilution is difficult to achieve in pactice and has the further disadvantage of reducing the overall sensitivity of the CLA by the dilution factor.

The sample gas must be dried to a dewpoint less than the CLA operating temperature to avoid plugging the sample capillary with condensation. However at 293K dewpoint the sample gas contains 2.3% H_2O vapor and as a result the CLA will indicate less than the actual NO concentration due to background and dilution effects. Lowering the dewpoint to 273K reduces the H_2O vapor concentration to 0.60% and reduces the error in indicated NO concentration.

In experiments involving combustion products of fuels in air, a low pressure reaction chamber CLA such as the TECO is preferred. However in experiments involving combustion in O_2/Ar or O_2/CO_2/Ar oxidants, high and low reaction chamber pressure CLAs perform equally well.

Small variations in CLA operating conditions such as adjustment of the sample gas or ozone flowrates and changes in the reaction chamber pressure do not have any clear advantages in reducing the effects of background gas composition variations. However if the reaction chamber pressure is maintained low, the sample gas flowrate is maintained constant and the ratio of O_2 to sample gas flowrates in high, the effects of background gas composition variations could be significantly reduced.

8.0 APPENDIX

This section shows the raw data for 150 data points taken over the course of the experimental study. The order in which these data are presented follows the same sequence as the test matrix (Table 3). The actual NO concentrations were determined from the NO concentrations in the compressed cylinders as diluted by the gas metering system (see Section 4.3). The indicated NO concentrations were those concentrations measured by the CLAs. Since the actual concentrations of NO in span and test gases were identical, the ratios of indicated to actual NO concentrations were direct measurements of background gas composition effects. The stoichiometry, ϕ, refers to the ratio of the actual fuel/air ratio and the stoichiometric fuel/air ratio.

EXPERIMENT NO. 1: Binary Background Gases

TEST NUMBER	THIRD BODY	CONCENTRATION OF THIRD BODY IN N_2 %	ACTUAL NO CONCENTRATION ppm	INDICATED TECO READING ppm NO	TECO $\left(\frac{NO_{Ind}}{NO_{Act}}\right)$	INDICATED BECKMAN READING ppm NO	BECKMAN $\left(\frac{NO_{Ind}}{NO_{Act}}\right)$
1 - 1	CO	10	200.0	202.8	1.014	203.0	1.015
1 - 2	CO	20	200.0	200.0	1.000	201.4	1.007
1 - 3	CO	30	200.0	200.0	1.000	203.2	1.016
1 - 4	CO	40	200.0	199.2	0.996	200.4	1.002
1 - 5	CO	50	200.0	199.8	0.999	200.9	1.005
1 - 6	H_2	10	200.0	200.0	1.000	200.0	1.000
1 - 7	H_2	20	200.0	200.0	1.000	197.5	0.988
1 - 8	H_2	30	200.0	207.5	1.038	207.3	1.037
1 - 9	H_2	40	200.0	214.0	1.070	213.0	1.065
1 - 10	H_2	50	200.0	213.0	1.065	213.0	1.065
1 - 11	CH_4	10	200.0	200.0	1.000	193.0	0.965
1 - 12	CH_4	20	200.0	200.0	1.000	184.0	0.920
1 - 13	CH_4	30	200.0	203.0	1.015	182.6	0.913
1 - 14	CH_4	40	200.0	200.0	1.000	176.5	0.883
1 - 15	CH_4	50	200.0	201.5	1.008	173.4	0.867

EXPERIMENT NO. 1: Binary Background Gases

TEST NUMBER	THIRD BODY	CONCENTRATION OF THIRD BODY IN N_2 %	ACTUAL NO CONCENTRATION ppm	INDICATED TECO READING ppm NO	TECO $\left(\frac{NO_{Ind}}{NO_{Act}}\right)$	INDICATED BECKMAN READING ppm NO	BECKMAN $\left(\frac{NO_{Ind}}{NO_{Act}}\right)$
1 - 16	O_2	10	200.0	193.0	0.965	193.0	0.965
1 - 17	O_2	20	200.0	184.0	0.920	186.0	0.930
1 - 18	O_2	30	200.0	183.5	0.918	187.5	0.938
1 - 19	O_2	40	200.0	174.0	0.870	180.0	0.900
1 - 20	O_2	50	200.0	173.0	0.865	178.9	0.895
1 - 21	CO_2	10	200.0	197.0	0.985	187.5	0.938
1 - 22	CO_2	20	200.0	192.0	0.960	179.0	0.895
1 - 23	CO_2	30	200.0	189.0	0.945	171.5	0.858
1 - 24	CO_2	40	200.0	186.0	0.930	165.0	0.825
1 - 25	CO_2	50	200.0	184.0	0.920	158.0	0.790
1 - 26	A	10	200.0	197.5	0.988	197.5	0.988
1 - 27	A	20	200.0	192.5	0.963	195.1	0.976
1 - 28	A	25	200.0	191.0	0.955		
1 - 29	A	30	200.0	189.0	0.945	195.0	0.975
1 - 30	A	40	200.0	186.0	0.930	194.0	0.970
1 - 31	A	50	200.0	183.5	0.918	193.5	0.968
1 - 32	A	75	200.0	175.4	0.877	190.4	0.952
1 - 33	A	100	200.0	169.0	0.845	187.0	0.935

EXPERIMENT NO. 2: Lean Complete Combustion Products, Dry

OXIDANT: 21% O_2, Balance N_2

TEST NUMBER	FUEL	STOICHIOMETRY ϕ	ACTUAL NO CONCENTRATION ppm	INDICATED TECO READING ppm NO	TECO $\left(\frac{NO_{Ind}}{NO_{Act}}\right)$	INDICATED BECKMAN READING ppm NO	BECKMAN $\left(\frac{NO_{Ind}}{NO_{Act}}\right)$
2 - 1	CH_0	1.0	200.0	194.4	0.972	178.4	0.892
2 - 2	CH_0	2.0	200.0	191.2	0.956	183.6	0.918
2 - 3	CH_0	3.0	200.0	192.4	0.962	187.6	0.938
2 - 4	CH_0	4.0	200.0	192.2	0.961	189.4	0.947
2 - 5	CH_0	5.0	200.0	190.4	0.952	189.6	0.948
2 - 6	CH_0	10.0	200.0	191.0	0.955	190.0	0.950
2 - 7	CH_4	1.0	200.0	198.6	0.993	186.6	0.933
2 - 8	CH_4	2.0	200.0	197.6	0.988	191.0	0.955
2 - 9	CH_4	3.0	200.0	195.0	0.975	192.0	0.960
2 - 10	CH_4	4.0	200.0	194.0	0.970	194.0	0.970
2 - 11	CH_4	5.0	200.0	193.0	0.965	193.4	0.967
2 - 12	CH_4	10.0	200.0	193.0	0.965	192.0	0.960

EXPERIMENT NO. 2: Lean Complete Combustion Products, Dry

OXIDANT: 21% O_2, Balance N_2

TEST NUMBER	FUEL	STOICHIOMETRY ϕ	ACTUAL NO CONCENTRATION ppm	INDICATED TECO READING ppm NO	TECO $\left(\frac{NO_{Ind}}{NO_{Act}}\right)$	INDICATED BECKMAN READING ppm NO	BECKMAN $\left(\frac{NO_{Ind}}{NO_{Act}}\right)$
2 - 13	CH_0	1.0	100.0	96.8	0.968	90.8	0.908
2 - 14	CH_0	1.25	100.0	95.5	0.955	90.7	0.907
2 - 15	CH_0	1.50	100.0	96.2	0.962	92.2	0.922
2 - 16	CH_0	1.75	100.0	95.5	0.955	92.8	0.928
2 - 17	CH_0	2.0	100.0	97.0	0.970	93.2	0.932
2 - 18	CH_0	2.5	100.0	96.8	0.968	93.8	0.938
2 - 19	CH_0	3.0	100.0	95.0	0.950	93.5	0.935
2 - 20	CH_0	4.0	100.0	95.8	0.958	93.8	0.938
2 - 21	CH_0	5.0	100.0	96.2	0.962	94.7	0.947
2 - 22	CH_0	10.0	100.0	97.5	0.975	97.2	0.972
2 - 23	CH_0	∞	100.0	96.5	0.965	96.8	0.968

EXPERIMENT NO. 3: Lean Complete Combustion Products, Wet

21% O_2, Balance N_2

TEST NUMBER	FUEL	STOICHIOMETRY ϕ	ACTUAL NO CONCENTRATION ppm	INDICATED TECO READING ppm NO	TECO $\left(\frac{NO_{Ind}}{NO_{Act}}\right)$	INDICATED BECKMAN READING ppm NO	BECKMAN $\left(\frac{NO_{Ind}}{NO_{Act}}\right)$	DEWPOINT °K
3 - 1	CH_0	1.0	196.8	190.0	0.965	176.7	0.898	287
3 - 2	CH_0	2.5	196.6	190.0	0.966	180.2	0.917	288
3 - 3	CH_0	1.0	197.0	190.3	0.966	171.5	0.871	287
3 - 4	CH_0	5.0	196.6	190.0	0.966	180.2	0.917	289
3 - 5	CH_0	2.5	198.2	192.1	0.969	183.6	0.926	279
3 - 6	CH_0	5.0	198.4	192.5	0.970	190.2	0.959	278
3 - 7	CH_0	1.0	198.4	193.5	0.975	178.6	0.900	276
3 - 8	CH_0	1.0	196.8	191.5	0.973	176.5	0.897	287
3 - 9	CH_0	1.0	196.2	190.0	0.968	170.7	0.870	290
3 - 10	CH_0	2.5	195.2	187.9	0.963	176.6	0.905	293
3 - 11	CH_0	5.0	195.0	188.4	0.966	176.0	0.903	295
3 - 12	CH_0	5.0				183.0	0.931	289
3 - 13	CH_0	1.0	199.3	193.5	0.971	179.6	0.901	Dry
3 - 14	CH_0	2.5	199.3	195.5	0.981	188.6	0.946	Dry
3 - 15	CH_0	5.0	199.3	195.0	0.978	192.2	0.964	Dry
3 - 16	CH_0	1.0	199.3	195.0	0.978	181.0	0.908	Dry

EXPERIMENT NO. 4: Lean Incomplete Combustion Products, Dry

OXIDANT: 21% O_2, Balance N_2

TEST NUMBER	FUEL	STOICHIOMETRY ϕ	ACTUAL NO CONCENTRATION ppm	INDICATED TECO READING ppm NO	TECO $\left(\frac{NO_{Ind}}{NO_{Act}}\right)$	INDICATED BECKMAN READING ppm NO	BECKMAN $\left(\frac{NO_{Ind}}{NO_{Act}}\right)$
4 - 1	CH_O	1.25	200.0	193.2	0.966	183.4	0.917
4 - 2	CH_O	1.50	200.0	192.2	0.961	185.4	0.927
4 - 3	CH_O	1.75	200.0	190.4	0.952	186.2	0.931
4 - 4	CH_O	2.00	200.0	190.8	0.956	188.2	0.941
4 - 5	CH_O	2.50	200.0	191.8	0.959	190.4	0.952
4 - 6	CH_O	3.00	200.0	192.0	0.960	190.8	0.956

EXPERIMENT NO. 5: Rich Combustion Products, Dry

OXIDANT: 21% O_2, Balance N_2

TEST NUMBER	FUEL	STOICHIOMETRY ϕ	ACTUAL NO CON-CENTRATION ppm	INDICATED TECO READING ppm NO	TECO $\left(\frac{NO_{Ind}}{NO_{Act}}\right)$	INDICATED BECKMAN READING ppm NO	BECKMAN $\left(\frac{NO_{Ind}}{NO_{Act}}\right)$
5 - 1	CH_3	0.9	200.0	192.8	0.964	182.6	0.913
5 - 2	CH_3	0.8	200.0	194.7	0.974	186.4	0.932
5 - 3	CH_3	0.7	200.0	195.4	0.977	189.8	0.949
5 - 4	CH_3	0.6	200.0	195.7	0.979	193.7	0.969
5 - 5	CH_4	0.8	200.0	195.5	0.978	191.5	0.958
5 - 6	CH_4	0.7	200.0	197.9	0.990	194.9	0.975
5 - 7	CH_4	0.6	200.0	199.0	0.995	198.0	0.990
5 - 8	CH_4	0.5	200.0	202.3	1.012	203.3	1.017

EXPERIMENT NO. 6 : Lean Complete Combustion Products, Dry

OXIDANT: 21% O_2, Balance A

TEST NUMBER	FUEL	STOICHIOMETRY ϕ	ACTUAL NO CON-CENTRATION ppm	INDICATED TECO READING ppm NO	TECO $\left(\frac{NO_{Ind}}{NO_{Act}}\right)$	INDICATED BECKMAN READING ppm NO	BECKMAN $\left(\frac{NO_{Ind}}{NO_{Act}}\right)$
6 - 1	CH_O	1.0	194.9	167.0	0.857	167.2	0.858
6 - 2	CH_O	2.0	194.9	167.5	0.859	174.0	0.893
6 - 3	CH_O	3.0	194.9	164.7	0.845	175.8	0.902
6 - 4	CH_O	4.0	194.9	168.5	0.865	179.2	0.919
6 - 5	CH_O	5.0	194.9	167.5	0.859	181.0	0.929
6 - 6	CH_O	∞	194.9	162.8	0.835	183.7	0.943
6 - 7	CH_4	1.0	194.9	168.4	0.864	176.1	0.904
6 - 8	CH_4	2.0	194.9	164.8	0.846	178.6	0.916
6 - 9	CH_4	3.0	194.9	165.0	0.847	181.7	0.932
6 - 10	CH_4	4.0	194.9	167.4	0.859	178.3	0.915
6 - 11	CH_4	∞	194.9	163.5	0.839	180.4	0.926

EXPERIMENT NO. 6: Lean Complete Combustion Products, Dry

OXIDANT: 21% O_2, 21% CO_2, Balance A

TEST NUMBER	FUEL	STOICHIOMETRY ϕ	ACTUAL NO CONCENTRATION ppm	INDICATED TECO READING ppm NO	TECO $\left(\frac{NO_{Ind}}{NO_{Act}}\right)$	INDICATED BECKMAN READING ppm NO	BECKMAN $\left(\frac{NO_{Ind}}{NO_{Act}}\right)$
6 - 12	CH_O	1.0	194.9	170.3	0.874	155.0	0.795
6 - 13	CH_O	2.0	194.9	168.7	0.866	159.4	0.818
6 - 14	CH_O	3.0	194.9	169.6	0.870	161.6	0.829
6 - 15	CH_O	4.0	194.9	168.8	0.866	162.0	0.831
6 - 16	CH_O	5.0	194.9	167.5	0.859	162.6	0.834
6 - 17	CH_O	10.0	194.9	167.0	0.857	163.8	0.840
6 - 18	CH_4	1.0	194.9	168.0	0.862	158.4	0.813
6 - 19	CH_4	2.0	194.9	168.8	0.866	161.8	0.830
6 - 20	CH_4	3.0	194.9	168.5	0.865	163.0	0.836
6 - 21	CH_4	4.0	194.9	167.0	0.857	163.5	0.839
6 - 22	CH_4	5.0	194.9	166.5	0.854	163.0	0.836
6 - 23	CH_4	10.0	194.9	166.5	0.854	165.3	0.848
6 - 24	CH_4	∞	194.9	166.5	0.854	164.5	0.844

EXPERIMENT NO. 7: Rich Combustion Products, Dry

OXIDANT: 21% O_2, Balance A

TEST NUMBER	FUEL	STOICHIOMETRY ϕ	ACTUAL NO CONCENTRATION ppm	INDICATED TECO READING ppm NO	TECO $\left(\frac{NO_{Ind}}{NO_{Act}}\right)$	INDICATED BECKMAN READING ppm NO	BECKMAN $\left(\frac{NO_{Ind}}{NO_{Act}}\right)$
7 - 1	CH_0	0.9	194.9	170.5	0.875	172.6	0.886
7 - 2	CH_0	0.8	194.9	172.7	0.886	176.0	0.903
7 - 3	CH_0	0.7	194.9	173.6	0.891	180.2	0.925
7 - 4	CH_0	0.6	194.9	174.3	0.894	183.7	0.943

EXPERIMENT NO. 7: Rich Combustion Products, Dry

OXIDANT: 21% O_2, 21% CO_2, Balance A

TEST NUMBER	FUEL	STOICHIOMETRY ϕ	ACTUAL NO CONCENTRATION ppm	INDICATED TECO READING ppm NO	TECO $\left(\frac{NO_{Ind}}{NO_{Act}}\right)$	INDICATED BECKMAN READING ppm NO	BECKMAN $\left(\frac{NO_{Ind}}{NO_{Act}}\right)$
7 - 5	CH_0	0.9	194.9	170.7	0.876	157.1	0.806
7 - 6	CH_0	0.8	194.9	172.2	0.884	161.4	0.828
7 - 7	CH_0	0.7	194.9	171.9	0.882	162.0	0.831
7 - 8	CH_0	0.6	194.9	171.1	0.878	166.1	0.852

EXPERIMENT NO. 8: Off Design Point Instrument Response

OXIDANT: 21% O_2, Balance N_2

FUEL: CH_0

STOICHIOMETRY: Constant at 125% T.A.

TEST NUMBER	SAMPLE VACUUM (in. HG)	O_2 PRESSURE (PSIG)	CHAMBER PRESSURE (TORR)	ACTUAL NO CONCENTRATION ppm	INDICATED TECO READING ppm NO	TECO $\left(\frac{NO_{Ind}}{NO_{Act}}\right)$
8 - 1	5.0	2.0	9.2	200.0	194.0	0.970
8 - 2	6.0	2.0	9.2	200.0	191.0	0.955
8 - 3	1.0	2.0	9.7	200.0	189.0	0.945
8 - 4	5.0	6.0	14.0	200.0	188.9	0.945
8 - 5	5.0	0.5	8.5	200.0	186.5	0.933
8 - 6	6.0	6.0	14.0	200.0	187.0	0.935
8 - 7	1.0	0.5	8.5	200.0	190.0	0.950
8 - 8	1.0	6.0	14.0	200.0	186.0	0.930
8 - 9	6.0	0.5	8.5	200.0	189.0	0.945

EXPERIMENT NO. 8: Off Design Point Instrument Response
OXIDANT: 21% O_2, Balance N_2
FUEL: CH_0
STOICHIOMETRY: Constant at 125% T.A.

TEST NUMBER	SAMPLE PRESSURE (PSIG)	O_2 PRESSURE (PSIG)	ACTUAL NO CONCENTRATION ppm	INDICATED BECKMAN READING ppm NO	BECKMAN $\left(\frac{NO_{Ind}}{NO_{Act}}\right)$
8 - 10	4.0	20.0	200.0	180.6	0.903
8 - 11	4.25	20.0	200.0	179.0	0.895
8 - 12	2.0	20.0	200.0	179.0	0.895
8 - 13	4.0	30.0	200.0	180.5	0.903
8 - 14	4.0	5.0	200.0	174.0	0.870
8 - 15	4.25	30.0	200.0	177.0	0.885
8 - 16	2.0	5.0	200.0	181.2	0.906
8 - 17	2.0	30.0	200.0	179.5	0.898
8 - 18	4.0	5.0	200.0	173.0	0.865

EXPERIMENT NO. 8: Off Design Point Instrument Response

OXIDANT: 21% O_2, Balance A

FUEL: CH_0

STOICHIOMETRY: Constant at 125% T.A.

TEST NUMBER	SAMPLE VACUUM (in. HG)	O_2 PRESSURE (PSIG)	CHAMBER PRESSURE (TORR)	ACTUAL NO CONCENTRATION ppm	INDICATED TECO READING ppm NO	TECO $\left(\frac{NO_{Ind}}{NO_{Act}}\right)$
8 - 19	5.0	2.0	8.5	194.9	167.2	0.858
8 - 20	6.0	2.0	8.5	194.9	166.7	0.855
8 - 21	1.0	2.0	8.5	194.9	169.2	0.868
8 - 22	5.0	6.0	13.0	194.9	167.2	0.858
8 - 23	5.0	0.5	7.5	194.9	170.8	0.876
8 - 24	5.5	6.0	11.0	194.9	162.9	0.836
8 - 25	1.0	0.5	7.5	194.9	172.6	0.886

EXPERIMENT NO. 8: Off Design Point Instrument Response

OXIDANT: 21% O_2, Balance A

FUEL: CH_0

STOICHIOMETRY: Constant at 125% T.A.

TEST NUMBER	SAMPLE PRESSURE (PSIG)	O_2 PRESSURE (PSIG)	ACTUAL NO CONCENTRATION ppm	INDICATED BECKMAN READING ppm NO	BECKMAN $\left(\frac{NO_{Ind}}{NO_{Act}}\right)$
8 - 26	4.0	20.0	194.9	169.8	0.871
8 - 27	4.0	20.0	194.9	172.0	0.883
8 - 28	2.0	20.0	194.9	169.1	0.868
8 - 29	4.0	30.0	194.9	169.4	0.869
8 - 30	4.0	6.0	194.9	177.4	0.910
8 - 31	4.25	30.0	194.9	168.8	0.866
8 - 32	2.0	5.0	194.9	179.7	0.922

9.0 REFERENCES

1. Clough, P.N., and Thrush, B.A., "Mechanism of Chemiluminescent Reaction Between Nitric Oxide and Ozone", Transactions of the Faraday Society, Vol. 63, No. 494, Part 4, Apr. 1967, pg. 915.

2. Fontijn, A., Sabadell, A.J., Ronco, J., "Homogeneous Chemiluminescent Measurement of Nitric Oxide with Ozone", Analytical Chemistry, Vol. 42, (1970), pg. 575.

3. Niki, H., Warnick, A. and Lord, R., "An Ozone - NO Chemiluminescence Method for NO Analysis in Piston and Turbine Engines", Proceedings of Automotive Engineering Congress, Detroit, Mich., (1971) pg. 246.

4. Maahs, H.G., "Interference of Oxygen, Carbon Dioxide and Water Vapor on the Analysis for Oxides of Nitrogen by Chemiluminescence", NASA Technical Memorandum NASA TM X-3229, Aug. 1975.

5. Mathews. R.D., Sawyer, R.F. and Schefer, R.W., "Interferences in Chemiluminescent Measurement of NO and NO_2 Emissions from Combustion Systems", Environmental Science and Technology, Vol. 11, No. 12, Nov. 1977, Pg. 1092.

6. Warren, G.S. and Babcock, F., Review of Scientific Instruments, Vol. 41, 1970, pg. 280.

7. Newitt, W.M., The Design of High Pressure Plant and Properties of Fluids at High Pressure, (1940), Pg. 20, Clarendon Press, Oxford, England.

8. Braker, W. and Mossman, A.L., Matheson Gas Data Book, Fifth Edition, Matheson Gas Products, East Rutherfore, New Jersey, 1971, Pg. 101.

9. Perry, John H., Chemical Engineers Handbook, McGraw-Hill, Fifth Edition, 1973.

10. Personal Communication with R.F. Sawyer, (June, 1978) and with R.D. Mathews, (October 1978), Authors of Reference 5.

II. MEASUREMENT OF NITROGENEOUS INTERMEDIATES TO OPTIMIZE A STAGED-COMBUSTION SYSTEM

by:

R. M. Winter
D. W. Pershing

Department of Chemical Engineering
University of Utah
Salt Lake City, Utah 84112

Prepared for:

Energy and Environmental Research Corporation

ABSTRACT

The overall objective of this work was to investigate the role of the thermal environment in the furnace on the optimization of staged combustion for NO_x emissions control. A supporting objective was to evaluate current NH_3 and HCN analytical technology and thereby experimentally define the technique appropriate for the measurement of TFN species in a rich flame.

The approach was experimental utilizing a 20.5 kW (70 x 10^3 Btu/hr) refractory-walled laboratory combustor. Specific-ion electrodes and gas chromatography were utilized for analytical measurement of NH_3 and HCN.

The NH_3-specific ion electrode was found suitable for reliable (±3 percent) and fast (10 minutes) NH_3 measurement. The HCN-specific ion electrode was suitable for HCN measurement when extreme accuracy was not required. Gas chromatography gave fast (5 minutes) and reliable (±1.0 percent) HCN measurements.

The combustion results indicated that the conversion of HCN to NO in the second stage of a staged combustor is low. Formation of thermal NO in the second stage was insignificant in the experimental system studied. Limited (12 percent) first-stage cooling significantly retarded the rate of NO decay in the first stage of CH_4/NH_3/air flames and increased NO in the exhaust. Additional cooling of the CH_4/NH_3/air flame had little effect on the first-stage NO, but

produced lower exhaust emissions than were measured with limited cooling.

CONTENTS

Page (II-)

ABSTRACT ii

LIST OF FIGURES vi

ACKNOWLEDGEMENTS ix

1. BACKGROUND 1

  1.1 Introduction 1
  1.2 Thermal NO Formation 1
  1.3 Fuel NO Formation 3
  1.4 Staged Combustion Mechanism 4

    1.4.1 Residence Time 7
    1.4.2 First-Stage Stoichiometry 7
    1.4.3 Degree of Mixing First Stage 9
    1.4.4 Thermal Environment 9

2. PURPOSE AND SCOPE 17

3. AMMONIA MEASUREMENT 19

  3.1 Background 19
  3.2 Theory 21
  3.3 Ammonia Probe Calibration 25
  3.4 Collection System Design 33
  3.5 Probe System Verification 50
  3.6 Species Interference Study 51

4. CYANIDE MEASUREMENT 57

  4.1 Background 57
  4.2 Theory 59
  4.3 Electrode Calibration 60
  4.4 Collection System 68
  4.5 Interference 70
  4.6 Conclusion 72

Chapter Page (II-)

5. ANALYTICAL SYSTEMS - FURNACE STUDIES 74

    5.1 Choke Temperature Measurement. 74
    5.2 NH_3 - HCN Waterspray Probe 76
    5.3 Gas Sampling System. 78

6. FURNACE SYSTEMS. 82

    6.1 Combustion Chamber 82
    6.2 Natural Gas/Air Flow System. 91
    6.3 Flame Safety System. 93

7. NATURAL GAS/AIR STAGED COMBUSTION. 94

    7.1 Introduction and Objectives. 94
    7.2 First-Stage NO 95
    7.3 First-Stage HCN. 95
    7.4 First-Stage NH_3. 95
    7.5 Exhaust NO 99
    7.6 Conclusions for Ch_4/Air Staged Combustion. 99

8. NATURAL GAS/AMMONIA/AIR STAGED COMBUSTION. 101

    8.1 Introduction and Objectives. 101
    8.2 First-Stage NO with NH_3 Addition 101
    8.3 First-Stage HCN with NH_3 Addition. 103
    8.4 First-Stage NH_3 with NH_3 Addition. 103
    8.5 Exhaust NO with NH_3 Addition. 103
    8.6 Exhaust NO with First- and Second-Stage NH_3 Doping . . . 108
    8.7 Conclusions for CH_4/NH_3/Air Staged Combustion. 108

9. CONCLUSION 112

NOMENCLATURE 114

APPENDIX: INTERNAL MEASUREMENT DATA 116

LIST OF REFERENCES 121

LIST OF FIGURES

Page (II-)

1.1 Conceptual schematic of staged combustion 6

1.2 Time history of nitrogen species 8

1.3 Nitrogen specie concentration versus first-stage stoichiometric ratio 10

1.4 Nitrogen species concentration v rsus first-stage stoichiometric ratio 11

1.5 Nitrogen species concentrations versus first-stage stoichiometric ratio 12

1.6 Effect of mixing on fixed-nitrogen species 13

1.7 Stack NO as a function of second-stage initial flame temperature 14

1.8 Influence of heat extraction profile 16

3.1 Schematic of ammonia-specific ion probe 22

3.2 Influence of pH on ammonia dissociation 26

3.3 Solution ammonia measurement apparatus 27

3.4 Influence of solution temperature on ammonia probe 28

3.5 Influence of pH on ammonia probe 30

3.6 25 °C-calibration curve of ammonia probe 32

3.7 Impinger designs 34

3.8 Gas-mixing system flow diagram 36

3.9 Experimental results on ammonia measurements 38

3.10 The effect of liquid height on the collection efficiency of the straight tube impinger 39

3.11 The effect of liquid height on the collection efficiency of the straight tube impinger with beads . . 40

Page (II-)

3.12 The effect of liquid height on the collection efficiency of the fritten cylinder impinger 41

3.13 Effect of final liquid concentration on collection efficiency 43

3.14 Effect of final liquid concentration on collection efficiency of the straight tube impinger with beads . . 45

3.15 Effect of final liquid concentration on collection efficiency, constant flow rate, varying impinger design 46

3.16 Liquid height versus collection efficiency for the second impinger 47

3.17 Percent deviation of contacting solutions 49

3.18 Probe verification schematic 52

3.19 Gaseous specie interference 54

3.20 Solids interference 56

4.1 Solution cyanide measurement apparatus 62

4.2 Influence of solution temperature on the cyanide electrode 63

4.3 Effect of solution pH on the percentage of cyanide 64

4.4 Influence of pH on the response of the cyanide electrode 66

4.5 Effect of ionic strength on the response of the cyanide electrode 67

4.6 Standard calibration curve for the cyanide electrode . . 69

4.7 $S^=$ interference removal 73

Page (II-)

5.1 Suction pyrometer schematic. 75

5.2 Flue and waterspray probe schematics 77

5.3 Intermediate species sampling flowsheet. 79

5.4 Gas-sampling system flow diagram 80

6.1 Gas/oil furnace schematic. 83

6.2 Diffusion burner, cross-sectional view 84

6.3 First-stage view port. 86

6.4 Combustion-gas cooling coils schematic 87

6.5 Choking section schematic. 89

6.6 Radial and axial second-stage air injection rings. 90

6.7 Natural gas/air-flow system schematic. 92

7.1 First-stage NO with CH_4/air. 96

7.2 First-stage HCN with CH_4/air 97

7.3 First-stage NH_3 with CH_4/air 98

7.4 Exhaust NO with CH_4/air. 100

8.1 First-stage NO with CH_4/NH_3/air. 102

8.2 First-stage HCN with CH_4/NH_3/air 104

8.3 First-stage NH_3 with CH_4/NH_3/air 105

8.4 Exhaust NO with CH_4/NH_3/air. 106

8.5 Temperature effect at the exhaust minimum ($SR_1 = 0.85$) 109

8.6 Exhaust NO with first- and second-stage doping 110

ACKNOWLEDGEMENTS

The authors gratefully acknowledge the assistance of T. D. Thacker, and J. Slama in obtaining the experimental data.

CHAPTER 1

BACKGROUND

1.1 Introduction

In the 1960s, man began to face the environmental dangers associated to his ever-increasing industrialization of the world, particularly the destruction of his habitat by pollution. Legislation during the 1970s prompted many technological advances in the abatement of pollutants. Technology has been applied to many sources of pollution, including direct fossil-fuel combustion. In addition to releasing energy, combustion results in significant amounts of atmospheric pollutants, including particulates, sulfur oxides (SO_x), and nitrogen oxides (NO_x). This work focuses on the abatement of nitrogen oxides by optimizing the thermal environment in a two-stage combustor, with special emphasis on the conversion of volatile fuel nitrogen to NO.

1.2 Thermal NO Formation

During the combustion of fuel, nitrogen oxides are formed by the high temperature, thermal fixation of molecular oxygen and nitrogen present in combustion air. Nitric oxide is the favored oxide form because the residence time in most stationary combustion processes is too short for the oxidation of NO to NO_2, even though NO_2 is thermodynamically favored at lower temperatures (Bartok, et al., 1964). NO, however, does oxidize in the atmosphere to NO_2, which is a primary participant in photochemical smog. NO resulting from the oxidation of atmospheric nitrogen, N_2, is defined as thermal NO.

For many years it was generally assumed that the thermal fixation of NO occurred according to the mechanism suggested by Zeldovich, et al. (1947):

$$O + N_2 = NO + N$$

$$N + O_2 = NO + O$$

$$N + OH = NO + H$$

taken together with the assumption that the combustion reactions have equilibrated prior to the onset of nitric oxide formation. The data of Fenimore (1971), Harris, et al. (1970), Bowman (1973), and Pershing and Berkau (1973) support this simplified picture for post combustion zone formation. Fenimore (1971) noted a substantial amount of "prompt" NO which formed very rapidly in the flame front of CH_4/air and C_2H_6/air flames and which could not be rationalized based on the extended Zeldovich mechanism with equilibrium radical concentrations. He postulated that this early NO formation was due to a -CN reaction involving hydrocarbon fragments.

At present thermal NO formation in gaseous flames is believed to occur primarily through the extended Zeldovich mechanism. This means that thermal NO is largely formed through a relatively slow, very temperature-dependent reaction, where the resultant thermal NO emissions are likely to depend on the time-temperature history throughout the entire length of the combustor. With light hydrocarbons the Zeldovich mechanism is also almost certainly coupled to the hydrocarbon chemistry indirectly via the nonequilibrium radical concentrations, and it is probably coupled directly via some type of Fenimore reaction (-CN) (Pershing, 1976).

1.3 Fuel NO Formation

For many years it was assumed that NO was formed only by high temperature fixation of atmospheric nitrogen and oxygen; recent experimental studies, however, have indicated that the conversion of bound nitrogen in the fuel to NO is potentially of equal or greater importance in the formation of NO_x during fuel combustion. In an EPA (NAPCA) evaluation of fuel additives in a small experimental furnace, Martin, et al. (1971), noted that certain nitrogen-containing additives, notably various amines and nitrates, increased NO_x emissions through approximately 50 percent conversion of the nitrogen in the additive to NO.

To date, a number of good experimental studies have been conducted on the addition of typical nitrogenous compounds to flat, laboratory flames. These data indicate that fuel nitrogen is a large potential source of NO emissions and that the oxidation of many nitrogen-containing compounds to NO is rapid, occurring on a time scale comparable to that of the combustion reactions (Bowman, 1973).

Pershing, et al. (1975), defined the relative importance of fuel NO formation by burning a bituminous coal and a low sulfur residual oil in both air and argon/oxygen atmospheres. Their data indicated that more than half of the total NO measured under normal combustion conditions was the result of fuel nitrogen oxidation. Other pilot-scale studies have indicated that fuel NO formation (1) increases with increasing fuel nitrogen content (Martin and Berkau, 1972), (2) is relatively insensitive to bulk gas temperatures (Pershing and Wendt, 1977), (3) does not depend strongly on nitrogen speciation with liquid fuels (Turner, et al., 1972; England, et al., 1981), and (4) is heavily dependent upon the rate of initial fuel/air contacting (Heap, et al., 1973).

In summary, the importance of fuel NO formation is now well established; therefore, nitrogen oxide abatement technologies for heavy liquid fuels and coals have focused on fuel nitrogen oxidation chemistry.

1.4 Staged Combustion Mechanisms

Combustion modifications have proven capable of reducing NO_x emissions significantly, and the most promising modification is two-stage combustion. This modified combustion scheme entails operating the primary combustion zone fuel rich by supplying a substoichiometric amount of air to it. The balance of the air is injected into the second stage to complete burnout of the fuel. Lack of sufficient oxygen in the first stage limits fuel NO_x formation. Removal of heat between the stages reduces the peak temperatures achieved, and this minimizes thermal NO_x formation in the second stage (McCann, 1972).

A variety of large-scale field tests have shown the utility of this combustion modification technique. Barnhart and Diehl (1960) reported a 27 percent reduction in NO_x emissions in a natural gas and oil-fired staged combustor when 95 percent of theoretical air was supplied to the primary combustion zone. A 47 percent reduction in NO_x emissions was achieved when 90 percent of theoretical air was fed to the primary combustion zone. In both cases, overall excess air was 15 percent. Bagwell, et al. (1971), reported reductions of 50-70 percent in emissions from two-stage combustion of natural gas in utility boilers. Bartok, et al. (1971), cited reductions as high as 90 percent in NO_x emissions in large gas-fired plants. A 62 percent reduction in NO_x emissions was achieved by Bienstock, et al. (1966), in a small experimental combustor firing 0.907 Kg (2 lbs) of pulverized coal per hour. One hundred five percent of theoretical air was supplied to the first stage. McCann, et al. (1972), reported a 50 percent reduction in NO_x emissions in a 226.8 Kg (500 lbs)-coal-per-hour pulverized coal staged combustor. In this investigation the first-stage air introduced into the primary combustion zone was varied from 105 to 95 percent of the stoichiometric air; and, for each case, excess air was adjusted from 8 to 22 percent.

In summary, staged combustion of a variety of fossil fuels has been domenstrated to be a plausible combustor-modification technique for the reduction of NO_x emissions; however, the technique has not been optimized. The four major combustor-design parameters in a two-stage system are (1) residence time in the primary combustion zone, (2) first-stage stiochiometry, (3) the degree of mixing in the first stage, and (4) the thermal environment of the combustor.

Figure 1.1 is a conceptual schematic of a staged-combustion system and it illustrates the chemical processes which are thought to be influenced by the combustor design parameters. The high-nitrogen fuel (heavy oil or coal) devolatilizes rapidly in the near burner region and the fuel nitrogen appears primarily as NO, HCN, NH_3 and N_2, and Char N (coal only). The reactive gas-phase nitrogen species ($NO + HCN + NH_3$) are collectively termed TFN (total fixed nitrogen); these species tend to decay to N_2 via free-radical mechanisms involving NH_i species. Char-nitrogen oxidizes heterogeneously at a much

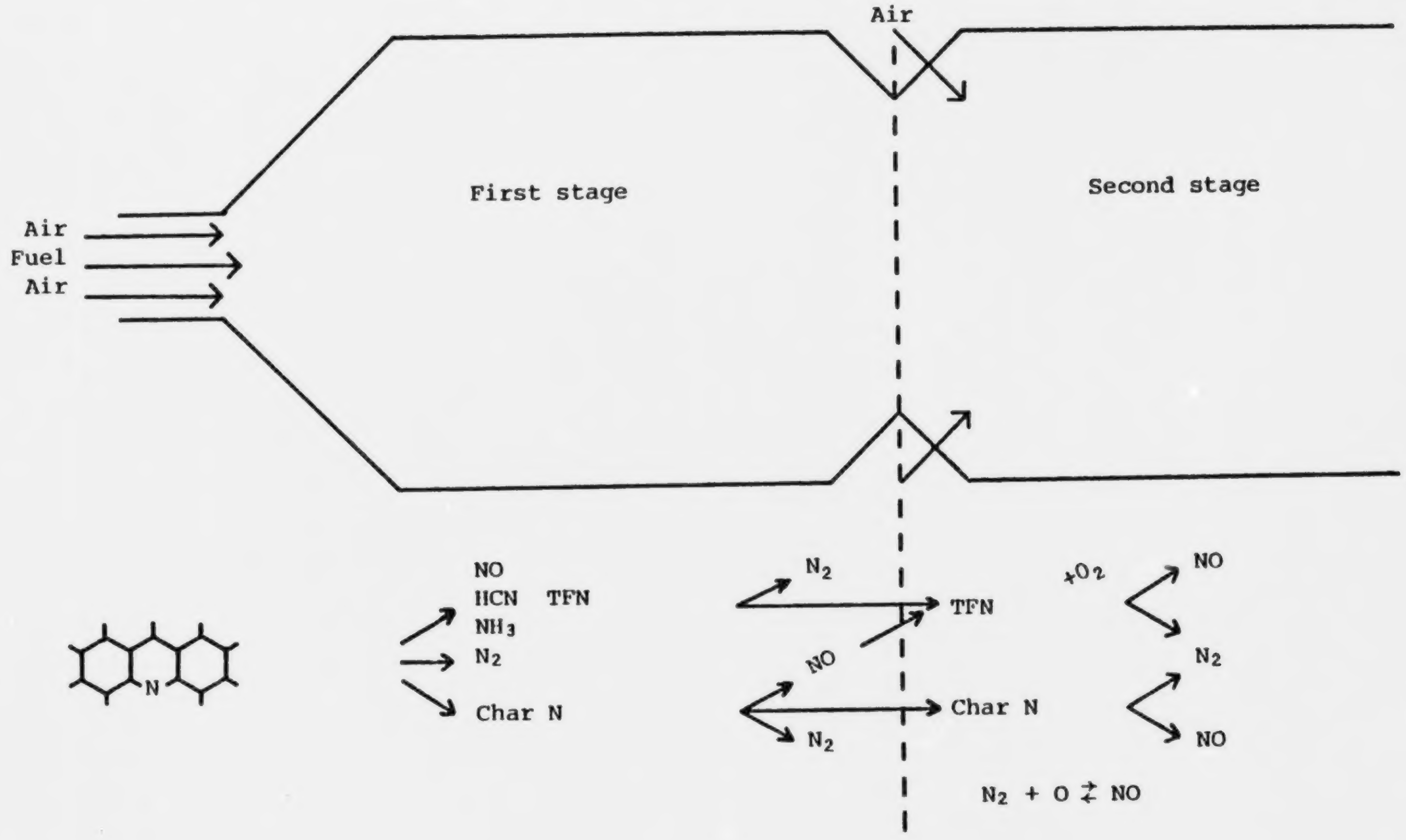
Air
Air
Fuel
Air
First stage
Second stage
NO
HCN TFN
NH3
N2
Char N
N2
TFN
NO
Char N
N2
+O2
NO
N2
NO
N2 + O ⇄ NO
N

Figure 1.1 Conceptual schematic of staged combustion.

slower effective rate and, under some conditions, it may even be carried into the fuel-lean second stage. The addition of the second-stage air promotes complete carbon burnout and enhances the conversion of TFN species and char-nitrogen (if any) to NO. Nitric oxide may also be formed in the second-stage flame by the thermal NO mechanism. The following sections discuss each of the major staged-combustion parameters in terms of their influence on the controlling chemistry.

1.4.1 Residence Time

Figure 1.2 is a typical time history of nitrogen species concentrations in the first stage of a premixed CH_4/NH_3/air flame (Song, et al., 1981). Foster and Keck (1980) observed similar species-concentration profiles in kerosene flames where the dopant was pyridine. The pyridine was added to the fuel to achieve a nitrogen concentration of 1 percent by mass. Initially the conversion of the dopant to HCN is very high; however, the conversion of the dopant to ammonia is very low. Also, an excess (with respect to the concentration of the dopant) of nitrogen-containing species may be observed due to the reaction of N_2 with hydrocarbon-free radicals. All species concentrations decay to relatively low asymptotic levels if the temperature and first-stage residence time are adequate. Hence, in a practical system, increasing the first-stage residence time results in decreased exhaust NO because of decreased TFN leaving the first stage.

1.4.2 First-Stage Stoichiometry

The stoichiometry in the first stage is an important parameter in the formation of HCN, NH_3, and NO in the first stage. First-stage

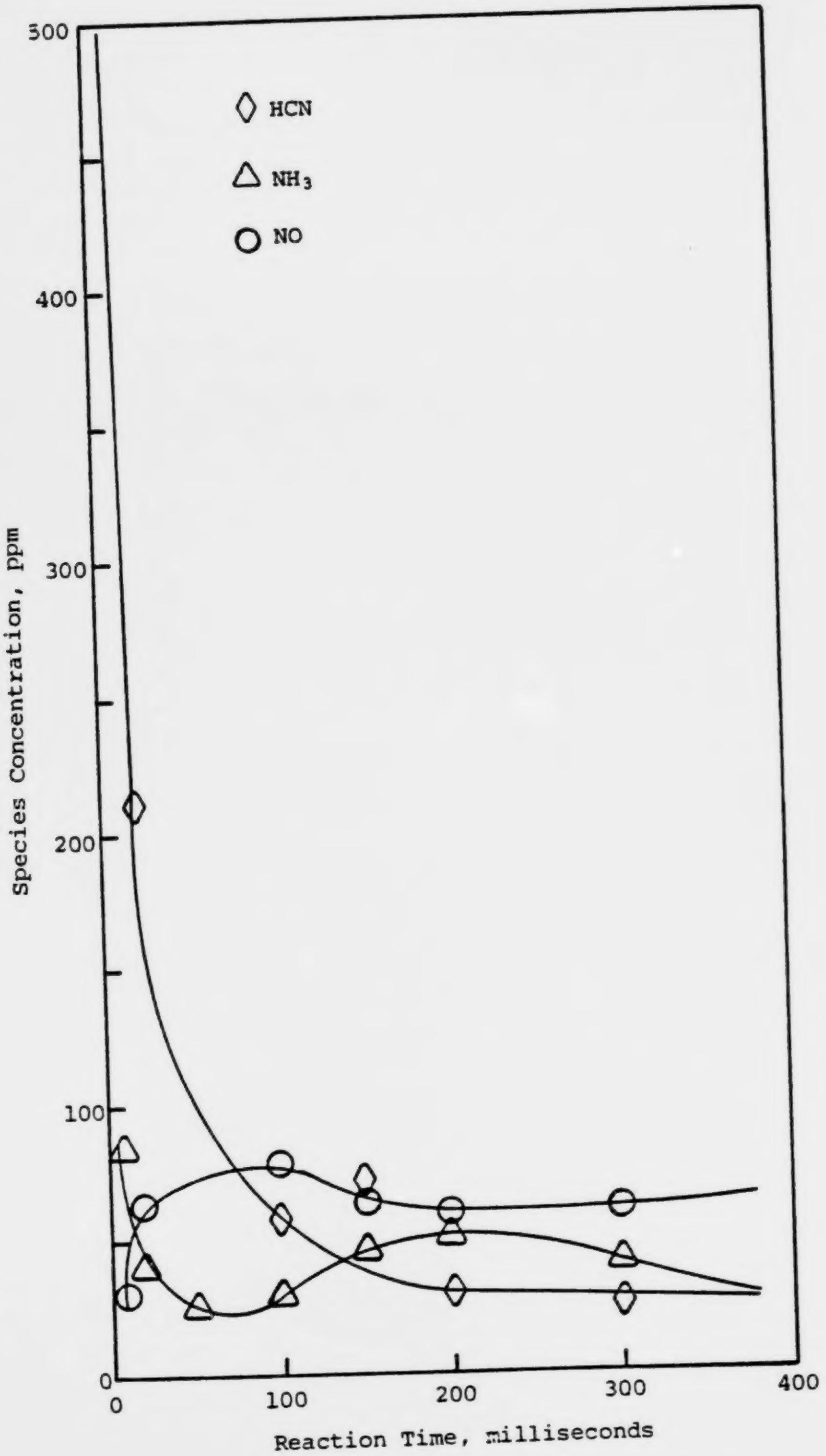

Figure 1.2 Time history of nitrogen species.

stoichiometry (SR_1) also greatly affects exhaust NO concentrations. Figures 1.3, 1.4 and 1.5 (Takagi, et al., 1979; England, et al., 1981; Chen, et al., 1981) illustrate the influence of first-stage stoichiometry on nitrogen-species distribution with gaseous, liquid, and solid fuels, respectively. In general, the behavior is remarkably similar. First-stage NO rapidly decreases as the SR is decreased; however, HCN and NH_3 begin to increase as SR_1 is decreased further. A minimum in both TFN and the exhaust NO is observed, but the stoichiometry at which this minimum occurs varies from fuel to fuel.

1.4.3 Degree of Mixing — First Stage

The degree of mixing in the first stage has a direct effect on the nitrogen-specie concentration. Foster and Keck have shown (Figure 1.6) that increased mixing (increased AP) decreases the total fixed-nitrogen specie concentration, most dramatically the HCN concentration. The work of England, et al. (1981), supports this conclusion and suggests that the effect may be related to both fuel/air mixing and droplet size.

1.4.4 Thermal Environment

The thermal environment of the combustor has proven to be a very important parameter for control of NO_x emissions. Johnson, et al. (1978), reported (Figure 1.7) a considerable reduction in stack NO as the initial second-stage flame temperature was reduced. The aforementioned work was performed in a 4.2E9 Joules (4 million Btu) per hour, two-stage pulverized-coal combustor. Chen, et al. (1980), has achieved similar results in a 7.38E7 Joules (70,000 Btu)/hour tunnel furnace firing pulverized coal.

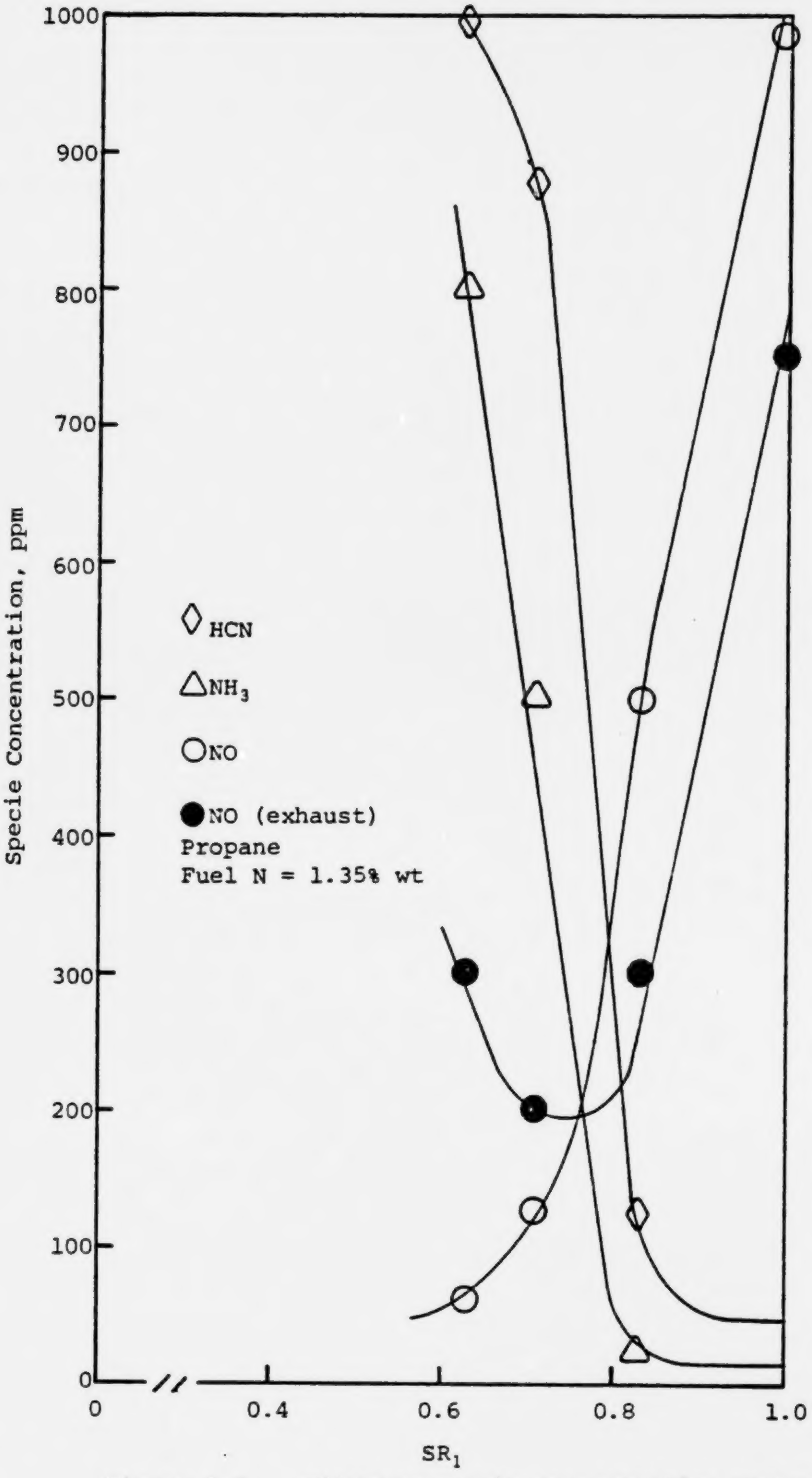

Figure 1.3 Nitrogen specie concentration versus first-stage stoichiometric ratio.

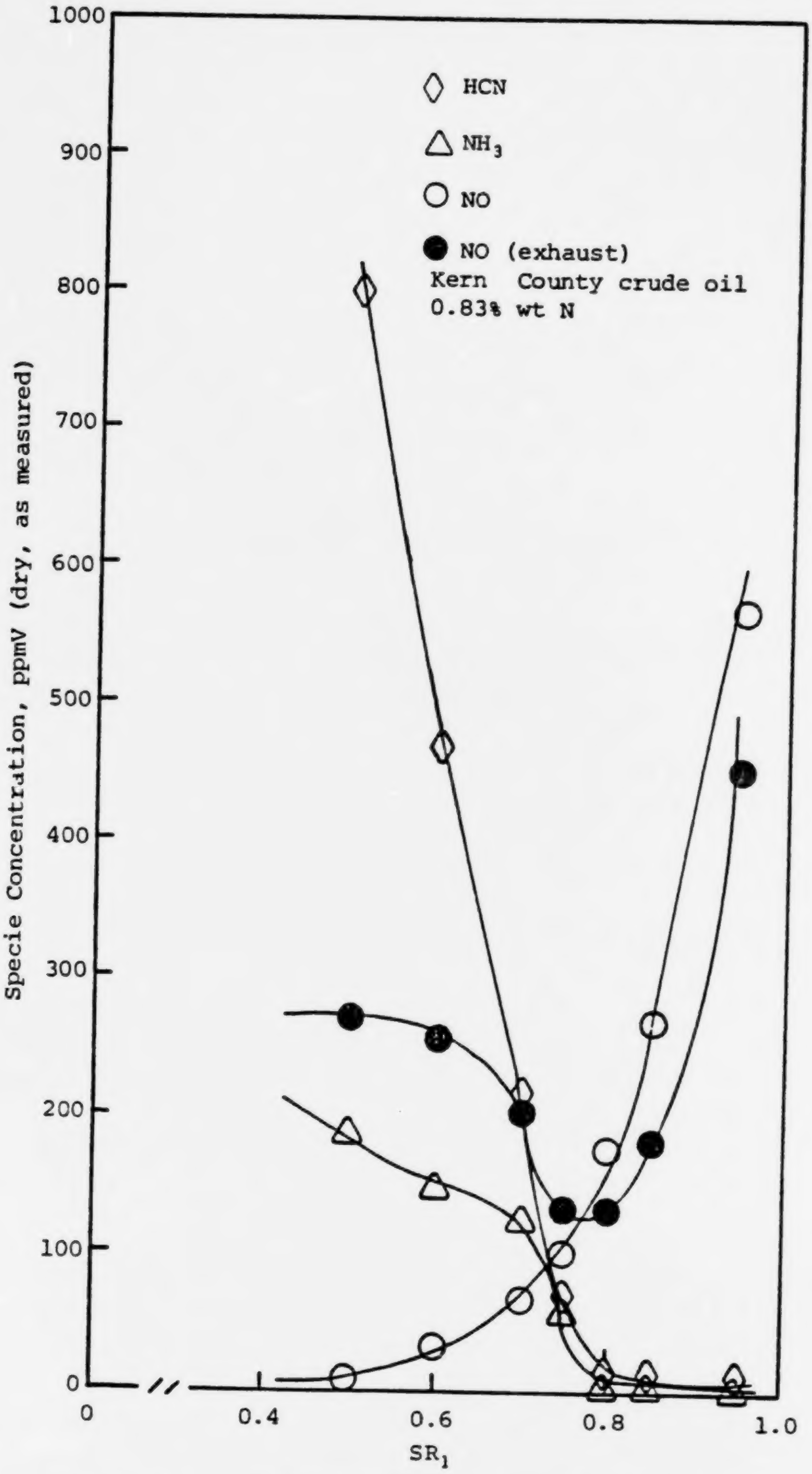

Figure 1.4 Nitrogen species concentration versus first-stage stoichiometric ratio.

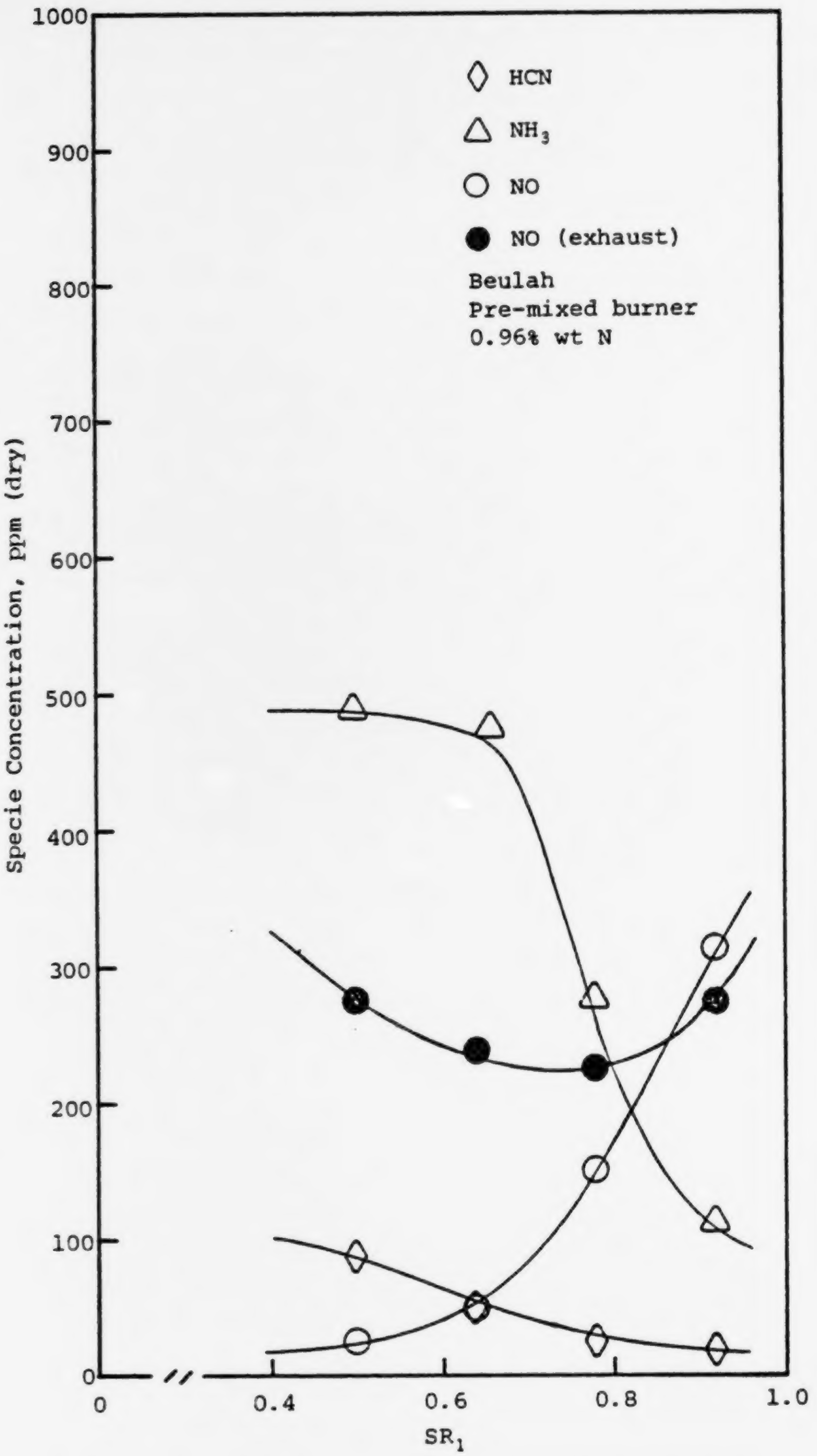

Figure 1.5 Nitrogen species concentrations versus first-stage stoichiometric ratio.

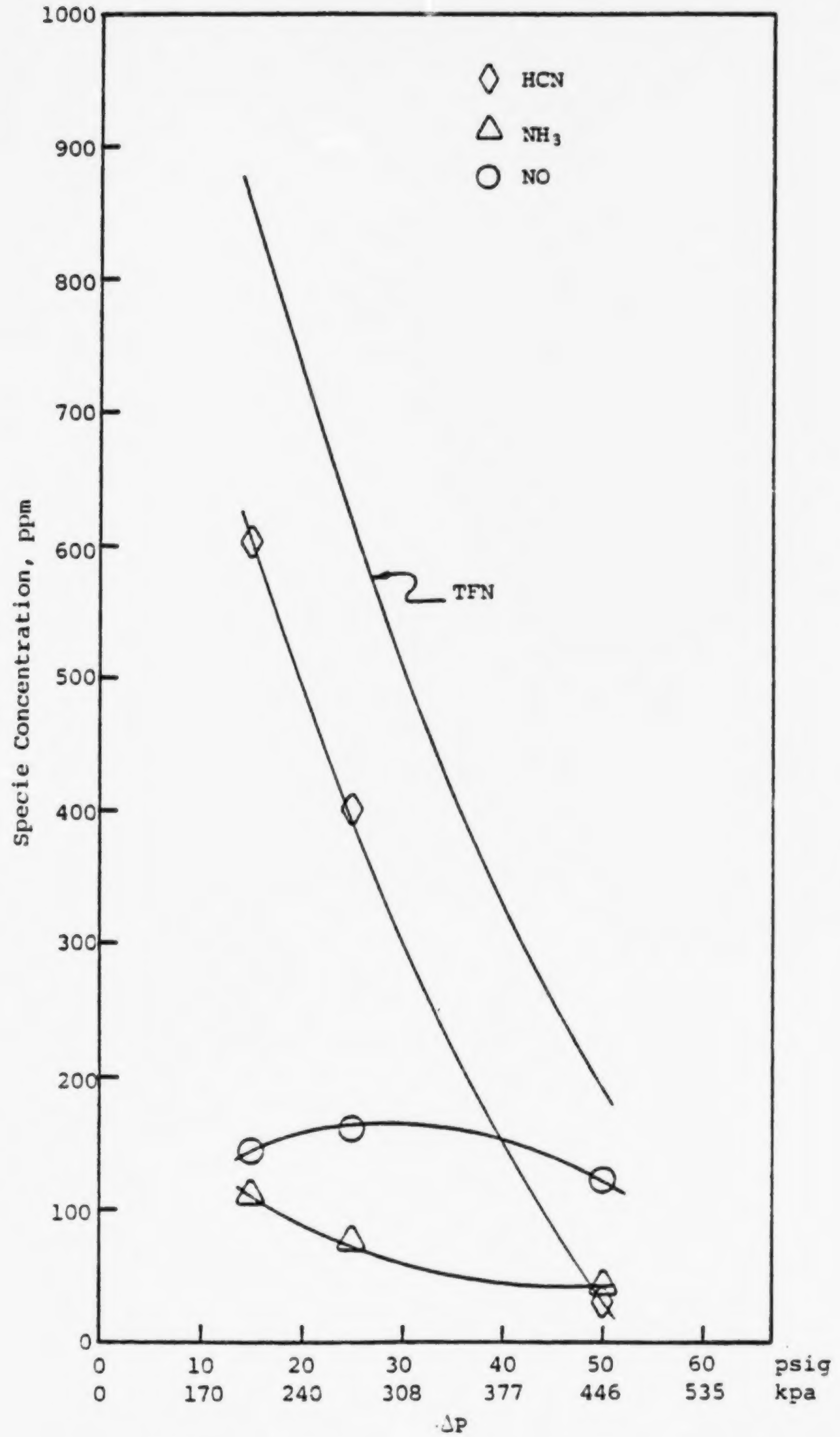

Figure 1.6 Effect of mixing on fixed-nitrogen species: kerosene, $\phi = 1.5$, $T_{inlet} = 600°K$, $X/D = 5.0$.

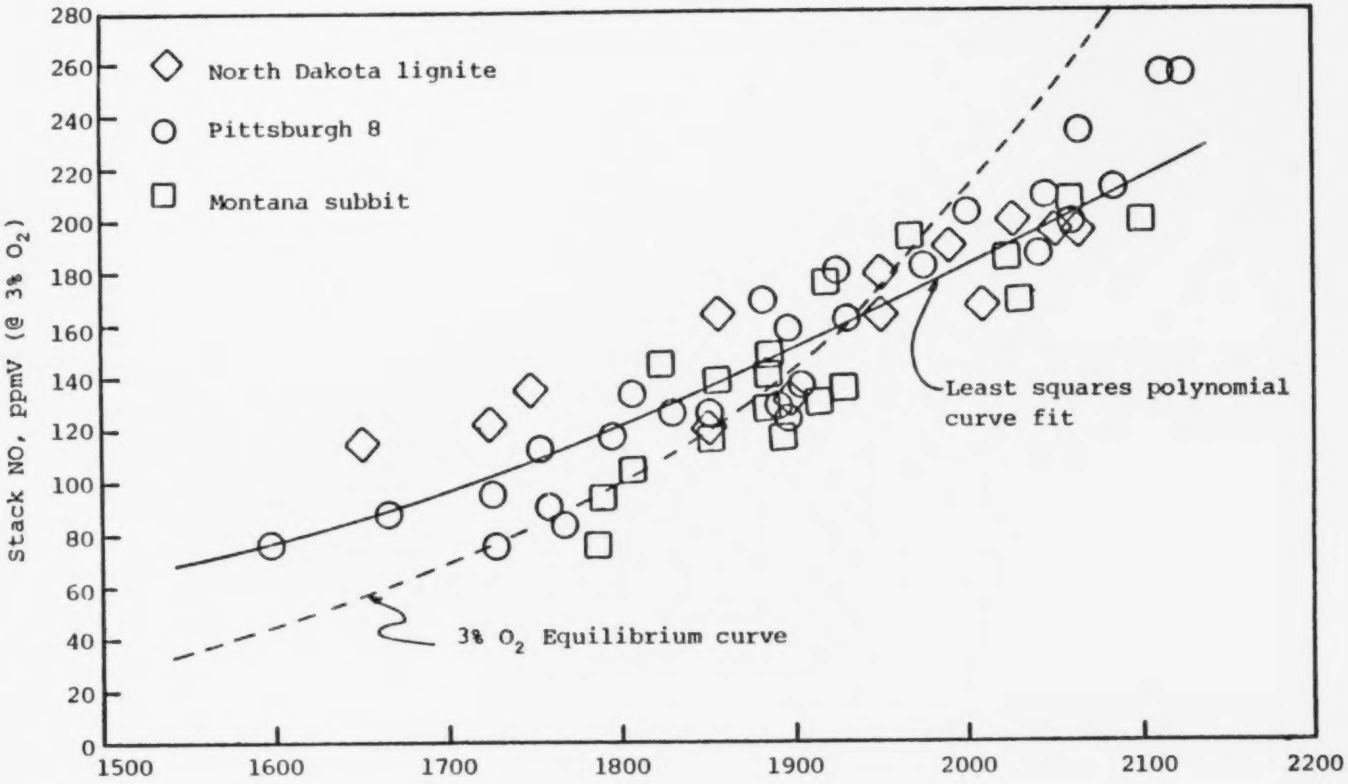

Figure 1.7 Stack NO as a function of second-stage initial flame temperature — optimum second-stage air slots.

Conversely, England, et al. (1981), reported a series of experiments in which the thermal environment of the first and second stages were changed systematically. The results show that decreasing the first stage temperature increased exhaust NO_x emissions and that the optimum thermal environment for liquid fuels has a high temperature vaporization zone, a hot, rich hold-up zone, and a cooled second stage (Figure 1.8). Reduction of total fixed nitrogen with increased first-stage temperature was also reported by Foster and Keck (1980). These latter results are in agreement with equilibrium calculations (Mason, 1980) and with finite rate kinetic modeling.

Thus, at present there is a major controversy over the optimum thermal environment in a staged combustor. Four sets of capable investigators have studied this parameter and reported exactly opposite results that cannot be rationalized simply on the basis of differences in combustion conditions or fuel composition.

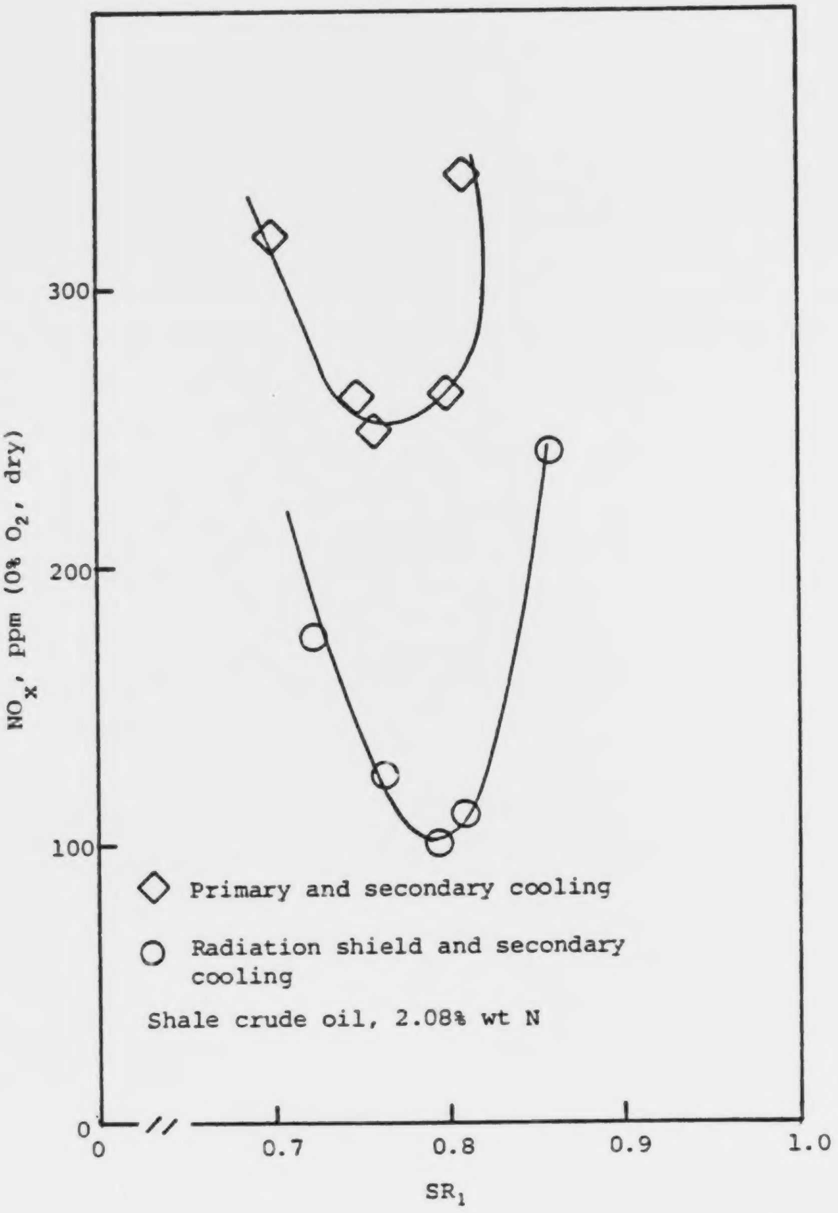

Figure 1.8 Influence of heat extraction profile in the first and second stages upon exhaust NO$_x$ emissions.

CHAPTER 2

PURPOSE AND SCOPE

The overall objective of this work was to investigate the role of the thermal environment in the furnace proper on the optimization of staged combustion for NO_x emissions control. The research concentrated on controlling first-stage thermal environment and evaluating the the impact of step changes in the thermal environment on first-stage NO, NH_3, and HCN and exhaust NO.

A supporting objective was to evaluate current NH_3 and HCN analytical technology and thereby experimentally define the techniques appropriate for the measurement of TFN species in a rich flame. Several analytical techniques had been previously implemented to detect NH_3 and HCN, but a detailed evaluation of the accuracy of the methods as applied to the detection of these species in furnace systems had not been completed. Therefore, prior to conducting the experimental studies on the influence of thermal environment in a staged combustor, it was necessary to develop and verify analytical techniques for HCN and NH_3.

The approach was experimental, utilizing a 25.5-kW (70×10^3 Btu/hr) refractory-walled laboratory combustor. Natural gas was the fuel, with air supplying the oxidizing agent. Pure ammonia gas was utilized as a nitrogen additive to the fuel.

Analytical technique development for NH_3 and HCN centered around the use of specific ion electrodes.

CHAPTER 3

AMMONIA MEASUREMENT

3.1 Background

A review of the available analytical chemistry literature was conducted to identify the various techniques available for ammonia quantification. An appropriate technique was selected after examination of this literature and discussions with other investigators in the field.

Most of the common techniques available are found under the broad heading of "wet chemistry." Titrametric and colormetric (Katz, 1977) methods are examples of these techniques. Both techniques involve capturing the gaseous ammonia in a liquid phase by bubbling the gas sample through impingers which contain an absorbing liquid medium. The absorbing liquid medium strips the ammonia from the gas phase. The liquid phase is then analyzed for ammonia as the method requires. These methods are certainly suitable; however, they are relatively time consuming.

Gunther, et al. (1956), developed a method to quantify ammonia gas directly, i.e., without absorption of ammonia into a liquid phase, by using spectrophotometry. An absorption maximum for ammonia at 204.3 mμ allowed determination of ammonia from 7 ppm to 1,000 ppm in air at atmospheric conditions; however, the interfering species present in fuel-rich furnace gas rendered this method unsuitable for the present study.

A chemiluminescent method developed by Axworthy, et al. (1976), was also considered. In this technique, NH_3 is catalytically oxidized to NO, which is subsequently measured by a chemiluminescent analyzer. Uncertainty of the oxidation efficiency left this technique questionable.

Gas chromatography was believed unsuitable because NH_3 is not detected by the N-P detector and because of the difficulty in separating the NH_3 from the other flue gas constituents when using the TC detector.

A method that appeared suitable was the specific ion electrode technique. The literature acclaimed this technique as fast, accurate, dependable, and appropriate for the operating range anticipated. After the specific ion method was selected for ammonia quantification, an in-depth literature review of this technique was executed. Both the ammonia selective electrode and the ammonia selective probe were investigated.

Early research by Mattock and Uncles (1964) displayed the ability of the glass for "selective" determination of ammonium and potassium ions in solution. Goodfellow and Webber (1972) later extrapolated Mattock and Uncles' work for the determination of ammonia in boiler feed water with the use of the ammonium selective glass electrode. Goodfellow and Webber (1972) found interferences to be negligible except for potassium and sodium ions and hydrazine which produced 1:1, 1:4, and 1:6 responses, respectively. Concern over these alkali interferences precluded the use of the ammonium-selective glass electrode in the current study, but the literature indicated that the ammonia selective probe did not respond to the alkali ions;

thus, this probe was believed to be appropriate for ammonia quantification.

Midgley and Torrance (1972) investigated the ammonia-specific probe as an instrument to quantify ammonia in condensed steam. The nomenclature of "probe" is distinguished from that of "electrode" in that the ammonia probe is a self-contained, electrochemical cell, whereas the ammonium electrode requires the use of a reference electrode. Midgley and Torrance found the probe to measure 0.1 ppm to 1.0 ppm ammonia in high-purity water from power stations within the required 10 percent accuracy margin. Amines were established as the only interfering species, unlike the ammonium electrode where alkali ions were a major interference. Beckett and Wilson (1974) and Midgley and Torrance found the precision of the ammonia probe to increase as the ammonia concentration increased; i.e., the relative total standard deviation of the results varied from 10 percent to 3 percent as the concentration of ammonia in solution ranged from 0.1 ppm to 4.0 ppm. Both Beckett and Wilson and Eagan and Dubois (1974) found good agreement between the ammonia probe and the Nesslerization method. Midgley and Torrance and other investigators detected a deviation from Nernstian performance of the probe at low ammonia concentrations (0.1 ppm to 8.0 ppm), pH effects, and temperature effects. All researchers noted that constant ionic strength, which is required for Nernstian response of the probe, was not a problem with ammonia levels of 0.1 ppm to 2,000 ppm when the samples were prepared properly.

3.2 Theory

The ammonia probe is an electrochemical cell (Figure 3.1) which is constructed of a glass pH electrode (cathode) pressed against a

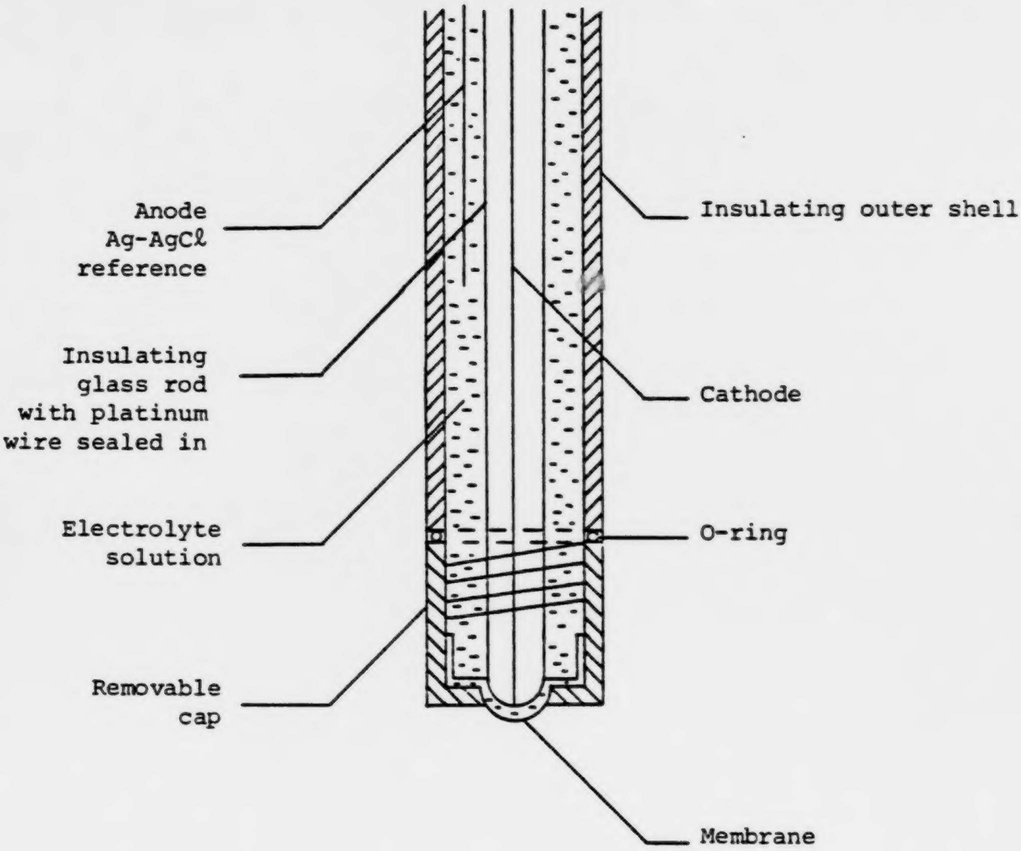
Anode
Ag-AgCℓ
reference
Insulating glass rod with platinum wire sealed in
Electrolyte solution
Removable cap
Insulating outer shell
Cathode
O-ring
Membrane

Figure 3.1 Schematic of ammonia-specific ion probe.

semi-permeable lipophilic membrane and an Ag-AgCℓ electrode (anode). Between the end of the glass pH electrode and the membrane is a very thin film of electrolyte solution, ammonium chloride. The Ag-AgCℓ electrode is also partially submerged in the electrolyte solution, thus completing the electrochemical circuit.

The membrane allows diffusion of free ammonia from the sample to the electrolyte solution. Ions cannot cross the membrane. Midgley and Torrance gave the following theoretical basis of the probe operation:

> . . . At equilibrium the partial pressures of ammonia on either side of the membrane are equal, and so changes in the ammonia concentration in the sample are reflected by activity changes in the film, and thus indirectly by pH changes arising from the ammonium-ammonia equilibrium:
>
> $$NH_4^+ \rightleftarrows NH_3 + H^+ \quad .$$
>
> The relationship between the e.m.f. of the probe and the ammonia concentration in the film can be established by considering the cell
>
> $$Ag|AgC\ell|\underset{\text{(bulk)}}{mM\ NH_4C\ell}|\underset{\text{(film)}}{mM\ NH_4C\ell,\ \nu\ M\ NH_3}|\text{glass electrode}$$
>
> where mM is the molar concentration of the ammonium chloride solution and ν is the number of moles of ammonia that have diffused through the membrane per liter of solution in the film. The potential (E) generated by this cell can be described by
>
> $$E = E^\circ_{glass} + k \log a_{H^+} - E^\circ_{Ag\text{-}AgC\ell} + k \log a_{C\ell^-} \qquad (1)$$
>
> where k = 2.303 RT/F.

R is the ideal gas constant, T is the absolute temperature, and F is Faraday's constant, 96,494 coulombs. The $\log a_{C\ell^-}$ term will be constant if the quantity of chloride ions in the electrolyte is large enough to overwhelm numerically any change that occurs by diffusion of ammonia and subsequent association as defined by $NH_4^+ \rightleftarrows NH_3 + H^+$.

. . . Collecting the constant terms, we obtain:

$$E = E' \; k \log a_{H^+} \qquad (2)$$

From its dissociation equilibrium the dissociation constant, K, of the ammonium ion is

$$K = a_{H^+} * a_{NH_3} / a_{NH_4^+} = 10^{-9.25} \qquad (3)$$

and we can substitute for a_{H^+} in equation (2) —

$$E = E' + k \log (K * a_{NH_4^+} / a_{NH_3}) \; . \qquad (4)$$

As the system is at constant ionic strength, the activity coefficients can be assumed to be constant.

The activity of ammonium ions and ammonia is described by

$$a_{NH_4^+} = \gamma_{NH_4^+} [NH_4^+]$$

$$a_{NH_3} = \gamma_{NH_3} [NH_3] \; .$$

". . . Collecting the constant terms in equation (4) we have

$$E = E'' + k \log [NH_4^+] - k \log [NH_3] \; . \qquad (5)"$$

The dissociation constant K is very small; therefore, the term $[NH_4^+]$ can be approximated to equal a constant. By assuming constant temperature and using a concentrated ammonium chloride solution for the electrolyte (i.e., concentrated relative to the NH concentration to be measured), equation (5) can be written

$$E = E''' - k * \log [NH_3] \; .$$

This equation displays the Nernstian response of the ammonia probe. Theoretically at 25°C the potential will decrease 59.2 millivolts for a ten-fold increase in ammonia concentration.

It should be emphasized that for the ammonia to be detected it must be free (i.e., not in a metal complex, etc.) and in the non-protonated form. Figure 3.2 exhibits clearly that the pH of the sample must be above eleven (11). The manufacturer of the probe recommends a pH above thirteen (13). Typically, concentrated sodium hydroxide is employed to reach the desired pH.

3.3 Ammonia Probe Calibration

The literature forewarns that it is necessary to have fine control of the sample temperature and probe temperature. Also, several investigators recommend avoiding magnetic stirrers, for they may liberate unwanted thermal energy. Hence, a constant temperature water bath with a water propelled magnetic stirrer (Figure 3.3) was employed in this work.

Initially temperature, pH effects, and ionic strength effects on the probe were investigated. All chemicals used were of analytical reagent grade. The probe was an HNU Systems, Inc., ammonia electrode model ISE-10-10-00. Corning's pH meter 130 was used to provide a digital read-out.

The influence of temperature on the operation of the probe was investigated by altering the set point of the constant temperature bath in which the probe and sample were held. Samples were prepared from a 10E-1 M (molar) $NH_4C\ell$ (ammonium chloride) solution by serial dilution. Sample concentration ranged by decades from 10E-1 M $NH_4C\ell$ to 10E-6 M $NH_4C\ell$. The hydroxide ion concentration in the sample was maintained with 10 M NaOH such that the sample pH was equal to or greater than thirteen (13). With the probe in contact with the sample, data was taken when equilibrium between the sample and the probe was achieved. The results of the experiments (Figure 3.4) show

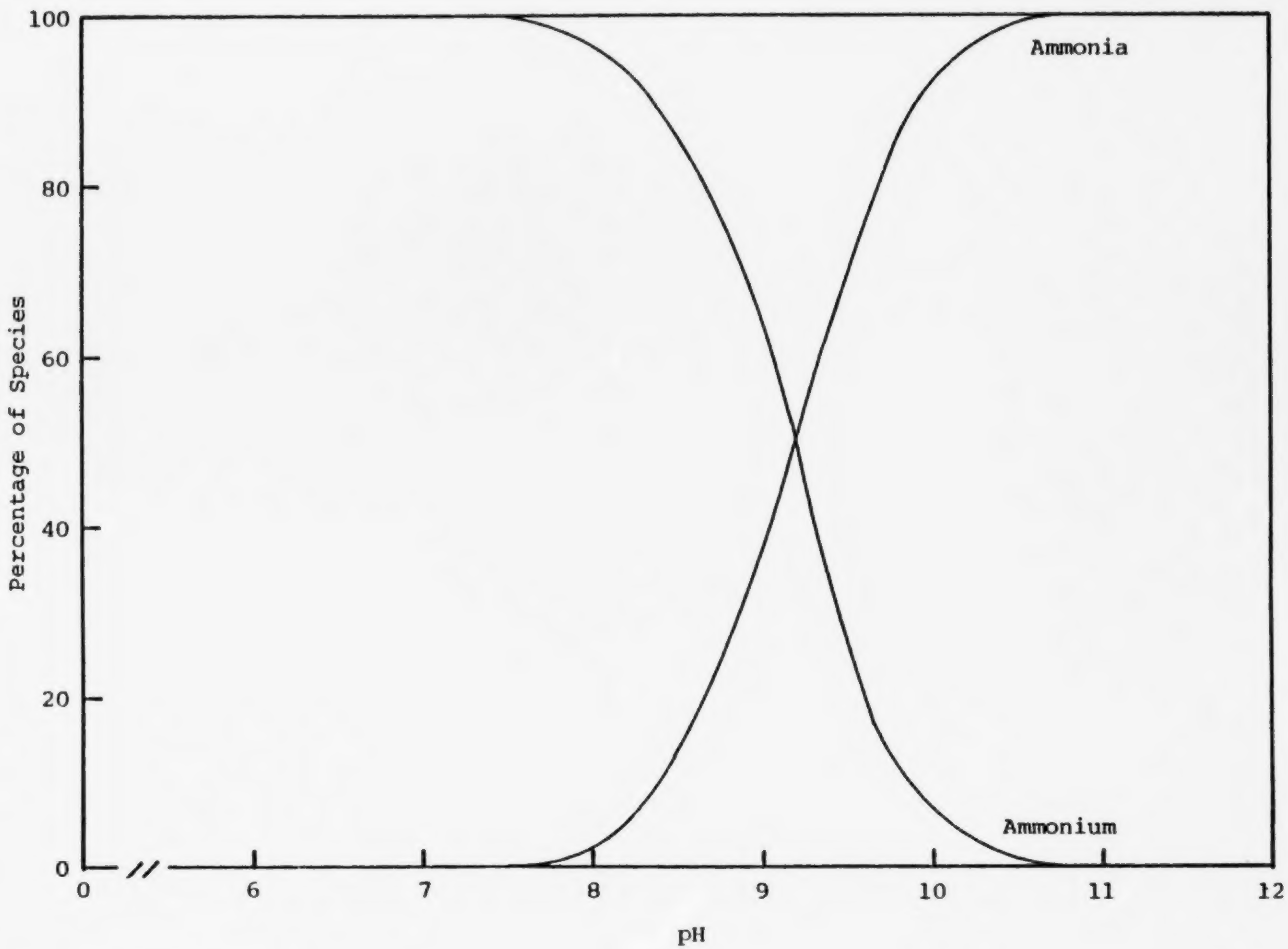

Figure 3.2 Influence of pH on ammonia dissociation.

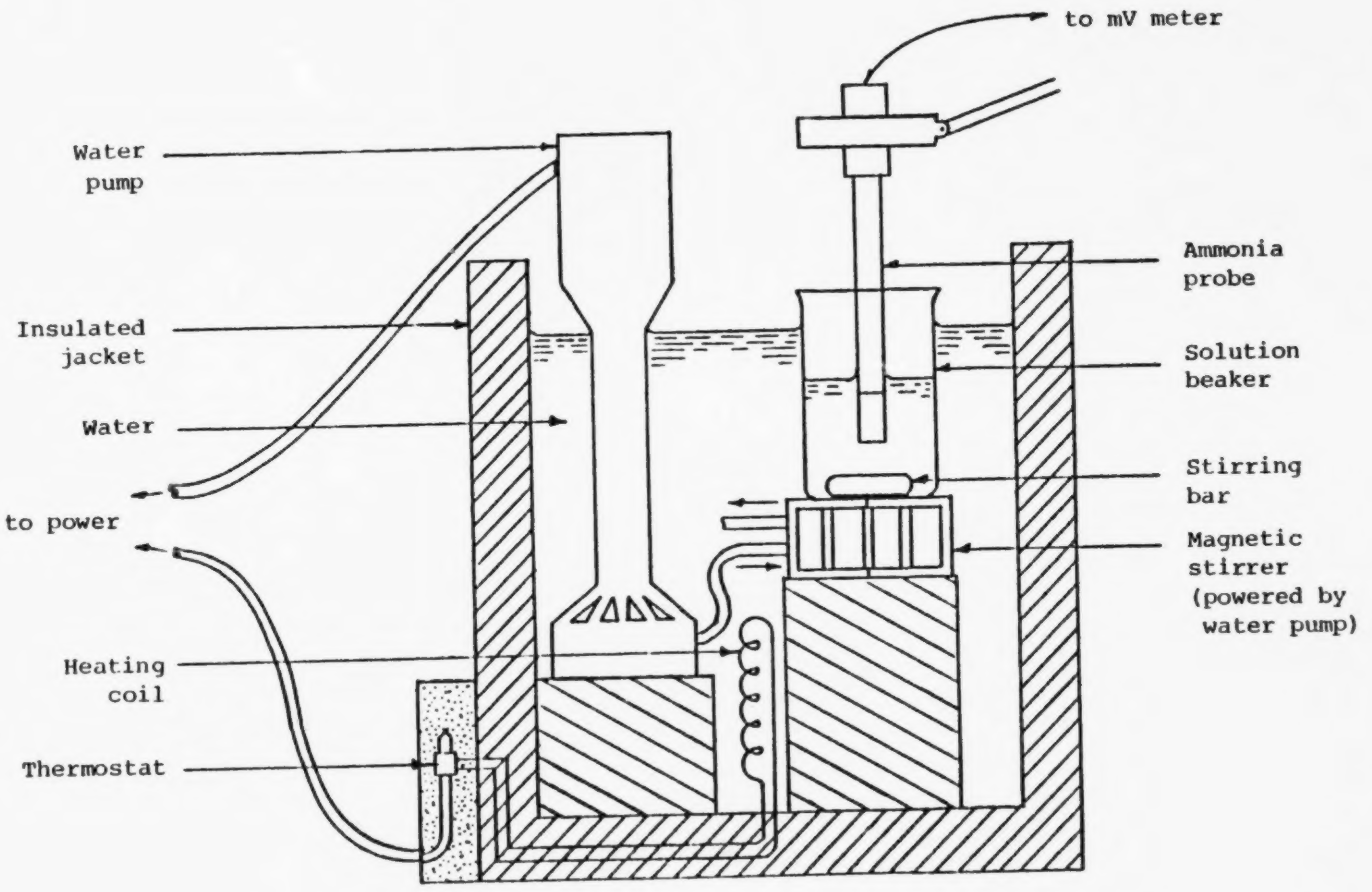
to mV meter
Water pump
Insulated jacket
Water
to power
Heating coil
Thermostat
Ammonia probe
Solution beaker
Stirring bar
Magnetic stirrer (powered by water pump)

Figure 3.3 Solution ammonia measurement apparatus.

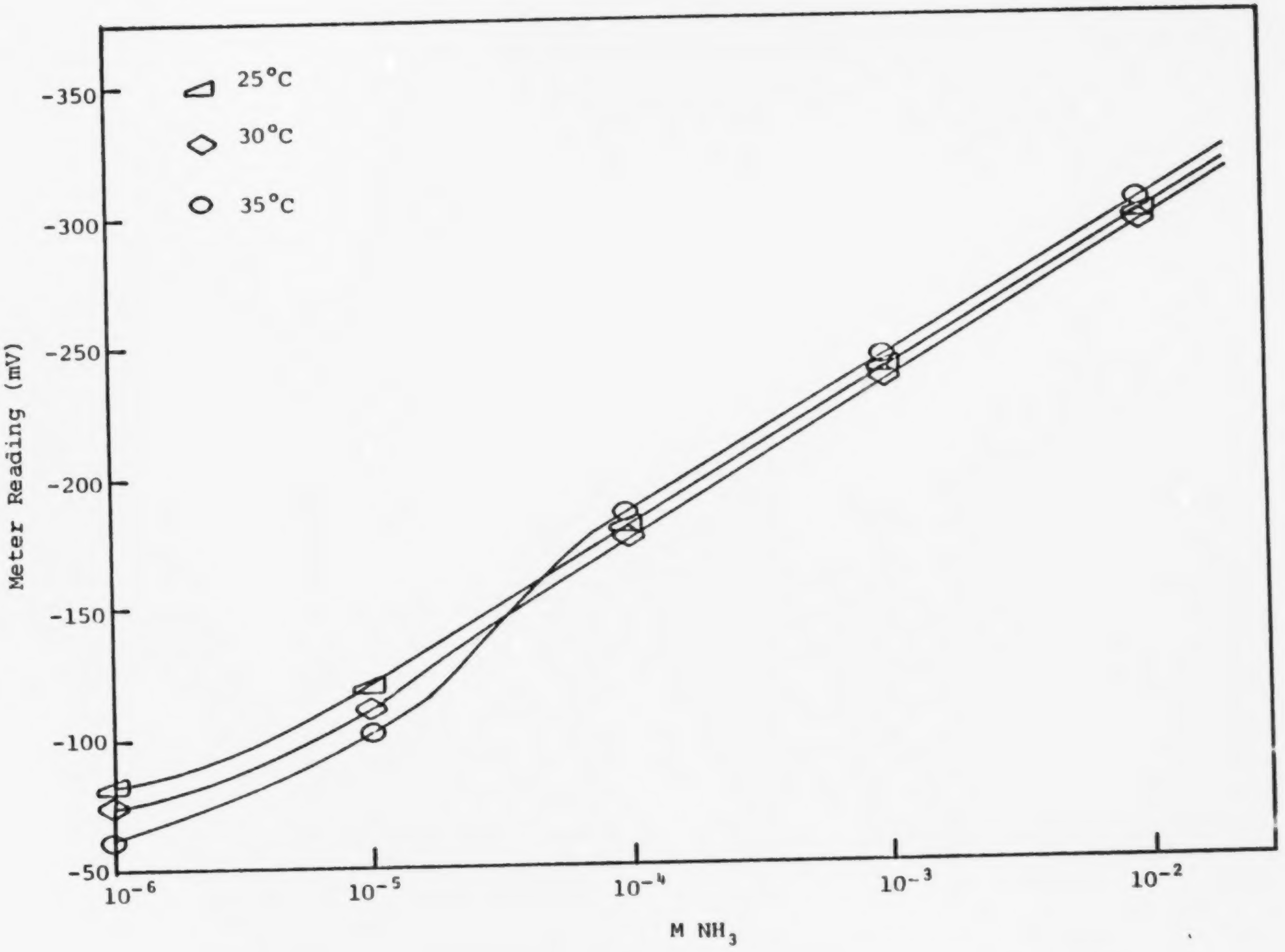

Figure 3.4 Influence of solution temperature on ammonia probe.

a major loss in linearity as the temperature is increased. The probable cause of linearity loss is the deviation of the probe from Nernstian response and the escape of ammonia from the sample. Because of this effect and the desire to maintain comparability of future data with existing literature results, 25 °C was selected as the standard operating temperature.

The manufacturer recommends that the sample be maintained at a pH of thirteen (13) using 10 M NaOH for proper functioning of the probe. Therefore, experiments were performed to determine the influence of pH on the probe. For a particular ammonia concentration, the pH was adjusted by drop-wise addition of 18 M H_2SO_4 and 10 M NaOH. Figure 3.5 presents the results obtained. All samples were initially adjusted to a pH of approximately thirteen (13). The arrows indicate the direction of varying pH. Clearly, pH has an effect on the response of the probe; as the pH is lowered, the response decreases. The 500 ppm NH_3 experiment shows that an asymptote in the response is reached at approximately 12.5 pH. It is believed that the varying total ionic strength of the samples caused the decrease in the response when the pH was returned to thirteen (13). These experiments demonstrated that if the pH is maintained near thirteen (13), the response reaches an asymptote which is desired.

For the probe to function with a Nernstian response background, ionic strength must be high and constant relative to the variable concentration of the ion added. The addition of 10 M NaOH to the solution to be analyzed, as specified by the manufacturer of the probe, keeps the background ionic strength high and relatively constant. Ionic strength is calculated by

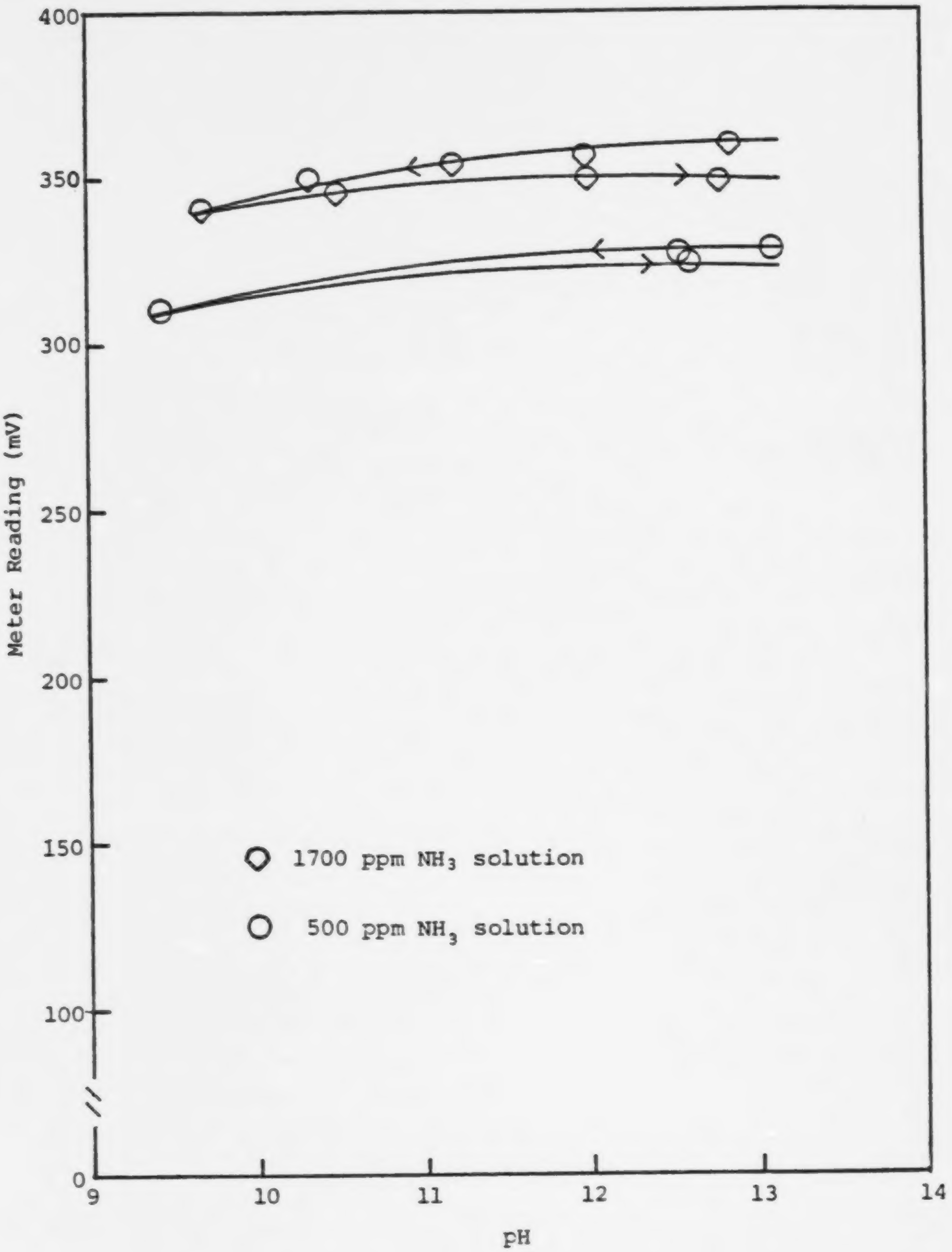

Figure 3.5 Influence of pH on ammonia probe.

$$\text{Ionic strength} = 1/2 \sum C_i Z_i^2$$

where C_i is the concentration of ion i and Z_i is the charge of ion i. Calculations indicate that the ionic strength increased two-fold during the experiments which were conducted to construct Figure 3.5. This supports the supposition above that changes in total ionic strength were partially responsible for the inability of the probe to give the same response after a high pH was re-achieved. This is in accordance with the Debye and Huckel equation relating the activity coefficient and ionic strenth proportionally.

A calibration curve was subsequently constructed with the appropriate attention to the temperature, pH, and ionic strength effects on the probe. The probe was calibrated with standard solutions prepared by dissolving 5.350 grams of $NH_4C\ell$ in 1.0 liter of 0.1 N H_2SO_4. Standard solutions ranging from 1.0E-2 M $NH_4C\ell$ to 1.0E-6 M $NH_4C\ell$ were prepared by serial dilution of the 0.1 M $NH_4C\ell$ solution. The sample was placed in the constant temperature bath and stirred. The pH was adjusted to 13.0 using 10 M NaOH. The probe was placed in the sample and data was taken when equilibrium was achieved. Figure 3.6 shows data obtained at 25°C which indicates that the response of the probe is log-linear down to a liquid concentration of 10E-05 moles per liter (0.1703 ppm (w/w)).

The feasibility of storing samples was also investigated. Concentrations of NH_3 ranged from 8.5 ppm (w/w) to 850.0 (w/w). Samples were prepared by adding 5.350 grams of $NH_4C\ell$ to 1.0 liter of 0.1 N H_2SO_4, then diluting this solution to the desired concentrations. A portion of each solution was analyzed immediately after preparation.

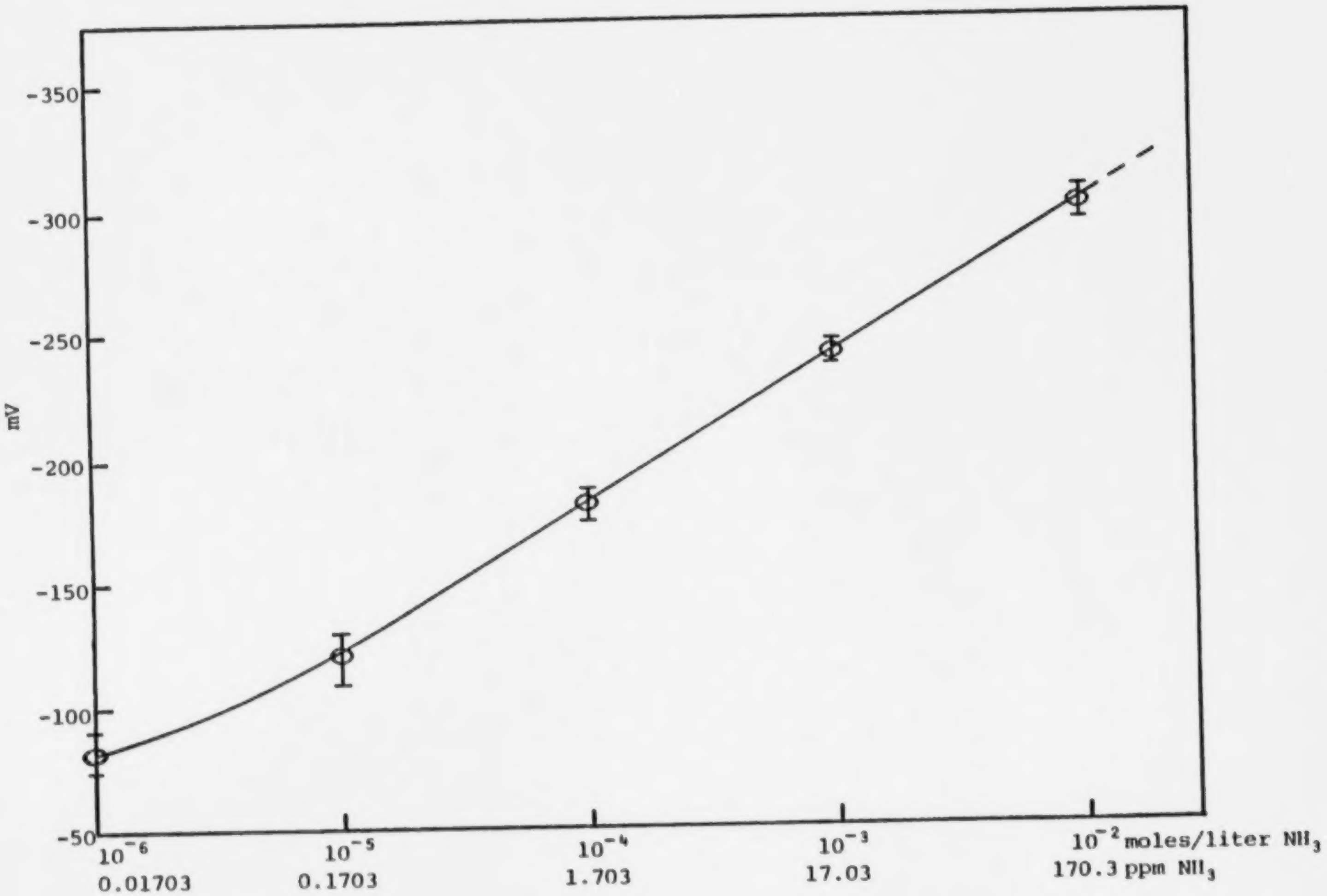

Figure 3.6 25 °C-calibration curve of ammonia probe.

The remaining portion of each solution was divided in half. One-half was stored under artificial light, while the other half was stored in darkness. The solutions were analyzed periodically for one week. No significant deviation of the response of the probe was found for either family of solutions. Storage under artificial light or without light did not have an effect on the final analysis of the sample. Although it is recommended that samples be analyzed soon after a sample is collected, delaying the analysis for short periods of time (one week) will not affect the outcome of the analysis. However, samples should be stored in containers providing very little volume above the sample to minimize ammonia loss to the gas phase.

3.4 Collection System Design

The collection system involved procuring a suitable sample from the furnace proper and then processing the sample so that the ammonia probe could be used. The furnace gas sampling probe was developed by Pershing, et al. (1977), and is described in detail in Chapter 6. The construction of the probe was such that the incoming gas sample was immediately quenched with an acid spray so that a gas phase and a liquid phase exited the probe. The collection system, therefore, necessarily consisted of several gas impingers to collect the incoming liquid phase from the gas sampling probe and to strip the ammonia remaining in the gas phase. The diameter of the impinger was 6.0 centimeters (2.4 inches) and the height was 29.0 centimeters (11.4 inches). To understand the effectiveness of the overall system, an impinger investigation was initiated.

Three gas-impinger designs (Figure 3.7) were investigated to establish their collection efficiency. Design A was a straight-tube

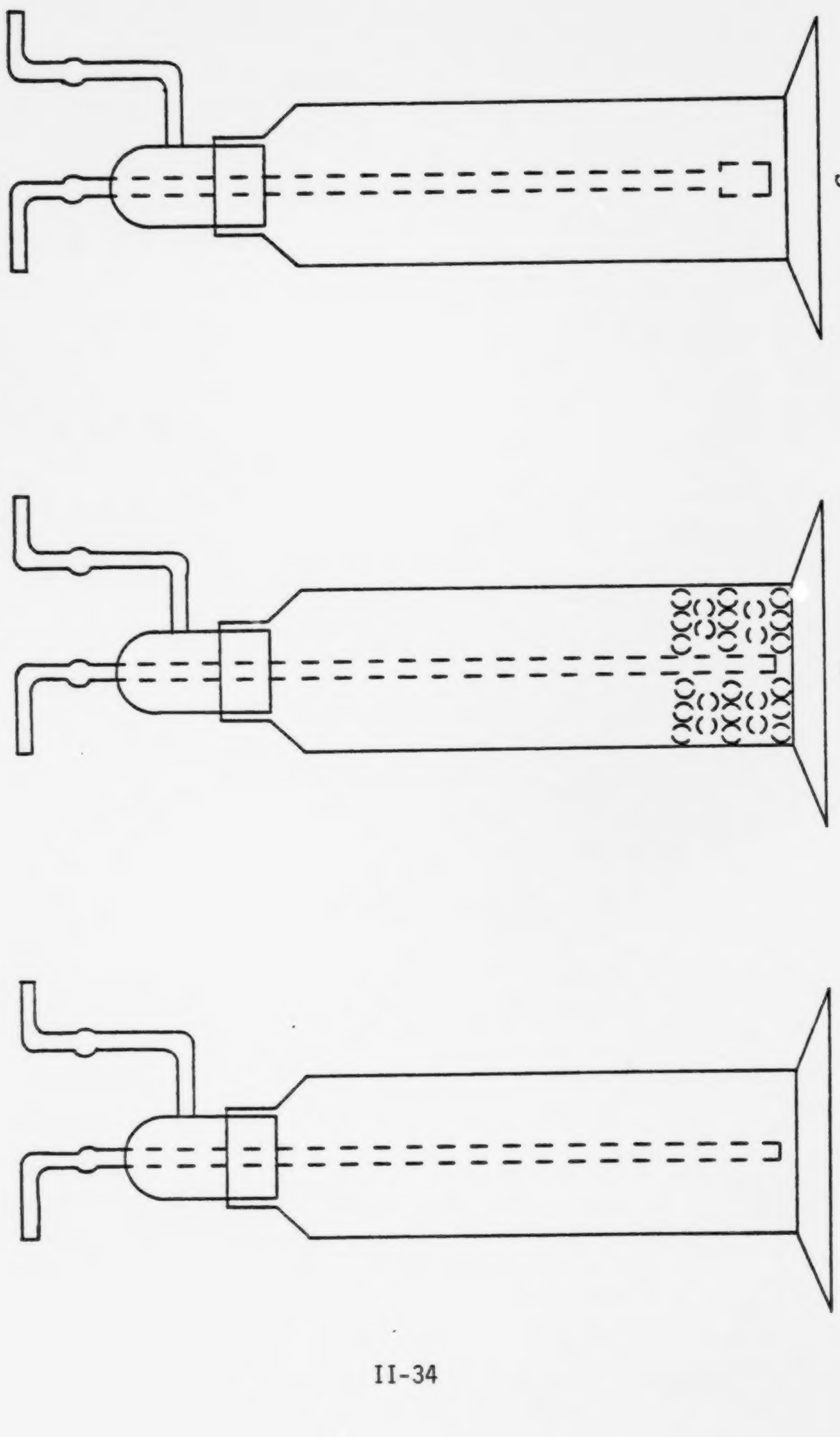

Figure 3.7 Impinger designs.

impinger. Gas entered the impinger through the straight tube which was located on the axis of the impinger. After leaving the tube, the gas bubbled through the liquid phase and exited at the top of the impinger. Design B was a straight-tube impinger inserted into a matrix of 6-millimeter (0.24-inch) glass beads. The glass-bead matrix was 8 centimeters (3.2 inches) deep. The glass beads were added to increase gas and liquid contacting. Design C was a straight-tube impinger with a fritted glass cylinder (12 coarse) attached to the end of the tube. The addition of the fritted glass cylinder was also to increase gas and liquid contacting. These designs were chosen because of perceived collection efficiency or previous usage by other investigators.

A gas-mixing system was used to accurately regulate the volume of ammonia standard gas entering the gas impingers. Mason (1980) described this system in detail; therefore, only a brief explanation will be given here. The system contains four identical flow measurement lines, one of which is illustrated in Figure 3.8. The temperature of the entering, standard gas is adjusted to 30°C by a long, tubular heat exchanger. The gas is then directed into one of five sapphire orifices which vary in size from 0.0762 millimeters (0.003 inches) to 0.635 millimeters (0.025 inches). This corresponds to a flow-rate range of 0.2 liter per minute to 62 liters per minute for N_2. The pressure upstream of the selected orifice is measured with a 15.24-centimeter (6-inch) pressure gauge and is adjusted to the desired value with a micro-needle valve. The gas temperature is maintained at 30°C throughout the orifice section with a constant-temperature bath. The system is operated such that the velocity at the jeweled

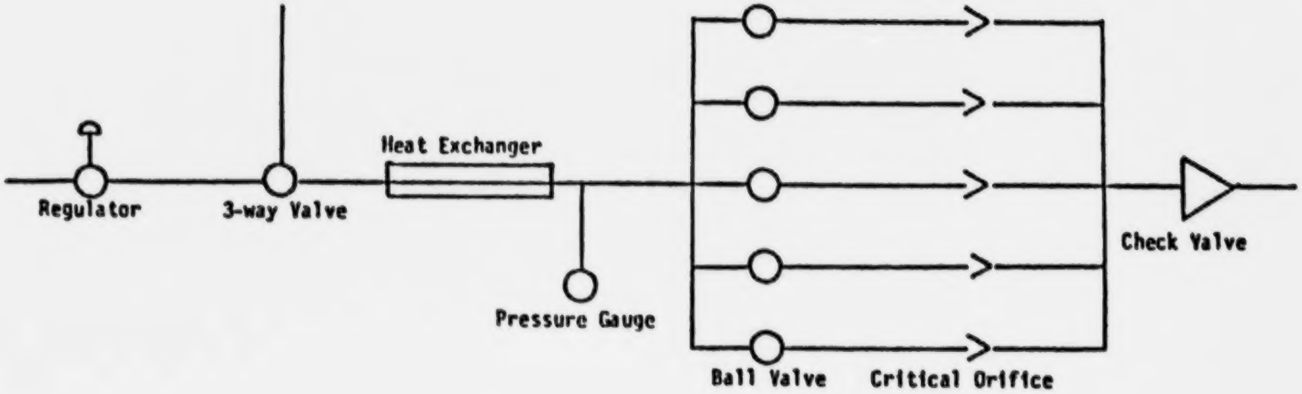
Heat Exchanger
Regulator
3-way Valve
Pressure Gauge
Ball Valve
Critical Orifice
Check Valve

Figure 3.8 Gas-mixing system flow diagram.

orifice is sonic; hence, the exit flow rate is directly related to the measured upstream pressure. Calibration curves were constructed for each orifice under sonic flow conditions.

The complete collection testing facility consisted of the gas-mixing system connected to a series of impingers. The exit gas from the impingers was released into an exhaust hood. To test this system, varying gas flow rates of 550 ppm NH_3 balance N_2 were passed through fritted impingers containing 150 milliliters of 0.1 N H_2SO_4. Figure 3.9 shows the results of these tests and indicates that with two impingers in series, approximately 97 percent collection efficiency was achieved.

Multiple combinations of liquid heights in the gas impingers and gas flow rates of 550 ppm NH_3 balance N_2 through the impingers were investigated. Throughout these investigations an 0.1 N H_2SO_4 solution was used as the liquid phase in the impingers. The acidic liquid phase was used to simulate the acidic phase which would exist in the gas sampling probe if the gas sampling probe was used in a flame from a fuel containing sulfur and other potential acid-producing compounds.

Figures 3.10 through 3.12 present the results obtained from these parametric investigations. The data indicate that each impinger design produces collection efficiencies of approximately 90 percent or better when the liquid height and gas flow rate are optimized. However, the performance of the various impingers varies widely at high gas rates and low liquid levels. The fritted tube impinger displayed the greatest efficiency (94 percent) for a flow rate of 4.48 ℓ/min at a liquid height of 5 inches.

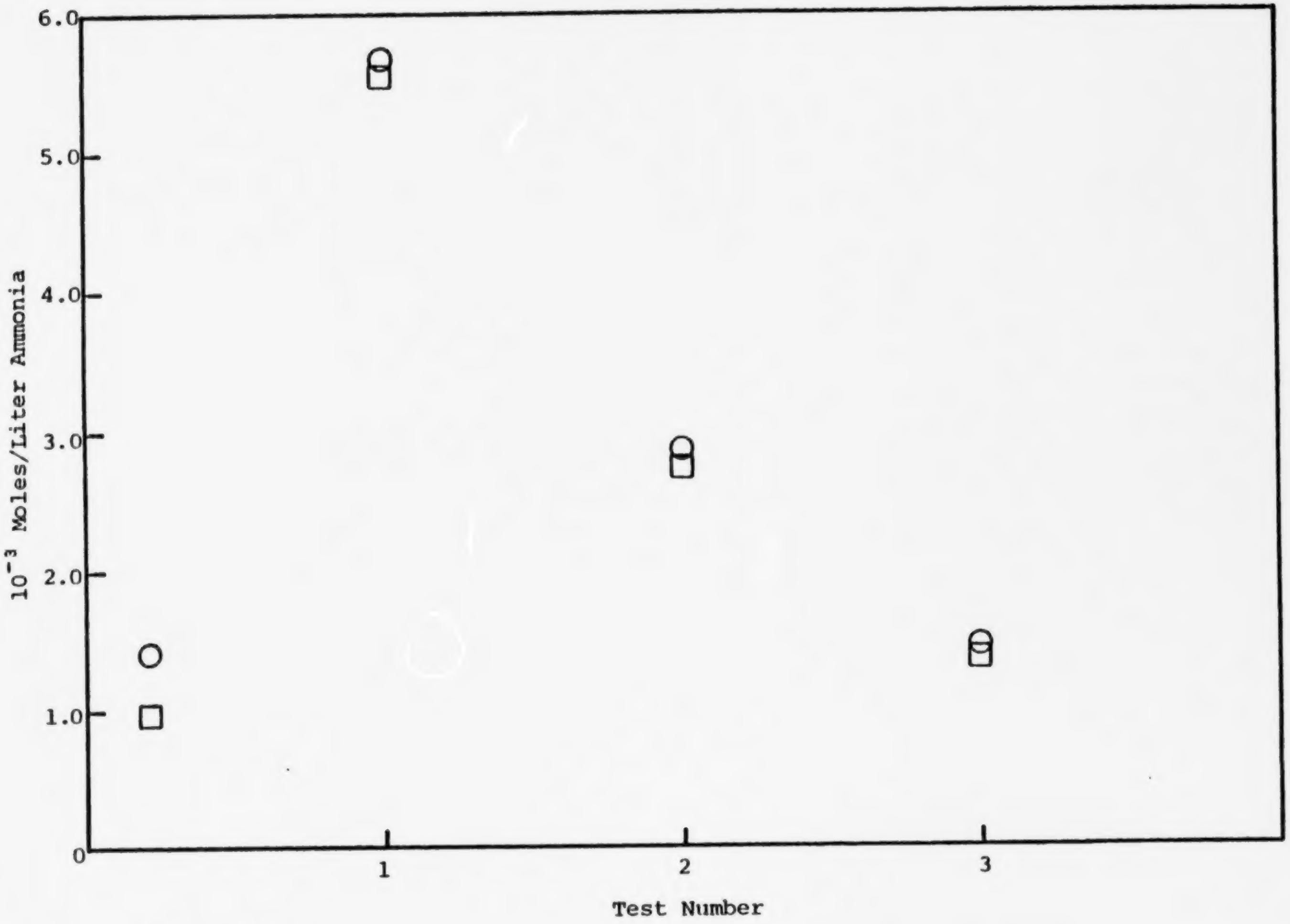

Figure 3.9 Experimental results on ammonia measurements.

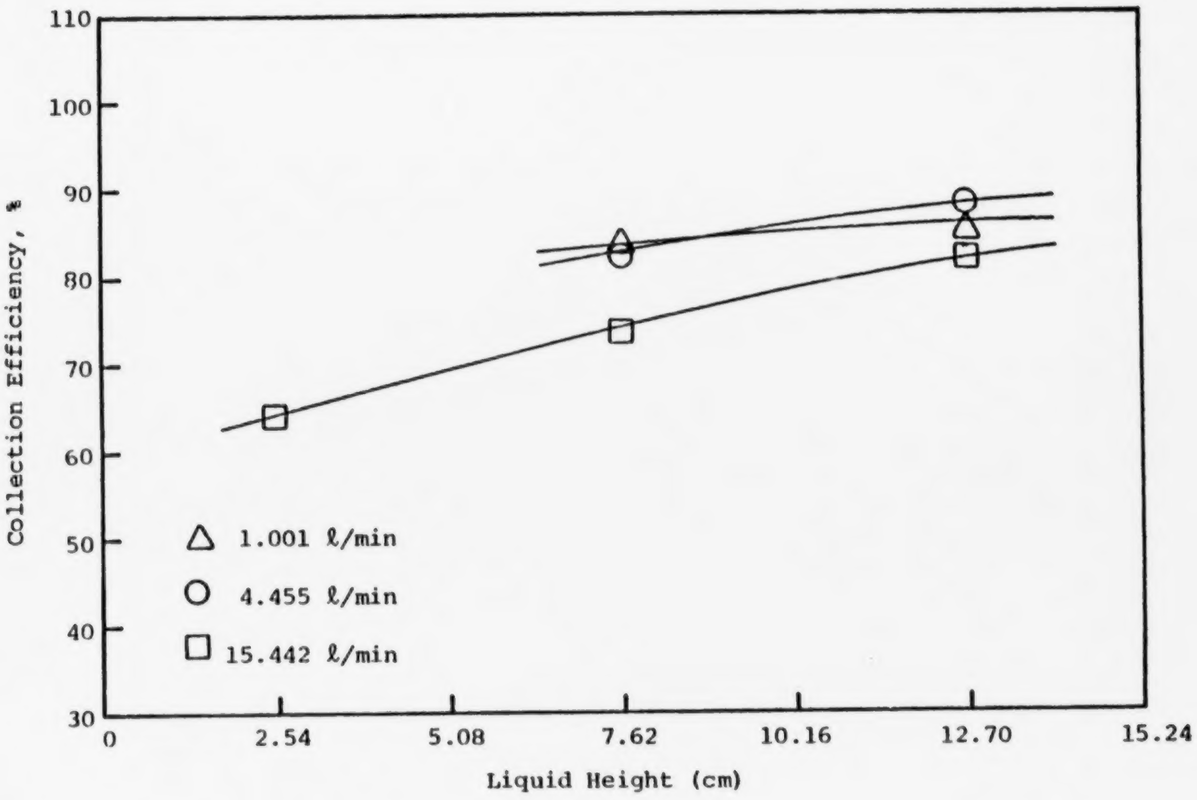

Figure 3.10 The effect of liquid height on the collection efficiency of the straight tube impinger.

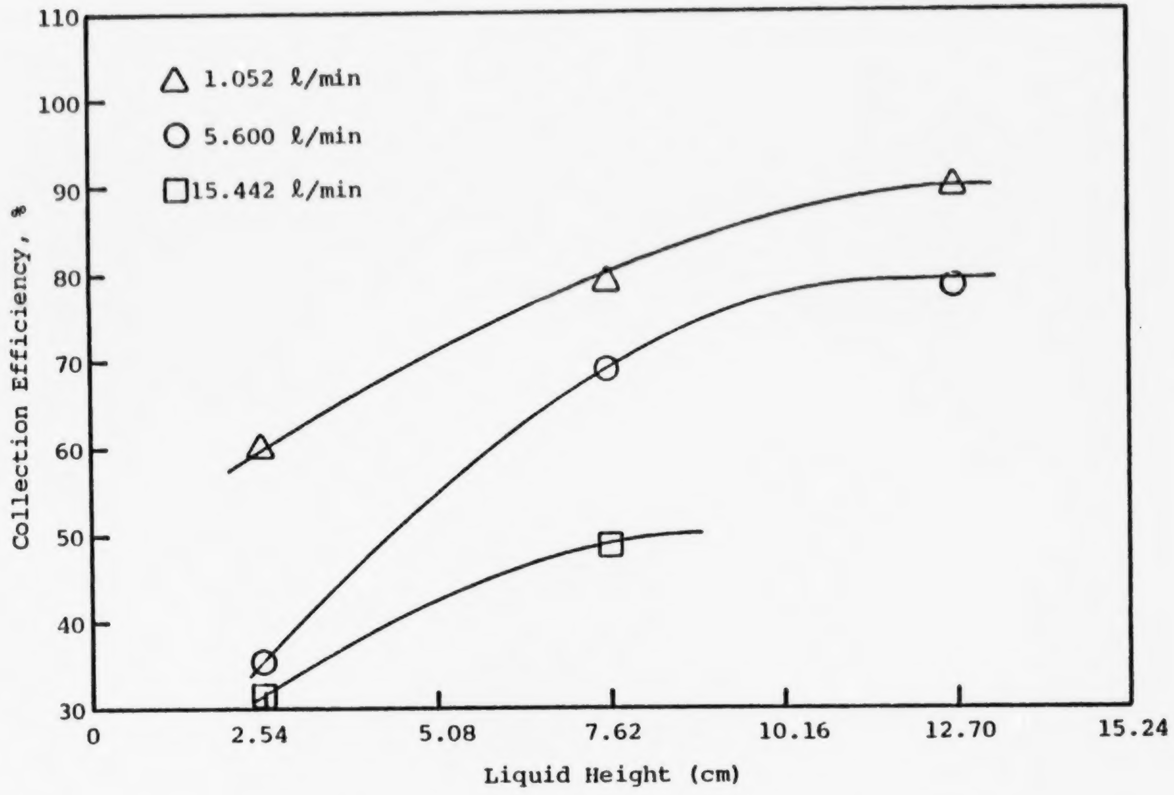

Figure 3.11 The effect of liquid height on the collection efficiency of the straight tube impinger with beads.

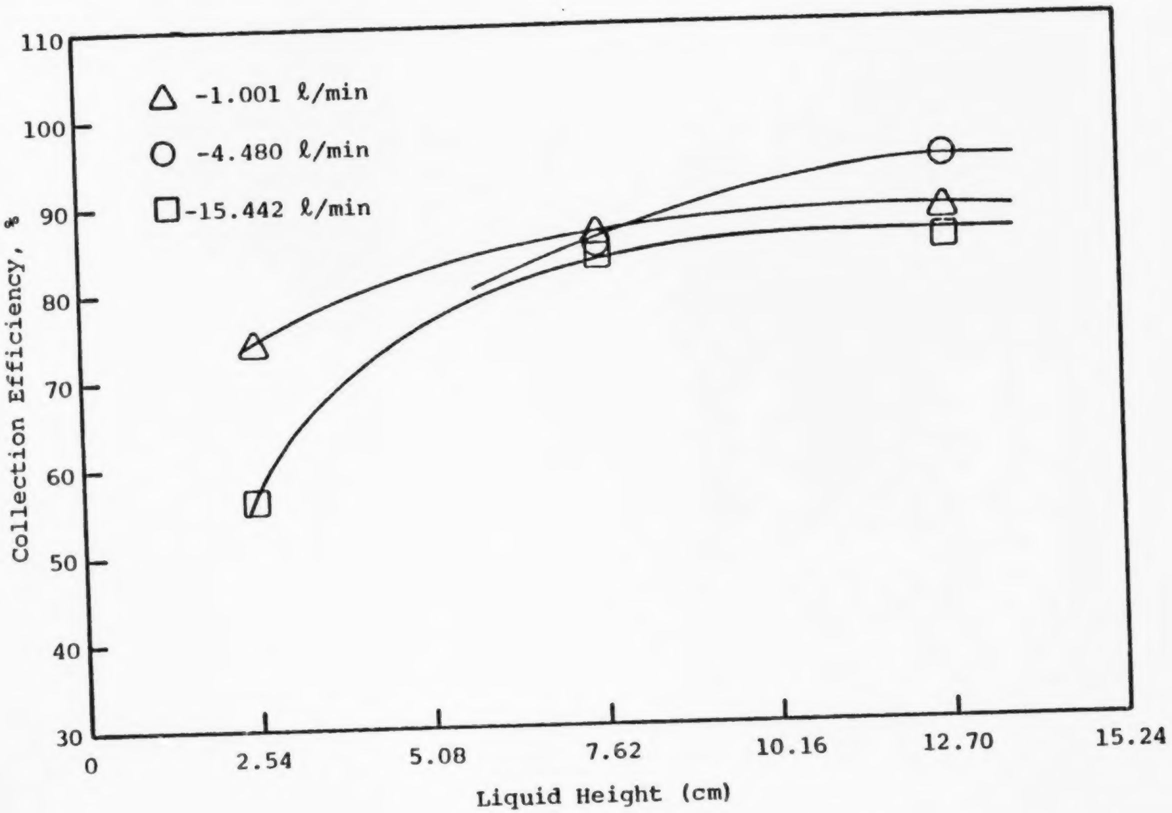

Figure 3.12 The effect of liquid height on the collection efficiency of the fritted cylinder impinger.

All of the figures indicate that, as the liquid height in the impinger is increased, the efficiency of collection increases. This is consistent with the associated increase in the number of overall transfer units.

In general, increasing the gas flow rate decreases the collection efficiency except in Figures 3.10 and 3.12 where the 4.48 ℓ/min curve lies above the other curves at a liquid height of 5 inches. Visual observation indicated that, in the straight tube and fritted tube impingers, the gas-liquid mixing was poor when the gas flow rate was as low as 1.0 ℓ/min. This results in increased local liquid-phase concentrations and, hence, a reduced driving force.

The straight-tube impinger with glass beads (Figure 3.11) exhibited strongest flow-rate dependence. Increased flow rate was accompanied by a dramatic decrease in ammonia absorption, which was caused by extensive gas-phase channeling in the glass-bead matrix.

Saturation of the liquid phase was investigated, using a fritted impinger with a liquid height of 1 inch of 0.1 N H_2SO_4 and a precisely measured flow rate of 15.0 liters per minute at 550 ppm ammonia balance nitrogen from the gas-mixing panel. Varying quantities of ammonia were passed through the impinger. The results presented in Figure 3.13 show that, as large quantities of NH_3 gas are contacted with the liquid phase, the collection efficiency decreases because of a decreased driving force. Although the magnitude of this dependence is a function of the incoming NH_3 gas concentration and amount of liquid phase, it is clear that, when designing a collection system, the approach to equilibrium (saturation) must be considered. (The dotted vertical line on Figure 3.13 indicates the equilibrium NH_3

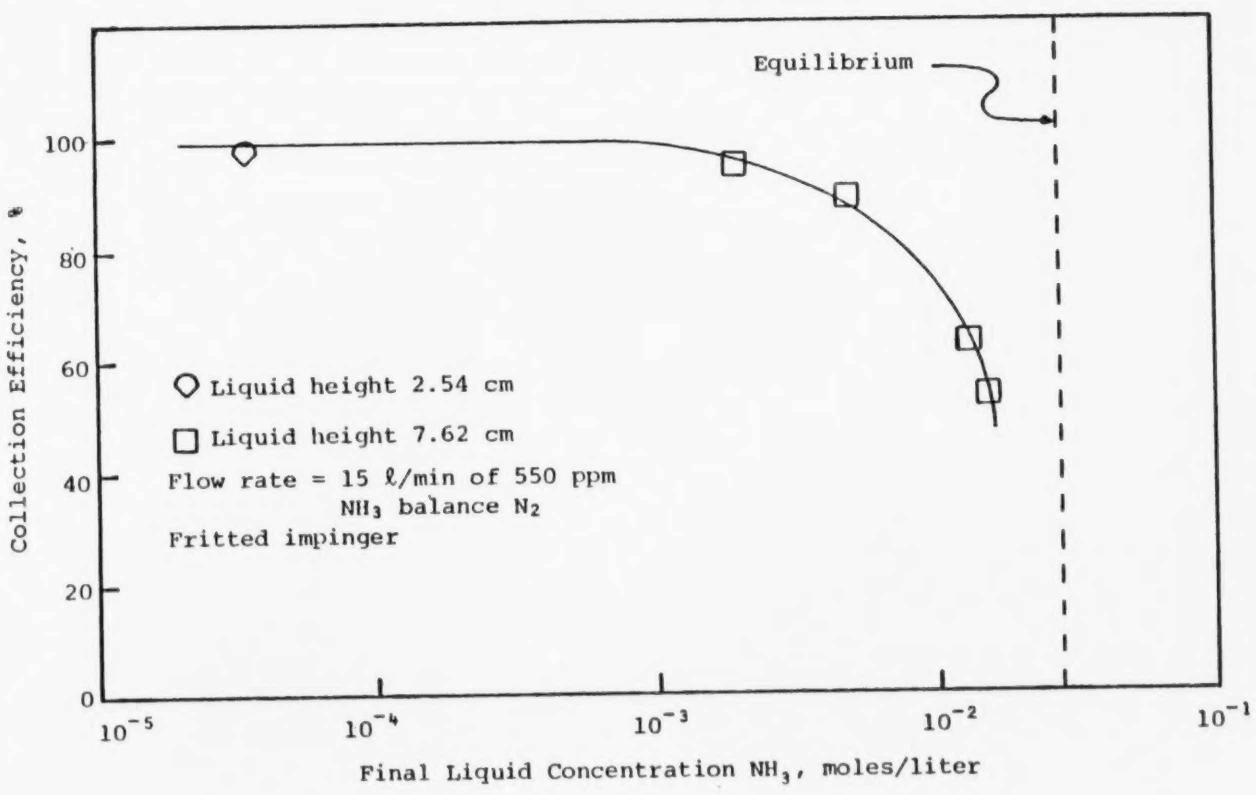

Figure 3.13 Effect of final liquid concentration on collection efficiency.

concentration in the liquid phase for a $NH_3/H_2O/N_2$ system with a gas phase NH_3 concentration of 550 ppm.)

The influence of gas flow rate can be considered in a similar fashion, as shown in Figure 3.14. These data were obtained for the straight-tube impinger with the glass beads, and they show a rather unusual dependence on flow rate. (For a constant flow rate, the various concentrations are associated with different liquid heights.) Note that all of the concentrations are far below the equilibrium concentration of 0.28 moles/ℓ. These data suggest that the liquid-phase mixing in this impinger system is relatively poor and that the NH_3 absorption may be limited by locally high-liquid phase concentrations. Comparison Figures 3.13 and 3.14 indicate that the steep decline in collection efficiency occurs at a much lower bulk liquid-phase concentration. Further, the 15 ℓ/min gas flow rate produced especially poor results; however, visual observation indicated that significant gas-phase channeling occurred in this case. In summary, these results suggest that the gas flow rate through the impinger must be selected to insure good gas-liquid contact and good liquid-phase mixing.

Figure 3.15 summarizes all of the data for the three impinger styles at a constant gas flow rate (4.48 ℓ/min). In general the data indicate that the performance of the straight-tube impinger with beads was not as good as the fritted design.

Clearly, one impinger cannot collect an acceptable percentage of the incoming ammonia at high flow rates and high gas concentrations; therefore, it was necessary to install several impingers in series. Figure 3.16 displays the results of the collection efficiency of

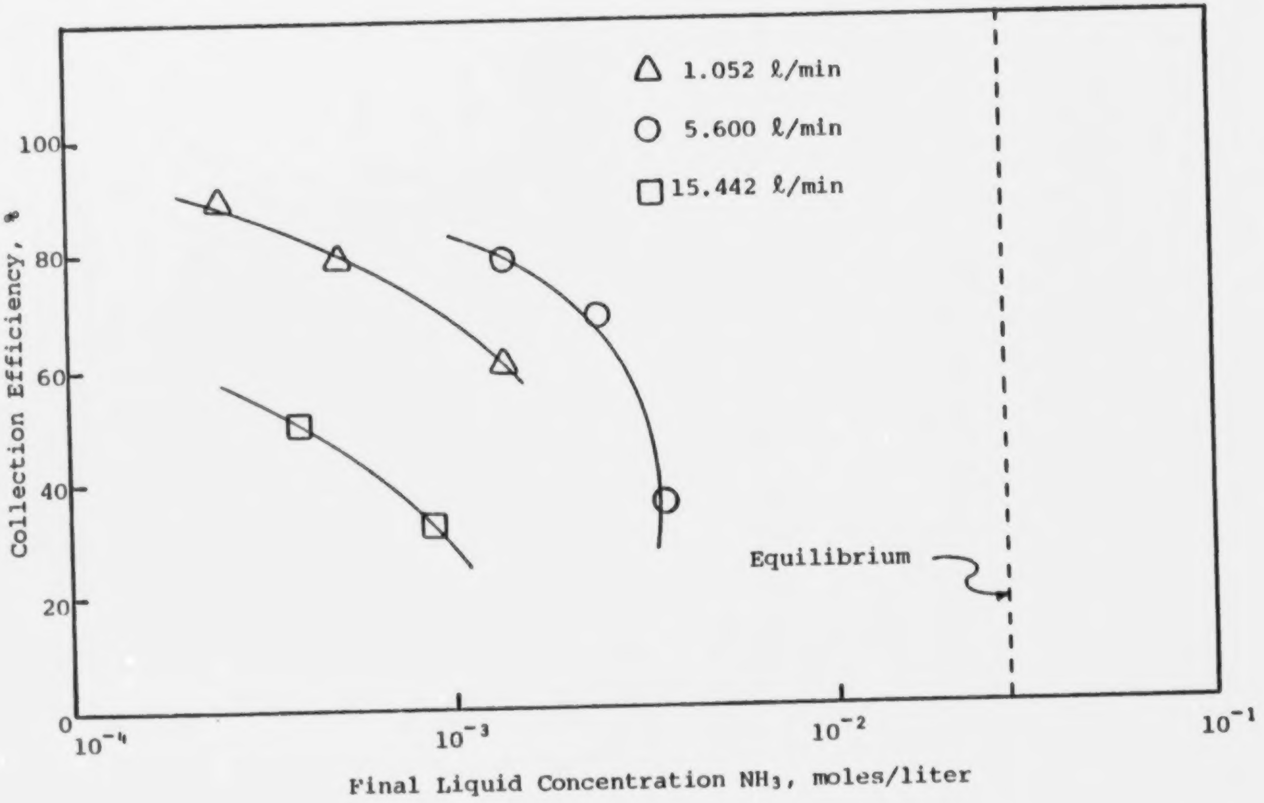

Figure 3.14 Effect of final liquid concentration on collection efficiency of the straight tube impinger with beads.

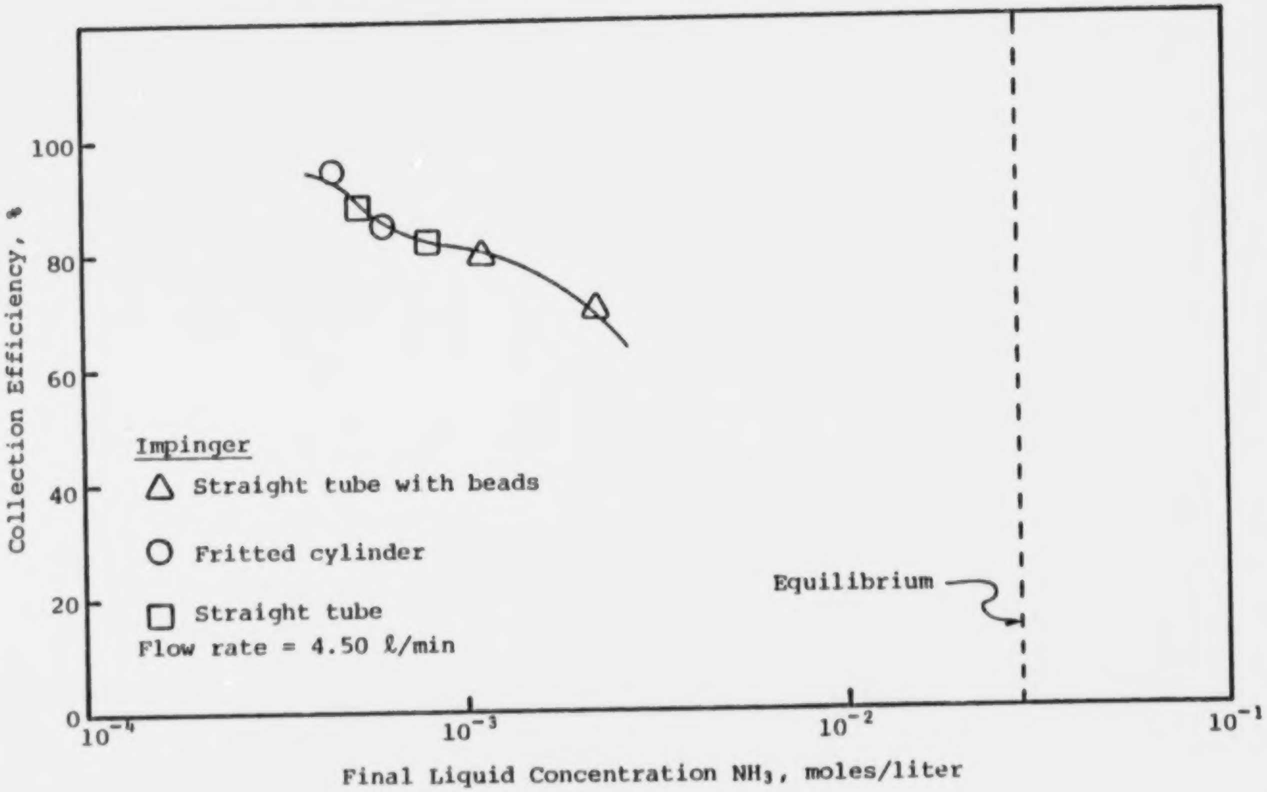

Figure 3.15 Effect of final liquid concentration on collection efficiency, constant flow rate, varying impinger design.

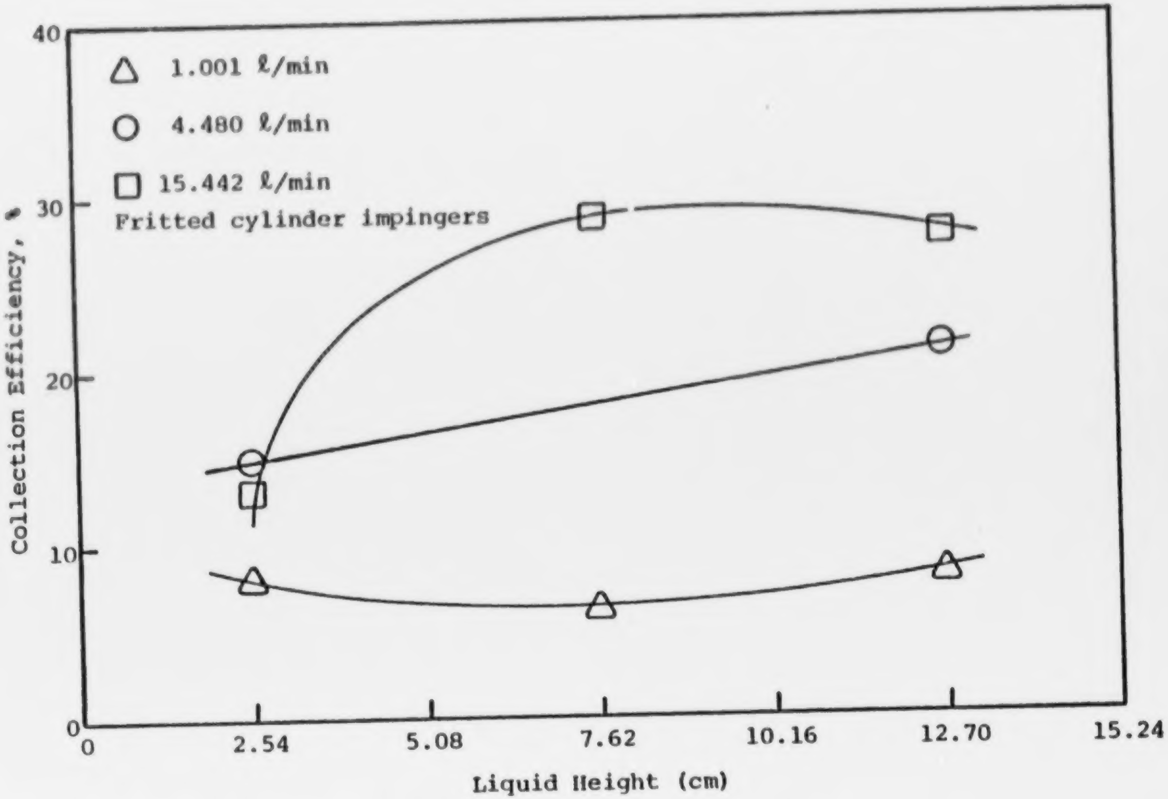

Figure 3.16 Liquid height versus collection efficiency for the second impinger in series.

the second impinger in series. The ordinate is the percent of ammonia collected that entered the second impinger. Five hundred fifty (550) ppm NH_3 balance N_2 entered the first impinger. As expected, when the flow rate increased, the efficiency increased. This was due in part to the higher concentration entering the second impinger from the first. The levels of ammonia in the second impinger were near the NH_3 probe's lower detection limit, and the levels in a third impinger in series were undetectable. Because of the inherent detection limit of the NH_3 probe and collection limit of the impingers, ammonia detection may not be 100 percent even with three impingers in series if the overall gas flow rate is too high for the impinger design and liquid level.

In the work presented thus far, 0.1 N H_2SO_4 was used as the scrubbing solution to simulate a furnace sample which would be acidic. Distilled and deionized (DD) water and 1.0 N NaOH were also investigated as alternative scrubbing solutions. DD water would be very convenient to use in the lab because no preparation is necessary and 1.0 NaOH would be convenient because it automatically compensates for the high-solution pH which is necessary for the operation of the NH_3 probe. Figure 3.17 shows collection efficiency of NH_3 for DD water and 1.0 N NaOH relative to 0.1 N H_2SO_4. DD water was found to collect 8 percent less NH_3 than the 0.1 N H_2SO_4 solution. 1.0 N NaOH collected 46 percent less NH_3 which was significantly lower than that collected by 0.1 N H_2SO_4. In conclusion, the 0.1 N H_2SO_4 was found to be the best scrubbing solution; but if necessary, DD water could be used.

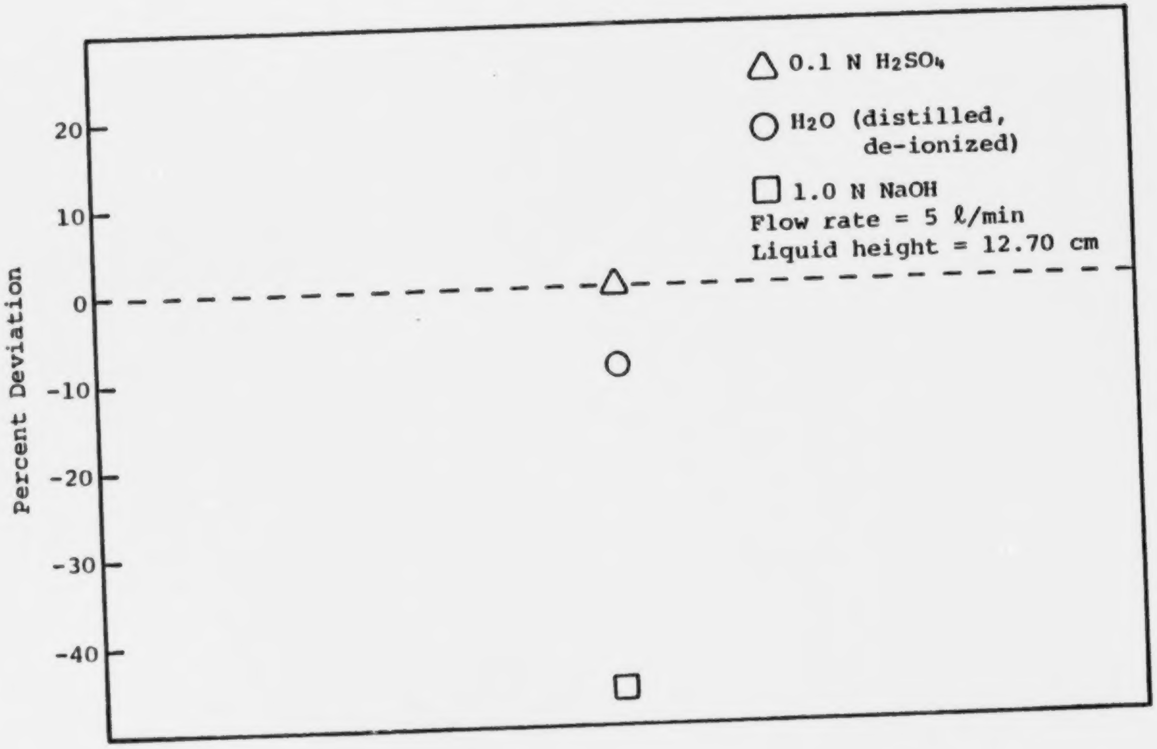

Figure 3.17 Percent deviation of contacting solutions using H_2SO_4 as the base case.

3.5 Probe System Verification

The gas-sampling waterspray probe was described earlier (Section 3.4). Therefore, only the modification of the probe will be treated here. A female-to-male Swagelok fitting was attached to the tip of the gas-sampling waterspray probe, enabling a gas-tight connection with the gas-mixing panel. This arrangement provided the flexibility required to characterize the waterspray probe.

The purpose of this test sequence was to check the efficiency of the waterspray probe without the aid of the collection system (i.e., impingers). DD water was selected as the spray solution. The incoming flow rate of ammonia to the probe was 5 liters per minute of 550 ppm NH_3 balance N_2. The collection efficiency of the waterspray probe was found to 97 percent. With two fritted impingers in series, collection efficiency rose to 98 percent. Changing the scrubbing solution to 0.1 N H_2SO_4 increased the collection efficiency to 99 percent. Without the spray and with the fritted impingers in series, the collection efficiency dropped to 95 percent.

Thus, with a 5.0 ℓpm sampling rate, the waterspray probe has very good collecting capabilities which are enhanced when the spray is 0.1 N H_2SO_4. Additional ammonia absorption will occur in the fritted impingers in series with the probe which increases the overall collection efficiency. The optimum total collection system, therefore, involves the waterspray probe with an 0.1 N H_2SO_4 spray followed by two fritted impingers connected in series. The second impinger would initially contain 300 mℓ of 0.1 N H_2SO_4, whereas the first impinger would collect the liquid phase exiting the waterspray probe.

3.6 Species Interference Study

Experiments were conducted to determine gas species which would interfere with the ammonia measurements. The experimental procedure was (1) prepare a precise mixture of the gas in question and the ammonia standard, (2) introduce this mixture into the water-spray probe with an 0.1 N H_2SO_4 spray, (3) collect the liquid phase exiting from the waterspray probe in the first fritted impinger, and (4) use a second fritted impinger containing 300 mℓ of 0.1 N H_2SO_4 for additional ammonia scrubbing. The collection system is shown in Figure 3.18. The gas mixture was prepared by utilizing the gas-mixing system described previously. The concentration of the gas in question was selected to simulate the levels expected in actual furnace systems. All of the gases used were certified standards supplied by Matheson Gas Products or by Linde. The liquid phase in the impingers was analyzed for ammonia by the ammonia probe. All of the experiments were also repeated with nitrogen in place of the investigated gas species to provide baseline data. The experiments with dimethylamine were conducted differently from those described above because dimethylamine was available in solution (25 percent dimethylamine in water). A 250 ppm dimethylamine in 0.1 N H_2SO_4 solution was prepared. The gas mixing system was connected directly to the two fritted impingers in series. The impingers contained 330 mℓ and 300 mℓ, respectively, of the prepared solution. A flow of 5 liters per minute of 135 ppm NH_3 in N_2 was provided to the impingers for 3 minutes from the gas-mixing system. The liquid phase in each impinger was then analyzed with the ammonia probe.

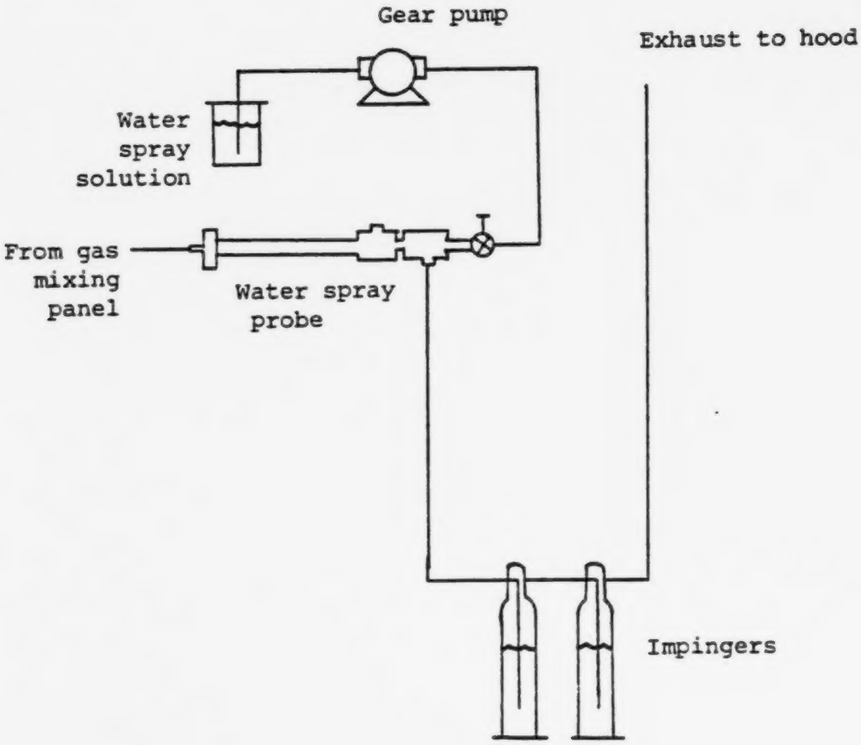
Gear pump
Exhaust to hood
Water spray solution
From gas mixing panel
Water spray probe
Impingers

Figure 3.18 Probe verification schematic.

Figure 3.19 displays the results of the aforementioned experiments. The ordinate represents the percent difference between experiments with the investigated gas species versus the baseline experiments. Sulfur dioxide and dimethylamine were found to alter the ammonia measurements significantly. The ammonia probe manufacturer warned of amine interference, and this admonishment was clearly substantiated. Interference from sulfur dioxide (SO_2) is due to the reactivity of SO_2 and NH_3 and the available residence time for mixing of those species between the gas-mixing system and the waterspray probe where these species were absorbed into the 0.1 N H_2SO_4 spray solution. When a much shorter residence time was provided, the amount of ammonia collected increased. These experiments demonstrate that two types of gas-phase interferences are of potential importance:

1. Other types of amine compounds produce a positive response, the probe is not entirely selective for NH_3 but also senses NH_i species;
2. Species such as SO_2 react with the NH_3 and therefore reduce the concentration of the free NH_3 measured by the probe.

The interferences of coal, coke and char on ammonia measurements were also investigated. The gas-mixing system was connected directly to two fritted impingers in series to perform these experiments. Each impinger contained 300 $m\ell$ of 0.1 N H_2SO_4 and 5 cm^3 of 1.6 millimeter (.063 inch) screenings of the solid in question. The ammonia standard of 550 ppm in N_2 was bubbled through the impingers at 5 liters per minute for 3 minutes. Baseline data were prepared by using the system as described, but without the addition of solids to

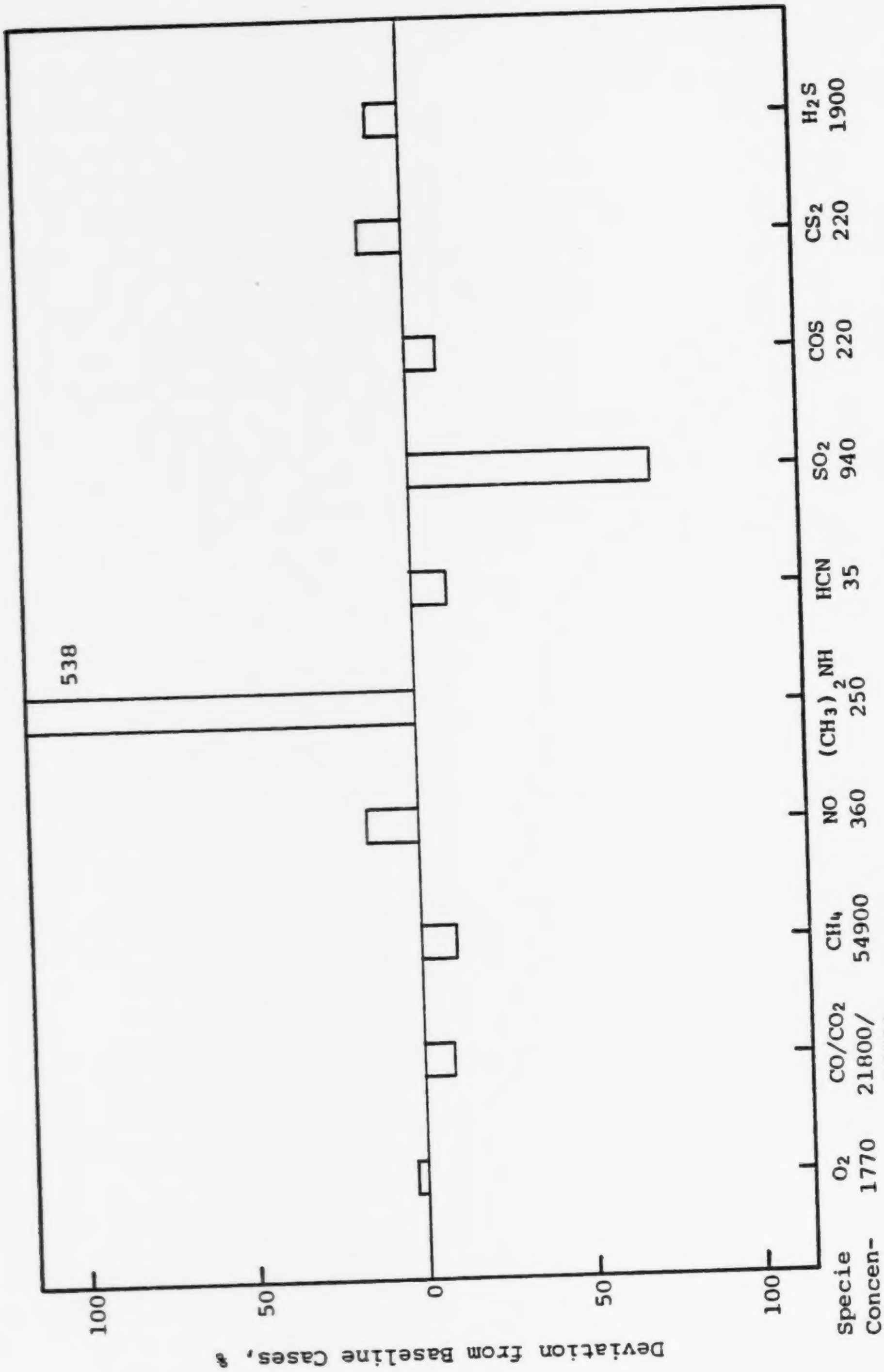

Figure 3.19 Gaseous specie interference.

the impingers. The liquid phase was then analyzed for ammonia with the ammonia probe. Figure 3.20 shows the result of the solids experiments which show no significant affect on the ammonia measurements.

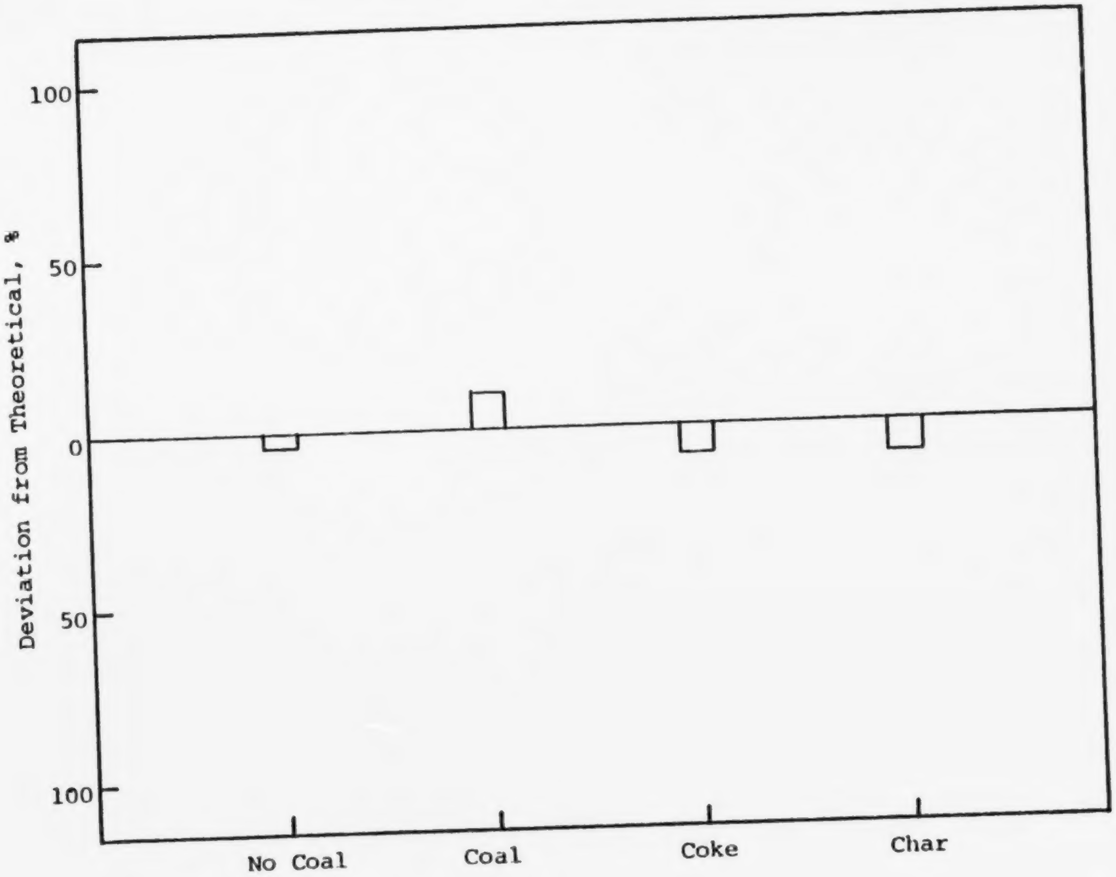

Figure 3.20 Solids interference.

CHAPTER 4

CYANIDE MEASUREMENT

4.1 Background

Hydrogen cyanide (HCN) and the cyanide ion (CN^-) are believed to play a major role in NO_x formation during combustion in furnaces. Because of the importance of hydrogen cyanide, an adequate technique for the measurement of it had to be developed anew or adapted from existing techniques.

Colormetric methods are available that will determine low levels of cyanide in aqueous solution, e.g., the pyridine-pyrozolone method, as described by Epstein (1947), and the similar method recommended in "Standard Methods for the Examination of Water and Wastewater" (1971). Both have a sensitivity of 33.3 μg per liter CN^- (33.3 ppb). To determine cyanide-ion concentrations in natural waters by the above methods, the cyanide must be separated from interfering substances. The separation is usually performed by distilling the cyanide from the acidified sample; this distillation will concentrate the cyanide and break down cyanide complexes.

Goulden, et al. (1972), found the aforementioned method did not give acceptable levels of cyanide recovery when the concentration of the initial solution was below 100 μg per liter CN^-. However, they outlined a modified version of Epstein's work which is capable of measuring cyanide concentrations down to 1.0 μg per liter.

Although the method by Goulden, et al., is as accurate as desired, the procedure required is time consuming and complex. A simpler and faster method involves the use of the specific ion electrode.

During the last decade, the cyanide ion electrode has been used increasingly by researchers for its fast, accurate, and dependable characteristics. Numerous advantages of the cyanide ion electrode over the colormetric methods are responsible for the extensive use of the electrode. Specifically, sample preparation is minimal, sample color and turbidity do not interfere with analysis, the electrode method is faster and simpler than colormetric methods (because laborious distillations are not required), and the electrode method is easily automated.

Of paramount concern are the selectivity of the cyanide ion electrode and anionic interferences. The cyanide ion electrode malfunctions if ions, forming soluble salts of silver, are present in sufficiently high levels. Possible anionic interferences that could form the aforementioned salts are sulfide, iodide, bromide, thiocyanide, and chorlide ions. Sekerka and Lechner (1976) noted that, as expected from the solubility products (K_{so}), the anions interfere in the order $S^{2-} > I^- > Br^- > CNS^- > CI^-$. The selectivity ratios of the interfering anions to the cyanide ion, as calculated by Sekerka and Lechner (1976) are <1 for S^{2-}, .1 for I^-, 10^3 for Br^-, and 10^5 for CNS^- and CI^-.

Cyanide will also complex with metal ions such as Cd^{++}, Zn^{++}, Ag^+, Ni^{++}, Ca^{++}, Fe^{++}, Fe^{+3}, Co^{+3}, and Hg^{++}. Cyanide must be in a free form to be detected by the cyanide ion electrode; therefore, a solution with cyanide complexes present must be treated to free the cyanide. To facilitate freeing of the cyanide ion from cyanide metal complexes, the complexes have been treated by acidification, by heating, and with EDTA, as detailed by Frant, et al. (1972). Sekerka and Lechner (1976) note there is a possibility of cyanide loss from evaporation by the aforementioned method; they outline another procedure for complex decomposition. Goulden, et al. (1972), have used UV irradiation successfully to decompose cyanide metal complexes. Several investigators believe this is the most reliable method for metal complex decomposition. In the present work, cyanide metal complex concentrations are negligible.

Sekerka and Lechner compared the cyanide electrode method to the ASTM (1970) colormetric method, and found the methods agreed within 10 percent down to a level of 2 ppb. Continuous monitoring of the mean level of cyanide was achieved by Fleet and Ho (1973) using a computerized Gran plot.

Because of the extensive literature on the suitability and speed of the electrode method for CN^- determination, this technique was chosen for initial evaluation as discussed in the following sections. Gas chromatography was also investigated in detail as a potential method for cyanide detection. Details of that investigation are contained in Chapter 5.

4.2 Theory

The cyanide electrode is constructed of a solid membrane which contains a mixture of silver sulfide and silver iodide bonded into the tip of the epoxy electrode body. When the membrane is in contact with a cyanide solution, silver ions dissolve from the membrane surface. Silver ions within the membrane migrate to the membrane surface to replace the dissolved ions, creating a potential difference. The potential difference is directly proportional to the cyanide ion concentration. This reaction is (Clysters and Adams, 1976]:

$$2CN^- + AgI \rightleftarrows Ag(CN)_2^- + I^- \quad .$$

The electrode follows the Nernst equation

$$E = E^\circ - k \ln a_{CN^-}$$

where E° is a reference potential and is constant, k is equal to RT/F, which is the electrode slope, and a_{CN^-} is the cyanide activity. The cyanide activity can be expressed

$$a_{CN^-} = \gamma_{CN^-} [CN^-] \qquad ,$$

where γ_{CN^-} is the ionic activity coefficient. If the total ionic strength is high and constant, relative to the detected ion concentration, the ionic activity coefficient will remain constant. Then the Nernst equation can be written

$$E = E^\circ - k \ln [CN^-]$$

where k is $RT/F \ln \gamma$, the modified electrode slope. The theoretical electrode slope at 25°C is 59.16 mV.

4.3 Electrode Calibration

The Orion Model 94-06 cyanide ion electrode was used throughout the studies. An Orion Model 90-02 double-junction reference electrode was used with the cyanide electrode. Constant-temperature experiments were achieved using a thermostated water bath. The solution was stirred by means of a magnetic stirrer, which was powered by the water recirculating pump in the water bath. Figure 4.1 is a schematic of the preliminary measurement system.

The initial parameters investigated were temperature, pH, and ionic strength. Analytic procedures were adhered to in the preparation of required solutions, and analytical reagent-grade chemicals were used throughout.

The effect of solution temperature on the electrode potential is shown in Figure 4.2. The three curves are linear to a cyanide concentration of .05 ppm and parallel throughout. The curve for 25°C lies approximately halfway between the curves for 20°C and 30°C; hence, it would be possible to interpolate between the curves for intermediate temperatures if necessary. For the purpose of standardization with the ammonia studies (Chapter 3), 25°C was chosen as the basis for further work. The slope of the 25°C curve is 56.4 ± 1.2 mV per decade of ppm. This slope is within 5 percent of the literature (Orion, 1977). All solutions were adjusted equally to a pH of 13 as recommended by Orion.

pH is a crucial parameter, for the cyanide electrode responds only to free cyanide ions. A pH of 11 is required for 98 percent of the cyanide present to be in the ionic state; this is shown in Figure 4.3. Fifty (50) percent of the cyanide present is in the ionic state at a pH of 9.2. Orion (1977) recommends using concentrated NaOH to accomplish the necessary pH adjustment to a pH of 13. Addition of NaOH also provides the necessary background ionic strength

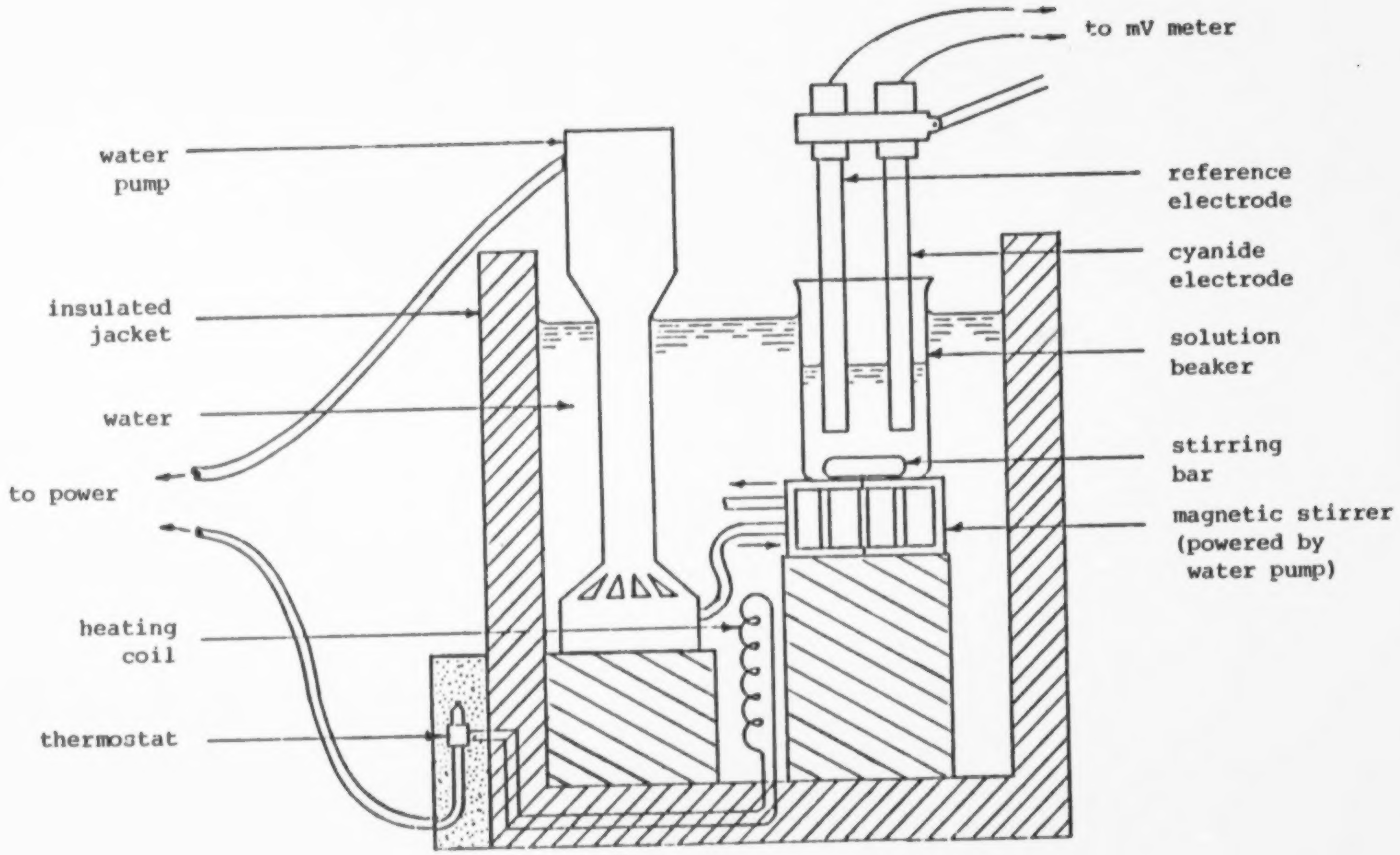
to mV meter
water pump
reference electrode
cyanide electrode
insulated jacket
solution beaker
water
stirring bar
to power
magnetic stirrer (powered by water pump)
heating coil
thermostat

Figure 4.1 Solution cyanide measurement apparatus.

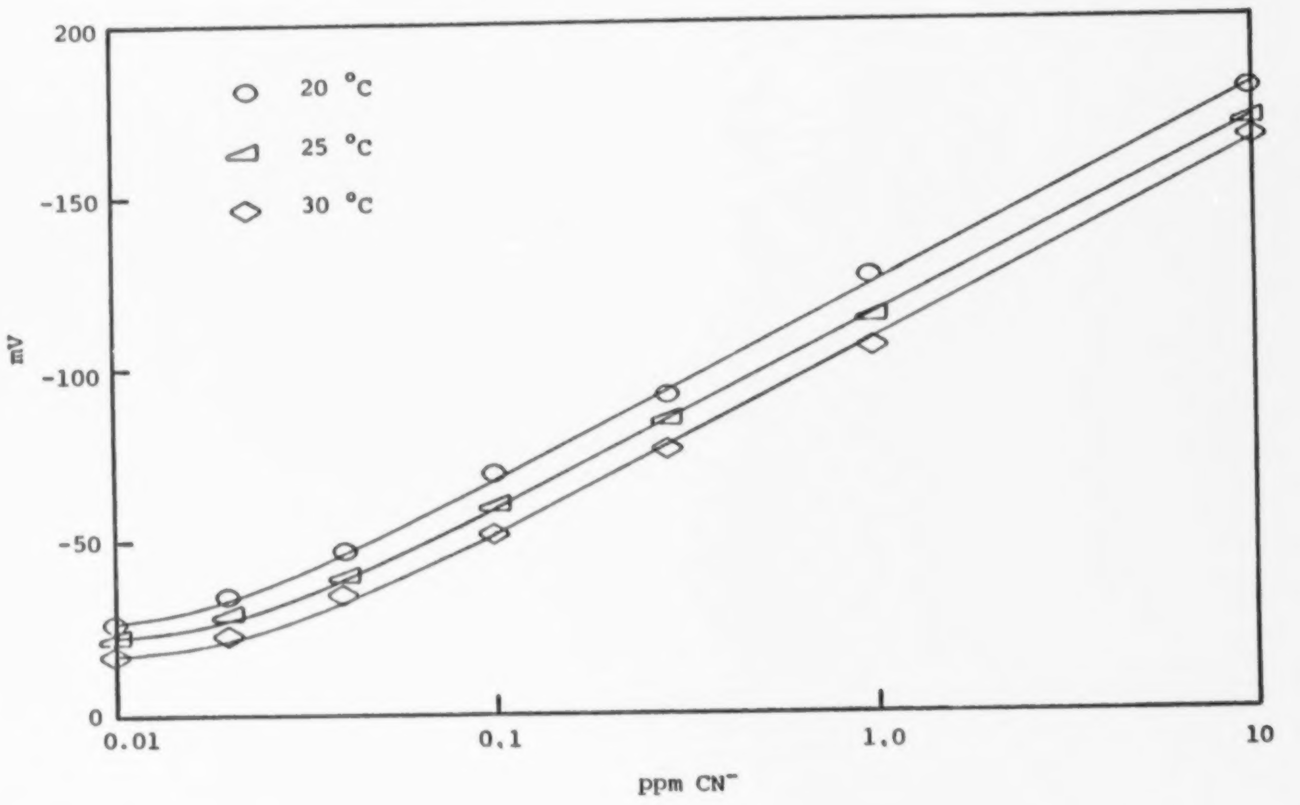

Figure 4.2 Influence of solution temperature on the cyanide electrode.

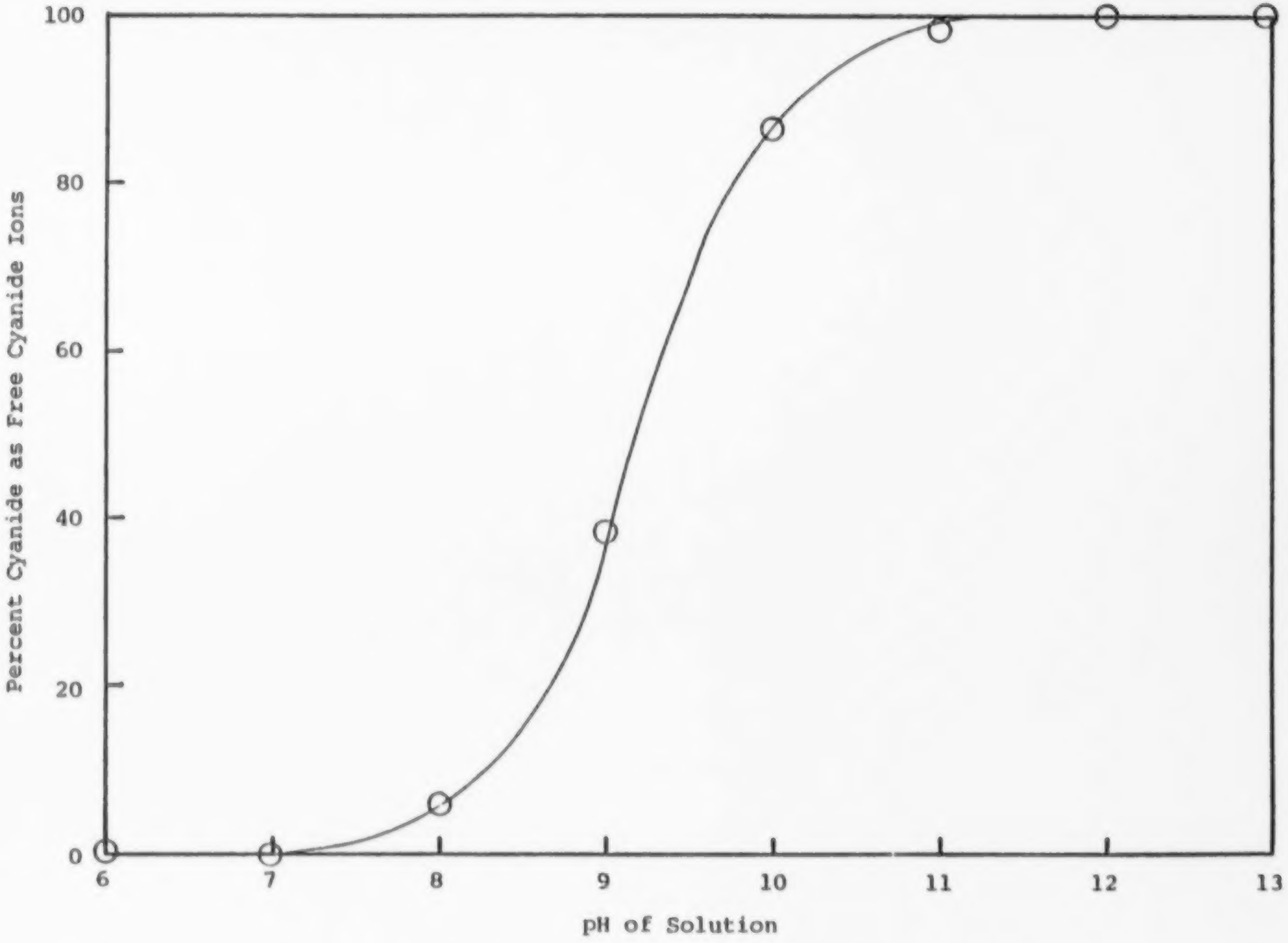

Figure 4.3 The effect of solution pH on the percentage of cyanide as free cyanide ions.

which is necessary for Nernstian behavior of the electrode. Figure 4.4 presents the results of a test series to define the influence of pH, and it shows a general decrease in the electrode potential as the pH is decreased. This is most dramatically represented by the .016 ppm CN^- curve. All solutions examined were initially adjusted to a pH of 13. The pH was then reduced by dropwise addition of 0.1 N H_2SO_4. When a pH of 13 was re-achieved after the stepwise increase of pH by NaOH addition, the electrode potential returned to its initial level. In conclusion, there is an effect of pH on the potential output of the electrode and it is most significant at low concentrations (<0.10 ppm CN^-). This effect is due in part to the total cyanide concentration not being in ionic form.

The same experimental procedure was conducted to examine ionic-strength effect on the electrode response. Figure 4.5 depicts the results of this experimentation. Initially, solutions of varying cyanide-ion concentration were adjusted to a pH of 12.9 with 10 M NaOH. The 2.0 and 10.0 ppm solutions were adjusted downward using 0.1 N H_2SO_4 to a pH of 5.9. The solutions were then adjusted upward to a pH of 11.9. As can be observed, the slope of each curve does not change significantly. But, as observed during the pH-related experiments, pH has a drastic effect on the potential output. In conclusion, although the ionic strength of ions added was increased ten-fold, there was no significant change in the slope of the curves, suggesting that the cyanide activity coefficient varied only slightly with the ionic-strength changes performed. Hence, the electrode followed Nernstian behavior when ionic strength was changed.

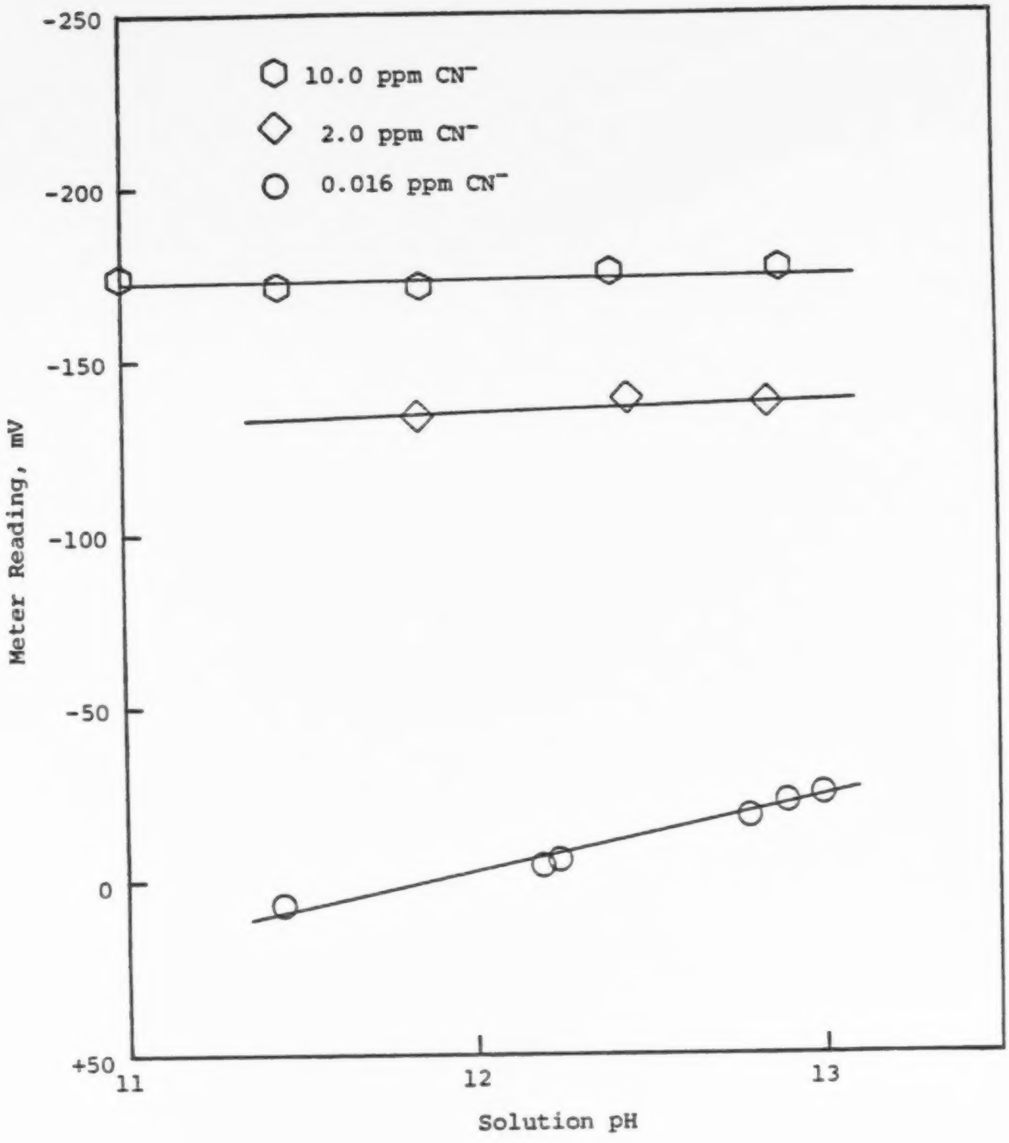

Figure 4.4 Influence of pH on the response of the cyanide electrode.

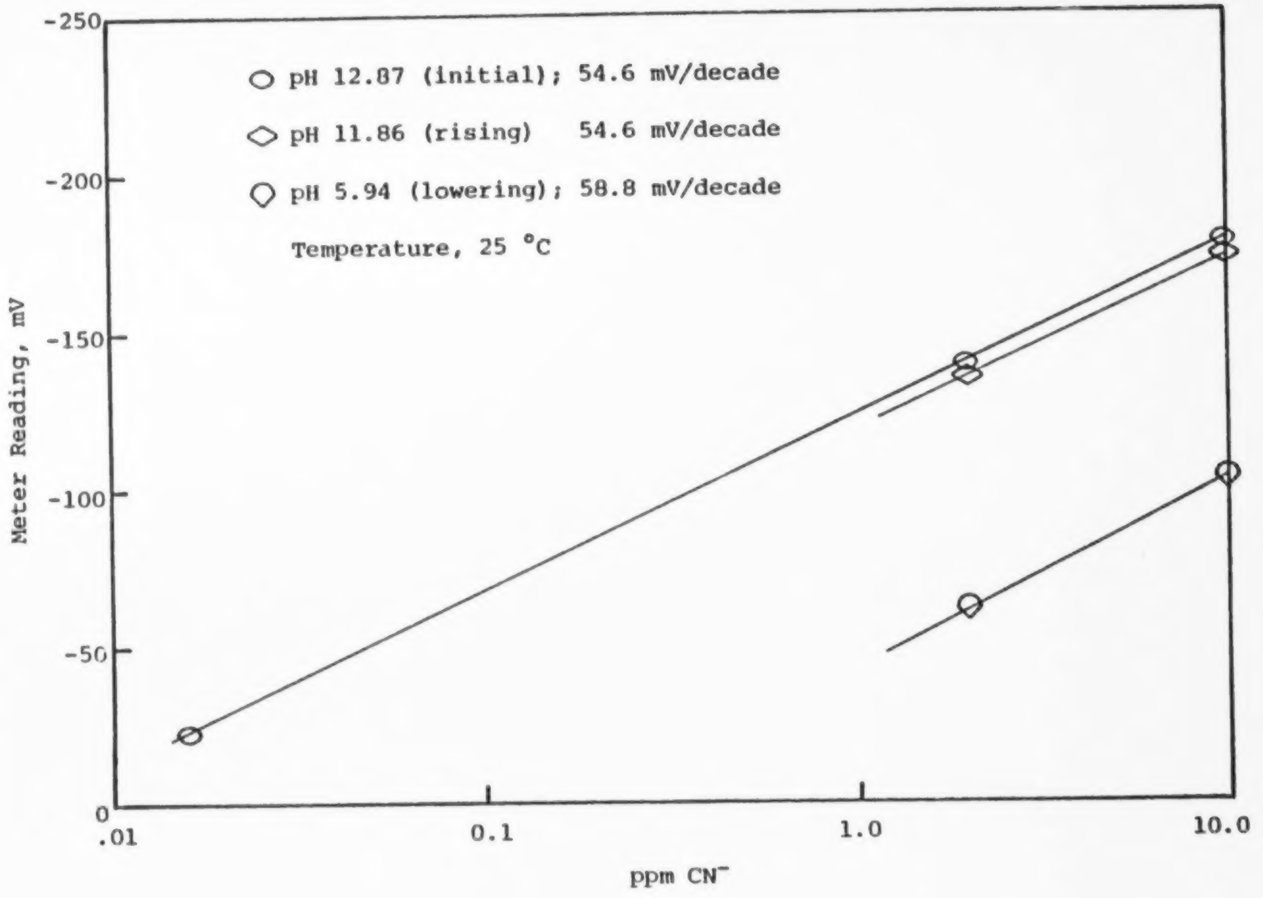

Figure 4.5 The effect of ionic strength on the response of the cyanide electrode.

A standard calibration curve for the cyanide electrode was prepared and is shown in Figure 4.6. Standard cyanide solutions were made using 0.1 N H_2SO_4 as the solute since ammonia absorption is enhanced by an acidic solute. Addition of 2.0 mℓ of 10 M NaOH to every 100 mℓ of solution was necessary to bring the pH to 12.8. The solution temperature was held at 25°C during electrode potential measurements. A straight-line calibration curve was obtained only if the potential measurements were made in the order from low concentrations to high concentrations. When electrode potential measurements were taken in reverse order, the calibration curve began to curve downward at 0.05 ppm. This effect is due to the membrane degradation of the electrode, which warrants polishing the membrane of the electrode, as specified by Orion (1977). In light of this observed hystersis effect, it is recommended that the cyanide electrode be conditioned with a solution of low cyanide concentration in comparison with the solution upon which measurements are to be made. This recommendation appears to be critical for solutions of less than 0.05 ppm cyanide-ion concentration.

4.4 Collection System

The collection system for cyanide was the optimum collection system developed for the previous ammonia studies. Thus, the system used was two fritted cylinder impingers in series containing 300 mℓ of contacting solution.

Contacting solutions were investigated. Those solutions were distilled deionized water, 0.1 N H_2SO_4, and 1.0 M NaOH. To test the efficiency of the bubblers as a function of contacting solution, a

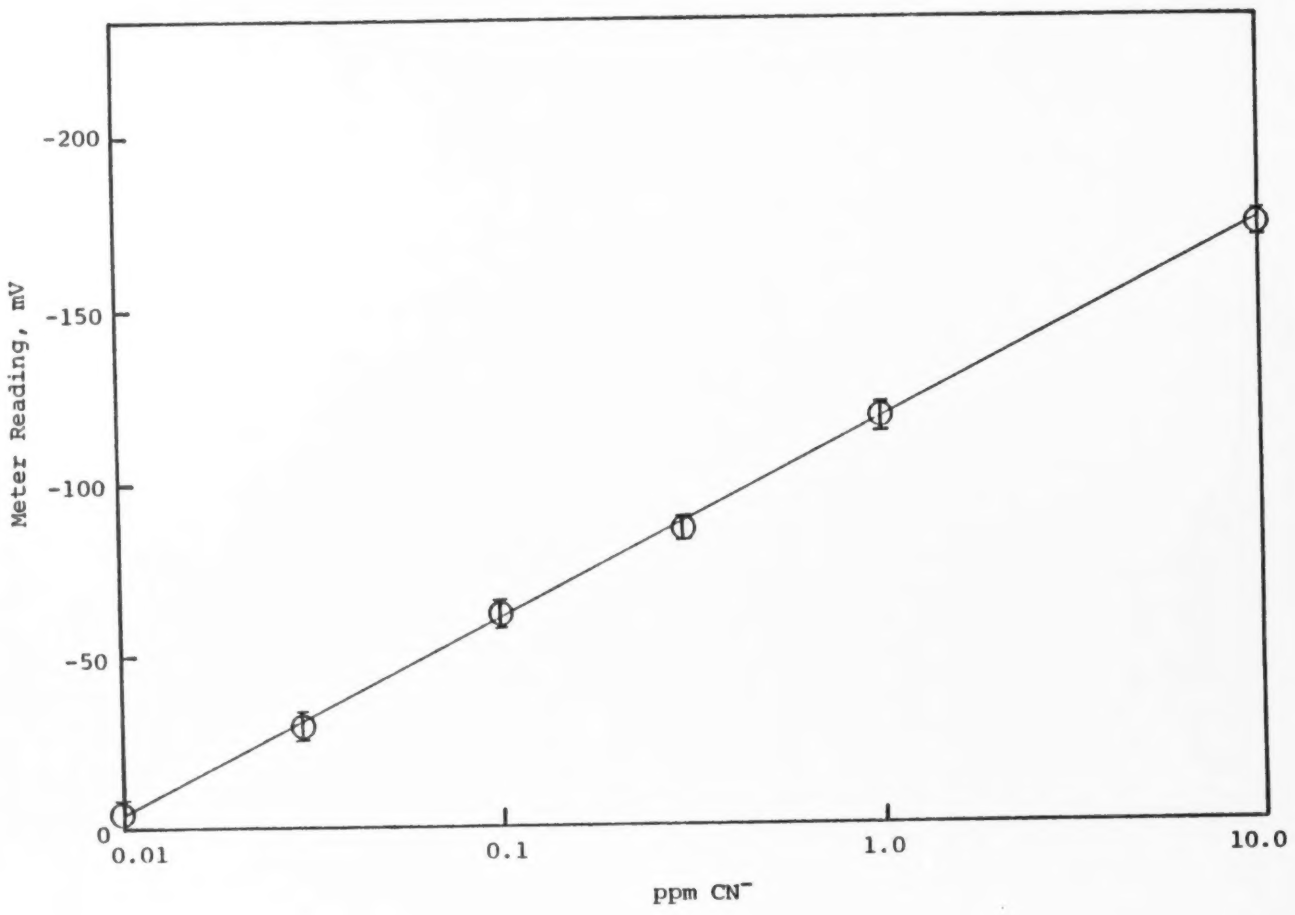

Figure 4.6 Standard calibration curve for the cyanide electrode at 25 °C.

known amount of hydrogen-cyanide gas was bubbled through two fritted cylinders in series. The gas-mixing panel was used to produce an accurate flow of cyanide gas to the impingers. The first bubbler accomplished 80 percent absorption and the second bubbler absorbed 5 percent of the total cyanide; therefore, a total of 85 percent of the incoming cyanide was absorbed (Table 4.1). Interestingly, there was no significant effect of contacting solution on collection efficiency. In addition, the same level of absorption was attained when the spray probe was connected in series with the impingers. The spray was the same as the contacting solution in the impingers.

As noted above, total absorption was not attained with any scrubbing solution; and this shortcoming must be taken into consideration when implementing this method. This method is, however, still very useful because of its simplicity and limited time requirements.

4.5 Interferences

Orion's list of possible interfering ions that would cause electrode malfunction includes $S^{=}$, I^{-}, Br^{-}, $C\ell^{-}$. The latter three ions are not available in combustion systems in concentrations that would cause the electrode to malfunction. However, the sulfide ion is a major concern, and it must be totally eliminated from the solution before the cyanide electrode is used. If sulfide ions are present, they will form an insoluble silver salt layer on the membrane surface of the electrode, rendering the electrode inoperable. Other potential interferants investigated were amines, NO, and SO_2, none of which caused significant deviation in the performance of the cyanide electrode.

Table 4-1

Contacting Solution	Theoretical 6.88 ppm		Theoretical 10.28 ppm	
	Imp. 1	Imp. 2	Imp. 1	Imp. 2
0.1 N H_2SO_4	5.43 ppm	0.18 ppm	8.20 ppm	0.51 ppm
H_2O	5.47 ppm	0.30 ppm	8.28 ppm	0.52 ppm
1.0 N NaOH	5.67 ppm	0.01 ppm	8.34 ppm	0.46 ppm

Sulfide removal has been addressed by several investigators. Riseman (1972) attempted sulfide removal by precipitation using a slight excess of lead. This method did not remove the sulfide ion satisfactorily. Sekerka and Lechner (1976) investigated Bi^{+3} addition to remove sulfide by precipitation, and found bismuth removed sulfide adquately. Additional studies were conducted as part of the present investigation to quantify the $Bi^{+3}/S^{=}$ ratio necessary to remove the sulfide ions adequately. Figure 4.7 shows the results of the investigation. A ratio of 4 ($Bi^{+3}/S^{=}$) is inadequate, but ratios of 33 and 100 are adequate to induce the necessary sulfide-ion capture. Degradation of the electrode membrane was not apparent when $Bi^{+3}/S^{=}$ ratios were kept above 30.

4.6 Conclusion

The simplicity and speed of the electrode method make it extremely attractive; the only major drawback appears to be a slightly low collection efficiency at the standard test conditions. With the spray probe, two fritted cylinder impingers in series, an 0.1 N H_2SO_4 absorbing solution, and a gas sample rate of 5 ℓ/min, the overall collection efficiency was found to be 85 percent. Further, this efficiency could not be improved significantly by changing the absorbing solution to either 1.0 N NaOH or H_2O.

The electrode exhibited a linear response from 0.01 through 10.0 ppm CN^- at 25°C. The only major interference was $S^{=}$ which was eliminated satisfactorily by the addition of excess bismuth trinitrate.

In conclusion, this method appears satisfactory for in-flame HCN measurements where extreme accuracy is not required.

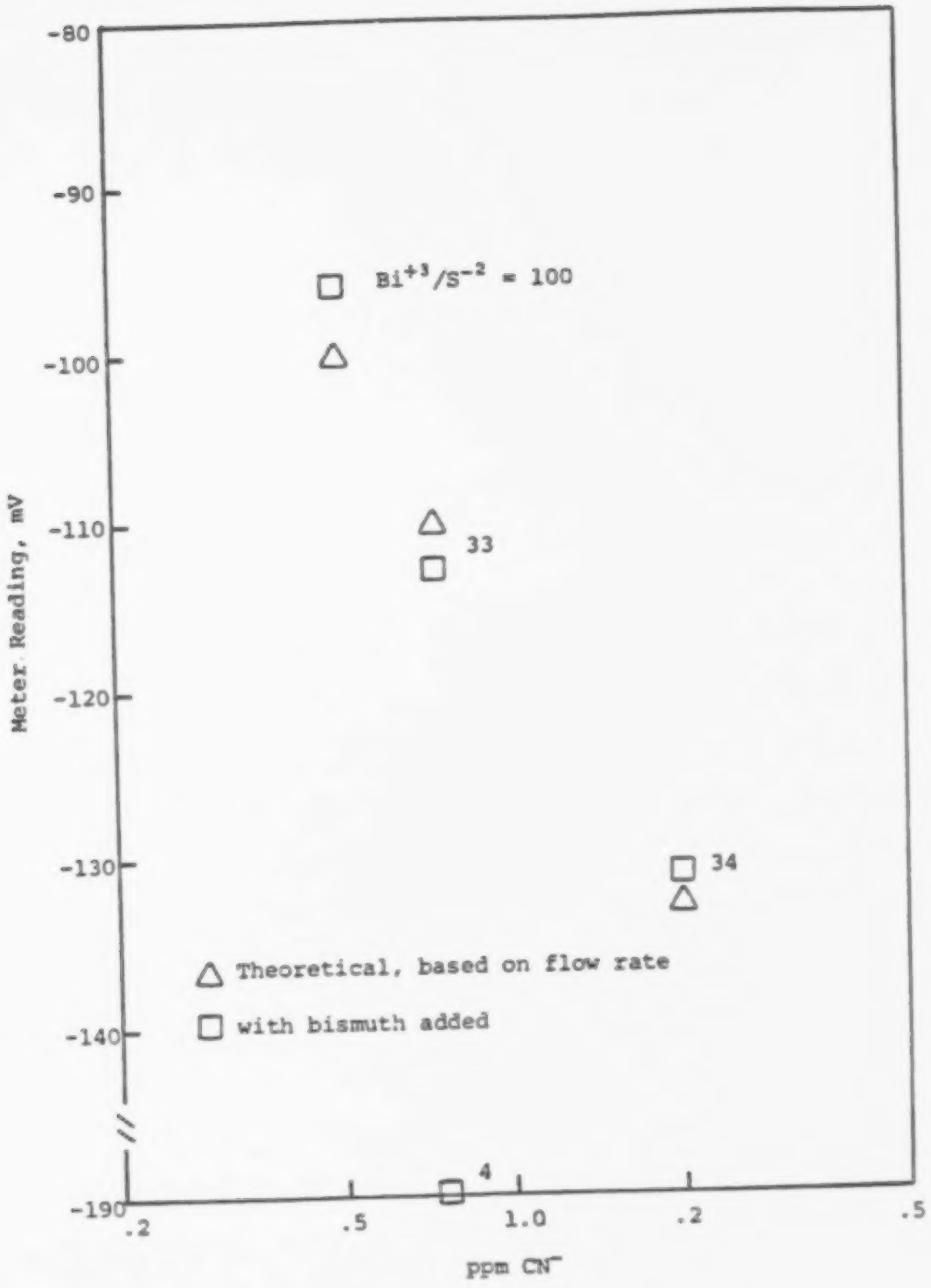

Figure 4.7 $S^=$ interference removal.

CHAPTER 5

ANALYTICAL SYSTEMS - FURNACE STUDIES

5.1 Choke Temperature Measurement

In past work by Mason (1980), a chromel-alumel thermocouple was inserted into the gas flow to measure the temperature of the combustion gases. In that study it was discussed that the thermocouple readings were lower than the true temperature of the gases because of radiation effects to the furnace walls. To obtain more precise gas temperature measurements at the end of the first combustion stage, a suction pyrometer designed and built by Purcell (1981) was used. The suction pyrometer (see Figure 5.1) uses a vacuum pump to draw the hot gases out of the main stream and through a 1.27-centimeter (1/2-inch), tubular, ceramic probe. Inside the ceramic probe are seven 0.48-centimeter (3/16 -inch) diameter ceramic tubes arranged in a honeycomb fashion. A platinum-platinum,

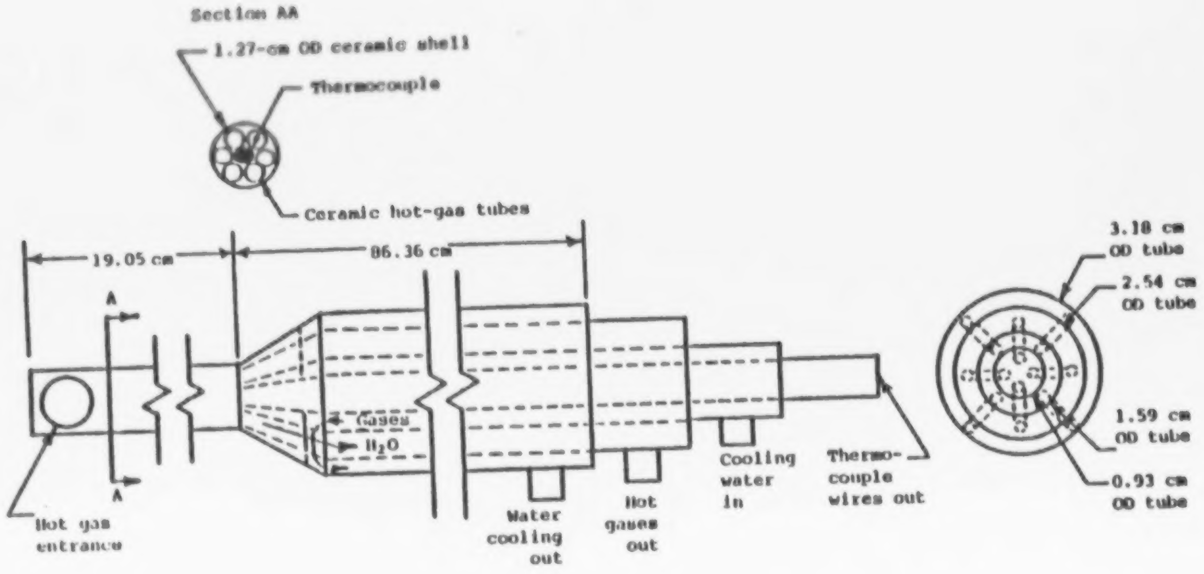
Section AA
1.27-cm OD ceramic shell
Thermocouple
Ceramic hot-gas tubes
19.05 cm
86.36 cm
A
A
Gases
H_2O
Hot gas entrance
Water cooling out
Hot gases out
Cooling water in
Thermo-couple wires out
3.18 cm OD tube
2.54 cm OD tube
1.59 cm OD tube
0.93 cm OD tube

Figure 5.1 Suction pyrometer schematic.

13-percent rhodium thermocouple is placed in the center tube with the hot gases passing through the peripheral tubes. This design insulates the thermocouple from possible radiation effects of the outside ceramic walls. The hot gases are then passed between two stainless-steel waterjackets, an outer jacket to protect the probe and an inner jacket to protect the thermocouple wires. Before it reaches the vacuum pump, the gas is cooled to 2 °C in an ice bath where the water vapor condenses. The water is then separated from the remaining gases in a knockout drum. This precaution is taken to protect the vacuum pump from possible contamination. The combustion gases are then vented from the vacuum pump. The temperature was monitored by a Doric Trendicator digital thermocouple readout.

5.2 NH_3 - HCN Waterspray Probe

This combustion study focused on the fate of the nitrogen molecules (added to the fuel in the form of ammonia) at the end of the primary combustion stage. This required that internal measurements be made in the choking section of the furnace for NO_x, NH_3, and HCN. The NO_x measurements are described in the following section. Because of the highly reactive nature of NH_3 and HCN, it was determined that these species could be more easily measured as ions in a water solution than as gases. For this purpose, a probe with a water spray feature was constructed.

The waterspray probe (see Figure 5.2) consists of an 0.95-centimeter (3/8-inch) I.D. stainless-steel, water-jacketed probe 1.52 meters (5 feet) long. This length enabled the probe to reach the choke from the rear of the furnace. Down the center of the probe was placed an 0.32-centimeter (0.125-inch) diameter stainless-steel

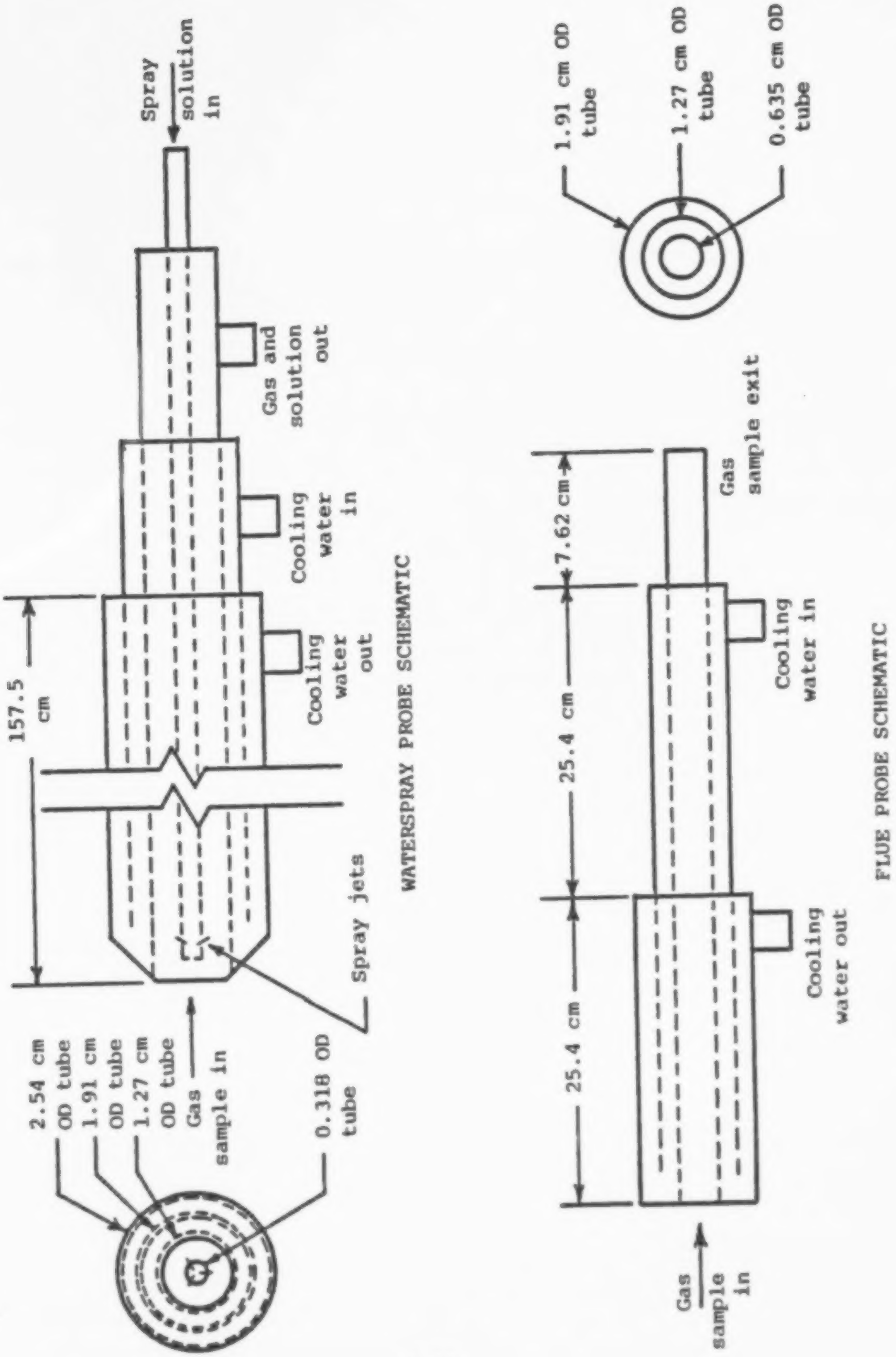
WATERSPRAY PROBE SCHEMATIC

FLUE PROBE SCHEMATIC

2.54 cm OD tube
1.91 cm OD tube
1.27 cm OD tube
Gas sample in
0.318 OD tube
Spray jets
157.5 cm
Cooling water out
Cooling water in
Gas and solution out
Spray solution in
Gas sample in
25.4 cm
25.4 cm
7.62 cm
Cooling water out
Cooling water in
Gas sample exit
1.91 cm OD tube
1.27 cm OD tube
0.635 cm OD tube

Figure 5.2 Flue and waterspray probe schematics.

tube supported at one-foot intervals. The end of the small tube was closed off and three equally spaced (0.0397 centimeters) holes, angled backward, were placed 0.32 centimeter (1/8 inch) from the closed end. As the sample pump draws a gas sample down the probe, an 0.1 N H_2SO_4 solution is pumped down the center tube by a Micro Pump, No. 120-411-10A, through the small holes near the end and into the gaseous stream sample. The NH_3 and HCN preferentially dissolve out of the gas into the solution. The gas and solution exiting from the rear of the probe are then separated in a stripping operation by two impingers in series. The solution is collected in the impingers while the gas continues on through an ice bath, knockout drum, glass-wool filter, desiccant dryer, Singer dry-gas meter, Model No. DTM 115, and sample pump (see Figure 5.3). The ice bath and knock-out drum are used to take the water vapor out of the gas and, with the glass-wool filter being used to take any particulates out of the gas, it is ensured that a clean gas stream is fed into the dry-gas meter. A bypass valve on the sample pump was used to vary the gas flow rate. Analysis for NH_3 and HCN in the captured liquid was performed as described in Chapters 3 and 4.

5.3 Gas Sampling System

The concentrations of NO, CO, CO_2, and O_2 were monitored at the end of the first stage in the choke and in the flue by methods previously described by Mason (1980).

The sample flow is diagrammed in Figure 5.4. A stainless-steel, water-jacketed probe (shown in Figure 5.2) is used for withdrawing a continuous sample from the furnace. The gas is then cooled to about 2 °C in a refrigerated, 0.95 centimeter (3/8 inch)

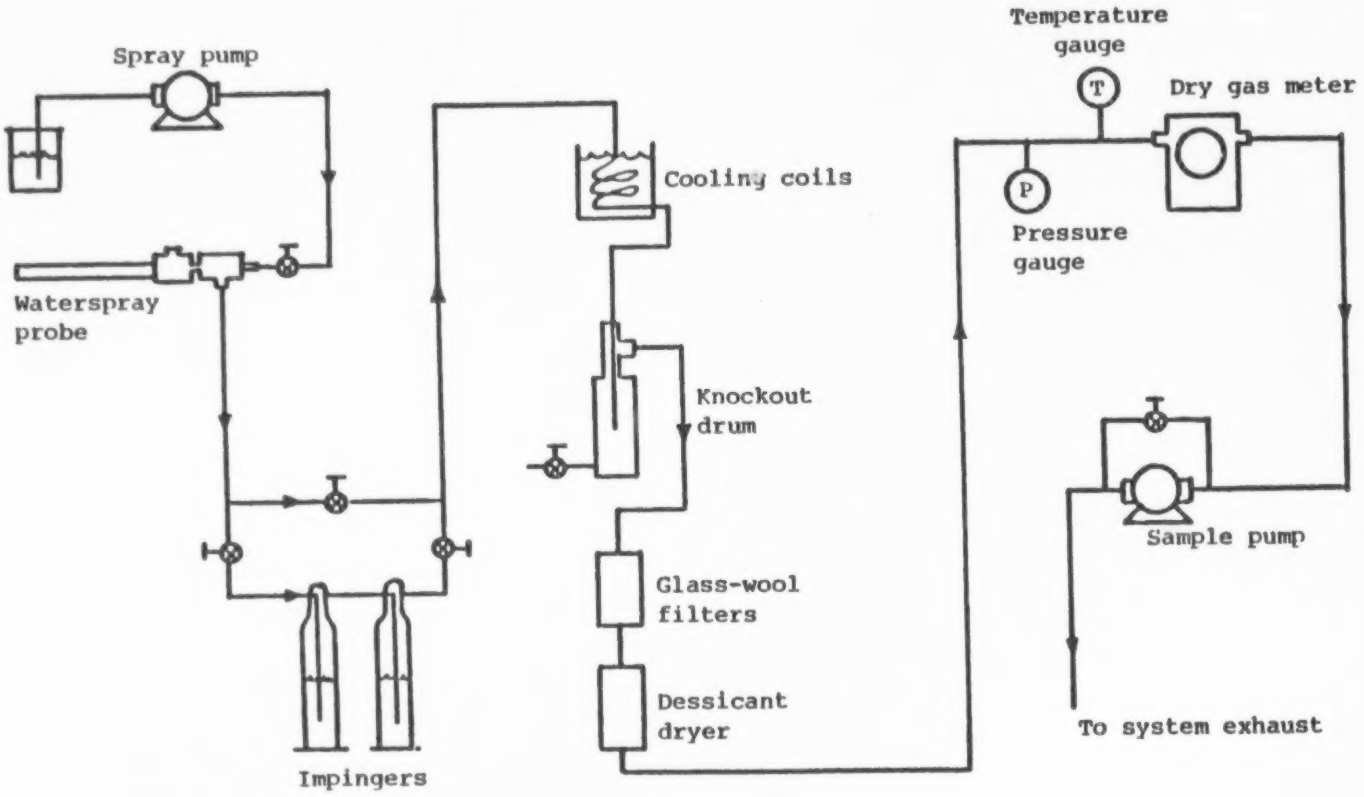

Spray pump
Waterspray probe
Impingers
Cooling coils
Knockout drum
Glass-wool filters
Dessicant dryer
Temperature gauge
T
Pressure gauge
P
Dry gas meter
Sample pump
To system exhaust

Figure 5.3. Intermediate species sampling flowsheet.

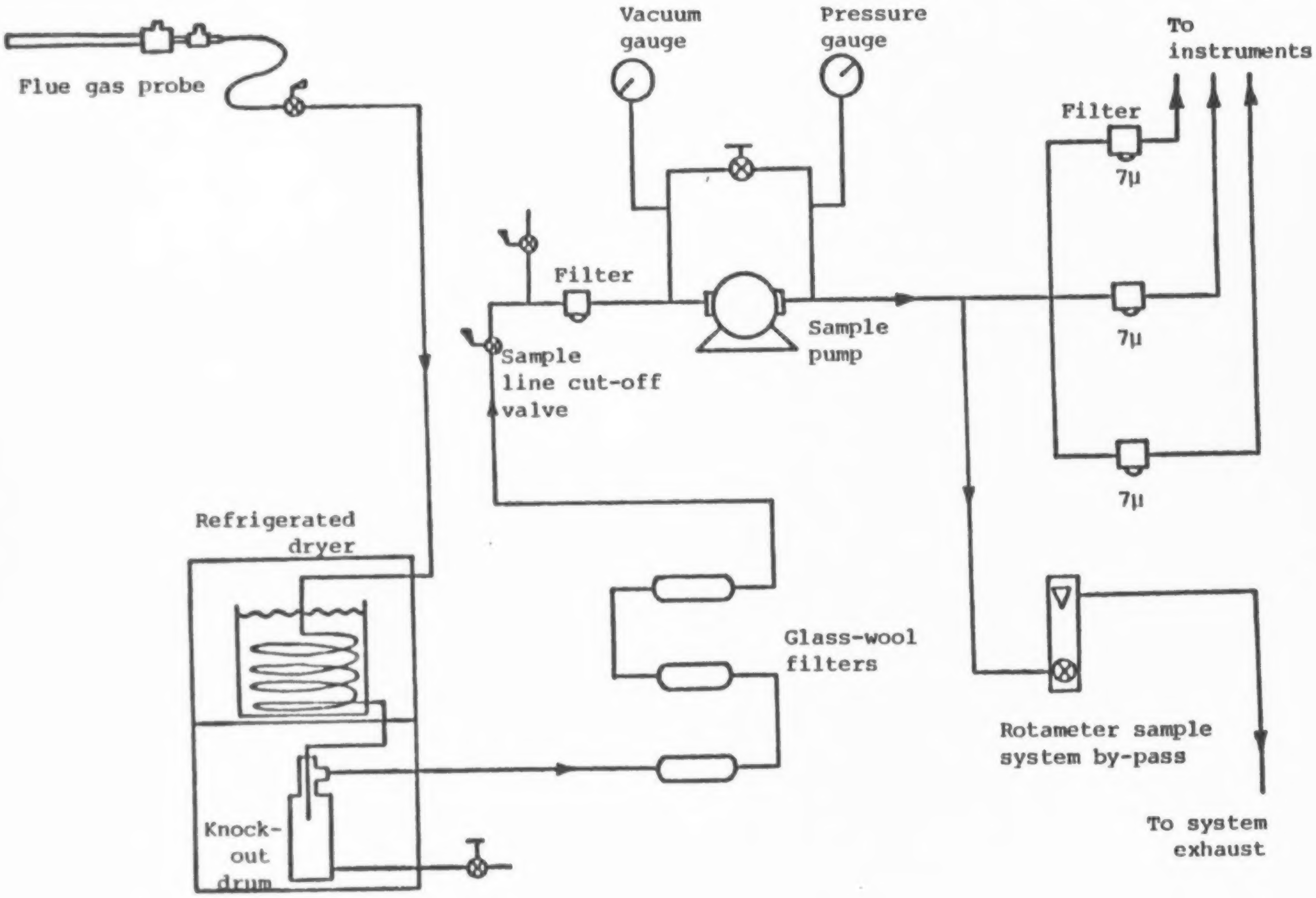
Flue gas probe
Vacuum gauge
Pressure gauge
To instruments
Filter
7µ
7µ
7µ
Filter
Sample line cut-off valve
Sample pump
Refrigerated dryer
Knock-out drum
Glass-wool filters
Rotameter sample system by-pass
To system exhaust

Figure 5.4. Gas-sampling system flow diagram.

stainless-steel coil upon which the water vapor condenses. Subsequently, the water is collected in the knockout drum and the sample is pulled through glass-wool filters and then through the stainless steel/teflon sample pump. The system is equipped with a bypass which accommodates the slow sample rate. This bypass allows a larger sample rate, thus decreasing the sample transport lag time. The sample pump (Thomas 727, diaphragm) also has a recycle bypass to decrease pump duty when only the instruments are passing sample.

The gas sample was analyzed continuously for NO, CO, CO_2, and O_2 concentrations. The analytical panel houses four principal instruments: a Thermo Electron, Model 10A Chemiluminescent NO-NO_x gas analyzer; an Anarad, Model AR-600 Infrared CO-CO_2 analyzer; a Beckman, Model 775 O_2 analyzer; and a Doric Trendicator 402A digital thermocouple readout. A stripchart recorder was used to record both the NO and O_2 concentrations. The CO and CO_2 percentages were read directly from the instruments. Various furnace thermocouples were monitored using the Trendicator readout. The toggle valves coupled the instruments with appropriate calibration and purge gases (stored in high-pressure cylinders), in addition to the sample gas.

CHAPTER 6

FURNACE SYSTEMS

6.1 Combustion Chamber

The experimental apparatus used in this work has been described in detail by Mason (1980). Therefore, only a brief summary of these furnace systems follows, with a detailed description of the modifications undertaken for this study.

The experimental work was carried out in a staged-combustion, horizontal, 11.43-centimeter (4.5-inch) diameter tunnel furnace. The dimensions of this furnace and various features are depicted schematically in Figure 6.1. The furnace is suitable for oil and gas combustion at firing rates up to 20.5 kW (70,000 Btu/hr). The six sections that comprise the furnace each have a mild steel shell to which copper cooling coils have been soldered. This provides cooling to the outside shell, thereby preventing possible hazardous conditions. The shell sections are lined with two inches of Insulblok 19 insulation block from A. P. Green Refractories. The central core was cast using the insulating refractory Casto-O-Lite 30, also by A. P. Green Refractories. A typical sectional view is shown in Figure 6.1.

Section (1) is the burner section. On the forward-end plate are six studs which provide the support for the burners. Various burners have been described by Mason (1980). In this study the diffusion Burner (Figure 6.2) was utilized and operated in the radial

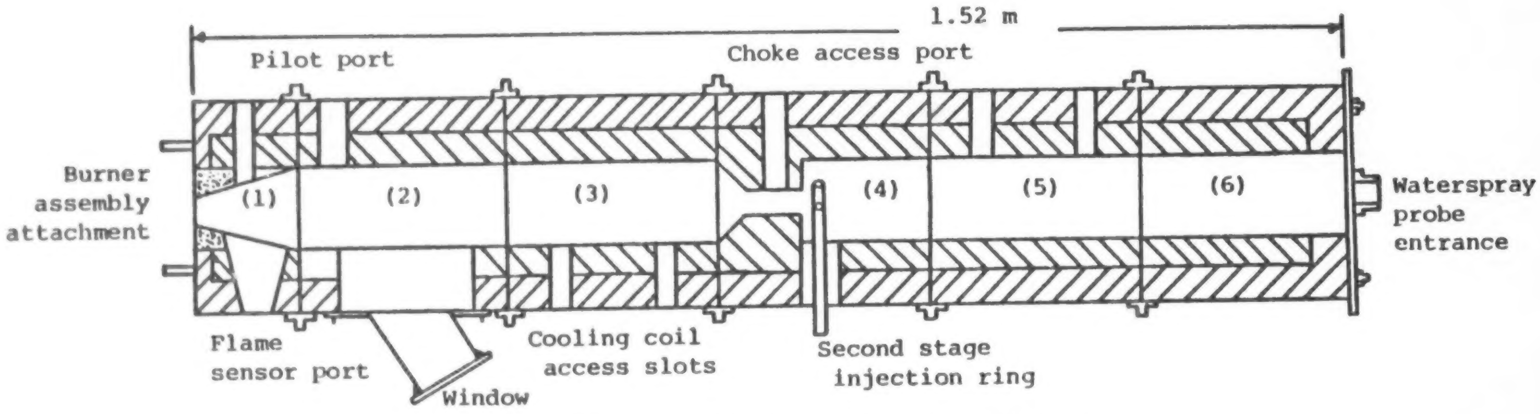
1.52 m
Pilot port
Choke access port
Burner assembly attachment
(1)
(2)
(3)
(4)
(5)
(6)
Waterspray probe entrance
Flame sensor port
Window
Cooling coil access slots
Second stage injection ring

BOTTOM SECTIONAL VIEW: FURNACE SCHEMATIC

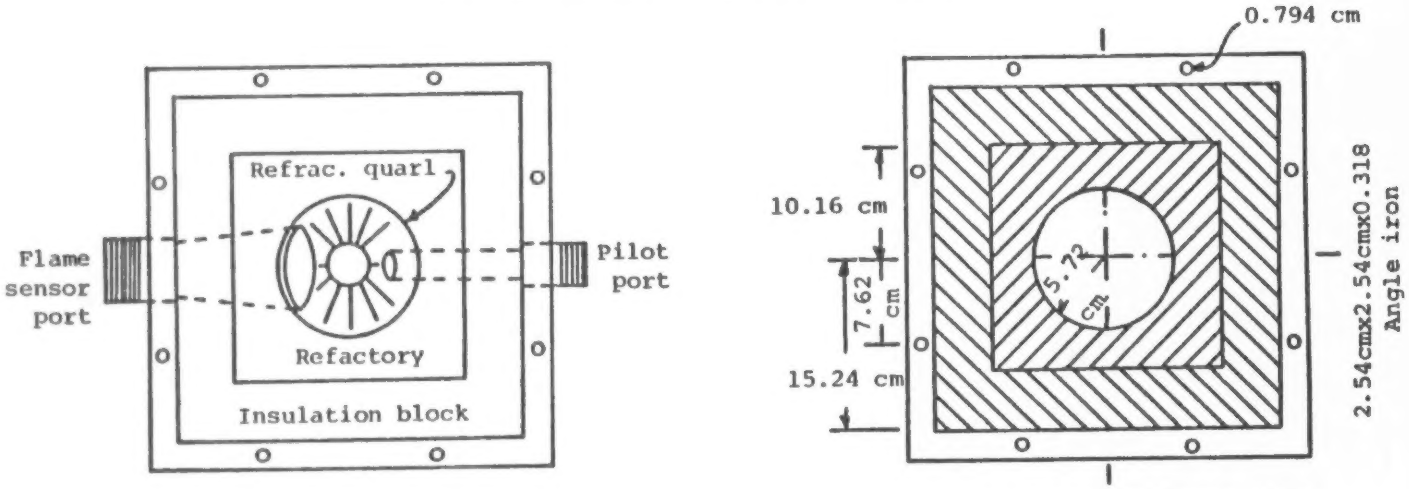
Refrac. quarl
Flame sensor port
Pilot port
Refactory
Insulation block
0.794 cm
10.16 cm
7.62 cm
15.24 cm
5.72 cm
2.54cmx2.54cmx0.318 Angle iron

FRONT BURNER SECTION, FLANGED-END VIEW

FURNACE CROSS-SECTIONAL VIEW

Figure 6.1 Gas/oil furnace schematic.

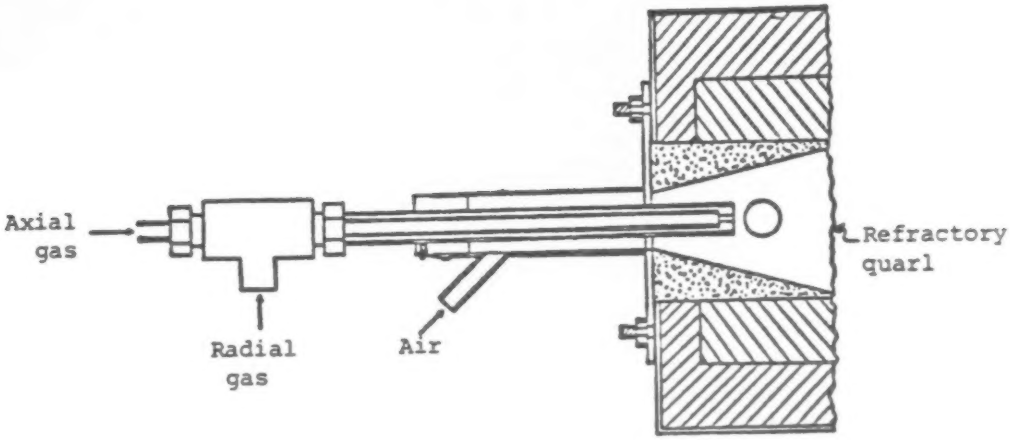
Axial gas
Radial gas
Air
Refractory quarl

Figure 6.2 Diffusion burner, cross-sectional view.

gas mode. The pilot port is attached perpendicular to the tunnel and primary-burner axis. The pilot port is equipped with a spark-plug ignition system. The ultraviolet detector for the flame safety system is also connected in line with the pilot assembly.

Section (2) has a quartz window to allow viewing of the first-stage combustion. In previous work a rectangular window was bolted to the outer shell. This proved to be ineffective as it placed the quartz window within 15.24 centimeters (6 inches) of the flame zone, which resulted in soot and other combustion products being deposited, blocking all sight. This problem was alleviated by replacing the rectangular window with a round viewing port extending away from the furnace shell. At the end of the port, 38.1 centimeters (15 inches) from the center of the flame zone, was placed an 11.43-centimeter (4.5-inch) diameter, 0.64 centimeter (0.25 inch)-thick quartz window. The port was placed at a 60° angle to the tunnel in the furnace to gain a better view angle of the initial flame area (see Figure 6.3). Cooling coils were soldered to the outside of the port to provide for the proper cooling. This new viewing port eliminated the previous problems associated with viewing the primary combustion area.

Section (3) has two rectangular access ports on the side for primary-stage gas-cooling coils. The cooling coils were made from 0.07 and 0.64 centimeter (0.125 and 0.25 inch) stainless steel tubes as shown in Figure 6.4 and were placed through the access ports in Section (3) as desired. Thermocouples were used to monitor the inlet and outlet cooling water temperatures, and the flow rates were noted to measure how much heat was taken out in the primary stage.

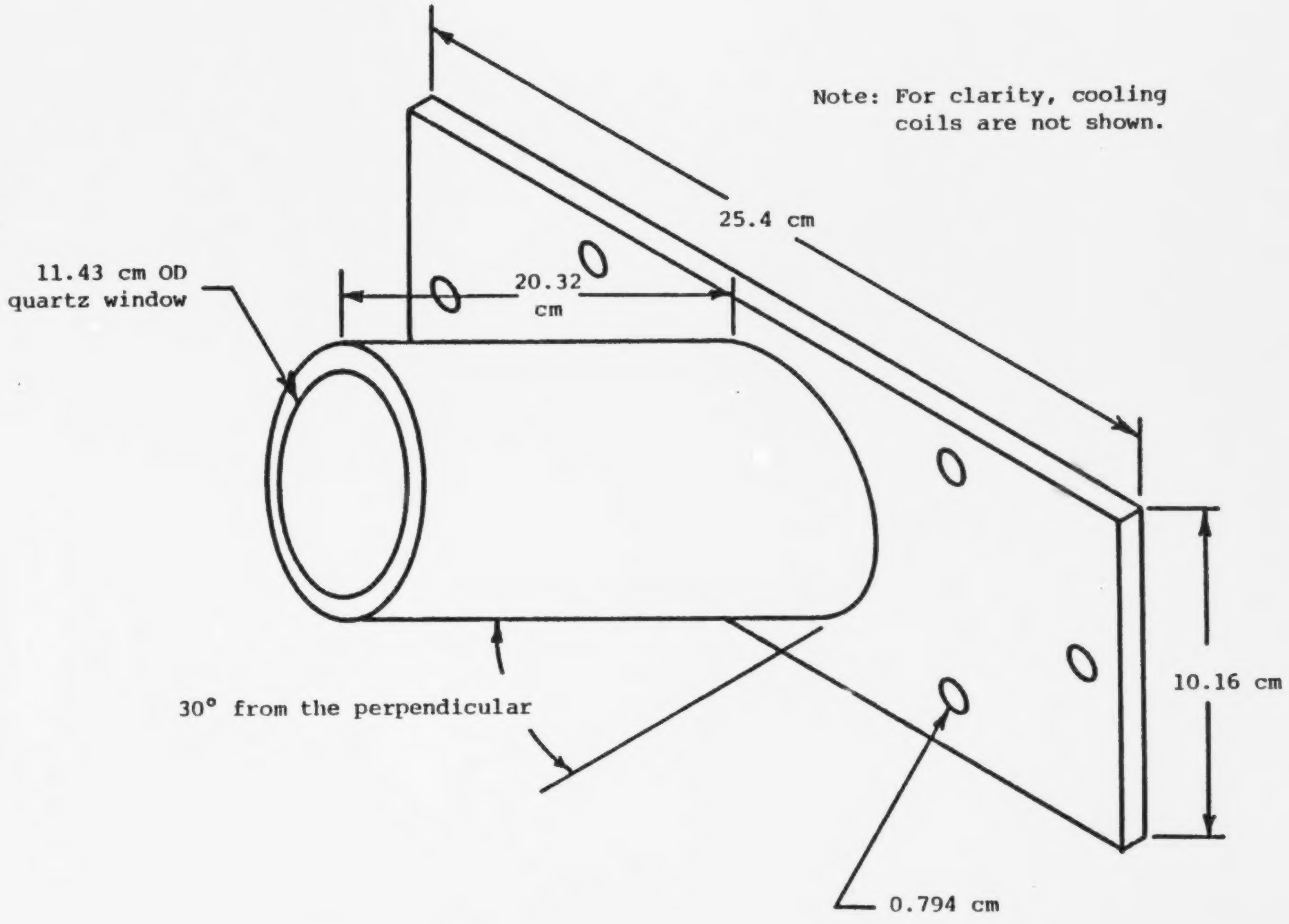
Note: For clarity, cooling
coils are not shown.
25.4 cm
11.43 cm OD
quartz window
20.32
cm
30° from the perpendicular
10.16 cm
0.794 cm

Figure 6.3 First-stage view port.

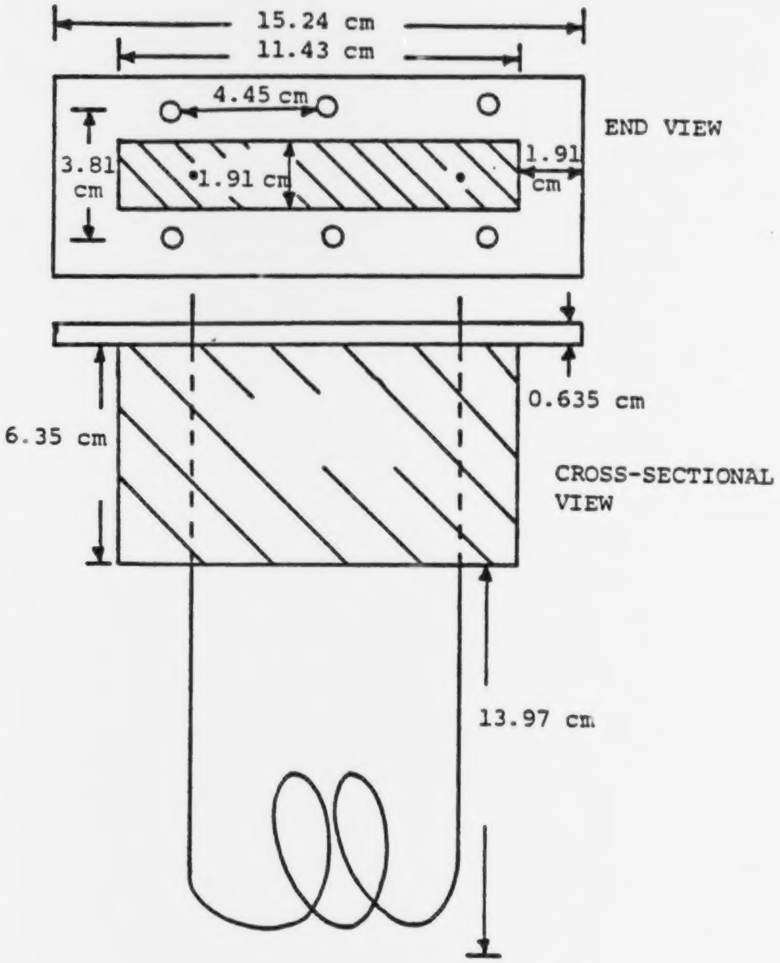
15.24 cm
11.43 cm
4.45 cm
END VIEW
3.81 cm
1.91 cm
1.91 cm
0.635 cm
6.35 cm
CROSS-SECTIONAL VIEW
13.97 cm

Figure 6.4 Combustion-gas cooling coils schematic.

Section (4) is the new choking section installed for this study. It divides the primary and secondary combustion zones by gradually choking the gaseous flow from the 11.43-centimeter (4.5-inch) tunnel to 5.08 centimeters (2 inches), then expanding again to the original tunnel size, at which point the second-stage air is injected (Figure 6.5).

A 3.81-centimeter (1.5-inch) diameter port was placed in the center of the choking area from one side to provide access for measurements at the end of the first stage of combustion. An 0.48-centimeter (3/16-inch) diameter hole for the insertion of a chromel-alumel thermocouple to measure the choke temperature was placed in line with the choke port from the top. The choking area extends for 6.35 centimeters (2.5 inches), behind which is a shoulder that extends back to the 11.43 centimeter (4.5 inch) tunnel diameter. The second-stage air injection ring is placed immediately after the choking area. Radial and axial modes of second-stage air were available (Figure 6.6). The second-stage air-injection ring was inserted through a 5.08 centimeter (2 inch)-by-10.16 centimeter (4 inch) slot in the shell on the opposite side from the choke port.

Section (5) provides the area for the sec[illegible]stage burnout to occur. A Magnehelic 0 to ±2.54 centimeters (±1 inch) of water-pressure gauge monitors the furnace pressure in this stage.

Section (6) is the base for the water-jacketed flue and the two rear access plates. One access plate has an 11.43-centimeter (4.5-inch) diameter quartz window and the other is an adjustable holder for the waterspray probe. The 1.07-meter (3.5-feet) long, water jacketed flue is made of 304 stainless-steel pipe. The

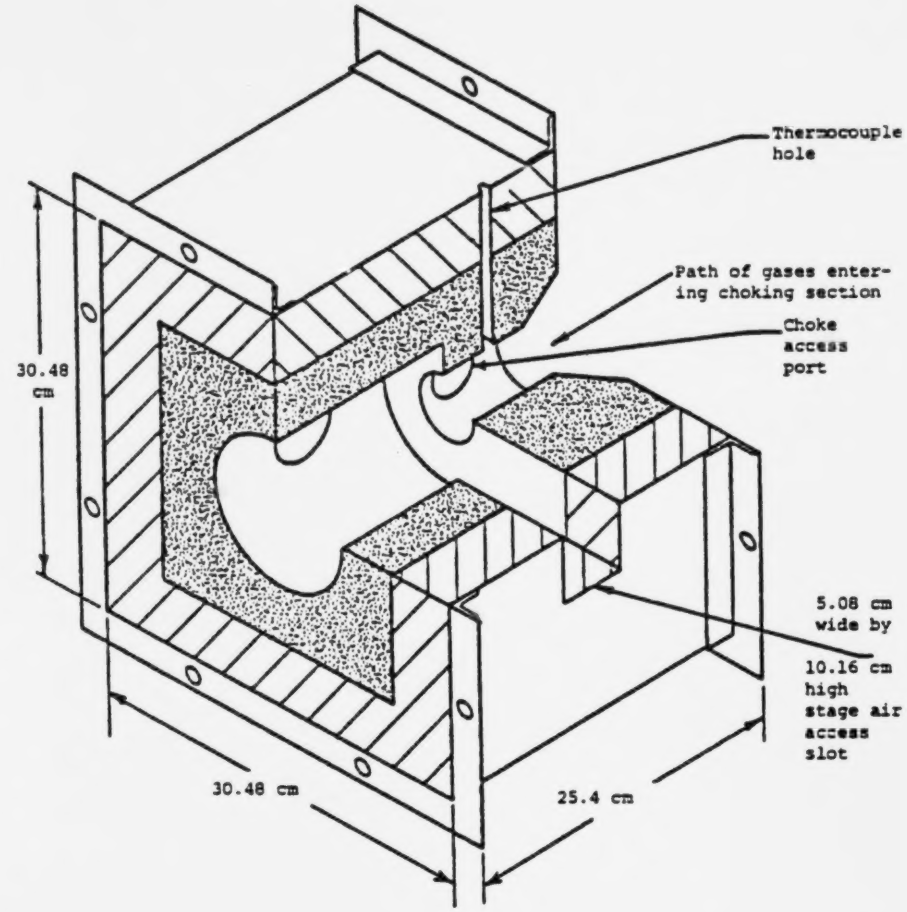
Thermocouple hole
Path of gases entering choking section
Choke access port
30.48 cm
5.08 cm wide by 10.16 cm high stage air access slot
30.48 cm
25.4 cm

Figure 6.5 Choking section schematic.

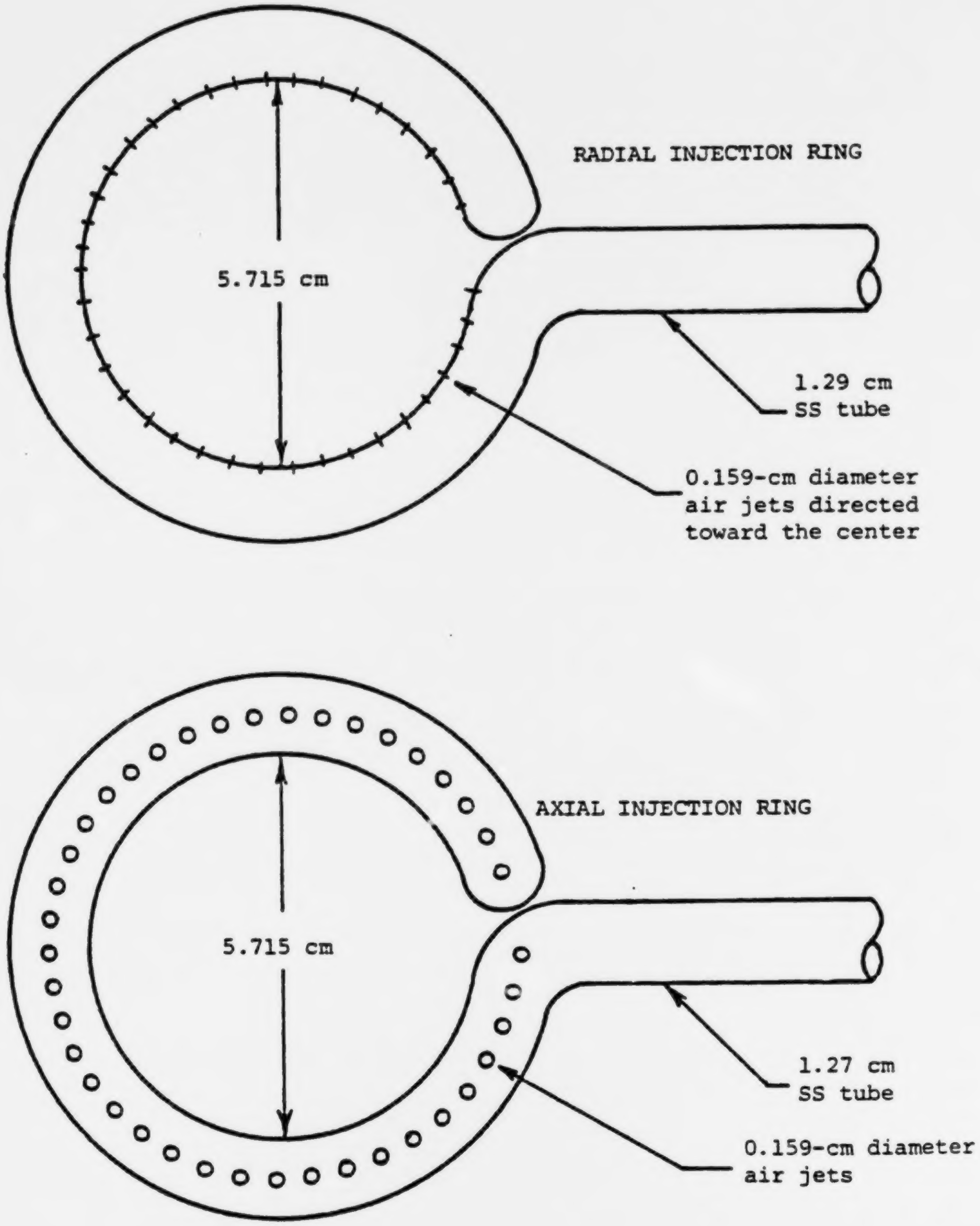
RADIAL INJECTION RING
5.715 cm
1.29 cm
SS tube
0.159-cm diameter
air jets directed
toward the center
AXIAL INJECTION RING
5.715 cm
1.27 cm
SS tube
0.159-cm diameter
air jets

Figure 6.6 Radial and axial second-stage air injection rings.

5.08 centimeters (4.5-inches) diameter flue exits into a pipe cross where gas samples are taken. The flue gas then passes through a gate valve which regulates furnace pressure. The exiting gases are drawn off by the main ventilation/flue system of the laboratory. The ventilation system has an induced-draft fan which tends to reduce the pressure inside the furnace chamber. Hence, careful regulation of the gate valve is required to ensure that a positive pressure of 0.5 to 0.64 centimeters (0.2 to 0.25 inches) of water is maintained inside the furnace during all testing.

6.2 Natural Gas/Air Flow System

The natural gas and air were metered through the gas/air flow system shown in Figure 6.7. This panel can provide the furnace with the following streams: pilot air, pilot gas, main-burner gas, primary (fuel-atomizing) air, secondary (main-burner) air, and second-stage air. This flow panel is capable of providing fuel and oxidant for firing rates up to about 20.5 kW (70,000 Btu/hr) and stoichiometric ratios of up to 2.0.

Compressed air 620-690 Kpa (90-100 psig) goes through two pressure regulators to achieve the desired rotameter calibration pressure of 138 Kpa (20 psig). The air line to the main burner can go through two rotameters; one for the low flow rates (0.0566-0.2832 meter^3/min; 2-10 ft^3/min) and the other rotameter for the large flow rates (0.1699-0.4531 meter^3/min; 6-16 ft^3/min). All air flow rates are controlled with brass needle valves. Low-pressure natural gas was used for the radial diffusion burner from the house natural gas system. The calibrations for each gauge are given by Mason (1980).

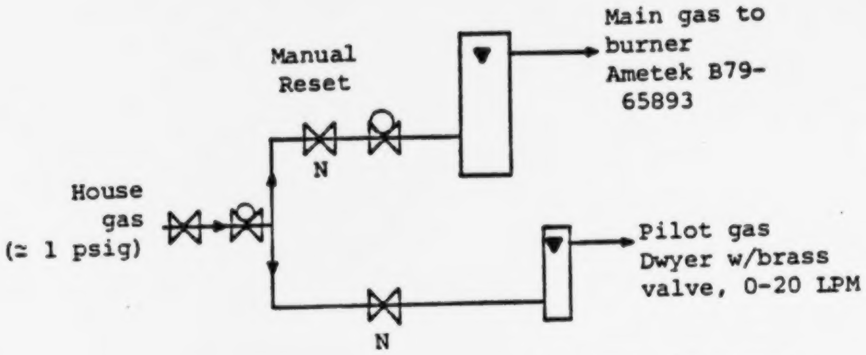
Main gas to
burner
Ametek B79-
65893
Manual
Reset
N
House
gas
(≃ 1 psig)
Pilot gas
Dwyer w/brass
valve, 0-20 LPM
N

FLOW DIAGRAM OF FURNACE NATURAL GAS SUPPLY

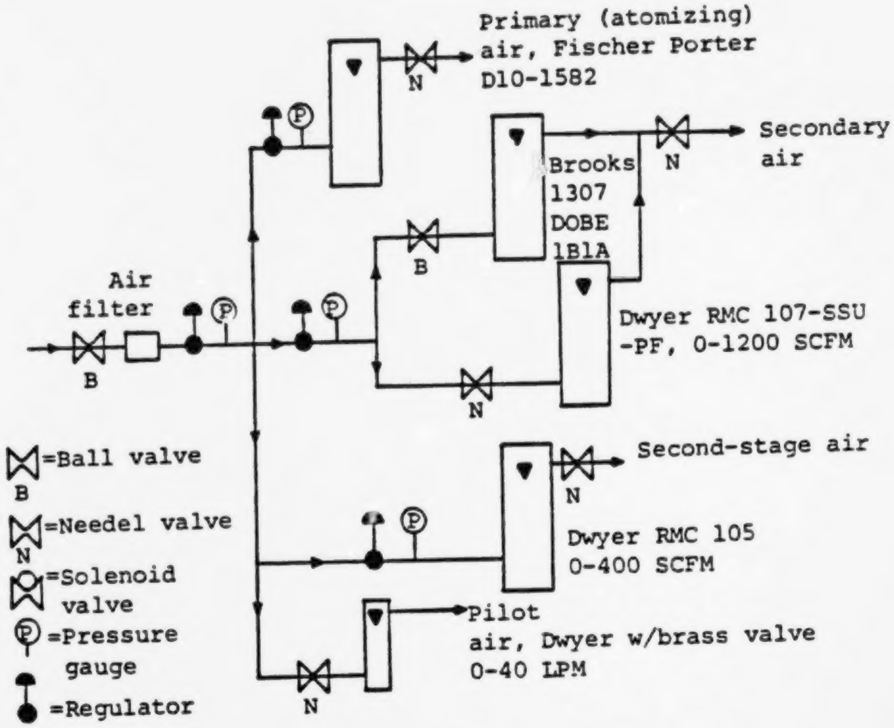
Primary (atomizing)
air, Fischer Porter
D10-1582
N
Secondary
air
N
Brooks
1307
DOBE
1B1A
B
Air
filter
B
Dwyer RMC 107-SSU
-PF, 0-1200 SCFM
N
Second-stage air
N
Dwyer RMC 105
0-400 SCFM
Pilot
air, Dwyer w/brass valve
0-40 LPM
N
B =Ball valve
N =Needel valve
=Solenoid
valve
=Pressure
gauge
=Regulator

FLOW DIAGRAM OF FURNACE AIR SUPPLY

Figure 6.7   Natural gas/air-flow system schematic.

To simulate the nitrogen chemically bound in coal, fuel nitrogen, ammonia was metered into the natural gas at the level which was desired. This was accomplished by using the critical orifice panel described in detail by Mason (1980).

6.3 Flame Safety System

The furnace was equipped with an electronic flame safeguard system to ensure an orderly shutdown of all natural gas in the event of a flame failure. The safety system consists of two solenoid valves and an amplifier in addition to the UV-light sensor mounted on the furnace. Should the UV-sensor not detect a flame or spark, the solenoid valves shut off both the main gas and pilot gas. In addition, the main gas valve must be reset manually prior to restarting the furnace.

CHAPTER 7

NATURAL GAS/AIR STAGED COMBUSTION

7.1 Introduction and Objectives

This chapter focuses on the study of a natural gas/air mixture under staged-combustion conditions. The thermal environment in the first stage was altered by the insertion of cooling coils. The baseline condition was zero cooling coils. One cooling coil produced an intermediate cooling environment by removing 12 percent of the input energy at an S.R. of 0.83. Two cooling coils produced the greatest cooling by removing 19 percent of the input energy at an S.R. of 0.83. With each thermal environment, measurements were taken at increments over a range of first-stage S.R.s of 0.62 to 1.0. The radial gas burner was fired at a rate of 20.51 kW (70,000 Btu/hr) with second-stage air added in the axial mode.

Internal measurements were taken in the choking area at the end of the first stage for temperature and NO, HCN, and NH_3 concentrations. Bulk-gas temperature was measured with the suction pyrometer, NH_3 and HCN were sampled by placing the waterspray probe in the choke from the rear, and the NO was sampled by placing the flue probe in the choke from the side port. The NO levels in the exhaust were found by placing the flue probe into the exhaust during duplicate runs of the ones used for internal measurements.

7.2 First-Stage NO

Figure 7.1 shows the NO concentrations exiting the first stage as they were measured over the range of S.R. and thermal environments. As the S.R. is reduced, the NO levels in the first stage decrease. At S.R.s below 0.95, cooling increases the NO concentration only very slightly over the no-cooling case. At S.R.s of 0.95 to 1.0, the no-cooling case is higher than the one- and two-cooling coil cases. This may be attributed to the higher temperature and oxygen concentrations at these points, which enhance the formation of thermal NO by the Zeldovich mechanism.

7.3 First-Stage HCN

The first-stage HCN concentration measurements are shown in Figure 7.2. As the S.R. is decreased, the HCN levels in the first stage increase significantly. No cooling results in the lowest HCN levels, addition of one cooling coil produces intermediate HCN levels, and addition of two cooling coils results in the highest HCN levels. From the increased HCN levels upon cooling, it can be assumed that cooling retards the decay of HCN.

7.4 First Stage NH_3

Figure 7.3 shows the NH_3 concentrations at the end of the first stage. As the S.R. in the first stage was decreased, only a slight increase in NH_3 levels was found. The levels of NH_3 are much lower than the HCN levels, and the NH_3 concentrations are essentially independent of the thermal environment in the first stage.

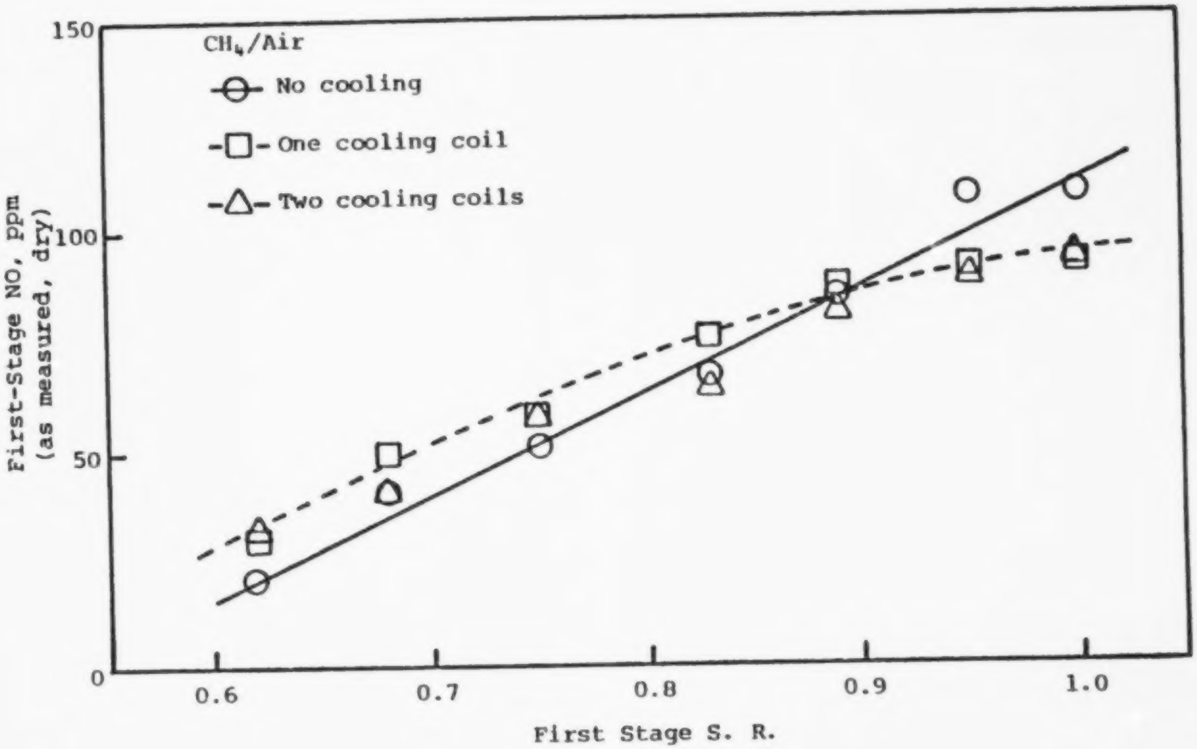

Figure 7.1 First-stage NO with CH$_4$/air.

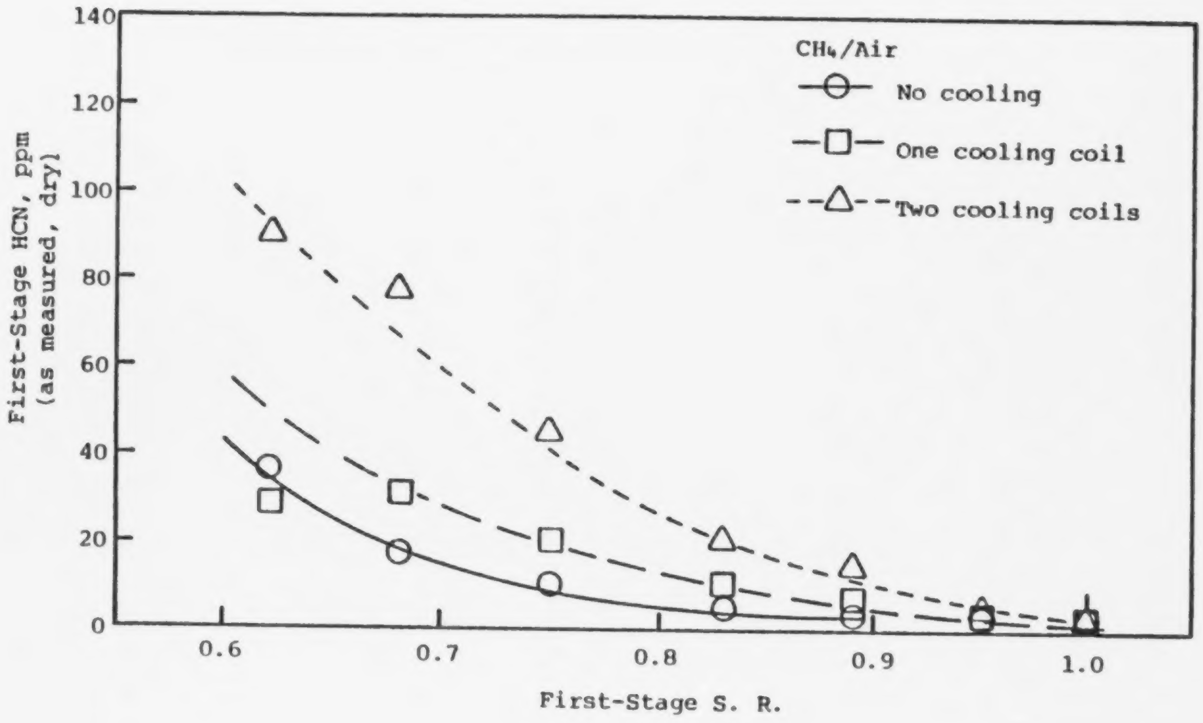

Figure 7.2 First-stage HCN with CH_4/Air.

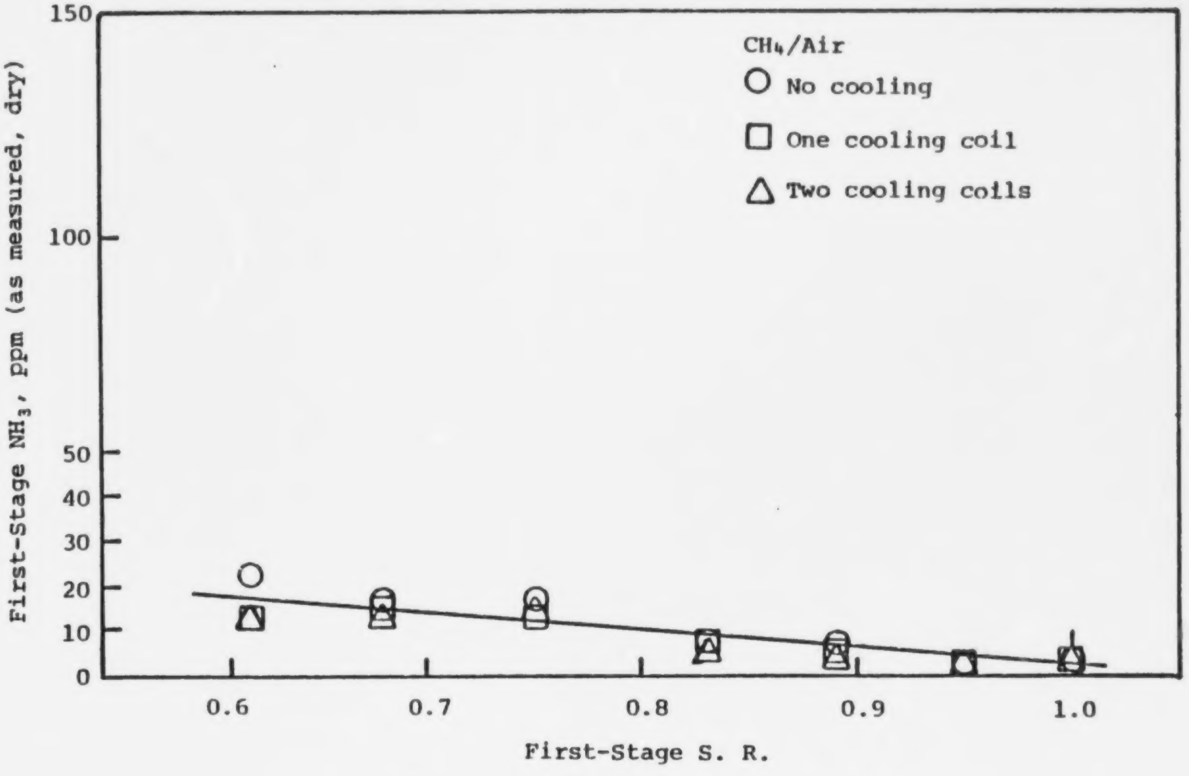

Figure 7.3 First-stage NH_3 with CH_4/air.

7.5 Exhaust NO

The NO levels in the exhaust are shown in Figure 7.4. This figure shows that the NO levels in the flue decrease with decreasing S.R. This result is significant when burning fuels with low nitrogen levels in stationary sources; staged combustion can reduce thermal NO emissions.

A comparison of Figure 7.4 with Figure 7.2 reveals another interesting conclusion. At low S.R., there are high HCN levels leaving the first stage, but no corresponding high levels of NO in the exhaust. This suggests that the conversion of HCN to NO in the second stage flame is small.

It can also be seen that reducing the second-stage flame temperature by cooling in the first stage does not significantly affect the NO levels in the exhaust. This leads to the conclusion that there is relatively little thermal NO formation by the Zeldovich mechanism in the second-stage flame. If second-stage thermal NO formation was significant, a temperature decrease should produce lower NO levels because of the slowing of the Zeldovich mechanism. This effect is not seen.

7.6 Conclusions for CH_4/Air Staged Combustion

Two important conclusions can be drawn from this chapter: (1) The conversion of HCN to NO is very low. HCN concentrations in the first stage were increased both by the addition of cooling coils and by lowering the S.R., but there was no corresponding increase in exhaust NO levels. (2) Thermal NO formation in the second-stage flame is small. Cooling had essentially no effect on NO levels in the exhaust.

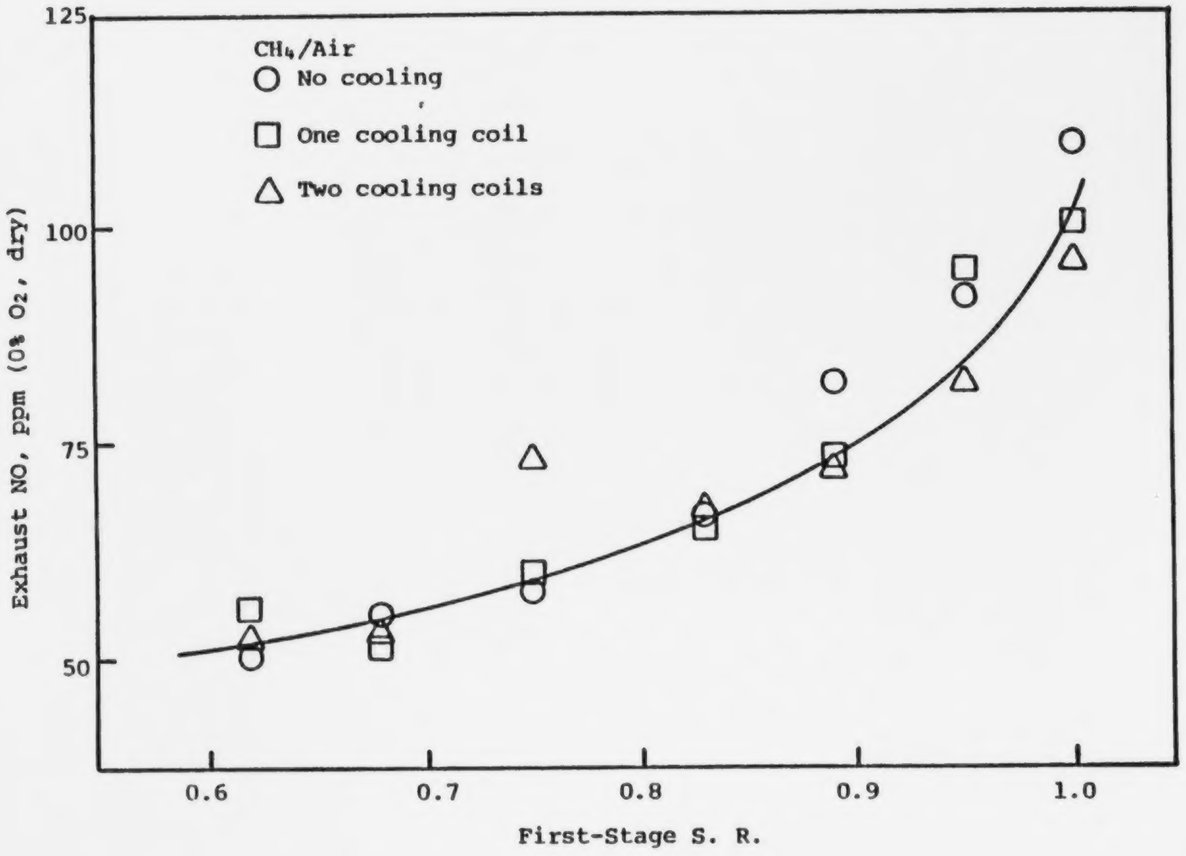

Figure 7.4 Exhaust NO with CH_4/air.

CHAPTER 8

NATURAL GAS/AMMONIA/AIR STAGED COMBUSTION

8.1 Introduction and Objectives

To simulate the effect of burning fuels with high nitrogen contents, the experiments of the previous chapter were repeated with the natural gas doped with 0.4 wt percent nitrogen in the form of ammonia. Ammonia was used to simulate the nitrogen volatiles given off when heteroatom-nitrogen compounds and amine groups in coal decompose upon heating. The ammonia was metered into the natural gas in precise levels using the critical orifice-meter panel described in Chapter 3. The same S.R. ranges were covered with the measurements of temperature, internal NO, HCN, and NH_3 concentrations along with flue NO concentrations being taken as previously described.

8.2 First-Stage NO with NH_3 Addition

The results of the first-stage NO measurements are presented in Figure 8.1. With ammonia addition, the NO levels exiting the first stage decrease almost linearly with decreasing S.R. All three lines start out together, but below an S.R. of 0.95, the one- and two-cooling-coil measurements lie together on the same line, which is higher and parallel to that for no cooling. This seems to indicate that as the initial first-stage cooling reduces the gas temperatures to below 1204 °C (2200 °F), it in essence "freezes" the NO-reduction reactions and any additional cooling has no effect. This

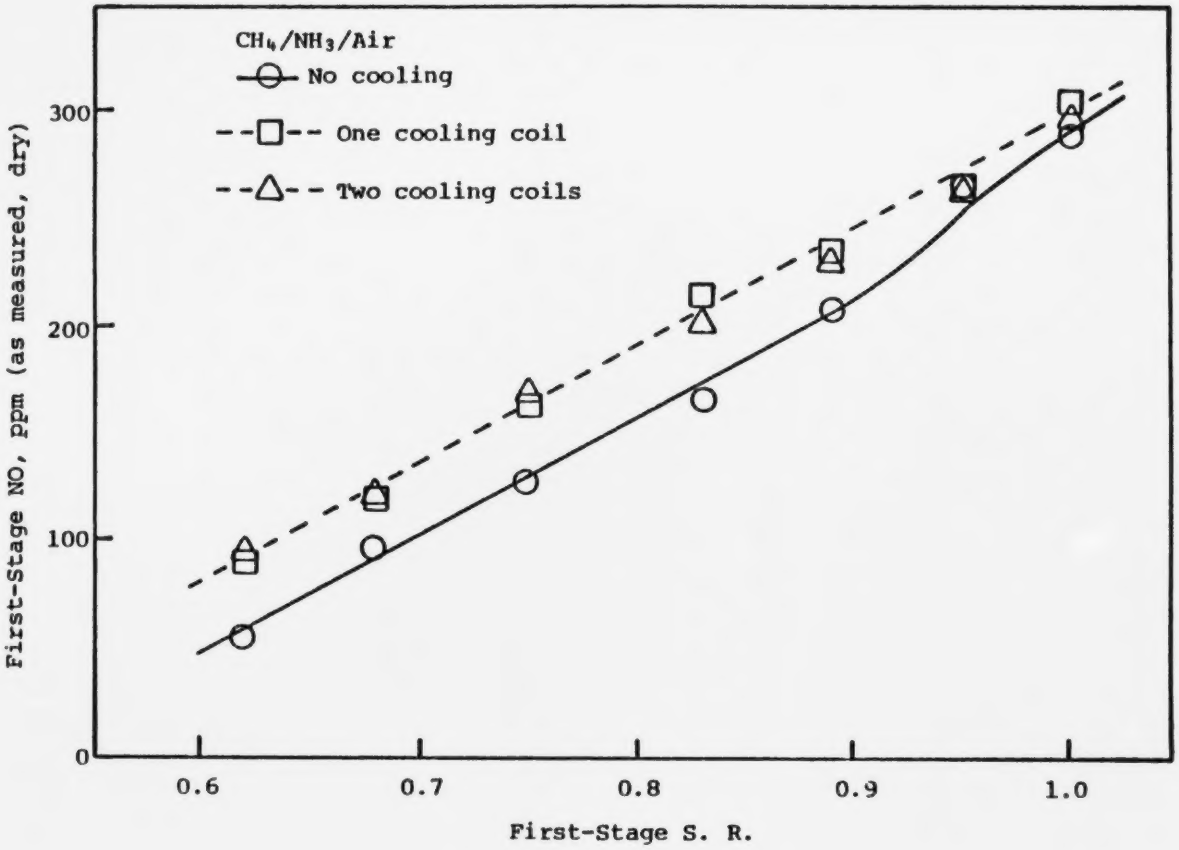

Figure 8.1 First-stage NO with CH_4/NH_3/air.

thermal-freezing effect was also observed, to a lesser extent, in ammonia-less flames (Figure 7.1). The cooling lines lie above the no-cooling level, indicating that the rate of NO destruction in the first stage is slowed by a decrease in temperature.

8.3 First-Stage HCN with NH_3 Addition

Figure 8.2 displays HCN concentrations leaving the first stage as a function of S.R. and thermal environment when NH_3 is added to the natural gas. The same general trends are, as noted, without NH_3 addition (see Figure 7.2) with two cooling coils giving the highest HCN level, one cooling coil giving an intermediate value and no cooling giving the lowest HCN levels, all increasing with decreasing S.R. The HCN levels did not increase to any great degree with NH_3 addition as opposed to no NH_3 addition. The three curves for the three thermal environments also show that the rate of HCN destruction still proceeds at an appreciable rate and does not slow to near zero upon cooling as does the NO decay (Figure 8.1).

8.4 First-Stage NH_3 with NH_3 Addition

The first-stage NH_3 levels with NH_3 addition to the fuel are shown in Figure 8.3. As the S.R. is decreased, the NH_3 levels rise. A relatively small temperature effect is shown, but it is not systematic. The highest NH_3 levels are found with no cooling; the lowest levels are produced with one cooling coil.

8.5 Exhaust NO with NH_3 Addition

The effects of first-stage S.R. and cooling on the NO levels in the exhaust of CH_4/NH_3 flames are shown in Figure 8.4. A minimum

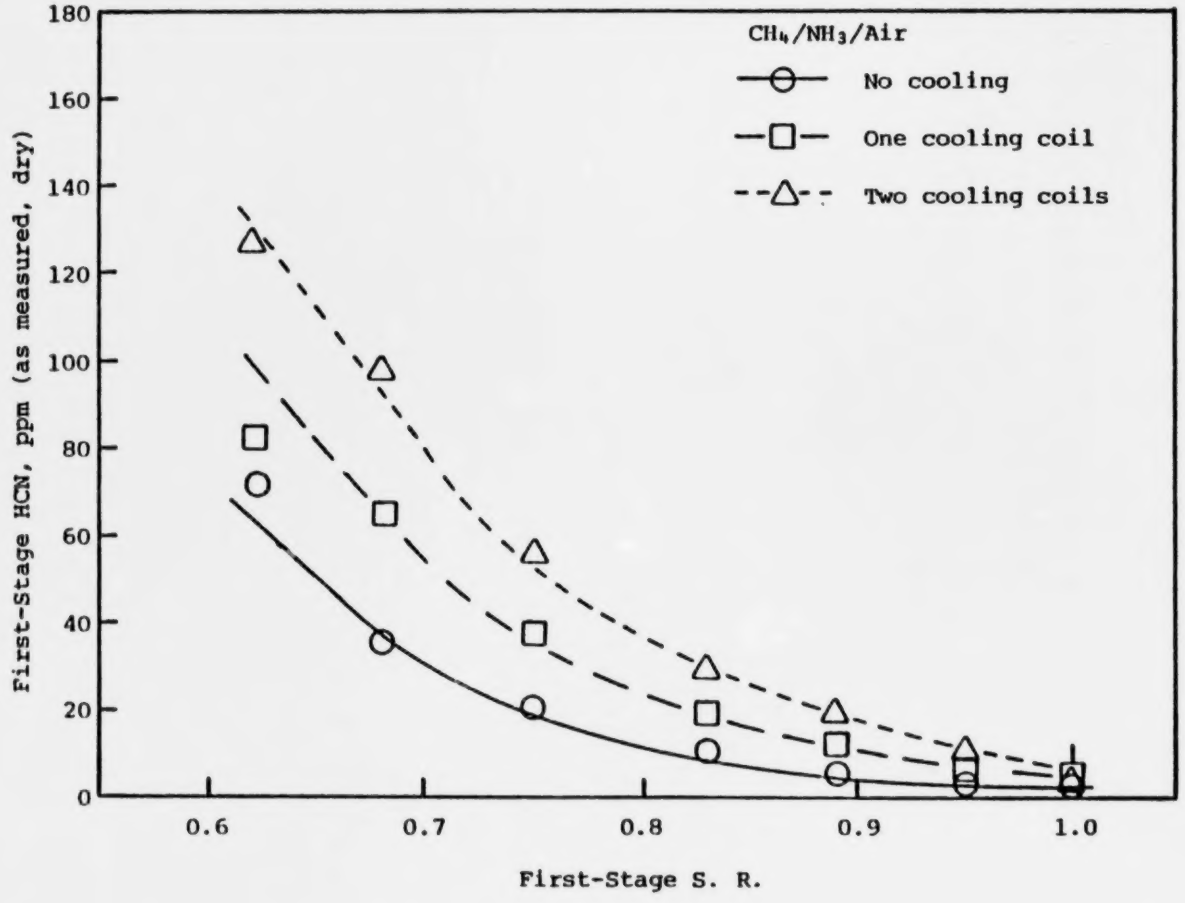

Figure 8.2 First-Stage HCN with $CH_4/NH_3/Air$.

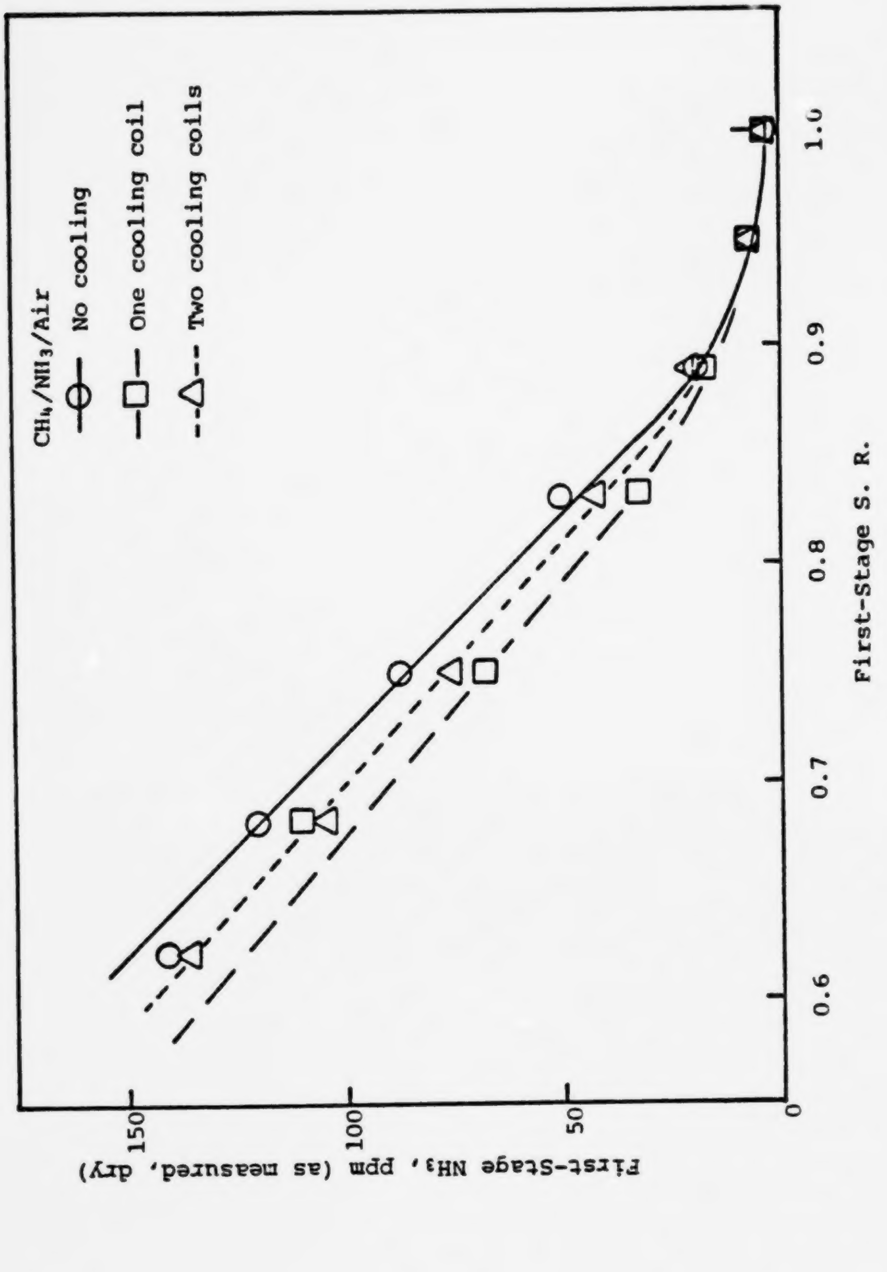

Figure 8.3 First-Stage NH_3 with CH_4/NH_3/Air.

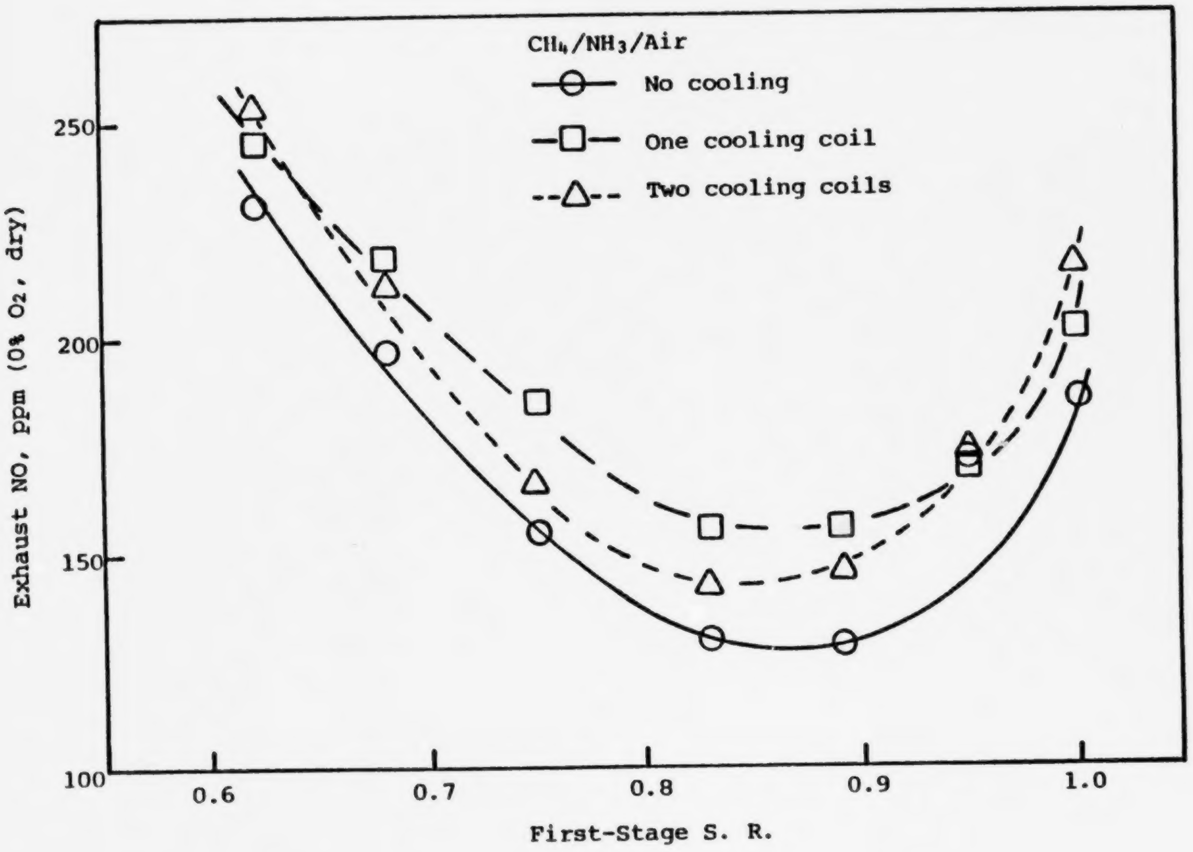

Figure 8.4 Exhaust NO with CH_4/NH_3/Air.

of NO emission is once again observed. From an S.R. of 1.0 to 0.85, the exhaust-NO levels decrease with decreasing S.R., after which they begin to increase as the S.R. is decreased further. It appears that the initial decrease below an S.R. of one may be attributed to the decreasing NO levels leaving the first stage as the NH_3 and HCN levels leaving the first stage are low and only slightly increasing in this range. The increasing exhaust NO levels below an S.R. of 0.85 may be attributed to increased NH_3 (leaving the first stage), which is subsequently converted to NO in the second stage. It was shown that the upturn in NO levels cannot be attributed to the increased HCN levels which would have been converted to NO in the second stage because this effect was not observed in the CH_4/air experiments. The upturn also cannot be attributed to increased levels of thermal NO in the second stage, as Figure 7.4 shows that there is no increase in NO levels at low S.R. in CH_4/air flames.

A very distinct thermal effect can also be seen in Figure 8.4. Decreasing the temperature by adding one cooling coil increases the exhaust NO level. This increase in exhaust NO is due to the increased NO levels exiting the first stage (Figure 8.1). The increased NO levels in the first stage are caused by a decreased rate of NO decay upon cooling. With this reasoning, one could assume that, since two cooling coils produce the same level of NO leaving the first stage as one cooling coil, both would have essentially the same NO levels in the exhaust. But two cooling coils produce an intermediate level of NO emissions. This cannot be due to varying levels of NH_3 leaving the first stage because no cooling produces the highest level of NH_3, with one cooling coil producing the lowest NH_3 levels, just the opposite effect is observed in the exhaust. Figure 8.5 shows how, at the minimum of exhaust emissions (at S.R. equal to 0.85), the first-stage NO, NH_3, and HCN concentrations, along with the exhaust NO levels, vary as the first-stage thermal environment is changed. From this figure, it appears that at the very lowest temperature shown the NO emissions are lower than what is expected from adding the first-stage NO and HCN together with NH_3. It is believed that this lowering may be due to some type of selective reduction reaction of NH_3, NO, and O_2 over the temperature range of 870 to 1100 °C in the second-stage flame. This reaction may be similar in nature to Exxon's "Thermal $DeNO_x$", the process in which NO emissions in the flue are reduced by selective reaction with injected NH_3 to form N_2.

8.6 Exhaust NO with First- and Second-Stage NH_3 Doping

A series of experiments were conducted in order to determine the validity of the occurrence of a selective reduction reaction of NH_3, NO, and O_2 in the second stage. Figure 8.6 shows that when NH_3 was added to the second stage at the choke, there was a considerable reduction in the exhaust NO at SR_1's greater than 0.75. This reduction in the exhaust NO concentration clearly supports the hypothesis that a reduction reaction occurred between NH_3 and NO.

8.7 Conclusions for CH_4/NH_3/Air Staged Combustion

From the results presented in this chapter, several interesting conclusions may be drawn. First, decreasing the first-stage temperature to below 1200 °C slows the rate of NO decay (to N_2) to near zero. Second, high levels of NH_3 in the fuel do not significantly increase the HCN concentration leaving the first stage. Third, intermediate

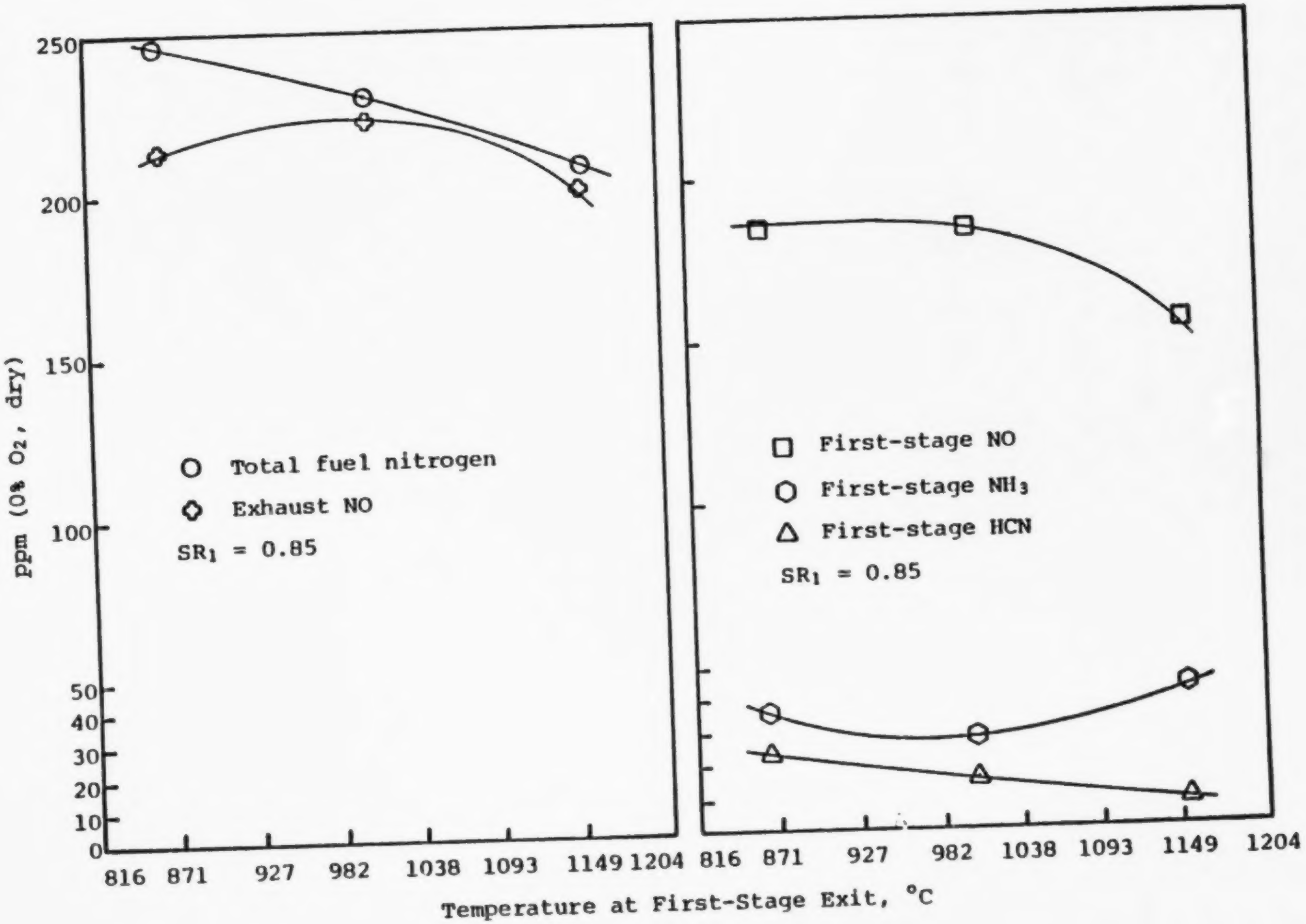

Figure 8.5 Temperature effect at the exhaust minimum (SR_1 = 0.85).

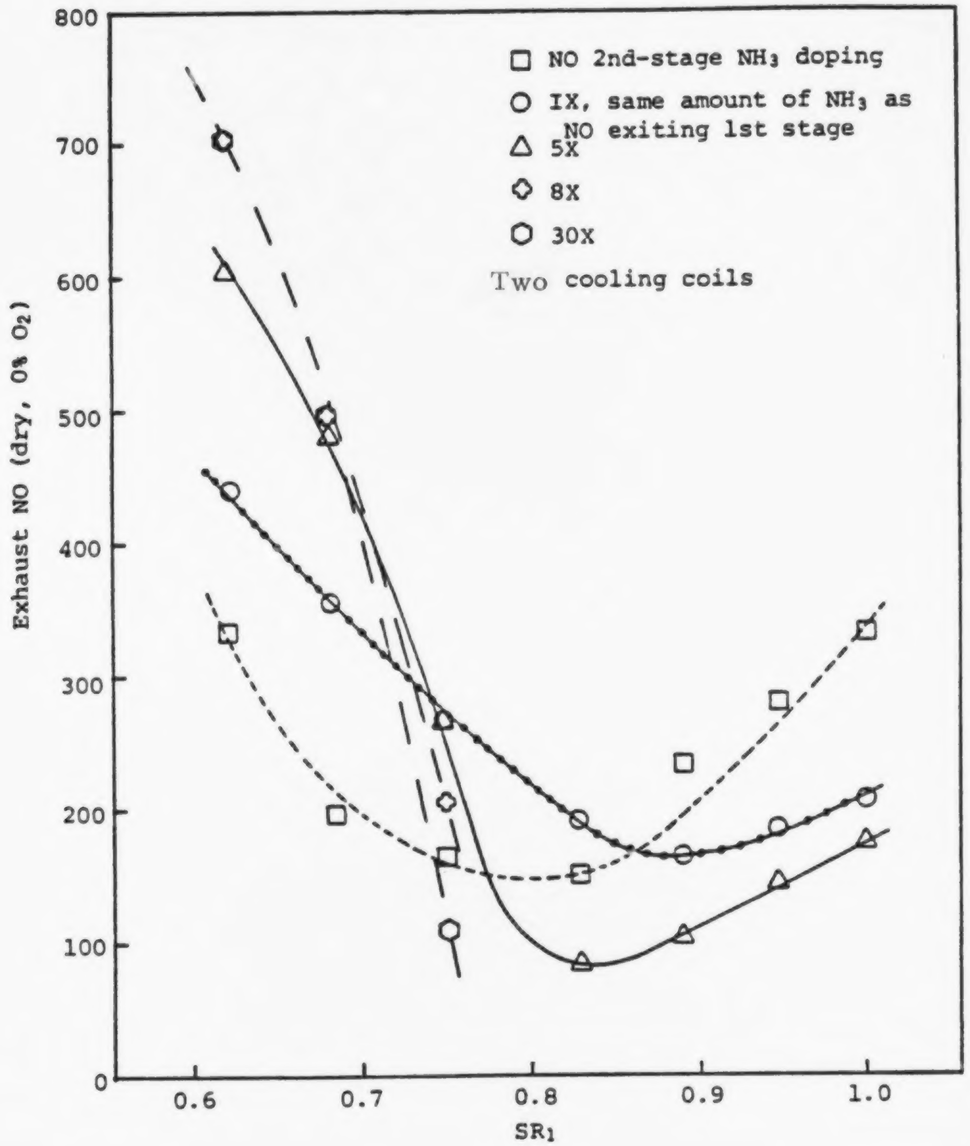

Figure 8.6 Exhaust NO with first- and second-stage doping.

levels of first-stage cooling increase exhaust NO emissions because of the associated increase in NO levels exiting the first stage. Fourth, additional cooling encourages a reduction reaction of NH_3, NO and O_2 in the second-stage flame to produce lower exhaust emissions than with intermediate cooling.

CHAPTER 9

CONCLUSION

From the results of this experimental study, the following conclusions may be drawn:

1. Gas-phase NH_3 concentration measurements can be made accurately and expeditiously with a gas-sensing, ion-specific electrode. The collection system should include a stainless-steel liquid spray probe, two 500-mℓ, fritted cylinder impingers and associated flow-metering equipment. The scrubbing solution of choice is 0.1 N H_2SO_4 and the gas flow rate should be approximately 5 ℓ/min. Collection efficiencies in excess of 98 percent can be expected with this system.
2. HCN can be successfully measured with either an ion-specific electrode system. HCN liquid-phase collection efficiencies are slightly lower (85 percent) than those observed with NH_3.
3. The conversion of HCN to NO in the second stage of a staged combustor is very low.
4. Thermal formation of NO in the second stage was insignificant in the experimental system studied.

5. Limited (12 percent), first-stage cooling retards the rate of decay of NO to near zero if the gas temperatures are reduced below 1200 °C.

6. Limited cooling in the first stage of CH_4/NH_3/air flames increases NO in the exhaust because the rate of NO destruction is significantly slowed in the first stage.

7. Additional cooling of CH_4/NH_3/air flames provides slightly lower emissions than initial cooling because the temperature minimum is reached in the second-stage flame, where NO, NH_3, and O_2 are reduced in a homogeneous gas-phase reaction. This produces lower NO levels in the exhaust.

These results suggest that the optimum staged-combustion system is one in which the first stage is operated essentially adiabatically to maximize TFN decay. Interstage cooling should also be used to reduce the second-stage flame temperature to below 1540 °C, thereby minimizing thermal NO formation in the second stage.

NOMENCLATURE

a_i	activity of ion i
c_i	concentration of ion_i
E	potential generated
E_i	standard potential of i at 25 °C
E'	$E^\circ_{glass} - E^\circ_{Ag-AgC\ell} + K \log a_{C\ell^-}$
E''	$E' + k \log K\gamma_{NH_4^+}/\gamma_{NH_3}$
E'''	$E'' + k \log [NH_4^+]$
F	Faraday's constant, 96494 coulombs
FID	flame ionization detector
[i]	concentration of i, moles/liter
K	dissociation constant
k	2.303 RT/F
M	molarity; moles/liter
mM	molar concentration of $NH_4C\ell$
mV	millivolts
N	normality; equivalents/liter
Nernstian response	log linear response
NPD	nitrogen-phosphorus detector
pH	$-\log [H^+]$
ppm	parts per million
R	ideal gas constant
Retention time	retention time of solute (measured from start)

SR	stoichiometric ratio; molar ratio of air to fuel
SR_1	stoichiometric ration in the first stage; molar ratio of air to fuel
T	absolute temperature
Z_i	charge of ion i
γ_i	activity coefficient of i
ν	number of moles of ammonia that have diffused through the membrane per liter of solution in the film

APPENDIX

INTERNAL MEASUREMENT DATA

The tables presented in this appendix tabulate the data for the optimization experiments conducted for this research.

TABLE A-1

NO COOLING COILS

	CH_4/Air			CH_4/NH_3/Air			Choke Temperature, °F
S.R.	NO	NH_3	HCN	NO	NH_3	HCN	
(All concentrations in ppm, as measured, dry)							
1.00	108	4	1	288	4	1	2283
0.95	108	3	1	265	6	2	2241
0.89	83	7	3	208	20	6	2223
0.83	67	10	6	165	50	12	2112
0.75	50	17	11	128	87	20	2015
0.68	40	18	18	96	120	36	2012
0.62	20	27	36	58	140	69	1955

TABLE A-2

ONE COOLING COIL

S.R.	CH_4/Air			CH_4/NH_3/Air			Heat Taken Out, Btu/hr	% of Input Energy Taken Out	Choke Temperature, °F
	NO	NH_3	HCN	NO	NH_3	HCN			
(All concentrations in ppm, as measured, dry)									
1.00	92	2	2	303	3	2	9154	13.1	2035
0.95	91	3	3	265	8	6	9049	13.0	2010
0.89	87	5	8	235	23	11	8677	12.4	1931
0.83	75	5	10	213	34	19	8355	11.9	1842
0.75	58	11	22	165	68	38	7353	10.5	1734
0.68	49	14	34	120	110	55	6229	8.9	1651
0.62	31	-	-	90	-	-	4972	7.1	1593

TABLE A-3

TWO COOLING COILS

S.R.	CH_4/Air NO	CH_4/Air NH_3	CH_4/Air HCN	CH_4/NH_3/Air NO	CH_4/NH_3/Air NH_3	CH_4/NH_3/Air HCN	Heat Taken Out, Btu/hr	% of Input Energy Taken Out	Choke Temperature, °F
(All concentrations in ppm, as measured, dry)									
1.00	93	2	2	295	5	6	14,932	21.3	1786
0.95	90	3	6	261	9	11	14,839	21.2	1757
0.89	80	4	14	232	20	19	14,126	20.2	1678
0.83	64	9	22	201	43	29	12,970	18.5	1586
0.75	58	16	46	170	91	56	11,293	16.1	1484
0.68	40	12	78	120	107	97	9,310	13.3	1427
0.62	33	13	91	96	139	128	7,651	10.9	1404

TABLE A-4

FLUE MEASUREMENT DATA

	No Cooling		One Cooling Coil		Two Cooling Coils	
S.R.	Thermal	With NH_3 Addition	Thermal	With NH_3 Addition	Thermal	With NH_3 Addition
(All concentrations in ppm, 0% O_2, dry)						
1.00	109	294	99	300	96	312
0.95	92	262	94	260	82	254
0.89	82	209	73	228	72	217
0.83	66	195	65	220	67	209
0.75	58	211	59	244	73	238
0.68	55	251	51	268	53	265
0.62	51	281	56	301	52	304

TABLE A-5

FLUE MEASUREMENT DATA FOR SECOND-STAGE AMMONIA DOPING

S.R.	Exhaust NO Concentration No Doping	1X*	5X	8X	30X
	(Two cooling coils, all concentrations in ppm, 0.0% O_2, dry)				
1.00	331	206	175	-	-
0.95	280	185	144	-	-
0.89	233	164	103	-	-
0.83	151	190	82	-	-
0.75	162	267	267	206	110
0.68	196	356	480	493	493
0.62	233	438	607	700	700

*1X = same amount of NH_3 added to second stage as NO exiting the first stage.

LIST OF REFERENCES

ASTM Standards 2B, 02036. Philadelphia: American Society for Testing and Materials (1970).

Axworthy, A. E.; Schneider, G. R.; Shuman, M. D.; and Dayan, V. H. "Chemistry of Fuel Nitrogen Conversion to Nitrogen Oxides in Combustion," EPA-600/2-76-039 (NTIS PB250373), February 1976.

Bagwell, F. A.; Rosenthal, K. E.; Teixeira, D. P.; Breen, B. P.; Bayard de Volo, N.; and Kerbo, S. "Utility Boiler Operating Modes for Reduced Nitric Oxide Emissions." Journal of the Air Pollution Control Association 21 (1971) : 702.

Barnhart, D. H.; and Diehl, E. K. "Control of Nitrogen Oxides in Boiler Flue Gases by Two-Stage Combustion." Journal of the Air Pollution Control Association 10 (1960) : 397.

Bartok, W.; Crawford, A. R.; Cunningham, A. R.; Hall, H. J.; Manny, E. H.; and Skopp, A. Systems Study of Nitrogen Oxide Control Methods for Stationary Sources, Volume II, EPA No. APTD-1286 (NTIS PB192789)(1969).

Bartok, W.; Crawford, A. R.; and Skopp, A. "Control of NO_x Emissions from Stationary Sources." Chemical Engineering Progress 67 (1971) : 64.

Beckett, M. J.; and Wilson, A. L. "The Manual Determination of Ammonia in Fresh Waters Using an Ammonia-Sensitive Membrane-Electrode." Water Research 8 (1974) : 333.

Bienstock, D.; Amsler, R. L.; and Bauer, E. R. "Formation of Oxides of Nitrogen in Pulverized Coal Combustion." Journal of the Air Pollution Control Association 16 (1966) : 442.

Bowman, C. T. "Kinetics of Nitric Oxide Formation in Combustion Processes." Fourteenth Symposium (International) on Combustion. Pittsburgh, Penn.: The Combustion Institute (1973).

Chen, S. L.; Heap, M. P.; and Pershing, D. W. "The Fate of Coal Nitrogen During Combustion," Fuel 61 (1982) : 1218.

Claeys, R. R.; and Fruend, H. "Gas Chromatographic Separation of HCN on Porapak Q - Analysis of Grace Aqueous Solutions." Environmental Science and Technology 2 (1968).

Clyster, H.; and Adams, F. "Potentionmetic Determinations With the Silver Sulfide Membrane Electrode, Part I - Determination of Cyanide." *Analytica Chimica* 83 (1976) : 27.

Eagan, M. L.; and Dubois, L. "The Determination of Ammonium Ion in Airborne Particulates with Selective Electrodes." *Analytica Chimica Acta* 70 (1974) : 157.

England, G. C.; Heap, M. P.; Pershing, D. W.; Nihart, R. K.; and Martin, G. B. "Mechanisms of NO_x Formation and Control: Alternative and Petroleum-Derived Liquid Fuels." *Eighteenth Symposium (International) on Combustion*. Pittsburgh, Penn.: The Combustion Institute (1981).

Epstein, J. "Estimation of Microquantities of Cyanide." *Analytical Chemistry* 19 (1947) : 272.

Fenimore, C. P. "Formation of Nitric Oxide in Premixed Hydrocarbon Flames." *Thirteenth Symposium (International) on Combustion*. Pittsburgh, Penn.: The Combustion Institute (1971).

Fleet, B.; and Ho, A. Y. "An Ion-Selective Electrode System for Continuously Monitoring Cyanide Ion, Based on a Computerized Gran Plot Technique." *Talanta 20* (1973) : 793.

Foster, D. E., and Keck, J. "Factors Affecting NO_x Formation from Nitrogen-Containing Fuels." *Combustion and Flame* 38 (1980) : 199.

Frant, M. S.; Ross, J. W. Jr.; and Riseman, J. H. "Electrode Indicator Technique for Measuring Low Levels of Cyanide." *Analytical Chemistry* 44 (1972).

Goodfellow, G. I.; and Webber, H. M. "The Determination of Ammonia in Boiler Feedwater With an Ammonium-Selective Glass Electrode." *Analyst* 97 (1972) : 95.

Goulden, P. D.; Afghan, B. K.; and Brooksbank, P. "Determination of Nanogram Quantities of Simple and Complex Cyanides in Water." Analytical Chemistry 44 (1972): 1845.

Gunther, F. A.; Barkley, J. H.; Kolbezen, M. J.; Blinn, R. C.; and Staggs, E. A. "Quantitative Microdetermination of Gaseous Ammonia by Its Absorption at 204.3 Mμ." *Analytical Chemistry* 28 (1956).

Harris, M. E.; Rowe, R.; Cook, E. G., and Grumer, J. *Reduction of Air Pollutants from Gas Burner Flames.* Bureau of Mines Bulletin 653 (EPA No. APTIC 28287) (1970).

Heap, M. P.; Lowes, T. M.; and Walmsley, R. "Nitric Oxide Formation in Pulverized Coal Flames." *Combustion Institute European Symposium 1973*. Edited by F. J. Weinberg. New York: Academic Press, 1973.

Johnson, S. A.; Cioffi, P. L.; Sommer, T. M.; and McElroy, M. W. The Primary Combustion Furnace System - An Adnvance Low-NO_x Concept for Pulverized Coal Combustion. Second EPRI NO_x Control Technology Seminar (1978).

Katz, M., ed. Methods of Air Sampling and Analysis. 2nd ed. Washington, D. C.: American Public Health Association, 1977.

Martin, G. B.; and Berkau, E. E. "An Investigation of the Conversion of Various Fuel Nitrogen Compounds to Nitrogen Oxides in Oil Combustion. AIChE Symposium Series No. 126 68 (1972).

Martin, G. B.; Pershing, D. W.; and Berkau, E. E. Effects of Fuel Additives on Air Pollutant Emissions from Distillate-Oil-Fired Furnaces. U. S. Environmental Protection Agency, Office of Air Programs Publication No. AP-87 (NTIS PB213-630), June, 1971.

Mason, V. D. B. S. Thesis, University of Utah Department of Chemical Engineering, 1980.

Mattock, G.; and Uncles, R. "The Response Properties of an Electrode Glass Sensitive to Potassium and Ammonium Ions." Analyst 89 (1964) : 350.

McCann, C. R.; Demeter, J. J.; Dzubay, J.; and Bienstock, D. "NO_x Emissions from Two-Stage Combustion of Pulverized Coal." 65th Annual Meeting of the Air Pollution Control Association, Miami Beach, Florida (1972).

Midgley, D.; and Torrance, K. "The Determination of Ammonia in Condensed Steam and Boiler Feed-Water With a Potentiometric Ammonia Probe." London Analyst 97 (1972) : 626.

Myerson, A. L.; and Chludzinski, J. J. Jr. "A Gas Chromatographic Determination of HCN in Combustion Effluents in the Low Ppm Range." Journal of Chromatographic Science 13 (1975).

Orion Research, Inc. Instruction Manual for the Cyanide Ion Electrode Model 94-06 (1977).

Pershing, D. W. Ph.D. Dissertation, University of Arizona Department of Chemical Engineering, 1976.

Pershing, D. W.; and Berkau, E. E. "The Chemistry of Nitrogen Oxides and Control Through Combustion Modifications." Pollution Control and Energy Needs. R. M. Jimeson and R. S. Spindt, eds. Washington, D. C.: American Chemical Society, 1973.

Pershing, D. W.; Lee, J; and Wendt, J. O. L. "Fate of Coal Nitrogen Under Fuel Rich and Staged Combustion Conditions." Paper presented at the 70th Annual AIChE Meeting, New York City, New York, 1977.

Pershing, D. W.; Martin, G. B.; and Berkau, E. E. "Influence of Design Variables on the Production of Thermal and Fuel NO from Residual Oil and Coal Combustion." AIChE Symposium Series No. 248 71 (1975).

Pershing, D. W.; and Wendt, J. O. L. "Pulverized Coal Combustion: The Influence of Flame Temperature and Coal Composition on Thermal and Fuel NO_x." Sixteenth Symposium (International) on Combustion. Pittsburgh, Penn.: The Combustion Institute (1977).

Riseman, J. H. "Electrode Techniques for Measuring Cyanide in Waste Waters." American Laboratory 4 (1972) : 63.

Sekerka, I.; and Lechner, J. F. "Potentiometric Determination of Low Levels of Simple and Total Cyanides." Water Research 10 (1976) : 479.

Song, Y. H.; Blair, D. W.; Siminski, U. J.; and Bartok, W. "Conversion of Fixed Nitrogen to N_2 in Rich Combustion." Eighteenth Symposium (International) on Combustion. Pittsburgh, Penn.: The Combustion Institute (1981).

Standard Methods for the Examination of Water and Wastewater. 13th ed. New York: American Public Health Association, American Water Works Association, and Water Pollution Control Federation, 1971.

Takagi, T.; Tatsumi, T.; and Ogasawara, M. "Nitric Oxide Formation from Fuel Nitrogen in Staged Combustion: Roles of HCN and NI_i." Combustion and Flame 35 (1979) : 17-25.

Turner, D. W.; Anderson, R. L.; and Siegmund, C. W. "Influence of Combustion Modification and Fuel Nitrogen Content on Nitrogen Oxides Emissions from Fuel Oil Combustion." AIChE Symposium Series No. 136 68 (1972).

Zeldovich, B. 1/a.; Sadovnikov, P. 1/a.; and Frank-Kamentskii, D. A. Oxidation of Nitrogen in Combustion. Translated by M. Shelef. Moscow, U.S.S.R.: Academy of Sciences, U.S.S.R. Institute of Chemical Physics, 1947.

III. SPRAY CHARACTERIZATION

by:

W. R. Seeker and G. S. Samuelsen

Energy and Environmental Research Corporation
18 Mason
Irvine, CA 92714

TABLE OF CONTENTS

Section Page (III-)

1.0 INTRODUCTION 1

2.0 BACKGROUND 4

2.1 IFRF Studies 4
2.2 Droplet Measurement Techniques 6
2.2.1 Mechanical Versus Optical 6
2.2.2 Optical Visualization Techniques 9
2.2.3 Optical Light Scattering Techniques 11
2.3 Present Study 12

3.0 APPROACH 13

4.0 EXPERIMENT 15

4.1 Spray Chamber 15
4.2 Laser Interferometry System 19
4.3 Laser Holography System 22
4.4 Laser Diffraction System 25
4.5 Test Matrix 25

5.0 RESULTS 34

5.1 Laser Interferometry Results 34
5.2 Assessment of Laser Interferometry Results 44
5.2.1 Laser Holography 44
5.2.2 Laser Diffraction 56

6.0 SUMMARY AND RECOMMENDATIONS 69

REFERENCES 71

APPENDIX A - Characterization of a Sonicore Nozzle . . . . A-i

APPENDIX B - Response of Spectron Development Laboratories for Clarification to Final Report . . . . B-i

APPENDIX C - Characterization of a Sonicore Nozzle (RAW DATA). . . . C-i

LIST OF FIGURES

Number Page (III-)

1 NO_x Emissions From a Firetube Combustor (England, et al., 1979) . . . 2

2 NO_x Emissions From a Tunnel Furnace (Heap, et al., 1979) . 3

3 IFRF Spray Performance Study (Flament and Payne, 1979) . . 5

4 IFRF Laser Diffraction Results (Flament and Payne, 1978) . 7

5 NO_x Emission--Relationship to Drop Size and Distribution . 8

6 Experimental Facility . . . 14

7 Cold Chamber . . . 16

8 Sonicore Nozzle . . . 20

9 Laser Interferometry System . . . 21

10 Laser Holography System . . . 23

11 Laser Diffraction System . . . 26

12 Laser Interferometry--Typical Tabulation . . . 35

13 Laser Interferometry--Spatial Variation of Number Density . 38

14 Laser Interferometry--Axial Variation of Volume Mean Diameter . . . 40

15 Laser Interferometry--Dependency of Volume Mean Diameter on Nozzle Atomizing Pressure . . . 42

16 Laser Interferometry--Dependency of Droplet Velocity on Droplet Size . . . 43

17 Laser Interferometry--Axial Variation in the Velocity of 52.7 μm Droplets . . . 45

18 Laser Interferometric and Holography Data--Number Density (1.34 atm) . . . 50

19 Laser Interferometry--Dynamic Range Limit . . . 55

20 Laser Interferometric and Holography Data--Weight Density (1.34 atm) . . . 57

LIST OF FIGURES

Number		Page (III-)
21	Interferometric and Diffraction (IFRF) Data	61
22	Interferometric, Diffraction (EER), and Holographic Data (1.34 atm, X = 20 cm)	66
23	Interferometric, Diffraction (IFRF), and Diffraction (EER) Data--Weight Density	68

LIST OF TABLES

Number		Page (III-)
1	Test Matrix	27
2	Experimental Tasks (Interferometry)	28
3	Experimental Tasks (Holography)	30
4	Experimental Tasks (Diffraction-EER)	33
5	Conditions for Comparison of Laser Holography to Laser Interferometry	48
6	Dynamic Range of Laser Interferometric Data	54
7	Conditions for Comparison of Laser Diffraction (IFRF) to Laser Interferometry	60
8	Conditions for Comparison of Laser Diffraction (EER) to Laser Interferometry	64

1.0 INTRODUCTION

The results from recent EPA Combustion Research Branch (CRB) studies indicate that the emission of NO_x from oil-fired furnaces and boilers are influenced by the type of nozzle employed, the operating condition of the nozzle, and the swirl of primary air (England, et al., 1979; Heap, et al., 1979). For example, the data of Figure 1 were obtained from a firetube boiler simulator operating with a variety of nozzle types under three swirl conditions. At low swirl, an increase in swirl number produces sharp reductions in the NO_x emitted. For most of the nozzles, NO_x then increases as the swirl number is raised to 0.8. A notable exception is the Monarch nozzle, the emissions for which continue to decrease as the swirl number is raised.

A second example (Figure 2) is data obtained from a tunnel furnace that was operated (a) in the absence of swirl, and (b) with a zero-nitrogen oxidizer (Ar, CO_2, O_2) as well as air to isolate the fuel NO_x produced. Here, the operating condition of the nozzle is shown to also influence the NO_x emission. Thermal NO_x, for example, decreases dramatically as atomizing pressure is reduced.

These data identify the need for characterizing those properties of sprays (e.g., droplet size distribution, droplet velocity, gas velocity, evaporation rate) that likely dictate the NO_x produced. Characterizations of this type require the measurement of local droplet size, local droplet velocities, and local gas velocities. Of the variety of techniques available to measure spray properties, only laser interferometry has the immediate potential to measure simultaneously the properties of interest. The present FCR study was established to test the applicability of laser interferometry in measuring spray properties for a variety of conditions, and to compare the results against the following two more conventional and extensively used but less versatile techniques: laser diffraction and laser holography. As a result, this study represents the first to systematically assess the performance of laser interferometry against that of laser diffraction and laser holography.

(a) Firetube Combustor

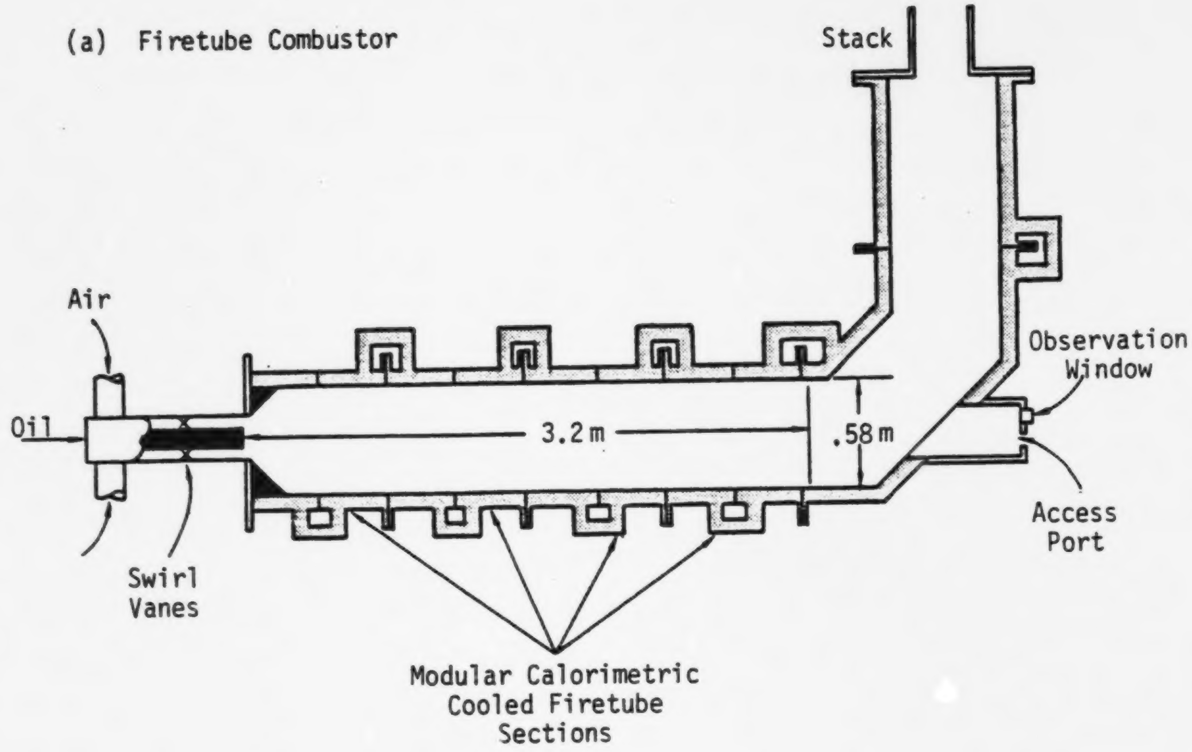
Stack
Air
Oil
Swirl Vanes
3.2 m
.58 m
Observation Window
Access Port
Modular Calorimetric Cooled Firetube Sections

(b) NO_x Emissions

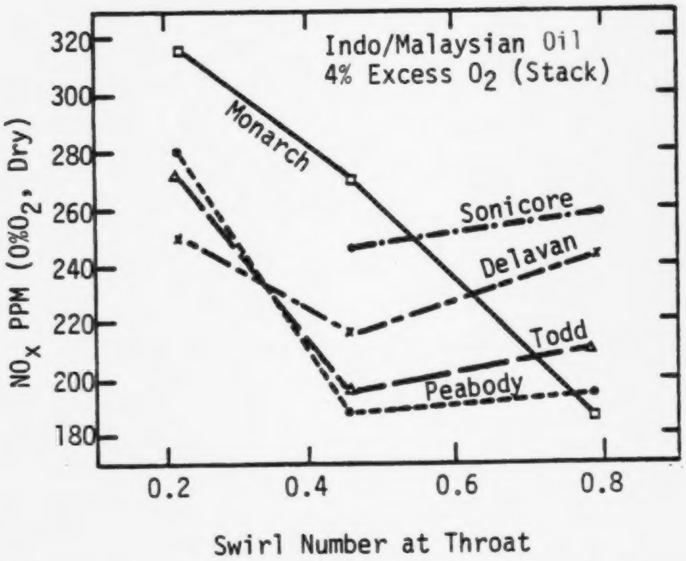

Figure 1. NO_x Emissions From a Firetube Combustor (England, et al., 1979).

(a) Tunnel Furnace

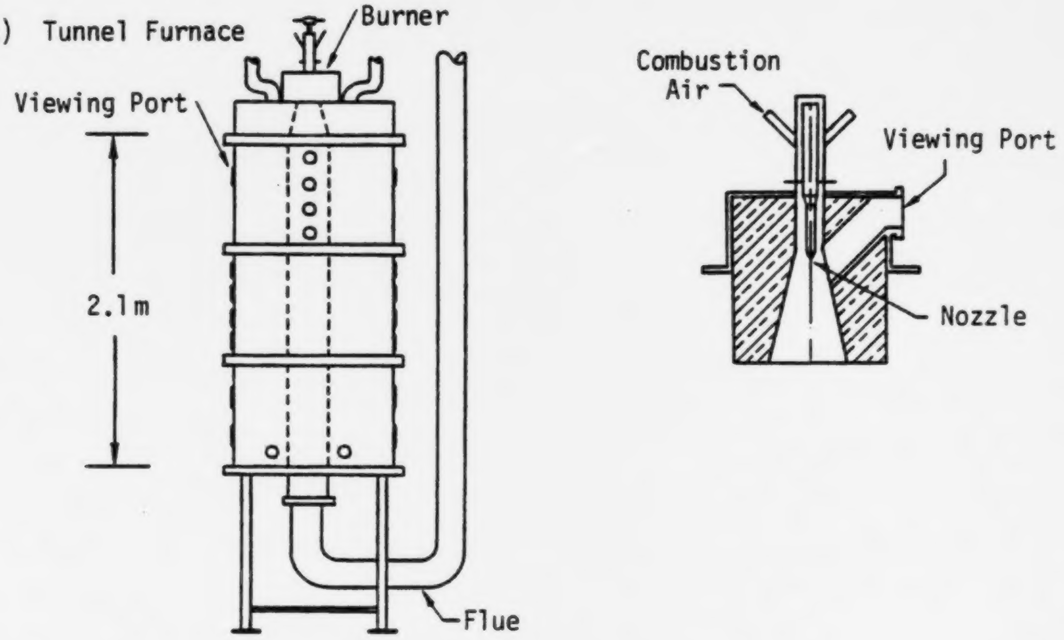
Burner
Viewing Port
2.1m
Flue
Combustion Air
Viewing Port
Nozzle

(b) NO_x Emissions

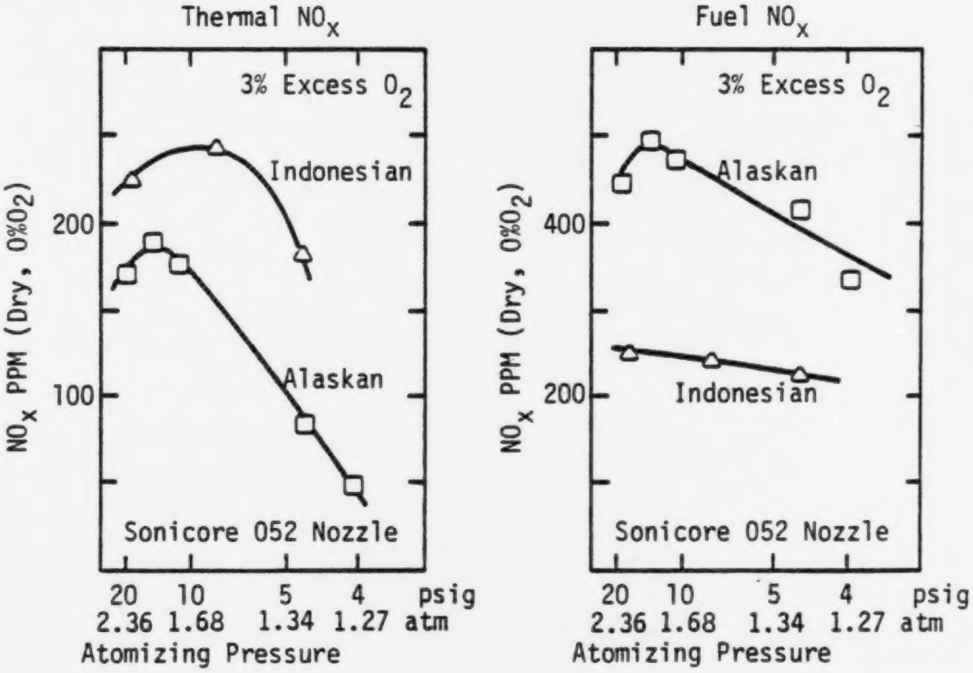

Figure 2. NO_x Emissions From a Tunnel Furnace (Heap, et al., 1979).

2.0 BACKGROUND

Before the present program was initiated, an exploratory study of spray behavior was conducted at the International Flame Research Foundation (IFRF) under EPA support (England et al., 1982). The goal was to obtain some initial indication of nozzle performance that might explain the data of Figures 1 and 2. A number of nozzles were analyzed in a cold spray chamber using a commercial laser diffraction diagnostic (Malvern Spray Analyzer). Though the data collected were both informative and enlightening, a major question raised concerned the adequacy of the droplet sizing technique employed, first with respect to accuracy, second with respect to the spatial detail provided, and third with respect to adequacy of the information obtained.

The following two sections review the IFRF results and the variety of techniques available for measuring spray performance. Emphasis is directed to those aspects of the IFRF study and diagnostics relevant to the present program.

2.1 IFRF Studies

The IFRF studies employed an existing cold-flow chamber (Figure 3a) in conjunction with a commercial laser diffraction particle sizing instrument (Malvern Model ST18005). The Malvern was fixed in position, and axial traverses were permitted by moving the nozzle assembly vertically. The laser diffraction technique, shown in schematic in Figure 3b, was developed at the University of Sheffield (Swithenbank, et al., 1976). A 2 mw laser beam is expanded and collimated to a 6.0 mm diameter beam for projection through the spray. Light from the beam is diffracted by droplets, the angle of diffraction depending on the particle size. (As the particle size decreases, the angle of diffracted light increases.)

The diffracted light is collected by a Fourier transform lens and focused on a 30-ring detector. The distribution of light energy across the 30 rings is read by a minicomputer and fit to a Rosin-Rammler distribution. The sweep time of the detector is approximately 13 ms. Usually 100 to 200 readings are required to obtain a representative, averaged reading.

The technique provides a size distribution for the droplets within the scattering volume. The technique does not measure individual drop sizes at

(a) Cold Chamber Experiment

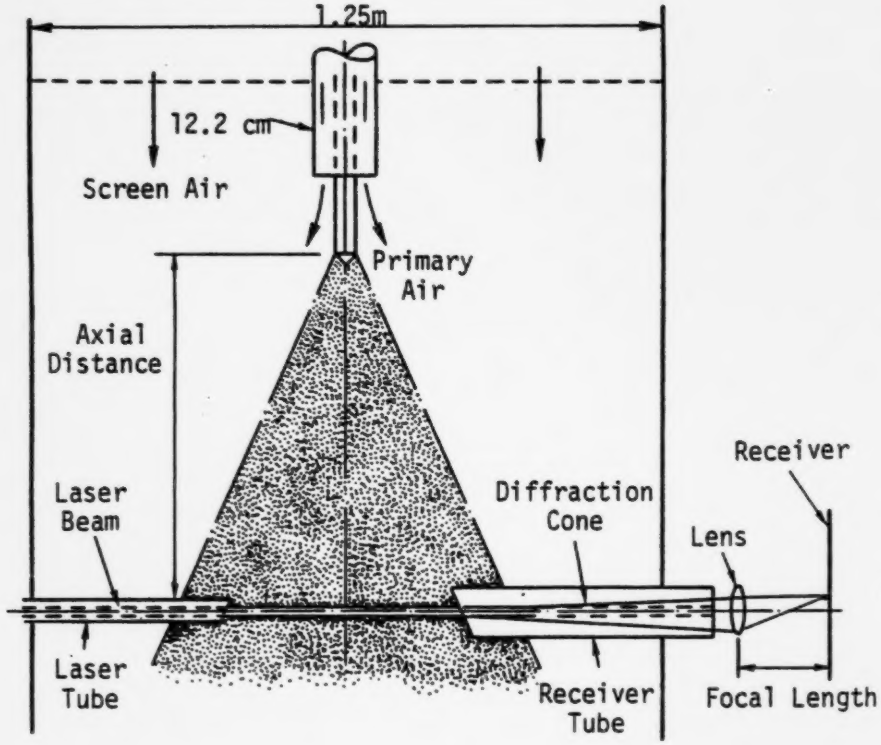
1.25m
12.2 cm
Screen Air
Primary Air
Axial Distance
Laser Beam
Diffraction Cone
Receiver
Lens
Laser Tube
Receiver Tube
Focal Length

(b) Laser Diffraction Diagnostic

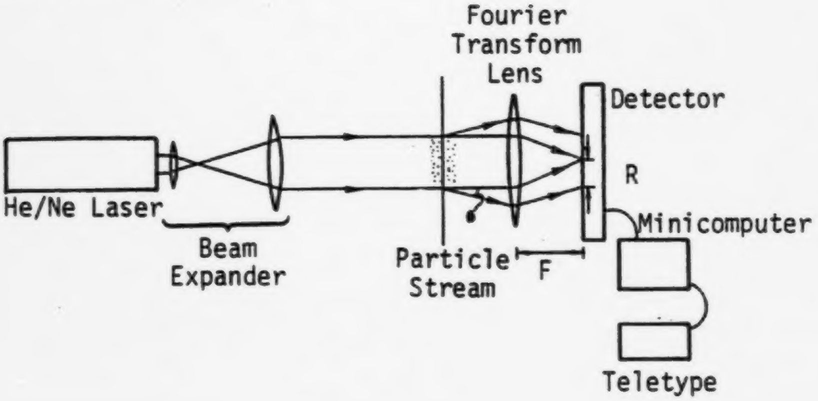
Fourier Transform Lens
Detector
R
He/Ne Laser
Minicomputer
Beam Expander
Particle Stream
F
Teletype

Figure 3. IFRF Spray Performance Study (England et al., 1982).

a point, nor does the technique provide velocity information. This notwithstanding, the Malvern has the advantage of (1) providing droplet size information within minutes, and (2) being relatively simple in both the hardware and software.

An example of data provided by the laser diffraction technique is presented in Figure 4. Droplet size distributions at one axial location are presented in Figure 4a for the Sonicore nozzle employed in the tunnel furnace studies of Figure 2. The parameter in the plot is atomizing pressure. The data indicate that both the mean droplet size and size distribution are strongly dependent on atomizing pressure.

In Figure 4b, the variation of Rosin-Rammler mean diameter with axial distance is shown. The effect of nozzle type on this variation is also demonstrated.

The information presented in Figure 4a can be applied to the NO_x emission data from the tunnel furnace to provide some insight into the causal-effect relationship between nozzle and emission. From Figure 5, it is apparent that larger droplets and/or broader size distribution contribute to lower NO_x emission. However, these data, though instructive, are not sufficient to fully assess the relationship of NO_x emission to nozzle performance. Additional information is required, including spatial (axial and radial) resolution of droplet size and velocity of individual droplets and fuel property effects such as viscosity. As background for the approach and measurement techniques employed in the present study, methods available for the acquisition of these data are summarized in the following section.

2.2 Droplet Measurement Techniques

2.2.1 Mechanical Versus Optical

Droplet sizing was first conducted using mechanical techniques. Optical methods were later introduced with the application of photographic techniques to spray analyses. Now, with the advent and advance of laser technology, the optical methods have expanded in number with a continual expansion in capability.

Mechanical methods include (1) droplet impaction on glass slides coated with such materials as oil, grease, soap, plastic film, and magnesium oxide

(a) Droplet Size Distribution

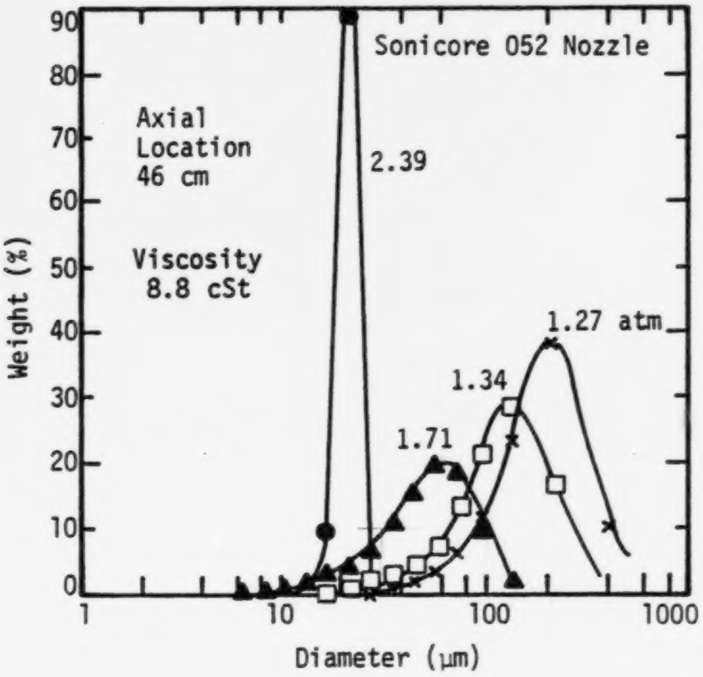

(b) Axial Variation

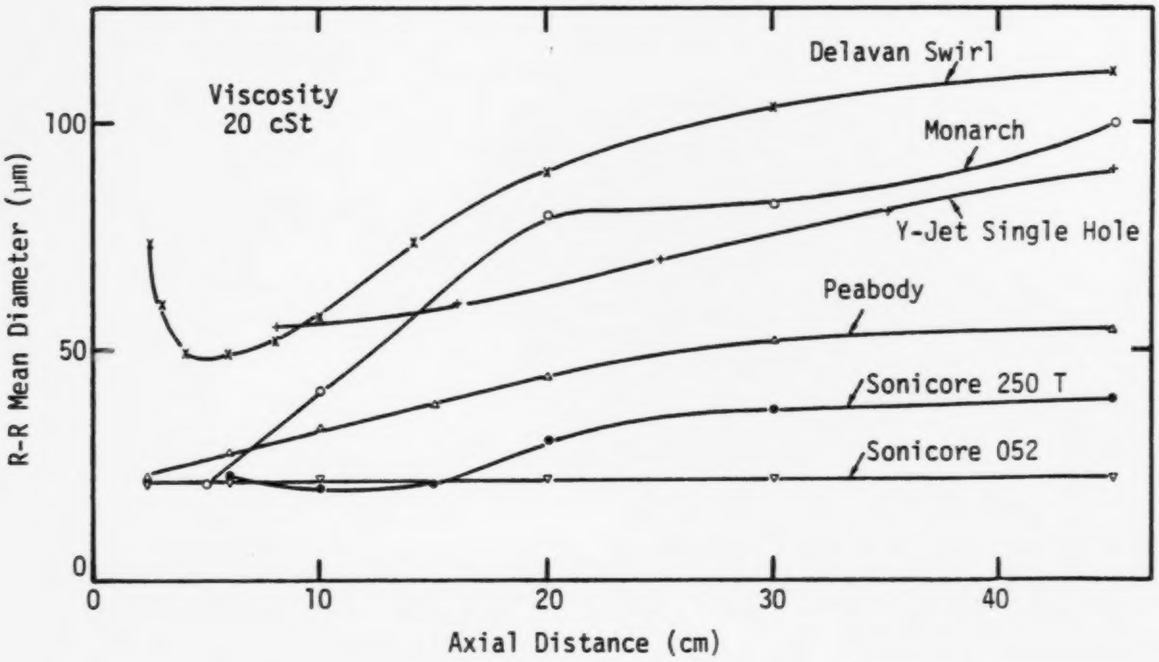

Figure 4. IFRF Laser Diffraction Results (England et al., 1982).

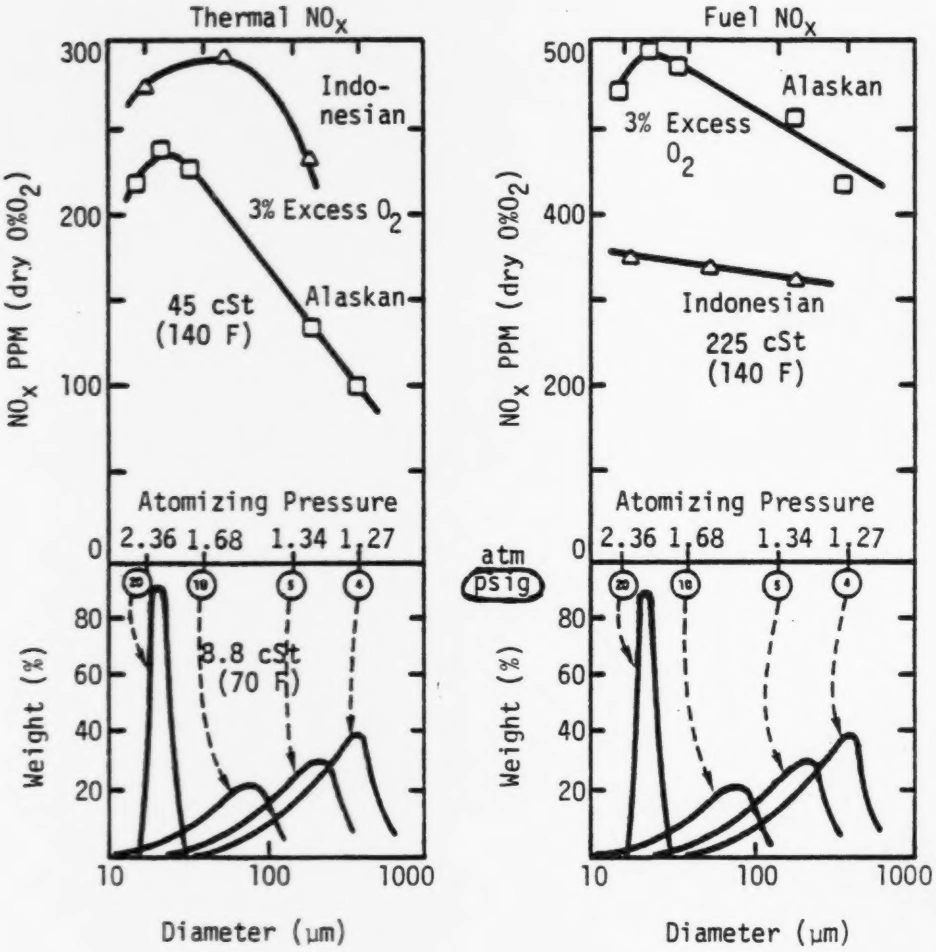

Figure 5. NO_x Emission--Relationship to Drop Size and Distribution.

(e.g., Kuhn, 1925; Lee, 1932; Nukiyama, 1938; Woolridge, 1959), (2) droplet impaction on an immersion fluid that is immersible with the sampled droplet (e.g., Tate, 1961), (3) freezing of atomized droplets (e.g., Taylor, 1954), (4) the use of molten wax as the atomizing fluid and the subsequent solidification and collection of wax particles (e.g., Joyce, 1946), and (5) aerodynamic separation of collected sprays (e.g., May, 1945). All these techniques require some means, usually tedious and time-consuming, of counting and sizing the collected droplets. In addition, the local flowfield and droplet properties can be perturbed by the collection techniques employed. Finally, the data cannot be readily resolved spatially nor temporally, and the velocity of individual droplets cannot be obtained.

Optical sizing techniques have four distinct advantages over mechanical techniques--they are nonintrusive and perturb neither the flow nor droplet conditions, measurements can be made in-situ, the droplet properties can be measured in relatively short periods, and droplet velocities can be obtained. From the variety available, optical techniques can be classified into two general groups: visualization and light scattering.

2.2.2 Optical Visualization Techniques

High-Speed Photography. High-speed photography has been used to measure size distributions in sprays and thereby avoid local perturbation by an intrusive probe (e.g., Subbs and York, 1952; DeCorso, 1958; Dobbins, et al., 1963; Ingebo, 1957). However, photography is not readily capable of giving the temporal distribution of the droplet sizes produced by the atomizer. In addition, the perceived size distribution is biased to the small particles. This is a result of the spray ballistics. The large droplets maintain a velocity after leaving the atomizer that is higher than the velocity of the smaller drops. As a result, the number concentration of the smaller droplets is disproportionately biased to a higher percentage. It is necessary to convert the apparent spatial distribution to the true distribution by multiplying the number of droplets of any given size by the droplet velocity for that size.

Analyses of spray photographs are also compromised by the interpretation of the depth of field. The question arises as to whether blurred images outside the field of focus should be counted. There is a tendency to count large droplets over a greater depth of field than would be covered when counting smaller droplets. One approach to this problem is to observe Fresnel diffraction rings around droplet images (DeCorso, 1958). The width of the diffraction ring can be correlated to the position of the droplet in the field of focus. The rejection or acceptance of a droplet, then, can be based on the appearance of the rings.

Holography. Holography has been used successfully in dilute spray systems in both isothermal (Polymeropoulos and Sernas, 1977) and reacting flows (Webster, et al., 1976). An advantage over photography is the provision of a 3-D recording which removes the depth of field uncertainty but still leaves the ambiguity associated with defining a sample volume for droplet sizing.

In dense sprays of the type encountered in boilers, the utility of holography is uncertain. In order for drops to be reconstructed clearly, the coherent light diffracted by each drop must pass unobstructed to the film plane. In dense sprays, secondary scattering of the light diffracted from the original source can occur and thereby create a hologram with ill-defined droplets.

As with photographic techniques, the analysis of holograms is tedious and dependent on judgment. Image analyzers have been employed to extract droplet size information (e.g. Feinstein and Girard, 1979), but the judgment of an operator is still required to determine which images are in focus and how many are not.

Flash TV. A high-speed flash-illuminated, television recording instrument has been designed (Simmons and Lapera, 1969) and used (e.g., Simmons, 1977) to measure local size distributions and, by spatial traverse, size distributions of whole sprays. A high-intensity (xenon) lamp is flashed at a preset frequency in the range from 100 to 1000 times with a 0.5 microsecond duration. The light is focused at a point in the spray producing a sampling volume, typically 10 mm^3. The illuminated droplet is transmitted to a 525-line TV camera Vidicon using appropriate optics.

The focus of the droplet is assessed electronically and rejected if not within prescribed constraints. The drop is then sized by the number of lines intercepted on the photosensitized surface of the Vidicon. The resolution is typically 4 μm. Sized particles are then classified into six size ranges and stored on magnetic tape. The tape can subsequently be fed for computer manipulation of the data, including various mathematical and statistical operations.

2.2.3 Optical Light Scattering Techniques

Light scattering methods can be divided into two categories, those that measure the light from a collection of particles in a collimated laser beam, and those that measure the light scattered from a highly focused laser beam by individual particles. A primary example of the former is the angular light distribution produced by droplets scattering light in the forward direction by diffraction. The primary example of the latter are droplets scattering light from an optical fringe produced by interferometry.

Diffraction. The standard example of droplet sizing using diffractive scattering is a technique described by Dobbins et al. (1963). The method is based on the forward scattering of a parallel beam of monochromatic light which has passed through a spray. The Sauter mean diameter is directly dependent upon the angular distribution of the light intensity. The technique has been applied satisfactorily to a number of practical problems (e.g., England et al., 1982 ; Tishkoff, et al., 1980; Negus and Azzopardi, 1978) to recover the spray Sauter mean diameter as a function of nozzle operating condition.

Although the angular distribution of the light intensity does not allow a distribution of droplet size to be inferred (Dobbins, et al., 1963), the angular distribution of light energy can be related to distribution (Swithenbank, et al., 1976). It is this method that is employed commercially in the Malvern instrument as described earlier with respect to the IFRF studies.

Interferometry. Interferometry utilizes a laser beam split into two parallel beams of equal intensity. The sampling volume is formed by focusing the two beams at a point. The intersection of the two beams establishes an interference fringe pattern (i.e., a row of equally-spaced columns of light varying in intensity in a Gaussian distribution). A droplet passing through the columns of light scatters light from each column in succession. Because the spacing between the columns can be calculated from the angle of intersection and the wavelength of the incident light, the velocity of the droplet passing through the fringe is a function of the frequency ("doppler signal") of the scattered light.

The relative amplitude modulation of the doppler signal is referred to as the visibility of the droplet producing the signal. The amount of modulation is a function of the particle size relative to the fringe spacing (i.e., a function of d/δ, where d is the particle diameter and δ is the fringe spacing) (Farmer, 1973).

Bachalo (1980) expanded the concept of visibility by utilizing light scattered in angles away from the forward direction. The net effect is to (a) reduce the size of the measurement volume, (b) reduce the background noise, and (c) increase the size limits over which the technique can be used. Rather than measuring the diffractive component of light scattered in the forward direction, the technique relies on the measurement of the reflected and refracted light, and is based on the measurement of the relative phase shift that occurs when two light waves pass through the droplets following different paths.

Additional information is provided in Appendix A.

2.3 Present Study

The present study was established to build upon the experience of the IFRF experiments, and to explore the utility and applicability of laser interferometry. The technique has the capability of providing the type of measurements required to address the relationship between NO_x emission and spray performance, namely:

- point measurement
- single droplet sizing
- droplet velocity
- gas velocity

The approach adopted is addressed in the following section.

3.0 APPROACH

The approach adopted for the present study was to obtain spray measurements under cold conditions in a chamber patterned after the firetube combustor (from which the data of Figure 1 were obtained) with respect to the diameter and the ability to later accommodate a variety of inlet geometries and swirl levels. Schematics of both the spray chamber and the firetube combustor are shown in Figure 6. The spray in the cold chamber is downward injected from a movable platform with respect to a fixed observation position. Details are presented in Section 4.

The following three nonintrusive laser techniques were used to characterize spray performance:

- interferometry
- holography
- diffraction

Interferometry is a point measurement technique and was selected because of the potential to (1) measure simultaneously droplet size and velocity, and (2) resolve spatially droplet size and velocity distributions. Holography provides an instantaneous, three-dimensional "picture" of the droplet field and was selected as a check for the interferometric and diffraction techniques. Diffraction was selected because, although velocity and spatial resolution are not provided, the technique has been extensively tested (e.g., Negus and Azzopardi, 1978) and is relatively fast in providing processed data. In addition, because diffraction was employed in the IFRF studies, the adaptation of diffraction to the present study had the added advantage of providing a check on reproducibility between two laboratories, including evaluation of chamber size. It is noteworthy that the diameters of the IFRF (Figure 3) and present (Figure 6) experiments are substantially different, 1.25m and 0.61m, respectively.

(a) Cold Chamber

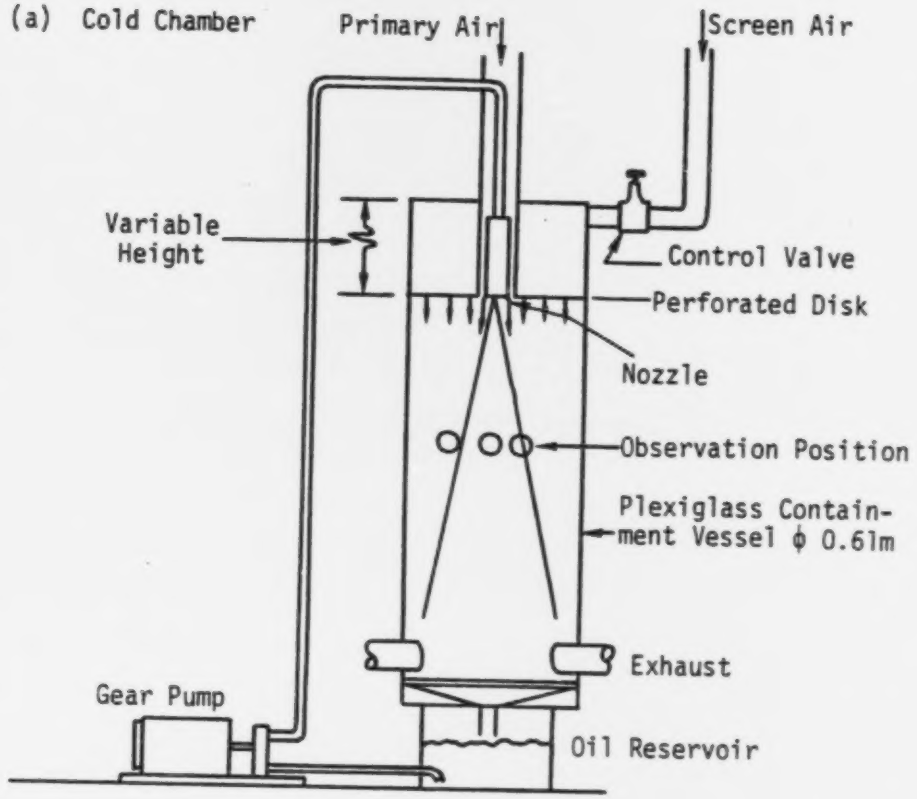
Primary Air
Screen Air
Variable Height
Control Valve
Perforated Disk
Nozzle
Observation Position
Plexiglass Containment Vessel ϕ 0.61m
Exhaust
Gear Pump
Oil Reservoir

(b) Firetube Combustor

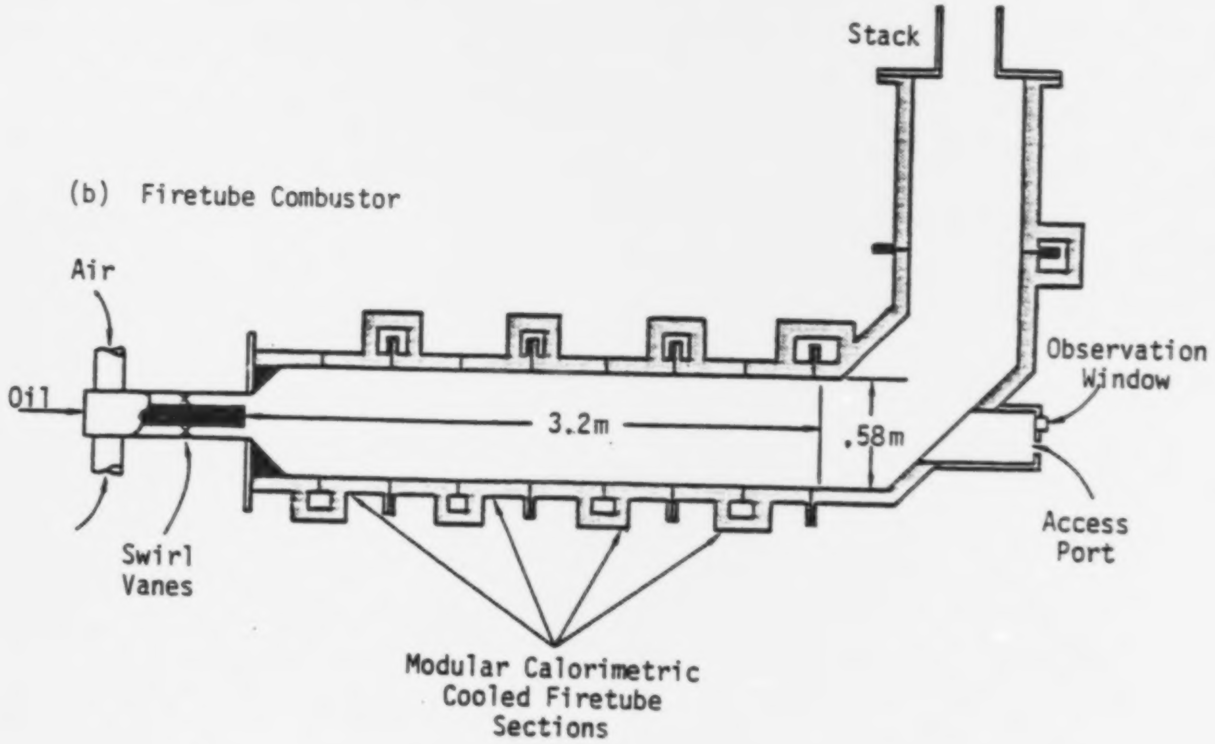
Stack
Air
Oil
3.2m
.58m
Observation Window
Access Port
Swirl Vanes
Modular Calorimetric Cooled Firetube Sections

Figure 6. Experimental Facility.

4.0 EXPERIMENT

4.1 Spray Chamber

A schematic of the nozzle characterization spray chamber is presented in Figure 7. The spray is directed downward in a plexiglass tube with an inner diameter of 0.61m and a height of 1.83m. Fuel oil is supplied to a Sonicore nozzle through the use of a Zenith pump metering system which allows fine control of the flow rate between 1.06 to 10.6 liters/hr (0.18 to 2.8 gal/hr). The pump can be exchanged for a larger one if higher flow rates are required in later applications.

Two separate air flow systems are used--a primary flow and a screen air flow. The primary air is directed coaxially around the nozzle holder. The screen air is used to minimize the concentration of the fine mist of oil which can develop around the spray. The screen air flow is directed downward uniformly across the vessel diameter through the use of a perforated plate. The flows are supplied by two high-pressure blowers which allow flow rates to 22.9 m^3/min (810 CFM) for the primary air and up to 11.2 m^3/min (395 CFM) for the screen air. In the present configuration these flow rates correspond to velocities up to 40.2 m/sec (132 ft/sec) for the primary and up to 0.67 m/sec (2.2 ft/sec) for the screen flow. The flow rates are measured using Barco venturis with the pressure drop measured with magnehelic differential pressure gauges. The venturis were chosen so as to minimize the pressure loss and to have as much of the pressure head available from the blowers (15.2 cm H_2O from the primary blower and 25.4 cm H_2O from the screen air blower) at the spray rig.

The apparatus has six 7.62 cm (3 inch) diameter windows mounted horizontally at a height of 94 cm (37 inches) from the bottom of the plexiglass container. The window material is ground and polished Optosil 1 fused silica with better than schlieren quality homogeneity, low birefringence and a minimum number of bubbles. These characteristics are all necessary for high quality holography. To allow for versatility in scattering angles and probing of portions of the spray, the windows are arranged, as demonstrated in Figure 7b, at 45^o and 30^o from the central path. The windows are inset slightly from the container walls to prevent direct spray impingement and have a uniform flow velocity across their face to minimize droplet accumulation (Figure 7c). Also, the windows can be easily removed for cleaning. The

(a) Detailed Overview

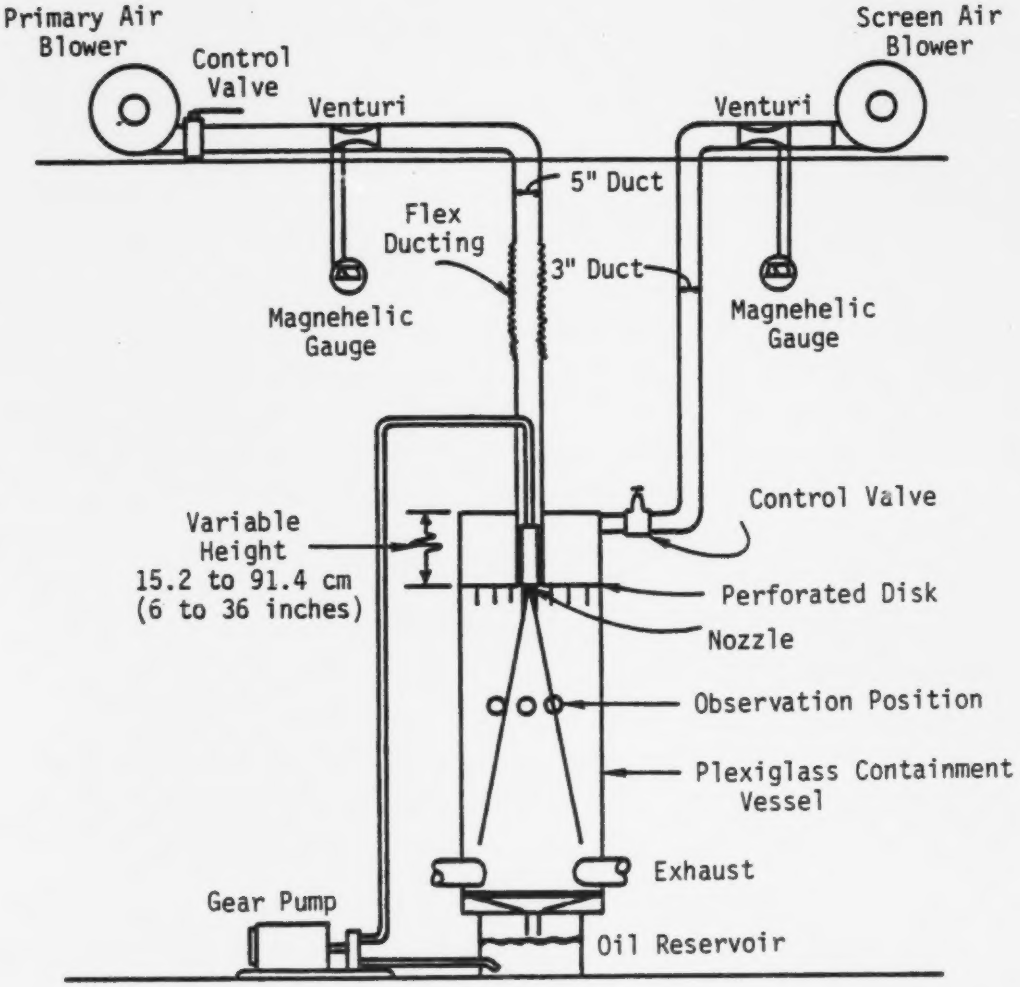
Primary Air Blower
Control Valve
Venturi
Screen Air Blower
Venturi
5" Duct
Flex Ducting
3" Duct
Magnehelic Gauge
Magnehelic Gauge
Control Valve
Variable Height 15.2 to 91.4 cm (6 to 36 inches)
Perforated Disk
Nozzle
Observation Position
Plexiglass Containment Vessel
Exhaust
Gear Pump
Oil Reservoir

Figure 7. Cold Chamber.

(b) Top view showing positioning of windows and available optical paths.

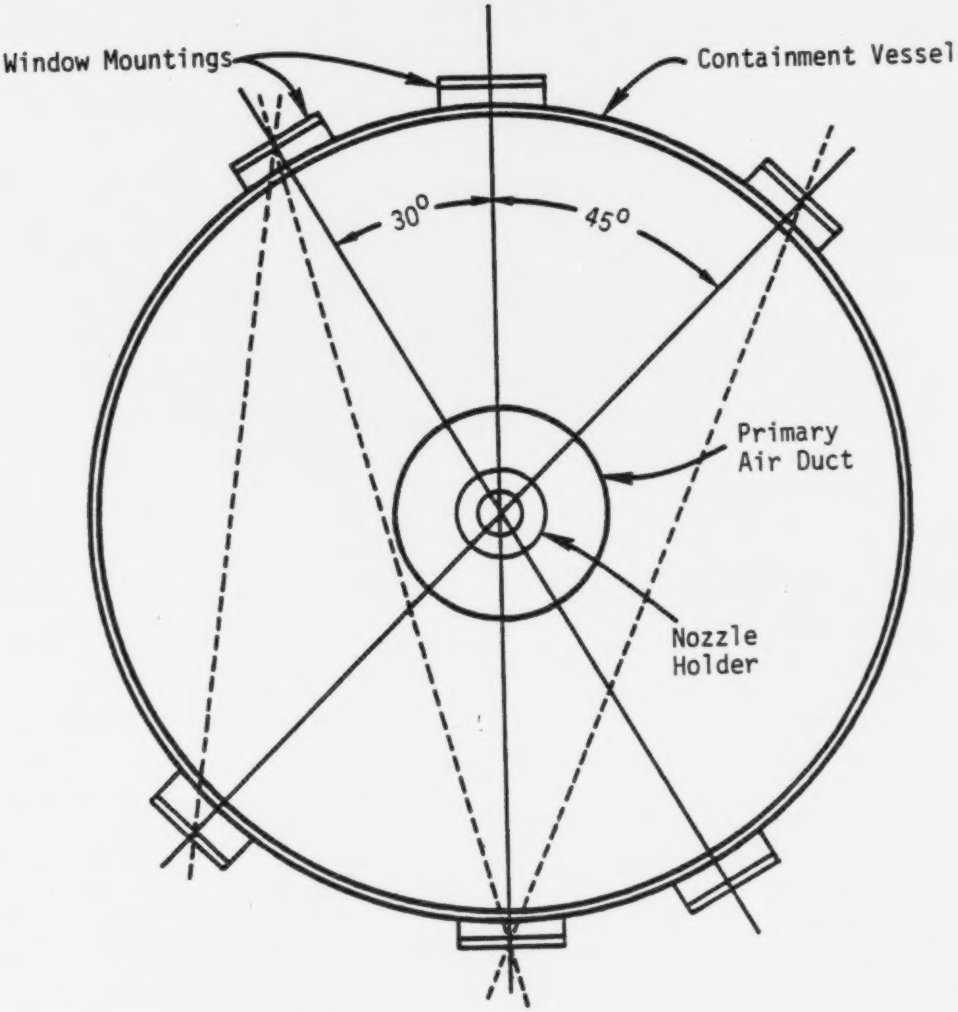
Window Mountings
Containment Vessel
30°
45°
Primary Air Duct
Nozzle Holder

Figure 7. Cold Chamber (Continued).

(c) Window Mounting Detail

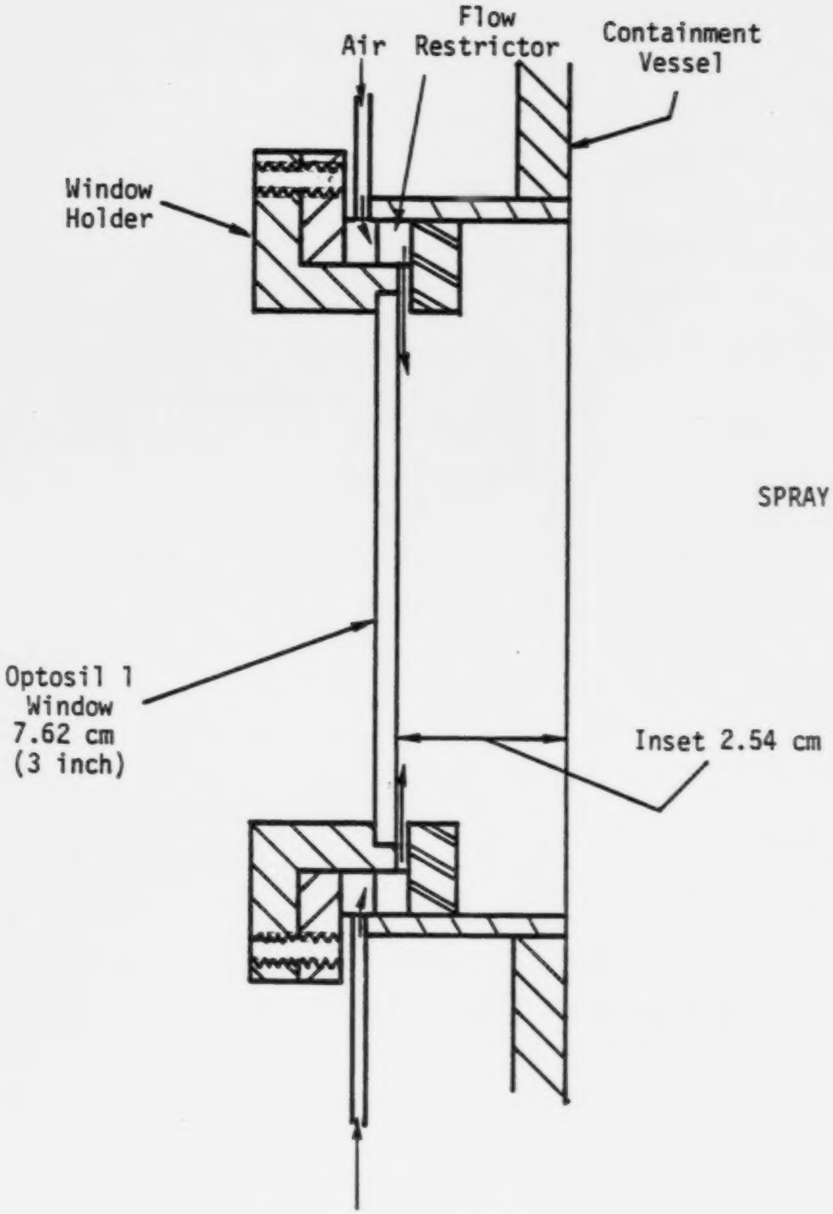
Air
Flow Restrictor
Containment Vessel
Window Holder
SPRAY
Optosil 1 Window 7.62 cm (3 inch)
Inset 2.54 cm

Figure 7. Cold Chamber (Concluded).

nozzle is positioned relative to the windows and optical systems by physically moving the nozzle holder/perforated screen air module. As designed, the axial position of the measurement can be varied from as close to the nozzle as allowed by the optical system to 76.2 cm away from the nozzle.

A Sonicore type 052 nozzle was selected because it is the only nozzle type common to both the tunnel furnace (Figure 1) and firetube furnace (Figure 2) data. In addition, the IFRF study included some limited data on the 052 model. The Sonicore 052 is a twin-fluid atomizer (Figure 8). Air is conveyed through the central core of the nozzle. The fuel oil is introduced downstream of the throat of a converging-diverging section. According to the manufacturer, "...as the gas expands through a converge-diverge section and into a reasonator cap at supersonic velocity, the reflected shockwaves focus the sonic energy between the resonator cap and the body of the nozzle. Fuel pumped into the shock wave is literally exploded into a fine, highly combustible mist."* The actual mechanism of liquid breakup is not certain as the nominal operating pressures for the Sonicore nozzles are substantially below those required to produce supersonic flow in the diverging section.

4.2 Laser Interferometry System**

The optical system for the laser interferometry was constructed on a breadboard, a schematic of which is presented in Figure 9. It consisted of a HeNe laser, transmitting lenses, a diffraction grating, transmitting mirrors, and collecting lenses. The lenses in both the transmitting and collecting optics are achromat in order to minimize aberrations. The transmitting mirrors are flat to one-quarter wavelength.

The laser beam was focused by lens L_1 on the diffraction grating and split into several beams according to the diffraction modes. Modes other than the $\underline{+}1$ modes were masked out. Since the lens L_2 is one focal distance from the diffraction grating, the beams coming out of L_2 were parallel and collimated. The ratio of L_2 to L_1 determined the beam diameter before it was focused by L_3. The separation of the beams was controlled by f_2. This provided an independent means of selecting the fringe spacing and the probe

---

* Oil Saving Combustion Systems with Sonicore Atomizing Nozzles, Bulletin F-300.

**Adapted from Appendix A.

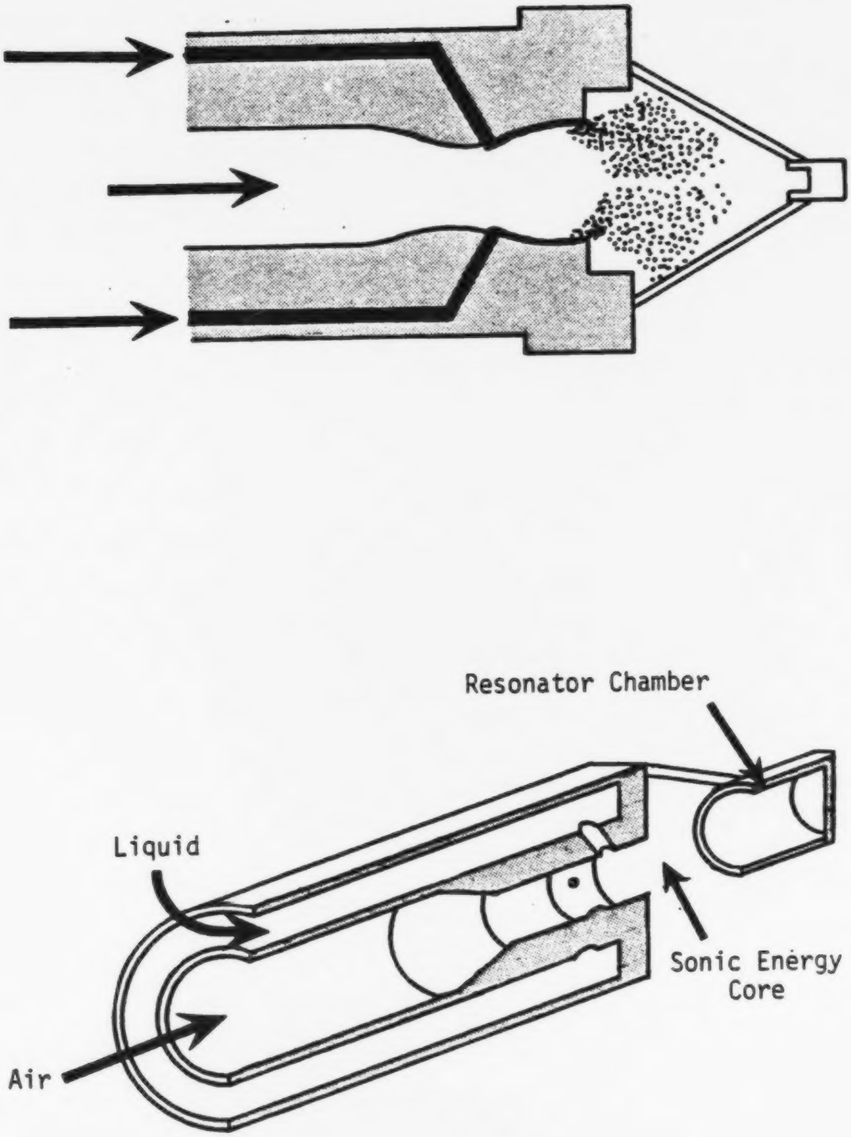
Resonator Chamber
Liquid
Sonic Energy Core
Air

Figure 8. Sonicore Nozzle.

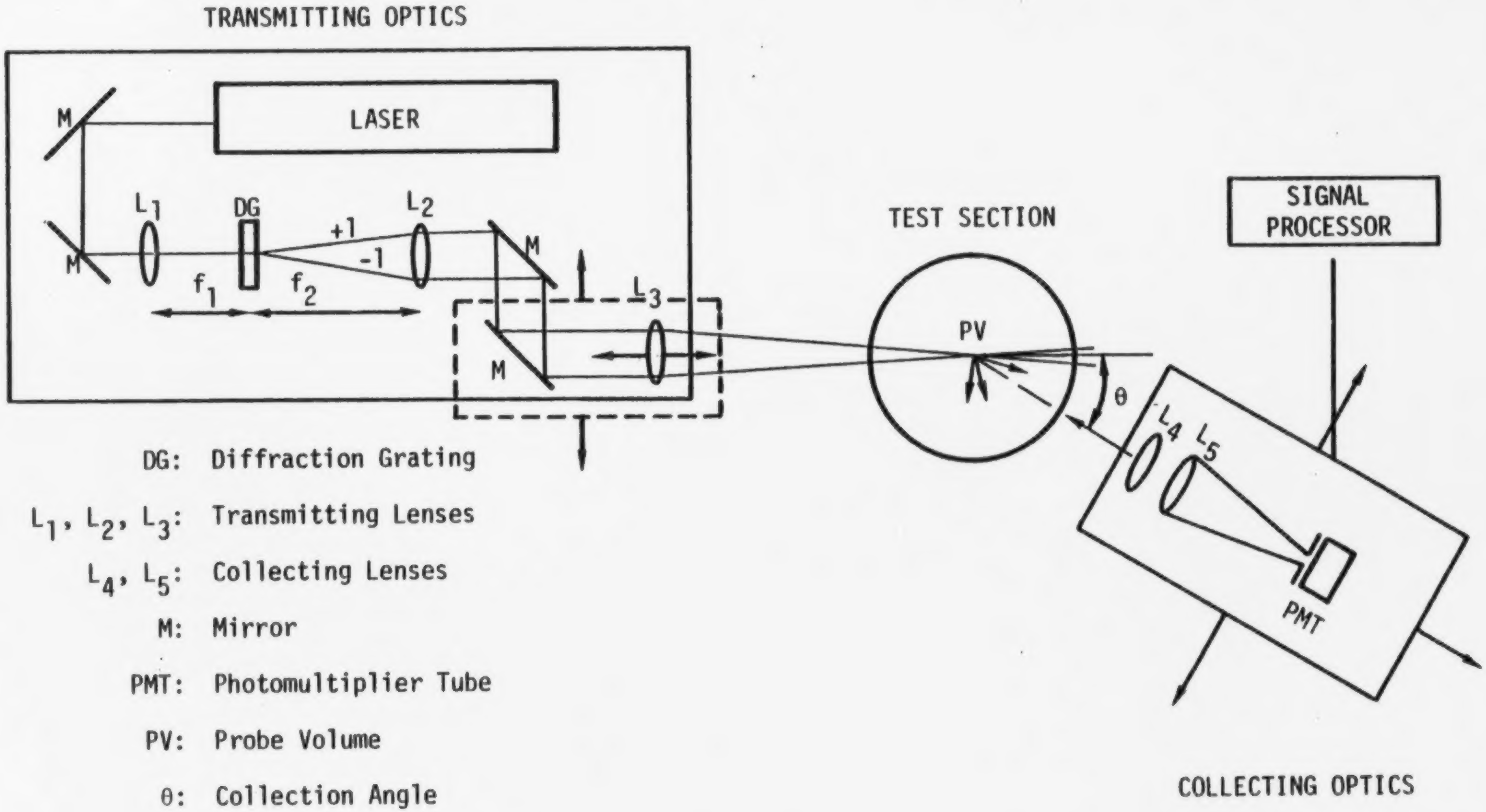
TRANSMITTING OPTICS
LASER
M
M
L1
DG
+1
-1
L2
M
M
f1
f2
L3
TEST SECTION
PV
θ
SIGNAL PROCESSOR
L4
L5
PMT
COLLECTING OPTICS

DG: Diffraction Grating

L_1, L_2, L_3: Transmitting Lenses

L_4, L_5: Collecting Lenses

M: Mirror

PMT: Photomultiplier Tube

PV: Probe Volume

θ: Collection Angle

Figure 9. Laser Interferometry System.

volume size. The laser beams were then focused by L_3 on the probe volume. For the present study, the probe volume was on the order of 0.01 mm^3.

The light scattered by the particles crossing the probe volume was collected by L_4 and then focused by L_5 on the photomultiplier tube. Both the transmitting and the receiving optics were mounted on traverse mechanisms which allowed radial scans to be conducted at any one axial position. Changes in axial positions were accommodated by moving the nozzle/screen air module.

The photomultiplier signal was analyzed by a SDL Model VP-1000 Visibility Processor to establish the Doppler period and visibility. For each particle signal processed, a data management system stored the visibility and period on a diskette for later processing and, for the total particle count, calculated and displayed histograms of particle size and velocity.

4.3 Laser Holography System*

The optical system used in the present experiment for the laser holography is presented in schematic in Figure 10. The system consisted of a HeNe laser for alignment and a ruby laser to take the hologram. The laser beam was split into an information beam and a reference beam. Both beams were expanded, spatially filtered, and collimated. The information beam went through the fuel spray while the reference beam bypassed the test section. The two beams were then mixed on a holoplate in the plate holder. The size of the probe volume was on the order of 10 cm^3.

The shutter in front of the plate holder allowed light to enter only while the recording was taking place and minimized the influence of extraneous light sources.

To align the holography system, a wire was hung inside the test facility at a known position with respect to the nozzle. It was placed far from the nozzle to avoid disturbing the flows. At axial positions downstream from the nozzle, this wire served as a reference. Flash photography on Polaroid film was performed at the beginning of each experiment. This served to confirm the alignment, to check the relative intensity of the reference and

---

*Adapted from Appendix A.

(a) Transmitter Module

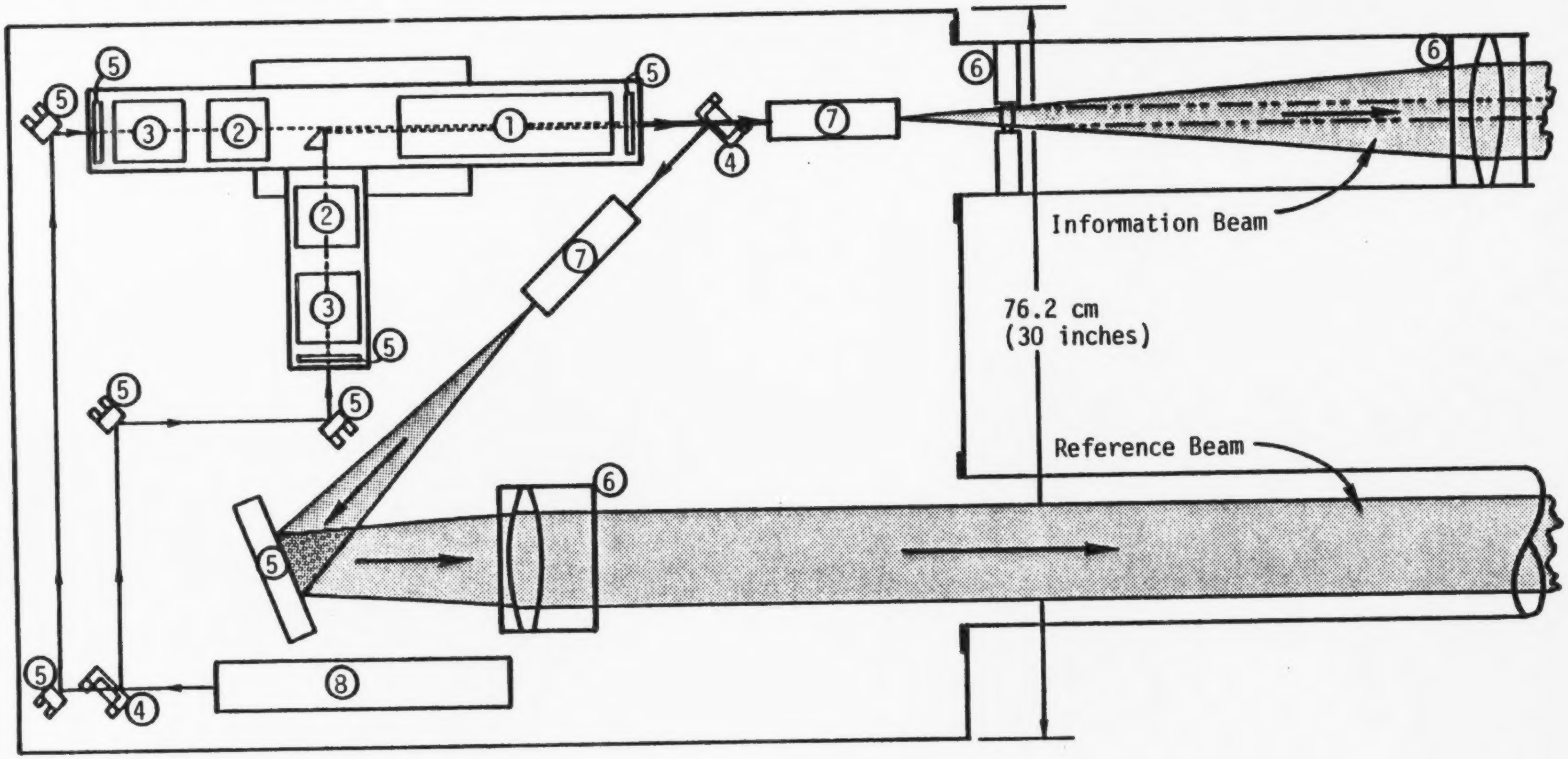
⑤
③
②
①
⑤
④
⑦
⑥
⑥
②
③
⑤
⑦
⑤
⑤
Information Beam
76.2 cm
(30 inches)
Reference Beam
⑥
⑤
⑤
④
⑧

① Ruby Laser
② Pockel's Cell
③ Brewster Stack
④ Beam Splitter
⑤ Mirror
⑥ Lens
⑦ Beam Expander/Spatial Filter
⑧ Alignment Laser (H_e-N_e)

Figure 10. Laser Holography System.

(b) Receiver Module

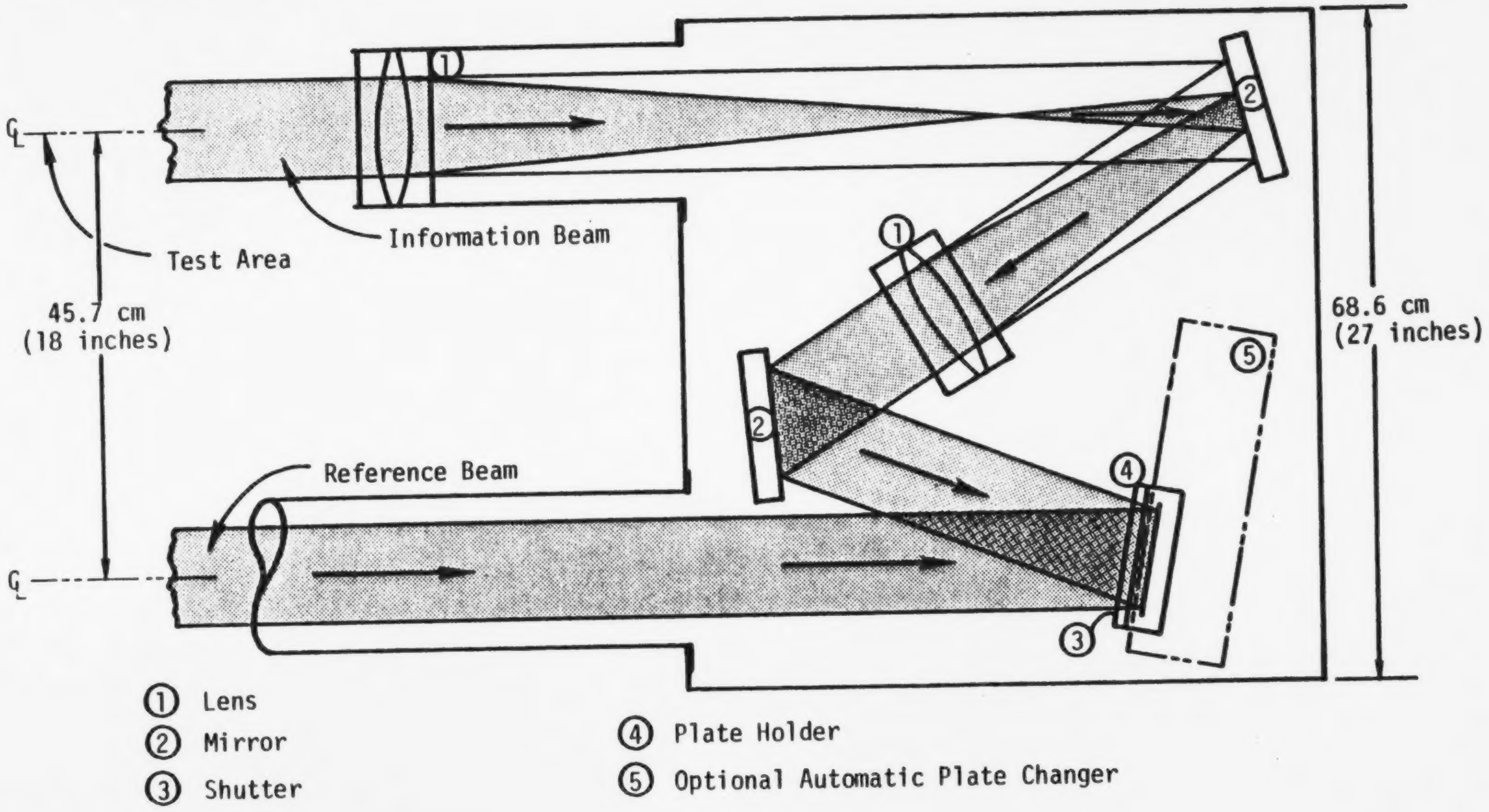
Information Beam
Test Area
45.7 cm
(18 inches)
Reference Beam
68.6 cm
(27 inches)
①
②
③
④
⑤
① Lens
② Mirror
③ Shutter
④ Plate Holder
⑤ Optional Automatic Plate Changer

Figure 10. Laser Holography System (Concluded).

objective waves, and to detect dirt on the optical windows.

4.4 Laser Diffraction System

The Malvern Model 1800, used in the IFRF studies, was transported to EER for use in the present study. A schematic is shown in Figure 11 of the experimental setup. The optical system was mounted on a specially designed support that (a) allowed the optical bench to be rotated out of the spray field and, when located in the spray field, to (b) traverse the spray radially by movement along rails fixed to the footing of the support structure.

4.5 Test Matrix

The experimental conditions used in the present experiment are presented in Table 1. Division of the conditions into experimental tasks is delineated in Tables 2, 3, and 4 for the three diagnostic methods: laser interferometry, laser holography, and laser diffraction, respectively.

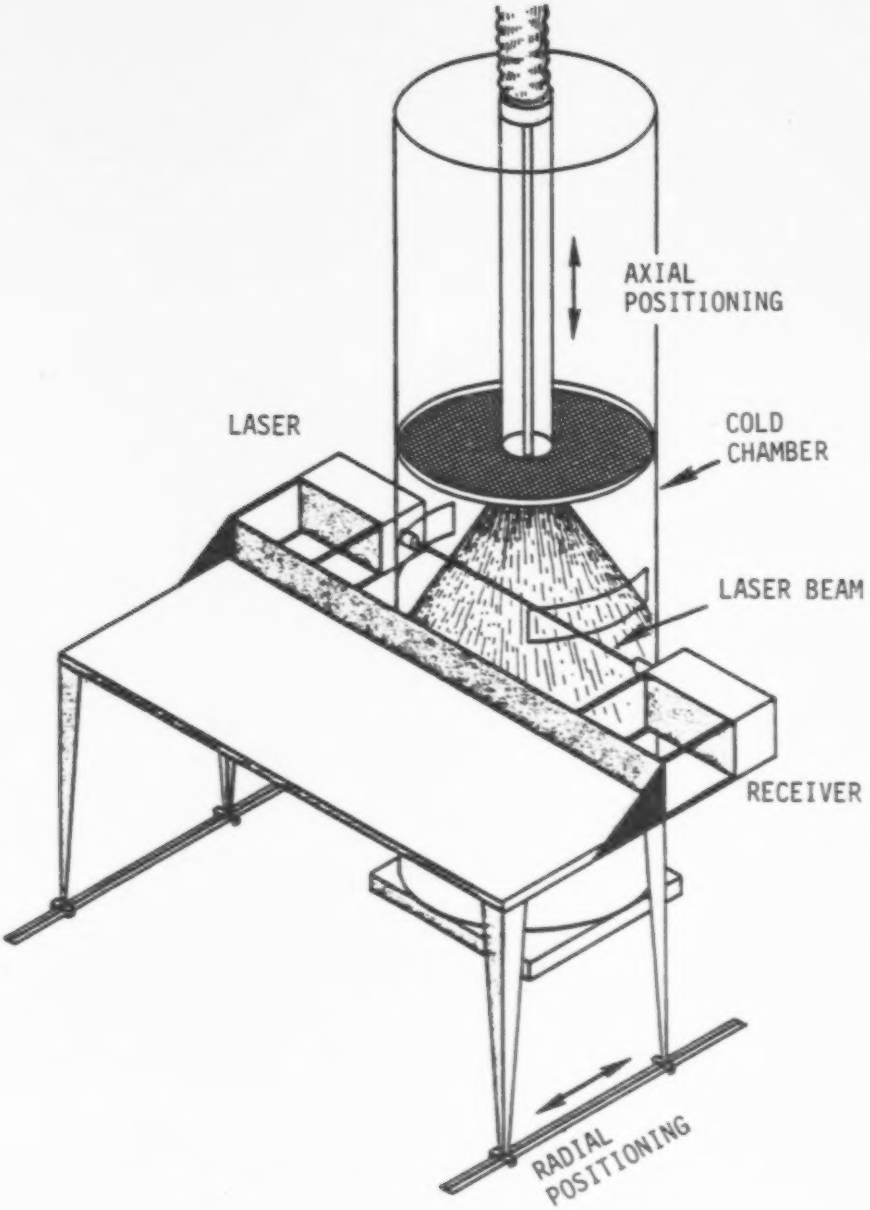
AXIAL POSITIONING
LASER
COLD CHAMBER
LASER BEAM
RECEIVER
RADIAL POSITIONING

Figure 11. Laser Diffraction System.

Table 1. Test Matrix

- NOZZLE: SONICORE 052
- FUEL: DIESEL #2, 1.3 cSt
- FUEL RATE (LITERS/HR): 0.95, 1.9*, 3.8
  (GAL/HR): 0.25, 0.5, 1.0
- ATOMIZING AIR PRESSURE (atm): 1.34, 1.68, 2.62, 2.36, 3.04
  (psig): 5, 10, 15, 20, 30
- PRIMARY AIR (m/s); 0, 2.2, 5, 10, 18
- SCREEN AIR (m/s): 0.4
- SAMPLING LOCATION
  - AXIAL: 2, 5, 10, 15, 20, 30, 40 cm
  - RADIAL: 0, ± 1.27, ± 2.54, ± 3.81 cm from center line

* Underline designates nominal condition.

Table 2. Experimental Tasks (Interferometry)

Task	Conditions			Sampling Location	Run							Comment
					Radial Distance from Center Line (r/2.54 cm)							
	Atomizing Pressure (atm)	Primary Air Velocity (mps)	Oil Flow Rate (liters/hr)	Axial (cm)	-1½	-1	-½	0	½	1	1½	
1	1.34	2.2	1.9	20		6	5 11	1	4	2 9	3 10	Radial Symmetry Check
2C	1.34	2.2	1.9	2			15	5	14			Position Analysis: 1.34 atm
				5			16	6	13			
				10			17	4	12	9		
				15				7				
				20				3	11	8		
				30			18	2	10	1		
				40				1				
3	1.68	2.2	1.9	5				1	6	9		Position Analysis: 1.68 atm
				10				2	5	8		
				20				3	4	7		
4	1.34	0	1.9	10				2	6	11		Parametric Variation: Primary Air Velocity
		5						3	7	12		
		10					1	4	8	13		
		18						5,9	10			
5	1.34	2.2	0.95	10				10				Parametric Variation: Oil Flow Rate and Atomizing Pressure
			3.8					11				
	1.68		0.95					9				
			1.9					7				
			3.8					8				
	2.02		0.95					2				
			1.9					1				
			3.8					3				
	2.36		0.95					5				
			1.9					4				
			3.8					6				

Table 2. Experimental Tasks (Interferometry)--Concluded

Task	Conditions			Sampling Location	Run							Comment
	Atomizing Pressure (atm)	Primary Air Velocity (mps)	Oil Flow Rate (liters/hr)	Axial (cm)	Radial Distance From Center Line (r/2.54 cm)							
					-1½	-1	-½	0	½	1	1½	
5C	1.34	2.2	1.9	10				5	18	26		Continuation of Task 5
			3.8					6	17	25		
	1.68		1.9					1	15	23		
			3.8					2	16	24		
	2.02		1.9					4	14	22		
			3.8					3	11	21		
	2.36		1.9					8	9	19		
			3.8					7	10	20		
	2.02		3.8						12			(Nozzle Rotated 90°)
	2.36		3.8						14			(Nozzle Rotated 90°)
6	1.68	2.2	2.4	5				2	6			Higher Viscosity Fluid: 25 CST
				10				1	5			
				20				3	4	7		
10	1.34	2.2	1.9	5				3	6	9		Velocity/Size Correlation: 1.34 atm
				10				2	5	8		
11	1.68	2.2	1.9	20				1	4	7		Velocity/Size Correlation: 1.68 atm
				5				3	6	9		
				10				2	5	8		
				20				1	4	7		
12	1.34	10	1.9	5				3	6	9		Velocity/Size Correlation: 10 m/s
				10				2	5	8		
				20				1	4	7		

Table 3. Experimental Tasks (Holography)

Task	Conditions			Sampling Location	Run	Comment
	Atomizing Pressure (atm)	Primary Air Velocity (mps)	Oil Flow Rate (Liters/hr)	Axial (cm)		
1	1.34	2.2	1.9	20	1,2	Position Analysis: 1.34 atm
				10	3,4	
				5	5,6	
				0	7,8,5F*	(*Flash Photography)
2	1.68	2.2	1.9	0	9,10,5F	Position Analysis: 1.68 atm
				5	11,12,13,4F	
				10	14,15,3F	
				20	16,17,2F	
3	1.34	2.2	1.9	5	1A,2A	Flash Photography Position Analysis: 1.34 atm
				10	3A	
				20	4A	
				5	5A	(Double Pulse, 75 μs Separation)
				10	6A	(Double Pulse, 75 μs Separation)
4	1.2	2.2	1.9	0	1B,2B	Injector Analysis: Parametric Variation in Atomizing Pressure, Oil Flow Rate, Primary Air Velocity
		10	1.9		7B,8B	
	1.34	2.2	3.8		15B	
	1.68	2.2	3.8		16B	
		10	1.9		9B,10B	
	2.36	10	1.9		11B,12B	
		2.2	1.9		3B,4B	
		2.2	3.8		17B	
	3.04	10	1.9		13B,14B	
		2.2	1.9		5B,6B	
		2.2	3.8		18B	

Table 3. Experimental Tasks (Holography)--Continued

Task	Conditions			Sampling Location	Run	Comment
	Atomizing Pressure (atm)	Primary Air Velocity (mps)	Oil Flow Rate (liters/hr)	Axial (cm)		
5	1.34	2.2	1.9	0	1C,2C	Near Field Injector Analysis: Parametric Variation in Atomizing Pressure, Primary Air Velocity
				5	9C	
		10		0	14C	
				5	18C	
	1.68	2.2		0	3C,4C	
				5	10C,11C	
		10		0	15C	
	2.36	2.2		0	5C,6C	
				5	12C	
		10		0	16C	
	3.04	2.2		0	7C,8C	
				5	13C	
		10		0	17C	
6	1.34	2.2	1.9	0	1D,2D,9D	Injector Analysis: Interferometric Holography
	1.68				3D,4D,10D	
	2.36				5D,6D	
	3.04				2D,8D	
7	1.34	2.2	1.9	0	11D,13D	Injector Analysis: Double Pulse With 35 μs Separation
	1.68				15D	
	1.34				12D	(Single Pulse)
	1.68				14D,16D,17D,18D	(Single Pulse)
76C	1.34	2.2	1.9	0	3E,4E	Injector Analysis: Interferometric Holography With High Magnification
	1.68				5E,6E,7E	
	1.34			0	2E	(Single Pulse)
				20	1E	(Single Pulse)
	1.68			0	8E	(Single Pulse)

Table 3. Experimental Tasks (Holography)--Concluded

Task	Conditions			Sampling Location	Run	Comment
	Atomizing Pressure (atm)	Primary Air Velocity (mps)	Oil Flow Rate (liters/hr)	Axial (cm)		
8	1.34	2.2	1.9	5	5H,6H	Position Analysis: High Magnification
				10	3H,4H	
				20	1H,2H	
		10		5	17H,18H	
				10	15H,16H	
				20	13H,14H	
	1.68	2.2		5	7H,8H	
				10	9H,10H	
				20	11H,12H	
9	1.34	2.2	1.9	0	1J,2J	Near Field Injector Analysis: High Magnification
				5	7J,8J	
		10		0	15J,16J	
				5	13J,14J	
	1.68	2.2		0	3J,4J	
				5	9J,10J	
	2.36			0	5J,6J	
				5	11J,12J	
	3.04			0	17J,18J	

Table 4. Experimental Tasks (Diffraction-EER)

Task	Conditions			Sampling Location	Run	Comment
	Atomizing Pressure (atm)	Primary Air Velocity (mps)	Oil Flow Rate (Liters/hr)	Axial		
1	1.34	2.2	1.9	10	1	Position Analysis: 1.34 atm
				15	2	
				20	3	
				30	4	
				40	5	
				46.5	6	
2	1.68	2.2	1.9	10	1	Parametric Variation: Atomizing Pressure
	2.02				2	
	2.36				3	

5.0 RESULTS

5.1 Laser Interferometric Results

The laser interferometric data were obtained and reduced by Spectron Development Laboratories (SDL). The results of their analyses are presented in Volume 1 of their final report, attached as Appendix A to this report. The data are provided in Appendix C.

An example of the data generated by the SDL interferometric system is presented in Figure 12a. The plot presents the frequency (the number of droplets, N_i, of diameter D_i, normalized by the total number of droplets, N, that pass through the sampling volume during a given sampling period at a single location in the spray). Below the plot, the total number of droplets recorded (N) is shown along with the following calculated parameters (the bold lettering has been added to the computer printout for clarity of presentation):

Linear mean diameter : $$D10 = \frac{\Sigma N_i D_i}{N} ,$$

Surface mean diameter : $$D20 = \left[\frac{\Sigma N_i D_i^2}{N}\right]^{1/2} ,$$

Volume mean diameter : $$D30 = \left[\frac{\Sigma N_i D_i^3}{N}\right]^{1/3} ,$$

Sauter mean diameter : $$D32 = \frac{\Sigma N_i D_i^3}{\Sigma N_i D_i^2} ,$$

Standard deviation : $$S = \left[\frac{\Sigma N_i (D_i - D10)^2}{N}\right]^{1/2} ,$$

Kurtosis : $$\Sigma \frac{N_i (D_i - D10)^3}{N} \bigg/ \left[\frac{\Sigma N_i (D_i - D10)^2}{N}\right]^{3/2} ,$$

In addition to size distribution data, the velocities of individual droplets were recorded for a select but limited number of tasks (Tasks 10, 11, and 12). An example of the data output for velocity is shown in Figure 12b. (The bold lettering has been added in this example as well.) The average velocity of each size group monitored is both plotted and tabulated.

(a) Droplet Sizing Data

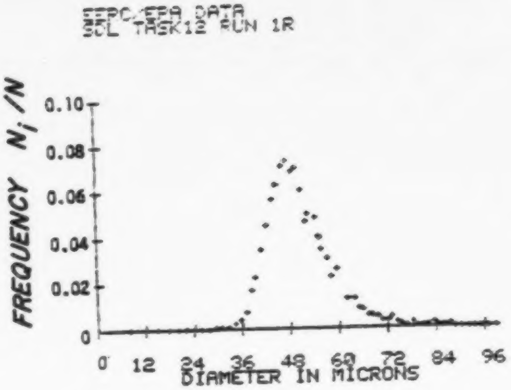

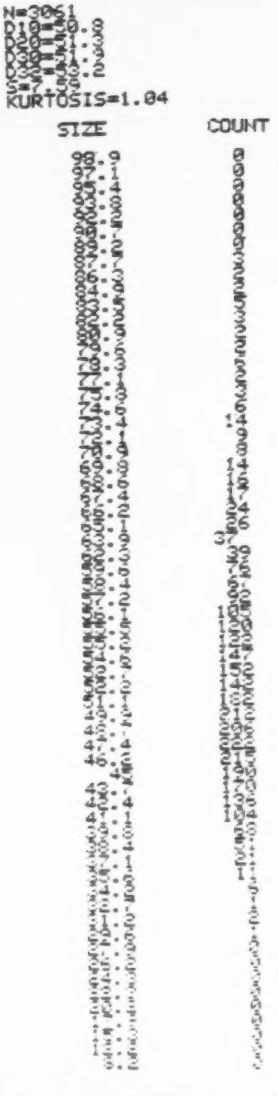

```
N=3061
D10=50.8
KURTOSIS=1.04
   SIZE          COUNT
   98.9            0
   97.1            0
```

(Source: Appendix C)

Figure 12. Laser Interferometry--Typical Tabulation.

(b) Droplet Size Velocity Data

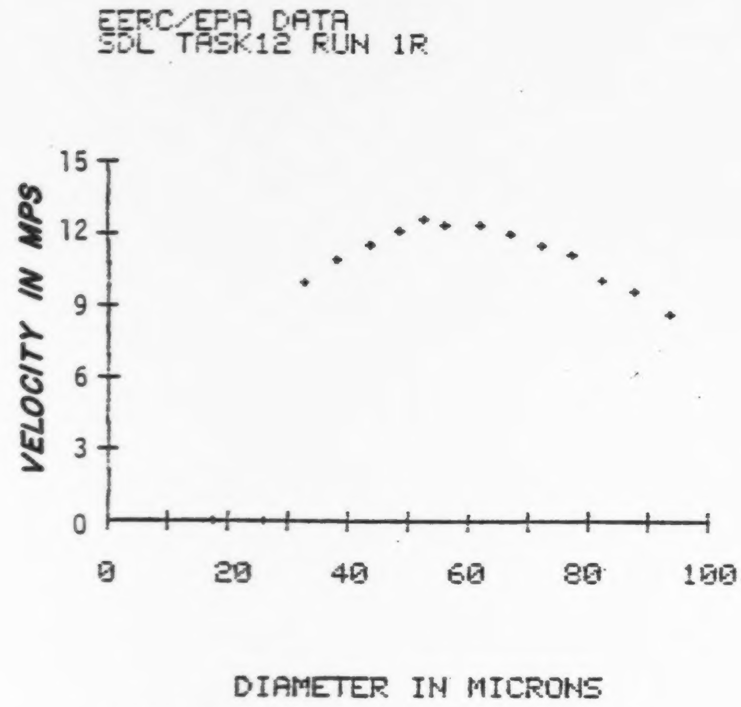

DIAMETER (MICRONS)	VELOCITY (M/SEC)
93.8	8.6
87.7	9.7
82.2	10.2
77.1	11.2
72.1	11.6
67.4	12.1
62.3	12.4
56.1	12.4
52.7	12.6
48.7	12.2
43.7	11.6
38.4	11
32.7	10

(Source: Appendix C)

Figure 12. Laser Interferometry--Typical Tabulation (Concluded).

To obtain a spatial distribution of the droplets in the spray, a composite of the local size distribution must be generated, an example of which is shown in Figure 13. This figure presents individual distributions obtained at different positions in the Sonicore nozzle spray field for two nozzle air pressures (1.34 and 1.68 atm, respectively). The sketch of the spray region was defined by visual observation prior to any optical measurements. Several trends are readily discernible; for example, no droplets of less than 24 μm or greater than about 90 μm are recorded. Secondly, there is a general broadening of size distributions towards larger droplets as the measuring point proceeds away from the spray field centerline. As the measuring point moves down in the spray field and away from the nozzle, there is a general narrowing of the distribution toward smaller droplets.

These same trends can be shown more explicitly when considering the volume mean diameter at different positions (Figure 14).* Droplet size decreases with axial distance from the nozzle. At a given axial location, the droplet size increases as the radial distance from the center line increases. These two observations can be explained in light of a general size segregation of larger droplets toward the edges of the spray field.

Figure 15 is a plot of the volume mean diameter against nozzle air pressures. In the center of the spray field there is little change in the mean size over the entire range of pressures. However, on the fringes of the spray there is a monotonic decrease in the mean size with increasing pressure.

Some of the data on velocity are shown in Figure 16 in which the mean velocity of a size class of droplets is plotted versus the class size. The data do not indicate any preferential relaxation of the smaller droplets from their ballistic velocity to the bulk gas velocity as would be expected by drag considerations. In fact, it appears that all droplets are moving with very close to the same velocity at any position independent of size.

---

*The precision of spray sizing data obtained with conventional optical methods is generally regarded to be in excess of 10 μm. Although the data plotted in Figures 14 and 15 should be interpreted in the context of this limit, the precision of interferometric data is markedly higher though the absolute value has yet to be established and verified.

(a) 1.34 atm

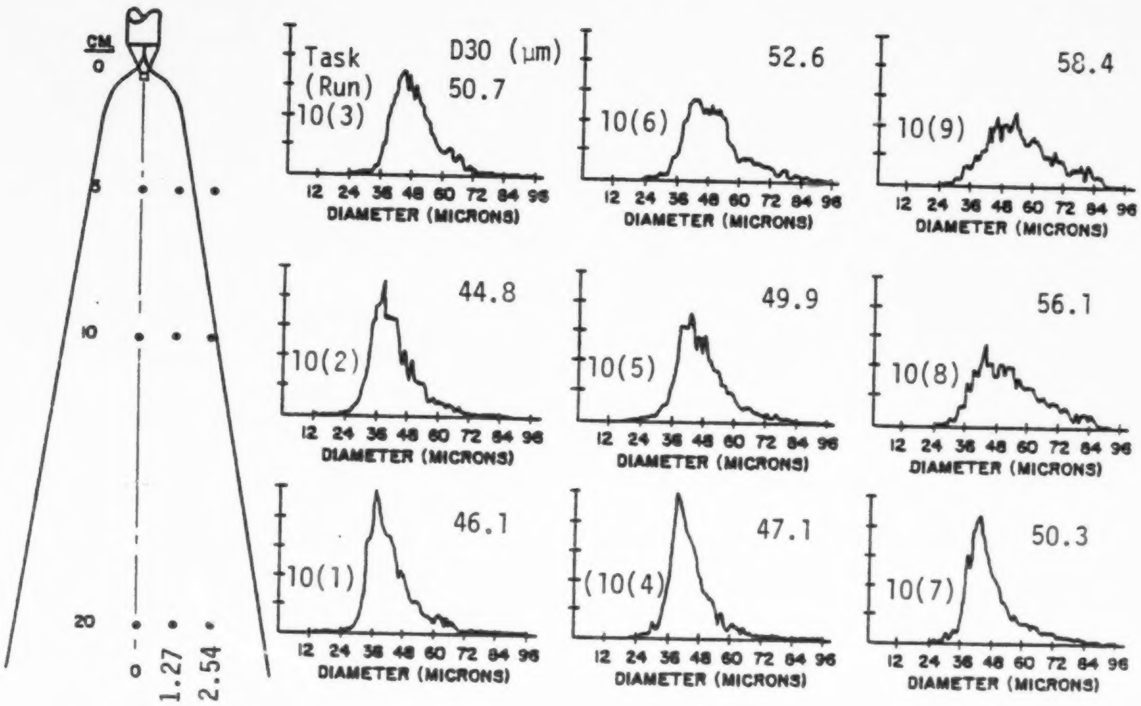

Figure 13. Laser Interferometry--Spatial Variation of Number Density.

(b) 1.68 atm

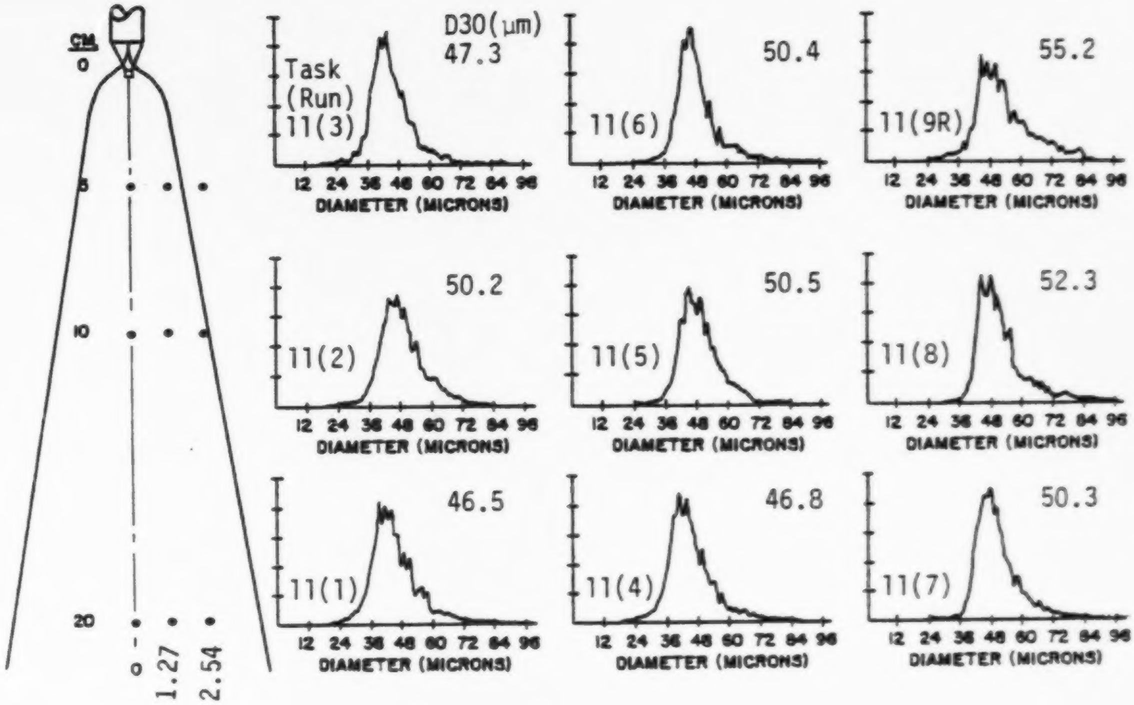

Figure 13. Laser Interferometry--Spatial Variation of Number Density (Concluded).

(a) 1.34 atm

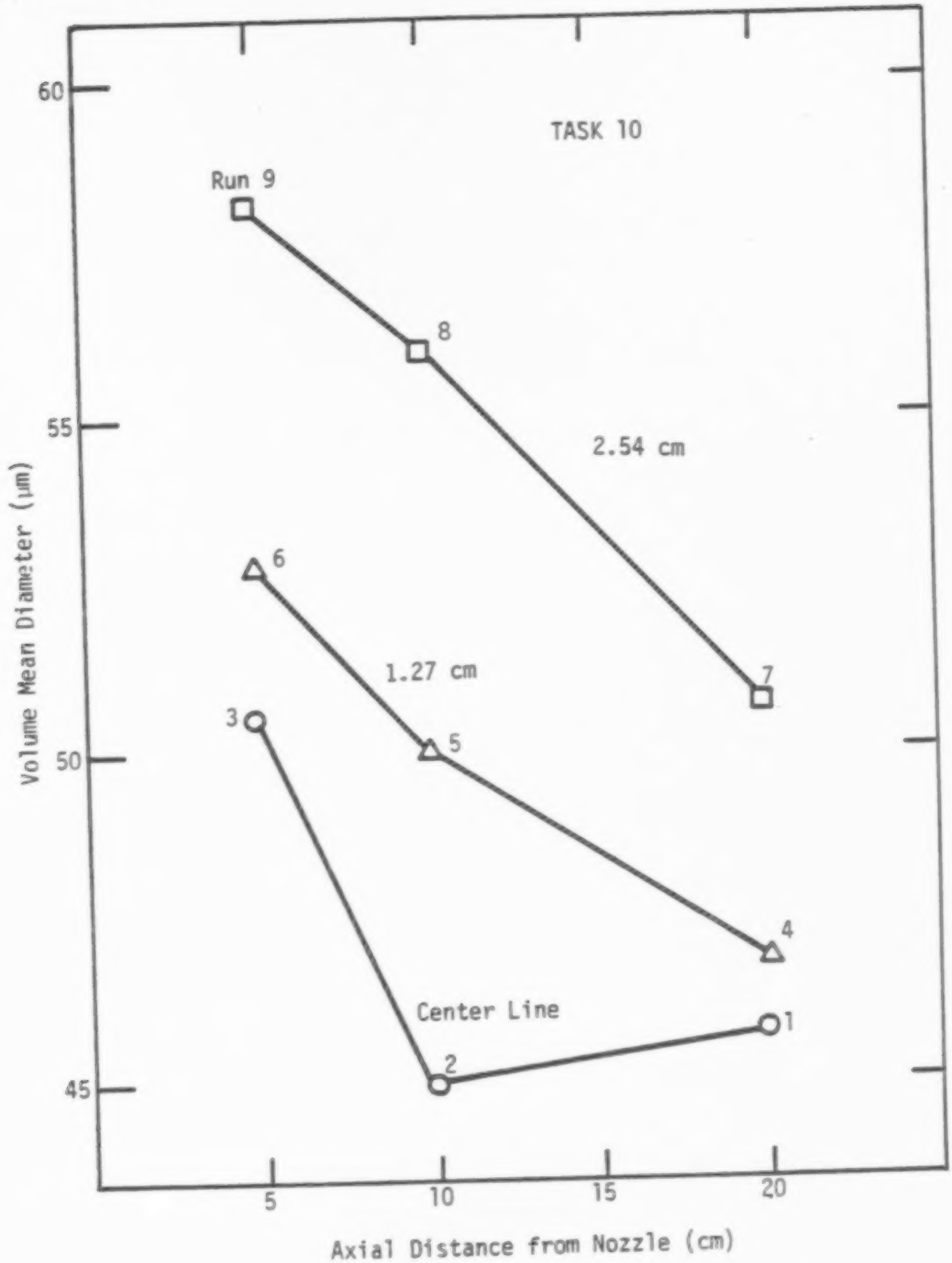

Figure 14. Laser Interferometry--Axial Variation of Volume Mean Diameter.

(b) 1.68 atm

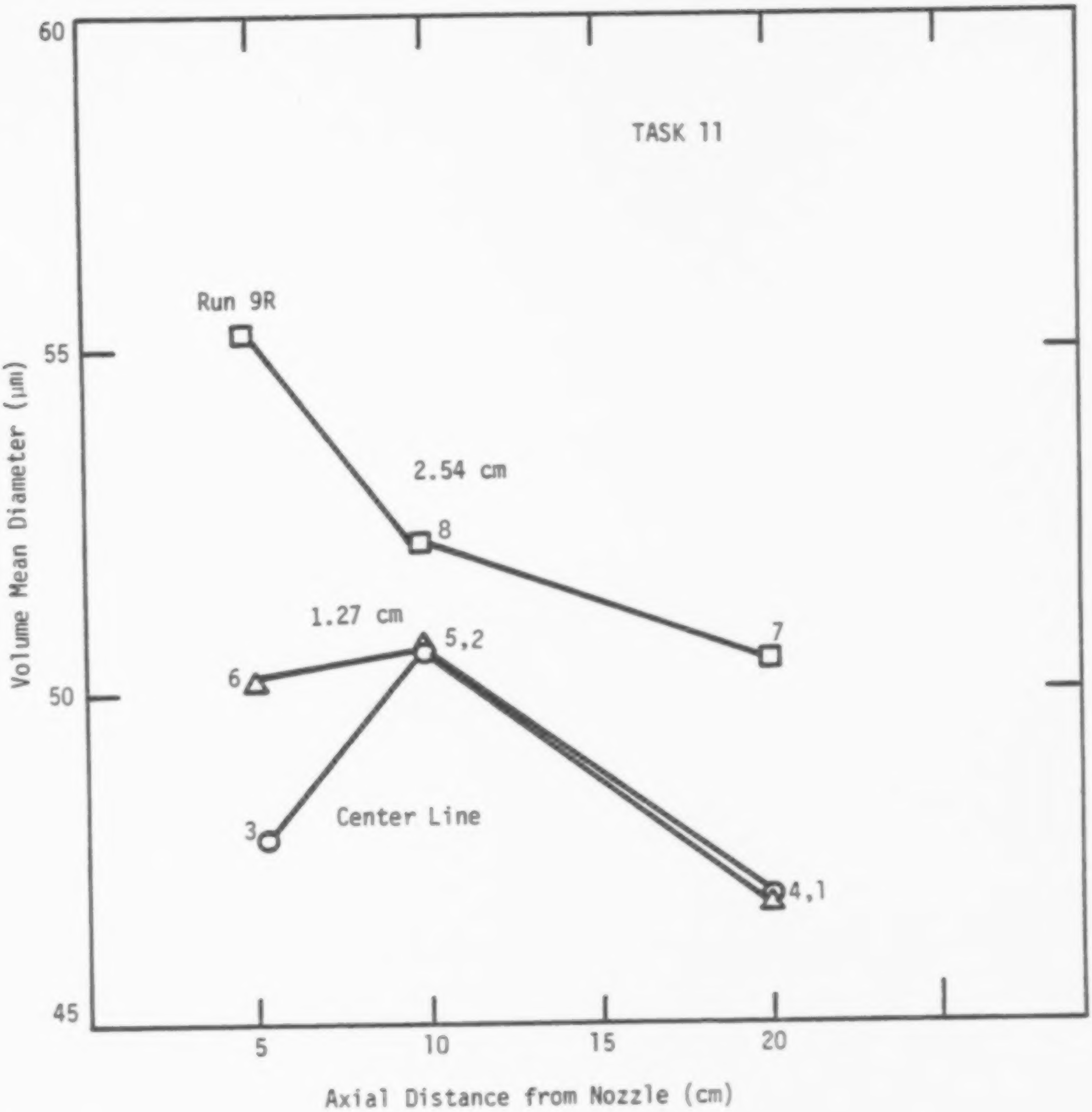

Figure 14. Laser Interferometry--Axial Variation of Volume Mean Diameter (Concluded).

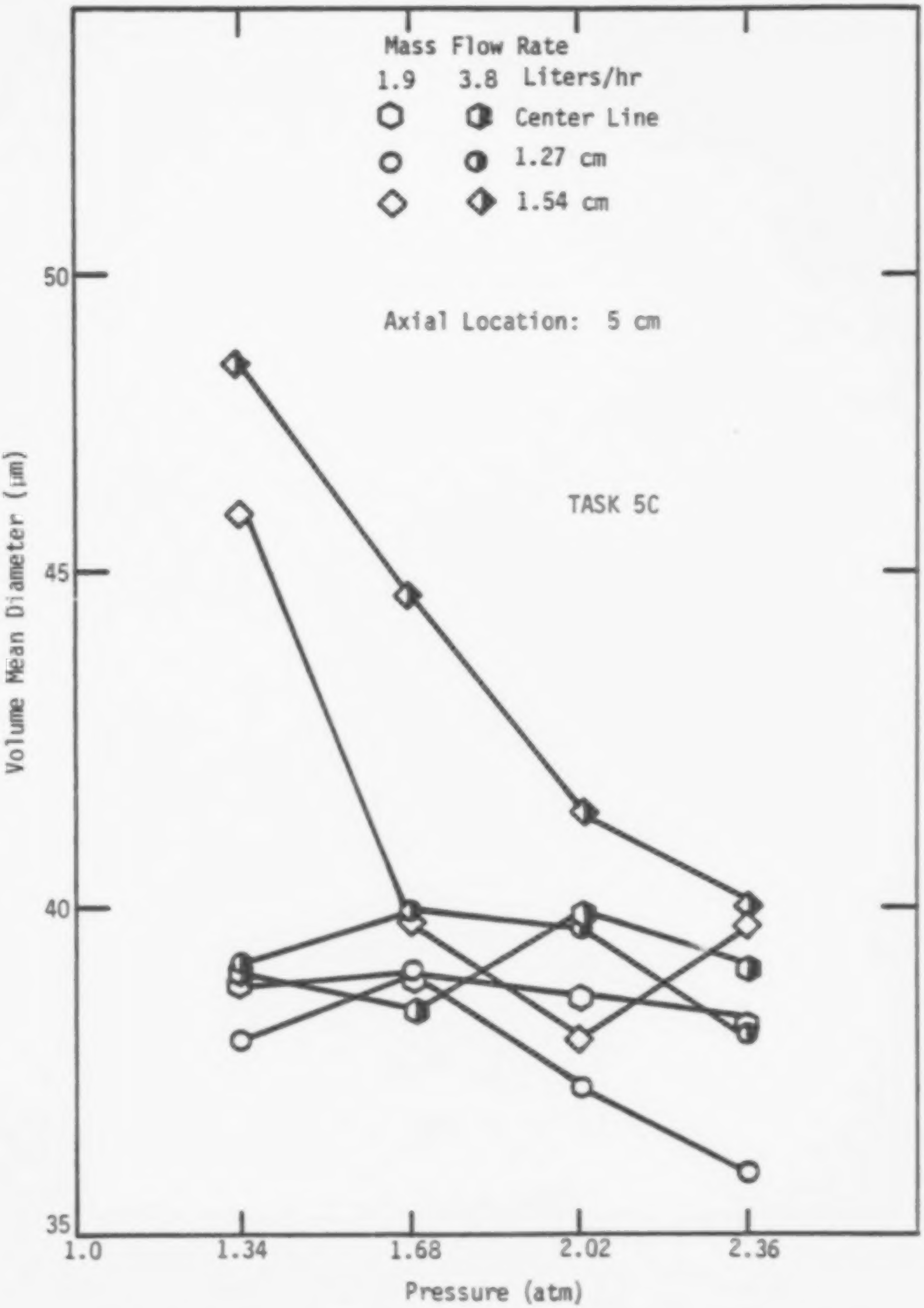

Figure 15. Laser Interferometry--Dependency of Volume Mean Diameter on Nozzle Atomizing Pressure.

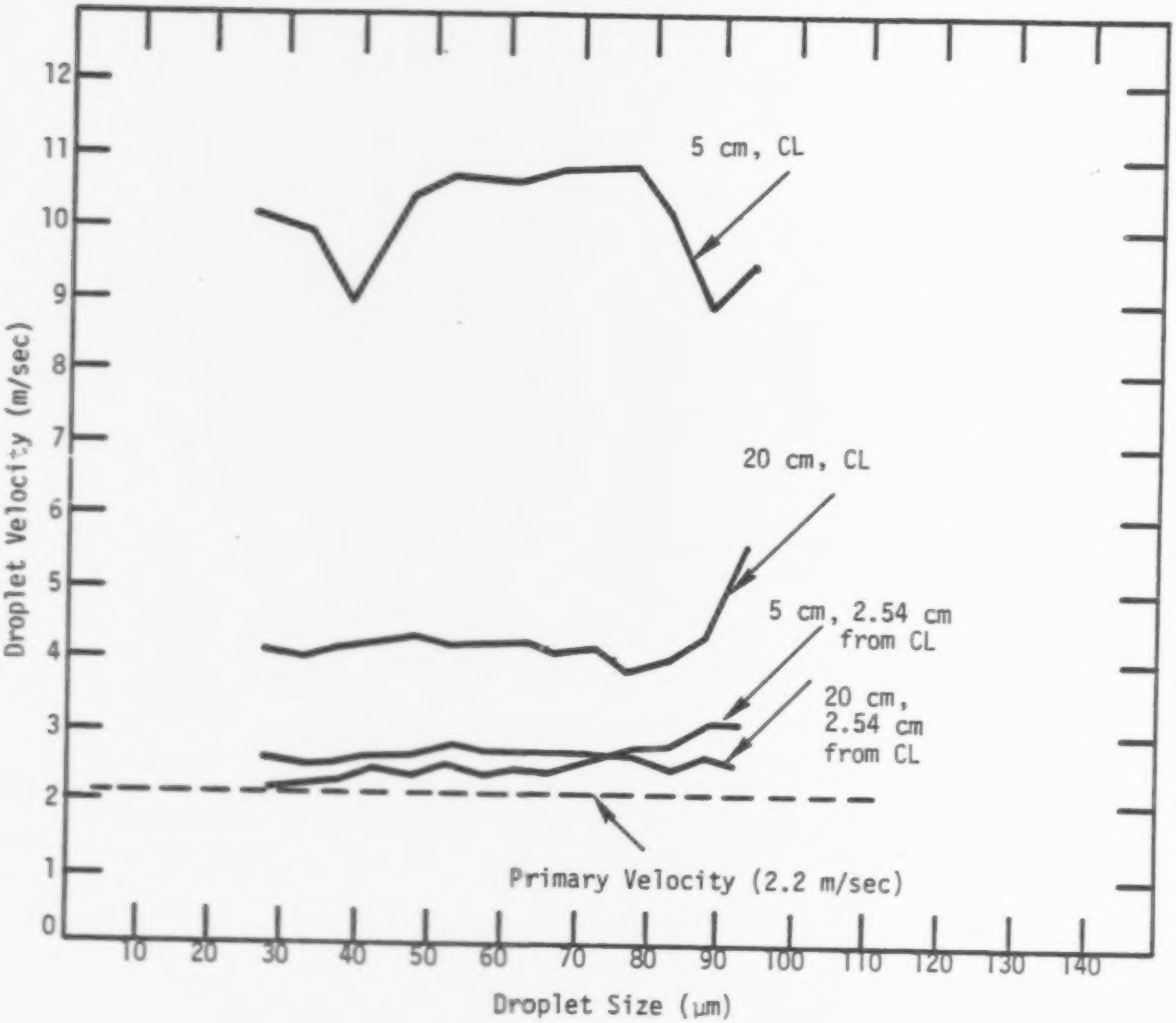

Figure 16. Laser Interferometry--Dependency of Droplet Velocity on Droplet Size.

There is, however, a very strong dependence of the particle field velocity on position. Figure 17 is an example of how a characteristic droplet velocity (taken as the size at 52.7 μm) behaves with position. It is clear that only on the spray field center line is there a substantial relaxation distance, while on the spray edges the droplets are moving relatively close to the bulk gas velocity. At higher bulk gas velocities, there is little influence of position on droplet velocity although there is some observable relaxation of center line droplets.

Such velocity behavior could plausibly be explained by considering that the atomizing air penetrates into the bulk flow to some finite distance. It would be expected that this high-velocity jet would penetrate further in the center and slow quickly on the edges to the bulk-flow velocity. This plume relaxation time is larger that the drag relaxation of any size droplet so that it controls the velocity of individual droplets which can be considered essentially at the local gas velocity.

Although these observations demonstrate some of the insights that can be gained from the broad capabilities of the interferometric measurements, a major premise to the present investigation was to test the applicability of laser interferometry by comparing the results against laser holography and laser diffraction. In the absence of such a test, the interferometric results must remain suspect.

5.2 Assessment of Laser Interferometric Results

Laser holography and laser diffraction were used at selected conditions as comparative tests to assess the performance of the laser interferometric technique. Below, the laser holography and laser diffraction results are presented and compared to the laser interferometric data.

5.2.1 Laser Holography

Holographic data were taken by SDL for the test matrix presented in Table 3. The holographic recordings for these conditions were first analyzed by SDL personnel, and subsequently and separately analyzed by EER personnel. Although all the holograms recorded were studied at one time or another by either SDL or EER personnel, a detailed analysis for direct comparison to the interferometric data was limited to the conditions listed in Table 5.

(a) 1.34 atm

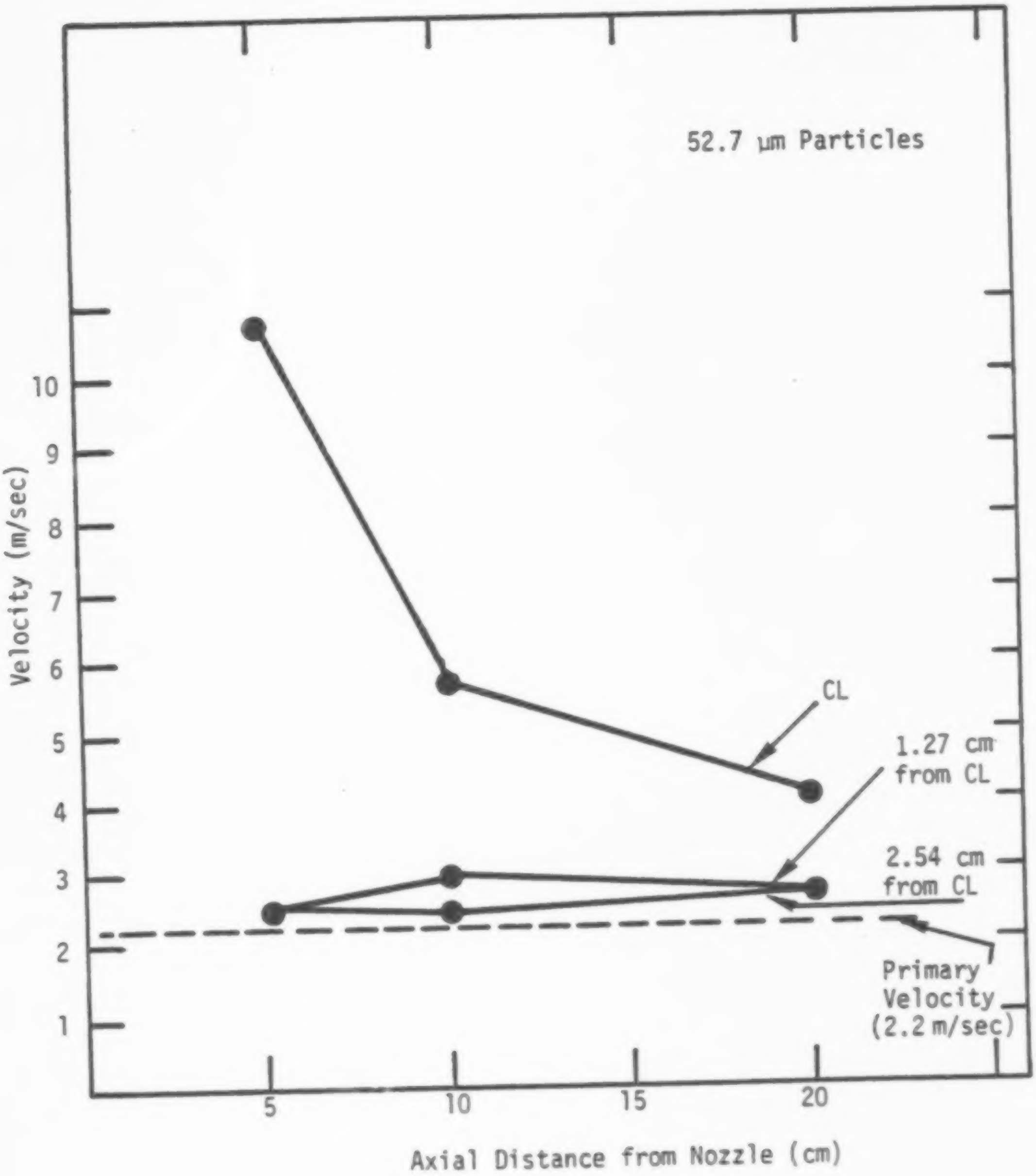

Figure 17. Laser Interferometry--Axial Variation in the Velocity of 52.7 μm Droplets.

(b) 1.68 atm

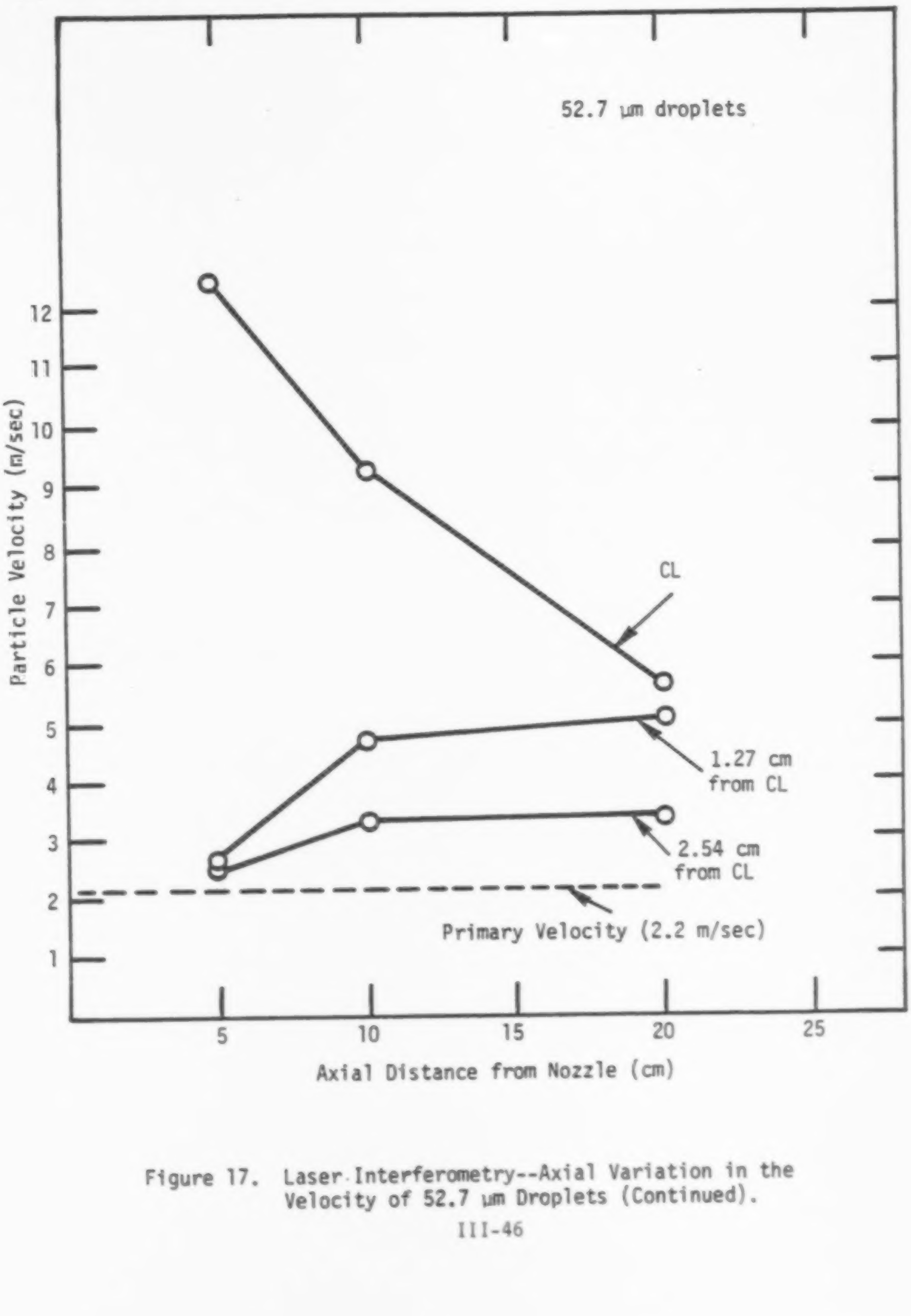

Figure 17. Laser Interferometry--Axial Variation in the Velocity of 52.7 μm Droplets (Continued).

(c) 10 m/sec Primary Velocity

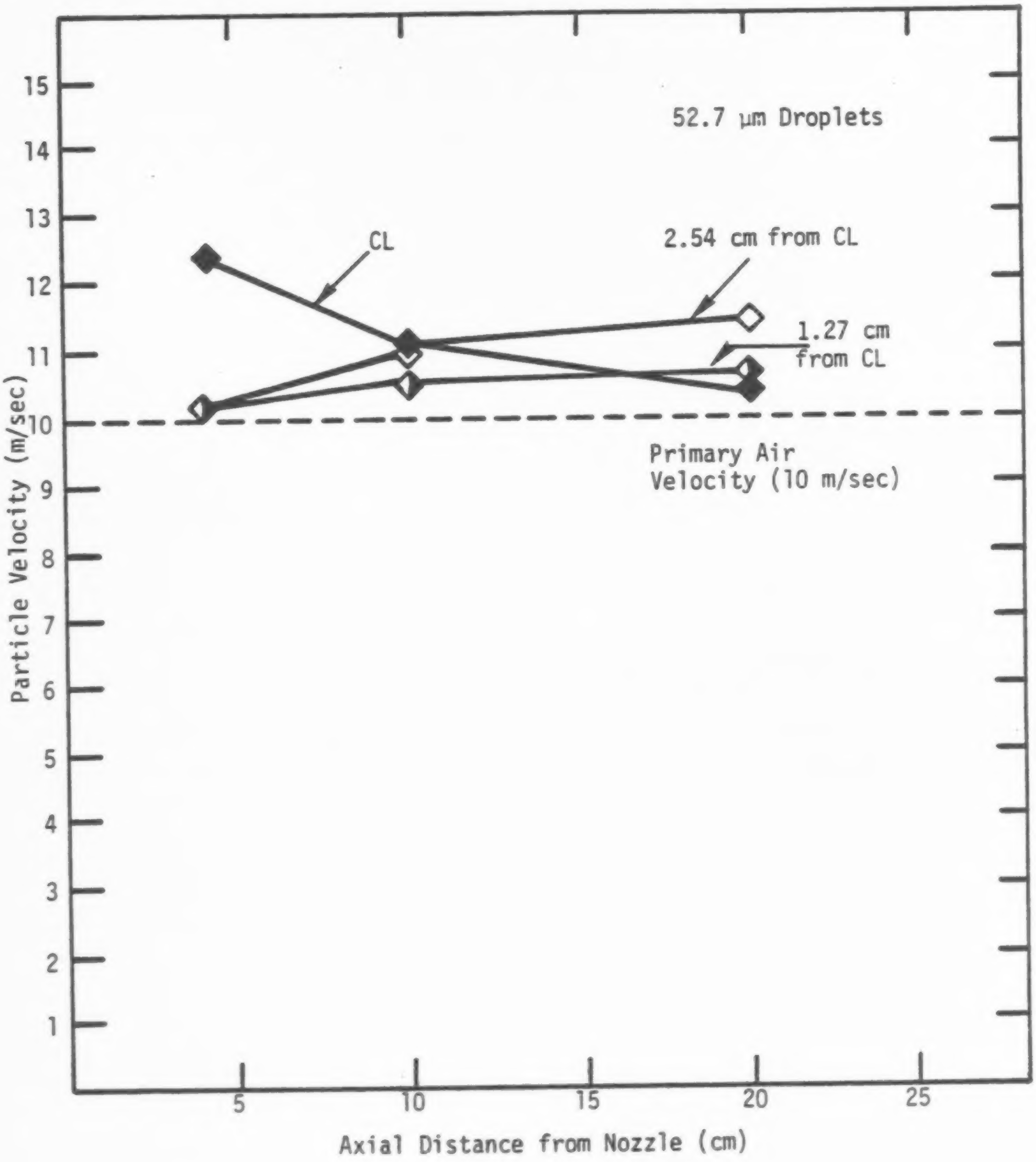

Figure 17. Laser Interferometry--Axial Variation in the Velocity of 52.7 μm Droplets (Concluded).

Table 5. Conditions for Comparison of Laser Holography to Laser Interferometry

FIXED CONDITIONS

$V_p = 2.2$ mps
$V_s = 0.4$ mps
$\dot{V}_f = 1.9$ liters/hr

PARAMETRIC VARIATION

Conditions	Task (Run)	
	Interferometry	Holography
p = 1.34 atm; x = 10 cm	10(2)	8(3H, 4H)
x = 20 cm	10(1)	8(1H, 2H)
p = 1.68 atm; x = 10 cm	11(2)	8(9H, 10H)
x = 20 cm	11(1)	8(11H, 12H)

SDL Analysis: The results of the comparison conducted by SDL are presented in Appendix A. A condensation of the results for one of the two atomizing pressures evaluated is presented in Figure 18a in terms of number density, f_{D_i}. The results of the holography analysis yield near identical number mean droplet diameters to those determined by interferometry. The most striking difference is the tail of the distributions at the large droplet side of the holography data. The SDL final report records the following explanation:

> The curve constructed with holography data is broader than the corresponding visibility one. This is due to the biased impression produced by the larger particles. This biasing arises because it is very easy to find the large particles in a hologram and quite difficult to find the very small ones. Hence, the total number of particles counted is usually smaller than the total number of particles present, while the total number of large particles is quite correct.

Source: Appendix A

EER Analysis: The analysis of the holograms by EER personnel yielded the following conclusions:

1. Human judgment in reading a hologram can dictate both the size distribution and number mean diameter within rather broad limits. A statistically acceptable reading would require a number of individuals, each of whom conduct many repetitious measurements.
2. Item 1 notwithstanding, the size distributions obtained from holographic observations by SDL are representative although the near superposition of the number mean diameters obtained from both the holographic and interferometric data may be more fortuitous than real. In the present case, for example, there were not enough data points taken around the mean to firmly fix the peak number density between 20 and 80 μm.
3. Large droplets (d_p > 90 μm), not represented in the interferometric data, are in fact present in the reconstructed holograms.
4. An analysis of all the holograms taken provides the following additional insights:

(a) x = 10 cm Source: Appendix A, Appendix C

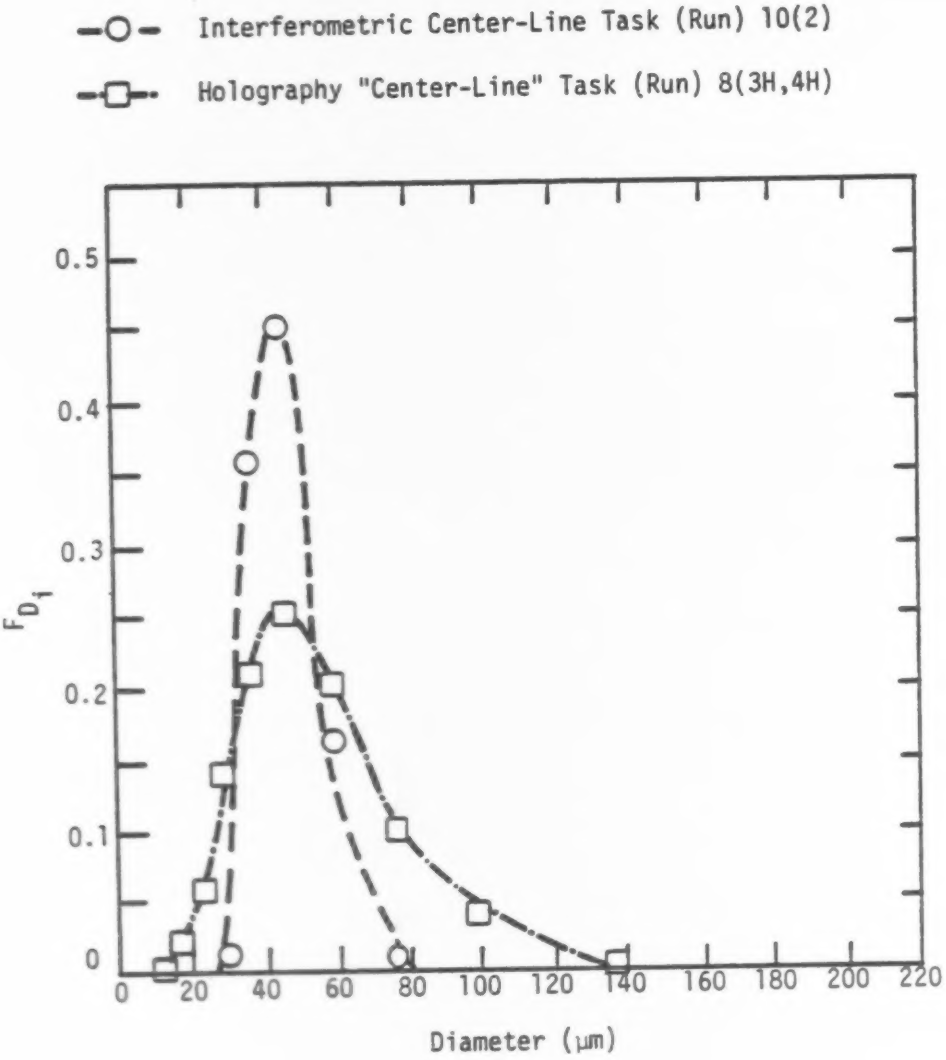

Figure 18. Laser Interferometric and Holography Data--Number Density (1.34 atm).

(b) x = 20 cm Source: Appendix A, Appendix C

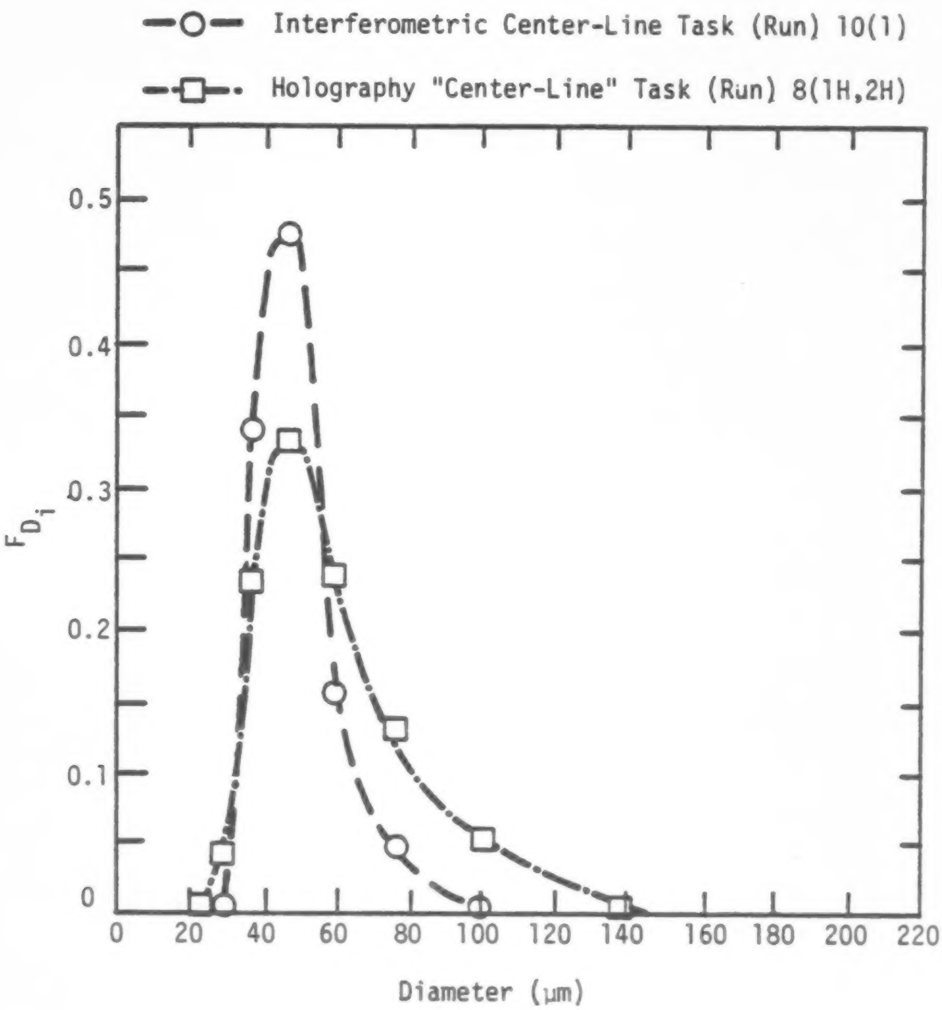

Figure 18. Laser Interferometric and Holography Data--Number Density (1.34 atm) (Continued).

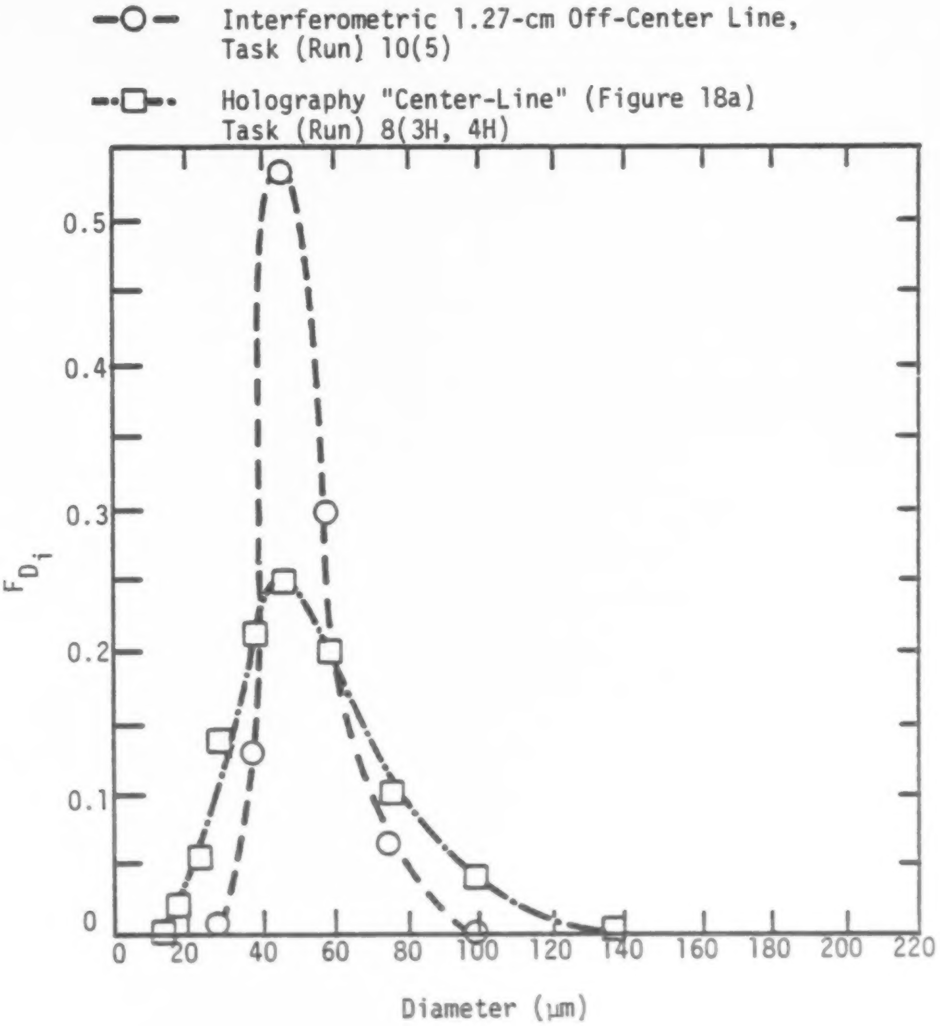

(c) x = 10 cm (Interferometric Data Displaced 1.27 cm)

Source: Appendix A, Appendix C

Figure 18. Laser Interferometric and Holographic Data--Number Density (1.34 atm) (Concluded).

- The population of large ($d_p > 90$ µm) droplets increases with radial displacement from the center line.
- Strong fluctuations of droplet number density appear to exist within the field, an event that was not recognized by the interferometric technique but potentially important in establishing causal-effect relationships between spray performance and pollutant production.

One explanation for the failure of the interferometric system to measure large particles rests with a difference in the measurement volume when compared to laser holography. The interferometric sampling volume is relatively small (~0.01 mm^3), as compared to 10 cm^3 for laser holography. As a result, the center line data of Figure 18 for the interferometric technique do not encompass the larger coverage of the holography. However, as shown in Figure 13, the interferometric data show very little broadening in the size distribution away from the center line. This is further demonstrated in Figure 18c where the holography data of Figure 18a are compared to interferometric data taken at a location displaced by 1.27 cm from the center line. Although a broadening of the interferometric-derived size distribution is evident, it is insufficient to provide an acceptable comparison to the holography observations.

The proper explanation for the failure of the interferometric technique to measure droplets greater than ~90 um appears to be the limited dynamic range of the instrument. The dynamic range for all the interferometric tasks is presented in Table 6. The upper limit of the dynamic range precluded the observation of droplets larger than the limit. In addition, another restriction further limits the dynamic range on the small end of the size range due to the sensitivity of the processor to measure small particles (see Figure 19 for diagrammatic representation). This sensitivity can be increased by an increase in the receiving PMT bias. However, this can result in the saturation of signals, thus restricting the large particle detection. It has been observed that if the PMT bias is increased, the processor will count many more small particles as the sensitivity limit is shifted downward.

One might expect that the sensitivity cutoff limit would result in a sharp drop in the distribution and not the slow tapering of the curve as

Table 6. Dynamic Range of Laser Interferometric Data

Task #	dmin(μm)	dmax(μm)
1	11.5	115
2C	11.5	115
3	7.5	75
4	11.5	115
5	11.5	115
5C	7.5	75
6	7.5	75
10	8.8	88
11	8.8	88
12	8.8	88

Source: Appendix B

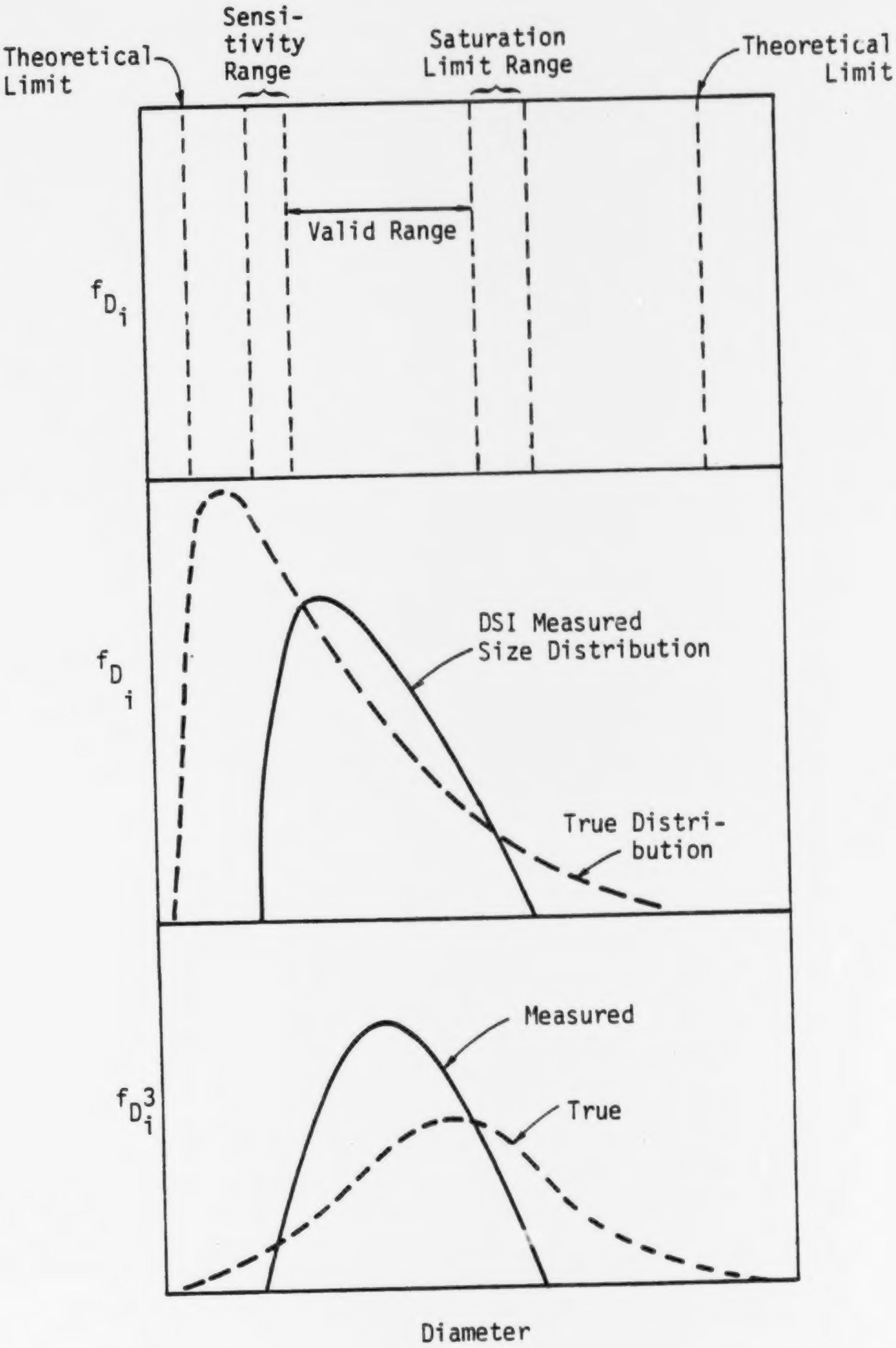
Theoretical Limit
Sensitivity Range
Saturation Limit Range
Theoretical Limit
Valid Range
f_{D_i}
f_{D_i}
DSI Measured Size Distribution
True Distribution
Measured
$f_{D_i^3}$
True
Diameter

Figure 19. Laser Interferometry--Diagrammatic Representation of Dynamic Range Limit.

observed. However, the limit is not at a set droplet size but rather at a set signal size. Because of the Gaussian beam intensity distribution of the measurement cross-section, the signal size will depend on both the size of the droplet and where the droplet passes through the probe volume. Particles scatter light in proportion to the square of their diameter and, because of the sensitivity limit, only the larger particles passing through the edge of the probe volume will score. The net result is a bias against the detection of small particles and, at the time the present data were collected, the reduction software had not progressed to the point of correcting for this bias. This signal size will depend on not only the size of the droplet but where it passes through the probe volume. The interferometric data do not depend on the signal size but just the ratio of AC to DC in the doppler burst; thus, a particle just at the sensitivity limit will result in a valid signal only if it passes at the center of the probe volume and not if it passes near the edge.

A similar phenomenon occurs on the large limit since the processor discriminates against saturated signals; however, there is again no specific cutoff but rather a range of values depending on where the droplet passes through the probe volume. A droplet may produce a saturated signal if it passes through the center and may not if it passes off center.

The impact of correctly representing the large diameter size of the distribution is no more evident than in the weight distribution. As shown in Figure 20, the dependency of the weight density, $f_{D_i}^3$, on the cubic power of diameter underlines the importance of correctly prescribing the size distribution on the side of large diameter. As a result, the interferometric operator must be aware of the sensitivity limit range as well as the saturation limit range. To obtain the full breadth of a spray droplet size distribution, several measurements with different PMT bias levels and fringe spacings may be required along with a procedure for combining the results.

5.2.2 Laser Diffraction

IFRF Data. A test matrix for the acquisition of the IFRF data is presented in Table 4. As described in Section 2, the IFRF experiments were conducted prior to the present experiments and, as a result, the condition of both experiments, though similar, are not identical. For the purposes of

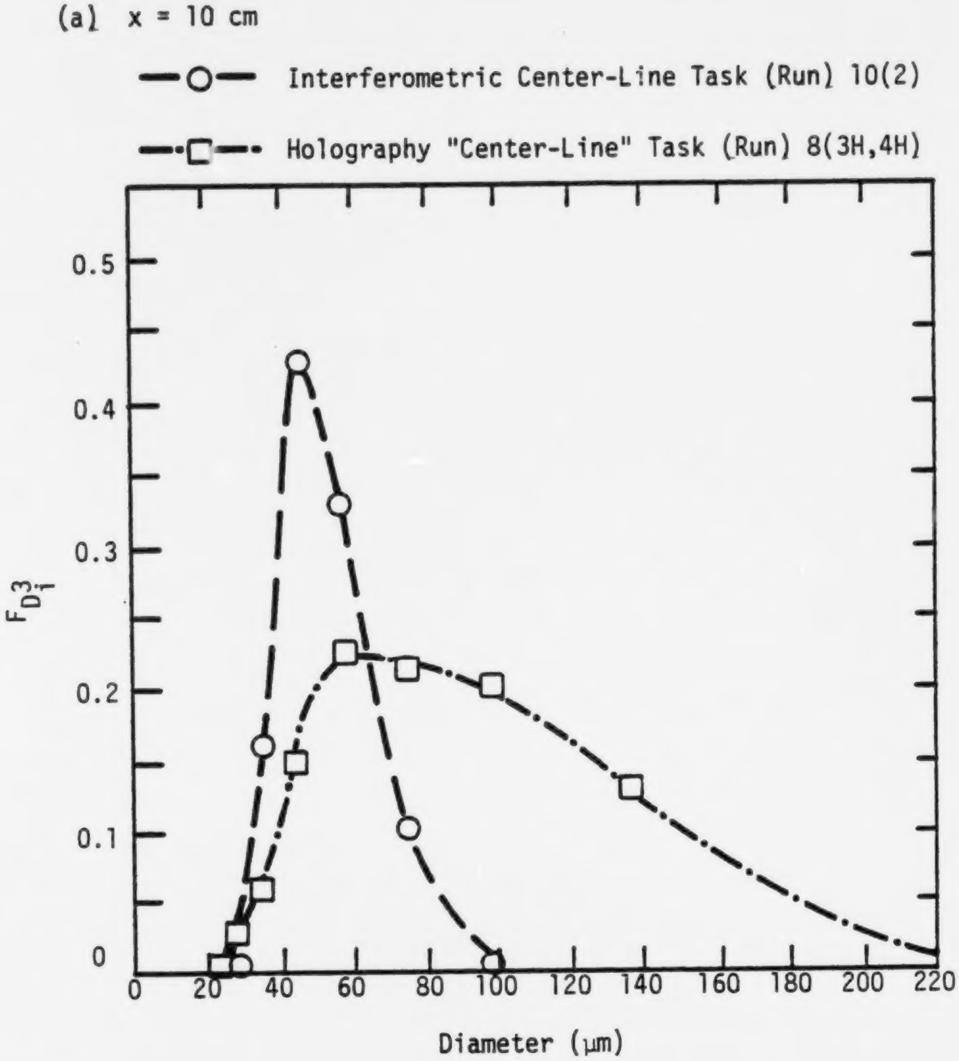

Figure 20. Laser Interferometric and Holography Data--Weight Density (1.34 atm).

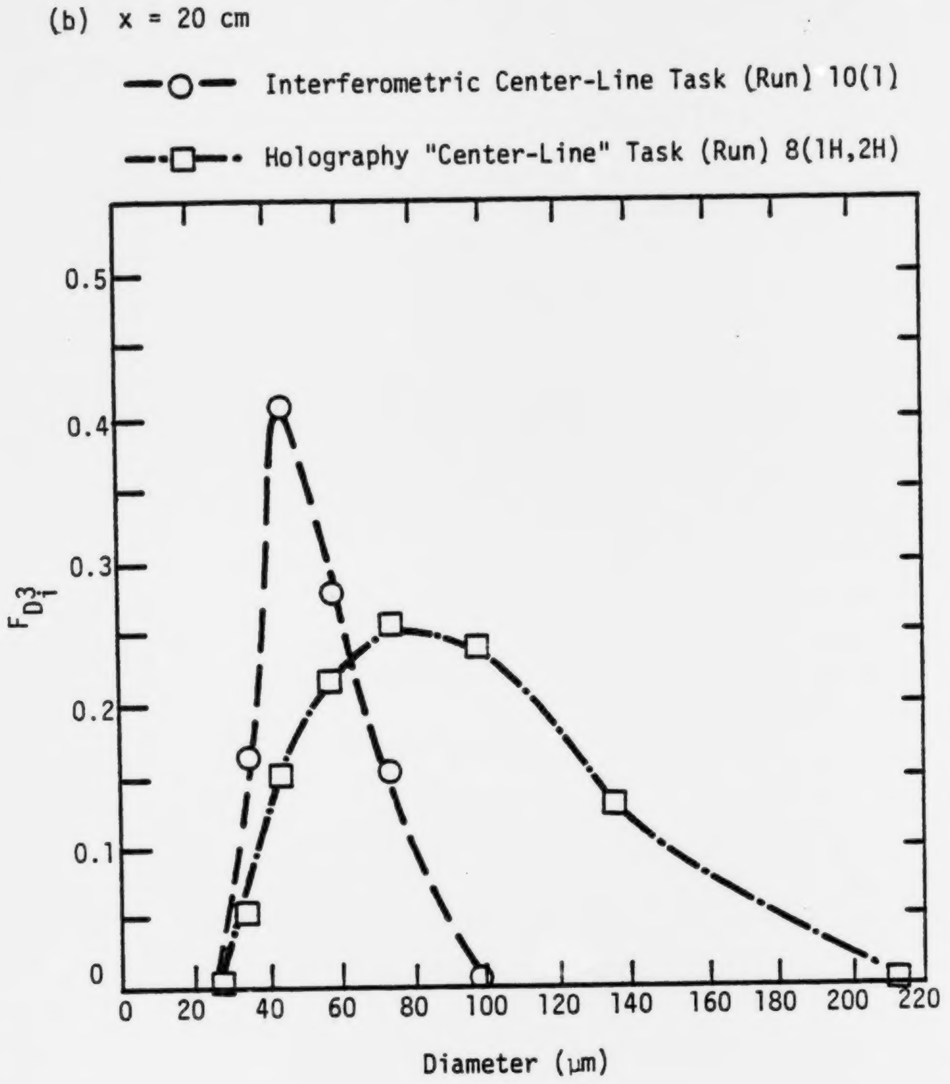

Figure 20. Laser Interferometric and Holography Data--
Weight Density (1.34 atm) (Concluded).

comparing results, the set of conditions listed in Table 7 are the most closely matched between the two experiments.

The comparison between the two experiments is presented in Figure 21 for both number density and weight density. The diffraction results indicate a much broader distribution in both number density and weight density. The majority of droplets, according to the diffraction data, are below the theoretical interferometric cutoff of approximately 10 μm (Table 5), and well below the apparent cutoff of approximately 20 μm. The presence of small droplets is not precluded by the holography results (Figure 18) as the small diameter cutoff for the holography data is estimated to be 15 μm (Appendix A).

The weight density measured by the diffraction method (Figure 21b) demonstrates the importance of measuring the large droplets, a result consistent with the holography data presented in the previous section.

The possible explanations for the differences observed between the interferometric and diffraction measurements include:

1. Problems associated with the comparison of the two techniques, and
2. Differences in the conduct of the two experiments.

With respect to the former, the IFRF diffraction data plotted in Figure 21 represent the aggregate number and weight density distribution across the entire spray, whereas the interferometric data represent the number and weight density distributions measured at the center line of the spray. The data of Figure 13 indicate that the interferometric data change little with radial distance. However, should a few large droplets ($d_p > 90$ μm) be present at radial distances greater than that included in the interferometric data set (2.54 cm from the center line), the interferometric-derived size distribution could significantly be broadened. The holography results demonstrate the existence of such large droplets, the number of which increase outside the radial bounds of the interferometric data set.

A second problem associated with the application of the techniques concerns the limited dynamic range of the interferometric method as employed in the present experiment. As noted in the previous section, the dynamic range was insufficient to discriminate particles greater than ~90 μm and

Table 7. Conditions for Comparison of Laser Diffraction (IFRF) to Laser Interferometry

FIXED CONDITIONS	
Diffraction (IFRF)	Interferometric
V_p = not specified	V_p = 2.2 mps
V_s = 0.2 mps	V_s = 0.4 mps
$\dot{V}_f$ = 1.9 liters/hr	$\dot{V}_f$ = 1.9 liters/hr
x = 46.5 cm	x = 20 cm
μ = 8.8 cSt	μ = 1.3 cSt
PARAMETRIC VARIATION	
Diffraction (IFRF)	Interferometric Task (Run)
P = 1.34 atm	P = 1.34 atm 10(1)
P = 1.68 atm	P = 1.68 atm 11(1)

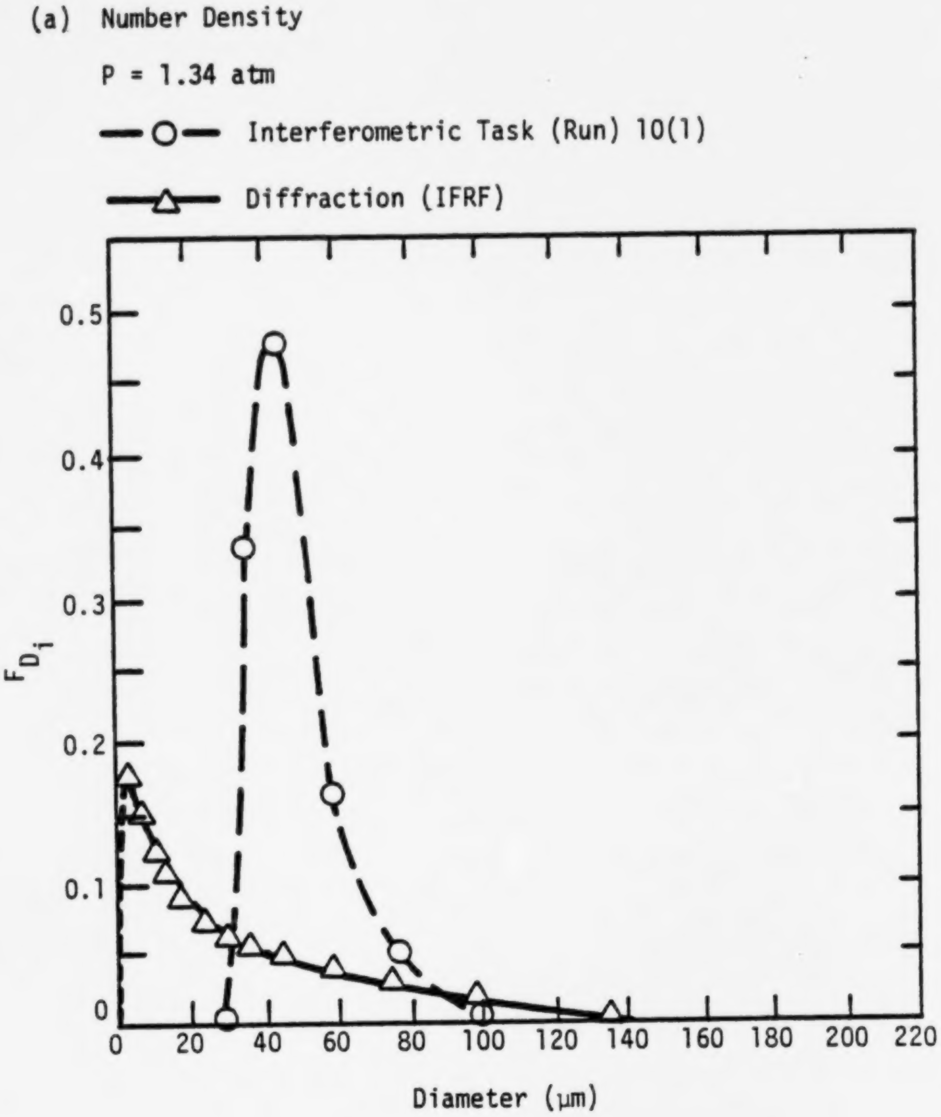

Figure 21. Interferometric and Diffraction (IFRF) Data.

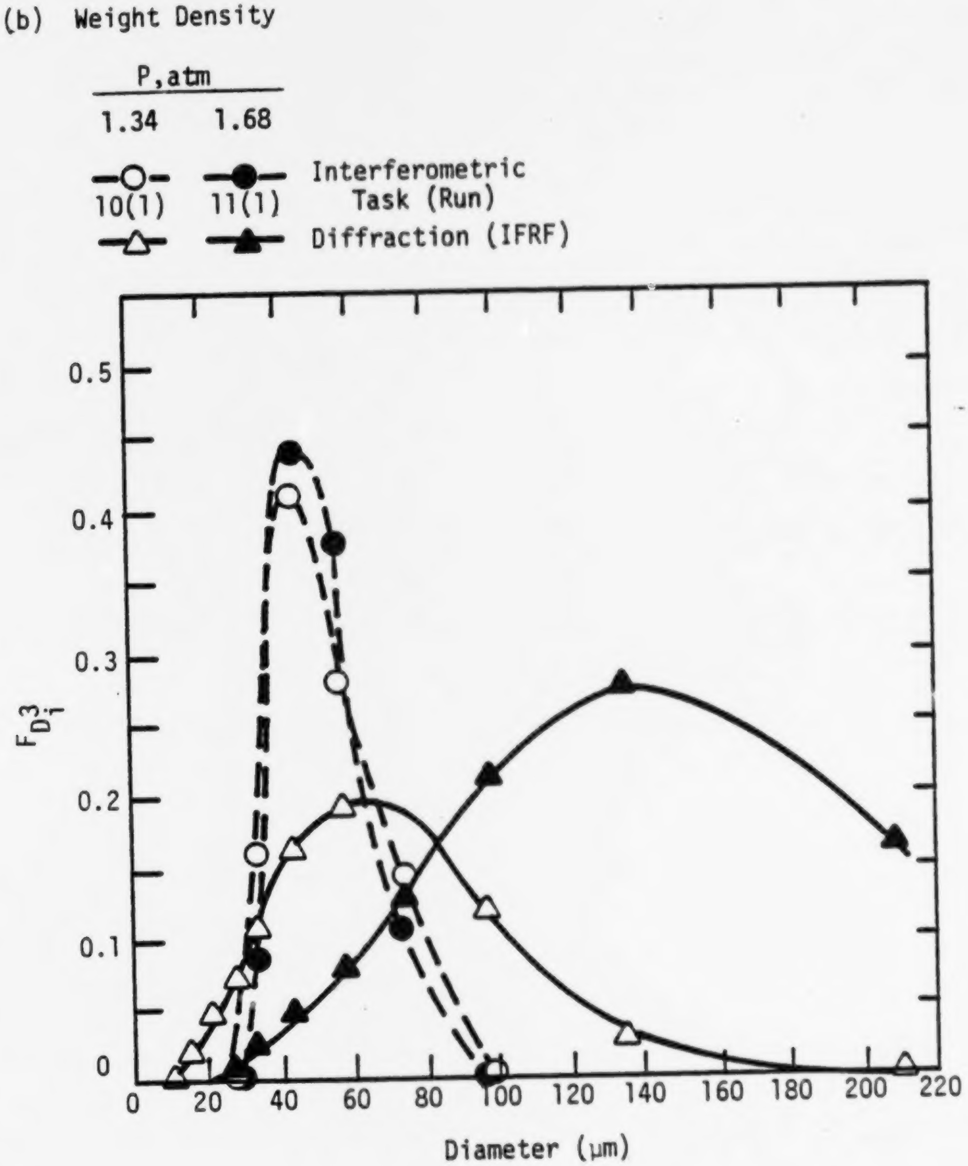

(b) Weight Density

Figure 21. Interferometric and Diffraction (IFRF) Data (Concluded).

less than 20 μm, and the steps taken to optimize the data rate may have preferentially filtered the larger size droplets.

A final question with respect to the application of the techniques concerns the droplet size distribution (Rosin Rammler) assumed in the Malvern technique. The forced fit may not accurately represent the actual size distribution.

With respect to the conduct of the two experiments, the following differences could potentially explain the discrepancies between the two sets of data:

- Different Facilities. The IFRF chamber is 1.52 meters (5 feet) in diameter whereas the EER chamber is approximately 0.61 meters (2 feet) in diameter.
- Different Operating Conditions. Significant differences occurred in the conduct of the two experiments, most notably the screen air and axial sampling location.
- Different Liquid Fuel Pressure Measurement Location. The liquid fuel pressure was measured approximately 3.0 and 6.1 meters (10 and 20 feet) from the nozzle in the EER and IFRF studies, respectively. Because of the sensitivity of the Sonicore performance to liquid-fuel pressure, the relative location of the pressure sampling point is important.
- Different Oil Type. The viscosities of the oils used for the EER and IFRF experiments were 1.3 and 8.8 cSt, respectively.

To provide a direct comparison to the interferometric data, the Malvern was transported to the EER test site, and laser diffraction measurements were made at the same condition and within the same chamber used for the earlier acquisition of the interferometric data.

EER Results. The test matrix for the acquisition of the EER data is presented in Table 5. For the purpose of direct comparison of the diffraction and the interferometric data, the conditions presented in Table 8 were selected.

Table 8. Conditions for Comparison of Laser Diffraction (EER) to Laser Interferometry

FIXED CONDITIONS		
$V_p = 2.2$ mps		
$V_s = 0.4$ mps		
$\dot{V}_f = 1.9$ liters/hr		
$P = 1.34$ atm		
$x = 20$ cm		
Interferometric	Task (Run)	10(1)
Diffraction	Task (Run)	1(3)

The results are presented in Figure 22 for both the number density and weight density in conjunction with the previously presented holography data.

The EER diffraction results show the same general trends as the IFRF diffraction results. In Figure 22a, for example, the diffraction measurement indicates a much higher population of small droplets than measured by either the interferometric or holography methods, both of which suffer from a small droplet cutoff in the range of 15 to 20 μm.

Because of the dependency of weight density of large droplets, the weight density distributions (Figure 22b) agree well for holography and diffraction, both of which measure the large droplets without restriction. The failure of the interferometric technique as applied in the present experiment to measure large droplets is again shown in these data.

Figure 23 compares the IFRF and EER results and shows that the IFRF weight-density distribution is broader with a higher mean diameter. The IFRF study evaluated a number of nozzles operating over a variety of oil mass flow rates, atomizing pressure, and fluid viscosity. On these variables, atomizing pressure and oil fuel rate were shown to have the greatest influence on mean droplet size and size distribution. Between the two experiments, the atomizing pressure at the nozzle is the highest uncertainty. Although measured and recorded in both cases, the distance from the measuring point to the nozzle (and hence the pressure drop) in the case of the IFRF studies is approximately twice that of the EER experiment. The difference in the diffraction data in Figure 23, as a result, is likely due to a lower nozzle pressure in the IFRF data. Viscosity is also an important variable, 1.3 cSt in the case of the EER experiments and 8.8 cSt in the case of the IFRF tests. However, in the IFRF studies, viscosity was varied from 8.8 to 19 cSt with little impact on either the mean diameter or distribution.

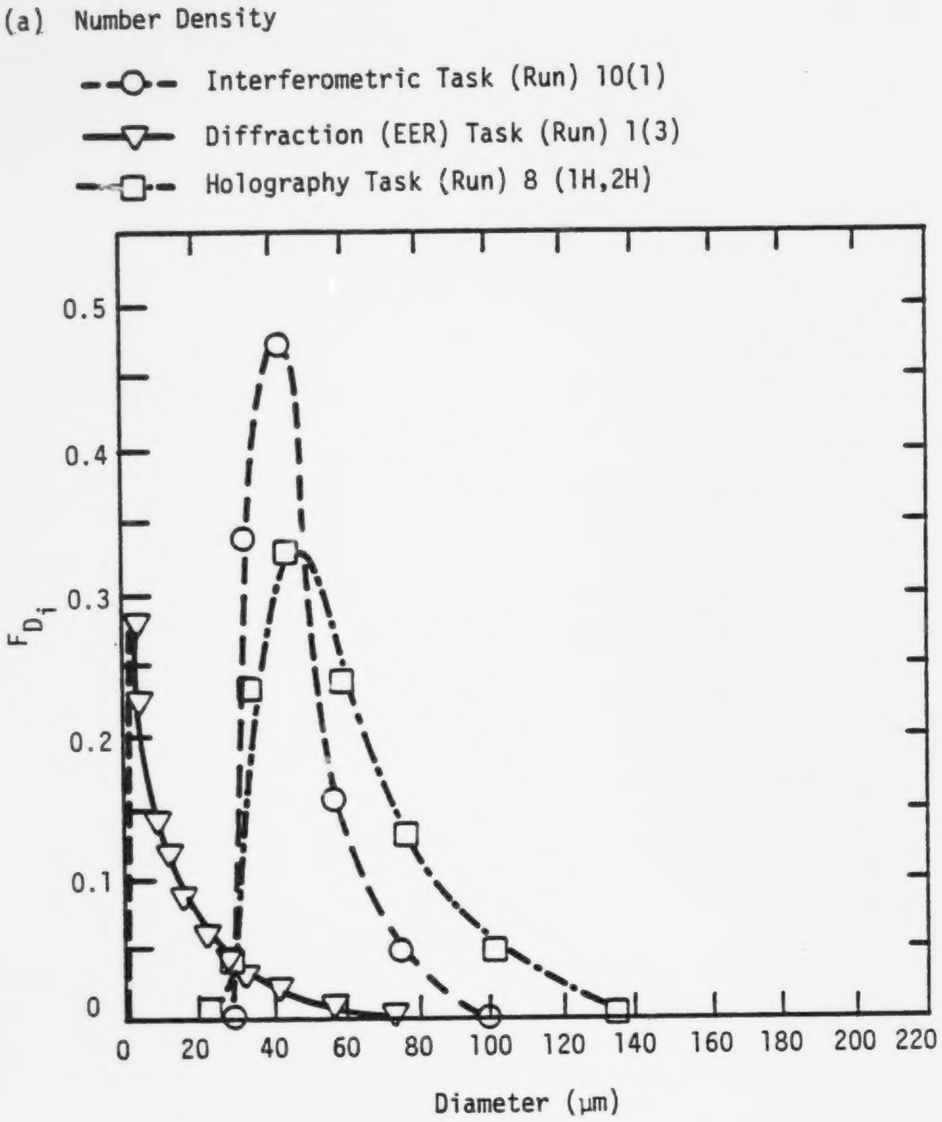

Figure 22. Interferometric, Diffraction (EER), and Holographic Data (1.34 atm, x = 20 cm).

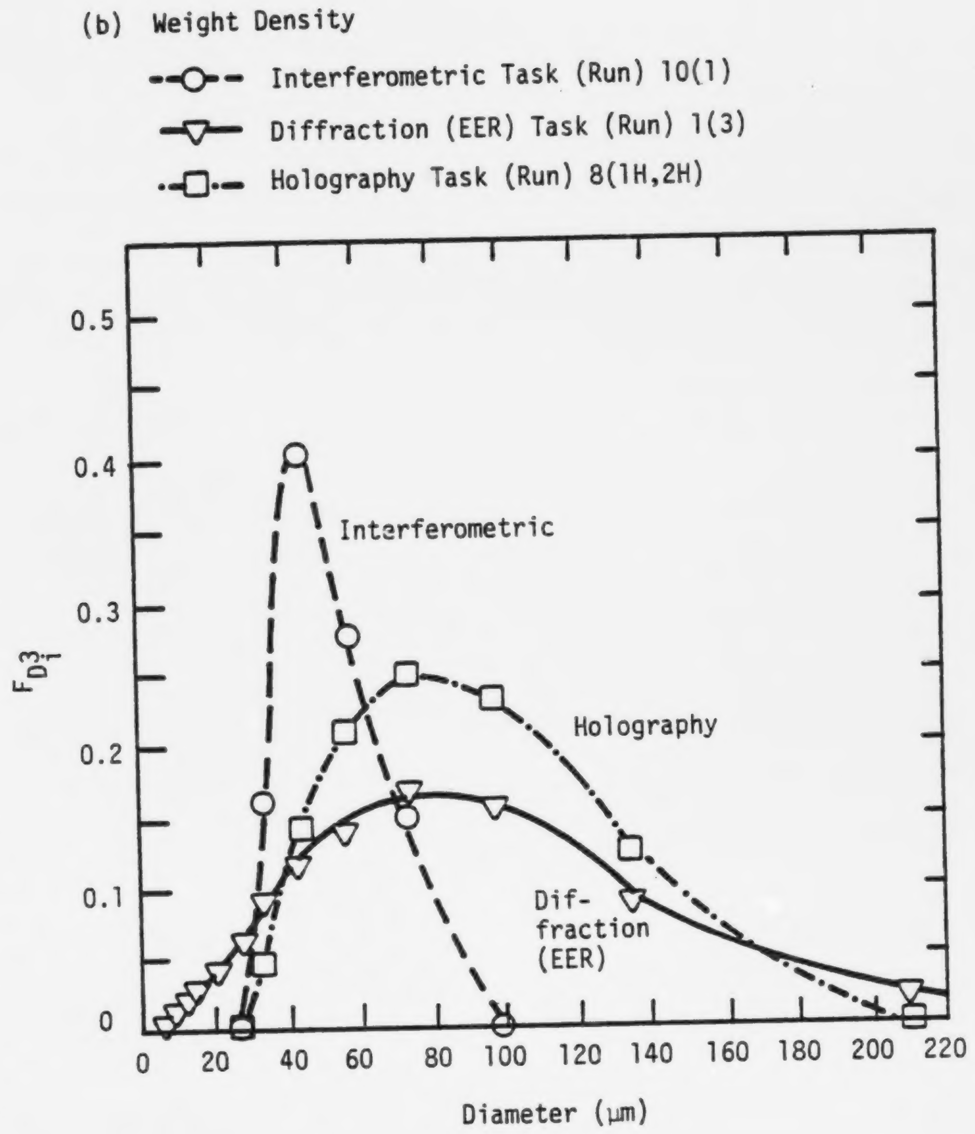

Figure 22. Interferometric, Diffraction (EER), and Holographic Data--Weight Density (1.34 atm, x = 20 cm) (Concluded).

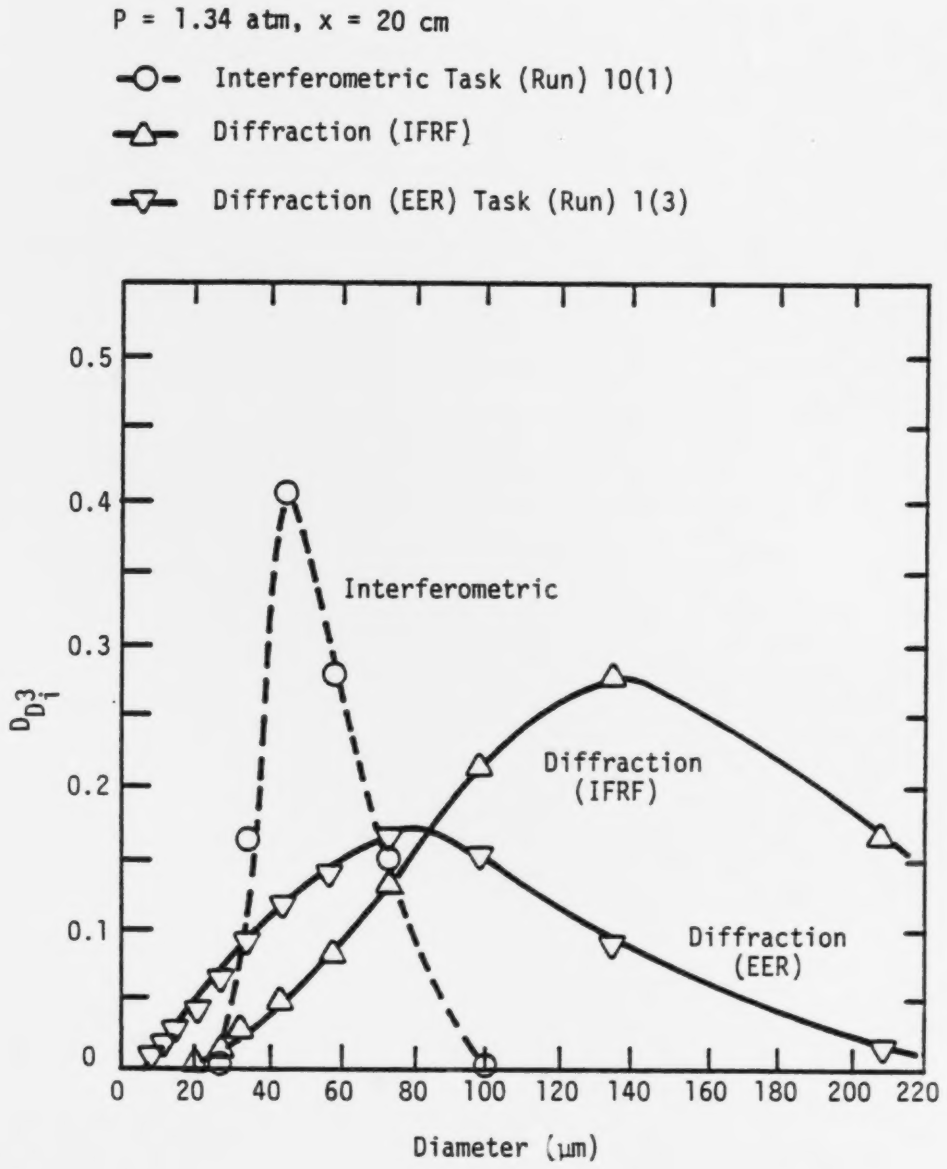

Figure 23. Interferometric, Diffraction (IFRF), and Diffraction (EER)--Weight Density.

6.0 CONCLUSIONS

The present study was undertaken to explore the utility and applicability of laser interferometry as a result of its potential to:

- Make point rather than path measurements and thereby provide spatial resolution.
- Measure single droplets rather than aggregates of droplets and thereby measure droplet velocity as well as exactly measure the number density.
- Measure droplet velocity and thereby obtain information concerning droplet ballistics and gas/droplet interaction.
- Measure gas velocity and thereby measure the aerodynamic flow activity on the droplet.

These types of measurements are necessary to the exploration of pollutant formation in combustors and boilers operating on both conventional and alternative fuels.

The conclusions of the study are:

1. Interferometry has a high potential for making the measurements described above.
2. Application of the technique requires that the dyanmic range (10:1) of the instrument be changed to accommodate large droplets (which are especially important to weight density distribution) and small droplets (which are especially important to number density distribution).
3. Both optical techniques used to assess the performance of the laser interferometric system in the present study established that the dynamic range was limited on the large droplet end ($d_p \sim 90\ \mu m$) and, as a result, the laser interferometric technique failed to measure large droplets.
4. The laser diffraction technique, in addition, indicated that droplets were indeed present below the lower cutoff (d_p = 15 to 20 μm) limit of both the holography and interferometry methods.

5. The interferometric operator must be very aware of the sensitivity limit range and the saturation limit range. It will require several measurements with different PMT bias levels and fringe spacings to obtain a broad size distribution. A sequence can be developed to measure the distribution by continually shifting the valid range and then combining results.

REFERENCES

Bachalo, W. D. (1980). "Method for Measuring the Size and Velocity of Spheres by Dual-Beam Light-Scatter Interferometry," Applied Optics, 19, 363.

Bexon, R., Bishop, G. D., and Gibbs, J. (1975). "News of Imano Equipment and Applications," No. 3.

Decorso, S. M. (1958). "A Photographic Method of Determining the Drop-Size Distribution of a Spray," Research Report 8-0524-R32, Westinghouse Research Laboratories, Pittsburgh, PA.

Dobbins, R. A., Crocco, L., and Glassman, L. (1963). "Measurement of Mean Particle Sizes of Sprays from Diffractively Scattered Light," AIAA Journal, 1, 1882.

England, G. C., Heap, M. P., Horton, R. T., Pershing, D. W., and Flament, G. (1979). "The Control of Pollutant Formation in Fuel Oil Flames-- The Influence of Oil Properties and Spray Characteristics," Proceedings of the Third Stationary Source Combustion Symposium; Volume II. Advanced Processes and Special Topics, EPA-600/7-79-050b, (NTIS PB292540) p. 41.

England, G. C., Pershing; D. W., Heap, M. P. and Cichanowicz, J. E. "Effects of Fuel Properties and Atomization Parameters of NO_x Control for Heavy Liquid Fuel Fired Package Boiler, EPA-600/7-82-029 (NTIS PB82-230715), April, 1982.

Farmer, W. M. (1973). The Interferometric Observation of Dynamic Particle size, Velocity, and Number Density," Ph.D. Thesis, University of Tennessee.

Feinstein, S. P. and Girard, M. A. (1979). "Feasibility of Automated Drop-size Distributions from Holographic Data Using Digital Image Processing Techniques," AIAA Paper 79-0297, presented at the 17th Aerospace Sciences Meeting, New Orleans.

Heap, M. P., Pershing, D. W., England, G. C., Lee, J. W., Chen, S. L. (1979). "The Influence of Fuel Characteristics on Nitrogen Oxide Formation-- Bench-Scale Studies, "Proceedings of the Third Stationary Source Combustion Symposium; Volume II. Advanced Processes and Special Topics, EPA-600/7-79-050b, (NTIS PB292540) p. 3.

REFERENCES (Continued)

Ingebo, R. D. (1957). "Atomization, Acceleration, and Vaporization of Liquid Fuels," Sixth Symposium (International) on Combustion, The Combustion Institute, New York, 684.

Joyce, J. R. (1946). "The Wax Method of Spray Particle Size Measurement," Tech. Rept. I. C. T./7, Shell Petroleum Co., Ltd., London, England.

Kuhn, R. (1925). "Atomization of Liquid Fuels," NACA Technical Memorandum 329-331.

Lee, D. W. (1932). "The Effect of Nozzle Design and Operating Conditions on the Atomization and Distribution of Fuel Sprays," NACA Report 425.

May, K. R. (1945). "The Cascade Impactor: An Instrument for Sampling Coarse Aerosols," Journal of Scientific Instrumentation, 22, 187.

Negus, C., and Azzopardi, B. J. (1978). "The Malvern Particle Size Distribution Analyzer: Its Accuracy and Limitations," Harwell Report AERE-R 9075.

Nukiyama, S., and Tanasawa, Y. (1938). "An Experiment on the Atomization of Liquid by Means of an Airstream," Transactions of the Society of Mechanical Engineers, 4, S-13.

Polymeropoulos, C. E. and Sernas, V. (1977). "Measurement of Droplet Size and Fuel-Air Ratio in Sprays," Combustion and Flame, 29, 123.

Simmons, H. C. (1977). "The Correlation of Drop-Size Distributions in Fuel Nozzle Sprays," Journal of Engineering for Power, 99 (3), 309.

Simmons, H. C. and Lapera, D. L. (1969). "A High-Speed Spray Analyzer for Gas Turbine Fuel Nozzles," Paper presented at ASME Gas Turbine Conference, Cleveland, March.

Stubbs, H. E. and York, J. L. (1952). "Photographic Analysis of Sprays," Transaction of the American Society of Mechanical Engineers, 74, 1157.

Swithenbank, J., Beer, J. M., Taylor, D. S., Abbot, D., and McCreath, G. C. (1976). "A Laser Diagnostic Technique for the Measurement of Droplet and Particle Size Distribution," University of Sheffield, Department of Chemical Engineering and Fuel Technology Report HIC 245.

Tate, R. W. (1961). "Immersion Sampling of Spray Droplets," AIChE Journal 7, 574.

Taylor, E. H. and Harmon, D. B. (1954). "Measuring Drop Sizes in Sprays," Industrial and Engineering Chemistry, 46, 1955.

Tishkoff, J. M., Hammond, D. C., and Chraplyvy, A. R. (1980). "Diagnostic Measurements of Fuel Spray Dispersion," presented at the ASME Winter Annual Meeting, Paper 80-WA/HT-3J.

REFERENCES (Concluded)

Webster, R. P., Weight, R. P., and Archenhold, E. (1976). "Holographic Size Analysis of Burning Sprays," Combustion and Flame, 27, 395.

Woolridge, A. L. (1959). "A Photographic Technique for the Determination of of Sizes of Liquid Droplets," CWL Special Publication 3-6, U.S. Army Chemical Warfare Laboratories.

APPENDIX A

CHARACTERIZATION OF A SONICORE NOZZLE

by:

C. F. Hess and W. D. Bachalo

Spectron Development Laboratories, Inc.
3303 Harbor Boulevard, Suite G-3
Costa Mesa, CA 92626

Prepared for:

Energy and Environmental Research Corporation
EER Subcontract No. EER-8318-9

TABLE OF CONTENTS

NO. PAGE (III-A-)

Table of Contents ii
List of Figures. iii
Introduction 1
1.0 Description of DSI Apparatus 3
1.1 Description of Experiments. 8
1.2 Task Matrix of Visibility Measurements. 9
1.3 Description of Holography Apparatus 17
1.4 Test Matrix of Holography Data. 17
2.0 Results and Discussion 22
2.1 Description of Size and Velocity Histograms 22
2.2 Definition of Size and Velocity Parameters. 23
2.3 Experimental Doppler Data 28
2.4 Experimental Holography Data. 33
2.5 Comparison Between Holography and Visibility Data 34
3.0 Brief Description of the Malvern Particle and Droplet Sizing System. 36
3.1 Principle of Operation. 36
4.0 Conclusions. 40
5.0 References 42
Appendix A-1
Theoretical Description A-1
Fraunhofer Diffraction. A-2
Size Determination by Diffractively Scattered Light A-3
Discussion. A-7
Inversion of the Measured Signal. A-13
Particle Velocity Effects A-16
Summary A-16
Future Work A-17
References. A-18

LIST OF FIGURES

NO. PAGE (III-A-)

1 Schmatic of Optical Apparatus for Droplet Size and Velocity Measurements 4

2 DSI Transmitting Optics 5

3 SDI Collecting Optics 6

4 Droplet Sizer and Velocimeter Apparatus in Test Facility 7

5 Polaroid Picture of Object and Reference Beams in Presence of Stream From Nozzle - Magnification = 1 10

6 Poloroid Picture of Object and Reference Beams in Presence of Atomizing Nozzle - Magnification = 3 11

7 Holocamera System Transmitting Module 15

8 Holocamera System Receiver Module 16

9 Sonicore Nozzle Spraying Fuel No. 2 and Crossing Laser Beams . . . 24

10 Test Rig 25

11 Mean Diameter and Standard Deviation as a Function of Position . . . 26

12 Max. and Min. Velocity as a Function of Position 27

13 Droplet Distribution Below Nozzle Tip Pressure of 5 PSI, Primary Velocity of 2.2 M/S 29

14 Ligament Formation at Nozzle Exit Pressure of 5 PSI, Primary Velocity of 2.2 M/S 30

15 Ligament Formation at Nozzle Exit Pressure of 10 PSI, Primary Velocity of 2.2 M/S 31

16 General View and Close-up of Spraying Nozzle Pressure of 5 PSI, Primary Velocity of 10 M/S 32

17 Holography and Visibility Data of Fuel Spray Nozzle Within 0.5 Inch of Centerline and Various Axial Positions 35

18 Cross Section of the Airy Pattern 38

19 Optical Arrangement of Fourier Transform Lens to Obtain the Size Distribution of Solid or Liquid Particles 39

A1 Cross Section of the Airy Pattern A-4

A2 Fraunhofer Diffraction Pattern of A Circular Aperture A-5

A3 Schematic of the Diffraction Patterns of a Polydisperse Particle Field A-6

LIST OF FIGURES (Continued)

PAGE (III-A-)

NO.

A4 Dual Beam Scatter by a Spherical Droplet A-8

A5 Van de Hulst, Anomolus Diffraction A-10

A6 Optical Arrangement of Fourier Transform Lens to Obtain the Size Distribution of Solid or Liquid Particles A-12

A7 Scatter From Various Stations Along the Beam A-14

INTRODUCTION

Two optical techniques were used to characterize the droplet field produced by a Sonicore nozzle under laboratory conditions. These techniques are droplet sizing interferometry (DSI) and holography. The first is a real time single droplet velocity and size measurement (Bachalo, et al., 1979). The second is a recording which stores for later reconstruction, all of the coherent optical information that has passed through or reflected from a volume and subsequently fell upon a holographic plate. This information is mixed with a reference wave to produce a three-dimensional field (Trolinger, 1975).

The purpose of this research is two-folded. First, it will be a demonstration of the droplet sizing interferometer (DSI) and how it compares to other optical techniques. Second is the characterization of the behavior of a Sonicore nozzle under various conditions. The techniques used to compare to DSI are particle field holography and multiple particle diffraction analysis (Malvern instrument). Measurements using DSI and holography were performed at the EERC combustion facilities. These provided a direct comparison between the two techniques. The analysis of the Malvern instrument was done theoretically. The Appendix contains the detailed description of such an analysis.

The conditions varied in the experiments are the pressure differential across the nozzle, the primary velocity, the screen velocity and the oil flow rate. The optical parameters varied on some of the experiments were the laser beam diameter and intersection angle. These have an influence on the probe volume size and fringe spacing. The size of the probe volume is important since the ability of measuring single droplets depends on how small this volume can be made. The fringe spacing determines the size interval where the instrument is sensitive. After optimizing these parameters, axial and radial profiles of the fuel spray were obtained under various conditions. The size and velocity of the droplets are thus obtained and they can then be related to evaporation rate, etc.

The DSI proved to be a very powerful instrument to study fuel sprays. It measured single droplet size and velocity even in the presence of high number densities. Its maximum processing rate is several times faster than the rate required by the experiments. The typical time to obtain a histogram with three thousand data points was in the order of five seconds. The results obtained with this technique compared very well with those obtained holographically.

Holography proved to be very adequate for measuring particles larger than 15 μm. Because of fuel accumulated on the windows and optical components, and because of the high number density of the spray, the speckle did not allow resolution of the smaller particles. This last problem can be considerably improved by using a sheet of light rather than a cylindrical beam.

This research program has been very successful. The instrumentation of SDL and test facilities of EERC performed very well under all the circumstances. The technical support of EERC was excellent. All these factors contributed to the successful completion of the proposed work.

1.0 DESCRIPTION OF DSI APPARATUS

The optical system was constructed on a breadboard. It consisted of a HeNe laser, transmitting lenses, a diffraction grating, transmitting mirrors and collecting lenses. The laser beam is focused by L_1 on the diffraction grating (Figure 1). There, it is split into several beams according to the diffraction modes. Only the ±1 modes are allowed through and the others are masked out. Since the lens L_2 is one focal distance from the diffraction grating, the beams coming out of L_2 are parallel and collimated. The ratio of L_2 to L_1 determines the beam diameter before it is focused by L_3. The separation of the beams is controlled by f_2. This provides an independent means of selecting the fringe spacing and the probe volume size. The laser beams are then focused by L_3 on the probe volume. This is the region in space where measurements are obtained.

The light scattered by the particles crossing the probe volume is collected by L_4 and then focused by L_5 on the photomultiplier tube. Both the transmitting and the receiving optics are mounted on traverse mechanisms which allows it to scan throughout the plume at any one axial position. To change axial positions the nozzle was moved up and down.

The signal coming out of the photomultiplier is then processed in the visibility processor. The Doppler frequency and the visibility is thus obtained. These parameters are then input to the data management system which displays histograms of size and velocity and stores in diskettes the visibility and period of each particle.

Photographs of the system are shown in Figures 2, 3 and 4. Figure 2 shows the transmitting optics used in the experiments. Note that this package is mounted in breaded board for maximum flexibility. The diffraction grating is mounted on an a.c. syncronous motor to provide frequency shift, if necessary. This feature was not used since the measured velocities were within the processor's range. The collecting optics and electronics are shown in Figure 3. The lenses and photomultiplier are mounted on a traversing platform.

SCHEMATIC OF DROPLET SIZING INTERFEROMETER

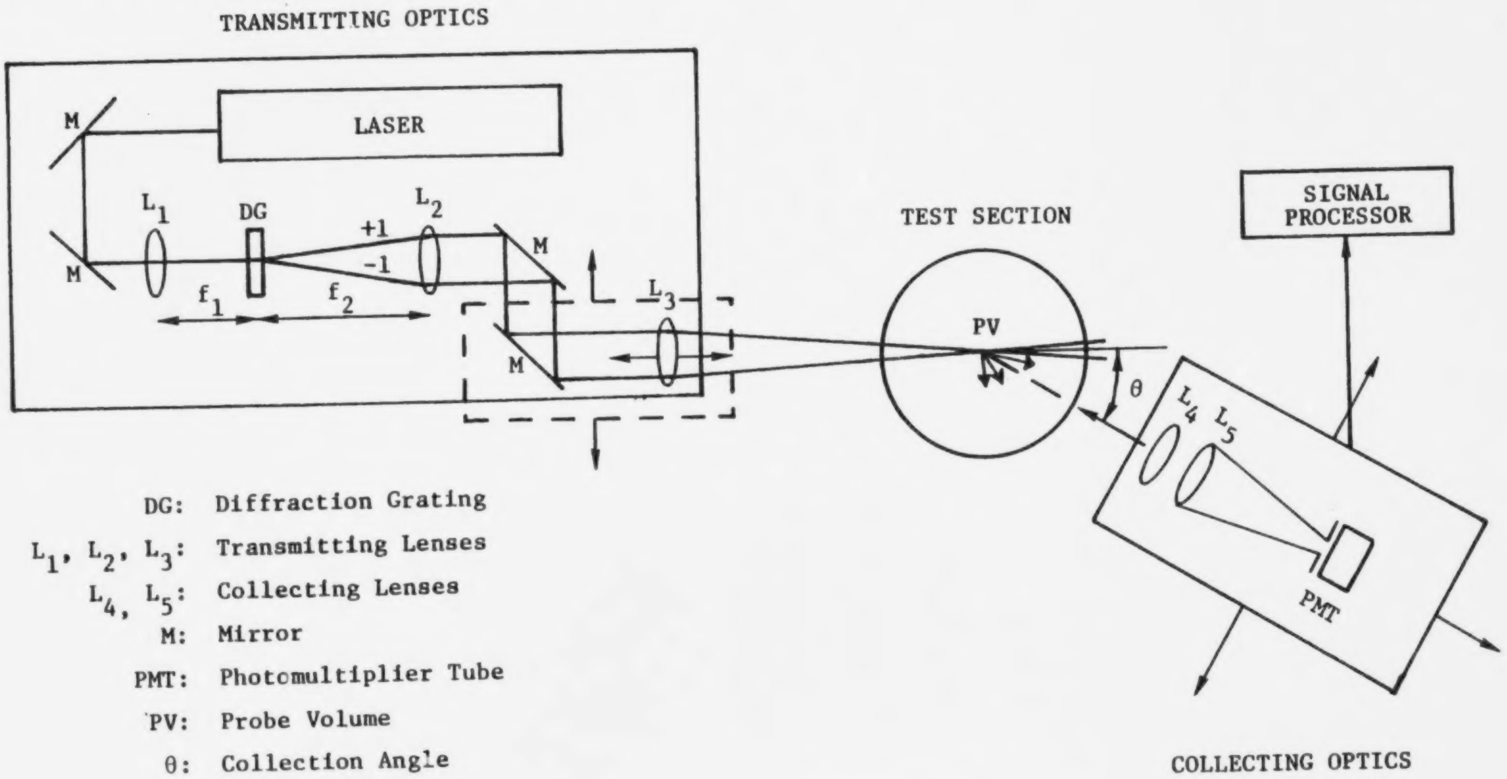
TRANSMITTING OPTICS
M
LASER
M
L_1
DG
+1
-1
L_2
M
f_1
f_2
L_3
M
TEST SECTION
PV
θ
SIGNAL PROCESSOR
L_4
L_5
PMT
COLLECTING OPTICS

DG:	Diffraction Grating
L_1, L_2, L_3:	Transmitting Lenses
L_4, L_5:	Collecting Lenses
M:	Mirror
PMT:	Photomultiplier Tube
PV:	Probe Volume
θ:	Collection Angle

Figure 1. SCHEMATIC OF OPTICAL APPARATUS FOR DROPLET SIZE AND VELOCITY MEASUREMENTS

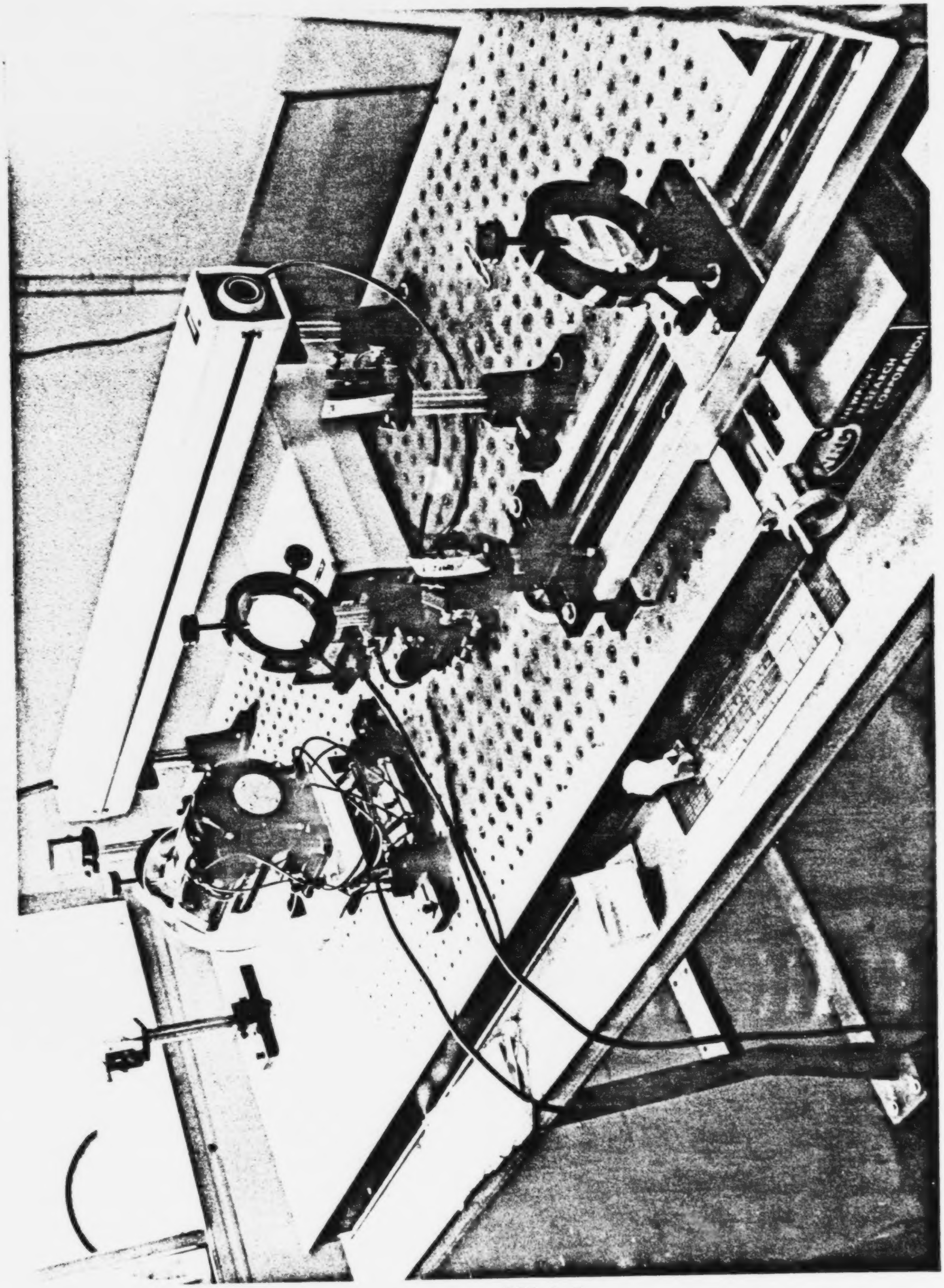
NEWPORT RESEARCH CORPORATION

Figure 2. DSI TRANSMITTING OPTICS

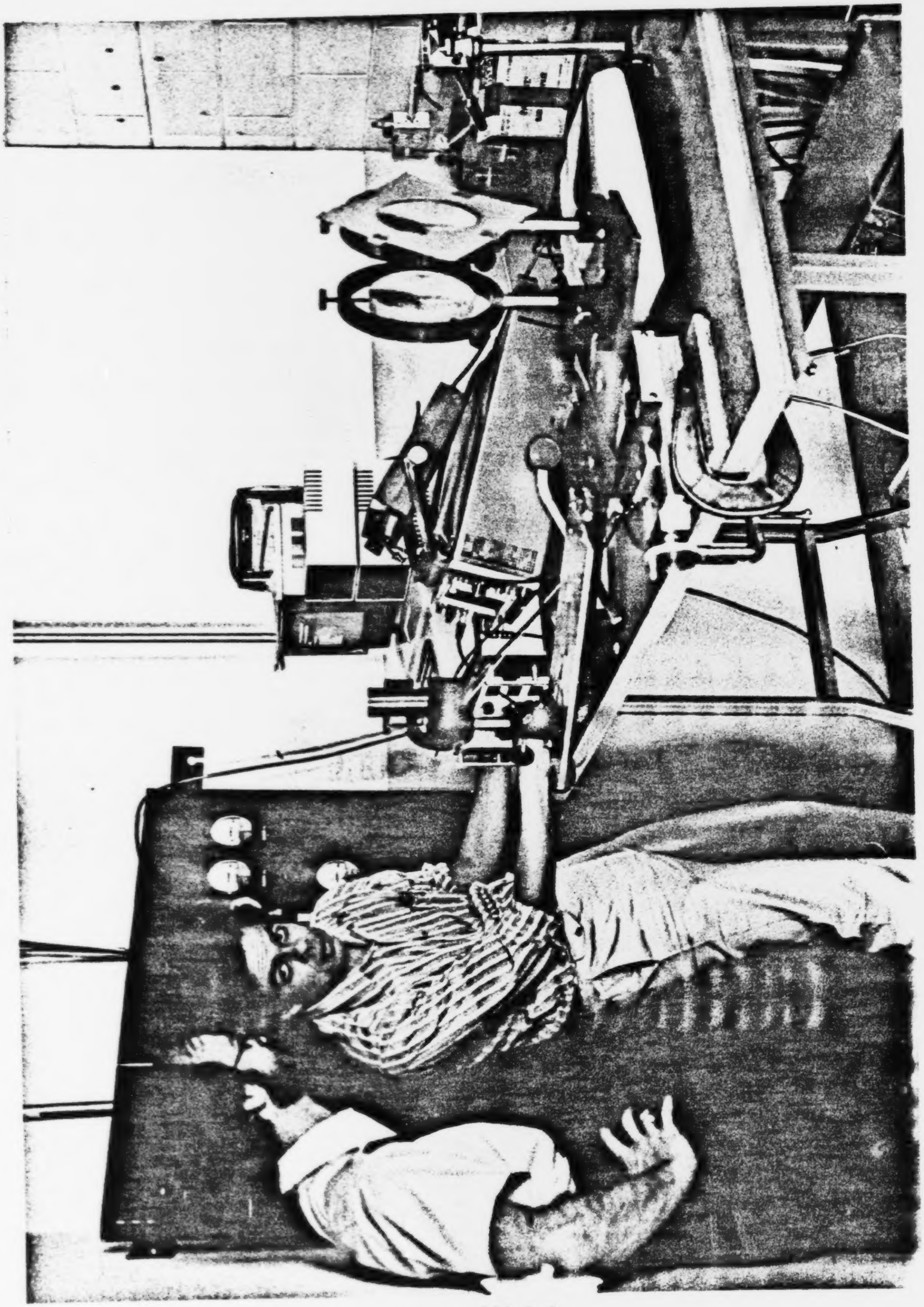

Figure 3. DSI COLLECTING OPTICS

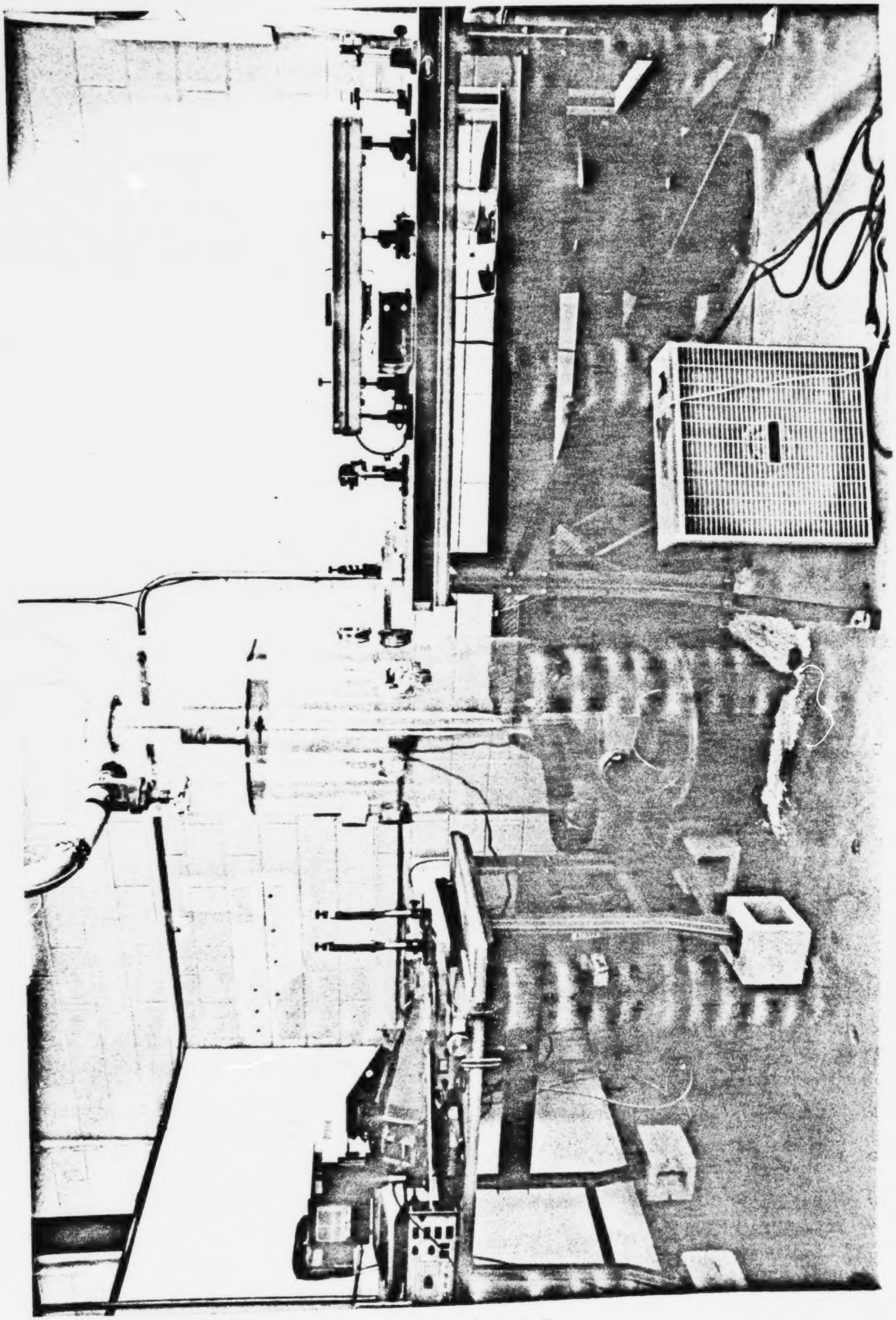

Figure 4. DROPLET SIZER AND VELOCIMETER APPARATUS IN TEST FACILITY

The lenses in both the transmitting and collecting optics are achromat in order to minimize aberrations. The transmitting mirrors are flat to one quarter wavelength.

The entire system including the test rig is shown in Figure 4. Notice that the incident laser beams and the scattered light travel through quartz windows located on the size of the plexiglass test rig. These windows were placed at a collection angle of 30° as specified by SDL, in order to obtain a small probe volume and a large scattered light intensity.

1.1 Description of Experiments

Two techniques are used to characterize the droplet size and velocity distributions of a fuel spray produced by a sonicore nozzle. They are scattered light interferometry and holography. The first one measures the visibility and Doppler period of individual particles crossing the probe volume. The second freezes in time the flow field in a given volume.

The two techniques were used for comparison and the experiments performed are now described.

The size and velocity of droplets of diesel fuel #2 were measured for various conditions as described in the task matrix below. The controlling parameters were the pressure difference across the nozzle, the surrounding air velocity and the fuel feed rate.

The droplet sizing interferometer was aligned with respect to the nozzle tip and that was assumed to be the zero axial and radial position. The optics were then translated to a different radial position and the nozzle was moved up and down to resolve the axial profiles. Unless otherwise specified, the dimensions of the axial position are given in centimeters and those of the radial position in inches.

To align the holography system, a wire was hung inside the test facility at a known position with respect to the nozzle. It was placed far from the nozzle to avoid disturbing the flows. At axial positions downstream from the nozzle, this wire served as a reference. Flash photography on polaroid film was performed at the beginning of each experiment. This served to confirm the alignment, to check the relative intensity of the reference and object waves and to detect dirt on the optical windows. A sample of these photographs is shown in Figure 5 and 6.

A task matrix of the performed experiments now follows.

1.2 Task Matrix of Visibility Measurements

Task 1: Radial Symmetry Check

Conditions: 20 cm axial, air pressure 5 psig, other parameters nominal

Radial (in):	-1,	-1/2,	CL,	1/2,	1,	1 1/2
Run:	6,	(5,11),	1,	4,	(2,9),	(3,10)

f_1 = 160 mm, f_2 = 330 mm, f_3 = 510 mm, δ = 15.8 μm, F# collection = 5.3

Total number of points: 6

Task 2C: Position Analysis at 5 psig

Conditions: air pressure 5 psig, other parameters nominal

Axial (cm):	2			5			10				15
Radial (in):	-.5	CL	.5	-.5	CL	.5	-.5	CL	.5	1	CL
Run:	15	5	14	16	6	13	17	4	12	9	

Axial (cm):	20			30				40
Radial (in):	CL	.5	1	-.5	CL	.5	1	CL
Run:	3	11	8	18	2	10	7	1

f_1 = 85 mm, f_2 = 330 mm, f_3 = 510 mm, δ = 15.8 μm, F# collection = 5.3

Total number of points: 19

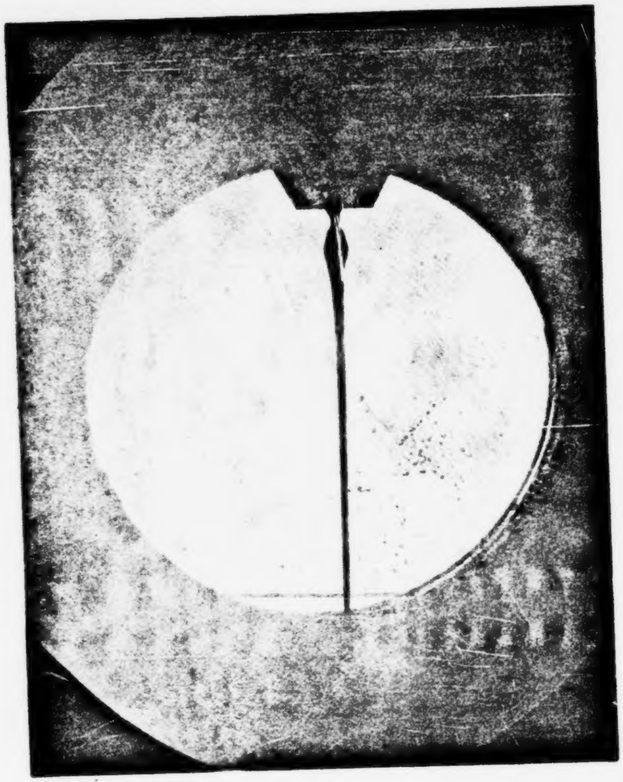

Figure 5. POLAROID PICTURE OF OBJECT AND REFERENCE BEAMS IN PRESENCE OF STREAM FROM NOZZLE MAGNIFICATION = 1

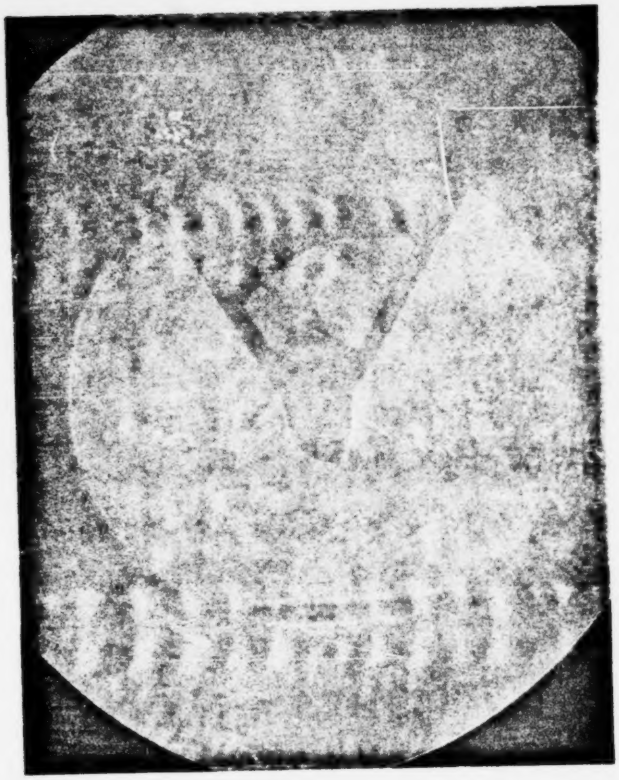

Figure 6. POLAROID PICTURE OF OBJECT AND REFERENCE BEAMS IN PRESENCE OF ATOMIZING NOZZLE MAGNIFICATION = 3

Task 3: Position Analysis at 10 psig

Conditions: nominal.

Axial (cm):	5			10			20		
Radial (in):	CL	.5	1	CL	.5	1	CL	.5	1
Run:	1	6	9	2	5	8	3	4	7

f_1 = 85 mm, f_2 = 510 mm, f_3 = 510 mm, δ = 10.2 μm, F# collection = 5.3

Total number of points: 9

Task 4: Variation of Primary Air Velocity

Conditions: 10 cm axial, air pressure 5 psig, other parameters nominal.

Primary Velocity (m/s):	0			5			10				18	
Radial (in):	CL	.5	1	CL	.5	1	.5	CL	.5	1	CL	.5
Run:	2	6	11	3	7	12	1	4	8	13	(5,9)	10

f_1 = 85 mm, f_2 = 330 mm, f_3 = 510 mm, δ = 15.8 μm, F# collection = 5.3

Total number of points: 11

Task 5: Parametric Nozzle Performance

Conditions: 10 cm axial, nominal velocities.

Air Pressure (psig):	5		10			15			20		
Oil Flow Rate (lbm/hr):	2	8	2	4	8	2	4	8	2	4	8
Radial (in):	CL	CL	CL	CL	CL	CL	CL	CL	CL	CL	CL
Run:	10	11	9	7	8	2	1	3	5	4	6

f_1 = 85 mm, f_2 = 330 mm, f_3 = 533 mm, δ = 15.8 μm, F# collection = 5.3

Total number of points: 11

Task 5C: Continuation Parametric Nozzle Performance

Conditions: 10 cm axial, nominal velocities.

Air Pressure (psig):	5						10					
Oil Flow (lbm/hr):	4			8			4			8		
Radial (in):	CL	.5	1	CL	.5	1	CL	.5	1	CL	.5	1
Run:	5	18	26	6	17	25	1	15	23	2	16	24

Air Pressure (psig):	15						20					
Oil Flow (lbm/hr):	4			8			4			8		
Radial (in):	CL	.5	1	CL	.5	1	CL	.5	1	CL	.5	1
Run:	4	14	22	3	11	21	8	9	19	7	10	20

Conditions: Same as above but nozzle rotated 90°.

Air Pressure (psig):	15	20
Oil Flow (lbm/hr):	8	8
Radial (in):	0.5	0.5
Run:	12	14

f_1: 85 mm, f_2 = 510 mm, f_3 = 533 mm, δ = 10.2 μm, F# collection = 5.3

Total number of points: 26

Task 6: Higher Viscosity Fluid Position Analysis

Conditions: Glycerin/water mixture; 25 cst, air pressure 10 psig, flow rate 5 lbm/hr

Axial (cm):	5		10		20		
Radial (in):	CL	.5	CL	.5	CL	.5	1
Run:	2	6	1	5	3	4	7

f_1: 85 mm, f_2 = 510 mm, f_3 = 533 mm, δ = 10.2 μm, F# collection = 5.3

Total number of points: 7

Task 10: Velocity/Size Correlation

Conditions: Air pressure 5 psig, other parameters nominal.

Axial (cm):	5			10			20		
Radial (in):	CL	.5	1	CL	.5	1	CL	.5	1
Run:	3	6	9	2	5	8	1	4	7

f_1 = 124 mm, f_2 = 330 mm, f_3 = 390 mm, δ = 12 μm, F# collection = 5.3

Total number of points: 9

Task 11: Velocity/Size Correlations

Conditions: Nominal

Axial (cm):	5			10			20		
Radial (in):	CL	.5	1	CL	.5	1	CL	.5	1
Run:	3	6	9	2	5	8	1	4	7

f_1 = 124 mm, f_2 = 330 mm, f_3 = 390 mm, δ = 12 μm, F# collection = 5.3

Total number of points: 9

Task 12: Velocity/Size Correlations

Conditions: Air pressure 5 psig, primary velocity 10 m/s, other parameters nominal.

Axial (cm):	5			10			20		
Radial (in):	CL	.5	1	CL	.5	1	CL	.5	1
Run:	3	6	9	2	5	8	1	4	7

f_1 = 124 mm, f_2 = 330 mm, f_3 = 390 mm, δ = 12 μm, F# collection = 5.3

Total number of points: 9

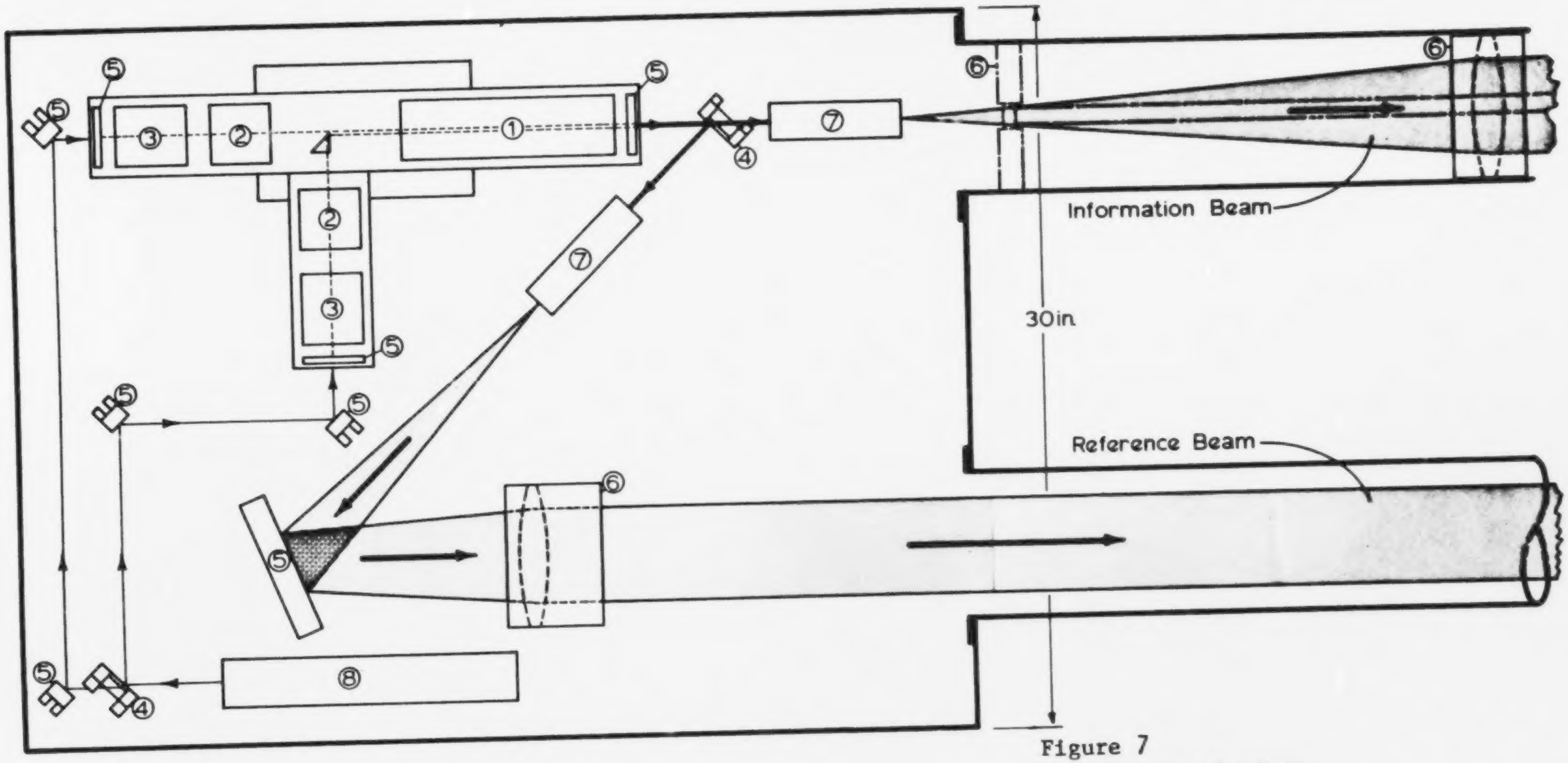
Information Beam
Reference Beam
30in
① Ruby Laser
② Pockel's Cell
③ Brewster Stack
④ Beam Splitter
⑤ Mirror
⑥ Lens
⑦ Beam Expander/Spatial Filter
⑧ Alignment Laser (H_e-N_e)

Figure 7
Holocamera System
Transmitter Module

Spectron
Development
Laboratories

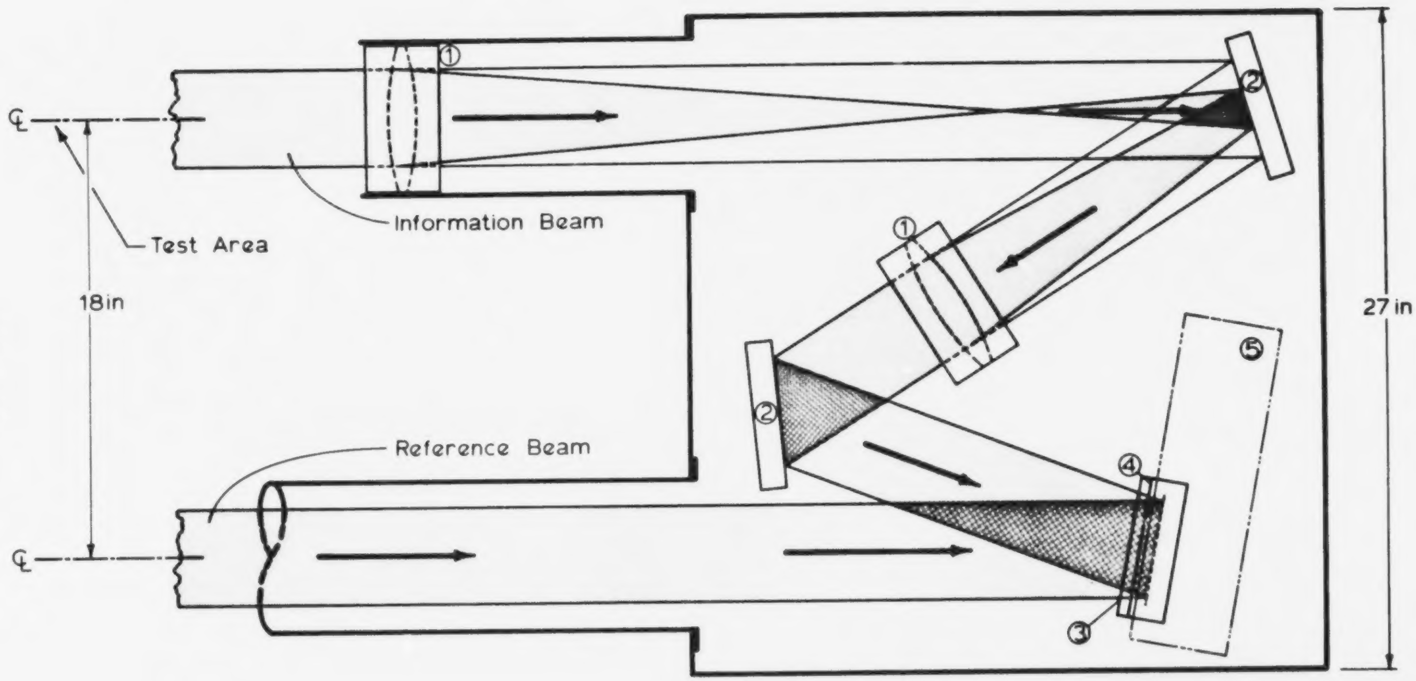
①
②
①
②
④
③
⑤
Information Beam
Reference Beam
Test Area
18in
27 in
℄
℄

① Lens
② Mirror
③ Shutter
④ Plate Holder
⑤ Optional Automatic Plate Changer

Figure 8 **Holocamera System**
Receiver Module

Spectron
Development
Laboratories

1.3 Description of Holography Apparatus

Figure 7 shows a schematic of the transmitter and Figure 8 one of the receiver. The information or object beam goes through two glass windows into the test volume.

The system consists of a HeNe laser for alignment and a ruby laser to take the hologram. The laser beam is split into an information beam and a reference beam. Either beam is expanded, spatially filtered and collimated. The information beam goes through the fuel spray while the reference beam bypasses the test section. The two beams are then mixed on a holoplate in the plate holder.

The shutter in front of the plate holder only allows light to enter while the recording is taking place. This minimizes the influence of extraneous light sources. The room was kept dark as a precaution.

1.4 Test Matrix of Holography Data

Task 1: Survey

Magnification: 1

Single Pulse

Conditions: Air pressure 5 psig, other parameters nominal.

Axial (cm):	20	10	5	0
Plate #:	1,2	3,4	5,6	7,8,5F*

* Flash Photography

Task 2: Axial Survey

Magnification: 1

Single Pulse

Conditions: Nominal

Axial (cm):	0	5	10	20
Plate #:	9,10,5F*	11,12,13,4F*	14,15,3F*	16,17,2F*

* Flash Photography

Task 3: Flash Photography Axial Survey

Magnification: 1

Single Pulse

Conditions: Air pressure 5 psig, other parameters nominal.

Axial (cm):	5	10	20
Plate #:	1A,2A	3A	4A

Double Pulse (75 μs separation)

Axial (cm):	5	10
Plate #:	5A	6A

Task 4: Parametric Analysis at Zero Axial Position

Magnification: 1

Single Pulse

Condition: Variable

Air pressure (psi):	3		5	10	
Oil Flow Rate (lbm/hr):	4		8	4	8
Primary Velocity (m/s):	2.2	10	2.2	10	2.2
Plate #:	1B,2B	7B,8B	15B	9B,10B	16B

Air Pressure (psi):	20			30		
Oil Flow Rate (lbm/hr):	4		8	4		8
Primary Velocity (m/s):	10	2.2	2.2	2.2	10	2.2
Plate #:	11B,12B	3B,4B	17B	5B,6B	13B,14B	18B

Task 5: Parametric Analysis

Magnification: 1

Single Pulse

Condition: Nominal oil flow rate and screen velocity

Task 5: Parametric Analysis (Continued)

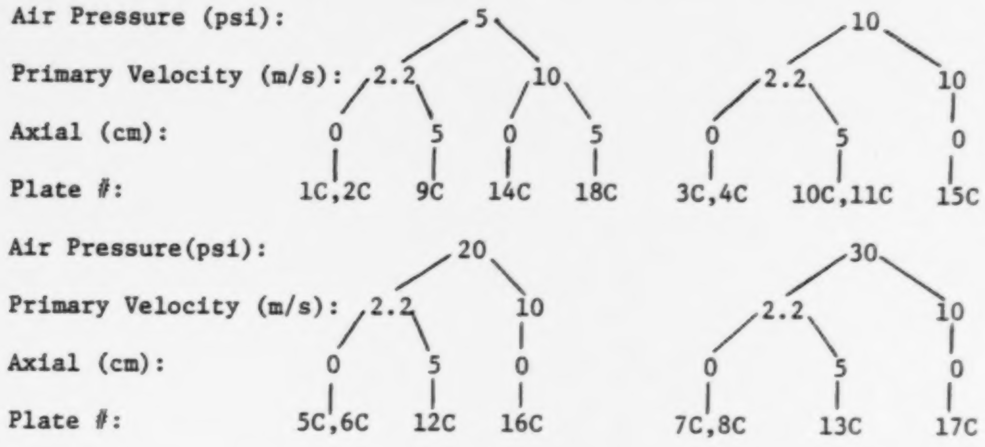

Air Pressure (psi):
5
10
Primary Velocity (m/s):
2.2
10
2.2
10
Axial (cm):
0
5
0
5
0
5
0
Plate #:
1C,2C
9C
14C
18C
3C,4C
10C,11C
15C
Air Pressure(psi):
20
30
Primary Velocity (m/s):
2.2
10
2.2
10
Axial (cm):
0
5
0
0
5
0
Plate #:
5C,6C
12C
16C
7C,8C
13C
17C

Task 6: Interferometric Holography at Zero Axial Position

Magnification: 1

Two Pulses

Condition: Variable air pressure, other parameters nominal.

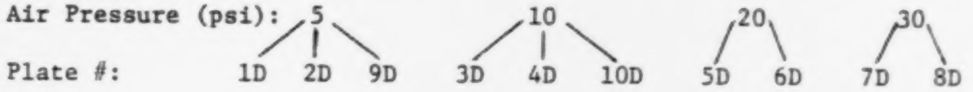

Air Pressure (psi):
5
10
20
30
Plate #:
1D
2D
9D
3D
4D
10D
5D
6D
7D
8D

Task 7: Double and Single Pulses at Zero Axial Position

Magnification: 1

Condition: Variable air pressure, other parameters nominal.

Double Pulse (35 μs separation)

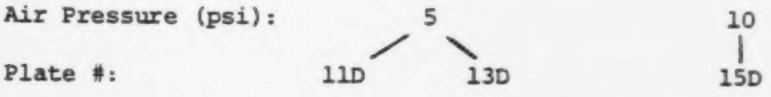

Air Pressure (psi):
5
10
Plate #:
11D
13D
15D

Single Pulse

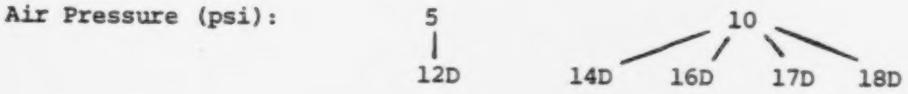

Air Pressure (psi):
5
12D
10
14D
16D
17D
18D

Task 7C: Interferometric Holography at Zero Axial Position

Magnification: 3

Two pulses

Conditions: Variable pressure, other conditions nominal

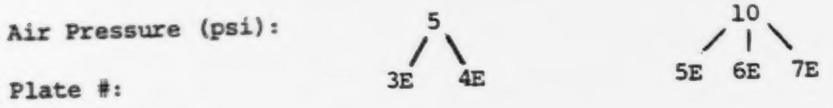
Air Pressure (psi):
Plate #:
5
3E
4E
10
5E
6E
7E

Single Pulse

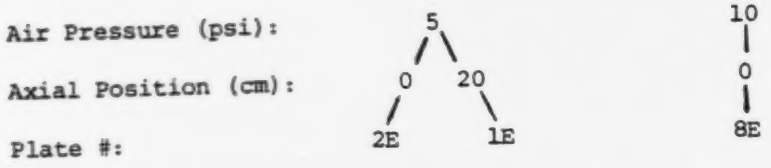
Air Pressure (psi):
Axial Position (cm):
Plate #:
5
0
20
2E
1E
10
0
8E

Task 8: Search of Particle Size

Magnification: 3

Single Pulse

Condition: Nominal oil flow rate and screen velocity

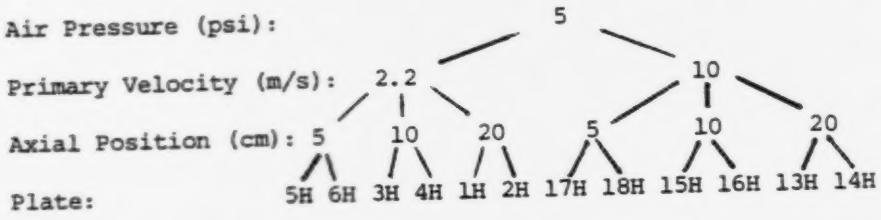
Air Pressure (psi):
Primary Velocity (m/s):
Axial Position (cm):
Plate:
5
2.2
10
5
10
20
5
10
20
5H
6H
3H
4H
1H
2H
17H
18H
15H
16H
13H
14H

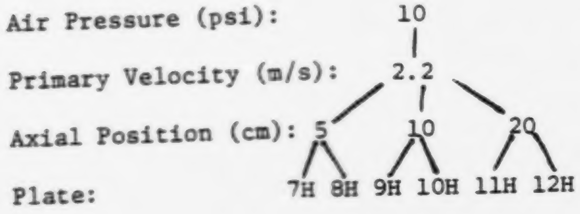
Air Pressure (psi):
Primary Velocity (m/s):
Axial Position (cm):
Plate:
10
2.2
5
10
20
7H
8H
9H
10H
11H
12H

Task 9: Survey Near Nozzle

Magnification: 3

Single Pulse

Condition: Nominal flow rate and screen velocity

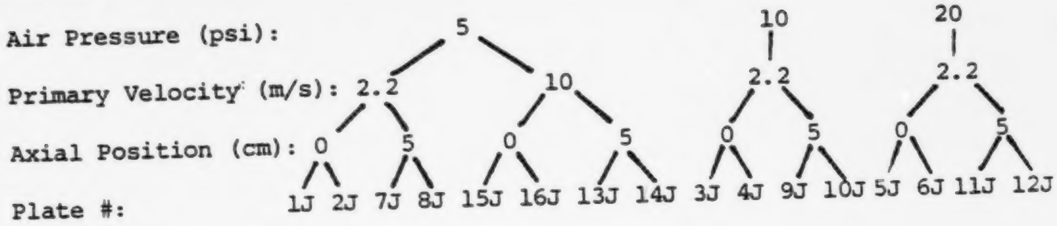
Air Pressure (psi):
5
10
20
Primary Velocity (m/s):
2.2
10
2.2
2.2
Axial Position (cm):
0
5
0
5
0
5
0
5
Plate #:
1J
2J
7J
8J
15J
16J
13J
14J
3J
4J
9J
10J
5J
6J
11J
12J

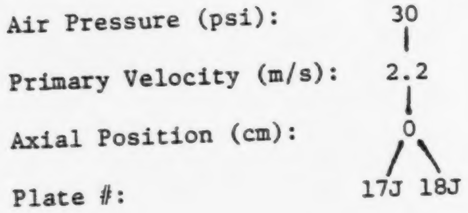
Air Pressure (psi):
30
Primary Velocity (m/s):
2.2
Axial Position (cm):
0
Plate #:
17J
18J

2.0 RESULTS AND DISCUSSION

A total of 116 visibility-Doppler histograms and 126 holograms were successfully made. Most of these data were repeated for statistical purpose. They are presented in Volume 2 of this report. These measurements represent the result of the first task of this research program: characterizing the Sonicore nozzle and comparing the holographic and interferometric techniques.

The size and velocity distributions obtained with the particle sizing interferometer are presented in the form of graphs and/or tables. Plots comparing the holography and the interferometry methods are also provided and discussed. A map of the size distributions and the velocity distributions are analyzed. Photographs of holograms at various positions of the plume are presented. The rest of the holographic data is in the form of glass plates which have been studied by EERC and SDL scientists and are available immediately upon request.

2.1 Description of Size and Velocity Histograms

The headings indicate the Task and Run numbers. These numbers relate to the conditions of the experiments as described in the section "Task Matrix of Visibility Measurements". The number of letters R following the Run number indicates the times this run was repeated.

The size histograms plot the frequency of particles of a certain size versus the corresponding size. This frequency is obtained by dividing the number of particles of a certain size by the total number collected. That is, the frequency $f_i = \frac{N_i}{N}$. The maximum frequency of the ordinate is then divided into five equal intervals.

The table below the graph shows the values that were used to construct the graph: the diameters of the particles and the number of particles with this diameter (count). Finally, there is a list of the size and velocity parameters of interest for this test. These parameters are defined below.

The velocity histograms indicate the velocity (ordinate) versus particle diameter (microns). The maximum ordinate is indicated below. It is typically 15m/sec. The ordinate is divided in five equal velocity intervals. Below the histogram there is a table of the values used to construct the graph.

2.2 Definition of Size and Velocity Parameters

Let:

D_i = diameter of droplet i,

N_i = number of i droplets collected,

U_i = velocity of droplet i, and

N = total collected droplets = ΣN_i .

The following can then be defined:

Linear mean diameter : $$D10 = \frac{\Sigma N_i D_i}{N} ,$$

Surface mean diameter: $$D20 = \left[\frac{\Sigma N_i D_i^2}{N}\right]^{1/2} ,$$

Volume mean diameter : $$D30 = \left[\frac{\Sigma N_i D_i^3}{N}\right]^{1/3} ,$$

Sauter mean diameter : $$D32 = \frac{\Sigma N_i D_i^3}{\Sigma N_i D_i^2} ,$$

Standard deviation : $$S = \left[\frac{\Sigma N_i (D_i - D10)^2}{N}\right]^{1/2} ,$$

Kurtosis : $$\Sigma \frac{N_i (D_i - D10)^3}{N} \Big/ \left[\frac{\Sigma N_i (D_i - D10)^2}{N}\right]^{3/2} ,$$

Mean velocity : $$\overline{U} = \Sigma N_i U_i / N ,$$

Turbulence intensity : $$T = \left[\frac{\Sigma N_i (U_i - \overline{U})^2}{N}\right]^{1/2} \Big/ \overline{U} .$$

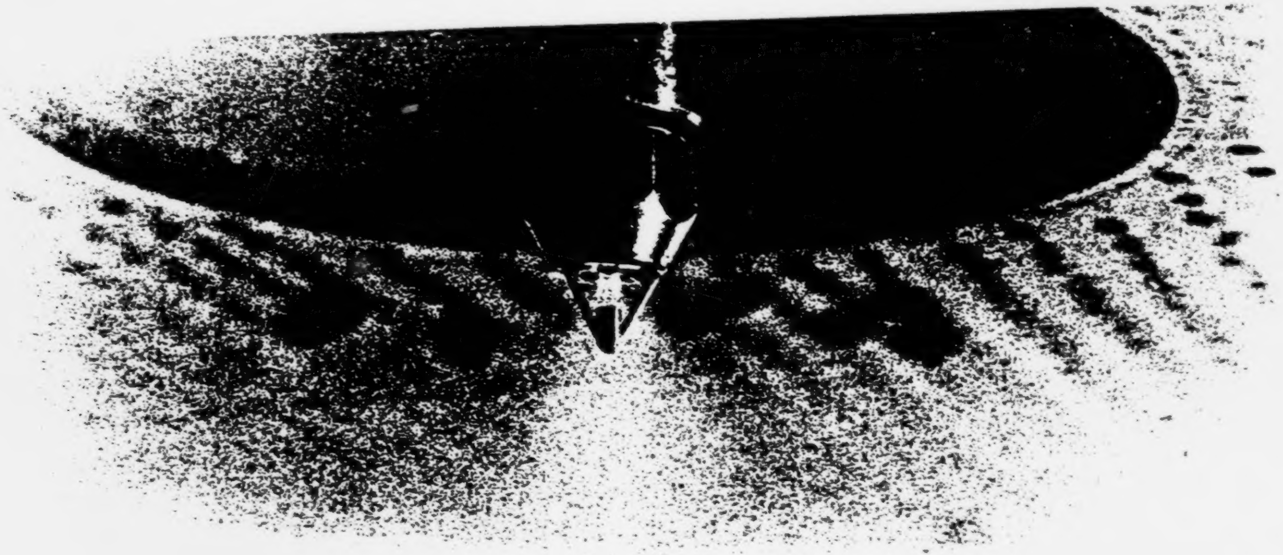

Figure 9. SONICORE NOZZLE SPRAYING FUEL NO. 2 AND CROSSING LASER BEAMS

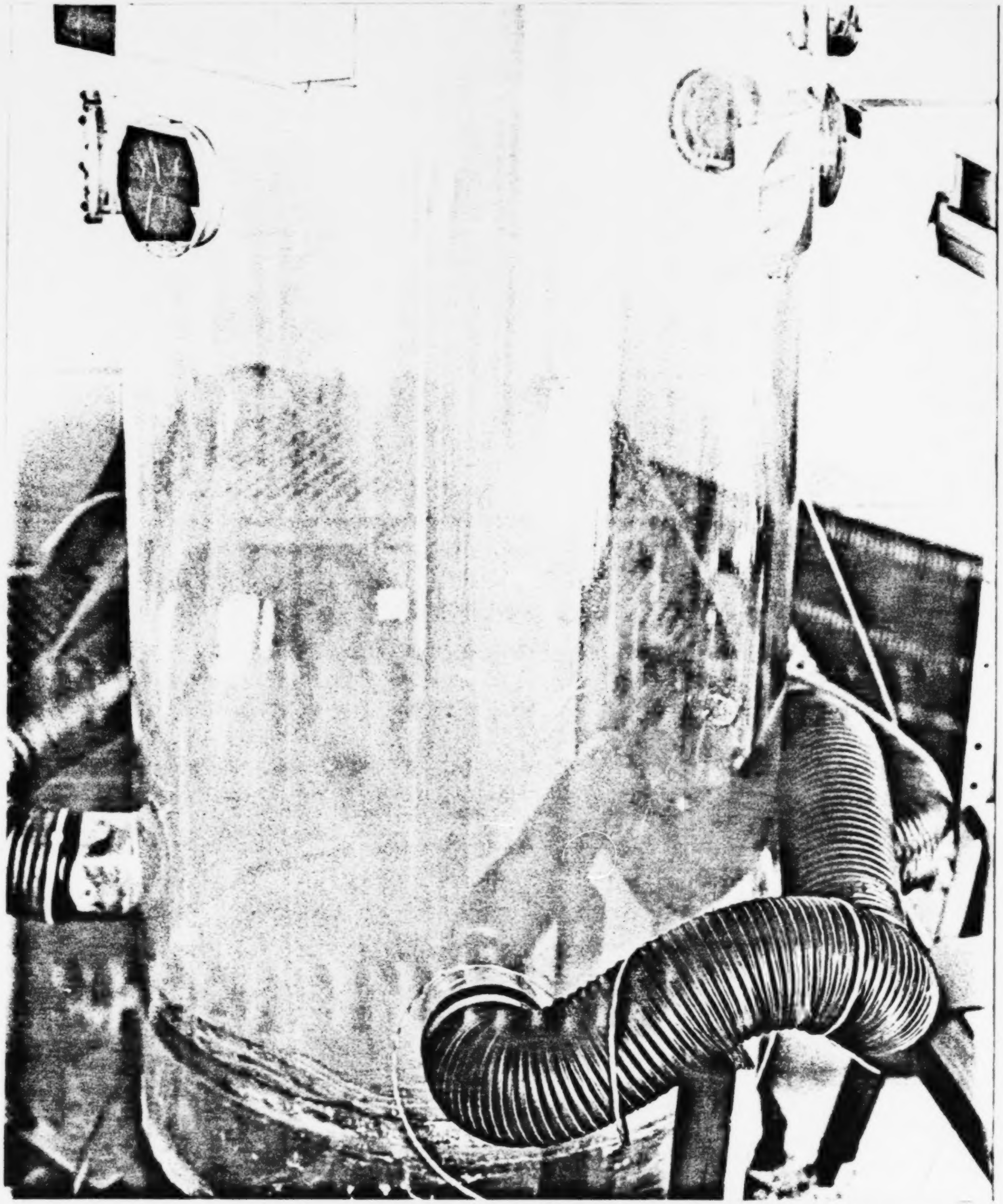

Figure 10. TEST RIG

SPECTRON DEVELOPMENT LABORATORIES

EPA/EERC SIZE DISTRIBUTION OF SONICORE NOZZLE

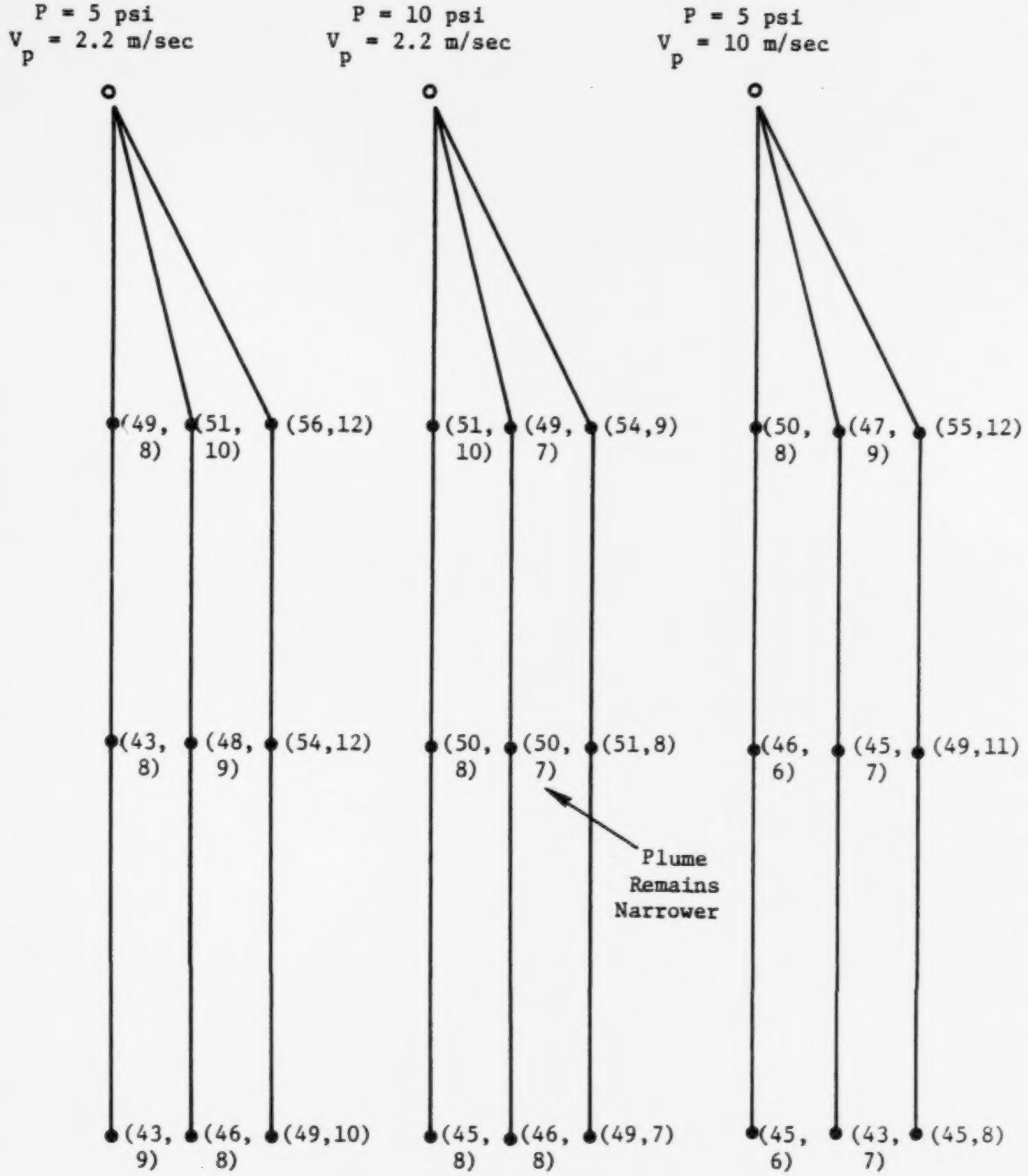
P = 5 psi
V_p = 2.2 m/sec
P = 10 psi
V_p = 2.2 m/sec
P = 5 psi
V_p = 10 m/sec
(49, 8)
(51, 10)
(56,12)
(51, 10)
(49, 7)
(54,9)
(50, 8)
(47, 9)
(55,12)
(43, 8)
(48, 9)
(54,12)
(50, 8)
(50, 7)
(51,8)
(46, 6)
(45, 7)
(49,11)
Plume Remains Narrower
(43, 9)
(46, 8)
(49,10)
(45, 8)
(46, 8)
(49,7)
(45, 6)
(43, 7)
(45,8)

Figure 11.
MEAN DIAMETER AND STANDARD DEVIATION (MICRONS) AS A FUNCTION OF POSITION

SPECTRON DEVELOPMENT LABORATORIES

EPA/EERC VELOCITY-SIZE CORRELATION OF SONICORE NOZZLE

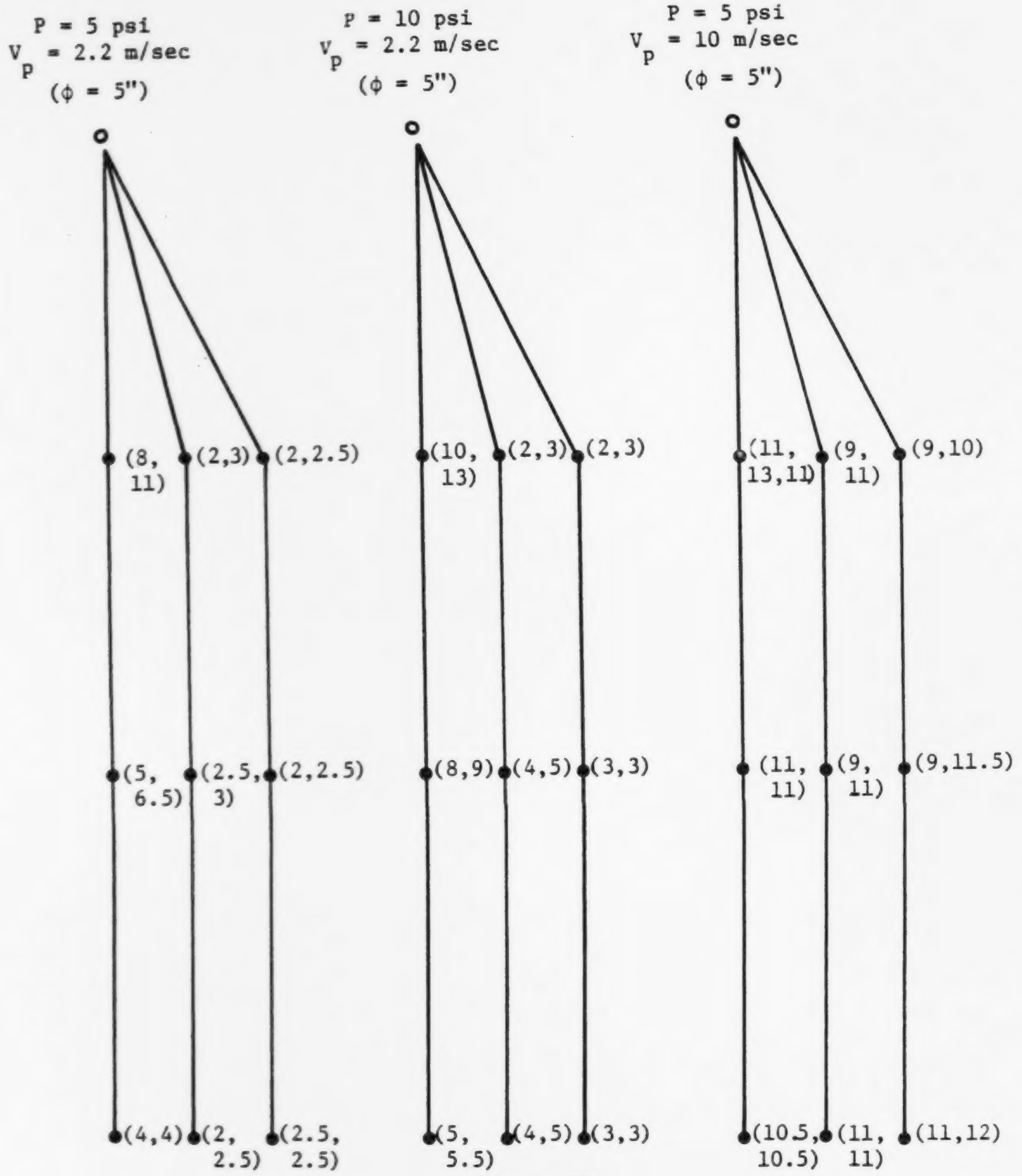

P = 5 psi
V_p = 2.2 m/sec
(ϕ = 5")
P = 10 psi
V_p = 2.2 m/sec
(ϕ = 5")
P = 5 psi
V_p = 10 m/sec
(ϕ = 5")
(8, 11)
(2,3)
(2,2.5)
(10, 13)
(2,3)
(2,3)
(11, 13,11)
(9, 11)
(9,10)
(5, 6.5)
(2.5, 3)
(2,2.5)
(8,9)
(4,5)
(3,3)
(11, 11)
(9, 11)
(9,11.5)
(4,4)
(2, 2.5)
(2.5, 2.5)
(5, 5.5)
(4,5)
(3,3)
(10.5, 10.5)
(11, 11)
(11,12)

Figure 12.

MAXIMUM AND MINIMUM VELOCITY (M/SEC) AS A FUNCTION OF POSITION

2.3 Experimental Doppler Data

Two sets of data were obtained in this phase of the project. In the first one (Tasks 1 through 6) the emphasis was made in the droplet size distribution as described in the proposal. In the second set (Tasks 10, 11 and 12) the software of the data management system was modified to measure both the size and velocity of individual droplets in order to correlate these parameters.

Figure 9 shows the Sonicore atomizing nozzle mounted in the spray rig. Measurements were made up to within 2 cm from the tip where very high number densities (>1000 particles/cm^3) are present. A close-up picture of the rig is shown in Figure 10.

The results of Tasks 10, 11 and 12 are condensed in Figures 11 and 12. Figure 11 shows the average diameter (D_{10}) and standard deviation (S) at various locations of the plume. Figure 12 shows the maximum and minimum particle velocities at the same location. Several observations can be drawn: (1) the average particle size decreases downstream; (2) the average particle size increases radially outwards; (3) the pressure, in the measured range, doesn't seem to have a very strong effect in the particle size. However, the plume is narrower and more uniform (smaller standard deviation) in the high pressure case. The explanation for this behavior, which is later confirmed by holography, is the following: the particles at the exit of the nozzle hit the resonator cup and are deviated outwards. The small particles are rapidly relaxed to the primary air flow and follow the general trajectory of the air. The large particles, however, have a much larger radial momentum and take longer to relax into the flow. These particles will be found in the outer edge of the plume (as later confirmed by holography). This relaxation time has another influence in the particle size distribution. The particles in the centerline decelerate very quickly (Figure 12) and since, in this region, there are many more small particles, the number density of small particles should increase as the velocity decreases. This effect produces differences in the size distributions determined by systems that measure over a collection of particles in a collimated laser beam and those that measure single particles.

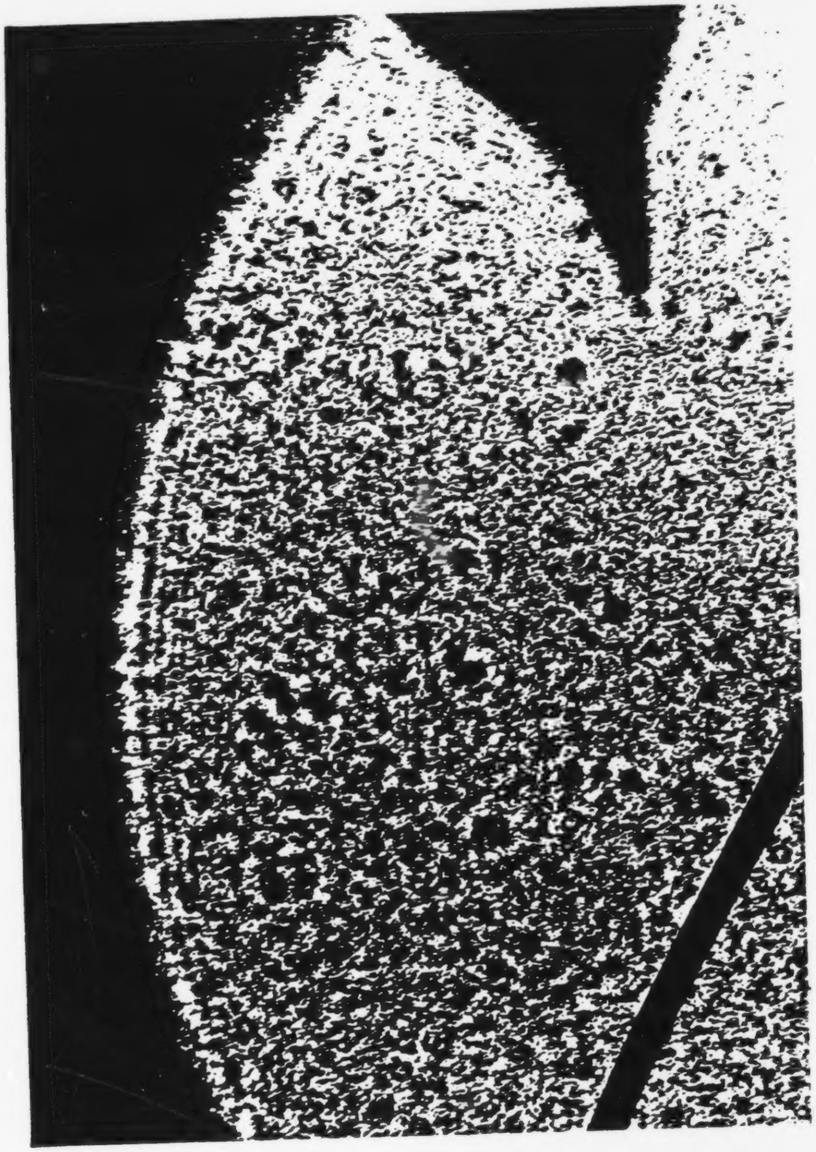

Figure 13. DROPLET DISTRIBUTION BELOW NOZZLE TIP
PRESSURE OF 5 PSI, PRIMARY VELOCITY OF 2.2 M/S

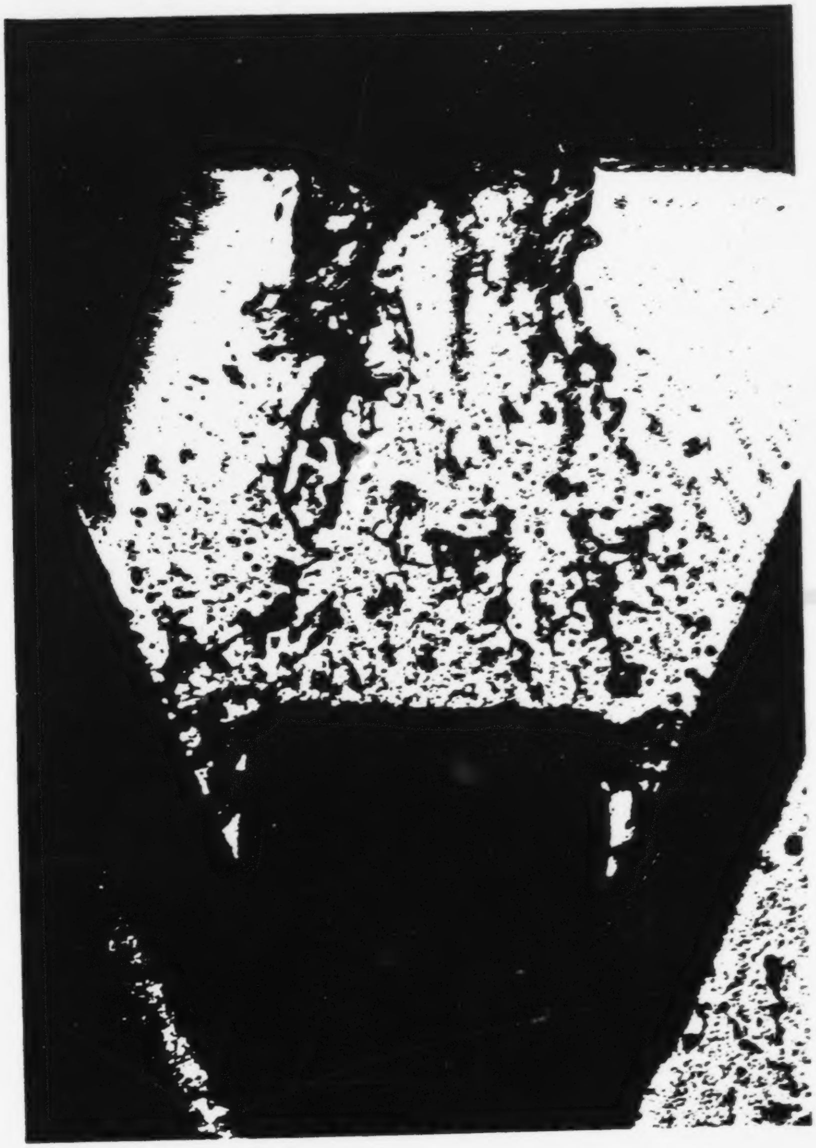

Figure 14. LIGAMENT FORMATION AT NOZZLE EXIT PRESSURE OF 5 PSI, PRIMARY VELOCITY OF 2.2 M/S

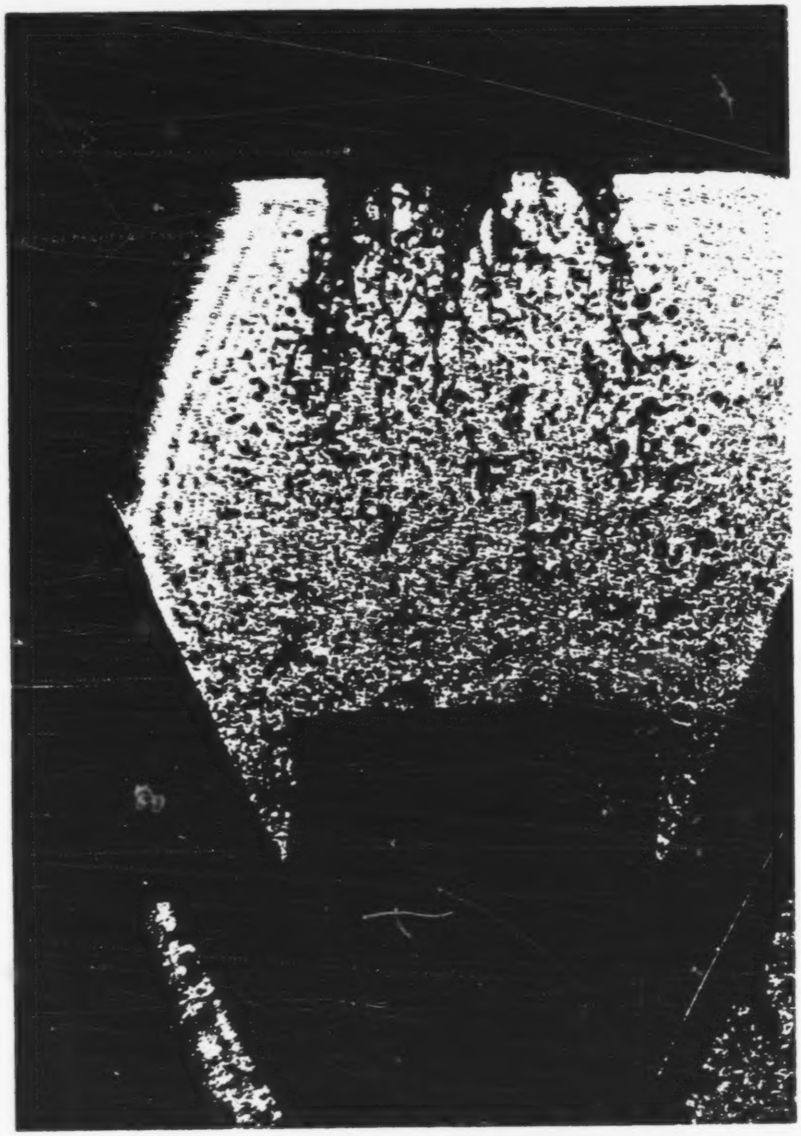

Figure 15.

LIGAMENT FORMATION AT NOZZLE EXIT
PRESSURE OF 10 PSI, PRIMARY VELOCITY OF 2.2 M/S

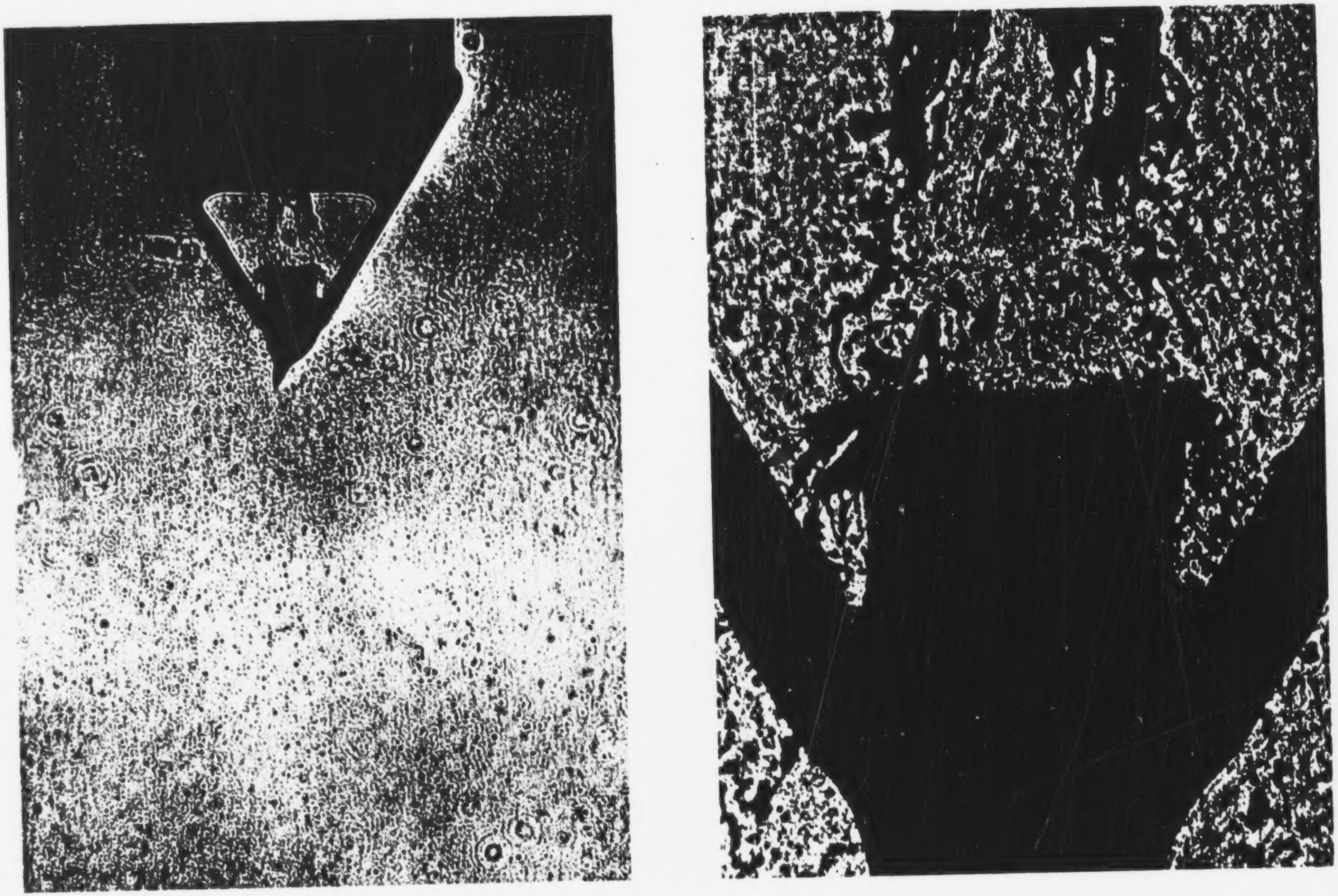

Figure 16. GENERAL VIEW AND CLOSE-UP OF SPRAYING NOZZLE PRESSURE OF 5 PSI, PRIMARY VELOCITY OF 10 M/S

2.4 Experimental Holography Data

Holography was also used to characterize the size distribution of the droplets formed by the sonicore nozzle. This technique employs a ruby laser beam of very short duration (~20 ns) and it is thus capable of freezing any motion in the flow.

When using holography in particle field diagnostics, the image of the particles over the field of view is recorded and subsequently reconstructed. The individual particle images can then be scanned and magnified in the reconstruction. This relaxes the need for the particles to be in the focal plane of the imaging system during the recording and one hologram reconstructs the images of particles over an entire volume of the particle field.

Holograms and flash photography were taken of both the particle field and the ligament formation region at the exit of the nozzle. The entire collection of data is summarized in the section "Test Matrix of Holography Data".

Some photographs of holograms at a given plane are presented. Figure 13 represents the size distribtuion immediately below the nozzle tip for a pressure of 5 psi and a primary velocity of 2.2 m/s. From this picture it becomes apparent that photographs lose considerable resolution and that the actual holoplate should be investigated. The wire showing at the lower right hand corner is a 250 μm wire used a size reference. The actual particle sizing was done using a microscope with a reticle on the actual holoplate. Using this technique, particles down to 15 μm could be resolved.

The ligament formation region for 5 psi and 2.2 m/s is shown in Figure 14. The equivalent region for 10 psi, 2.2 m/s is presented in Figure 15. Notice that the pressure output has a very strong influence in the droplet formation. In the 5 psi case, the ligaments are still long and forming when hitting the resonator cup. In the 10 psi case the droplets are virtually all formed before hitting the cup. Some ligaments, however, can be observed in this region. Figure 16 shows an overview of the particle field (right) and the detail of the ligament breakage for 5 psi, 10m/sec. Three kinds of images can be observed: (1) clearly defined black dots; they represent particles that are in focus on the plane of the photograph; (2) fuzzy, grey dots; these are particles out of focus but yet close to the photography plane; (3) concentric rings; they are the diffraction pattern of particles very far from the focusing plane. In many instances they represent particles accumulated on the quartz windows.

2.5 Comparison Between Holography and Visibility Data

Figures 17a and 17b show the size distribution as obtained by holography and visibility for two different conditions. The pressure across the nozzle was changed from 10 psi (Figure 17a) to 5 psi (Figure 17b) with all the other conditions remaining constant. These conditions are: primary velocity (2.2 m/s), screen air velocity (0.4 m/s), fuel mass rate (4 lb. m/hr). Since the number of samples analyzed by both techniques was considerably different, the number of particles of any size range was nondimensionalized dividing them by the maximum number of any one size. Thus defining a frequency (f) that varies from zero to one.

The two techniques compare very well. The mode is always the same, the shapes of the curves are very similar and the tendencies are equal. Some general observations:

(a) Near the centerline of the plume, the size distribtuion downstream of the nozzle is almost invariable,

(b) The curve constructed with holography data is broader than the corresponding visibility one. This is due to the biased impression produced by the larger particles. This biasing arises because it is very easy to find the large particles in a hologram and quite difficult to find the very small ones. Hence, the total number of particles counted is usually smaller than the total number of particles present, while the total number of large particles is quite correct.

There was some speckle on the holograms due to the windows on the nozzle rig being dirty. This speckle limited the resolution to about 10 μm. The smallest particles clearly detectable were about 15 μm in diameter.

Figure 17. HOLOGRAPHY AND VISIBILITY DATA OF FUEL SPRAY NOZZLE WITHIN 0.5 INCH OF CENTERLINE AND VARIOUS AXIAL POSITIONS. (SDL/EER)

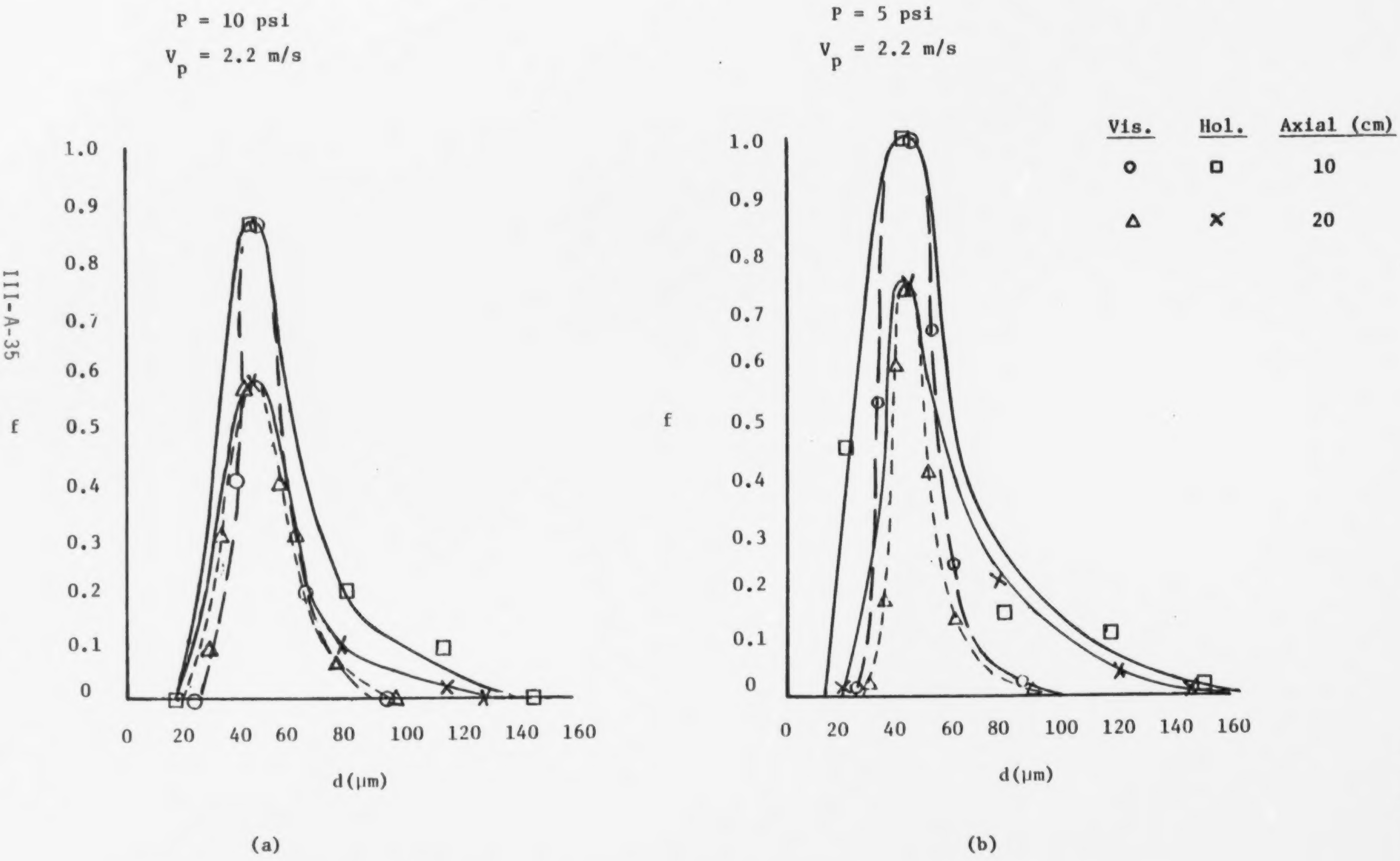

3.0 BRIEF DESCRIPTION OF THE MALVERN PARTICLE AND DROPLET SIZING SYSTEM

Particle sizing instruments based on light scattering methods can be divided into two categories: single particle counters and multiple particle scattering techniques. Single particle counters typically produce more information about the size distribution but have difficulties with measuring in high particle number densities. The multiple particle scattering methods work best in such environments.

In the present discussion, the Malvern Particle and Droplet Sizer, which is of the latter type, will be described and some of its limitations and operating characteristics identified.

3.1 Principle of Operation

When plane waves of light from a collimated or focused laser beam fall onto a particle, the light is scattered or deflected by the particle. For particles larger than the wavelength of light ($\alpha = \frac{2\pi a}{\lambda} > 10$), where a is the particle radius and λ is the laser wavelength), then the scattered light can be described by the simplified laws of reflection, refraction, and diffraction. The light reflected and refracted by the particle are scattered through all angles and it is assumed that only an insignificant amount of them is scattered in the forward direction compared to the diffracted light. Diffraction, which is described using the wave theory of light, is an edge phenomena with the particle scattering like an opaque disk of similar projected cross-section. Light scattered by diffraction is intense and confined to the forward direction.

The diffracted light is described by the Fraunhofer diffraction theory. Light scattered in the near-forward direction is proportional to the particle diameter squared (or the projected cross-sectional area). The angular width of the scatter distribution or radius of the scattered light intensity rings is given by

$$r = \frac{mf\lambda}{2a} \qquad (1)$$

where m is the number of the ring being considered and f is the collecting lens focal length. It is apparent from the behavior of the scattered light with particle size that the particle size could be determined by measuring the scattered light intensity or the angular distribution or both.

Figure 18 is the scattering intensity distribution for a single particle. When particles of different diameters are present in the laser beam, patterns of scattered light from each of the particles are superimposed with the scattered intensity adding linearly.

A schematic of an optics system utilizing this concept is shown in Figure 19. The beam is expanded and collimated to a diameter of approximately 6 mm. The collecting lens produces the Fourier transform of the scatter distribution at the rear focal plane of the lens. Note that the transmitted beam is focused to a small spot on the detector where it must be dumped completely. Particles located anywhere in the beam between the transmitting and collecting lenses scatter light to the detector. All light scattered at an angle θ by the particles reaches the detector at radius r.

The detector consists of a series of concentric rings that measure the energy scattered at incremental radii. Each detector ring is constructed such that it has the maximum sensitivity for the size increments measured. The detectors are typically scanned electronically and read into the system's processor.

Scattered light energy measured by the detector must be used to reconstruct the particle size distribution. One method of recovering the size distribution from the measured energy distribution is to use a particle size distribution function such as the Rosin-Rammler function. The two-parameter distribution is adjusted to produce a theoretical energy distribution that approximates that measured. Other methods have also been used (see Appendix) including the use of eigenfunctions.

The method has been applied to several measurement situations with reasonably good success. A more detailed description of the method is given in the Appendix along with description of some of the limitations of the system.

Table 1

x	$\left[2\frac{J_1(\pi x)}{\pi x}\right]^2$	max or min
0	1	max
1.220	0	min
1.635	0.0175	max
2.233	0	min
2.679	0.0042	max
3.238	0	min
3.699	0.0016	max

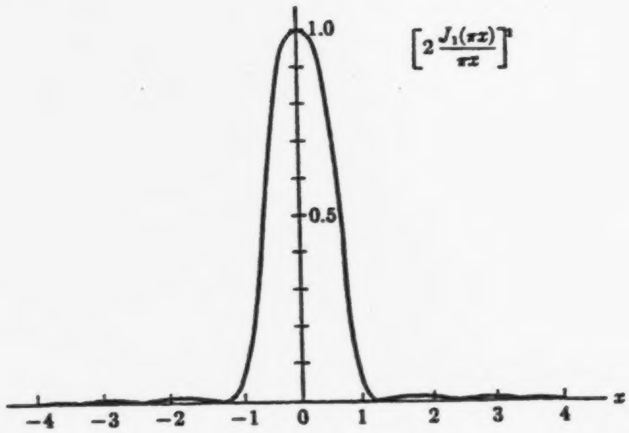

Figure 18. CROSS SECTION OF THE AIRY PATTERN

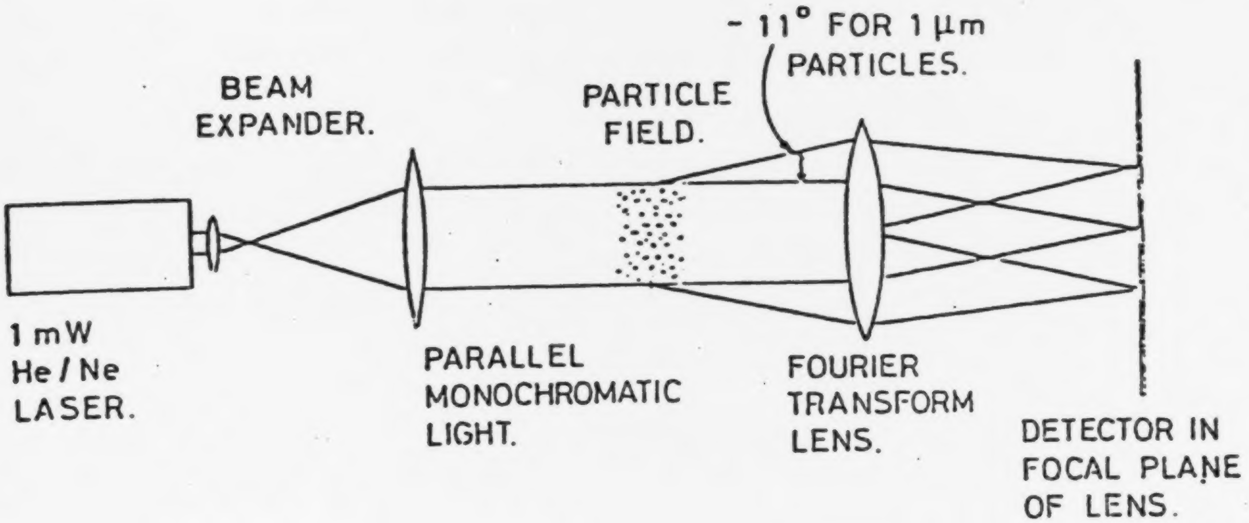
~ 11° FOR 1 μm
PARTICLES.
BEAM
EXPANDER.
PARTICLE
FIELD.
1 mW
He / Ne
LASER.
PARALLEL
MONOCHROMATIC
LIGHT.
FOURIER
TRANSFORM
LENS.
DETECTOR IN
FOCAL PLANE
OF LENS.

Figure 19. OPTICAL ARRANGEMENT OF FOURIER TRANSFORM LENS TO OBTAIN THE SIZE DISTRIBUTION OF SOLID OR LIQUID PARTICLES

4.0 CONCLUSIONS

The conclusions and observations listed below are based on the optical diagnostics work of this research program. The analysis and interpretation of the spray will be done by EERC scientists. Some observations of the spray behavior are given since they relate to the optical techniques. These conclusions and observations now follow:

(1) The DSI instrument proved to be very powerful to study fuel sprays, since both the size and velocity distributions of the droplets are necessary.

(2) The limitations of the DSI would be extremely high number density and velocity.

(3) Holography is adequate for sizing droplets but the analysis of holograms is very time consuming.

(4) Windows must be kept very clean to produce high quality holograms. The speckle generated in these experiments allowed to resolve particles larger than 15 μm.

(5) The results obtained using holography and DSI compared very well.

(6) Average particle size decreases with axial position.

(7) Average particle size increases with radial position.

(8) The pressure difference across the nozzle didn't seem to have a very strong effect on the particle size distribution of the region of interest (near center of plume). However, the plume is narrower and more uniform (smaller standard deviation).

(9) Particles in the centerline decelerate faster.

The following conclusions are as a result of a theoretical study of the Malvern system.

(1) The technique is well suited for sizing opaque particles. Transparent particles result in anomalous diffraction that can create the impression that the measured particles are larger or smaller than the actual particles.

(2) The instrument works very well in high number density environments. It is limited, however, by low number densities.

(3) Stray light reflected or scattered by the optical components can produce measurement difficulties.

(4) The spatial resolution is limited.

(5) Present inversion techniques require a fit to a size distribution function.

(6) It is limited to measure size only and cannot measure velocity, flux or number density.

5.0 REFERENCES

Bachalo, W. D., C. F. Hess, and C. A. Hartwell, (1979). "An Instrument for Spray Droplet Size and Velocity Measurements", ASME Paper 79-WA/GT-13.

Trolinger, J. D. (1975). "Particle Field Holography", Optical Engineering, Vol. 14, No. 5, September-October.

APPENDIX

A DISCUSSION OF THE SMALL ANGLE LIGHT SCATTERING METHOD FOR PARTICLE SIZING

INTRODUCTION

The measurement of particle and droplet size and velocity is of great importance in combustion research. Producing real time in situ measurements of the particle or droplet size distributions is especially important in evaluating the combustion processes and particulate formation. Several light scatter detection methods have evolved to fulfill this need. The light scatter methods can be divided into two categories; those that measure the light scattered from a highly focused laser beam by individual particles and those that measure the light scattered from a collection of particles in a collimated laser beam. Both methods have merit in specific applications and their suitability depends upon the information that is required.

In this report a description of the technique utilizing small angle scattering from a polydispersion of particles is given. The description of the method will be given in sufficient detail, it is hoped, to be understood by the layman. The method will also be evaluated to identify the strengths and weaknesses of the technique. This information should be useful to the potential user for the selection of the device over other techniques and for establishing its limitations.

Theoretical Description

The scattering of light by dielectric spherical particles of arbitrary size is treated formally by solutions of the Maxwell's equations with the appropriate boundary conditions. Mie obtained a solution of the equations for the case of a plane wave of linearly polarized incident radiation on a sphere of arbitrary size and refractive index. However, for many applications the formal Mie solution is unnecessary. In the present analysis we are concerned with particles larger in diameter than the light wavelength, λ, and with index of refraction $m>1$ which allows certain approximations to be used that greatly simplify the calculations.

Particle size is typically described in dimensionless form given by

$$\alpha = \frac{2\pi a}{\lambda} \tag{1}$$

where a is the particle radius. For the approximations used in the present technique to be valid, two conditions must be satisfied. The size parameter $\alpha >> 1$ and the phase shift $\rho = 2\alpha(m-1)$ must be large before simplifications to the theory can be used. Under these restrictions the light scattered can be described by the simple geometric optics laws which are asymptotic laws on electromagnetic waves and by Fraunhofer diffraction around the sphere.

Of the total radiation scattered, which equals twice energy incident on the geometrical cross section of the particle, πa^2, (assuming no absorption), one half is scattered by reflection and refraction by the sphere and the other half by diffraction around the sphere. The geometric-optics pattern arising from the reflection and refraction of rays by the sphere forms a wide pattern of moderate intensity. The diffraction pattern is narrow, very intense, and concentrated about the forward (in the direction of the transmitted beam) direction. It is the light scattered by diffraction that has been most commonly used for determination of particle size.

Fraunhofer Diffraction

Diffraction has been defined by Sommerfield as "any deviation of light rays from rectilinear paths which cannot be interpreted as reflection or refraction". Physicists became cognizant of the diffraction phenomena when an aperture in an opaque screen was illuminated by a light source and was observed some distance from the screen. Light and dark rings were observed extending far into the geometric shadow of the screen. Huygens (1678) wave theory of light suggested a means of accounting for this scatter. He postulated that each point on the wavefront of light disturbance was a new source of a secondary spherical disturbance. Subsequent wavefronts could then be described by reconstructing the envelope of the secondary wavelets. Fresnel (1818) later used Huygens' envelope construction with the principle of interference and some arbitrary assumptions about the effective amplitudes and phases of the secondary sources to calculate the distribution of light in diffraction patterns.

Approximations by Fresnel and Fraunhofer have been made to the general diffraction theory which allow diffraction pattern calculations to be simplified under certain restrictions. For the Fraunhofer approximation

$$z >> \frac{ka^2}{2} \qquad (2)$$

where z is the distance from the aperture to the observation plane and $k = \frac{2\pi}{\lambda}$. When the conditions for the approximation are satisfied the intensity of the light scattered from a parallel beam of monochromatic light by a uniformly illuminated particle of diameter, 2a through an angle ω is given by

$$I = I_o \ {\frac{2J_1(k\ a \sin \omega)}{k\ a \sin \omega}}^{2} \qquad (3)$$

for $a >> \lambda$. ω is the scattering angle and J_1 is the Bessel function of the first kind and order 1. The pattern formed is the well-known Airy pattern shown in cross section in Figure A1 and the actual diffraction pattern is shown in Figure A2. It should be noted that the light scattered in the forward direction is assumed to be much greater than that scattered by refraction or near-forward reflection. This is not always true and will be discussed later.

Size Determination by Diffractively Scattered Light

The optical method used is, in principle, the same as the Young's eriometer. With this method the separate diffraction patterns formed by light scattered from particles (Figure A3) in a collimated monochromatic beam of light are superimposed with a lens on the plane of the lens. In general, the particles will be of different sizes. The resultant amplitude of the diffraction pattern is a function of the phase of each component. If there are only a few particles in the beam, destructive and constructive interference effects in the form of interference patterns would be observable. However, when there are a large number of particles in the beam at random positions the irradiance rather than the field amplitudes of the diffraction patterns will be detected as a linearly additive sum. In this case, the N particles in the collimated monochromatic beam will scatter N diffraction patterns that produce an irradiance at the detector plane equal to the sum.

Table 1

x	$\left[2\frac{J_1(\pi x)}{\pi x}\right]^2$	max or min
0	1	max
1.220	0	min
1.635	0.0175	max
2.233	0	min
2.679	0.0042	max
3.238	0	min
3.699	0.0016	max

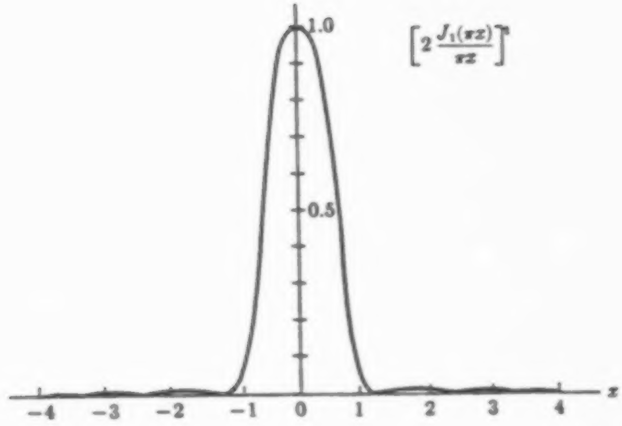

Figure A1. CROSS SECTION OF THE AIRY PATTERN

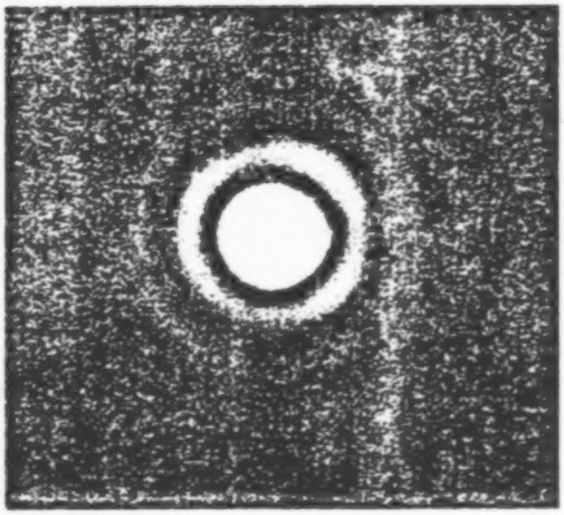

Figure A2. FRAUNHOFER DIFFRACTION PATTERN OF A CIRCULAR APERTURE

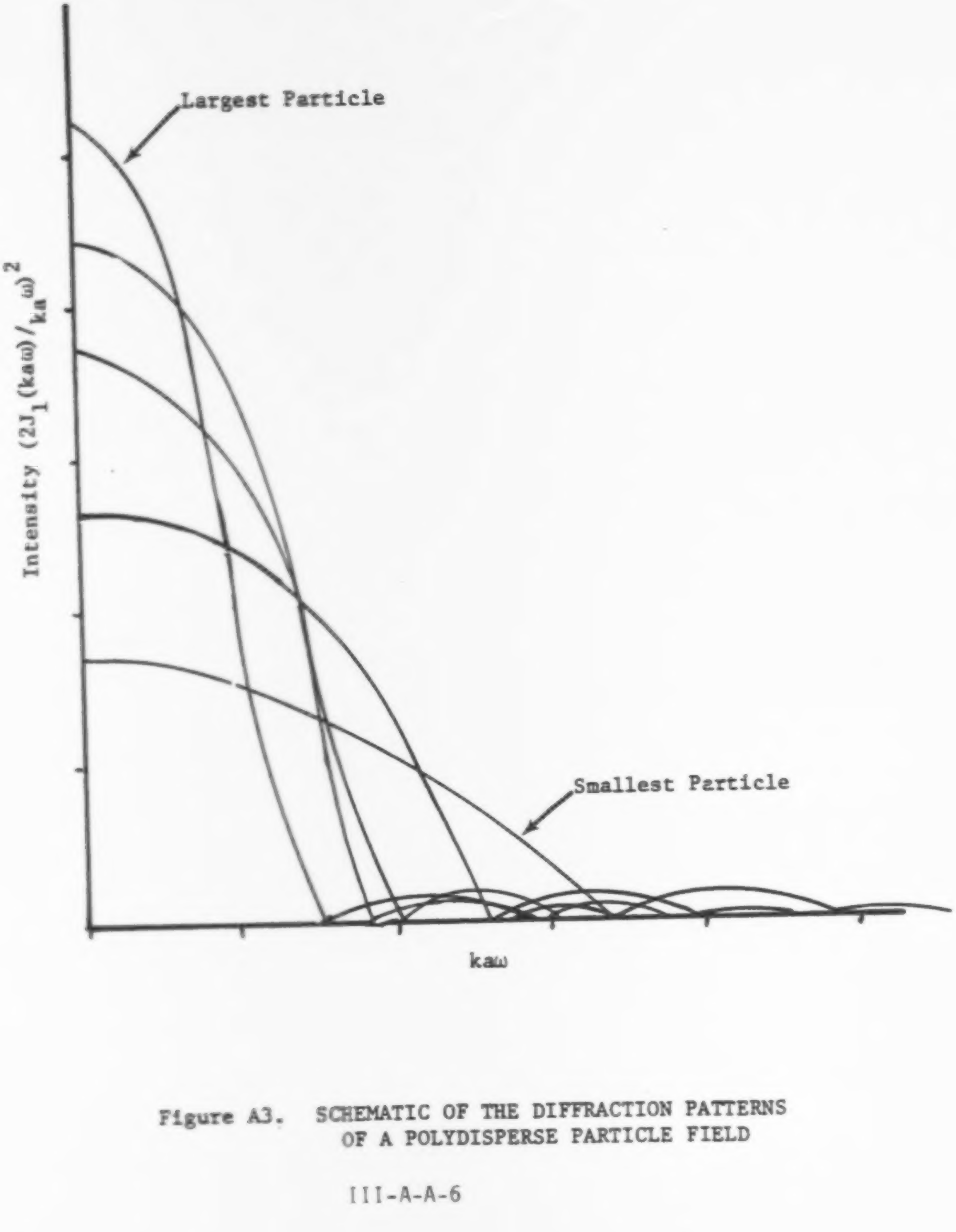

Figure A3. SCHEMATIC OF THE DIFFRACTION PATTERNS OF A POLYDISPERSE PARTICLE FIELD

The distinctive rings of the Fraunhofer diffraction pattern are typically smoothed out for a polydisperse sample. If the measurements can be made with adequate precision, the detected pattern can be inverted to produce the size distribution of the particle field that produced the pattern. The analysis of the detector configuration has been treated by Swithenbank et al.[1] in some detail. In that work, it was recognized that any droplet or particle diffracts light to all radii but that the energy distribution peaks at a specific radius. Since the energy distribution varies as $\frac{2J_1^2(ka\omega)}{\omega^2}$ and ω can be approximated by $\omega \cong \sin^{-1} \frac{s}{f} \simeq \frac{s}{f}$ for small where s is the radius of the detector ring and f is the lens focal length. The expression for the energy peak can then be written as $x = 2 \frac{\pi a}{\lambda}(\frac{s}{f})$.

Discussion

At this point it may be useful to the understanding of the method if the concept is described free from the more complex mathematical expressions. In addition, some comments and restrictions to the method so far described will be given.

Particles passing through a monochromatic collimated beam (typically, a laser beam) will scatter (or deflect) light from the beam in all directions. If the particles are spherical droplets with insignificant absorption (clear or transparent) half of the light will be scattered by reflection and refraction. This part of the incident radiation falling on the particle cross sectional area, πa^2, can be described by simple geometric optics using ray tracing. The rays (narrow beams of width small compared to the radius of the spherical droplet but larger than the wavelength, λ) can be traced for each point of incidence on the sphere.

When a ray strikes the spherical particle, a reflected and a refracted ray occurs, Figure A4. The deflection angles, taken with respect to the sphere tangents are described by the simple law of reflection (angle of incidence equals the angle of reflection) and by Snell's law for the refraction

$$m \cos \tau = m' \cos \tau' \tag{4}$$

where τ' and τ are given on Figure A4, m and m' are the refractive indices of the surrounding medium (1.0 for air) and the droplet material respectively.

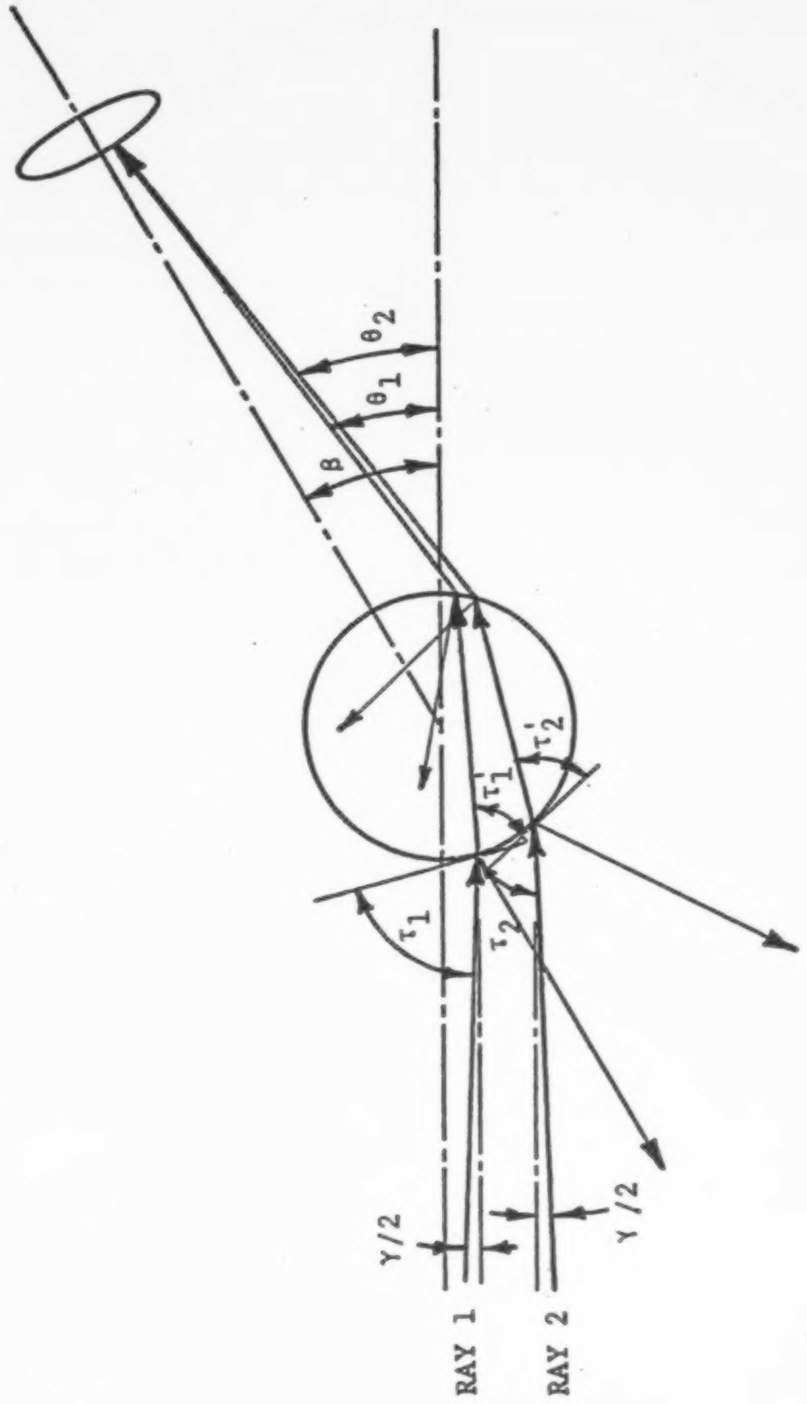
θ2
θ1
β
τ'2
τ'1
τ1
τ2
γ/2
γ/2
RAY 1
RAY 2

Figure A4. DUAL BEAM SCATTER BY A SPHERICAL DROPLET

The other half of the light beam incident on the sphere cross sectional area, πa^2 is scattered by diffraction. To describe the diffraction mechanism, the wave theory of light propagation must be used (although results have also been obtained using a ray optics approach) to mathematically describe the angular intensity distribution. If the Huygens' envelope construction was used, the planar light wave incident on the aperture can be assumed as giving rise to secondary spherical waves emmitting through the aperture. The spherical wave at one edge will differ in phase from the wave scattered from the diametrically opposed edge and hence will cause interference at the plane of observation. Rings of the Fraunhofer diffraction are a result of this interference (Figure A1). It should be noted that although the Fraunhofer diffraction pattern was calculated for an aperture, Babinet showed that the diffraction pattern (intensity distribution) is the same for a sphere when taken as an opaque disk of equal projected cross sectional area.

When the particles are not opaque as in the case of liquid droplets of many materials, a phenomenon occurs called anomalous diffraction. In a range of drop sizes the amplitude of the diffracted light is comparable in magnitude to the reflected and refracted light in the near forward direction. Interference of the diffracted light with the light passing through the droplet (refracted) and that reflected from the edge of the droplet occurs. This interference can significantly change the diffraction pattern. Van de Hulst[2] describes this phenomenon with some examples for water droplets in the size range 6 to 10 µm in diameter. For example, the ratios of the peak scattering intensities for a droplet 7 µm in diameter computed from the Fraunhofer diffraction formula to that including the anomalous diffraction is (p. 261 Van de Hulst)

$$R = \frac{I_{\text{diff.}}}{I_{\text{anal. diff.}}} = \frac{0.625}{1.225} = 0.5 \qquad (5)$$

The secondary intensity peaks are significantly changed, Figure A5. Note that the intensity is the square of the ordinate in this figure.

Anomalous diffraction was not accounted for in the analysis of Swithenbank, et al. and it does not appear that the effect has been included in the software of instruments based on the small angle scatter

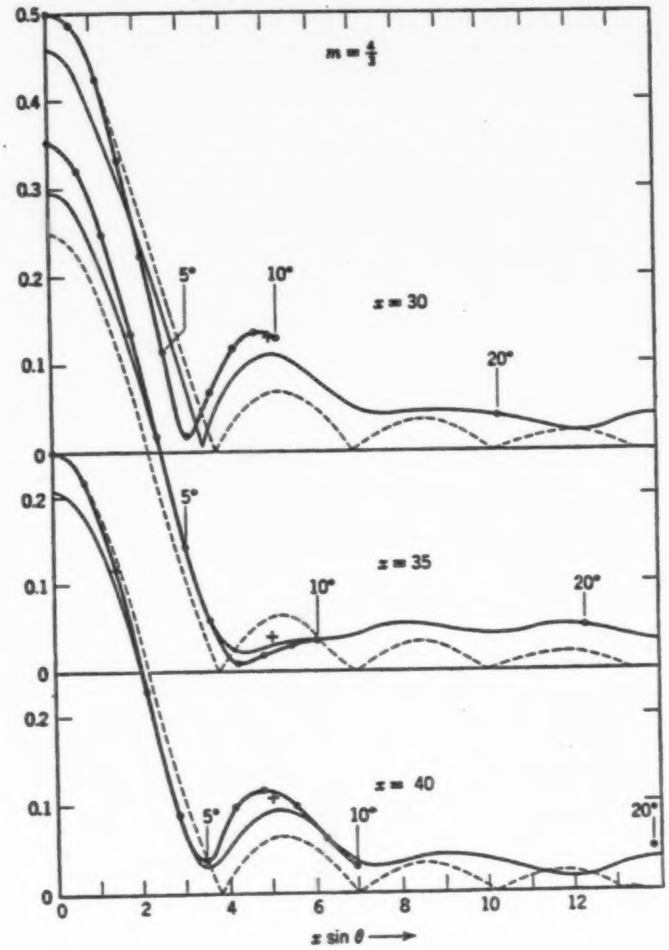

Figure A5. VAN DE HULST, ANOMOLUS DIFFRACTION

- Thick line with dots - Rigorous data for m = 1.33
- Crosses - Approximation formula for m = 1.33
- Dotted Line - Fraunhofer diffraction formula

techniques (e.g. Malvern). When not included in the analysis, anomalous diffraction can cause the measured droplet size to be either larger or smaller than the actual size.

The question of anomalous diffraction was addressed by Jones[3]. Calculations of the light scatter intensity distribution were carried out using both the diffraction theory and the exact Mie approach. The Mie theory includes the scatter by diffraction, reflection, and refraction. The size range $\frac{\lambda}{\pi} < 2a < \frac{40\lambda}{\pi}$ was examined. It was found that the difference in particle size between that determined by the Mie theory and diffraction theory increases with decreasing particle size and does so in a slightly oscillatory fashion. For glass spheres with little or no absorption, the error approached 20% at the minimum size range of 2 µm.

Assuming that the scatter from individual particles has been correctly formulated, the next stage of the size determination can be considered. Because the laser beam is collimated at a relatively large diameter (1 to 10 mm) and only a small portion of the light is scattered by a single particle, a number of particles are required to be in the beam to scatter sufficient light to be detected. With only a few particles in the beam interference effects between the scatter patterns would be observed. When there are a number of particles in the beam at one time the patterns will add linearly by intensity rather than complex field amplitudes and phases. A random polydisperse sample of particles will produce an intensity distribution which is the sum of the individual diffraction patterns.

The optical arrangement for the method is shown in Figure A6. A detector array is located in the rear focal plane of the lens. Since the laser beam is collimated, it will focus in the rear focal plane at the center of the array detector. It is very important that the transmitted beam be properly dumped since light reflections back to the lens will, in turn, be reflected back to the detector array and superimposed on the scattered light distribution. If air-spaced achromatic lenses are used, reflections between the elements can also produce background illumination.

It is interesting to note that although the particles along the entire exposed beam contribute to the signal, light scattered at a specific angle,

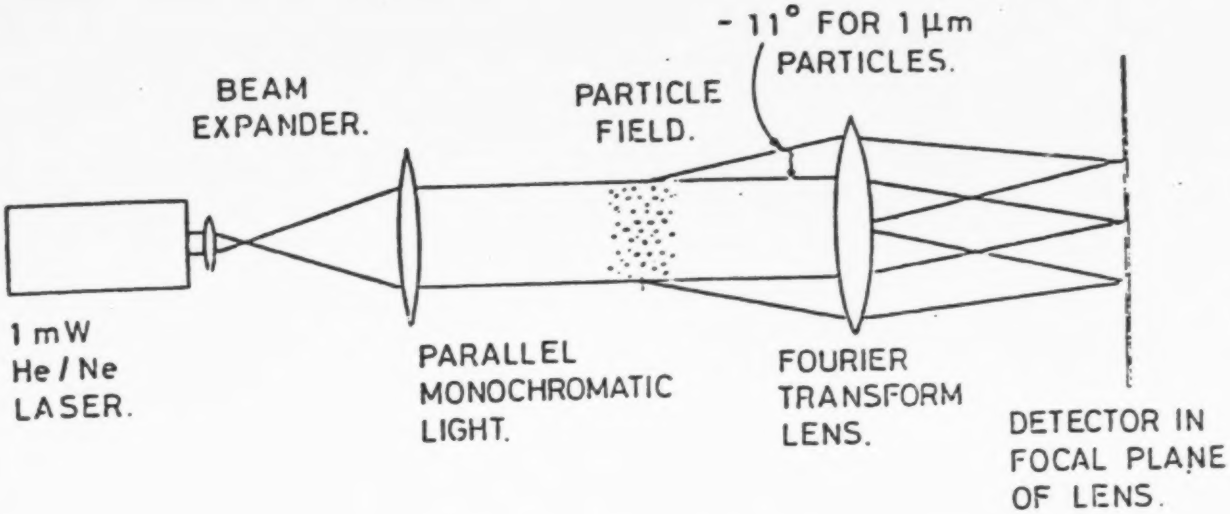

- 11° FOR 1 µm PARTICLES.
BEAM EXPANDER.
PARTICLE FIELD.
1 mW He / Ne LASER.
PARALLEL MONOCHROMATIC LIGHT.
FOURIER TRANSFORM LENS.
DETECTOR IN FOCAL PLANE OF LENS.

Figure A6. OPTICAL ARRANGEMENT OF FOURIER TRANSFORM LENS TO OBTAIN THE SIZE DISTRIBUTION OF SOLID OR LIQUID PARTICLES

θ, by the particles is imaged at the same radius on the rear focal plane (Fourier transform plane). This is shown diagrammatically in Figure A7. Clearly, it is important that the detector be accurately positioned at the rear focal plane of the lens. Otherwise, the location of the particle along the beam would affect the scattered light distribution on the detector.

Unfortunately, the system makes no discrimination on where the scattered light originates. Even the slightest facility window contamination can be detected as "particles" by systems based on this method. Since many particle measurements must be made through the windows of an enclosure, this problem is serious. One example has been cited (NASA Lewis) wherein the instrument was confounded by small inclusions in quartz windows. The instrument manufacturer has been made aware of this problem and they are working on window purging methods.

Windows can also produce multiple reflections that might enter the detector if both windows are not normal to the transmitted beam. Background light produced by such reflections can be accounted for if it remains at a constant level.

Because particles are detected along the entire beam path, the instrument is insensitive to the spatial variations of the spray. If the spray plume was axisymmetric, the distribution could be determined by making measurements at the incremental radii of the spray and using the Abel inversion technique. This would be a very tedious process due to the amount of data and processing time required.

Inversion of the Measured Signal

The description of the scattered light intensity from a distribution of particle in the sample volume (in the collimated beam) can be posed in the form of an integral equation:

$$I = \int_{a_1}^{a_2} n(a)\, G\, (r,a)\, da \tag{7}$$

where n(a) is some distribution function.

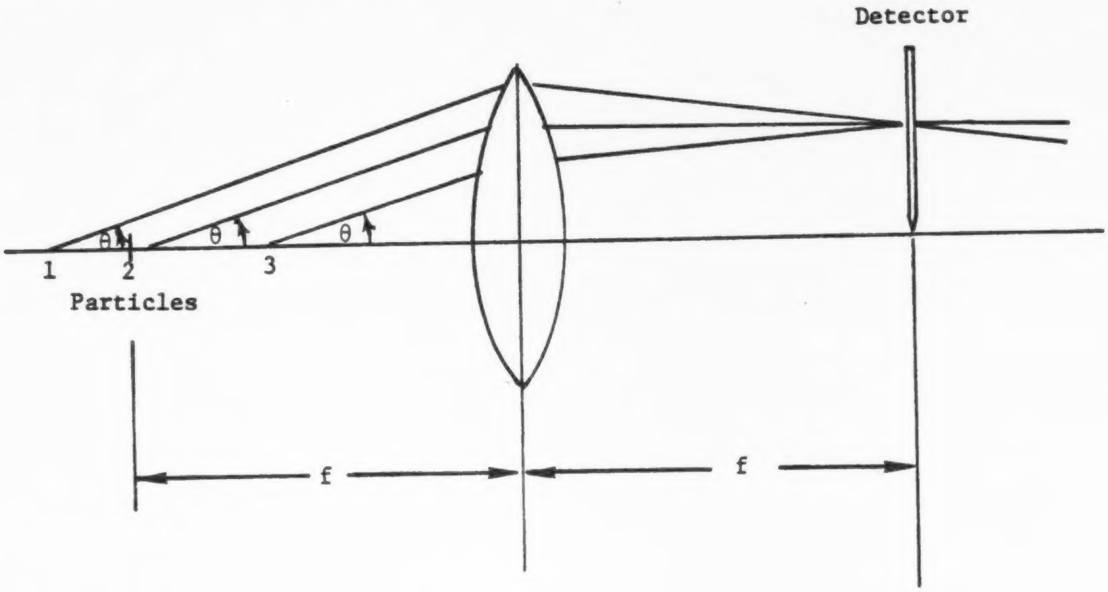
Detector
θ
θ
θ
1
2
3
Particles
f
f

Figure A7. SCATTER FROM VARIOUS STATIONS ALONG THE BEAM

$$F(r,a) = I_o\left(\frac{ka^2}{f}\right)^2 \left[\frac{J_1(kar/f)}{kar/f}\right]^2 \qquad (8)$$

To obtain the size distribution, Equation (7) must be inverted so that n(a) is given as an explicit function of the measured intensity distribution.

One method of solving this problem is to assume that the measured size distribution can be described by a suitable particle distribution function (e.g. the two-parameter Rosin-Rammler function). This method has been used in practice but unnecessarily limits the capability of the instrument.

The problem has been formulated in matrix notation by Anderson and Beissner[4] as

$$I = GN \qquad (9)$$

where I is a column matrix whose elements are the irradiance measurements at a set radial distance, G is a rectangular matrix of the function G(r,a) and N is a column matrix whose elements are the number of particles as a function of size.

To obtain a solution of the matrix equation for N, the values of the size distribution, the following matrix relationship can be used:

$$N = (G^T G)^{-1}\, G^T I \qquad (10)$$

where G^T is the transpose matrix. The accurate solution of this equation is restricted by the requirement that the difference in the diffraction pattern produced by particles in adjacent intervals be large in comparison with the experimental error in the irradiance measurement.

Another inversion method attributed to Shifrin[5] is described by Abbiss[6]. In that report, the details of the method are given along with an error analysis. Monodispersions are also treated in the analyses.

The existing inversion methods are still relatively slow. Although the inversion technique that requires the use of a distribution function limits the method, it can be accomplished with a minicomputer in a reasonable amount of time. Undoubtedly, inversion methods that are both fast enough for use on microcomputers and that produce the actual size distribution will be developed.

Particle Velocity Effects

It is important to recognize that the techniques which measure over a collection of particles in a collimated laser beam are responding to the particle number density distribution, N(a). Single particle counters respond to the particle flux:

$$F = A(a)\,N(a)\,V(a) \tag{11}$$

where A(a) is the probe cross sectional area which is dependent upon the particle size and V(a) is the velocity of particles of radius, a. If the particles of different sizes are moving at different speeds at the various locations, then the relative number density will change. Thus, the mean size measured by the multiple particle scatter detection method will differ from that measured by single particle counters. The measurements can be compared only if the velocity of the particles in each size increment is measured as well.

The particle number density or flux cannot be measured with instruments based on the multiple particle scatter detection method.

SUMMARY

The small angle light scattering method has been reviewed and its applicability to particle sizing discussed. A summary of the observations and conclusions are presented below.

- Anomalus Diffraction - When using the method to size transparent particles, e.g. liquid droplets, the light transmitted through the particle will interact with the diffractive scatter. This can significantly change the apparent diffraction pattern.
- Particle Number Density - Although the method works in high number density environments, it will not work well in low number density environments. A sufficient number of particles are required in the beam at one time to "smooth" the diffraction pattern and to provide adequate signal for the detector.
- Stray Light - Light reflected or scattered from the lenses and facility windows will contribute to the background noise and measurement error. Some of the stray light could be "zeroed" out but transient contamination on

the optics will be most troublesome and can introduce sizable errors. The fixed background will lower the signal-to-noise ratio.

- Spatial Resolution - The instrument measures particles along the beam path and hence has limited spatial resolution. Spatial distributions can be determined for axisymmetric sprays but the process is very tedious.
- Size Distributions - Presently, the inversion method requires the use of distribution functions using a two-parameter fit. Actual distributions can be determined but the process is time consuming and probably requires more accuracy than Malvern has.
- Particle Velocity Effects - If the droplets have velocities that depend on their size, the measured sized distribution will be affected. The size measurement is based on the size number density in the volume of the laser beam.
- Number Density - Particle flux or number density cannot be measured with the method.
- Alignment - Because the diffraction pattern is very narrow for large particles, the system is very sensitive to the alignment.

Although the method has some limitations, it has been used to make satisfactory size measurements. It appears that the instrument is best suited for sizing opaque particles in environments where window contamination is not a problem.

Several users of the Malvern instrument were contacted and their observations and experiences were discussed. Despite the limitations documented here, they were satisfied with the instrument's capabilities and their measurements in most part agreed with the results determined by independent means. The applications were typically in unconfined nozzle sprays.

Future Work

Experimental verification of some of the points made in this analysis would be very useful. These could be established to assess the measurement errors produced. For example, the effects of anomalous diffraction could be determined by using a water spray and then adding an absorbing dye to the water and repeating the measurement. The spray would be held at constant conditions and the size distributions compared.

REFERENCES

1. Swithenbank, J., Bear, J. M., Taylor, D. S., Abbot, D., and McCreath, G. C., "A Laser Diagnostics Technique for the Measurement of Droplet and Particle Size Distribution", AIAA, No. 76-69, Washington, D.C., January 26, 1976.

2. Van DeHulst, H. C., Light Scattering by Small Particles, John Wiley and Sons, 1957.

3. Jones, A. R., "Error Contour Charts Relevant to Particle Sizing by Forward Scattered Lobe Methods", J. Phys. D: Applied Physics, Vol 10, Pg. 163, 1977.

4. Anderson, W. L. and Beissner, R. E., "Counting and Classifying Small Objects by Far-Field Light Scattering", Applied Optics, 10, 1503, 1971.

5. Shifrin, K. S., "Calculations of a Certain Class of Definite Integrals Containing the Square of a First-Order Bessel Function", Trudy Vsesoyuznogo Zaochnogo Lesotekhnicheskogo Instituta, 2, 1956.

6. Abbiss, J. B., "Theoretical Aspects of the Determination of Particle-Size Distributions from Measurements of Scattered Light Intensity", RAE Technical Report 70151, August 1970.

APPENDIX B

RESPONSE OF SPECTRON DEVELOPMENT LABORATORIES FOR CLARIFICATION TO FINAL REPORT

1. What is the expected dynamic size range of the DSI instrument and how was that dynamic range determined? Specifically, what is the dynamic size range of each data set (Task 1 - 12)?

2. What were the fringe spacings employed for each data set and how was the best fringe spacing selected? How does the fringe spacing influence the dynamic size range?

3. What is the meaning of the data in squares in Task 2 - 5C?

4. There was a concern about the accuracy of the early data, Task 1 - 5C. Is this still the case or have the problems been resolved? Which data sets are valid and which are of concern? What were the problems and how were they resolved?

5. How was the data taken? What special techniques were employed to assure the data were valid? How was alignment verified for the receiving optics? What justification is there for maximizing visibility?

6. What were the DC offset problems which were encountered? How were they circumvented? How was the technique used, verified?

7. What is the meaning of the number of invalids encountered by the DSI processor? Does this have any implications to the accuracy of the data? Is there any way of telling if the invalids were due to multiple droplets, oversized droplets or undersized droplets? How does the processor discriminate against droplets not passing through the center of the probe volume?

8. On what sized droplet did the signal detector system output a saturated signal? Was this maximum particle size determined for every data set? How would the DSI processor handle a saturated signal?

9. What experiments were run to verify the DSI technique? Were any additional tests run for the processor checkout? Were any additional experiments performed (other than with mono-disperse sprays) on samples with known size distributions?

10. How were the size distributions obtained from the holograms? Are the tabulated data available?

11. How was the physical positioning of probe volume performed? What was

the relative accuracy of the positioning technique and the impact of the accuracy on the probe volume size?

12. The trends in the data (e.g., average size decreases downstream, size increases radially, etc.) are relatively small changes as compared to the distribution standard deviation. Can such conclusions be drawn from the data in view of that observation?

13. What is the resolution limit of the holography? How will the resolution limit impact the measured size distribution?

RESPONSE TO EER-EPA QUESTIONNAIRE ON TASK I

1. The dynamic range of the DSI instrument is about 10:1 and it is given by $d = .086\delta$ CF to 0.86δ CF. Where δ is the fringe spacing and CF is the value of the abscissae where the visibility is zero. For the collection F# = 5.3 and off-axis angle, $\theta = 30^0$, the collection factor CF = 8.54 (obtained from visibility curve). Hence, $d = .73\delta$ to 7.3δ. Looking at the values of δ given in the report, the following dynamic ranges are then obtained:

TASK #	δ(μm)	dmin(μm)	dmax(μm)
1	15.8	11.5	115
2C	15.8	11.5	115
3	10.2	7.5	75
4	15.8	11.5	115
5	15.8	11.5	115
5C	10.2	7.5	75
6	10.2	7.5	75
10	12	8.8	88
11	12	8.8	88
12	12	8.8	88

The value of δ is selected during the experiment to centralize the visibility distribution. If the histogram is truncated on both sides, more than one δ may be necessary.

2. The answer to this question is given in Item 1.

3. In the presence of incomplete size distributions, more than one size range should be used in order to obtain the entire distribution. However, in many cases, most of the distribution can be obtained and the rest can be inferred by extrapolation. This technique is better when the missing sizes are on the small side since they contribute the least to the mean size parameters. The squares on the histograms represent the values obtained by extrapolation.

4. In the early data, there was no clear way of setting up the high voltage into the photomultiplier tube. This will not change the value of

the visibilities obtained, but will have an effect on the dynamic range. If too little gain is used, the small particles will not be seen, while, if too much gain is used, the signals from the large particles will saturate the electronics and will be rejected. For the early data, care was exercised to avoid saturated signals. This may have resulted in not seeing the small particles. As a consequence, the early histograms needed a certain amount of extrapolated points to complete the distribution.

The validity of the results is definitely questionable in Tasks 1 through 3. The best results are those of Tasks 10, 11 and 12. In future programs, this problem will not be encountered since the new processors have an automatic high voltage gain control that sets the signals to the optimum level.

5. The visibility of a particle or droplet crossing the probe volume is given by $V = Vo/\cos h\ (2yz\ \alpha/b^2)$, where Vo is the visibility corresponding to the middle of the probe volume, y and z are distances away from the middle of the probe volume, α is the beam intersection angle, and b the waist radius. Hence, $V \leq Vo$, and to minimize the error and optimize the alignment, V (which is measured) must be maximized. To assure the validity of the data, a storage scope was used in conjunction with the processor. Some of the signals were displayed and analyzed. The intensity level and the DC level, the symmetry of the Doppler burst and the visibility were checked. After all these tests were performed, the data were taken electronically by the processor, displayed on the CRT and stored in diskettes.

6. In addition to the Doppler signal, extraneous light can enter the PM tube causing a DC offset. The Doppler signal, however, must be integrated with respect to the ground level. In order to achieve that, the DC offset produced by the noisy signals must be subtracted electronically. In the early EER experiments, this was done manually by observing the signal on the scope. A human error is obviously present using this methodology and to minimize it, the DC offset was corrected several times and the data compared. We should mention that the new generation of processors have an automatic DC offset compensator.

7. The invalid signals correspond to droplets with a visibility outside the dynamic range. Notice that visibilities smaller than about 15%

should not be measured to avoid the ambiguity zone and those with a visibility larger than 99% may present large conversion errors. The invalid signals are not erroneous signals or bad data; they are outside the measurement range, that is, larger or smaller droplets.

The total number of processor starts (on out-of-range droplets or multiples) is output to a BNC terminal at the rear of the processor. A minor addition could be made to provide information as to why the signal was rejected.

Signals that saturate the amplifiers or do not meet the periodicity check were eliminated by the processor and were not accounted for. The processor does not discriminate against droplets outside the center of the probe volume. This must be done during the alignment by using a pinhole that only "sees" light scattered from such center.

8. The amplifiers saturate when an input signal of 1 V ground to peak is present. It was the duty of the operator to control the PM tube voltage supply to prevent saturation from happening. The fringe spacing must also be selected such that the largest signal to be measured has a visibility of 15%. Combining these last two statements, the signals with 15% visibility should almost saturate the amplifiers. This maximum size was determined for every data set. The DSI processor threw out saturated signals and they were not accounted for.

9. The experiments to verify the DSI techniques were based on monodispersed sprays. The size of the droplets was measured with an independent method and the visibility signals were observed on a scope and processed by the VP-1000. Other tests to the processor include the use of real sprays to check the processor in the presence of high data rates. However, the size distribution of the spray is not known. Tests using signal generators and other electronic equipment are also performed as part of the routine tests.

10. The size distributions obtained from the holograms were made magnifying the reconstructed image and using an eyepiece with a calibrated reticle. The handwritten tables that generated these graphs are not available anymore.

11. The beam crossover was intersected on the tip of the resonator cup.

Then the nozzle was raised and the spray turned on. The crossover could then be seen just below the tip. This positioning was performed visually by two or three people independently and the difference was in the order of 1 mm.

The size of the probe volume is a function of the transmission and collection lenses and does not depend on where the beams are crossed.

12. Several histograms were taken at the same point, each containing around 3,000 samples. Many of these repeated histograms were stored in diskettes and are shown in the final report. It can be observed that the mean parameters do not change significantly between repeated runs. That is, the mean and standard deviations are almost invariable. This leads to indicate that the changes observed as a function of position or condition are significant.

13. For the setup and conditions run at EERC, the resolution limit was about 10 μm, and the smallest particles clearly detectable were about 15 μm. The effect on the size distribution is explained in Part (b) of page 38 of the final report.

APPENDIX C

CHARACTERIZATION OF A SONICORE NOZZLE
(RAW DATA)

by:

C. F. Hess and W. D. Bachalo

Spectron Development Laboratories, Inc.
3303 Harbor Boulevard, Suite G-3
Costa Mesa, CA 92626

Prepared for:

Energy and Environmental Research Corporation
EER Subcontract No. EER-8318-9

EERC/EPA DATA
SDL TASK1 RUN 1

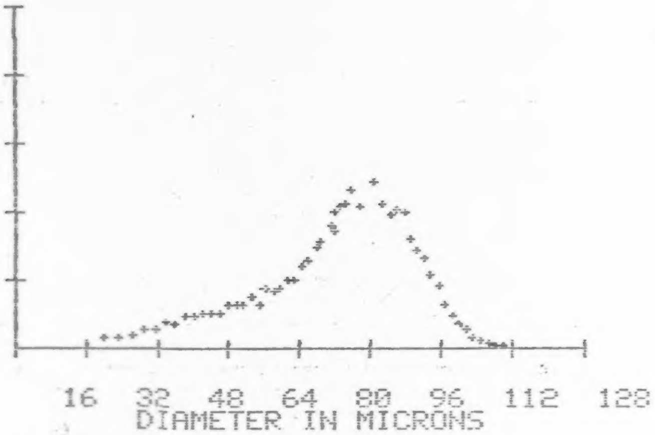

```
MAXIMUM FREQUENCY=.1

 N=25906
 D10=73.1
 D20=74.8
 D30=76.3
 D32=79.4
 S=16.24
 KURTOSIS=-.71
```

SDL TASK1 RUN 1R

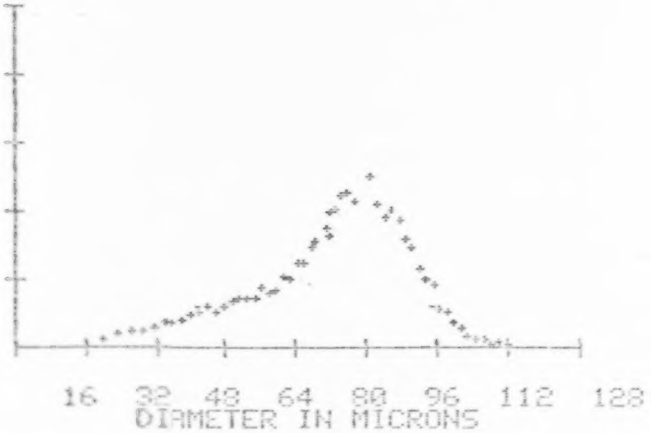

```
MAXIMUM FREQUENCY=.1

 N=25240
 D10=73
 D20=74.8
 D30=76.2
 D32=79.3
 S=16.19
 KURTOSIS=-.67
```

SDL TASK1 RUN 2

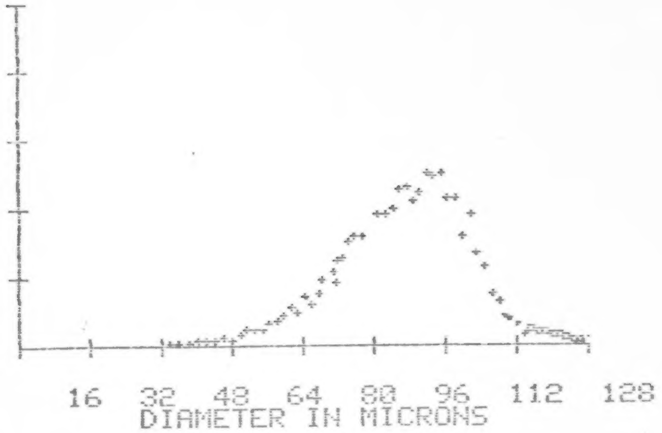

MAXIMUM FREQUENCY=.1

N=12526
D10=86.8
D20=88
D30=89.1
D32=91.4
S=14.49
KURTOSIS=-.32

EERC/EPA DATA
SDL TASK1 RUN 2R

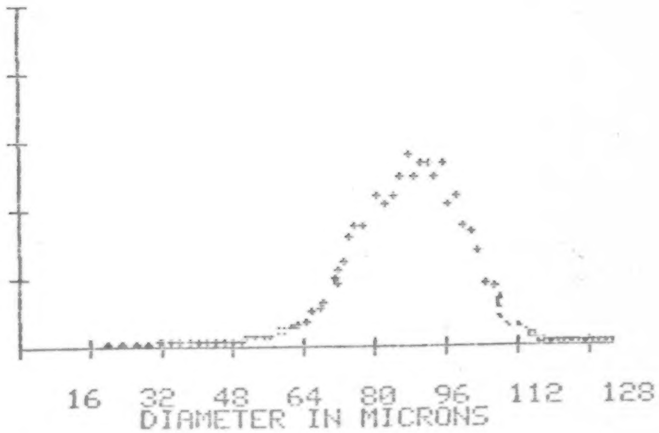

MAXIMUM FREQUENCY=.1

N=15386
D10=87.2
D20=88.2
D30=89.2
D32=91.1
S=13.64
KURTOSIS=-.64

EERC/EPA DATA
SDL TASK1 RUN 2RR

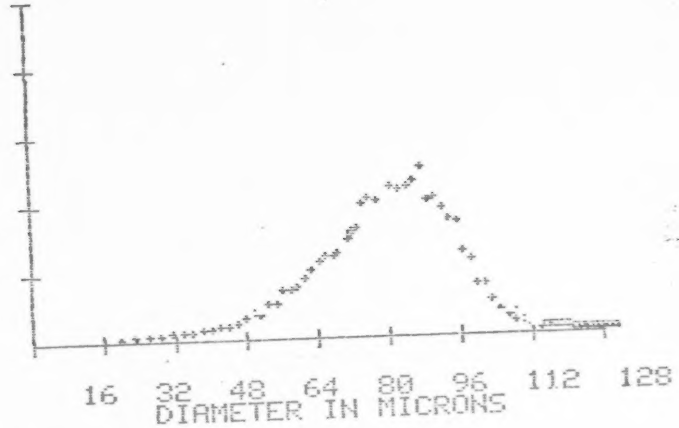

MAXIMUM FREQUENCY=.1

N=15321
D10=80
D20=81.6
D30=83
D32=86
S=16.07
KURTOSIS=-.21

SDL TASK1 RUN 3

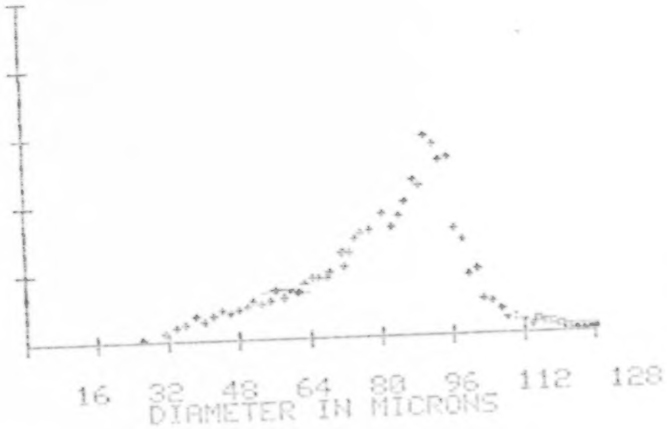

MAXIMUM FREQUENCY=.1

N=11794
D10=81.1
D20=82.9
D30=84.5
D32=87.7
S=17.07
KURTOSIS=-.5

EERC/EPA DATA
SDL TASK1 RUN 3R

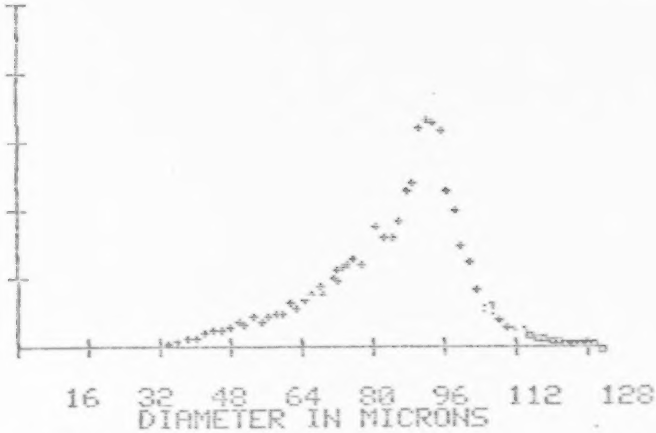

MAXIMUM FREQUENCY=.1

N=12762
D10=85.1
D20=86.4
D30=87.6
D32=90
S=15.05
KURTOSIS=-.65

EERC/EPA DATA
SDL TASK1 RUN 4

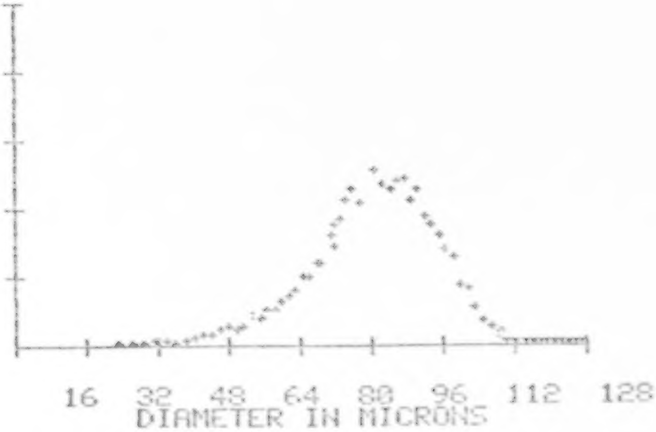

MAXIMUM FREQUENCY=.1

N=12316
D10=80.5
D20=81.7
D30=82.8
D32=85.1
S=13.93
KURTOSIS=-.39

```
]RUPR#0

     EERC/EPA DATA
     SDL  TASK1  RUN  5
```

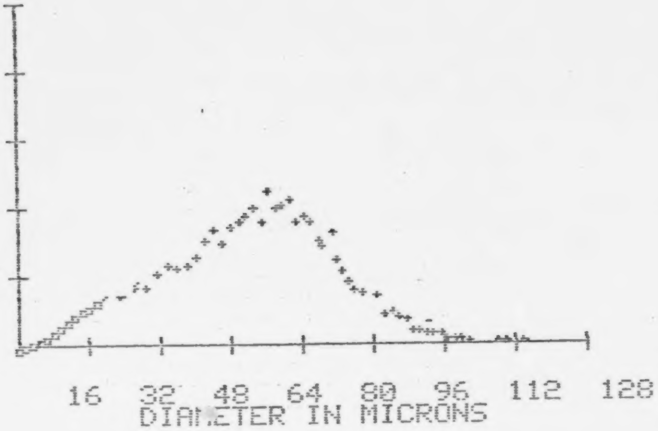

```
MAXIMUM FREQUENCY=.1

 N=13068
 D10=55
 D20=57.9
 D30=60.3
 D32=65.3
 S=18.25
 KURTOSIS=-.34
```

```
     SDL  TASK1  RUN  5R
```

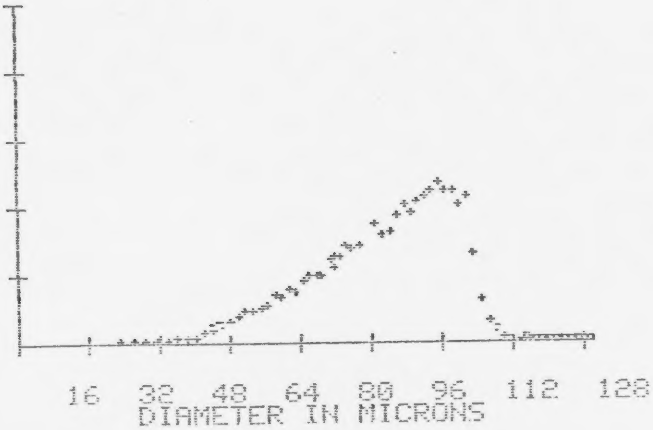

```
MAXIMUM FREQUENCY=.1

 N=27407
 D10=83.1
 D20=84.6
 D30=85.9
 D32=88.7
 S=15.78
 KURTOSIS=-.47
```

EERC/EPA DATA
SDL TASK1 RUN 5RR

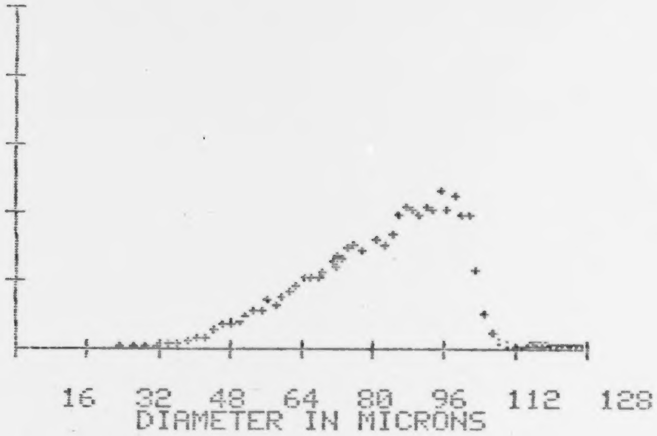

MAXIMUM FREQUENCY=.1

N=22775
D10=82
D20=83.5
D30=84.9
D32=87.6
S=15.8
KURTOSIS=-.5

SDL TASK1 RUN 6

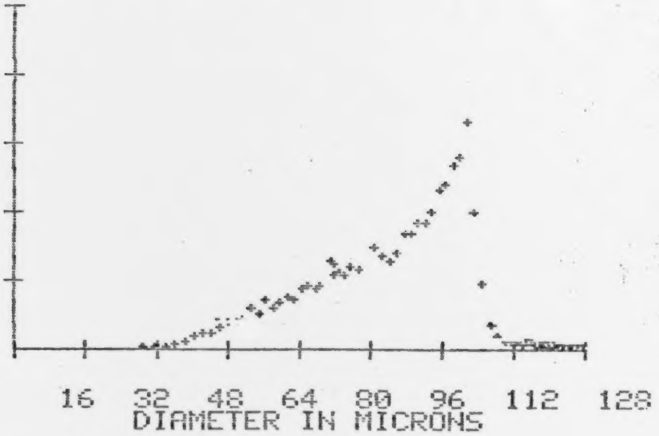

MAXIMUM FREQUENCY=.1

N=9476
D10=84.1
D20=85.8
D30=87.2
D32=90.2
S=16.81
KURTOSIS=-.59

EERC/EPA DATA
SDL TASK1 RUN 6R

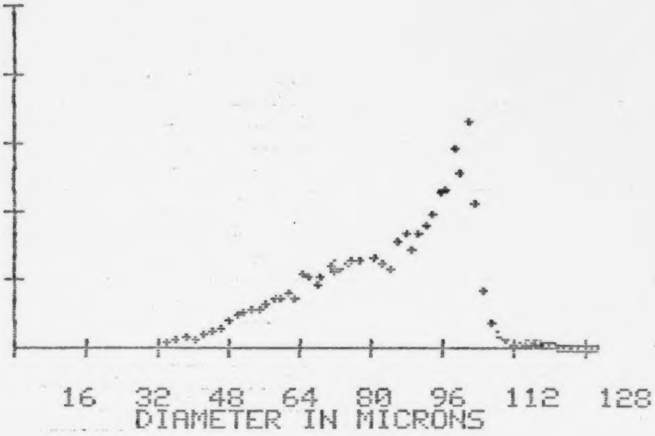

MAXIMUM FREQUENCY=.1

N=10001
D10=83.6
D20=85.2
D30=86.6
D32=89.5
S=16.57
KURTOSIS=-.58

SDL TASK1 RUN 7

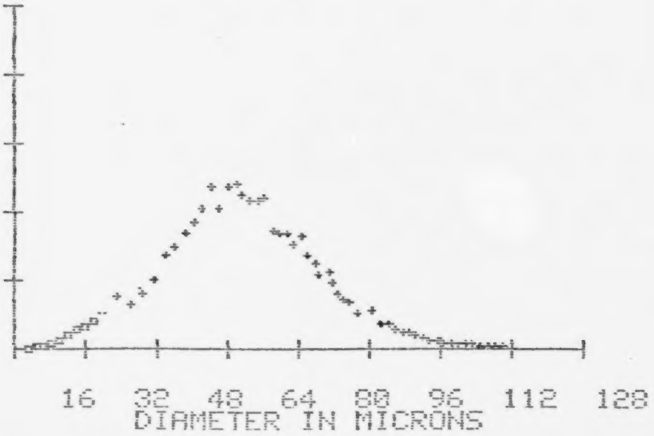

MAXIMUM FREQUENCY=.1

N=16762
D10=53.8
D20=56.3
D30=58.5
D32=63.3
S=16.68
KURTOSIS=.05

SDL TASK1 RUN 7RR

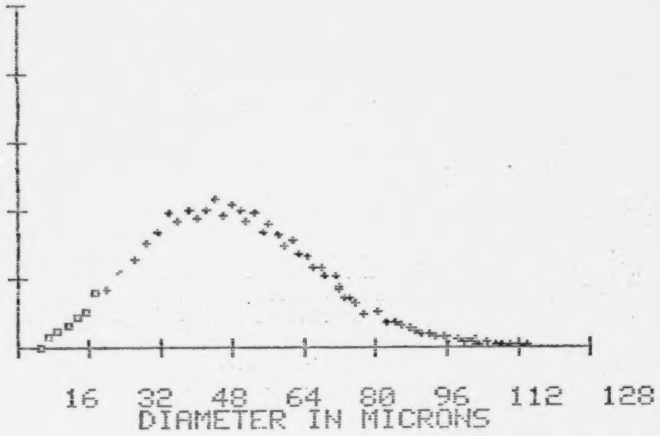

```
MAXIMUM FREQUENCY=.1

 N=30067
 D10=51
 D20=54.3
 D30=57.1
 D32=63.1
 S=18.46
 KURTOSIS=.13
```

EERC/EPA

SDL TASK1 RUN 8

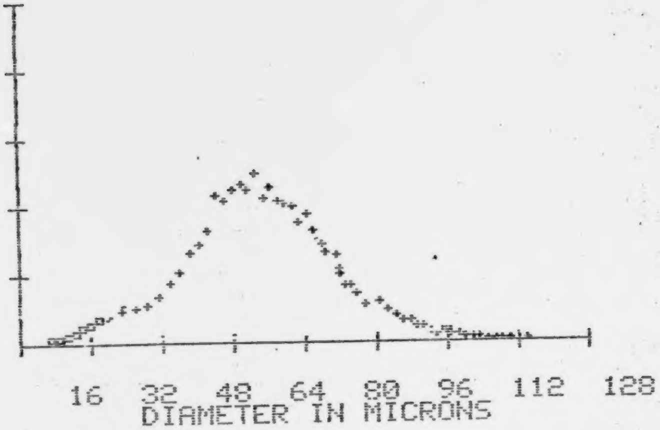

MAXIMUM FREQUENCY=.1

N=25973
D10=56
D20=58.3
D30=60.3
D32=64.5
S=16.11
KURTOSIS=-.08

SDL TASK1 RUN 8RR

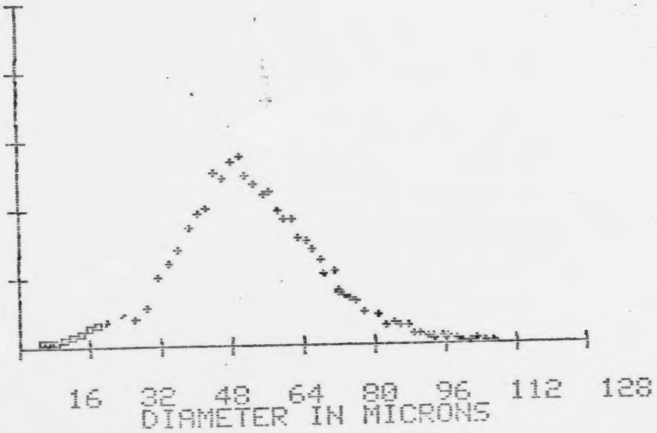

MAXIMUM FREQUENCY=.1

N=16673
D10=53.7
D20=55.9
D30=57.8
D32=61.9
S=15.47
KURTOSIS=0

SDL TASK1 RUN 9

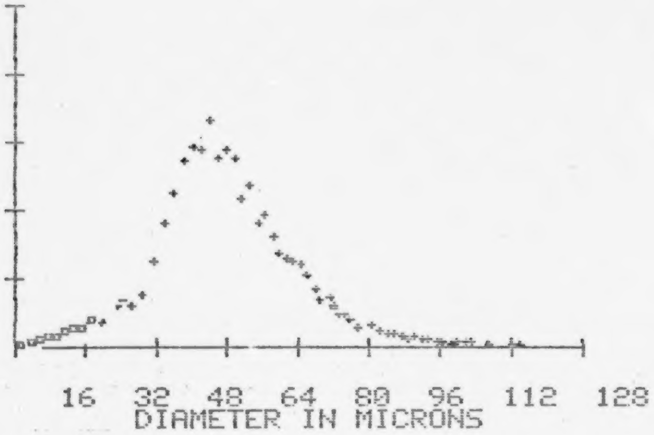

MAXIMUM FREQUENCY=.1

N=19184
D10=50
D20=52.3
D30=54.5
D32=59.1
S=15.45
KURTOSIS=.28

SDL TASK1 RUN 9R

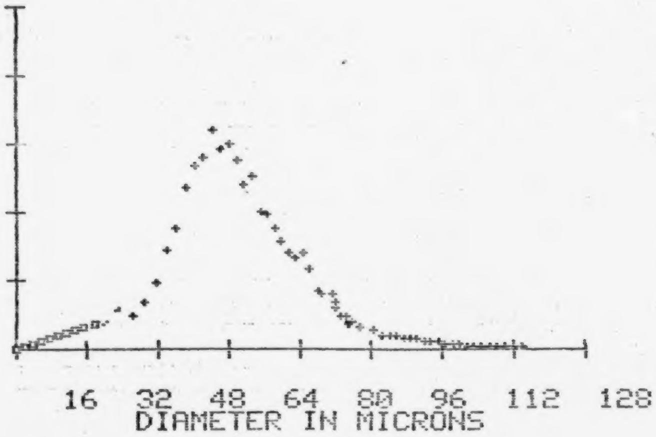

MAXIMUM FREQUENCY=.1

N=19944
D10=50.9
D20=53.2
D30=55.3
D32=59.8
S=15.49
KURTOSIS=.2

SDL TASK1 RUN 10

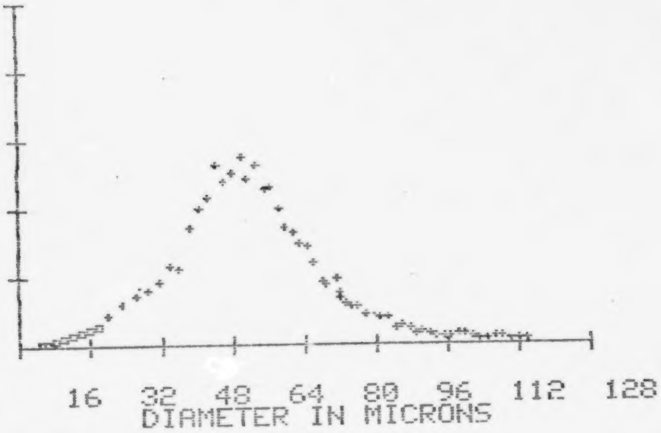

MAXIMUM FREQUENCY=.1

N=12707
D10=53.9
D20=56.3
D30=58.7
D32=63.7
S=16.51
KURTOSIS=.42

EERC/EPA DATA
SDL TASK1 RUN 10R

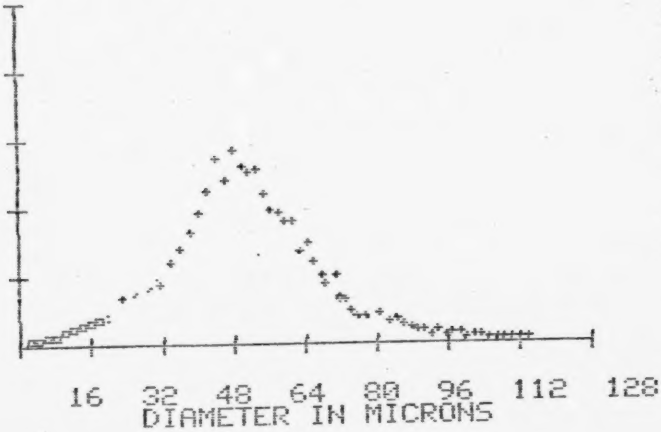

MAXIMUM FREQUENCY=.1

N=9644
D10=53.1
D20=55.7
D30=58.2
D32=63.5
S=17.11
KURTOSIS=.27

EERC/EPA DATA
SDL TASK1 RUN 11R

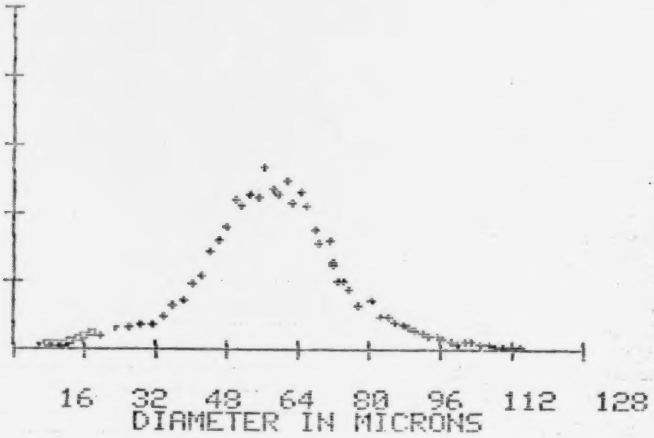

MAXIMUM FREQUENCY=.1

N=21282
D10=59.6
D20=61.6
D30=63.3
D32=67
S=15.49
KURTOSIS=-.14

EERC/EPA DATA
SDL TASK1 RUN 12R

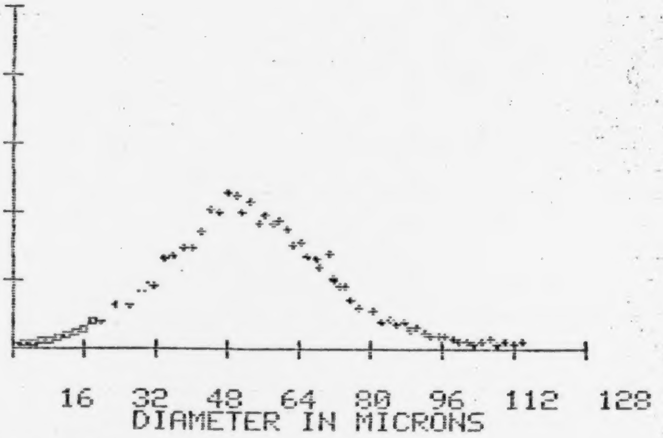

MAXIMUM FREQUENCY=.1

N=11602
D10=55.7
D20=58.6
D30=61.2
D32=66.8
S=18.33
KURTOSIS=.12

EERC/EPA DATA
SDL TASK2 RUN 1R

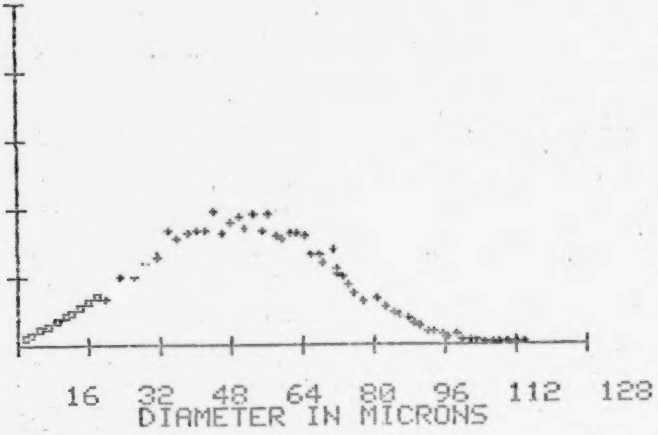

MAXIMUM FREQUENCY=.1

N=33970
D10=52.4
D20=56
D30=58.9
D32=65.2
S=19.91
KURTOSIS=-.17

SDL TASK2 RUN 2R

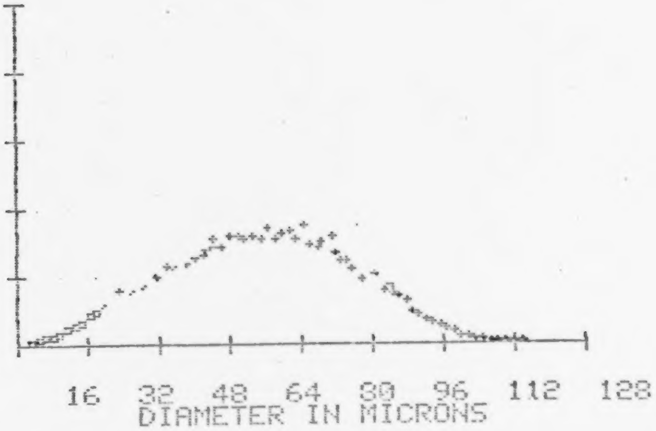

MAXIMUM FREQUENCY=.1

N=37469
D10=57.8
D20=61.1
D30=63.7
D32=69.2
S=19.57
KURTOSIS=-.24

EERC/EPA DATA
SDL TASK2 RUN 3R

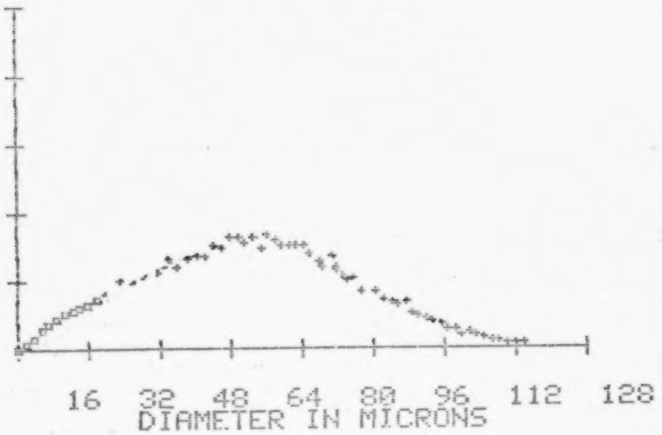

MAXIMUM FREQUENCY=.1

N=41195
D10=55.5
D20=59.8
D30=63.2
D32=70.6
S=22.36
KURTOSIS=-.13

EERC/EPA DATA
SDL TASK2 RUN 4

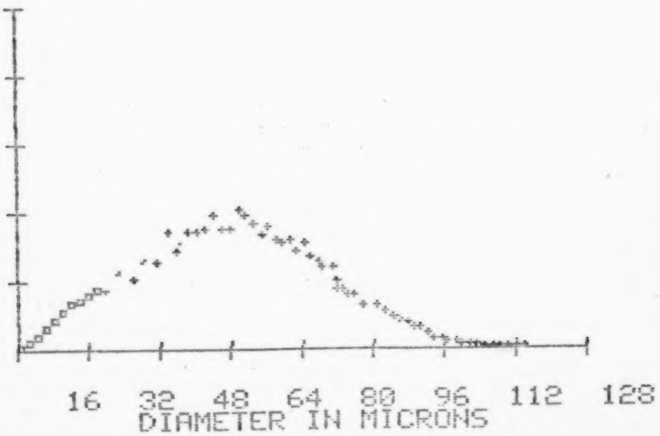

MAXIMUM FREQUENCY=.1

N=31534
D10=51.4
D20=55.3
D30=58.4
D32=65.1
S=20.43
KURTOSIS=-.11

EERC/EPA DATA
SDL TASK2 RUN 5R

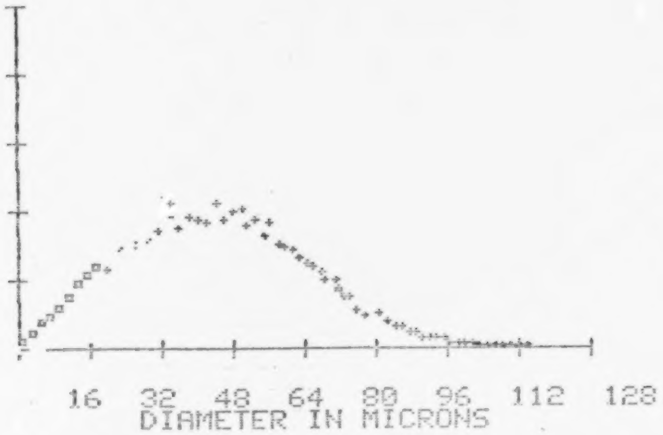

MAXIMUM FREQUENCY=.1

N=31992
D10=47.9
D20=52
D30=55.3
D32=62.4
S=20.26
KURTOSIS=-.01

EERC/EPA DATA
SDL TASK2 RUN 6R

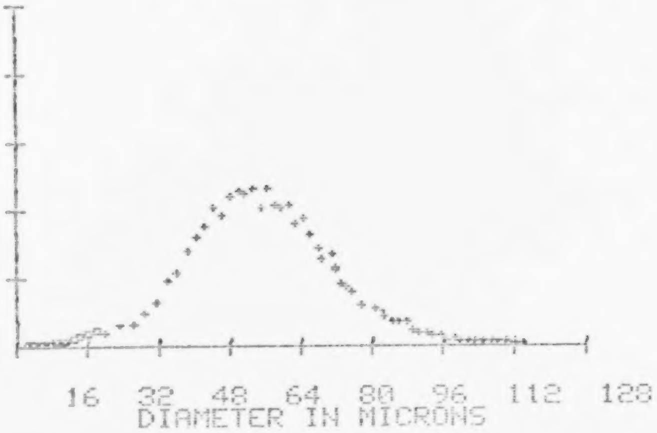

MAXIMUM FREQUENCY=.1

N=27638
D10=56.9
D20=59
D30=61
D32=65.1
S=15.81
KURTOSIS=.06

EERC/EPA DATA
SDL TASK2 RUN 7R

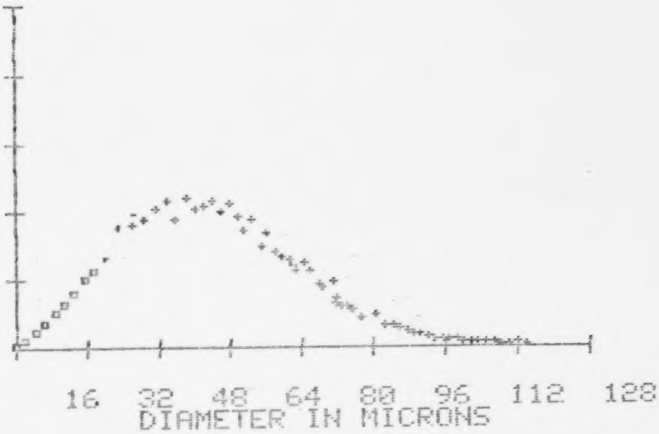

MAXIMUM FREQUENCY=.1

N=30757
D10=47.3
D20=51.3
D30=54.7
D32=62.2
S=19.95
KURTOSIS=.2

EERC/EPA DATA
SDL TASK2C RUN 1R

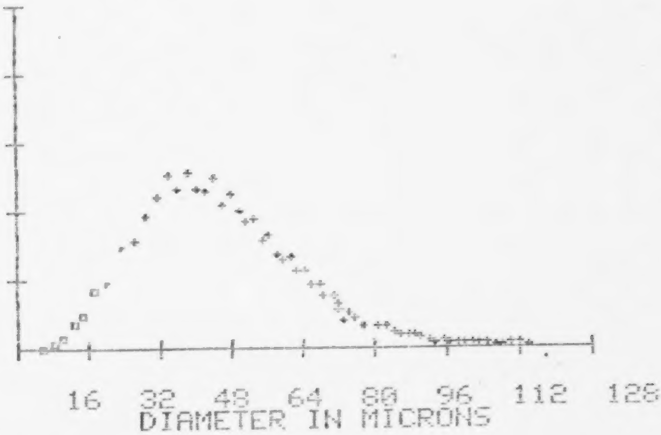

MAXIMUM FREQUENCY=.1

N=24828
D10=48.2
D20=51.3
D30=54.2
D32=60.5
S=17.59
KURTOSIS=.46

SDL TASK2C RUN 2R

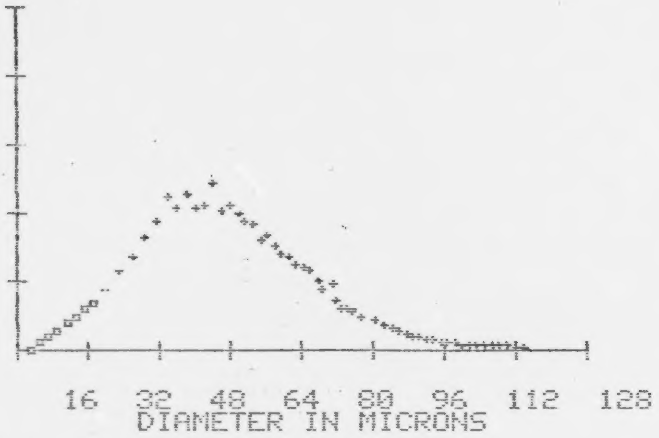

```
MAXIMUM FREQUENCY=.1

 N=26845
 D10=49.6
 D20=53
 D30=56
 D32=62.5
 S=18.62
 KURTOSIS=.25
```

SDL TASK2C RUN 3R

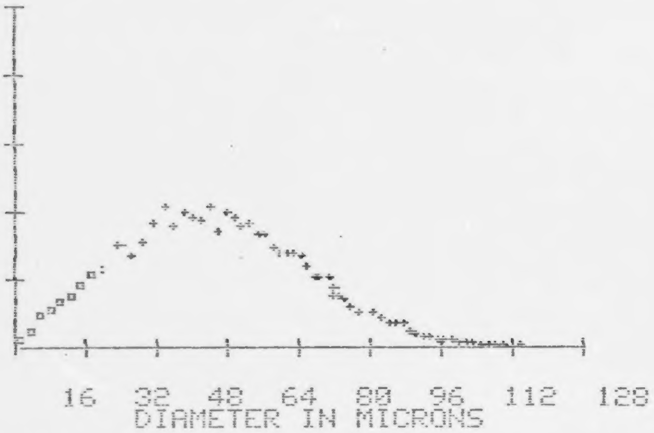

```
MAXIMUM FREQUENCY=.1

 N=29041
 D10=48.8
 D20=52.8
 D30=56
 D32=63.1
 S=20.2
 KURTOSIS=.03
```

SDL TASK2C RUN 4R

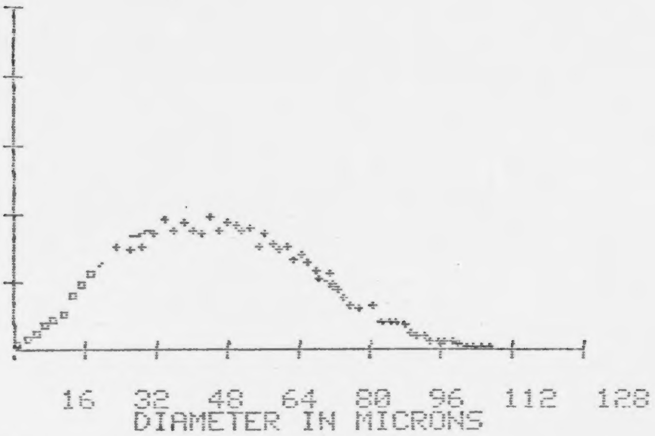

```
MAXIMUM FREQUENCY=.1

 N=34285
 D10=49.3
 D20=53.2
 D30=56.3
 D32=63
 S=19.97
 KURTOSIS=-.05
```

SDL TASK2C RUN 5R

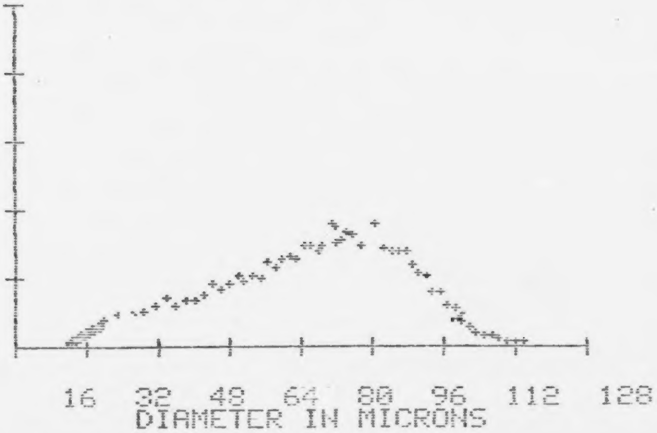

```
MAXIMUM FREQUENCY=.1

 N=29455
 D10=64.4
 D20=68.2
 D30=71
 D32=77
 S=22.53
 KURTOSIS=-.56
```

EERC/EPA DATA
SDL TASK2C RUN 6R

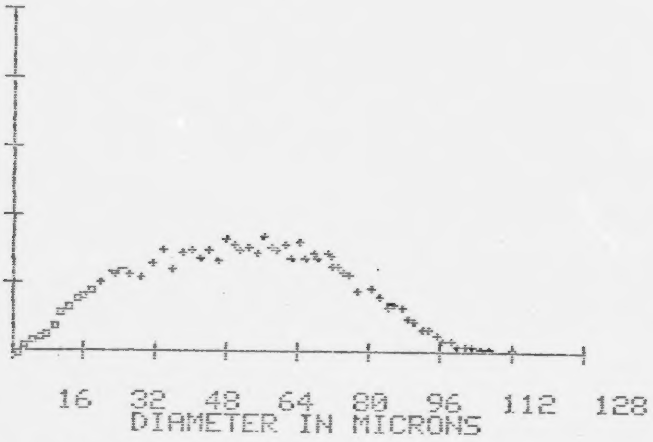

MAXIMUM FREQUENCY=.1

N=20584
D10=53.9
D20=58.1
D30=61.2
D32=68.1
S=21.55
KURTOSIS=-.23

SDL TASK2C RUN 7R

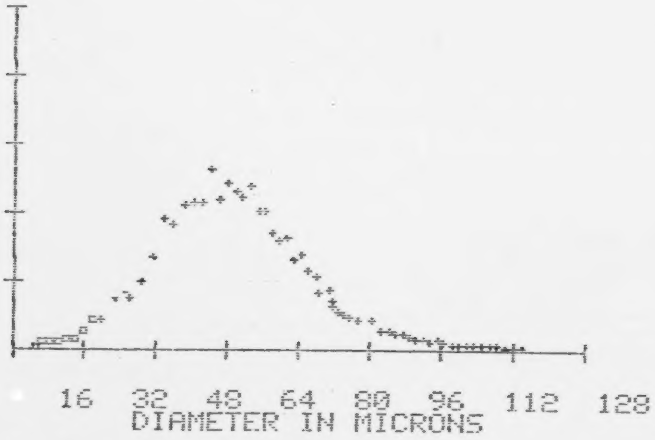

MAXIMUM FREQUENCY=.1

N=24102
D10=51.8
D20=54.5
D30=56.9
D32=62.1
S=16.74
KURTOSIS=.29

```
EERC/EPA DATA
SDL TASK2C RUN 8R
```

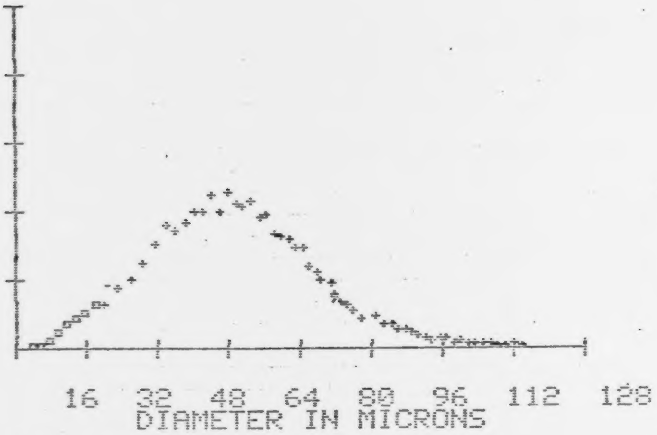

```
MAXIMUM FREQUENCY=.1

N=28703
D10=51.8
D20=54.9
D30=57.5
D32=63.3
S=18.08
KURTOSIS=.15
```

```
EERC/EPA DATA
SDL TASK2C RUN 9R
```

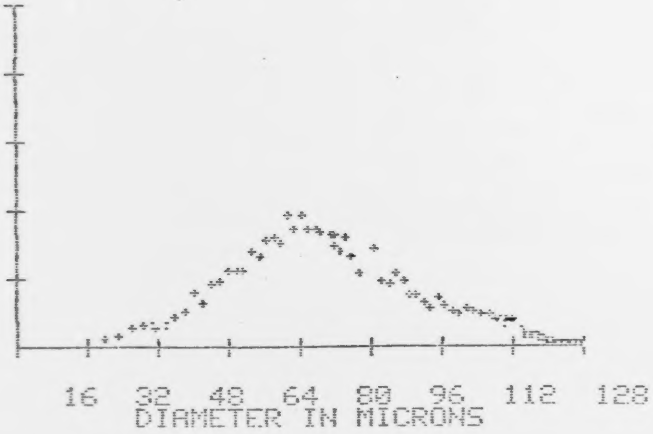

```
MAXIMUM FREQUENCY=.1

N=9490
D10=64.5
D20=68.8
D30=72.2
D32=79.4
S=23.99
KURTOSIS=-.25
```

EERC/EPA DATA
SDL TASK2C RUN 10R

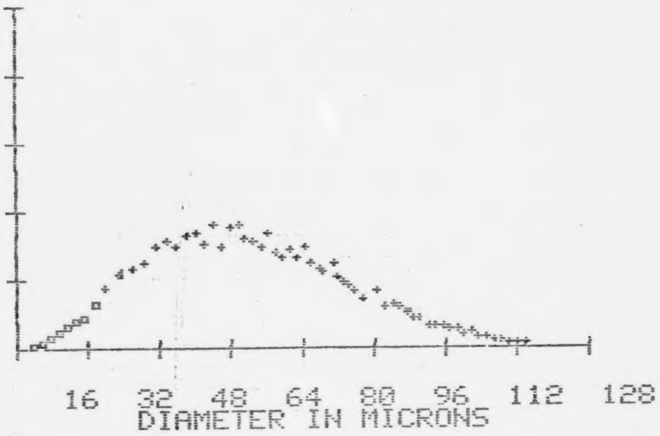

MAXIMUM FREQUENCY=.1

N=35587
D10=55.2
D20=59
D30=62.3
D32=69.5
S=20.98
KURTOSIS=.13

EERC/EPA DATA
SDL TASK2C RUN 11R

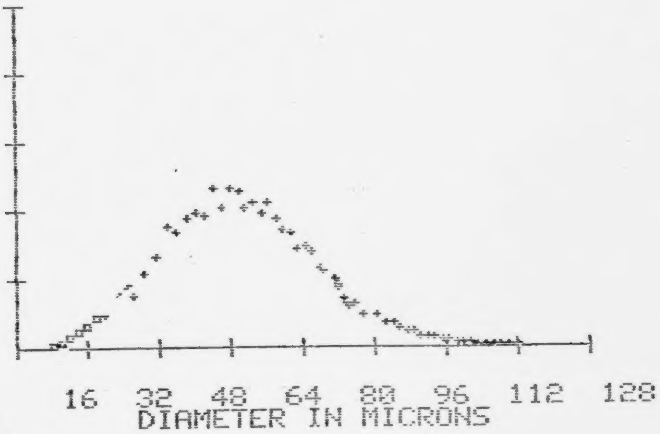

MAXIMUM FREQUENCY=.1

N=26660
D10=53
D20=55.6
D30=57.9
D32=62.7
S=16.63
KURTOSIS=.15

EERC/EPA DATA
SDL TASK2C RUN 12R

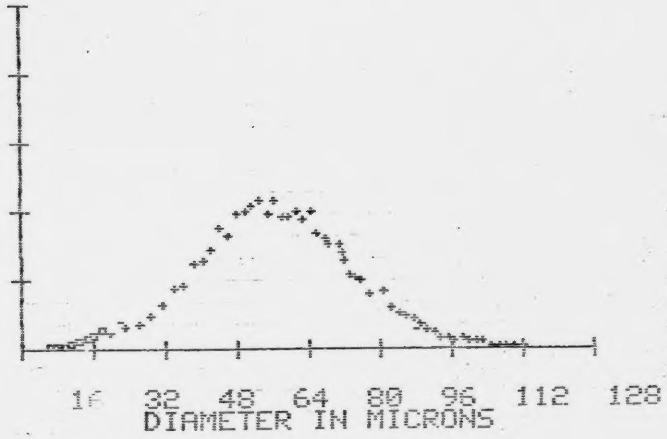

```
MAXIMUM FREQUENCY=.1

 N=29627
 D10=58.7
 D20=60.9
 D30=62.8
 D32=66.9
 S=16.11
 KURTOSIS=-.06
```

SDL TASK2C RUN 13R

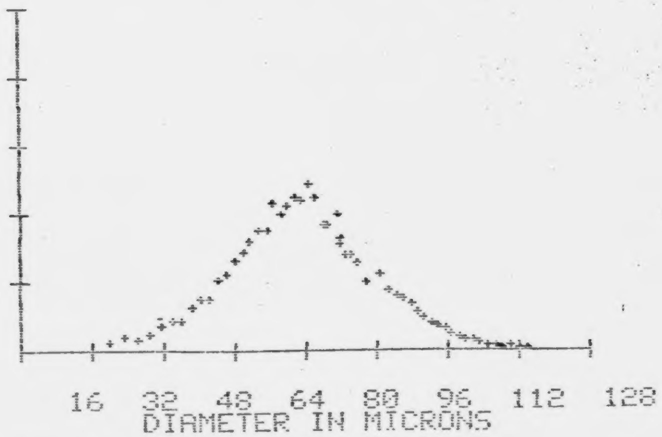

```
MAXIMUM FREQUENCY=.1

 N=28894
 D10=59.4
 D20=62.7
 D30=65.2
 D32=70.4
 S=19.9
 KURTOSIS=-.52
```

```
EERC/EPA DATA
SDL TASK2C RUN 14R
```

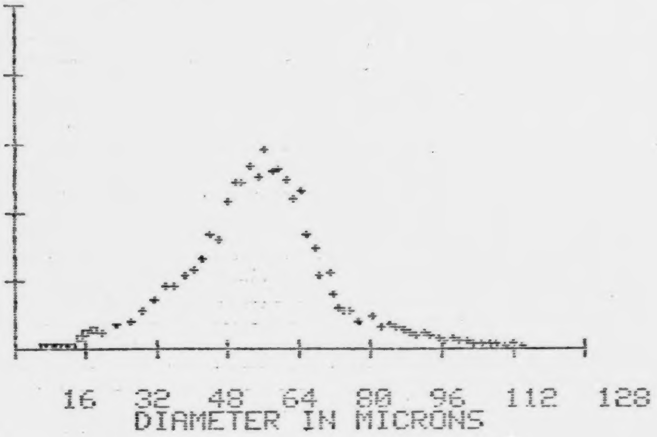

```
MAXIMUM FREQUENCY=.1

N=21894
D10=57
D20=59
D30=60.8
D32=64.7
S=15.2
KURTOSIS=.17
```

```
EERC/EPA DATA
SDL TASK2C RUN 15
```

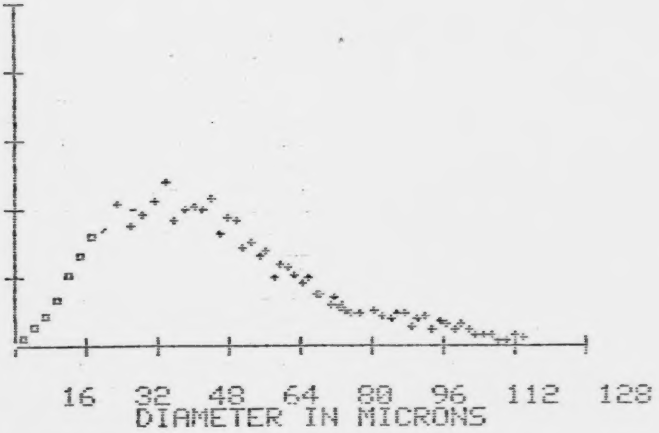

```
MAXIMUM FREQUENCY=.1

N=5878
D10=48.2
D20=53.3
D30=57.8
D32=67.8
S=22.86
KURTOSIS=.45
```

EERC/EPA DATA
SDL TASK2C RUN 16R

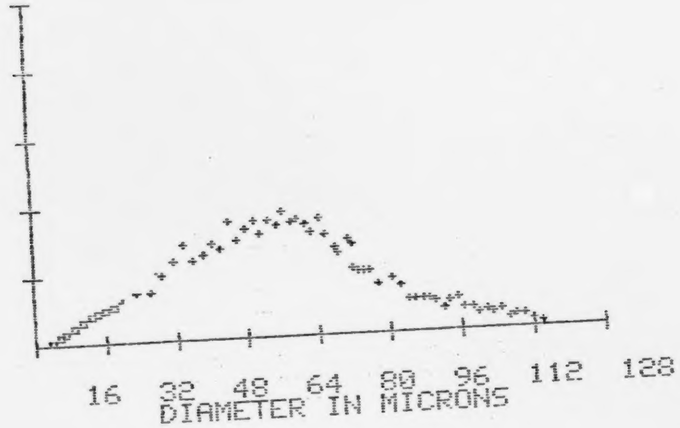

MAXIMUM FREQUENCY=.1

N=5693
D10=57.5
D20=61.3
D30=64.5
D32=71.4
S=21.27
KURTOSIS=.05

EERC/EPA DATA
SDL TASK2C RUN 17R

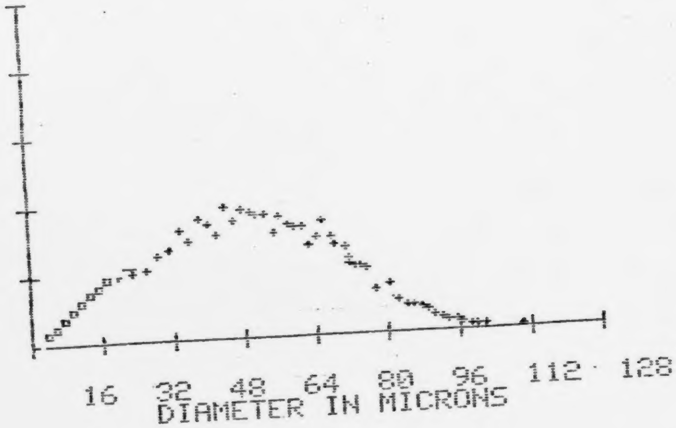

MAXIMUM FREQUENCY=.1

N=10379
D10=51.9
D20=55.6
D30=58.5
D32=64.8
S=19.99
KURTOSIS=-.18

```
EERC/EPA DATA
SDL TASK2C RUN 18R
```

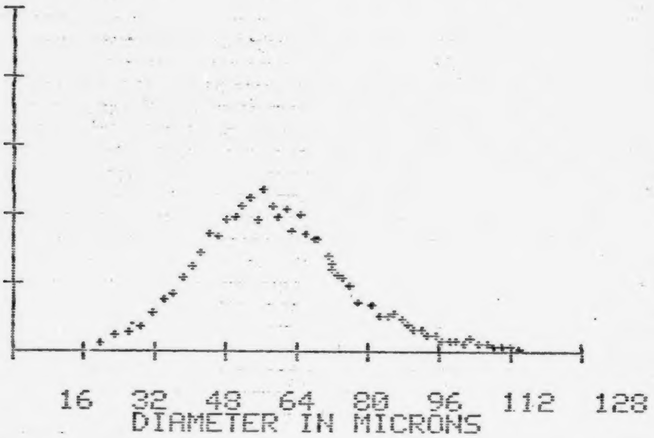

```
MAXIMUM FREQUENCY=.1

 N=8986
 D10=55.9
 D20=59.3
 D30=62
 D32=67.9
 S=19.71
 KURTOSIS=-.19
```

SDL TASK3 RUN 1R

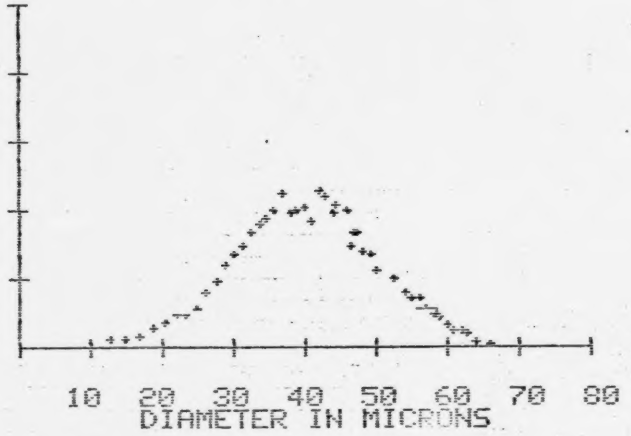

MAXIMUM FREQUENCY=.1

N=8308
D10=41
D20=42
D30=42.9
D32=44.8
S=9.07
KURTOSIS=-.08

EERC/EPA DATA
SDL TASK3 RUN 2R

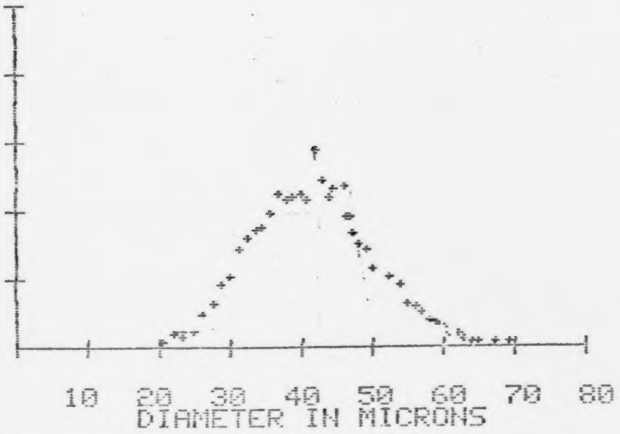

MAXIMUM FREQUENCY=.1

N=6568
D10=42.2
D20=42.9
D30=43.6
D32=45
S=7.87
KURTOSIS=.18

EERC/EPA DATA
SDL TASK3 RUN 3R

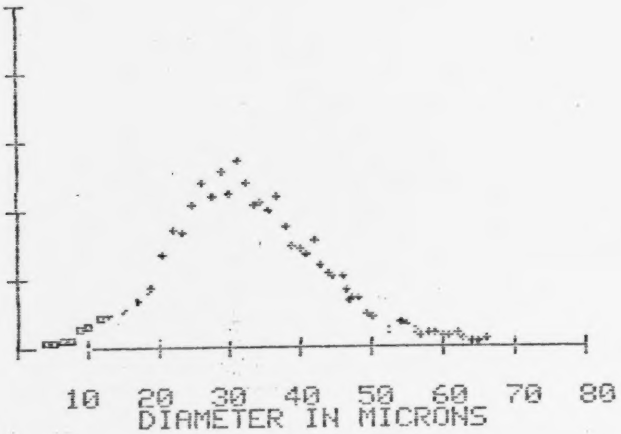

MAXIMUM FREQUENCY=.1

N=7023
D10=33.9
D20=35.5
D30=36.9
D32=40
S=10.51
KURTOSIS=.15

SDL TASK3 RUN 4R

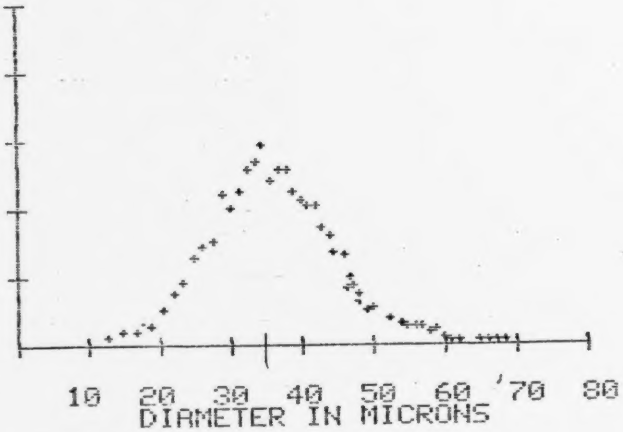

MAXIMUM FREQUENCY=.1

N=7259
D10=34.5
D20=36.3
D30=37.7
D32=40.7
S=11.23
KURTOSIS=-.39

SDL TASK3 RUN 5R

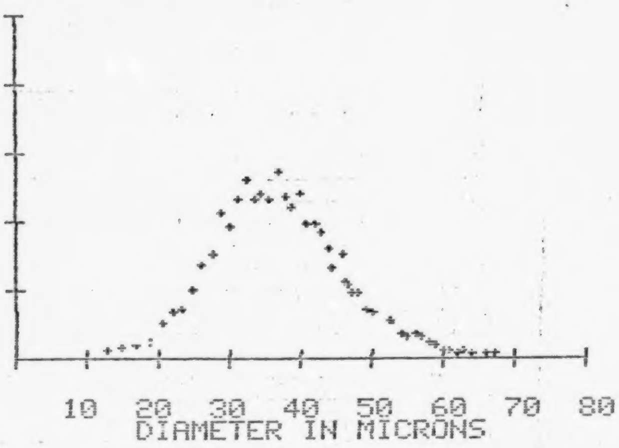

MAXIMUM FREQUENCY=.1

N=7751
D10=35.1
D20=36.9
D30=38.3
D32=41.4
S=11.44
KURTOSIS=-.44

EERC/EPA DATA
SDL TASK3 RUN 6R

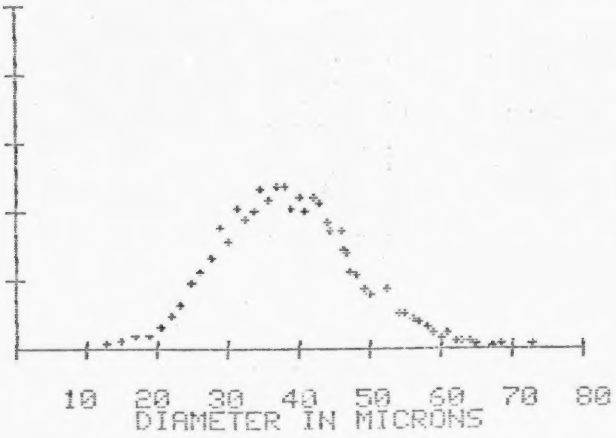

MAXIMUM FREQUENCY=.1

N=8957
D10=36.4
D20=38.4
D30=39.8
D32=43
S=12
KURTOSIS=-.47

SDL TASK3 RUN 7R

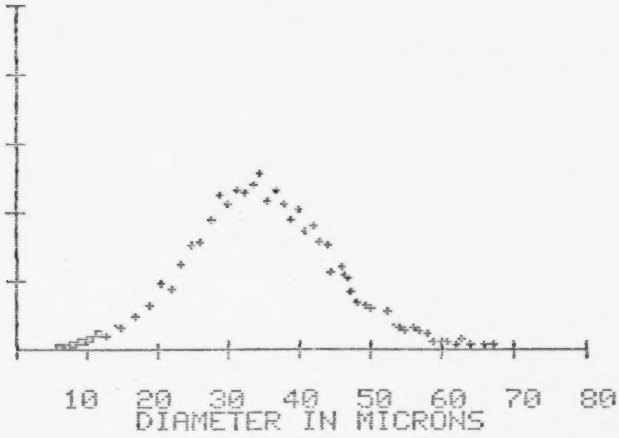

MAXIMUM FREQUENCY=.1

N=7487
D10=36.1
D20=37.4
D30=38.5
D32=41
S=9.68
KURTOSIS=.03

EERC/EPA DATA
SDL TASK3 RUN 8R

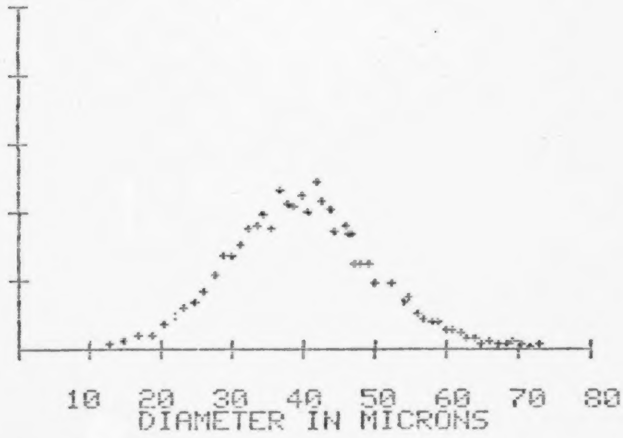

MAXIMUM FREQUENCY=.1

N=8755
D10=37.7
D20=39.8
D30=41.3
D32=44.6
S=12.54
KURTOSIS=-.49

EERC/EPA DATA
SDL TASK3 RUN 9R

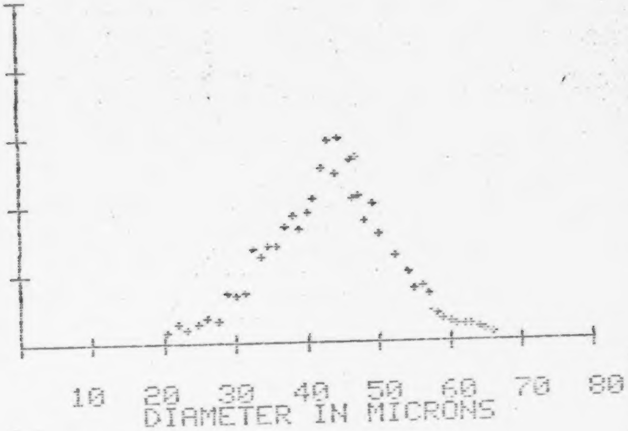

```
MAXIMUM FREQUENCY=.1

 N=3926
 D10=40.2
 D20=42
 D30=43.3
 D32=46
 S=12.23
 KURTOSIS=-1.02
```

EERC/EPA DATA
SDL TASK4 RUN 1R

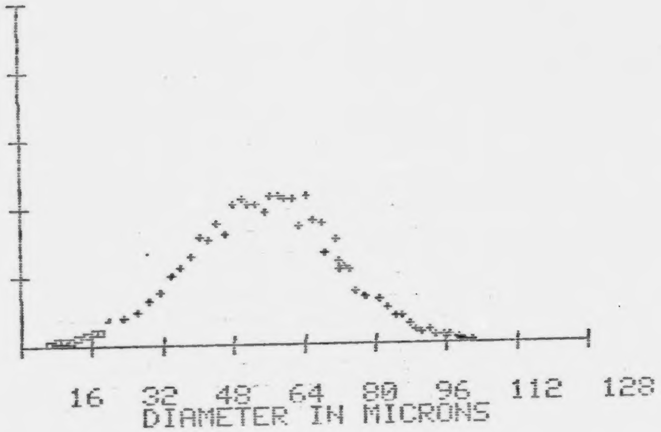

MAXIMUM FREQUENCY=.1

N=8889
D10=56.9
D20=59
D30=60.8
D32=64.6
S=15.65
KURTOSIS=-.23

EERC/EPA DATA
SDL TASK4 RUN 2R

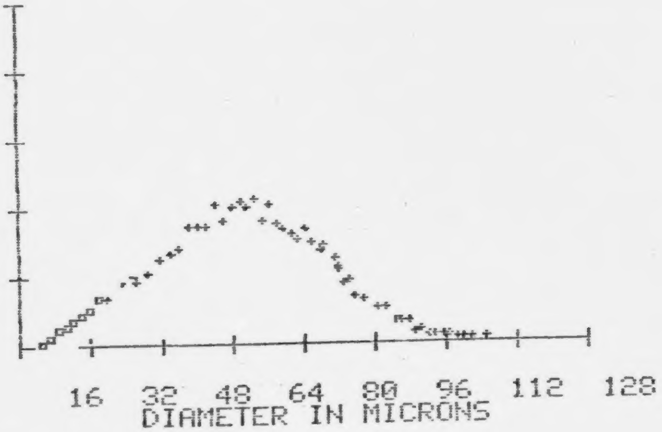

MAXIMUM FREQUENCY=.1

N=9301
D10=52.9
D20=55.9
D30=58.4
D32=63.6
S=18.01
KURTOSIS=-.18

SDL TASK4 RUN 3R

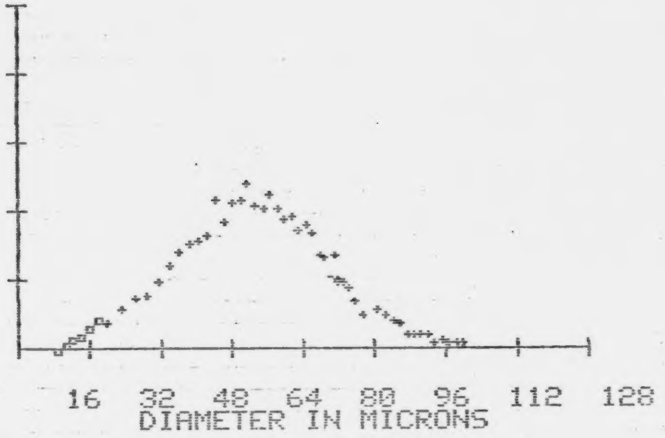

MAXIMUM FREQUENCY=.1

N=7915
D10=55.1
D20=57.3
D30=59.2
D32=63.2
S=15.64
KURTOSIS=-.11

SDL TASK4 RUN 4R

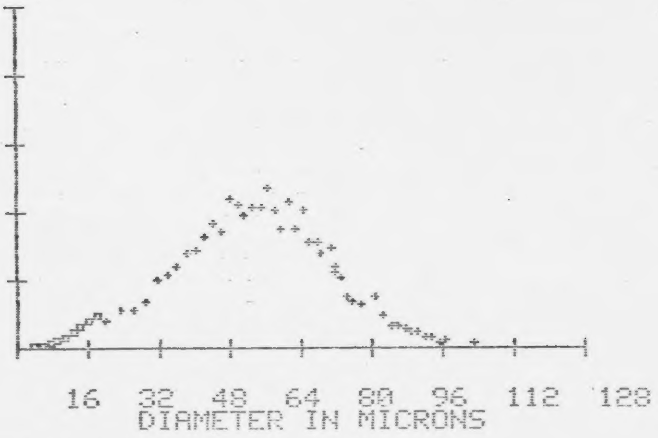

MAXIMUM FREQUENCY=.1

N=5344
D10=55.3
D20=57.8
D30=59.8
D32=64
S=16.54
KURTOSIS=-.29

SDL TASK4 RUN 5R

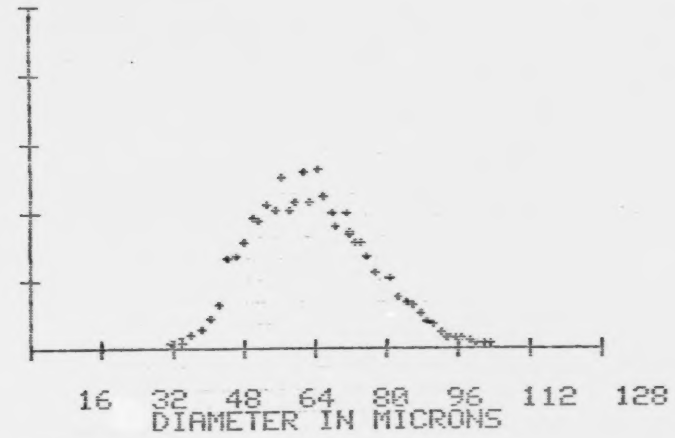

MAXIMUM FREQUENCY=.1

N=7985
D10=59.2
D20=61.9
D30=63.9
D32=68.2
S=18.25
KURTOSIS=-.78

SDL TASK4 RUN 6R

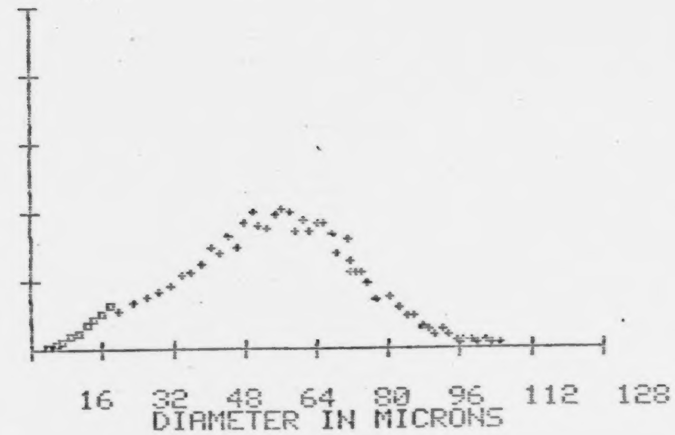

MAXIMUM FREQUENCY=.1

N=9750
D10=55.7
D20=58.6
D30=61
D32=65.9
S=18.2
KURTOSIS=-.33

SDL TASK4 RUN 7R

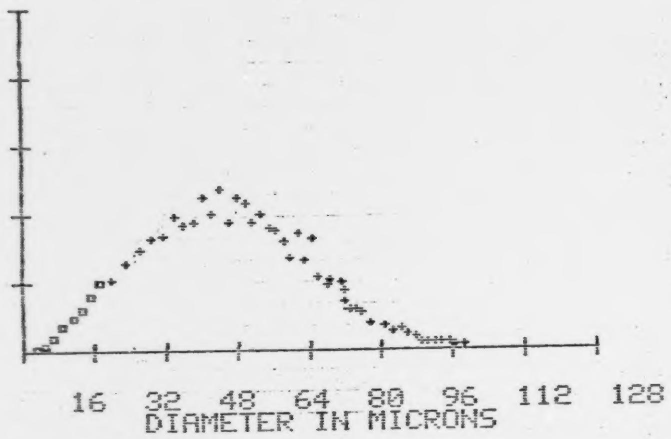

MAXIMUM FREQUENCY=.1

N=6470
D10=48.7
D20=51.9
D30=54.5
D32=60.2
S=17.9
KURTOSIS=-.05

EERC/EPA DATA
SDL TASK4 RUN 8R

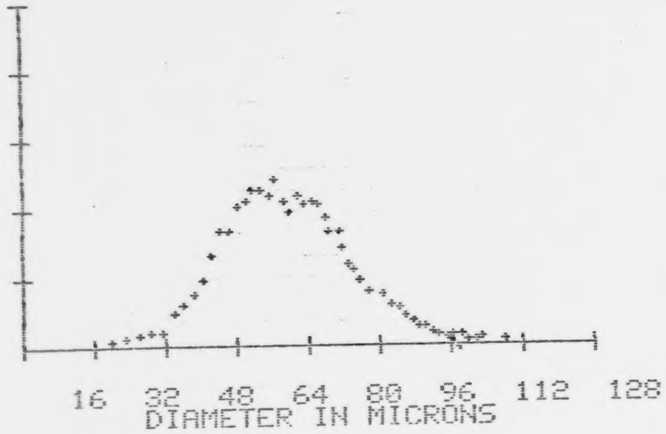

MAXIMUM FREQUENCY=.1

N=7160
D10=56.4
D20=59.3
D30=61.6
D32=66.4
S=18.47
KURTOSIS=-.49

35

EERC/EPA DATA
SDL TASK4 RUN 9R

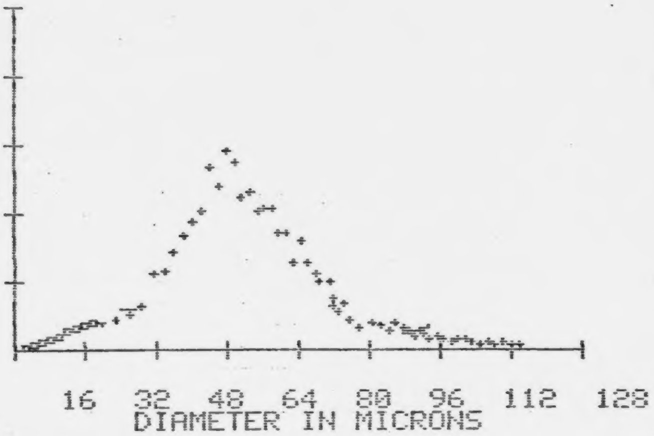

MAXIMUM FREQUENCY=.1

N=6620
D10=53.8
D20=56.6
D30=59.1
D32=64.6
S=17.5
KURTOSIS=.29

SDL TASK4 RUN 10R

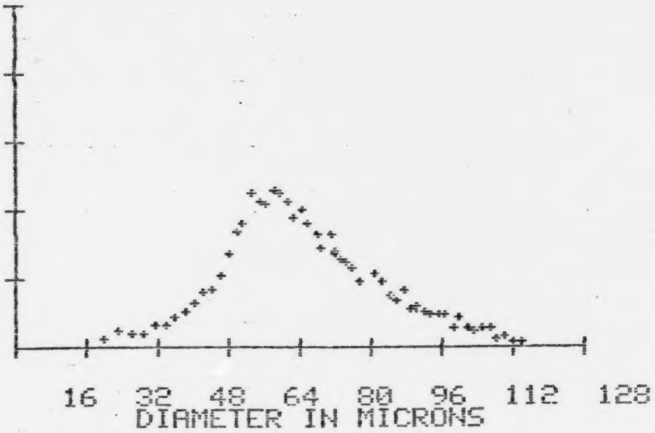

MAXIMUM FREQUENCY=.1

N=8513
D10=60.5
D20=64.1
D30=66.9
D32=73.1
S=21.28
KURTOSIS=-.31

SDL TASK4 RUN 11R

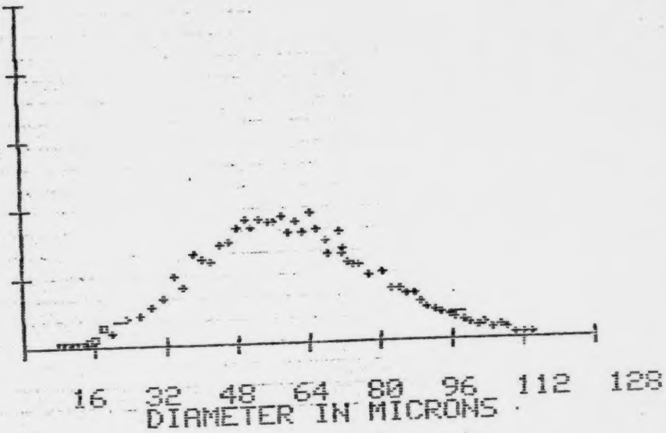

MAXIMUM FREQUENCY=.1

N=10163
D10=61.4
D20=64
D30=66.4
D32=71.4
S=18.13
KURTOSIS=.12

SDL TASK4 RUN 12R

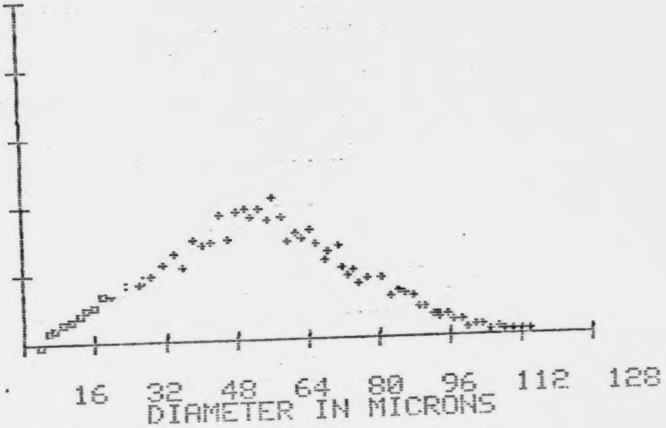

MAXIMUM FREQUENCY=.1

N=7848
D10=55.6
D20=59.3
D30=62.2
D32=68.7
S=20.4
KURTOSIS=-.06

SDL TASK4 RUN 13R

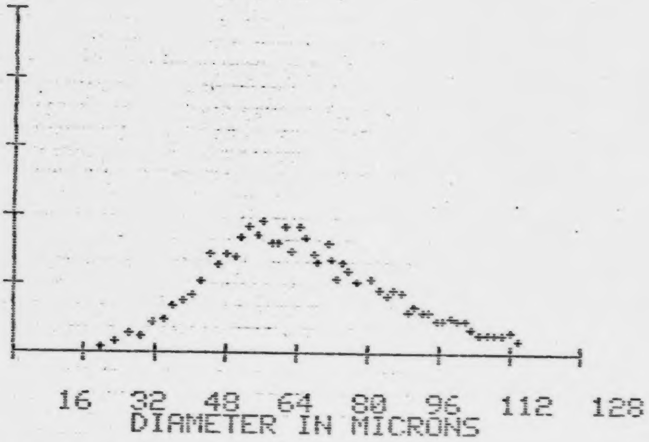

MAXIMUM FREQUENCY=.1

N=7751
D10=61.2
D20=65.4
D30=68.7
D32=75.8
S=22.86
KURTOSIS=-.15

EERC/EPA DATA
SDL TASK5 RUN 1R

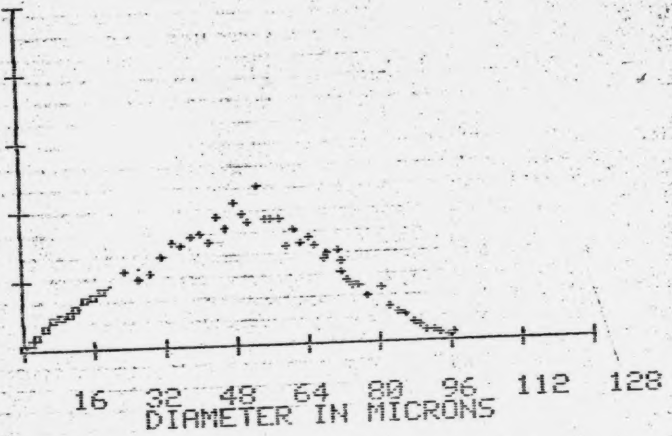

MAXIMUM FREQUENCY=.1

N=9002
D10=50.9
D20=54.6
D30=57.4
D32=63.4
S=19.78
KURTOSIS=-.34

EERC/EPA DATA
SDL TASK5 RUN 2R

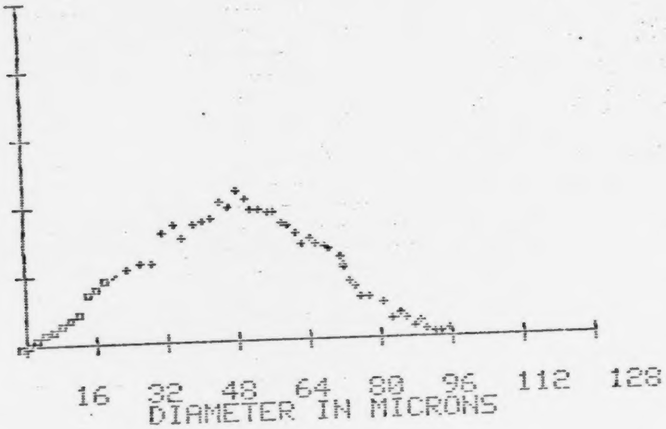

MAXIMUM FREQUENCY=.1

N=9171
D10=50.3
D20=53.5
D30=56.1
D32=61.5
S=18.37
KURTOSIS=-.26

EERC/EPA DATA
SDL TASK5 RUN 3R

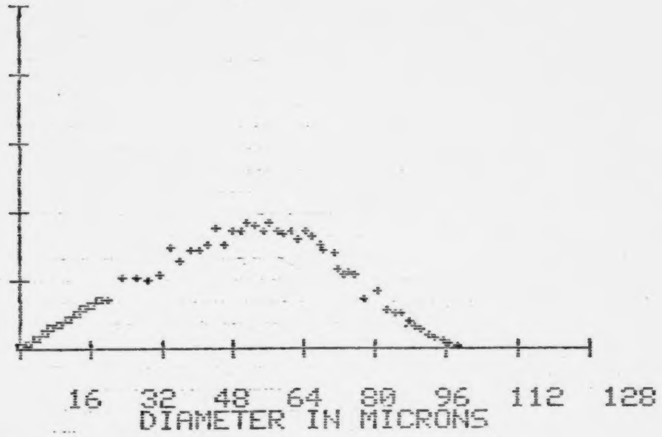

MAXIMUM FREQUENCY=.1

N=10998
D10=53.2
D20=56.7
D30=59.3
D32=65
S=19.66
KURTOSIS=-.38

EERC/EPA DATA
SDL TASK5 RUN 4R

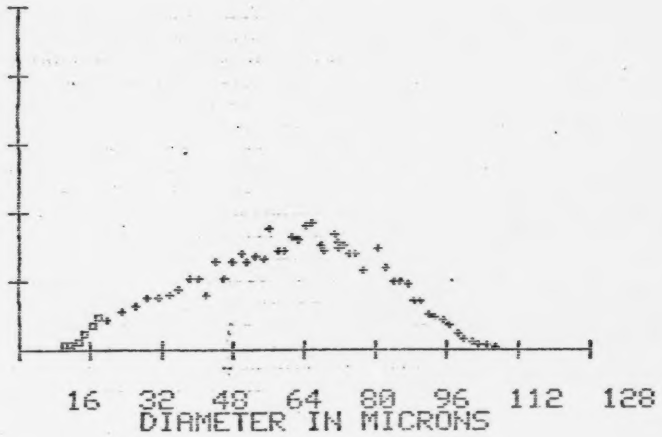

MAXIMUM FREQUENCY=.1

N=10683
D10=62.1
D20=64.9
D30=67.2
D32=72.1
S=18.97
KURTOSIS=-.37

EERC/EPA DATA
SDL TASK5 RUN 5R

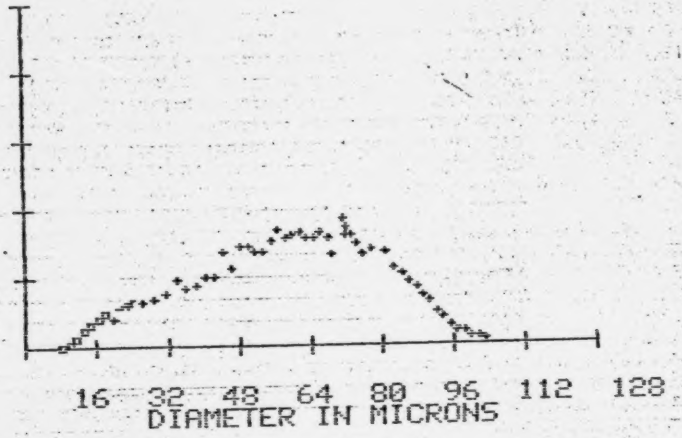

MAXIMUM FREQUENCY=.1

N=10673
D10=61.2
D20=64
D30=66.3
D32=71
S=18.78
KURTOSIS=-.41

EERC/EPA DATA
SDL TASK5 RUN 6R

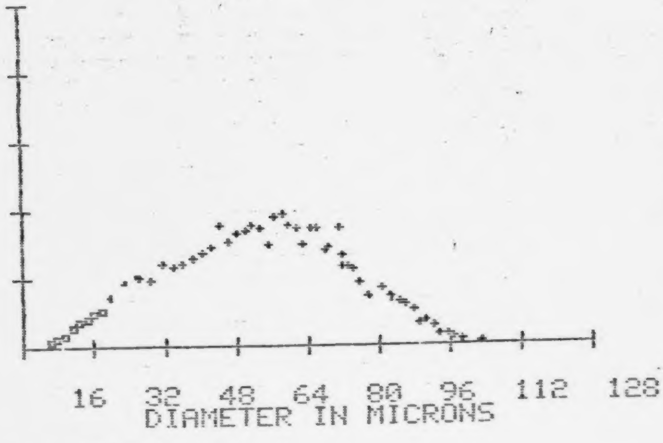

MAXIMUM FREQUENCY=.1

N=10323
D10=55.5
D20=58.6
D30=61
D32=66.3
S=18.73
KURTOSIS=-.29

EERC/EPA DATA
SDL TASK5 RUN 7R

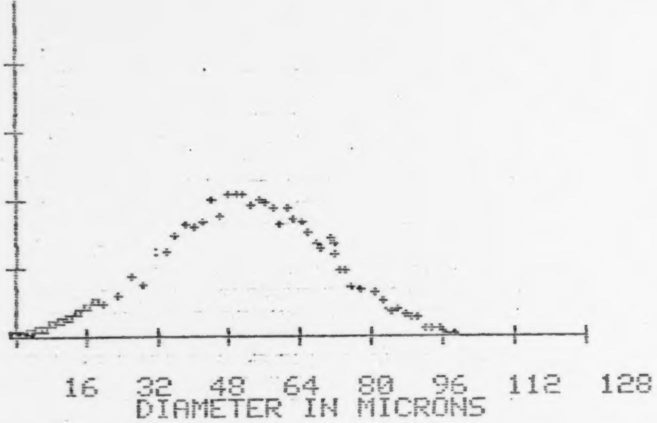

MAXIMUM FREQUENCY=.1

N=9343
D10=54
D20=56.7
D30=59
D32=63.7
S=17.4
KURTOSIS=-.32

SDL TASK5 RUN 8R

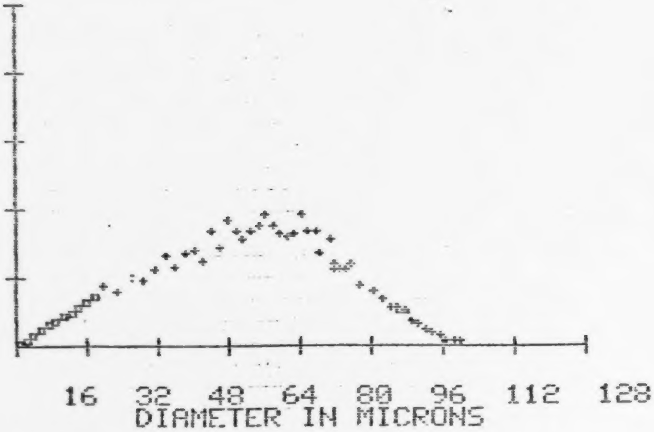

MAXIMUM FREQUENCY=.1

N=10523
D10=54.1
D20=57.7
D30=60.4
D32=66.2
S=19.97
KURTOSIS=-.4

EERC/EPA DATA
SDL TASK5 RUN 9R

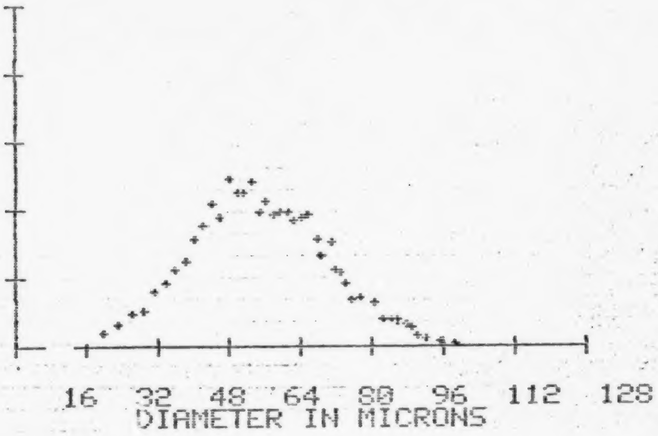

MAXIMUM FREQUENCY=.1

N=8553
D10=53
D20=55.9
D30=58.2
D32=63.2
S=17.91
KURTOSIS=-.37

EERC/EPA DATA
SDL TASK5 RUN 10R

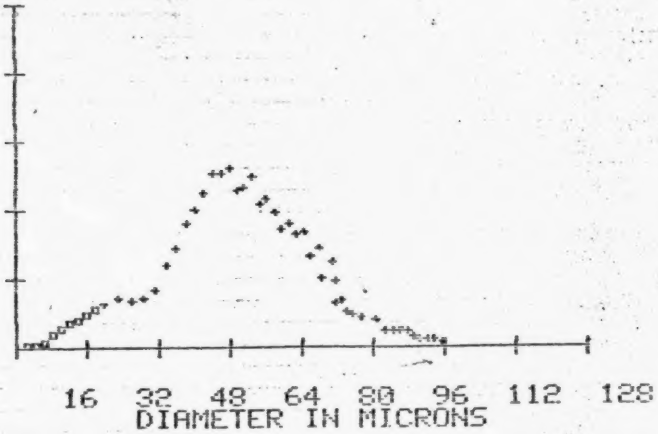

MAXIMUM FREQUENCY=.1

N=7473
D10=51.7
D20=54.2
D30=56.2
D32=60.4
S=16.06
KURTOSIS=-.29

SDL TASK5 RUN 11R

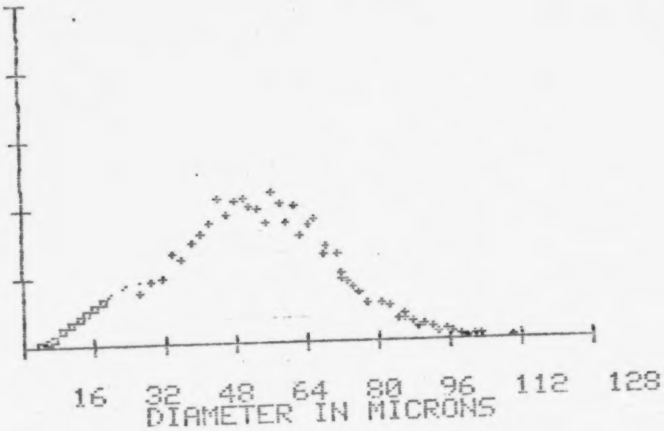

MAXIMUM FREQUENCY=.1

N=9039
D10=53.5
D20=56.5
D30=58.9
D32=64.1
S=18.05
KURTOSIS=-.2

SDL TASK5C RUN 1R

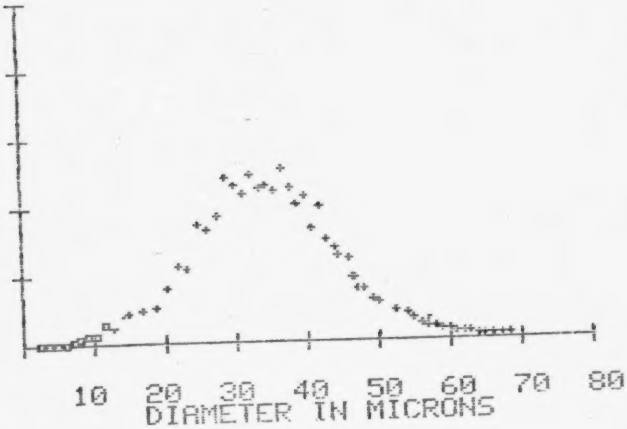

MAXIMUM FREQUENCY=.1

N=7521
D10=36
D20=37.3
D30=38.4
D32=40.9
S=9.59
KURTOSIS=.1

SDL TASK5C RUN 3R

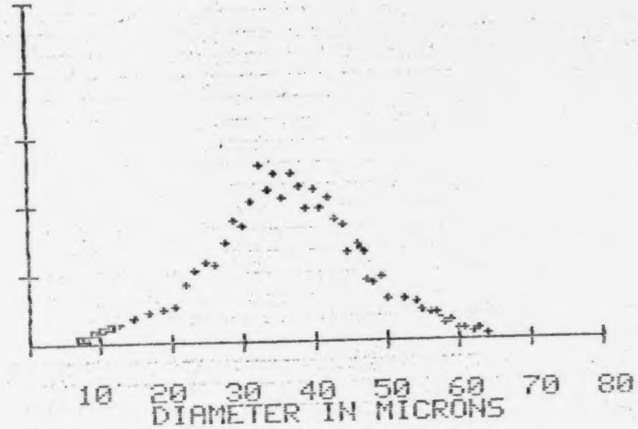

MAXIMUM FREQUENCY=.1

N=7410
D10=37.4
D20=38.7
D30=39.8
D32=42.1
S=9.76
KURTOSIS=-.16

EERC/EPA DATA
SDL TASK5C RUN 5R

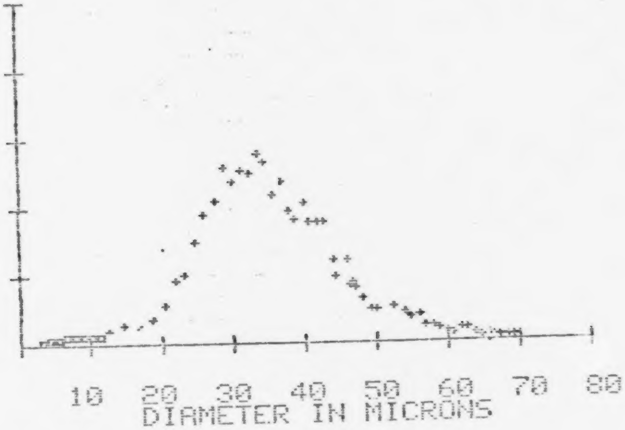

MAXIMUM FREQUENCY=.1

N=6855
D10=36.3
D20=37.6
D30=38.8
D32=41.4
S=9.82
KURTOSIS=.2

SDL TASK5C RUN 4R

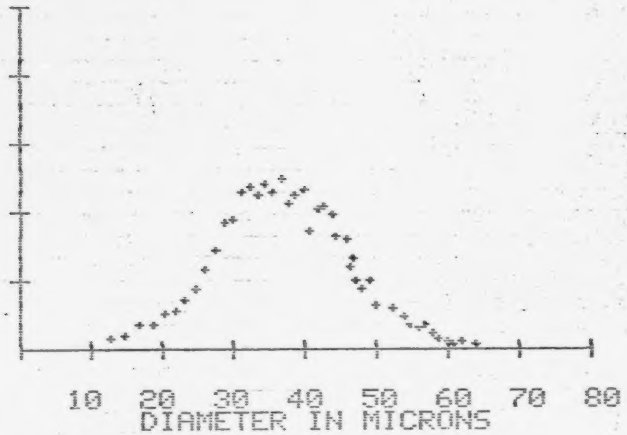

```
MAXIMUM FREQUENCY=.1

 N=8460
 D10=35.3
 D20=37.2
 D30=38.6
 D32=41.5
 S=11.49
 KURTOSIS=-.54
```

EERC/EPA DATA
SDL TASK5C RUN 6

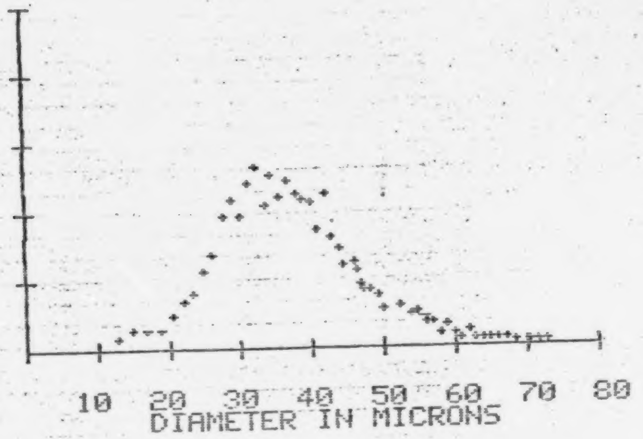

MAXIMUM FREQUENCY=.1

N=7940
D10=35.2
D20=37.3
D30=38.9
D32=42.5
S=12.12
KURTOSIS=-.16

EERC/EPA DATA
SDL TASK5C RUN 7R

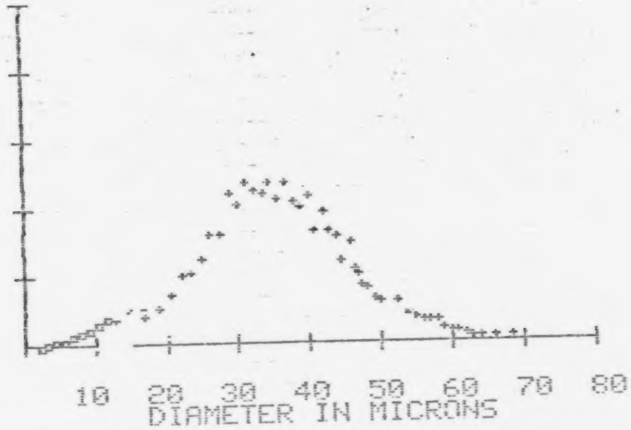

MAXIMUM FREQUENCY=.1

N=8091
D10=36.4
D20=37.8
D30=39
D32=41.5
S=10.16
KURTOSIS=-.12

EERC/EPA DATA
SDL TASK5C RUN 8R

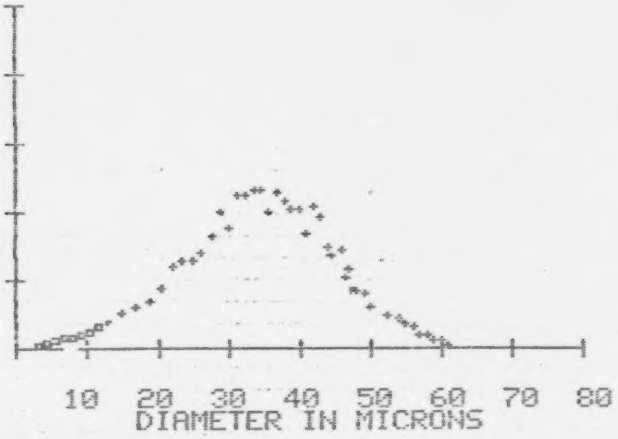

MAXIMUM FREQUENCY=.1

N=8289
D10=35.7
D20=37.1
D30=38.2
D32=40.6
S=9.98
KURTOSIS=-.38

EERC/EPA DATA
SDL TASK5C RUN 9R

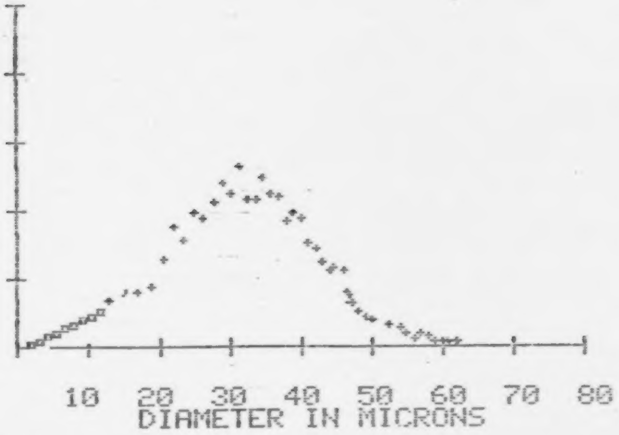

MAXIMUM FREQUENCY=.1

N=7377
D10=33
D20=34.7
D30=36
D32=38.8
S=10.46
KURTOSIS=-.27

SDL TASK5C RUN 10R

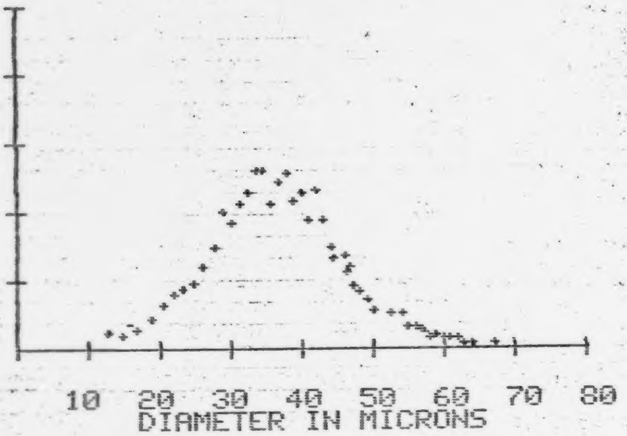

MAXIMUM FREQUENCY=.1

N=8057
D10=34.9
D20=36.8
D30=38.2
D32=41.3
S=11.55
KURTOSIS=-.42

EERC/EPA DATA
SDL TASK5C RUN 11

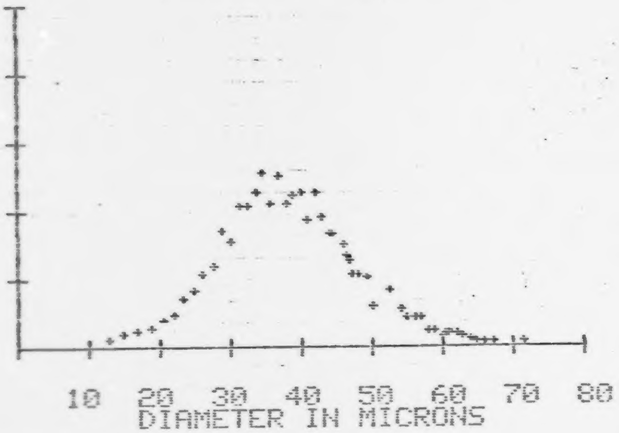

MAXIMUM FREQUENCY=.1

N=8294
D10=36.2
D20=38.1
D30=39.6
D32=42.8
S=11.95
KURTOSIS=-.45

EERC/EPA DATA
SDL TASK5C RUN 12R

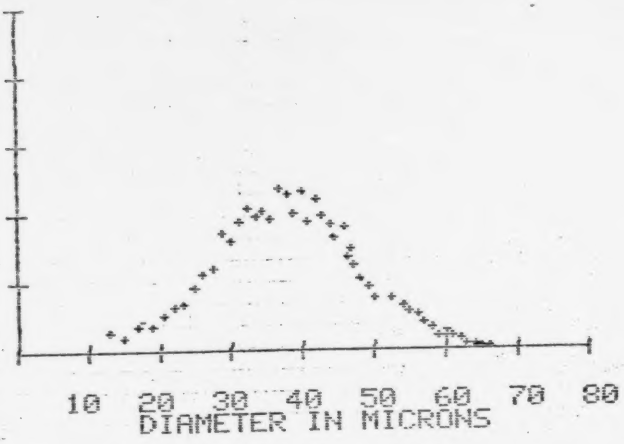

```
MAXIMUM FREQUENCY=.1

 N=8892
 D10=36
 D20=38
 D30=39.5
 D32=42.7
 S=12.06
 KURTOSIS=-.5
```

EERC/EPA DATA
SDL TASK5C RUN 13R

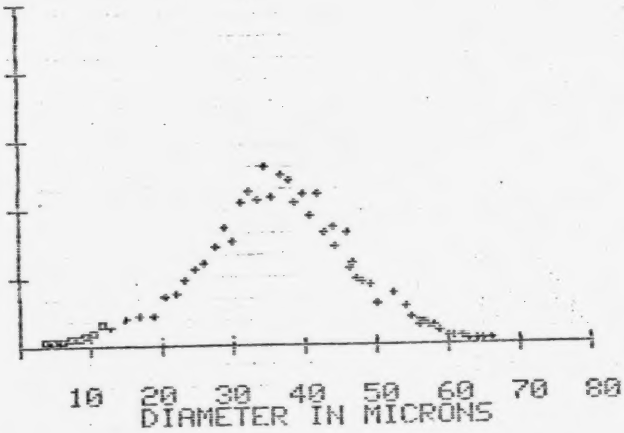

```
MAXIMUM FREQUENCY=.1

 N=7368
 D10=37.2
 D20=38.5
 D30=39.6
 D32=41.9
 S=9.9
 KURTOSIS=-.33
```

EERC/EPA DATA
SDL TASK5C RUN 14R

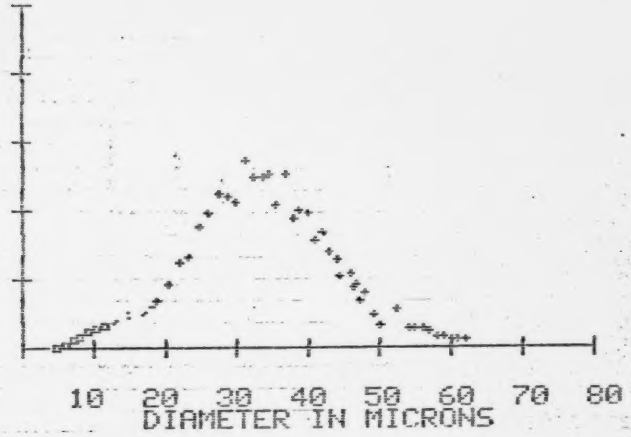

MAXIMUM FREQUENCY=.1

N=7043
D10=34.8
D20=36.1
D30=37.3
D32=39.8
S=9.69
KURTOSIS=-.11

EERC/EPA DATA
SDL TASK5C RUN 15R

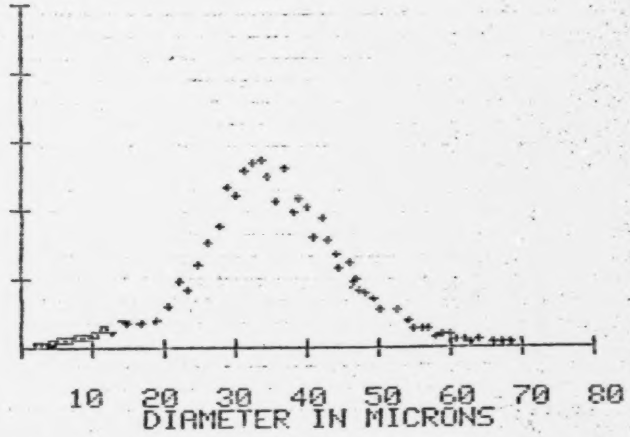

MAXIMUM FREQUENCY=.1

N=7046
D10=36.3
D20=37.6
D30=38.7
D32=41.2
S=9.87
KURTOSIS=-.09

SDL TASK5C RUN 16R

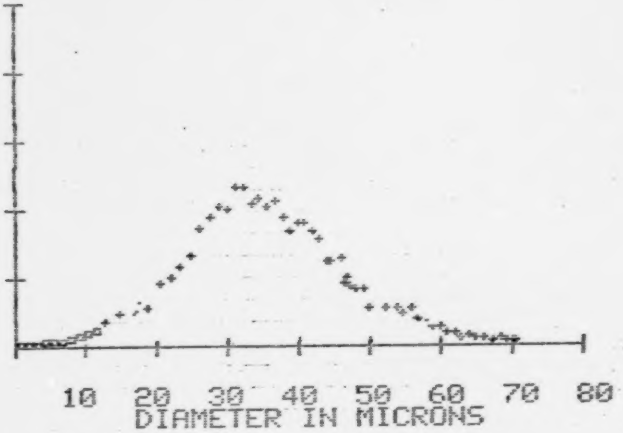

MAXIMUM FREQUENCY=.1

N=8173
D10=36.7
D20=38.3
D30=39.7
D32=42.7
S=10.93
KURTOSIS=.07

EERC/EPA DATA
SDL TASK5C RUN 17R

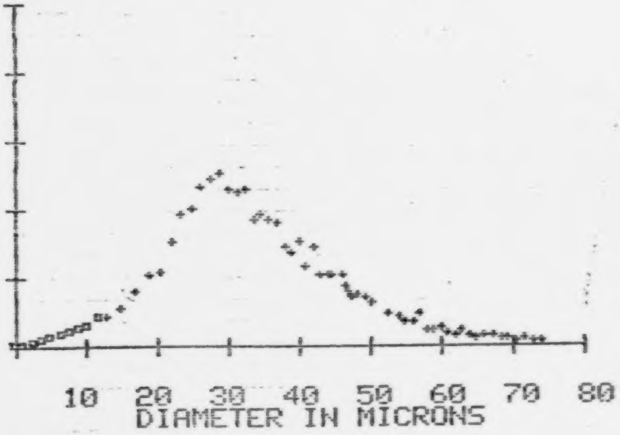

MAXIMUM FREQUENCY=.1

N=7608
D10=34.8
D20=36.8
D30=38.7
D32=42.7
S=12.1
KURTOSIS=.31

SDL TASK5C RUN 18R

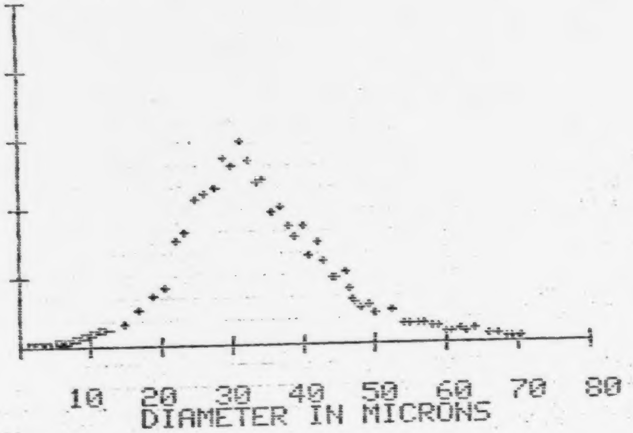

MAXIMUM FREQUENCY=.1

N=6417
D10=34.9
D20=36.4
D30=37.9
D32=40.9
S=10.37
KURTOSIS=.44

EERC/EPA DATA
SDL TASK5C RUN 19R

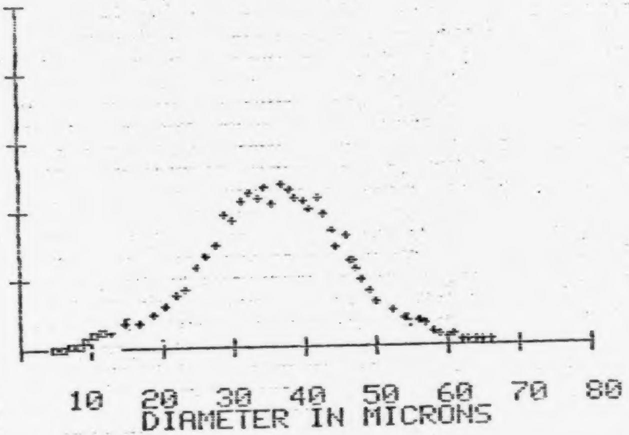

MAXIMUM FREQUENCY=.1

N=8165
D10=37.4
D20=38.5
D30=39.6
D32=41.7
S=9.4
KURTOSIS=-.17

EERC/EPA DATA
SDL TASK5C RUN 20R

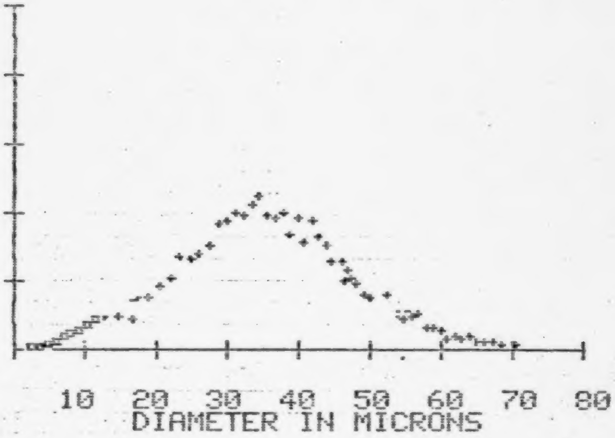

MAXIMUM FREQUENCY=.1

N=7365
D10=36.7
D20=38.4
D30=39.9
D32=43.1
S=11.52
KURTOSIS=-.11

EERC/EPA DATA
SDL TASK5C RUN 21R

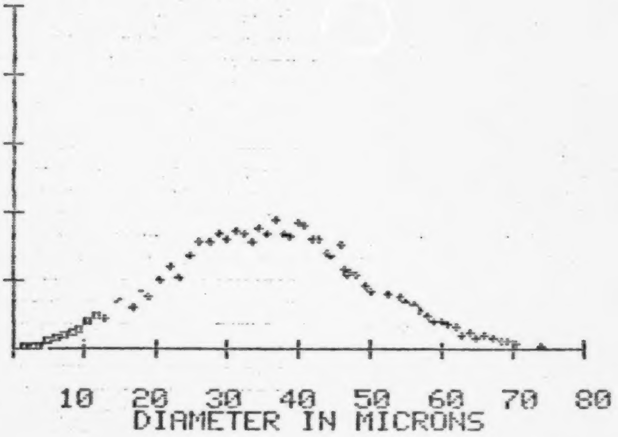

MAXIMUM FREQUENCY=.1

N=8737
D10=37.5
D20=39.6
D30=41.3
D32=44.9
S=12.5
KURTOSIS=-.07

EERC/EPA DATA
SDL TASK5C RUN 22R

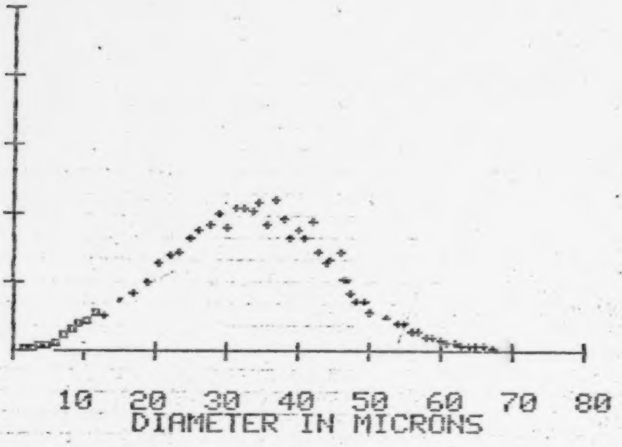

MAXIMUM FREQUENCY=.1

N=8969
D10=34.7
D20=36.4
D30=37.9
D32=41
S=11.18
KURTOSIS=-.17

EERC/EPA DATA
SDL TASK5C RUN 23R

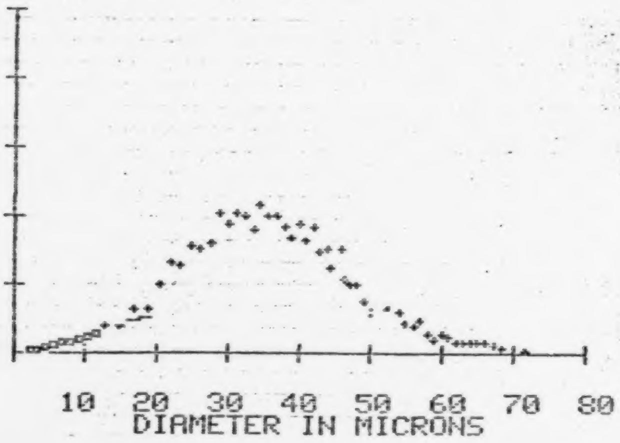

MAXIMUM FREQUENCY=.1

N=7993
D10=36.6
D20=38.3
D30=39.8
D32=42.9
S=11.24
KURTOSIS=.01

EERC/EPA DATA
SDL TASK5C RUN 24R

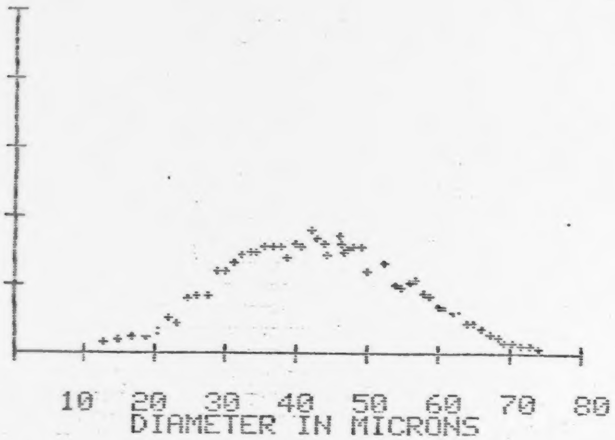

MAXIMUM FREQUENCY=.1

N=11869
D10=40.2
D20=42.7
D30=44.7
D32=48.8
S=14.51
KURTOSIS=-.37

SDL TASK5C RUN 25R

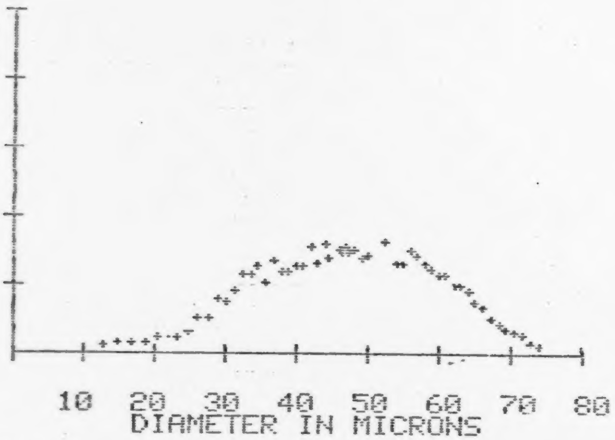

MAXIMUM FREQUENCY=.1

N=11666
D10=43.6
D20=46.3
D30=48.2
D32=52.4
S=15.55
KURTOSIS=-.56

SDL TASK5C RUN 26R

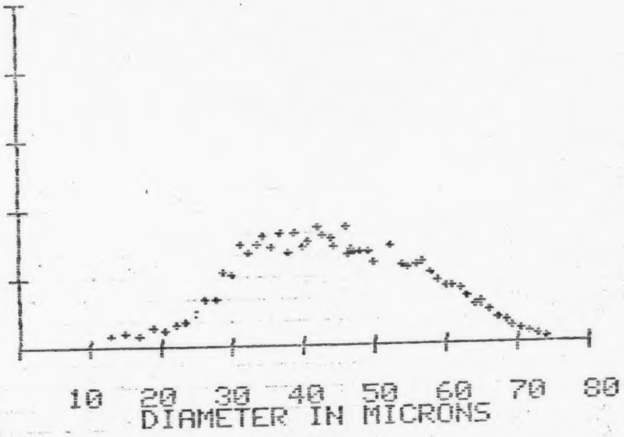

MAXIMUM FREQUENCY=.1

N=12267
D10=41.2
D20=43.8
D30=45.8
D32=50.1
S=14.92
KURTOSIS=-.39

SDL TASK5C RUN 2R

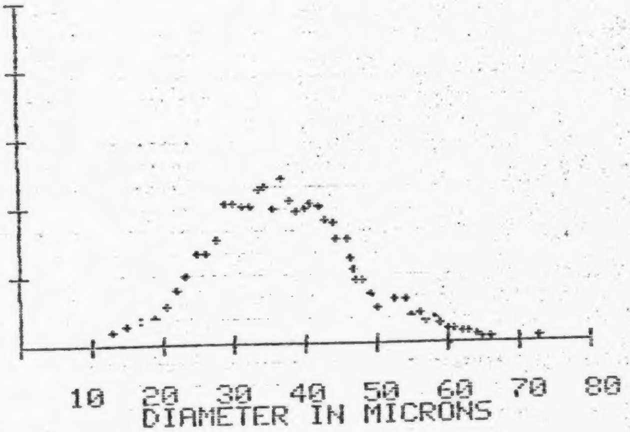

MAXIMUM FREQUENCY=.1

N=8766
D10=35.3
D20=37.3
D30=38.9
D32=42.4
S=12.13
KURTOSIS=-.28

EERC/EPA DATA
SDL TASK6 RUN 1R

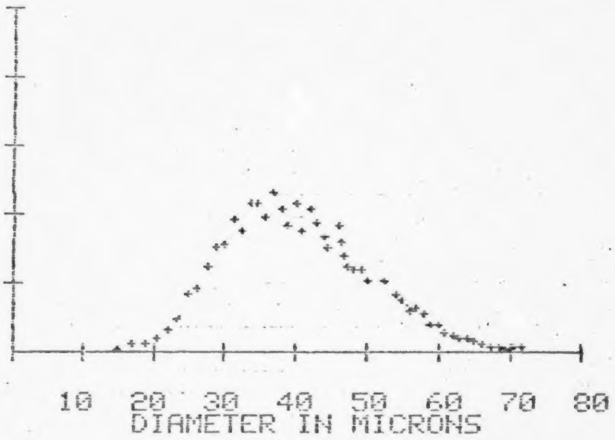

MAXIMUM FREQUENCY=.1

N=8185
D10=40.9
D20=41.9
D30=43
D32=45.2
S=9.43
KURTOSIS=.32

EERC/EPA DATA
SDL TASK6 RUN 2R

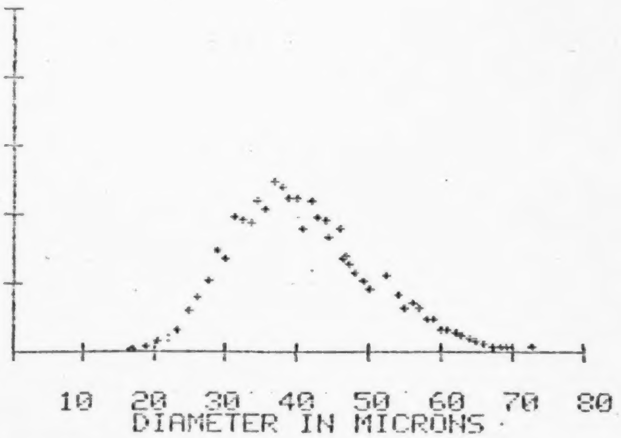

MAXIMUM FREQUENCY=.1

N=7612
D10=41.2
D20=42.2
D30=43.2
D32=45.2
S=9.1
KURTOSIS=.42

SDL TASK6 RUN 3R

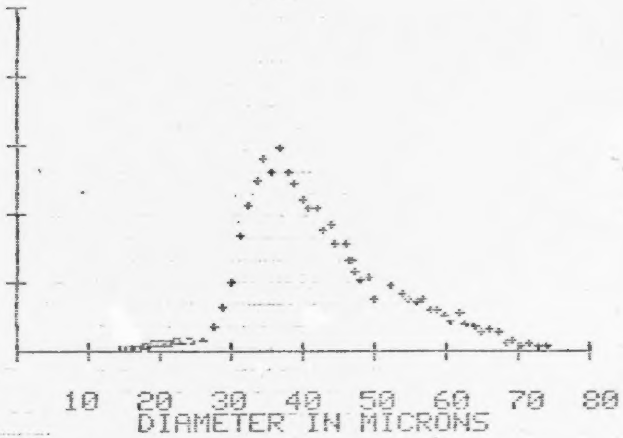

```
MAXIMUM FREQUENCY=.1

 N=6445
 D10=42.6
 D20=43.7
 D30=44.8
 D32=47.1
 S=9.63
 KURTOSIS=.68
```

SDL TASK6 RUN 4R

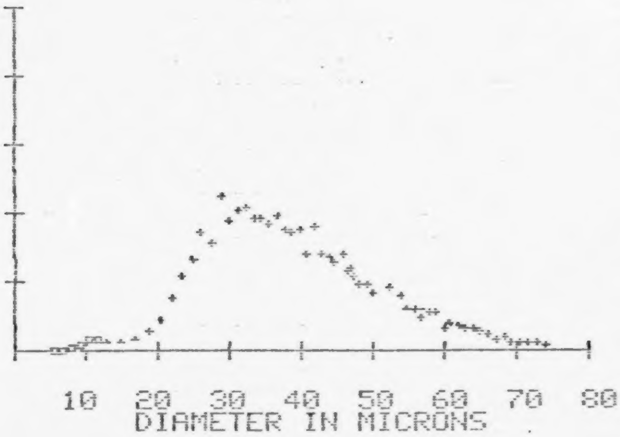

```
MAXIMUM FREQUENCY=.1

 N=8390
 D10=39.5
 D20=41.1
 D30=42.6
 D32=45.8
 S=11.3
 KURTOSIS=.39
```

SDL TASK6 RUN 5R

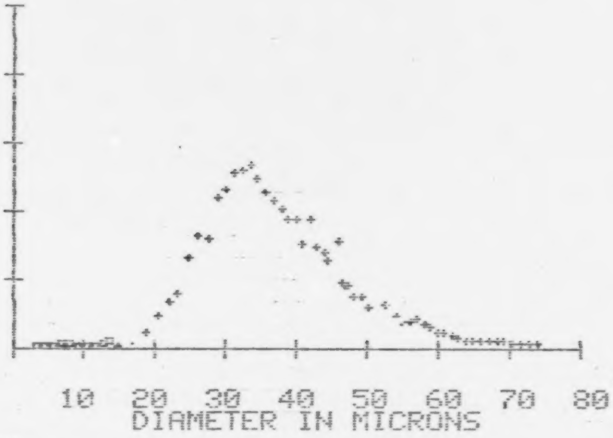

MAXIMUM FREQUENCY=.1

N=7131
D10=38
D20=39.3
D30=40.6
D32=43.4
S=10.15
KURTOSIS=.44

SDL TASK6 RUN 6R

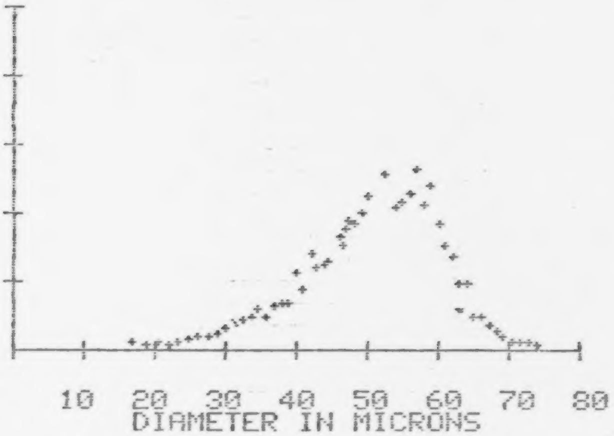

MAXIMUM FREQUENCY=.1

N=8162
D10=46.9
D20=49
D30=50.5
D32=53.6
S=14.3
KURTOSIS=-1.08

```
EERC/EPA DATA
SDL TASK10 RUN 1
```

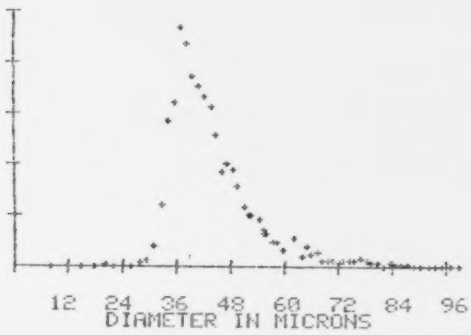

```
MAXIMUM FREQUENCY=0.1

N=3055
D10=44.2
D20=45.1
D30=46.1
D32=48.2
S=8.95
KURTOSIS=1.41

    SIZE         COUNT

    98.9           0
    97.1           0
    95.4           0
    93.8           0
    92.2           0
    90.7           0
    89.2           0
    87.7           2
    86.3           2
    84.9           1
    83.5           4
    82.2           0
    80.9           4
    79.6           3
    78.3           6
    77.1           8
    75.8           7
    74.6           5
    73.4           6
    72.1           3
    70.9           7
    69.8           7
    68.6           5
    67.4          17
    66.2          14
    65.1          22
    63.9         10
    62.3          33
    59.6          19
    58.4          27
    57.2          27
    56.1          38
    55.5          38
    55.2          44
    54.6          54
    53.7          51
    52.2          59
    51.1          69
    49.9          95
    48.7         114
    47.4         122
    46.2         112
      45         156
    43.7         169
    42.4         202
    41.1         215
    39.8         226
    38.4         265
    37.1         285
    35.6         194
    34.2         173
    32.7          72
    31.2          23
    29.6           7
    27.9           4
    26.2           0
    24.3           0
    22.3           0
    20.2           1
    17.9           0
    15.3           0
    12.2           0
     8.2           0
```

```
EERC/EPA DATA
SDL TASK10 RUN 1R
```

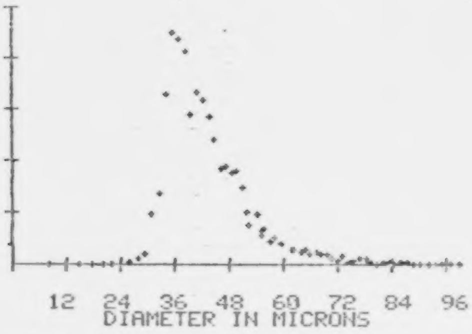

```
MAXIMUM FREQUENCY=0.1

N=3055
D10=43.6
D20=44.5
D30=45.5
D32=47.5
S=8.81
KURTOSIS=1.28

     SIZE         COUNT

     98.9           0
     97.1           0
     95.4           0
     93.8           0
     92.2           0
     90.7           0
     89.2           0
     87.7           2
     86.3           3
     84.9           1
     83.5           2
     82.2           2
     80.9           0
     79.6           1
     78.3           6
     77.1           5
     75.8           3
     74.6           2
     73.4           8
     72.1           4
     70.9           5
     69.8          11
     68.6          11
     67.4          14
     66.2          12
     65.1          17
     63.9         13
     62.3          15
     59.6          23
     58.4          30
     57.2          26
     56.1          40
     55.5          34
     55.2          39
     54.6          58
     53.7          46
     52.2          61
     51.1          90
     49.9         108
     48.7         107
     47.4         114
     46.2         111
       45         147
     43.7         171
     42.4         192
     41.1         202
     39.8         175
     38.4         251
     37.1         265
     35.6         273
     34.2         200
     32.7          82
     31.2          58
     29.6          11
     27.9           5
     26.2           2
     24.3           0
     22.3           0
     20.2           0
     17.9           0
     15.3           0
     12.3           0
      8.2           0
```

EERC/EPA DATA
SDL TASK10 RUN 2

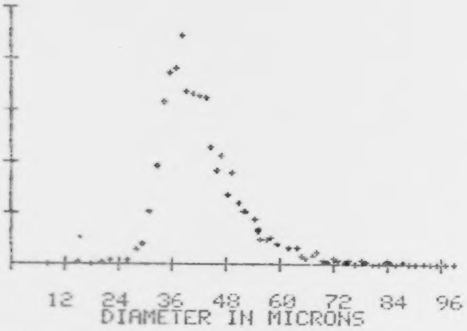

```
MAXIMUM FREQUENCY=0.1

N=3051
D10=43.1
D20=43.9
D30=44.8
D32=46.6
S=8.37
KURTOSIS=1.04

       SIZE           COUNT

       98.9             0
       97.1             0
       95.4             0
       93.8             0
       92.2             0
       90.7             0
       89.2             0
       87.7             1
       86.3             0
       84.9             1
       83.5             1
       82.2             0
       80.9             0
       79.6             1
       78.3             4
       77.1             0
       75.8             4
       74.6             2
       73.4             4
       72.1             6
       70.9             1
       69.8             3
       68.6            13
       67.4             9
       66.2             7
       65.1             9
       63.9            19
       62.3           19
       59.6            23
       58.4            31
       57.2            28
       56.1            29
       55.5            40
       55.2            38
       54.6            53
       53.7            63
       52.2            62
       51.1            71
       49.9           108
       48.7            83
       47.4           128
       46.2           111
         45           138
       43.7           195
       42.4           199
       41.1           201
       39.8           205
       38.4           270
       37.1           230
       35.6           226
       34.3           191
       32.7           117
       31.2            63
       29.6            24
       27.9            15
       25.9             3
       24.3             0
       22.3             3
       20.2             1
       17.8             0
       15.3             1
       12.2             0
        8.2             0
```

```
EERC/EPA DATA
SDL TASK10 RUN 2R
```

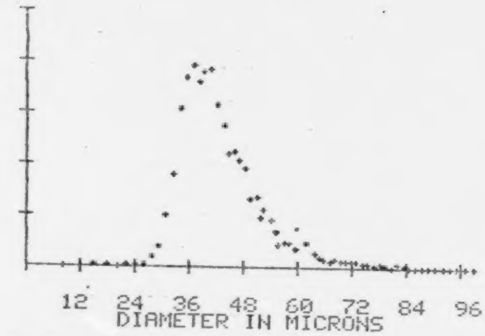

```
MAXIMUM FREQUENCY=0.1

N=3056
D10=43.4
D20=44.2
D30=45.1
D32=46.9
S=8.5
KURTOSIS=1.08

       SIZE           COUNT

       98.9             0
       97.1             0
       95.4             0
       93.8             0
       92.2             0
       90.7             0
       89.2             0
       87.7             0
       86.3             0
       84.9             0
       83.5             1
       82.2             3
       80.9             0
       79.6             2
       78.3             4
       77.1             2
       75.8             3
       74.6             3
       73.4             6
       72.1             6
       70.9             5
       69.8             7
       68.6             8
       67.4             7
       66.2             8
       65.1            12
       63.9            15
       62.3           28
       59.6            20
       58.4            27
       57.2            28
       56.1            26
       55.5            40
       55.2            43
       54.6            56
       52.7            67
       52.2            58
       51.1            83
       49.9            80
       48.7           116
       47.4           127
       46.2           135
         45           133
       43.7           168
       42.4           191
       41.1           232
       39.8           230
       38.4           220
       37.1           238
       35.6           223
       34.2           188
       32.7           109
       31.2            59
       29.6            23
       27.9            10
       26.2             1
       24.3             2
       22.3             2
       20.2             0
       17.3             1
       15.3             1
       12.2             0
        8.2             0
```

```
CERC/EPA DATA
SDL TASK10 RUN 3
```

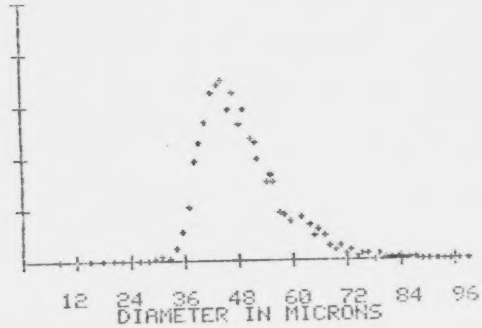

```
MAXIMUM FREQUENCY=0.1

N=3060
D10=49.3
D20=50
D30=50.7
D32=52.1
S=8.21
KURTOSIS=.93

     SIZE          COUNT

     98.9            0
     97.1            0
     95.4            0
     93.8            0
     92.2            0
     90.7            0
     89.2            0
     87.7            1
     86.3            2
     84.9            2
     83.5            2
     82.2            1
     80.9            2
     79.6            5
     78.3            0
     77.1            5
     75.8            5
     74.6            4
     73.4           12
     72.1            6
     70.9           15
     69.8           12
     68.6           15
     67.4           27
     66.2           35
     65.1           27
     63.9           48
     62.3           50
     59.6           46
     58.4           53
     57.2           56
     56.1           91
     55.5          101
     55.2           99
     54.6           93
     52.7          119
     52.2          139
     51.1          144
     49.9          177
     48.7          160
     47.4          196
     46.2          177
       45          211
     43.7          206
     42.4          196
     41.1          162
     39.8          137
     38.4          115
     37.1           63
     35.6           33
     34.2           13
     32.7            2
     31.2            3
     29.6            1
     27.9            0
     26.2            0
     24.3            0
     22.3            0
     20.2            0
     17.9            0
     15.3            0
     12.2            0
      8.2            0
```

```
EERC/EPA DATA
SDL TASK10 RUN 3R
```

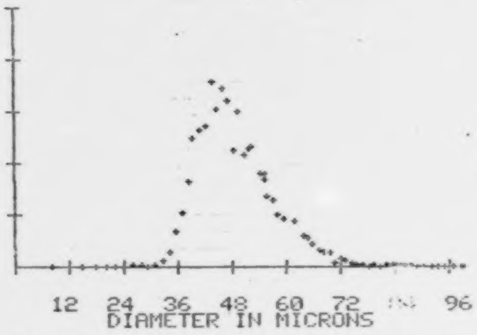

```
MAXIMUM FREQUENCY=0.1

N=3062
D10=49.2
D20=49.8
D30=50.4
D32=51.7
S=7.84
KURTOSIS=.69

    SIZE         COUNT

     98.9          0
     97.1          0
     95.4          0
     93.8          0
     92.2          0
     90.7          0
     89.2          0
     87.7          1
     86.3          1
     84.9          1
     83.5          1
     82.2          2
     80.9          0
     79.6          1
     78.3          0
     77.1          2
     75.8          2
     74.6          3
     73.4          5
     72.1          9
     70.9          4
     69.8         17
     68.6         16
     67.4         19
     66.2         26
     65.1         34
     63.9         35
     62.3         52
     59.6         55
     58.4         59
     57.2         77
     56.1         83
     55.5        109
     55.2        102
     54.6        108
     52.7        142
     52.2        139
     51.1        132
     49.9        184
     48.7        137
     47.4        194
     46.2        208
       45        185
     43.7        216
     42.4        164
     41.1        160
     39.8        150
     38.4         98
     37.1         64
     35.6         41
     34.2         15
     32.7          5
     31.2          2
     29.6          0
     27.9          2
     26.2          1
     24.3          0
     22.3          0
     20.2          0
     17.9          0
     15.3          0
     12.2          0
      8.2          0
```

```
EERC/EPA DATA
SDL TASK10 RUN 4
```

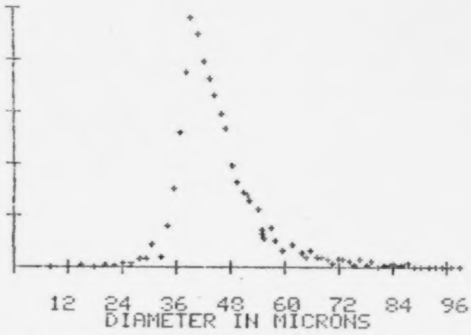

```
MAXIMUM FREQUENCY=0.1

N=3053
D10=45.5
D20=46.3
D30=47.1
D32=48.8
S=8.35
KURTOSIS=1.3

     SIZE           COUNT

      98.9             0
      97.1             0
      95.4             0
      93.8             0
      92.2             0
      90.7             0
      89.2             0
      87.7             3
      86.3             2
      84.9             1
      83.5             2
      82.2             1
      80.9             0
      79.6             5
      78.3             2
      77.1             9
      75.8             1
      74.6             7
      73.4             8
      72.1             8
      70.9             4
      69.8             9
      68.6            11
      67.4            11
      66.2            18
      65.1            11
      63.9           17
      62.3            26
      59.6            19
      58.4            31
      57.2            46
      56.1            33
      55.5            42
      55.2            39
      54.6            67
      53.7            76
      52.2            85
      51.1            87
      49.9            99
      48.7           120
      47.4           162
      46.2           178
        45           200
      43.7           221
      42.4           240
      41.1           271
      39.8           291
      38.4           229
      37.1           158
      35.6            91
      34.2            49
      32.7            11
      31.2            25
      29.6             8
      27.9             9
      26.2             3
      24.3             3
      22.3             2
      20.2             1
      17.9             0
      15.3             1
      12.3             0
       8.2             0
```

```
EERC/EPA DATA
SDL TASK10 RUN 4R
```

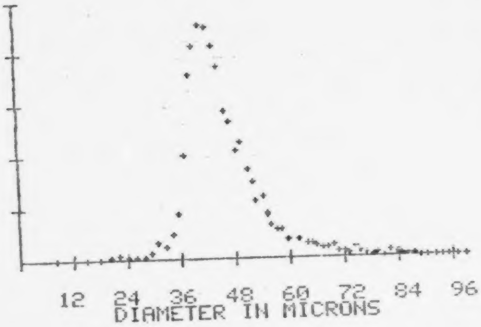

```
MAXIMUM FREQUENCY=0.1

N=3057
D10=46.1
D20=46.8
D30=47.6
D32=49.2
S=8.1
KURTOSIS=1.35

     SIZE        COUNT

     98.9          0
     97.1          0
     95.4          0
     93.8          0
     92.2          0
     90.7          0
     89.2          0
     87.7          1
     86.3          1
     84.9          1
     83.5          4
     82.2          5
     80.9          0
     79.6          4
     78.3          2
     77.1          3
     75.8          6
     74.6         10
     73.4          4
     72.1          6
     70.9          6
     69.8         14
     68.6         11
     67.4         11
     66.2         14
     65.1         16
     63.9        17
     62.3          21
     59.6          20
     58.4          32
     57.2          33
     56.1          39
     55.5          51
     55.2          53
     54.6          73
     53.7          68
     52.2          90
     51.1         103
     49.9         136
     48.7         127
     47.4         159
     46.2         173
       45         225
     43.7         250
     42.4         274
     41.1         276
     39.8         251
     38.4         218
     37.1         121
     35.6          52
     34.2          29
     32.7          14
     31.2          18
     29.6           7
     27.9           2
     26.2           1
     24.3           1
     22.3           3
     20.3           1
     17.9           0
     15.3           0
     12.3           0
      8.2           0
```

```
EERC/EPA DATA
SDL TASK10 RUN 4RR
```

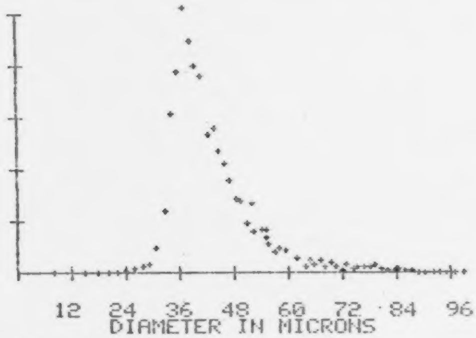

```
MAXIMUM FREQUENCY=0.1

N=3050
D10=43.7
D20=44.6
D30=45.6
D32=47.7
S=8.96
KURTOSIS=1.52
     SIZE          COUNT

      98.9           0
      97.1           0
      95.4           0
      93.8           0
      92.2           0
      90.7           0
      89.2           0
      87.7           1
      86.3           2
      84.9           3
      83.5           2
      82.2           2
      80.9           4
      79.6           8
      78.3           6
      77.1           5
      75.8           7
      74.6           4
      73.4           9
      72.1           2
      70.9           6
      69.8          10
      68.6           6
      67.4          13
      66.2           8
      65.1          14
      63.9          7
      62.3          17
      59.6          25
      58.4          29
      57.2          23
      56.1          33
      55.5          50
      55.2          40
      54.6          49
      52.7          47
      52.2          81
      51.1          58
      49.9          84
      48.7          86
      47.4         109
      46.2         129
         45        144
      43.7         168
      42.4         163
      41.1         231
      39.8         242
      38.4         271
      37.1         310
      35.6         237
      34.2         186
      32.7          72
      31.2          29
      29.6           9
      27.9           5
      26.2           3
      24.3           2
      22.3           0
      20.2           0
      17.5           0
      15.3           0
      12.2           0
       8.2           0
```

```
TERC/EPA DATA
SDL TASK10 RUN 5
```

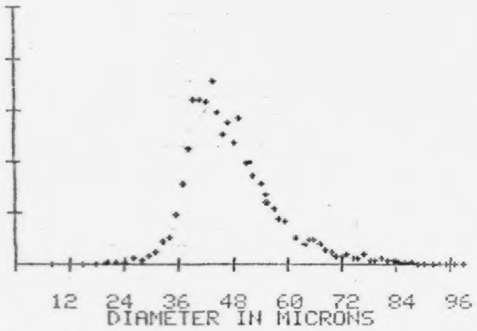

```
MAXIMUM FREQUENCY=0.1

N=3054
D10=48.2
D20=49
D30=49.9
D32=51.7
S=9
KURTOSIS=.92
     SIZE          COUNT

      98.9            0
      97.1            0
      95.4            0
      93.8            0
      92.2            0
      90.7            0
      89.2            0
      87.7            2
      86.3            2
      84.9            2
      83.5            3
      82.2            3
      80.9            6
      79.6            3
      78.3            3
      77.1           10
      75.8            7
      74.6            5
      73.4           11
      72.1            9
      70.9            9
      69.8           13
      68.6           16
      67.4           24
      66.2           27
      65.1           29
      63.9          23
      62.3           31
      59.6           50
      58.4           53
      57.2           64
      56.1           73
      55.5           72
      55.2           81
      54.6           95
      53.7          103
      52.2          120
      51.1          118
      49.9          173
      48.7          143
      47.4          167
      46.2          154
        45          178
      43.7          216
      42.4          192
      41.1          194
      39.8          195
      38.4          136
      37.1           94
      35.6           56
      34.2           30
      32.7           25
      31.2           14
      29.6            8
      27.9            4
      26.2            7
      24.3            1
      22.3            1
      20.2            1
      17.9            0
      15.3            0
      12.2            0
       8.2            0
```

```
EERC/EPA DATA
SDL TASK10 RUN 5R
```

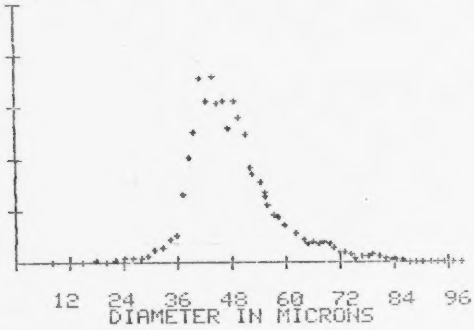

```
MAXIMUM FREQUENCY=0.1

N=3055
D10=48.5
D20=49.3
D30=50.2
D32=51.9
S=8.76
KURTOSIS=.94

   SIZE         COUNT

    98.9          0
    97.1          0
    95.4          0
    93.8          0
    92.2          0
    90.7          0
    89.2          0
    87.7          0
    86.3          1
    84.9          1
    83.5          1
    82.2          4
    80.9          5
    79.6          8
    78.3          7
    77.1          5
    75.8          4
    74.6          9
    73.4         11
    72.1         12
    70.9         15
    69.8         20
    68.6         23
    67.4         21
    66.2         23
    65.1         20
    63.9        26
    62.3         32
    59.6         42
    58.4         53
    57.2         55
    56.1         66
    55.5         77
    55.2         83
    54.6         94
    52.7        105
    52.2        112
    51.1        151
    49.9        169
    48.7        190
    47.4        156
    46.2        189
      45        187
    43.7        218
    42.4        189
    41.1        217
    39.8        152
    38.4        122
    37.1         79
    35.6         31
    34.2         25
    32.7         15
    31.2         13
    29.6          5
    27.9          3
    26.2          4
    24.3          3
    22.3          1
    20.2          0
    17.9          1
    15.3          0
    12.2          0
     8.2          0
```

```
EERC/EPA DATA
SDL TASK10 RUN 5R
```

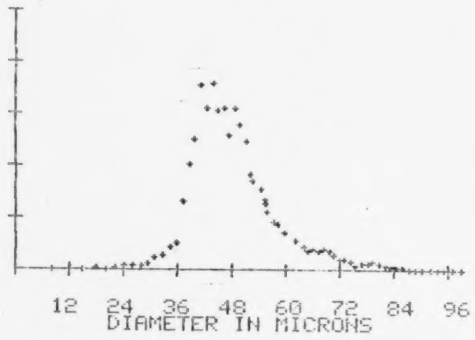

```
MAXIMUM FREQUENCY=0.1

N=3055
D10=48.5
D20=49.3
D30=50.2
D32=51.9
S=8.76
KURTOSIS=.94

     SIZE         COUNT

      98.9          0
      97.1          0
      95.4          0
      93.8          0
      92.2          0
      90.7          0
      89.2          0
      87.7          0
      86.3          1
      84.9          1
      83.5          1
      82.2          4
      80.9          5
      79.6          8
      78.3          7
      77.1          5
      75.8          4
      74.6          9
      73.4         11
      72.1         12
      70.9         15
      69.8         20
      68.6         23
      67.4         21
      66.2         23
      65.1         20
      63.9        26
      62.3         32
      59.6         42
      58.4         53
      57.2         55
      56.1         66
      55.5         77
      55.2         83
      54.6         94
      53.7        105
      52.2        112
      51.1        151
      49.9        169
      48.7        190
      47.4        156
      46.2        189
        45        187
      43.7        218
      42.4        189
      41.1        217
      39.8        152
      38.4        122
      37.1         79
      35.6         31
      34.2         25
      32.7         15
      31.2         13
      29.6          5
      27.9          3
      26.2          4
      24.3          3
      22.3          1
      20.2          0
      17.9          1
      15.3          0
      12.2          0
       8.2          0
```

```
EERC FPA DATA
SDL TASK10 RUN 6
```

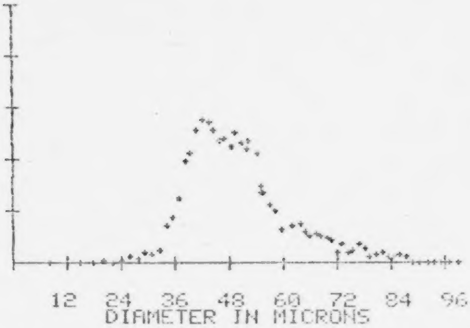

```
MAXIMUM FREQUENCY=0.1

N=3050
D10=50.4
D20=51.4
D30=52.6
D32=54.9
S=10.43
KURTOSIS=.89

     SIZE          COUNT

      98.9            0
      97.1            0
      95.4            0
      93.8            0
      92.2            0
      90.7            0
      89.2            0
      87.7            5
      86.3            8
      84.9            5
      83.5            6
      82.2           11
      80.9            9
      79.6            7
      78.3           17
      77.1           20
      75.8           14
      74.6           11
      73.4           21
      72.1           11
      70.9           26
      69.8           27
      68.6           30
      67.4           34
      66.2           30
      65.1           35
      63.9          46
      62.3           42
      59.6           37
      58.4           59
      57.2           66
      56.1           81
      55.5           90
      55.2           82
      54.6          129
      52.7          143
      52.2          132
      51.1          140
      49.9          153
      48.7          135
      47.4          146
      46.2          144
        45          155
      43.7          163
      42.4          167
      41.1          154
      39.8          129
      38.4          117
      37.1           76
      35.6           52
      34.2           42
      32.7           14
      31.2            8
      29.6           11
      27.9            4
      26.2            6
      24.3            [illegible]
      22.3            0
      20.2            1
      17.9            0
      15.3            0
      12.3            0
       8.2            0
```

EERC/EPA DATA
SDL TASK10 RUN 6R

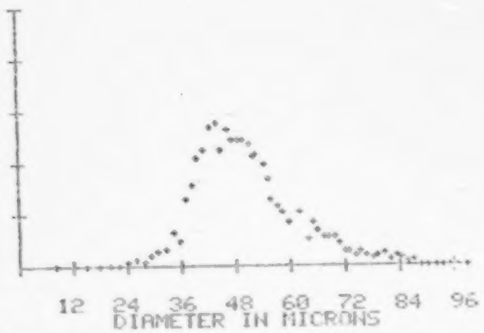

MAXIMUM FREQUENCY=0.1

N=3054
D10=50.9
D20=51.9
D30=53
D32=55.3
S=10.43
KURTOSIS=.84

SIZE	COUNT
98.9	0
97.1	0
95.4	0
93.8	0
92.2	0
90.7	0
89.2	0
87.7	6
86.3	4
84.9	9
83.5	12
82.2	7
80.9	13
79.6	11
78.3	9
77.1	12
75.8	15
74.6	12
73.4	15
72.1	16
70.9	26
69.8	33
68.6	33
67.4	34
66.2	41
65.1	51
63.9	30
[illegible]	62
[illegible]	50
59.6	63
58.4	69
57.2	77
[illegible]	102
[illegible]	102
[illegible]	119
[illegible]	131
52.2	129
51.1	142
49.9	148
48.7	149
47.4	148
46.2	159
45	138
43.7	168
42.4	166
41.1	136
39.8	125
38.4	93
37.1	76
35.6	28
34.2	39
32.7	19
31.2	15
29.8	10
[illegible]	8
[illegible]	5
[illegible]	3
[illegible]	8
[illegible]	0
[illegible]	0
[illegible]	0
[illegible]	0
8.2	0

```
CERC/EPA DATA
SDL TASK10 RUN 7
```

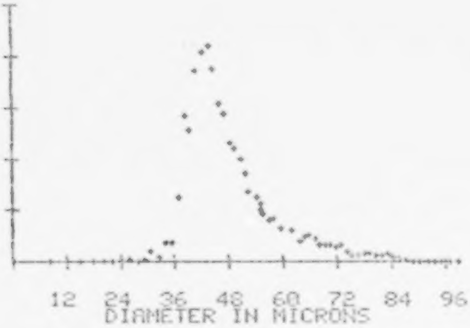

```
MAXIMUM FREQUENCY=0.1

N=3054
D10=48.5
D20=49.4
D30=50.3
D32=52.3
S=9.26
KURTOSIS=1.3

     SIZE           COUNT

     98.9             0
     97.1             0
     95.4             0
  [illegible]         0
  [illegible]         0
  [illegible]         0
     89.2             0
     87.5             1
     86.3             3
     84.9             3
     83.5             9
     82.3             5
     80.9             5
     79.6             8
     78.3             9
     77.1             6
     75.8             7
     74.6            10
     73.4            18
     72.1            17
     70.9            18
     69.8            19
     68.6            19
     67.4            26
     66.2            30
     65.1            27
     63.9         [illegible]
  [illegible]        35
  [illegible]        39
  [illegible]        49
  [illegible]        48
  [illegible]        54
  [illegible]        59
  [illegible]     [illegible]
  [illegible]     [illegible]
  [illegible]        83
  [illegible]       104
     51.1           121
     49.9           133
     48.7           140
     47.4           174
     46.2        [illegible]
     45             258
     43.7           256
     42.4           249
     41.1           227
     39.8           155
     38.4           172
     37.1         [illegible]
  [illegible]     [illegible]
  [illegible]        22
  [illegible]         4
  [illegible]        10
  [illegible]         1
  [illegible]         0
  [illegible]         2
  [illegible]         1
  [illegible]         0
  [illegible]         0
  [illegible]         0
  [illegible]         0
  [illegible]         0
```

EERC/EPA DATA
SDL TASK10 RUN 7R

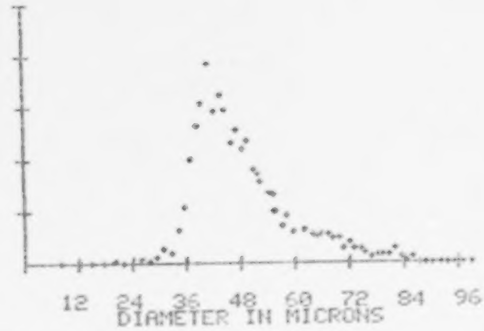

```
MAXIMUM FREQUENCY=0.1

N=3050
D10=48.8
D20=49.8
D30=51
D32=53.4
S=10.23
KURTOSIS=1.09

     SIZE         COUNT

     98.9           0
     97.1           0
     95.4           0
     93.8           0
     92.2           0
     90.7           0
     89.2           0
     87.7           0
     86.3           6
     84.9           2
     83.5           6
     82.2          16
     80.9           9
     79.6           8
     78.3           9
     77.1           7
     75.9          12
     74.6          15
     73.4          15
     72.1          12
     70.9          16
     69.8          22
     68.6          27
     67.4          22
     66.2          33
     65.1          31
     63.9         34
     [illegible]   37
     59.6          35
     [illegible]   54
     [illegible]   42
     56.1          53
     [illegible]   61
     [illegible]   80
     54.6          81
     [illegible]   94
     52.2         103
     51.1         109
     49.9         146
     48.7         134
     47.4         156
     46.2         140
          [illegible]   138
     43.7         137
     42.4         177
     41.1         232
     39.8         188
     38.4         161
     37.1         121
     [illegible]    55
     [illegible]    37
     [illegible]    10
     31.2           15
     [illegible]     7
     [illegible]     2
     [illegible]     3
     [illegible]     0
     [illegible]     1
     [illegible]     0
     [illegible]     0
     [illegible]     0
     [illegible]     0
     [illegible]     0
      8.2            0
```

```
EERC/EPA DATA
SDL TASK10 RUN 8
```

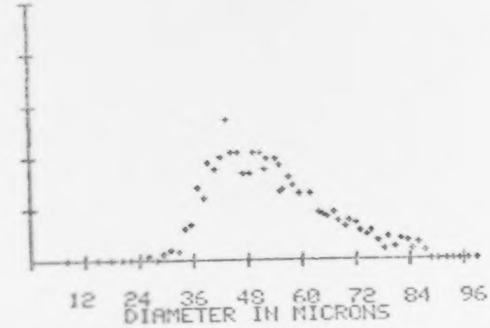

```
MAXIMUM FREQUENCY=0.1

N=2285
D10=53.5
D20=54.8
D30=56.1
D32=58.9
S=11.92
KURTOSIS=.67

      SIZE          COUNT

      98.9            0
      97.1            0
      95.4            0
      93.8            0
      92.2            0
      90.5            0
      88.9            0
      87.5            6
      86.3           14
      84.6            9
      83.5           16
      82.2           18
      80.9           10
      79.5           19
      78.3            9
      77.1           15
      75.8           24
      74.6           21
      73.4           24
      72.1           33
      70.9           33
      69.8           29
      68.6           33
      67.4           42
      66.2           37
      65.1           40
      63.9           42
      62.8           57
      61.7           58
      60.6           64
      59.4           72
      58.4           61
      57.2           83
      56.1           59
      55.1           88
      54.0           88
      53.1           80
      52.1           95
      51.1           95
      49.2           77
      48.7           76
      47.4           95
      46.4           94
      43.7          123
      42.4           91
      41.1           79
      39.8           84
      38.4           55
      [illegible]    64
      [illegible]    39
      [illegible]    27
      [illegible]     7
      [illegible]     8
      [illegible]     4
      [illegible]     0
      [illegible]     0
      [illegible]     0
      [illegible]     0
      [illegible]     0
      [illegible]     0
      [illegible]     0
      [illegible]     0
      16.2            0
```

```
EERC/EPA DATA
SDL TASK10 RUN 8R
```

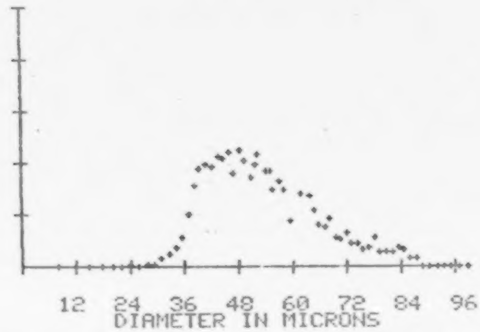

```
MAXIMUM FREQUENCY=0.1

N=2301
D10=53.5
D20=54.7
D30=55.9
D32=58.5
S=11.48
KURTOSIS=.69

      SIZE          COUNT

       98.9           0
       97.1           0
       95.4           0
       93.8           0
       92.2           0
       90.7           0
       89.2           0
       87.7           6
       86.3           7
       84.9          13
       83.5          15
       82.2          12
       80.9          12
       79.6          12
       78.3          24
       77.1          16
       75.8          13
       74.6          19
       73.4          19
       72.1          29
       70.9          23
       69.8          24
       68.6          42
       67.4          34
       66.2          35
       65.1          48
       63.9         62
       62.3          63
       59.6          39
       58.4          68
       57.2          75
       56.1          68
       55.5          83
       55.2          84
       54.6          84
       53.7          98
       52.2          89
       51.1          79
       49.9          93
       48.7         103
       47.4          83
       46.2         100
         45          96
       43.7          97
       42.4          88
       41.1          83
       39.8          85
       38.4          71
       37.1          45
       35.6          25
       34.2          16
       32.7          11
       31.2           6
       29.6           1
       27.9           1
       26.2           0
       24.3           1
       22.3           0
       20.2           0
       17.9           0
       15.3           0
       12.2           0
        8.2           0
```

```
EERC/EPA DATA
SDL TASK10 RUN 9
```

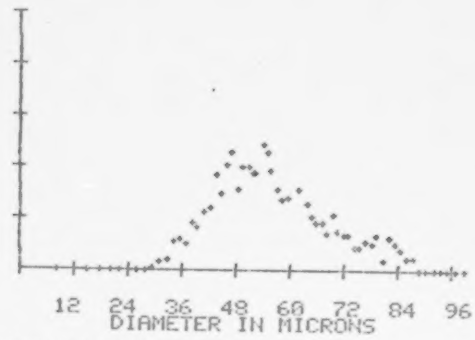

```
MAXIMUM FREQUENCY=0.1

N=1328
D10=55.9
D20=57.1
D30=58.4
D32=61
S=11.89
KURTOSIS=.56

   SIZE        COUNT

   98.9          0
   97.1          0
   95.4          0
   93.8          0
   92.2          0
   90.7          0
   89.2          0
   87.7          6
   86.3          6
   84.9         10
   83.5         13
   82.2         16
   80.9          5
   79.6         18
   78.3         13
   77.1         14
   75.8         11
   74.6         11
   73.4         18
   72.1         18
   70.9         20
   69.8         28
   68.6         19
   67.4         24
   66.2         24
   65.1         27
   63.9        33
   62.3         41
   59.6         37
   58.4         36
   57.2         41
   56.1         50
   55.5         60
   55.2         60
   54.6         64
   52.7         50
   52.2         49
   51.1         53
   49.9         53
   48.7         41
   47.4         60
   46.2         54
     45         39
   43.7         48
   42.4         32
   41.1         29
   39.8         22
   38.4         24
   37.1         13
   35.6         16
   34.5         15
   32.7          5
   31.2          4
   29.6          1
   27.9          0
   26.2          0
   24.3          0
   22.3          0
   20.2          0
   17.9          0
   15.3          0
   12.2          0
    8.2          0
```

```
EERC/EPA DATA
SDL TASK10 RUN 9R
```

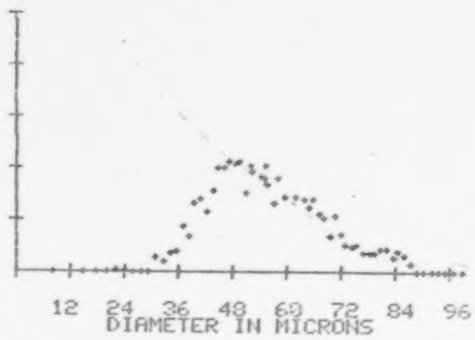

```
MAXIMUM FREQUENCY=0.1

N=1390
D10=55.5
D20=56.8
D30=58
D32=60.5
S=11.75
KURTOSIS=.49

     SIZE        COUNT

     98.9          0
     97.1          0
     95.4          0
     93.8          0
     92.2          0
     90.7          0
     89.2          0
     87.7          4
     86.3          8
     84.9         11
     83.5          7
     82.2         12
     80.9         12
     79.6          9
     78.3         10
     77.1         10
     75.8         14
     74.6         13
     73.4         14
     72.1         20
     70.9         30
     69.8         18
     68.6         28
     67.4         31
     66.2         38
     65.1         34
     63.9        38
     62.3         40
     59.6         39
     58.4         50
     57.2         36
     56.1         46
     55.5         56
     55.2         50
     54.6         51
     53.7         53
     52.2         56
     51.1         42
     49.9         59
     48.7         58
     47.4         59
     46.2         55
       45         55
     43.7         43
     42.4         32
     41.1         39
     39.8         36
     38.4         19
     37.1         24
     35.6         11
     34.2          9
     32.7          5
     31.2          7
     29.6          0
     27.9          0
     26.3          0
     24.3          1
     22.3          1
     20.2          0
     17.9          0
     15.3          0
     12.3          0
      8.2          0
```

```
[illegible] DATA
SDL TASK(1 RUN 1
```

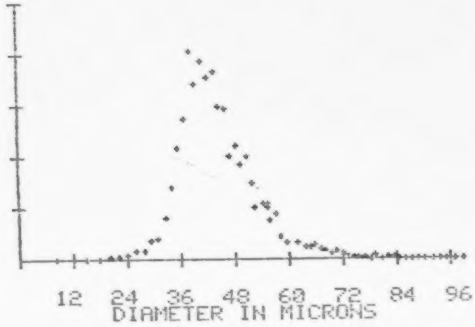

```
MAXIMUM FREQUENCY=0.1

N=3054
D10=45
D20=45.8
D30=46.5
D32=48
S=8.09
KURTOSIS=.78

    SIZE        COUNT

    98.9          0
    97.1          0
    95.4          0
    93.8          0
    92.2          0
    90.7          0
    89.2          0
    87.7          0
    86.3          0
    84.9          0
    83.5          1
    82.2          1
    80.9          0
    79.6          3
    78.3          0
    77.1          2
    75.8          2
    74.6          1
    73.4          4
    72.1          5
    70.9          8
    69.8          7
    68.6          9
    67.4         11
    66.2         17
    65.1         14
    63.9        13
    62.3         18
    59.6         18
    58.4         25
    57.2         53
    56.1         45
    55.5         59
    55.2         64
    54.6         66
    52.7         61
    52.2         90
    51.1        122
    49.9        112
    48.7        134
    47.4        122
    46.2        176
      45        178
    43.7        221
    42.4        213
    41.1        233
    39.8        207
    38.4        245
    37.1        164
    35.6        130
    34.2         83
    32.7         49
    31.2         24
    29.6         22
    27.9          8
    26.2          9
    24.3          3
    22.3          3
    20.2          2
    17.9          0
    15.3          0
    12.2          0
     8.2          0
```

```
LERC/EPA DATA
SPL TASK11 RUN IR
```

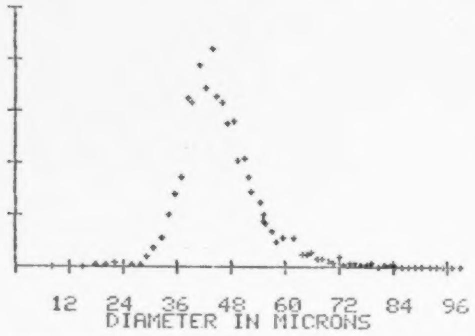

```
MAXIMUM FREQUENCY=0.1

N=3056
D10=46.1
D20=46.8
D30=47.5
D32=48.9
S=7.87
KURTOSIS=.83

     SIZE         COUNT

     98.9            0
     97.1            0
     95.4            0
     93.8            0
     92.2            0
     90.7            0
     89.2            0
     87.7            0
     86.3            0
     84.9            0
     83.5            2
     82.2            2
     80.9            0
     79.6            3
     78.3            2
     77.1            1
     75.8            4
     74.6            3
     73.4            2
     72.1           12
     70.9            4
     69.8            5
     68.6            8
     67.4            9
     66.2           17
     65.1           14
     63.9          13
     62.3           34
     59.6           33
     58.4           29
     57.2           41
     56.1           50
     55.5           53
     55.2           60
     54.6           74
     53.7           88
     52.2          105
     51.1          127
     49.9          123
     48.7          169
     47.4          168
     46.2          192
       45          198
     43.7          256
     42.4          210
     41.1          235
     39.8          193
     38.4          196
     37.1          103
     35.6           83
     34.2           60
     32.7           33
     31.2           20
     29.6           11
     27.9            2
     26.2            2
     24.3            0
     22.3            3
     20.2            1
     17.9            2
     15.3            0
     12.2            0
      8.2            0
```

```
CERC/EPA DATA
SDL TASK11 RUN 2
```

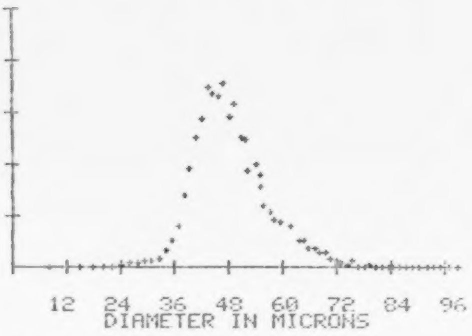

```
MAXIMUM FREQUENCY=0.1

N=3060
D10=49
D20=49.6
D30=50.2
D32=51.4
S=7.55
KURTOSIS=.51

      SIZE           COUNT

       98.9            0
       97.1            0
       95.4            0
       93.8            0
       92.2            0
       90.7            0
       89.2            0
       87.7            0
       86.3            0
       84.9            0
       83.5            0
       82.2            0
       80.9            0
       79.6            2
       78.3            0
       77.1            0
       75.8            5
       74.6            1
       73.4            4
       72.1            5
       70.9            8
       69.8           16
       68.6           17
       67.4           20
       66.2           21
       65.1           30
       63.9          30
       62.3           48
       59.6           53
       58.4           55
       57.2           66
       56.1           73
       55.5           95
       55.2          109
       54.6          122
       52.7          114
       52.2          152
       51.1          154
       49.9          193
       48.7          178
       47.4          217
       46.2          201
         45          205
       43.7          211
       42.4          175
       41.1          153
       39.8          116
       38.4           84
       37.1           47
       35.6           31
       34.2           18
       32.7            9
       31.2            7
       29.6            6
       27.9            4
       26.2            3
       24.3            2
       22.3            0
       20.2            0
       17.9            0
       15.3            0
       12.2            0
        8.2            0
```

```
EERC/EPA DATA
SDL TASK11 RUN 2R
```

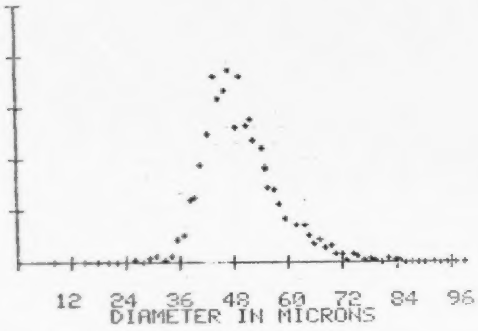

```
MAXIMUM FREQUENCY=0.1

N=3064
D10=50.1
D20=50.6
D30=51.2
D32=52.4
S=7.53
KURTOSIS=.73

     SIZE          COUNT

      98.9           0
      97.1           0
      95.4           0
      93.8           0
      92.2           0
      90.7           0
      89.2           0
      87.7           0
      86.3           0
      84.9           1
      83.5           1
      82.2           3
      80.9           0
      79.6           1
      78.3           3
      77.1           1
      75.8           6
      74.6           8
      73.4           2
      72.1           9
      70.9           8
      69.8          19
      68.6          16
      67.4          26
      66.2          21
      65.1          31
      63.9         43
      62.3          44
      59.6          50
      58.4          68
      57.2          84
      56.1          87
      55.5         112
      55.2         110
      54.6         133
      52.7         143
      52.2         169
      51.1         161
      49.9         220
      48.7         157
      47.4         226
      46.2         203
        45         191
      43.7         220
      42.4         151
      41.1         114
      39.8          75
      38.4          74
      37.1          32
      35.6          25
      34.2           6
      32.7           2
      31.2           5
      29.6           3
      27.9           0
      26.2           1
      24.3           0
      22.3           0
      20.2           0
      17.9           0
      15.3           0
      12.2           0
       8.2           0
```

```
ELRC/EPA DATA
SDL TASK11 RUN 3
```

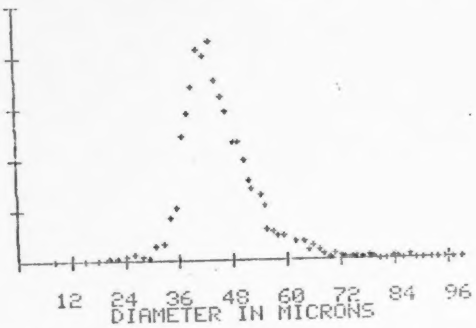

```
MAXIMUM FREQUENCY=0.1

N=3058
D10=46
D20=46.6
D30=47.3
D32=48.6
S=7.58
KURTOSIS=1.01
       SIZE          COUNT

       98.9           0
       97.1           0
       95.4           0
       93.8           0
       92.2           0
       90.7           0
       89.2           0
       87.7           3
       86.3           0
       84.9           2
       83.5           2
       82.2           0
       80.9           0
       79.6           2
       78.3           3
       77.1           1
       75.8           3
       74.6           1
       73.4           2
       72.1           3
       70.9           6
       69.8           2
       68.6           7
       67.4          11
       66.2          15
       65.1          11
       63.9         20
       62.8           20
       61.2           29
       59.6           28
       58.4           34
       57.2           36
       56.1           66
       55.5           65
       54.6           76
       52.2           84
       52.2           94
       51.1          118
       49.9          140
       48.7          140
       47.4          178
       46.2          194
         45          214
       43.7          260
       42.4          243
       41.1          251
       39.8          208
       38.4          176
       37.1          147
       35.6           61
       34.2           51
       32.5           19
       31.2           17
       29.6            2
       27.9            3
       26.2            6
       24.3            3
       22.3            1
       20.2            1
       17.9            0
       15.3            0
       12.2            0
        8.2            0
```

```
EERC/EPA DATA
SDL TASK11 RUN 3R
```

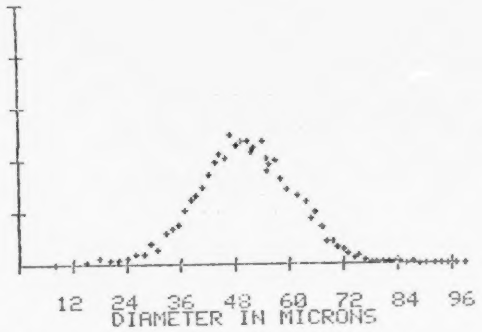

```
MAXIMUM FREQUENCY=0.1

N=3057
D10=50.9
D20=51.9
D30=52.8
D32=54.6
S=9.84
KURTOSIS=-.05
      SIZE          COUNT

      98.9            0
      97.1            0
      95.4            0
      93.8            0
      92.2            0
      90.7            0
      89.2            0
      87.7            2
      86.3            0
      84.9            2
      83.5            2
      82.2            1
      80.9            1
      79.6            2
      78.3            1
      77.1            3
      75.8            9
      74.6            7
      73.4           10
      72.1           17
      70.9           19
      69.8           26
      68.6           26
      67.4           42
      66.2           60
      65.1           52
      63.9          72
      62.3           79
      59.6           86
      58.4           98
      57.2          121
      56.1          116
      55.5          124
      55.2          109
      54.6          144
      52.7          137
      52.2          130
      51.1          143
      49.9          143
      48.7          139
      47.4          151
      46.2          123
        45          129
      43.7          ~~126~~
      42.4          103
      41.1           88
      39.8           79
      38.4           75
      37.1           63
      35.6           45
      34.2           41
      32.7           37
      31.2           16
      29.6           23
      27.9           12
      26.2           11
      24.3            7
      22.3            5
      20.3            4
      17.3            6
      15.2            6
      12.2            6
       8.2            0
```

```
EERC/EPA DATA
SDL TASK11 RUN 4
```

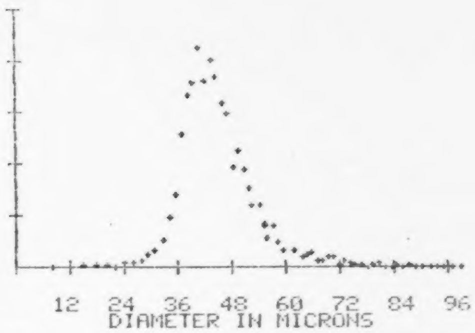

```
MAXIMUM FREQUENCY=0.1

N=3057
D10=45.4
D20=46.1
D30=46.8
D32=48.2
S=7.76
KURTOSIS=.87
      SIZE          COUNT

      98.9            0
      97.1            0
      95.4            0
      93.8            0
      92.2            0
      90.7            0
      89.2            0
      87.7            1
      86.3            0
      84.9            1
      83.5            0
      82.2            0
      80.9            3
      79.6            1
      78.3            0
      77.1            1
      75.8            1
      74.6            4
      73.4            7
      72.1            2
      70.9           10
      69.8           12
      68.6            7
      67.4            5
      66.2           16
      65.1           13
      63.9          11
      62.3           19
      59.6           19
      58.4           28
      57.2           48
      56.1           33
      55.5           47
      55.2           51
      54.6           73
      52.7           73
      52.2           91
      51.1          113
      49.9          137
      48.7          117
      47.4          180
      46.2          191
        45          223
      43.7          242
      42.4          219
      41.1          258
      39.8          218
      38.4          203
      37.1          156
      35.6           85
      34.2           58
      32.7           31
      31.2           18
      29.6           13
      27.9            5
      26.2            4
      24.3            4
      22.3            0
      20.2            2
      17.9            2
      15.3            2
      12.3            0
       8.2            0
```

EERC/EPA DATA
SDL TASK11 RUN 4R

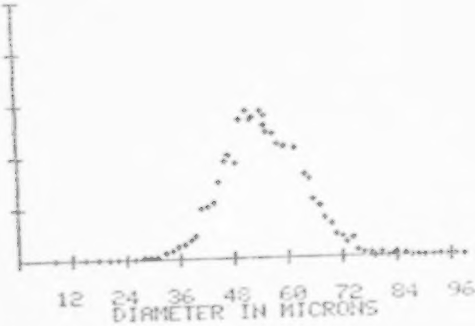

MAXIMUM FREQUENCY=0.1

N=3066
D10=54.7
D20=55.3
D30=55.9
D32=57.1
S=8.06
KURTOSIS=.22

SIZE	COUNT
98.9	0
97.1	0
95.4	0
93.8	0
92.2	0
90.7	0
89.2	0
87.7	0
86.3	1
[illegible]	0
83.5	1
82.2	0
80.9	4
79.6	0
78.3	4
77.1	4
75.8	5
74.6	[illegible]
73.4	17
72.1	23
70.9	28
69.8	38
68.6	45
67.4	61
66.2	67
65.1	91
63.9	98
[illegible]	109
[illegible]	122
59.6	133
58.4	146
57.2	148
56.1	168
55.5	155
[illegible]	174
[illegible]	[illegible]
[illegible]	165
[illegible]	164
[illegible]	173
[illegible]	164
48.7	112
47.4	122
46.[illegible]	114
45	91
43.7	66
42.4	50
41.1	57
39.8	26
38.4	20
37.1	15
35.6	14
34.2	9
32.7	5
31.2	1
29.6	2
27.9	0
26.3	0
[illegible]	0
[illegible]	0
[illegible]	0
[illegible]	0
[illegible]	[illegible]
[illegible]	[illegible]
8.2	[illegible]

```
EERC/EPA DATA
SDL TASK11 RUN 5
```

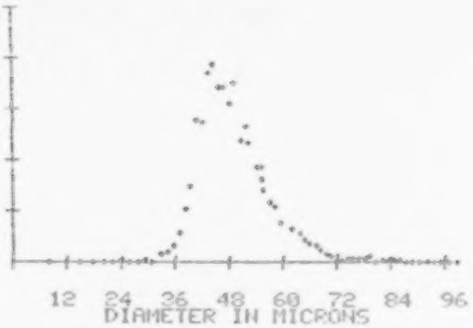

```
MAXIMUM FREQUENCY=0.1

N=3059
D10=49.4
D20=50
D30=50.5
D32=51.7
S=7.36
KURTOSIS=.86

     SIZE          COUNT

      98.9            0
      97.1            0
      95.4            0
[illegible]
       8.2            0
```

EERC/EPA DATA
SDL TASK11 RUN 5R

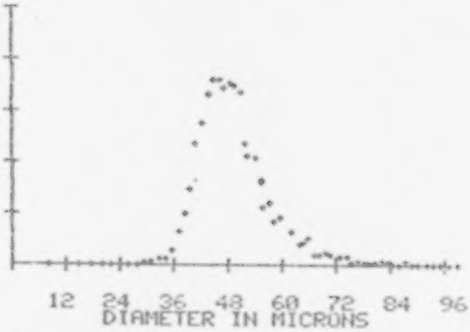

MAXIMUM FREQUENCY=0.1

N=3061
D10=49.7
D20=50.2
D30=50.8
D32=52
S=7.44
KURTOSIS=1.02

SIZE	COUNT
98.9	0
97.1	0
95.4	0
93.8	0
92.2	0
90.7	0
89.2	0
87.7	4
86.3	0
84.9	0
83.5	2
82.2	3
80.9	2
79.6	1
78.3	2
77.1	3
75.8	8
74.6	8
73.4	6
72.1	12
70.9	13
69.8	12
68.6	12
67.4	30
66.2	26
65.1	24
63.9	39
62.8	56
61.6	49
60.4	73
59.2	68
58.1	97
56.5	100
55.2	127
53.7	128
52.2	144
51.1	206
49.9	213
48.7	213
47.4	208
46.2	220
45	219
43.7	201
42.4	167
41.1	143
39.8	89
38.4	60
37.1	39
35.6	17
34.2	6
32.7	3
31.2	3
29.6	1
27.9	0
26.2	0
24.3	0
22.3	0
20.3	0
17.5	0
14.3	0
12.2	0
8.2	0

EERC/EPA DATA
SDL TASK11 RUN 6

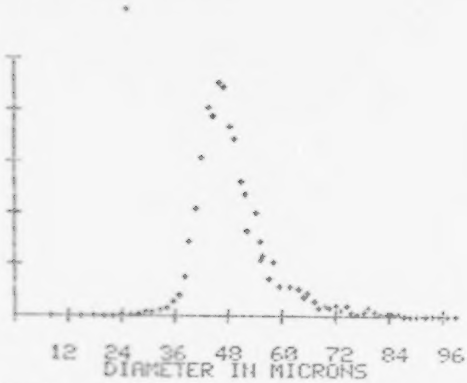

```
MAXIMUM FREQUENCY=0.1

N=3063
D10=49.3
D20=49.8
D30=50.4
D32=51.7
S=7.48
KURTOSIS=1.19

      SIZE         COUNT

      98.9            0
      97.1            0
      95.4            0
      93.8            0
      92.2            0
      90.7            0
      89.2            0
      87.7            0
      86.3            1
      84.9            1
      83.5            2
      82.2            2
      80.9            4
      79.6            9
      78.3            4
      77.1            2
      75.8            4
      74.6           10
      73.4            5
      72.1           11
      70.9            8
      69.8           10
      68.6            9
      67.4           16
      66.2           25
      65.1           22
      63.9          38
      [illegible]    34
      [illegible]    33
      [illegible]    62
      [illegible]    43
      [illegible]    69
      [illegible]    66
      [illegible]    86
      54.6          122
      [illegible]   100
      [illegible]   144
      51.1          158
      49.9          209
      48.7          223
      47.4          271
      46.[illegible] 276
      45            236
      43.[illegible] 245
      42.4          188
      41.1          125
      39.8           87
      38.4           46
      37.1           23
      [illegible]    16
      [illegible]     8
      [illegible]     5
      [illegible]     4
      [illegible]     4
      [illegible]     2
      [illegible]     2
      [illegible]     1
      [illegible]     0
      [illegible]     0
      [illegible]     0
      [illegible]     0
      [illegible]     0
```

```
EERC/EPA DATA
SDL TASK11 RUN 6R
```

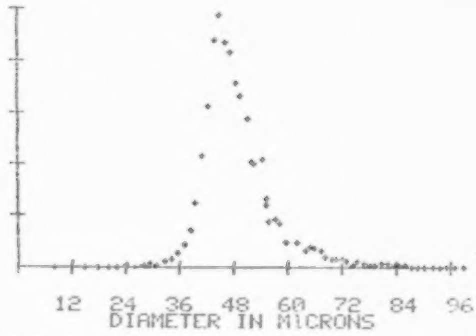

```
MAXIMUM FREQUENCY=0.1

N=3061
D10=48.9
D20=49.4
D30=50
D32=51.1
S=7.05
KURTOSIS=1.18

    SIZE         COUNT

    98.9           0
    97.1           0
    95.4           0
    93.8           0
    92.2           0
    90.7           0
    89.2           0
    87.7           0
    86.3           1
    84.9           2
    83.5           1
    82.2           3
    80.9           3
    79.6           1
    78.3           2
    77.1           3
    75.8           5
    74.6           1
    73.4           6
    72.1           9
    70.9           8
    69.8           9
    68.6          11
    67.4          18
    66.2          21
    65.1          23
    63.9          19
    62.3          27
    59.6          27
    58.4          49
    57.2          55
    56.1          53
    55.5          72
    55.2          88
    54.6         126
    53.7         122
    52.2         124
    51.1         175
    49.9         202
    48.7         216
    47.4         254
    46.2         255
      45         297
    43.7         269
    42.4         189
    41.1         130
    39.8          76
    38.4          43
    37.1          27
    35.6          16
    34.2           8
    32.7           6
    31.2           2
    29.6           4
    27.9           1
    26.2           0
    24.5           2
    22.3           0
    [illegible]    0
    17.9           0
    15.3           0
    12.2           0
     8.2           0
```

```
EERC/EPA DATA
SDL TASK11 RUN 7
```

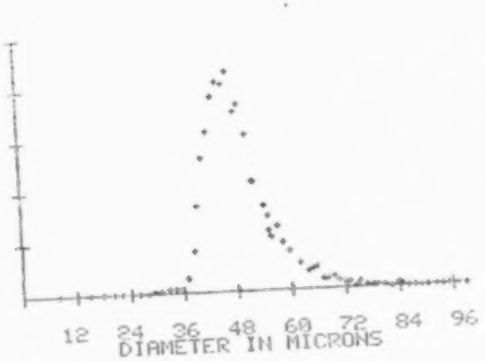

```
MAXIMUM FREQUENCY=0.1

N=3061
D10=49.2
D20=49.7
D30=50.3
D32=51.3
S=7
KURTOSIS=1.14
     SIZE          COUNT

     98.9            0
     97.1            0
     95.4            0
     93.8            0
     92.2            0
     90.7            0
     89.2            0
     87.7            0
     86.3            0
     84.9            2
     83.5            2
     82.2            0
     80.9            2
     79.6            2
     78.3            2
     77.1            2
     75.8            7
     74.6            2
     73.4            5
     72.1            6
     70.9            9
     69.8           14
     68.6           18
     67.4           12
     66.2           25
     65.1           33
  [illegible]       22
  [illegible]       30
  [illegible]       46
  [illegible]       56
  [illegible]       74
  [illegible]       63
  [illegible]       71
  [illegible]       87
  [illegible]      100
  [illegible]      130
  [illegible]      128
  [illegible]      186
  [illegible]      221
  [illegible]      211
  [illegible]      260
  [illegible]      247
     45            248
     43.7          230
     42.4          189
     41.1          157
  [illegible]      102
  [illegible]       47
  [illegible]       17
  [illegible]        3
  [illegible]        3
  [illegible]        4
  [illegible]        2
  [illegible]        1
  [illegible]        0
  [illegible]        0
  [illegible]        0
  [illegible]        0
  [illegible]        0
  [illegible]        0
  [illegible]        0
  [illegible]        0
```

```
EERC/EPA DATA
SDL TASK11 RUN 7R
```

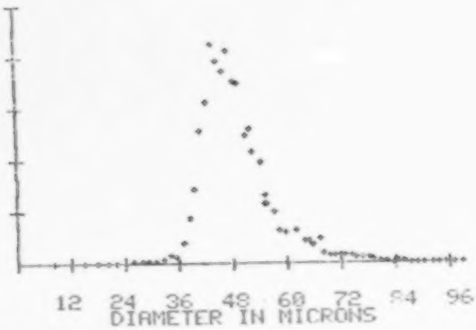

```
MAXIMUM FREQUENCY=0.1

N=3061
D10=49.3
D20=49.9
D30=50.5
D32=51.7
S=7.4
KURTOSIS=1.2

     SIZE          COUNT

     98.9            0
     97.1            0
     95.4            0
     93.8            0
     92.2            0
     90.7            0
     89.2            0
     87.7            0
     86.3            1
     84.9            3
     83.5            0
     82.2            2
     80.9            1
     79.6            3
     78.3            5
     77.1            5
     75.8            5
     74.6            9
     73.4            8
     72.1            8
     70.9            9
     69.8            9
     68.6           11
     67.4           27
     66.2           22
     65.1           26
     63.9          25
     62.3           38
     59.6           35
     58.4           37
     57.2           60
     56.1           71
     55.5           69
     55.2           79
     54.6          118
     52.7          132
     52.2          157
     51.1          152
     49.9          211
     48.7          215
     47.4          252
     46.2          226
        45         233
     43.7          259
     42.4          190
     41.1          156
     39.8           86
     38.4           54
     37.1           22
     35.8            7
     34.5            8
     [illegible]     4
     [illegible]     1
     [illegible]     1
     [illegible]     1
     [illegible]     1
     [illegible]     0
     [illegible]     0
     [illegible]     0
     [illegible]     0
     [illegible]     0
     [illegible]     0
```

```
EERC/EPA DATA
SDL TASK11 RUN 8
```

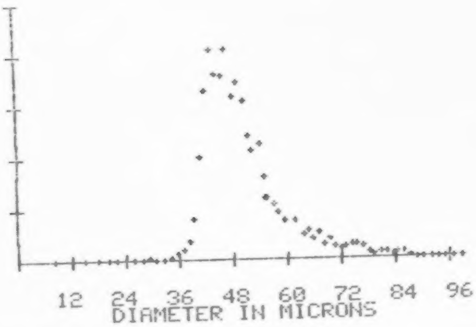

```
MAXIMUM FREQUENCY=0.1

N=3061
D10=50.8
D20=51.5
D30=52.3
D32=53.8
S=8.32
KURTOSIS=1.44

      SIZE           COUNT

      98.9             0
      97.1             0
      95.4             0
      93.8             0
      92.2             0
      90.7             0
      89.2             0
      87.7             2
      86.3             5
      84.9             6
      83.5             4
      82.2             6
      80.9             6
      79.6             3
      78.3             7
      77.1            13
      75.8            15
      74.6            15
      73.4            13
      72.1            11
      70.9            13
      69.8            24
      68.6            15
      67.4            30
      66.2            24
      65.1            32
      63.9           29
      62.3            45
      59.6            46
      58.4            55
      57.2            64
      56.1            72
      55.5            72
      55.2            98
      54.5           137
      52.7           128
      52.2           146
      51.1           188
      49.9           210
      48.7           192
      47.4           249
      46.2           216
      [illegible]    218
      43.7           249
      42.4           199
      41.1           128
      39.8            48
      38.4            20
      37.1            10
      35.6             5
      34.5             1
      32.2             0
      31.2             0
      29.9             1
      [illegible]      0
      [illegible]      0
      [illegible]      0
      [illegible]      0
      [illegible]      0
      [illegible]      0
      [illegible]      0
      [illegible]      0
       8.2             0
```

```
EERC/EPA DATA
SDL TASK11 RUN 8R
```

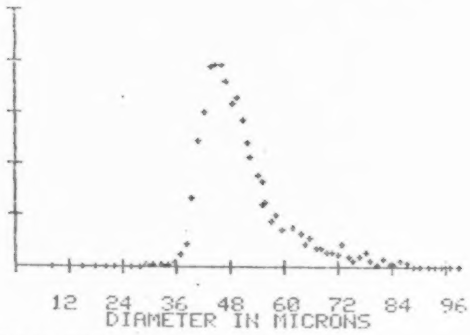

```
MAXIMUM FREQUENCY=0.1

N=3062
D10=50.6
D20=51.3
D30=52.1
D32=53.7
S=8.46
KURTOSIS=1.38

    SIZE          COUNT

    98.9            0
    97.1            0
    95.4            0
    93.8            0
    92.2            0
    90.7            0
    89.2            0
    87.7            3
    86.3            5
    84.9            1
    83.5            2
    82.2            9
    80.9            2
    79.6            6
    78.3           16
    77.1           10
    75.8            6
    74.6           12
    73.4           25
    72.1           14
    70.9           17
    69.8           16
    68.6           21
    67.4           20
    66.2           32
    65.1           26
    63.9          39
    62.3           45
    59.6           44
    58.4           59
    57.2           53
    56.1           74
    55.5           72
    55.2          100
    54.6          106
    53.7          130
    52.2          147
    51.1          172
    49.9          199
    48.7          192
    47.4          218
    46.2          239
       43         238
    43.7          236
    42.4          183
    41.1          147
    39.8           79
    38.4           25
    37.1           13
    35.6            4
    34.2            1
    32.7            2
    31.2            1
    29.6            1
    27.9            0
    26.2            0
    24.3            0
    22.3            0
    20.2            0
    17.9            0
    15.3            0
    12.2            0
     8.2            0
```

EERC/EPA DATA
SDL TASK11 RUN 9R

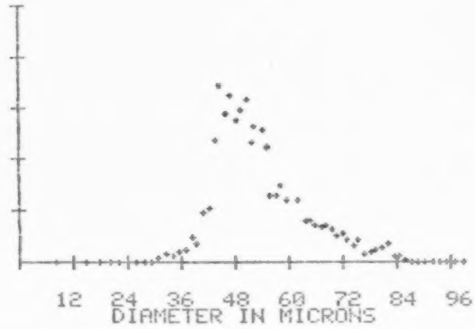

MAXIMUM FREQUENCY=0.1

N=1837
D10=53.5
D20=54.3
D30=55.2
D32=56.9
S=9.31
KURTOSIS=.96

SIZE	COUNT
98.9	0
97.1	0
95.4	0
93.8	0
92.2	0
90.7	0
89.2	0
87.7	0
86.3	1
84.9	4
83.5	3
82.2	12
80.9	9
79.6	8
78.3	6
77.1	5
75.8	15
74.6	11
73.4	15
72.1	20
70.9	18
69.8	23
68.6	26
67.4	24
66.2	25
65.1	29
63.9	29
62.3	44
59.6	44
58.4	54
57.2	46
56.1	46
55.5	80
55.2	83
54.6	93
53.7	97
52.2	84
51.1	116
49.9	108
48.7	101
47.4	113
46.2	105
45	122
43.7	87
42.4	38
41.1	35
39.8	13
38.4	17
37.1	8
[illegible]	6
[illegible]	5
[illegible]	5
[illegible]	5
[illegible]	2
[illegible]	0
[illegible]	0
[illegible]	0
[illegible]	0
[illegible]	0
[illegible]	0
[illegible]	0
[illegible]	0
8.2	0

```
EERC/EPA DATA
SDL TASK12 RUN 1
```

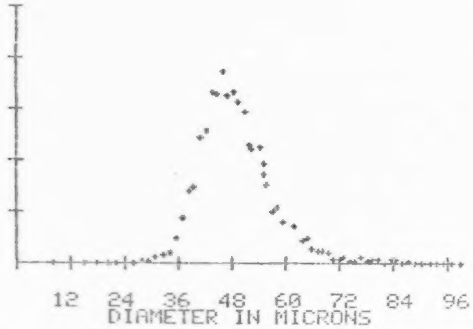

```
MAXIMUM FREQUENCY=0.1

N=3059
D10=49.4
D20=49.9
D30=50.5
D32=51.7
S=7.48
KURTOSIS=.82

    SIZE         COUNT

    98.9           0
    97.1           0
    95.4           0
    93.8           0
    92.2           0
    90.7           0
    89.2           0
    87.7           1
    86.3           0
    84.9           3
    83.5           4
    82.2           0
    80.9           3
    79.6           3
    78.3           1
    77.1           6
    75.8           2
    74.6           1
    73.4           6
    72.1           3
    70.9           3
    69.8          12
    68.6          13
    67.4          14
    66.2          17
    65.1          28
    63.9         25
    62.3          44
    59.6          47
    58.4          65
    57.2          61
    56.1          92
    55.5         104
    55.2         116
    54.6         136
    53.7         134
    53.2         138
    51.1         172
    49.9         190
    48.7         201
    47.4         197
    46.2         226
      45         200
    43.9         231
    42.4         155
    41.1         145
    39.8          88
    38.4          83
    37.1          52
    35.6          28
    34.2          11
    32.7           5
    31.2           4
    29.6           2
    27.9           1
    26.3           0
    24.5           0
    22.3           0
    20.3           0
    17.5           0
    15.3           0
    12.2           0
     8.2           0
```

```
EERC/EPA DATA
SDL TASK12 RUN 1R
```

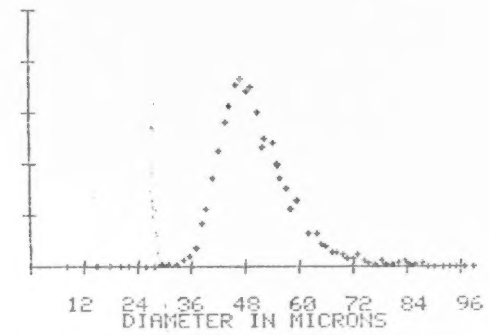

```
MAXIMUM FREQUENCY=0.1

N=3061
D10=50.8
D20=51.3
D30=51.9
D32=53.2
S=7.59
KURTOSIS=1.04

     SIZE          COUNT

     98.9            0
     97.1            0
     95.4            0
     93.8            0
     92.2            0
     90.7            0
     89.2            0
     87.7            3
     86.3            2
     84.9            2
     83.5            5
     82.2            3
     80.9            2
     79.6            2
     78.3            6
     77.1            2
     75.8            3
     74.6            6
     73.4           14
     72.1            9
     70.9            8
     69.8           14
     68.6           16
     67.4           17
     66.2           24
     65.1           26
     63.9          37
     62.3           39
     59.6           76
     58.4           67
     57.2           92
     56.1          105
     55.5          120
     55.2          122
     54.6          147
     52.7          152
     52.2          142
     51.1          182
     49.9          212
     48.7          206
     47.4          222
     46.2          215
       45          190
     43.7          170
     42.4          136
     41.1          104
     39.8           69
     38.4           51
     37.1           21
     35.6           11
     34.2            6
     32.7            1
     31.2            2
     29.6            1
     27.9            0
     26.2            0
     24.3            0
     22.3            0
     20.2            0
     17.9            0
     15.3            0
     12.2            0
      8.2            0
```

```
JPR#0      EERC/EPA DATA
     SDL 12 RUN 2
```

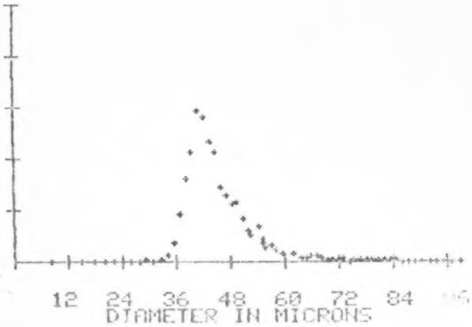

```
MAXIMUM FREQUENCY=.2

N=3057
D10=45.6
D20=46.1
D30=46.7
D32=47.8
S=6.8
KURTOSIS=1.54
      SIZE          COUNT

      98.9            0
      97.1            0
      95.4            0
      93.8            0
      92.2            0
      90.7            0
      89.2            0
      87.7            0
      86.3            0
      84.9            1
      83.5            1
      82.2            1
      80.9            3
      79.6            2
      78.3            4
      77.1            2
      75.8            3
      74.6            0
      73.4            6
      72.1            3
      70.9            1
      69.8            2
      68.6            9
      67.4           12
      66.2           11
      65.1            8
      63.9           7
      62.8           15
      59.6           16
      58.4           25
      57.2           36
      56.1           31
      55.5           41
      55.2           51
      54.6           81
      53.3           62
      52.2           72
      51.1           98
      49.9          148
      48.7          135
      47.4          155
      46.2          175
        45          259
      43.7          279
      42.4          342
      41.1          357
      39.8          257
      38.4          191
      37.1          109
      35.6           40
      34.2           12
      32.7            5
      31.2            [illegible]
      29.6            1
      27.9            0
      26.2            0
      24.3            0
      22.3            0
      20.3            0
      17.9            0
      15.3            0
      12.3            0
       8.2            0
```

```
EERC/EPA DATA
SDL 12 RUN 2R
```

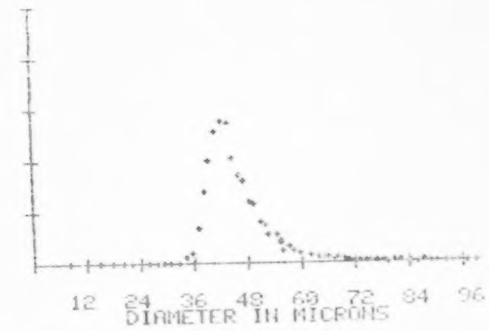

```
MAXIMUM FREQUENCY=.2

N=3060
D10=46
D20=46.4
D30=46.9
D32=47.9
S=6.46
KURTOSIS=1.36

     SIZE          COUNT

     98.9            0
     97.1            0
     95.4            0
     93.8            0
     92.2            0
     90.7            0
     89.2            0
     87.7            1
     86.3            0
     84.9            0
     83.5            0
     82.2            1
     80.9            2
     79.6            0
     78.3            1
     77.1            1
     75.8            1
     74.6            1
     73.4            1
     72.1            3
     70.9            4
     69.8            5
     68.6           10
     67.4            8
     66.2           11
     65.1           12
     63.9           10
     62.8           16
     61.6           [illegible]
     60.4           [illegible]
     59.2           [illegible]
     58.1           [illegible]
     [illegible]    27
     [illegible]    49
     [illegible]    54
     [illegible]    [illegible]
     [illegible]    69
     52.2           93
     51.1           96
     49.9          139
     48.7          147
     47.4          193
     46.2          210
     [illegible]   245
     [illegible]   331
     42.4          335
     41.1          305
     39.8          243
     38.4          169
     37.1          [illegible]
     [illegible]   [illegible]
     [illegible]    21
     [illegible]    11
     [illegible]     0
     [illegible]     0
     [illegible]     0
     [illegible]     0
     [illegible]     0
     [illegible]     0
     [illegible]     0
     [illegible]     0
     [illegible]     0
     [illegible]     0
     [illegible]     0
      8.2            0
```

```
EERC/EPA DATA
SDL 12 RUN 3
```

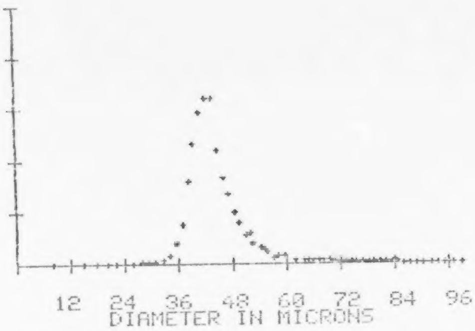

```
MAXIMUM FREQUENCY=.2

N=2968
D10=44.8
D20=45.2
D30=45.7
D32=46.7
S=6.25
KURTOSIS=1.84
    SIZE        COUNT

    98.9          0
    97.1          0
    95.4          0
    93.8          0
    92.2          0
    90.7          0
    89.2          0
    87.7          0
    86.3          0
    84.9          1
    83.5          1
    82.2          1
    80.9          1
    79.6          3
    78.3          1
    77.1          1
    75.8          4
    74.6          2
    73.4          4
    72.1          1
    70.9          3
    69.8          7
    68.6          5
    67.4          6
    66.2          9
    65.1          6
    63.9         5
    62.3          5
    59.6         17
    58.4         15
    57.2         14
    56.1         26
    55.5         31
    55.2         32
    54.6         38
    53.7         44
    52.2         69
    51.1         65
    49.9         93
    48.7        117
    47.4        159
    46.2        198
      45        261
    43.7        376
    42.4        379
    41.1        346
    39.8        274
    38.4        188
    37.1         87
    35.6         44
    34.2         16
    32.7          8
    31.2          2
    29.6          2
    27.9          2
    26.2          0
    24.3          0
    22.3          0
    20.2          0
    17.9          0
    15.3          0
    12.2          0
     8.2          0
```

```
EERC/EPA DATA
SDL 12 RUN 3R
```

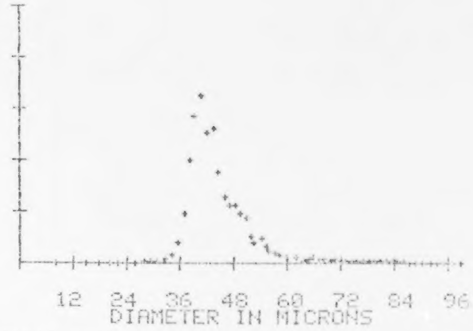

```
MAXIMUM FREQUENCY=.2

N=2923
D10=44.9
D20=45.5
D30=46.1
D32=47.3
S=6.86
KURTOSIS=1.85

     SIZE          COUNT

     98.9            0
     97.1            0
     95.4            0
     93.8            0
     92.2            0
     90.7            0
     89.2            0
     87.7            0
     86.3            2
     84.9            3
     83.5            1
     82.2            1
     80.9            1
     79.6            3
     78.3            4
     77.1            1
     75.8            2
     74.6            2
     73.4            4
     72.1            3
     70.9            9
     69.8            1
     68.6            5
     67.4            7
     66.2           11
     65.1            7
     63.9            4
     62.3           13
     59.6           13
     58.4           17
     57.2           22
     56.1           27
     55.4           35
     55.2           37
     54.6           53
     53.7           45
     52.2           60
     51.1          103
     49.9          109
     48.7          129
     47.4          128
     46.2          149
       45          203
     43.7          304
     42.4          292
     41.1          379
     39.8          330
     38.4          229
     37.1          109
     35.6           43
     34.2           15
     32.7            6
     31.2            3
     29.6            1
     27.9            1
     26.2            0
     24.3            0
     22.3            0
     20.2            0
     17.9            0
     15.3            0
     12.2            0
      8.2            0
```

```
CERC/EPA DATA
SDL 12 RUN 4
```

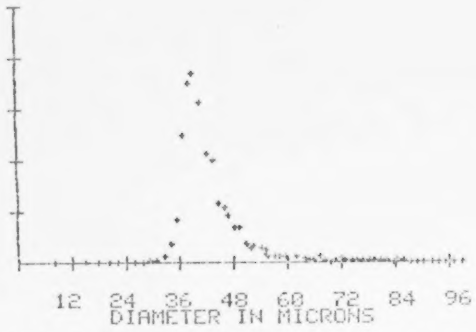

```
MAXIMUM FREQUENCY=.2

N=2588
D10=42.9
D20=43.4
D30=44
D32=45.2
S=6.6
KURTOSIS=2.21
      SIZE          COUNT

       98.9            0
       97.1            0
       95.4            0
       93.8            0
       92.2            0
       90.7            0
       89.2            0
       87.7            0
       86.3            1
       84.9            1
       83.5            0
       82.2            1
       80.9            4
       79.6            1
       78.3            2
       77.1            2
       75.8            2
       74.6            1
       73.4            2
       72.1            3
       70.9            3
       69.8            0
       68.6            4
       67.4            9
       66.2            4
       65.1            4
       63.9          7
       62.3           10
       59.6            9
       58.4           11
       57.2           10
       56.1            9
       55.5           15
       55.2           23
       54.6           28
       52.7           33
       52.2           26
       51.1           37
       49.9           69
       48.7           70
       47.4           94
       46.2          109
         45          117
       43.7          205
       42.4          217
       41.1          321
       39.8          379
       38.4          360
       37.1          253
       35.6           85
       34.2           34
       32.7           10
       31.2            2
       29.6            1
       27.9            0
       26.2            0
       24.3            0
       22.3            0
       20.2            0
       17.9            0
       15.3            0
       12.2            0
        8.2            0
```

```
EERC/EPA DATA
SDL 12 RUN 4R
```

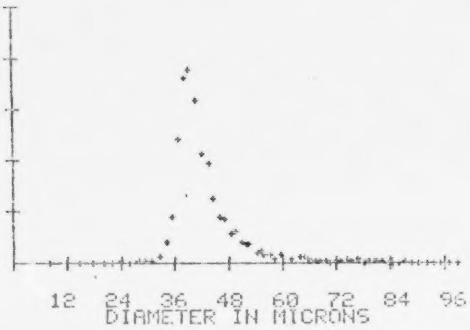

```
MAXIMUM FREQUENCY=.2

N=2540
D10=42.9
D20=43.4
D30=44
D32=45.2
S=6.66
KURTOSIS=2.13

     SIZE         COUNT

     98.9           0
     97.1           0
     95.4           0
     93.8           0
     92.2           0
     90.7           0
     89.2           0
     87.7           1
     86.3           0
     84.9           0
     83.5           0
     82.2           2
     80.9           1
     79.6           2
     78.3           0
     77.1           5
     75.8           3
     74.6           5
     73.4           1
     72.1           2
     70.9           0
     69.8           2
     68.6           2
     67.4           4
     66.2           5
     65.1          11
     63.9         10
     62.3           5
     59.6          14
     58.4           8
     57.2          16
     56.1          14
     55.5          20
     55.2          21
     54.6          20
     52.7          34
     52.2          34
     51.1          38
     49.9          61
     48.7          56
     47.4          84
     46.2          89
       45         124
     43.7         191
     42.4         214
     41.1         318
     39.8         379
     38.4         363
     37.1         242
     35.6          89
     34.2          37
     32.7          10
     31.2           2
     29.6           1
     27.9           1
     26.2           0
     24.3           1
     22.3           0
     20.2           0
     17.9           0
     15.3           0
     12.2           0
      8.2           0
```

EERC/EPA DATA
SDL 12 RUN 5

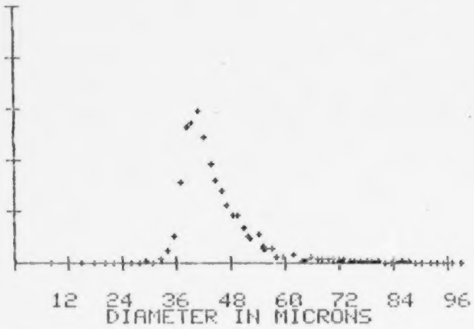

MAXIMUM FREQUENCY=.2

N=3057
D10=44.7
D20=45.3
D30=45.9
D32=47.3
S=7.19
KURTOSIS=1.74

SIZE	COUNT
98.9	0
97.1	0
95.4	0
93.8	0
92.2	0
90.7	0
89.2	0
87.7	1
86.3	2
84.9	1
83.5	0
82.2	0
80.9	1
79.6	4
78.3	4
77.1	2
75.8	1
74.6	4
73.4	7
72.1	4
70.9	6
69.8	9
68.6	5
67.4	8
66.2	14
65.1	7
63.9	4
62.3	18
59.6	13
58.4	14
57.2	32
56.1	31
55.5	31
55.2	39
54.6	64
52.7	56
52.2	63
51.1	79
49.9	108
48.7	109
47.4	136
46.2	167
45	192
43.7	233
42.4	296
41.1	361
39.8	332
38.4	320
37.1	187
35.6	59
34.2	25
32.7	9
31.2	0
29.6	1
27.9	0
26.2	0
24.3	0
22.3	0
20.2	0
17.9	0
15.3	0
12.2	0
8.2	0

```
EERC/EPA DATA
SDL 12 RUN 5R
```

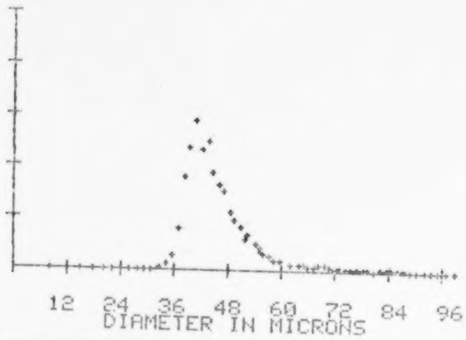

```
MAXIMUM FREQUENCY=.2

N=3057
D10=45.8
D20=46.4
D30=47
D32=48.4
S=7.2
KURTOSIS=1.73

      SIZE          COUNT

      98.9            0
      97.1            0
      95.4            0
      93.8            0
      92.2            0
      90.7            0
      89.2            0
      87.7            2
      86.3            2
      84.9            1
      83.5            2
      82.2            3
      80.9            0
      79.6            2
      78.3            2
      77.1            2
      75.8            3
      74.6            4
      73.4            8
      72.1            3
      70.9            7
      69.8           10
      68.6           10
      67.4            9
      66.2            9
      65.1           11
      63.9          12
      62.8           12
      59.6           20
      58.4           20
      57.2           34
      56.1           38
      55.5           41
      55.2           49
      54.6           62
      53.7           80
      52.2           69
      51.1          108
      49.9          115
      48.7          133
      47.4          182
      46.           196
        45          226
      43.7          303
      42.4          283
      41.1          282
      39.8          284
      38.4          216
      37.1           96
      35.6           33
      34.5           10
      32.7            2
      31.2            0
      29.6            0
      27.9            0
      25.9            0
      24.3            0
      22.3            0
      20.3            0
      17.3            0
      15.3            0
      12.2            0
       8.2            0
```

EERC/EPA DATA
SDL 12 RUN 6

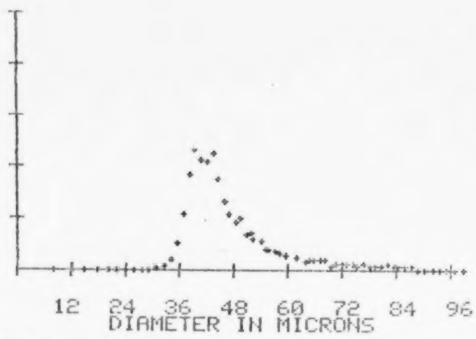

```
MAXIMUM FREQUENCY=.2

N=3037
D10=47.2
D20=48.1
D30=49.2
D32=51.5
S=9.59
KURTOSIS=1.64

     SIZE          COUNT

      98.9            0
      97.1            0
      95.4            0
      93.8            0
      92.2            0
      90.7            0
      89.2            0
      87.7            8
      86.3            5
      84.9            7
      83.5            7
      82.2           10
      80.9            7
      79.6            5
      78.3            6
      77.1           13
      75.8            6
      74.6           10
      73.4           11
      72.1           11
      70.9           12
      69.8            8
      68.6           20
      67.4           23
      66.2           23
      65.1           23
      63.9           19
      62.3           27
      59.6           34
      58.4           35
      57.2           40
      56.1           45
      55.5           45
      55.2           45
      54.6           64
      52.7           69
      52.2           87
      51.1           79
      49.9          119
      48.7          111
      47.4          127
      46.2          156
        45          212
      43.7          272
      42.4          252
      41.1          257
      39.8          280
      38.4          223
      37.1          129
      35.6           61
      34.2           23
      32.7            9
      31.2            3
      29.6            0
      27.9            0
      26.2            0
      24.3            0
      22.3            0
      20.3            0
      17.9            0
      15.3            0
      12.2            0
       8.2            0
```

```
EERC/EPA DATA
SDL 12 RUN 6R
```

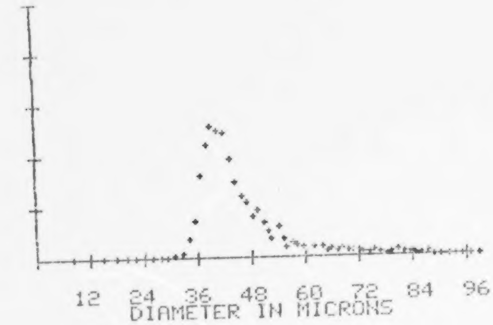

```
MAXIMUM FREQUENCY=.2

N=3033
D10=45.9
D20=46.9
D30=47.9
D32=50.2
S=9.26
KURTOSIS=1.81
      SIZE          COUNT

      98.9            0
      97.1            0
      95.4            0
      93.8            0
      92.2            0
      90.7            0
      89.2            0
      87.7            7
      86.3            3
      84.9            3
      83.5            8
      82.2            7
      80.9           10
      79.6            5
      78.3            3
      77.1            8
      75.8           12
      74.6            7
      73.4            7
      72.1           11
      70.9           14
      69.8           13
      68.6           16
      67.4           11
      66.2           19
      65.1           10
      63.9           23
      62.3           22
      59.6           20
      58.4           26
      57.2           32
      56.1           23
      55.5           43
      55.2           41
      54.6           69
      52.7           43
      52.2           63
      51.1           79
      49.9          110
      48.7           95
      47.4          129
      46.2          146
        45          176
      43.7          232
      42.4          292
      41.1          299
      39.8          309
      38.4          263
      37.1          191
      35.6           85
      34.2           40
      32.7            7
      31.2            3
      29.5            0
      27.9            0
      26.2            0
      24.3            0
      22.3            0
      20.2            0
      17.9            0
      15.3            0
      12.2            0
       8.2            0
```

```
EERC/EPA DATA
SDL 12 RUN 7
```

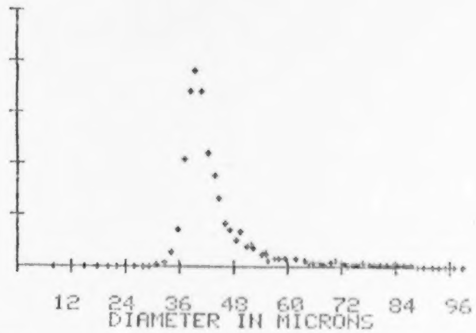

```
MAXIMUM FREQUENCY=.2

N=2503
D10=43.6
D20=44.3
D30=45.1
D32=46.7
S=7.64
KURTOSIS=2.29

     SIZE          COUNT

     98.9             0
     97.1             0
     95.4             0
     93.8             0
     92.2             0
     90.7             0
     89.2             0
     87.7             1
     86.3             2
     84.9             2
     83.5             2
     82.2             4
     80.9             3
     79.6             1
     78.3             3
     77.1             5
     75.8             4
     74.6             2
     73.4             3
     72.1             5
     70.9            10
     69.8             5
     68.6             4
     67.4             6
     66.2             5
     65.1             6
     63.9           12
     62.3            14
     59.6            15
     58.4            14
     57.2            13
     56.1            12
     55.5            22
     55.2            26
     54.6            23
     52.7            36
     52.2            43
     51.1            39
     49.9            66
     48.7            49
     47.4            71
     46.2            83
       45           129
     43.7           174
     42.4           220
     41.1           339
     39.8           379
     38.4           339
     37.1           207
     35.6            71
     34.2            28
     32.7             5
     31.2             3
     29.6             0
     27.9             0
     26.2             0
     24.3             0
     22.3             0
     20.2             0
     17.9             0
     15.3             0
     12.2             0
      8.2             0
```

```
EERC/EPA DATA
SDL 12 RUN 7R
```

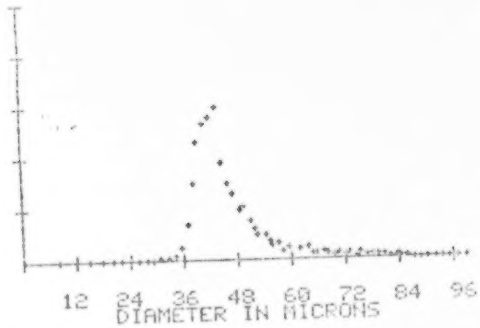

```
MAXIMUM FREQUENCY=.2

N=3055
D10=46.5
D20=47.2
D30=48
D32=49.7
S=8.14
KURTOSIS=1.8
        SIZE          COUNT

        98.9            0
        97.1            0
        95.4            0
        93.8            0
        92.2            0
        90.7            0
        89.2            0
        87.7            0
        86.3            2
        84.9            3
        83.5            2
        82.2            1
        80.9            6
        79.6            8
        78.3            6
        77.1            5
        75.8           14
        74.6            3
        73.4           11
        72.1            8
        70.9           14
        69.8            6
        68.6           10
        67.4           17
        66.2           13
        65.1           14
        63.9          29
        [illegible]    24
        59.6           27
        58.4           19
        [illegible]    35
        56.1           31
        [illegible]    42
        [illegible]    41
        54.6           57
        [illegible]    58
        52.2           73
        51.1           89
        49.9          126
        48.7          115
        47.4          156
        46.2          176
          45          228
         43.7         358
         42.4         333
         41.1         320
         39.8         276
         38.4         177
        [illegible]    79
        [illegible]    28
        [illegible]     8
        [illegible]     4
        [illegible]     2
        [illegible]     0
        [illegible]     0
        [illegible]     0
        [illegible]     0
        [illegible]     0
        [illegible]     0
        [illegible]     0
        [illegible]     0
          8.2           0
```

EERC/EPA DATA
SDL 12 RUN 8

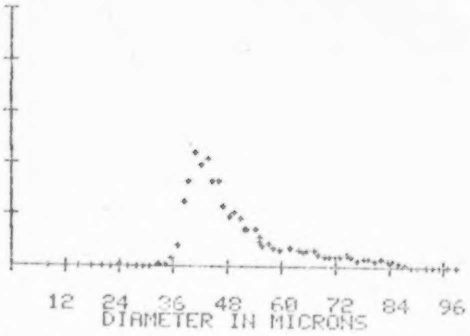

MAXIMUM FREQUENCY=.2

N=3032
D10=50
D20=51.2
D30=52.4
D32=55.1
S=10.78
KURTOSIS=1.32

SIZE	COUNT
98.9	0
97.1	0
95.4	0
93.8	0
92.2	0
90.7	0
89.2	0
87.7	4
86.3	9
84.9	10
83.5	12
82.2	16
80.9	14
79.6	15
78.3	17
77.1	12
75.8	20
74.6	25
73.4	23
72.1	23
70.9	24
69.8	22
68.6	28
67.4	36
66.2	34
65.1	30
63.9	36
62.8	42
59.6	34
58.4	41
57.2	51
56.1	47
55.5	65
55.2	56
53.5	84
52.7	87
52.2	84
51.1	111
49.9	124
48.7	112
47.4	137
46.2	196
45	197
43.7	248
42.4	234
41.1	262
39.8	198
38.4	147
37.1	44
35.6	16
34.2	3
32.7	3
31.2	0
29.6	0
27.9	0
26.2	0
24.3	1
22.3	0
20.1	0
17.7	0
15.3	0
12.2	0
8.2	0

```
EERC/EPA DATA
SDL 12 RUN 6R
```

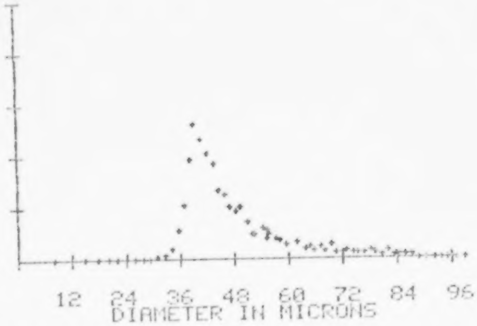

```
MAXIMUM FREQUENCY=.2

N=3035
D10=47.8
D20=49
D30=50.3
D32=53
S=10.5
KURTOSIS=1.52
    SIZE          COUNT

    98.9            0
    97.1            0
    95.4            0
    93.8            0
    92.2            0
    90.7            0
    89.2            0
    87.7            9
    86.3            9
    84.9            6
    83.5            7
    82.2           15
    80.9            8
    79.6           14
    78.3           16
    77.1           11
    75.8           12
    74.6           11
    73.4           15
    72.1           13
    70.9           13
    69.8           30
    68.6           17
    67.4           29
    66.2           15
    65.1           25
    63.9           23
    62.3           35
    59.6           38
    58.4           40
    57.2           46
    56.1           54
    55.5           64
    55.2           45
    54.6           70
    52.7           57
    52.2           54
    51.1           84
    49.9          119
    48.7          112
    47.4          118
    46.2          151
      45          157
    43.7          221
    42.4          245
    41.1          280
    39.8          313
    38.4          230
    37.1          123
    35.6           63
    34.2           20
    32.7            5
    31.2            2
    29.6            0
    27.9            0
    26.2            0
    24.3            0
    22.3            0
    20.2            0
    17.9            0
    15.3            0
    12.3            0
     8.2            0
```

EERC/EPA DATA
SDL TASK10 RUN 1R

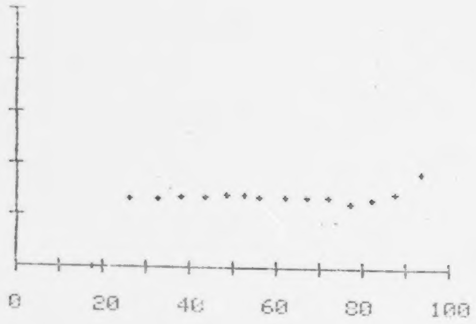

MAXIMUM VELOCITY = 15 M/SEC

DIAMETER IN MICRONS

DIAMETER (MICRONS)	VELOCITY (M/SEC)
93.8	5.6
87.7	4.3
82.2	4
77.1	3.8
72.1	4.2
67.4	4.1
62.3	4.2
56.1	4.2
52.7	4.2
48.7	4.3
43.7	4.2
38.4	4.2
32.7	4
26.2	4.1

EERC/EPA DATA
SDL TASK10 RUN 2R

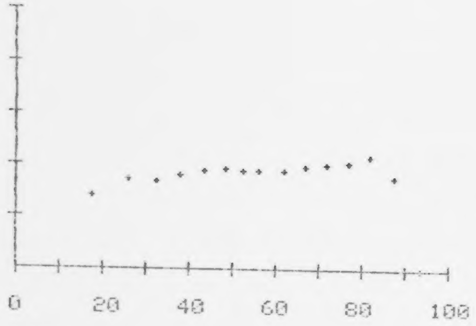

MAXIMUM VELOCITY ~~= 15 M/SEC~~

DIAMETER IN MICRONS

DIAMETER (MICRONS)	VELOCITY (M/SEC)
87.7	5.4
82.2	6.6
77.1	6.2
72.1	6.1
67.4	5.9
62.3	5.7
56.1	5.7
52.7	5.7
48.7	5.8
43.7	5.7
38.4	5.5
32.7	5.2
26.2	5.3
17.9	4.3

EERC/EPA DATA
SDL TASK10 RUN 3R

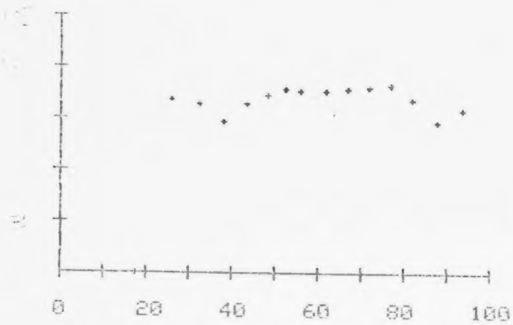

MAXIMUM VELOCITY = 15 M/SEC

DIAMETER IN MICRONS

DIAMETER (MICRONS)	VELOCITY (M/SEC)
93.8	9.5
87.7	8.8
82.2	10.1
77.1	10.9
72.1	10.9
67.4	10.8
62.3	10.6
55.1	10.6
52.7	10.7
48.7	10.4
43.7	9.8
38.4	8.9
32.7	9.9
26.2	10.2

EERC/EPA DATA
SDL TASK10 RUN 4R

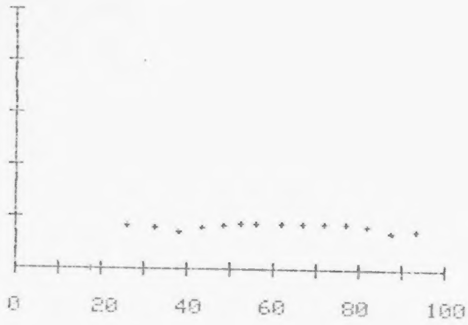

MAXIMUM VELOCITY = 15 M/SEC

DIAMETER IN MICRONS

DIAMETER (MICRONS)	VELOCITY (M/SEC)
93.8	2.4
87.7	2.2
82.2	2.5
77.1	2.7
72.1	2.7
67.4	2.7
62.3	2.7
55.1	2.7
52.7	2.6
48.7	2.7
43.7	2.6
38.4	2.6
32.7	2.5
26.2	2.5
	2.5

EERC/EPA DATA
SDL TASK10 RUN 5R

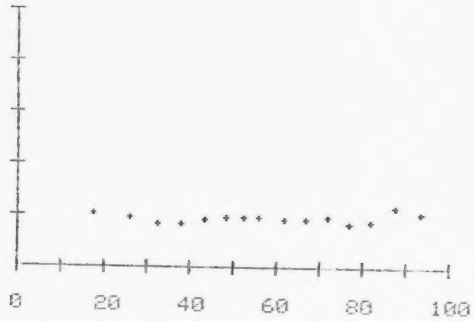

MAXIMUM VELOCITY = 15 M/SEC

DIAMETER IN MICRONS

DIAMETER (MICRONS)	VELOCITY (M/SEC)
93.8	3.2
87.7	3.6
82.2	2.7
77.1	2.6
72.1	2.9
67.4	2.9
62.3	2.9
56.1	2.9
52.7	2.9
48.7	2.9
43.7	2.8
38.4	2.6
32.7	2.6
26.2	3
17.9	3.2

EERC/EPA DATA
SDL TASK10 RUN 6R

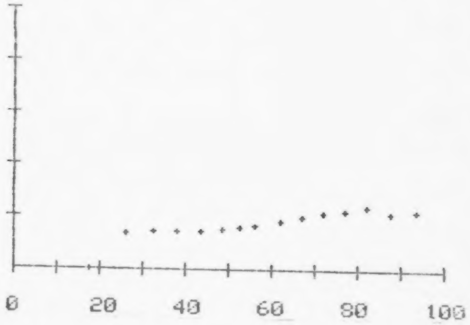

MAXIMUM VELOCITY = 15 M/SEC

DIAMETER IN MICRONS

DIAMETER (MICRONS)	VELOCITY (M/SEC)
93.8	3.5
87.7	3.4
82.2	3.6
77.1	3.4
72.1	3.4
67.4	3.1
62.3	2.9
56.1	2.7
52.7	2.5
48.7	2.3
43.7	2.3
38.4	2.2
32.7	2.2
26.2	2.1

EERC/EPA DATA
SDL TASK10 RUN 7R

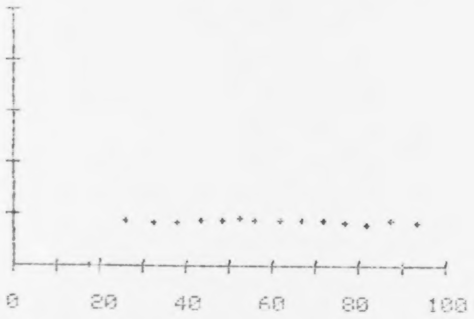

MAXIMUM VELOCITY = 15 M/SEC

DIAMETER IN MICRONS

DIAMETER (MICRONS)	VELOCITY (M/SEC)
93.8	2.6
87.7	2.7
82.2	2.5
77.1	2.6
72.1	2.7
67.4	2.7
62.3	2.7
56.1	2.7
52.7	2.8
48.7	2.7
43.7	2.7
38.4	2.6
32.7	2.6
26.2	2.7

EERC/EPA DATA
SDL TASK10 RUN 8R

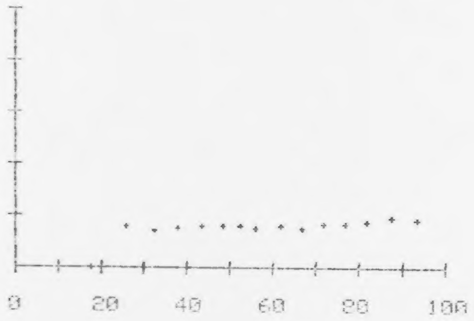

MAXIMUM VELOCITY = 15 M/SEC

DIAMETER IN MICRONS

DIAMETER (MICRONS)	VELOCITY (M/SEC)
93.8	2.8
87.7	[illegible]
82.2	2.8
77.1	2.5
72.1	2.6
67.4	2.4
62.3	2.4
56.1	2.4
52.7	2.5
48.7	2.4
43.7	2.4
38.4	2.3
32.7	2.3
26.2	2.4

EERC/EPA DATA
SDL TASK10 RUN 9R

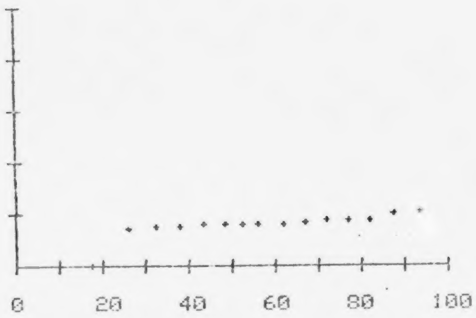

MAXIMUM VELOCITY = 15 M/SEC

DIAMETER IN MICRONS

DIAMETER (MICRONS)	VELOCITY (M/SEC)
93.8	3.1
87.7	3.1
82.2	2.8
77.1	2.7
72.1	2.7
67.4	2.5
62.3	2.5
56.1	2.4
52.7	2.5
48.7	2.4
43.7	2.5
38.4	2.4
32.7	2.3
26.2	2.2

EERC/EPA DATA
SDL TASK11 RUN 1R

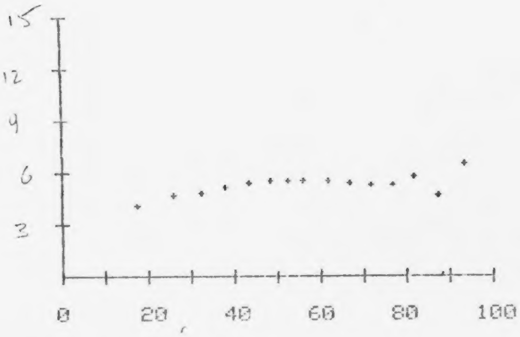

MAXIMUM VELOCITY = 15 M/SEC

DIAMETER IN MICRONS

DIAMETER (MICRONS)	VELOCITY (M/SEC)
93.8	6.5
87.7	4.7
82.2	5.9
77.1	5.4
72.1	5.4
67.4	5.4
62.3	5.6
56.1	5.6
52.7	5.6
48.7	5.6
43.7	5.5
38.4	5.2
32.7	4.9
26.2	4.8
17.9	4.1

EERC/EPA DATA
SDL TASK11 RUN 2R

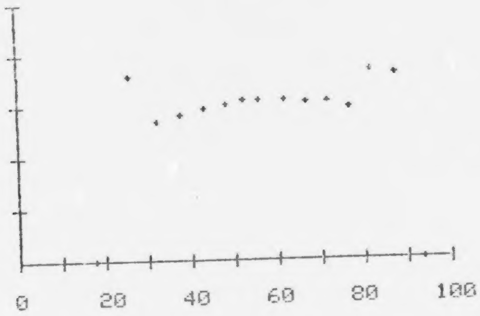

MAXIMUM VELOCITY = 15 M/SEC

DIAMETER IN MICRONS

DIAMETER (MICRONS)	VELOCITY (M/SEC)
87.7	10.8
82.2	11
77.1	8.8
72.1	9.1
67.4	9.2
62.3	9.3
56.1	9.3
52.7	9.3
48.7	9
43.7	8.8
38.4	8.5
32.7	8.1
26.2	10.8

EERC/EPA DATA
SDL TASK11 RUN 3R

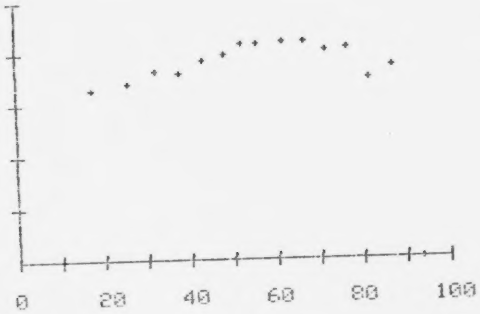

MAXIMUM VELOCITY = 15 M/SEC

DIAMETER IN MICRONS

DIAMETER (MICRONS)	VELOCITY (M/SEC)
87.7	11.2
82.2	10.5
77.1	12.3
72.1	12.2
67.4	12.6
62.3	12.7
56.1	12.6
52.7	12.5
48.7	11.9
43.7	11.6
38.4	10.9
32.7	10.9
26.2	10.2
17.9	9.9

EERC/EPA DATA
SDL TASK11 RUN 4R

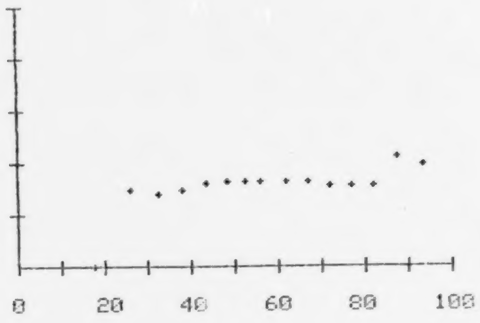

MAXIMUM VELOCITY = 15 M/SEC

DIAMETER IN MICRONS

DIAMETER (MICRONS)	VELOCITY (M/SEC)
93.8	6
87.7	6.4
82.2	4.8
77.1	4.8
72.1	4.7
67.4	5
62.3	5
56.1	5
52.7	5
48.7	5
43.7	4.9
38.4	4.6
32.7	4.4
26.2	4.5

EERC/EPA DATA
SDL TASK11 RUN 5R

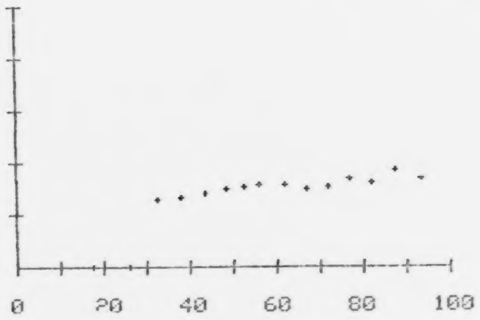

MAXIMUM VELOCITY = 15 M/SEC

DIAMETER IN MICRONS

DIAMETER (MICRONS)	VELOCITY (M/SEC)
93.8	5.1
87.7	5.5
82.2	4.8
77.1	5.1
72.1	4.6
67.4	4.5
62.3	4.7
56.1	4.8
52.7	4.6
48.7	4.5
43.7	4.2
38.4	4
32.7	3.9

EERC/EPA DATA
SDL TASK11 RUN 6R

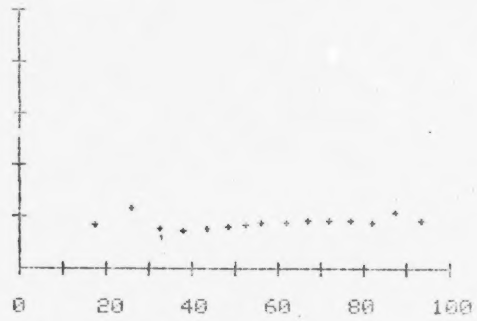

MAXIMUM VELOCITY = 15 M/SEC

DIAMETER IN MICRONS

DIAMETER (MICRONS)	VELOCITY (M/SEC)
93.8	2.8
87.7	3.3
82.2	2.7
77.1	2.8
72.1	2.8
67.4	2.8
62.3	2.7
56.1	2.7
52.7	2.6
48.7	2.4
43.7	2.3
38.4	2.2
32.7	2.3
26.2	3.5
17.9	2.6

EERC/EPA DATA
SDL TASK11 RUN 7R

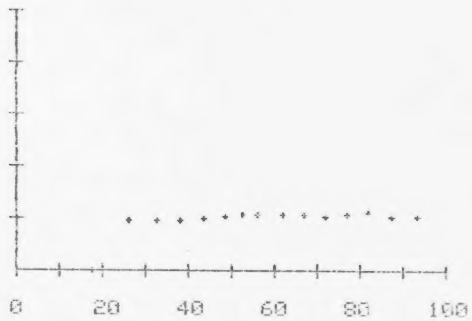

MAXIMUM VELOCITY = 15 M/SEC

DIAMETER IN MICRONS

DIAMETER (MICRONS)	VELOCITY (M/SEC)
93.8	3.2
87.7	3.2
82.2	3.4
77.1	3.3
72.1	3.1
67.4	3.3
62.3	3.3
56.1	3.3
52.7	3.3
48.7	3.2
43.7	3.1
38.4	2.9
32.7	3
26.2	3

EERC/EPA DATA
SDL TASK11 RUN 8R

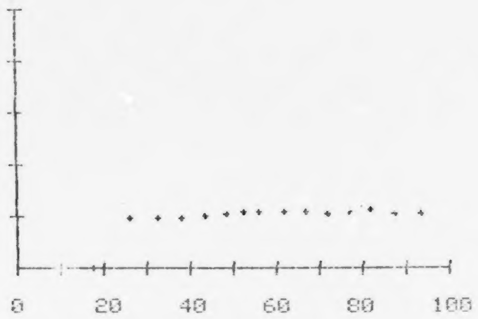

MAXIMUM VELOCITY = 15 M/SEC

DIAMETER IN MICRONS

DIAMETER (MICRONS)	VELOCITY (M/SEC)
93.8	3.2
87.7	3.2
82.2	3.4
77.1	3.3
72.1	3.1
67.4	3.3
62.3	3.3
56.1	3.3
52.7	3.3
48.7	3.2
43.7	3.1
38.4	2.9
32.7	3
26.2	3

EERC/EPA DATA
SDL TASK11 RUN 9R

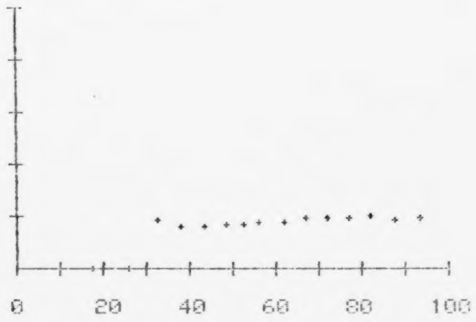

MAXIMUM VELOCITY = 15 M/SEC

DIAMETER IN MICRONS

DIAMETER (MICRONS)	VELOCITY (M/SEC)
93.8	3
87.7	2.9
82.2	3.1
77.1	2.9
72.1	2.9
67.4	2.9
62.3	2.8
55.1	2.7
52.7	2.6
48.7	2.5
43.7	2.5
38.4	2.5
32.7	2.8

EERC/EPA DATA
SDL TASK12 RUN 1R

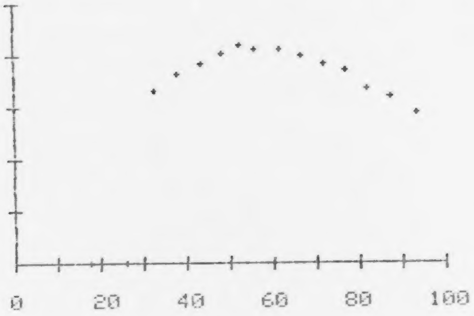

MAXIMUM VELOCITY = 15 M/SEC

DIAMETER IN MICRONS

DIAMETER (MICRONS)	VELOCITY (M/SEC)
93.8	8.6
87.7	9.7
82.2	10.2
77.1	11.2
72.1	11.6
67.4	12.1
62.3	12.4
56.1	12.4
52.7	12.6
48.7	12.2
43.7	11.6
38.4	11
32.7	10

EERC/EPA DATA
SDL 12 RUN 2R

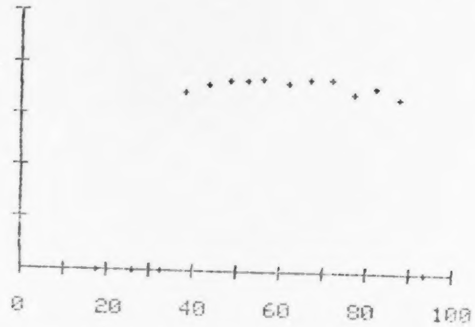

MAXIMUM VELOCITY = 15 M/SEC

DIAMETER IN MICRONS

DIAMETER (MICRONS)	VELOCITY (M/SEC)
87.7	10.2
82.2	10.7
77.1	10.4
72.1	11.2
67.4	11.2
62.3	11
56.1	11.2
52.7	11.1
48.7	11.1
43.7	10.9
38.4	10.4

EERC/EPA DATA
SDL 12 RUN 3R

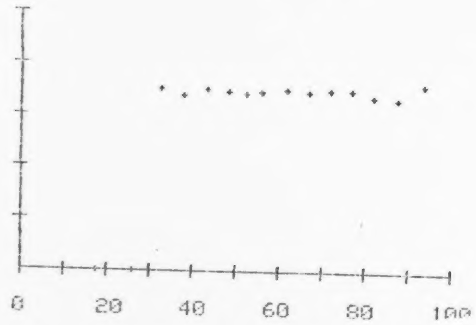

MAXIMUM VELOCITY = 15 M/SEC

DIAMETER IN MICRONS

DIAMETER (MICRONS)	VELOCITY (M/SEC)
93.8	10.9
87.7	10.1
82.2	10.3
77.1	10.6
72.1	10.7
67.4	10.5
62.3	10.7
56.1	10.5
52.7	10.4
48.7	10.5
43.7	10.6
38.4	10.3
32.7	10.6

EERC/EPA DATA
SDL 12 RUN 4R

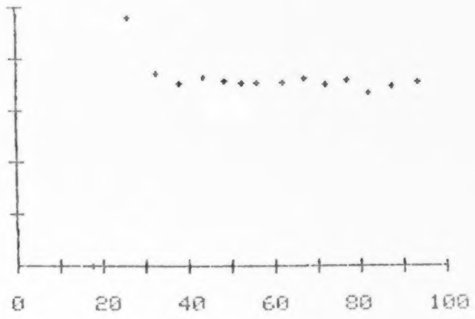

MAXIMUM VELOCITY = 15 M/SEC
DIAMETER IN MICRONS

DIAMETER (MICRONS)	VELOCITY (M/SEC)
93.8	10.6
87.7	10.3
82.2	10
77.1	10.7
72.1	10.5
67.4	10.9
62.3	10.7
56.1	10.6
52.7	10.6
48.7	10.8
43.7	10.9
38.4	10.6
32.7	11.3
26.2	14.5

EERC/EPA DATA
SDL 12 RUN 5R

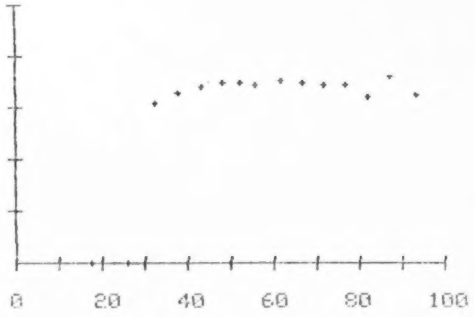

MAXIMUM VELOCITY = 15 M/SEC
DIAMETER IN MICRONS

DIAMETER (MICRONS)	VELOCITY (M/SEC)
93.8	9.8
87.7	10.9
82.2	9.6
77.1	10.3
72.1	10.3
67.4	10.5
62.3	10.6
56.1	10.4
52.7	10.5
48.7	10.5
43.7	10.3
38.4	9.8
32.7	9.4

EERC/EPA DATA
SDL 12 RUN 6R

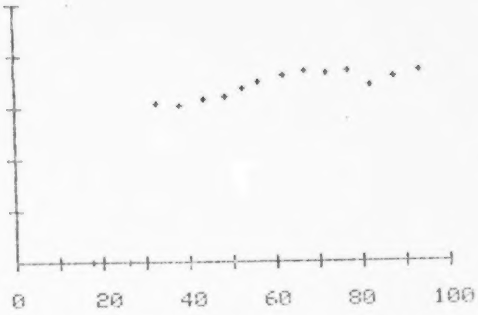

MAXIMUM VELOCITY = 15 M/SEC
DIAMETER IN MICRONS

DIAMETER (MICRONS)	VELOCITY (M/SEC)
93.8	11.1
87.7	10.7
82.2	10.2
77.1	11.1
72.1	11
67.4	11.1
62.3	10.9
56.1	10.5
52.7	10.1
48.7	9.7
43.7	9.6
38.4	9.1
32.7	9.3

EERC/EPA DATA
SDL 12 RUN 7R

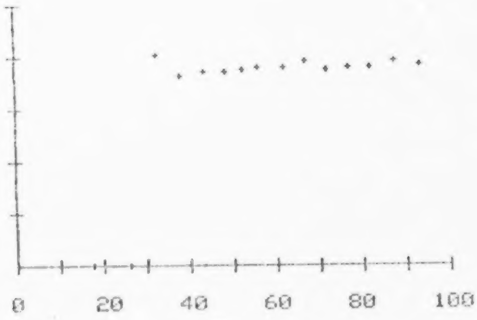

MAXIMUM VELOCITY = 15 M/SEC
DIAMETER IN MICRONS

DIAMETER (MICRONS)	VELOCITY (M/SEC)
93.8	11.5
87.7	11.8
82.2	11.4
77.1	11.5
72.1	11.4
67.4	11.8
62.3	11.4
56.1	11.4
52.7	11.3
48.7	11.2
43.7	11.2
[illegible].4	11
[illegible].7	12.2

[illegible] DATA
SDL 12 RUN 8F

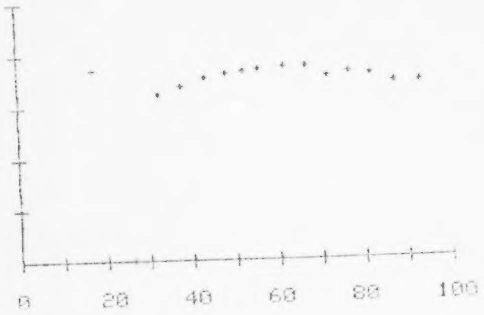

MAXIMUM VELOCITY = 15 M/SEC
DIAMETER IN MICRONS

DIAMETER (MICRONS)	VELOCITY (M/SEC)
93.8	10.3
87.9	10.4
82.2	10.9
77.1	11
72.1	10.8
67.4	11.3
62.3	11.4
56.1	11.2
52.7	11
48.7	10.9
43.7	10.7
38.4	10.2
32.7	9.7
17.9	11.3

EERC/EPA DATA
SDL 12 RUN 9R

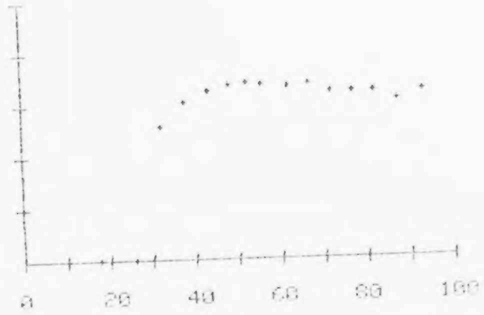

MAXIMUM VELOCITY = 15 M/SEC
DIAMETER IN MICRONS

DIAMETER (MICRONS)	VELOCITY (M/SEC)
93.8	9.7
87.9	9.6
82.2	9.6
77.1	9.6
72.1	9.7
67.4	10.1
62.3	10
56.1	10.2
52.7	10.2
48.7	10.1
43.7	9.7
38.4	9.2
32.7	7.7

EERC/EPA DATA
SDL 12 RUN 9

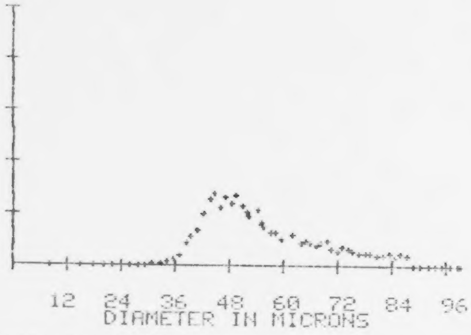

MAXIMUM FREQUENCY=.2

N=3020
D10=54.9
D20=56.2
D30=57.5
D32=60.1
S=11.67
KURTOSIS=.87

SIZE	COUNT
98.9	0
97.1	0
95.4	0
93.8	0
92.2	0
90.7	0
89.2	0
87.7	20
86.3	25
84.9	18
83.5	25
82.2	20
80.9	23
79.6	25
78.3	25
77.1	27
75.8	34
74.6	36
73.4	39
72.1	31
70.9	36
69.8	55
68.6	52
67.4	47
66.2	49
65.1	54
63.9	53
62.3	68
59.6	61
58.4	74
57.2	77
56.1	87
55.5	95
55.2	98
54.6	130
53.7	113
52.2	125
51.1	136
49.9	160
48.7	143
47.4	156
46.2	135
45	165
43.7	154
42.4	116
41.1	78
39.8	68
38.4	55
37.1	20
35.6	13
34.2	6
32.7	3
31.2	2
29.6	0
27.9	0
26.2	0
24.5	0
22.3	0
20.2	0
17.9	0
15.3	0
12.2	0
8.2	0

```
EERC/EPA DATA
SDL 12 RUN 9R
```

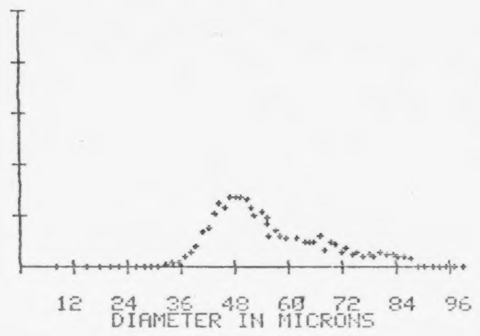

```
MAXIMUM FREQUENCY=.2

N=2826
D10=55.6
D20=56.8
D30=58
D32=60.6
S=11.55
KURTOSIS=.86

      SIZE          COUNT

      98.9            0
      97.1            0
      95.4            0
      93.8            0
      92.2            0
      90.7            0
      89.2            0
      87.7           18
      86.3           19
      84.9           22
      83.5           23
      82.2           24
      80.9           31
      79.6           22
      78.3           27
      77.1           20
      75.8           30
      74.6           25
      73.4           40
      72.1           29
      70.9           46
      69.8           54
      68.6           35
      67.4           64
      66.2           50
      65.1          54
      63.9           53
      62.3           61
      59.6           63
      58.4           66
      57.2           77
      56.1           67
      55.5          105
      55.2           95
      54.6          118
      52.7          109
      52.2          127
      51.1          146
      49.9          151
      48.7          154
      47.4          153
      46.2          131
        45          139
      43.7          116
      42.4           85
      41.1           75
      39.8           44
      38.4           30
      37.1           20
      35.6            6
      34.2            6
      32.7            1
      31.2            0
      29.6            0
      27.9            0
      26.2            0
      24.3            0
      22.3            0
      20.2            0
      17.9            0
      15.3            0
      12.2            0
       8.2            0
```